Volume 94 Number 1 MAY 1998 ISSN 0026-8976

MOLECULAR PHYSICS

An international journal in the field of chemical physics

Special Issue:
The Coupled Cluster Theory Electron Correlation Workshop
'Fifty Years of the Correlation Problem'
Cedar Key, Florida, 15–19 June 1997
Guest Editor: R. J. Bartlett

TAYLOR & FRANCIS
ALERE FLAMMAM
1798 - 1998

MOPHAM 94 (1) 1-248 (1998)

MOLECULAR PHYSICS

An international journal in the field of chemical physics

Recognized by the European Physical Society

Subscription Information

Molecular Physics is published semi-monthly, except one issue in January, March, May, July, September and November (total eighteen issues), by Taylor & Francis Ltd, One Gunpowder Square, London EC4A 3DE, UK.

Annual Subscriptions 1998

Print	ISSN 0026–8976	$2395	£1452
Online	ISSN 1362–3028	$2395	£1452
Combined	MPHOP	$2874	£1742

For more information on our journals and books publishing, visit our website: http://www.tandf.co.uk/

Periodical postage paid at Jamaica, New York 11431. US Postmasters: Send address changes to *Molecular Physics*, Publications Expediting Inc., 200 Meacham Avenue, Elmont, New York 11003. Air freight and mailing in the USA by Publications Expediting Inc., 200 Meacham Avenue, Elmont, New York 11003.

Typeset in the UK by Keyword Publishing Services Ltd. and printed by Cambridge University Press, Cambridge, UK. The paper used in this publication is 'acid free' and conforms to the American National Standards Institute requirements in this respect.

Dollar rates apply to subscribers in all countries except the UK and the Republic of Ireland where the pound sterling price applies. All subscriptions are payable in advance and all rates include postage. Journals are sent by air in the USA, Canada, Mexico, India, Japan and Australasia. Subscriptions are entered on an annual basis, i.e. January to December. Payment may be made by sterling cheque, dollar cheque, international money order, National Giro, or credit card (Amex, Visa, Mastercard).

Orders originating in the following territories should be sent to the local distributor. **India:** Universal Subscription Agency Pvt. Ltd, 101–102 Community Centre, Malviya Nagar Extn, Post Bag No. 8, Saket, New Delhi 110017. **Japan:** Kinokuniya Company Ltd, Journal Department, PO Box 55, Chitose, Tokyo 156. **USA, Canada and Mexico:** Taylor and Francis, Inc., 1900 Frost Road, Suite 101, Bristol, Pennsylvania 19007. **UK and other territories:** Taylor & Francis Ltd, Rankine Road, Basingstoke, Hampshire RG24 8PR.

Advertising in Taylor & Francis journals: Di Owen Marketing, 15 Upper Grove Road, Alton, Hampshire GU34 1NW, UK, Tel/Fax +44 (0)1420 89142 (for the world excluding the USA), or Advertising Department, Taylor & Francis Inc., 1900 Frost Road, Suite 101, Bristol, PA 19007, USA, Tel: +215 785 5800, Fax: +215 785 5515 (for USA and North America).

REPORT DOCUMENTATION PAGE

AFRL-SR-BL-TR-98-

0582

1. AGENCY USE ONLY (Leave blank)	2. REPORT DATE	3. REPORT TYPE AND DATES COVERED
		Final 15 Feb 97 To 14 Aug 97

4. TITLE AND SUBTITLE

1997 COUPLED CLUSTER AND ELECTRON CORRELATION WORKSHOP "FIFTY YEARS OF THE CORRELATION PROBLEM"

5. FUNDING NUMBERS

F49620-97-1-0091

2303/FS

61102F

6. AUTHOR(S)

Dr Rodney J. Bartlett

7. PERFORMING ORGANIZATION NAME(S) AND ADDRESS(ES)

Dept of Chemistry & Physics
University of Florida
P.O. Box 118435
Gainesville FL 32611-8435

8. PERFORMING ORGANIZATION REPORT NUMBER

9. SPONSORING MONITORING AGENCY NAME(S) AND ADDRESS(ES)

AFOSR/NL
110 Duncan Ave Room B115
Bolling AFB DC 20332-8050

Dr Michael R. Berman

10. SPONSORING MONITORING AGENCY REPORT NUMBER

11. SUPPLEMENTARY NOTES

12a. DISTRIBUTION AVAILABILITY STATEMENT

Approved for public release;
distribution unlimited.

12b. DISTRIBUTION CODE

The Coupled Cluster Theory Electron Correlation Workshop "Fifty Years of the Correlation Problem" was held at Cedar Key, Florida, from June 15-19, 1997, to recognize the essential developments for one of the dominant topics in the quantum theory of atoms, molecules, and solids. The instantaneous Coloumbic interactions among electrons that correlate their motion (the electron correlation problem) has been the focal point of ab initio quantum chemistry and physics for many years. Only with the proper inclsion of electron correlation in approximate solutions of the Schroedinger (or Dirac-Fock) equation is it possible to provide predictive accuracy for most properties of atoms and molecules. Such quantities include energetics (involving multiplets, dissociation pathways, and activation barriers), excited states and first- and second-order properties (like moments, field, gradients, polarizabilities, and magnetic susceptibilities), and vibrational, electronic, EPR and NMR spectra, among others.

14. SUBJECT TERMS

15. NUMBER OF PAGES

16. PRICE CODE

17. SECURITY CLASSIFICATION OF REPORT	18. SECURITY CLASSIFICATION OF THIS PAGE	19. SECURITY CLASSIFICATION OF ABSTRACT	20. LIMITATION OF ABSTRACT
(U)	(U)	(U)	(UL)

Coupled Cluster Theory
and
Electron Correlation Workshop

50 Years of the Correlation Problem

June 15-19, 1997

Lion's Club
Cedar Key, Florida

SPONSORS

Air Force Office of Scientific Research
Army Research Office
Office of Naval Research

~

IBM Corporation

~

University of Florida
Division of Sponsored Research
Quantum Theory Project

LIST OF PARTICIPANTS

SECTION 4

Address List

Adamowicz, Ludwik,
University of Arizona
Chemistry Department

Tucson AZ 85721
USA
Phone: 520-621-6607
Fax: 520-621-8407
ludwik@ccit.arizona.edu

Balkova, Anna,
University of Florida
Quantum Theory Project
P.O. Box 118435
Gainesville FL 32611
USA
Phone: 352-392-1597
Fax: 352-392-8722
BALKOVA@QTP.UFL.EDU

Bartlett, Rodney, J.
University of Florida
Quantum Theory Project
381 Williamson Hall, P.O. Box 118435
Gainesville FL 32611-8435
USA
Phone: 352-392-1597
Fax: 352-392-8722
BARTLETT@QTP.UFL.EDU

Becker, Klaus, W..
Technische Universität Dresden
Institut fur Theoretische Physik
TU Dresden Mommsenstr. 13
Dresden D-01062
Germany
Phone: 49-351-463-3852
Fax: 49-351-463-7079
becker@physik.tu-dresden.de

Bishop, Raymond, F.
University of Manchester
Physics
P.O. Box 88
Manchester M6O1QD
UNITED KINGDOM
Phone: 44/61-200-3674
Fax: 44/161-200-3669
R.F.BISHOP@UMIST.AC.UK

Bonacic-Koutecky, Vlasta,
Humboldt-Universität Berlin
Chemistry
Bunsenstrasse 1
Berlin D-10117
GERMANY
Phone: 49-30-2265-1007
Fax: 49-30-2265-1008
vbk@kirk.chemie.hu-berlin.de

Bukowski, Robert
University of Delaware
Department of Physics

Newark DE 19716
USA
Phone: 302-831-2662
Fax: 302-831-1637
bukowski@mp5.physics.udel.edu

Cernusák, Ivan
Comenius University
Dept of Phys Chem
Mlynska dolina CH-1
Bratislava SK-842 15
Slovakia
Phone: 421-7-796429
Fax: 421-7-729064
cernusak@fns.uniba.sk

Christiansen, Ove
Aarhus University
Chemistry
Langelandsgade 140
Aarhus C DK-8000
Denmark
Phone: 45-8942-3833
Fax: 45-8619-6199
ove@aauc32.uni-c.dk

Cízek, Jiri
University of Waterloo
Department of Applied Mathematics

Waterloo Ontario N2L 3G1
CANADA
Phone: 519/885-1211
Fax: 519/746-4319
JCIZEK@THEOCHEM.UWATERLOO.CA

Crawford, T., Daniel.
University of Georgia
Dept of Chemistry
1001 Cedar Street
Athens GA 30602
USA
Phone: 706-542-7738
Fax: 706-542-0406
CRAWDAD@OTANES.CCQC.UGA.EDU

De Jong, Wibe, Albert.
University of Groningen
Chemical Physics
Nijenborgan 4
Groningen 9747 AG
Netherlands
Phone: 31-503634377
Fax: 31-503634447
bert@chem.rug.nl

Dufty, James
University of Florida
Dept of Physics
215 Williamson Hall P O Box 118440
Gainesville FL 32611
USA
Phone: 352-3926693
Fax: 352-392-0524
DUFTY@PHYS.UFL.EDU

Dykstra, Clifford,
Indiana University-Purdue Univ. at Indianapolis
Chemistry Department
402 N. Blackford Street
Indianapolis IN 46202-3274
USA
Phone: 317/274-6872
Fax: 317-274-4701
dykstra@chem.iupui.edu

Eguiluz, Adolfo,
University of Tennessee
Dept. of Physics and Astronomy
1408 Circle Drive
Knoxville TN 37996-1200
USA
Phone: 423-974-9642
Fax: 423-974-7843
eguiluz@utk.edu

Eliav, Ephraim,
Tel Aviv University
School of Chemistry
Ramat Aviv
Tel Aviv 69978
ISRAEL
Phone: 972-3-6408902
Fax: 972-3-6409293
ephriam@chemlb6.tau.ac.il

Fasano, Mike
University of Florida
Quantum Theory Project
P O Box 118435
Gainesville FL 32611-8435
USA
Phone: 352-392-6365
Fax: 352-392-8722
fasano@qtp.ufl.edu

Fernández, Berta
Universidade de Santiago de Compostela
Dept. of Physical Chemistry
Faculty of Chemistry, Avda. de las Ciencias
Santiago de Compostela D-15706
Spain
Phone: 34-81-563100
Fax: 34-81-595012
qfberta@usc.es

Füsti-Molnár, László
Eotvos Lorand University
Dept of Theor Chem
PO Box 32
Budapest H-1518
HUNGARY
Phone: 36-1-209-0555
Fax: 36-1-209-0602
fusti@para.elte.hu

Gauss, Jürgen
Universität Mainz
Inst für Physikalische Chemie
Mainz D 55099
GERMANY
Phone: 49-6131-393736
Fax: 49-6131-393768
gauss@spock.chemie.uni-mainz.de
slater.chemie.uni-mainz.de

Gdanitz, Robert,
Gesamthochschule Kassel
Dept. of Physics
FB 18
Kassel D-34109
GERMANY
Phone: 49-561-804-4120
Fax: 49-561-804-4006
gdanitz@hrz.uni-kassel.de

Gulhery, Nathalie
Universite Paul Sabatier
IRSAMC
148 route de Narbonne
Toulouse 31062
France
Phone: 33-5-61556098
Fax: 33-5-61556065
nathalie@irsamc1.ups-tlse.fr

Gutsev, Gennady, L.
University of Florida
Quantum Theory Project
370 Williamson Hall P.O. Box 118435
Gainesville FL 32611-8435
USA
Phone: 352-392-1597
Fax: 352-392-8722
GUTSEV@QTP.UFL.EDU

Gwaltney, Steven, R..
University of Florida
Quantum Theory Project
345 Williamson Hall, P.O. Box 118435
Gainesville FL 32611-8435
USA
Phone: 352-392-6365
Fax: 352-392-8722
GWALTNEY@QTP.UFL.EDU

Handy, Nicholas, C.
University of Cambridge
Dept. of Chemistry
Lensfield Road
Cambridge CB2 1EW
UK
Phone: 44-1223-336373
Fax: 44-1223-336362
nch1@cam.ac.uk

Harris, Frank
University of Utah
Dept of Chemistry
Salt Lake City UT 84112
USA
Phone: 801-581-8445
Fax: 801-585-3207
HARRIS@DIRAC.CHEM.UTAH.EDU

Hirao, Kimihiko
University of Tokyo
Dept of Applied Chemistry
Tokyo 113
Japan
Phone: 81-3-5802-3335
Fax: 81-3-5802-3335
hirao@qcl.t.u-tokyo.ac.jp

Ho, Jia-Jen
National Taiwan Normal University
Dept. of Chemistry
88 sec. 4 Tingchow Road
Taipei 117
Taiwan ROC
Phone: 886-2-9309085
Fax: 886-2-9324249
jjh@proton.chem.ntnu.edu.tw

Hubac, Ivan,
Comenius University
Dept of Chem Physics & Biophys
Bratislava SK-842 15
SLOVAKIA
Phone: 42-7-728100
Fax: 42-7-725882
hubac@fmph.uniba.sk

Hunt, Patricia
University of Auckland
Dept. of Chemistry
Private Bag 92019
Auckland
New Zealand
Phone: 64-9-3737999
Fax: 64-9-3737422
p.hunt@auckland.ac.nz

Jankowski, Karol,
Nicholas Copernicus University
Physics
ul. Grudziadzka 5
Torun PL 87-100
POLAND
Phone: 48/56-210-65
Fax: 48/56-25397
karoljan@phys.uni.torun.pl

Jankowski, Piotr
University of Delaware
Dept. of Physics & Astronomy
307 Sharp Laboratory
Newark DE 19716
USA
Phone: 302-831-8767
Fax: 302-831-1637
jankowsk@udel.edu

Jayasuriya, Keerthi,
U.S. Army Res Devlp & Eng Ctr

Bldg 3028
Picatinny Arsenal NJ 07806-5000
USA
Phone: 201/724-5810
Fax:

Jayatilaka, Dylan
University of Western Australia
Dept. of Chemistry

Nedlands 6009
Western Australia
Phone: 61-09-3803515
Fax: 61-09-3803515
dylan@crystal.uwa.edu.au

Kais, Sabre,
Purdue University
Chemistry Department
1393 Brown Building
West Lafayette IN 47907
USA
Phone: 317-494-5965
Fax: 317-494-0239
SABRE@SALAM.CHEM.PURDUE.EDU

Kaldor, Uzi,
Tel-Aviv University
Chemistry
Institute of Chemistry
Tel Aviv 69978
ISRAEL
Phone: 972-3-6408590
Fax: 972-3-640293
kaldor@chemib2.tau.ac.il

Kladko, Konstantin
Max Planck Institute

Bayreuther Str 40, Haus 16
Dresden D-01187
Germany
Phone: 49-351-463-6214
Fax: 49-351-463-7279
kladko@mpidks-dresden.mpg.de

Klopper, Wim,
University of Oslo

Kjemisk Institute P.O. Box 1033 Blindern
Oslo N-0315
Norway
Phone: 47/22855433
Fax: 47/22855441
w.m.klopper@kjemi.uio.no

Knowles, Peter,
University of Birmingham
Chemistry

Birmingham B15 2TT
UNITED KINGDOM
Phone: FAX:44-121-414-7471
Fax: 44-121-414-7471
P.J.Knowles@bham.ac.uk

Koch, Henrik,
Aarhus University
Department of Chemistry
845 Page Mill Road
Aarhus C DK-8000
DENMARK
Phone: 45-86-78-4444
Fax: 45-86-196199
koch@ws4.kemi.aau.dk

Korkin, Anatoli,
University of Florida
Quantum Theory Project
362 WM Hall PO Box 118435
Gainesville FL 32611-8435
USA
Phone: 352-392-6113
Fax: 352-392-8722
korkin@qtp.ufl.edu

Koutecky, Jaroslav,
Freie Universität Berlin
Inst für Physikalische und Theor Chemie
FU-Berlin Takustr.3
Berlin D-14195
GERMANY
Phone: 49-30-838-3757
Fax:
jbk@kirk.chemie.hu-berlin.de

Kucharski, Stanislaw,
Silesian University
Department of Chemistry
Szkolna 9
Katowice 40-006
POLAND
Phone: 48-32-588211
Fax: 48-32-599978
saketc3.ich.us.edu.pl

Kutzelnigg, Werner,
Ruhr-Universität
Lehrstuhl für Theoretische Chemie
Universitatsstr. 150
Bochum 1 D-44780
GERMANY
Phone: 49-234-7006485
Fax: 49-234-7094109
werner.kutzelnigg@rz.ruhr-uni-bochum.de

Ladik, Janos
Universität Erlangen-Nürnberg
Inst. of Theoretical Chemistry
Egerlandstrasse 3
Erlangen D-97058
Germany
Phone: 49-9131-857766
Fax: 49-9131-857736
ladik@pctc.chemie.uni-erlangen.de

Linderberg, Jan,
Aarhus University
Chemistry Department
Langelandsgade 140
Aarhus C DK-8000
DENMARK
Phone: 45/89423829
Fax: 45-8619-6199
jan@kemi.aau.dk

Lindgren, Ingvar,
Chalmers University of Technology
Department of Physics

Goteborg S-41296
SWEDEN
Phone: 46-31-772-3272
Fax: 46-31-772-3496
ingvar.lindgren@stratresearch.se

Lindh, Roland,
University of Lund
Dept of Theoretical Chemistry
P.O. Box 124
Lund S-221 00
SWEDEN
Phone: 46-46-108237
Fax:

Löwdin, Per-Olov
Uppsala University
Quantum Chemistry Group
Box 518
Uppsala S-75120
SWEDEN
Phone: 46 18 183260
Fax:

Maslen, Paul
University of California at Berkeley
Chemistry

Berkeley CA 94705
USA
Phone:
Fax: 510-623-1255
maslen@bastille.cchem.berkeley.edu

Maynau, Daniel,
Université Paul Sabatier
Laboratoire de Physique Quantique
118, Route de Narbonne
Toulouse Cedex 31062
FRANCE
Phone: 33-561-556-835
Fax: 33-561-556-065
daniel@irsamc1.ups-tlse.fr

Meissner, Leszek,
Nicolas Copernicus University
Physics Institute
Grudziadzka 5
Torun PL-87-100
POLAND
Phone: 48-56-21065
Fax: 48-56-25397
meissner@phys.uni.torun.pl

Merchán, Manuela
Universitat de València
Physics
Dr. Moliner 50
Burjassot Valencia 46100
Spain
Phone: 34-6-3864332
Fax: 34-6-3864564
merchan@vm.ci.uv.es

Mishra, Manoj, K.
Indian Institute of Technology Bombay
Department of Chemistry

Powai Mumbai 400076
INDIA
Phone: 091/225782545
Fax: 91-22-578-3480
mmishra@chem.iitb.ernet.in

Monkhorst, Hendrik, J.
University of Florida
Quantum Theory Project
362 Williamson Hall, P.O. Box 118435
Gainesville FL 32611-8435
USA
Phone: 352-392-1597
Fax: 352-392-8722
monkhors@qtp.ufl.edu

Morrison, John, C.
University of Louisville
Dept. of Physics

Louisville KY 40292
USA
Phone: 502-852-0916
Fax: 502-852-0742
jcmorr01@homer.louisville.edu

Mukherjee, Debashis,
Indian Association for the Cultivation of Science
Dept. of Physical Chemistry
Raja S.C. Mullicle Road
Calcutta Jadavpur 700-032
INDIA
Phone: 91-33-473-5374
Fax: 91-33-473-2805
pcdm@iacs.ernet.in

Noga, Jozef
Slovak Academy of Sciences
Inst. of Inorganic Chemistry
Dubravska cesta 9
Bratislava SK-84236
SLOVAKIA
Phone: 421-7-375170
Fax: 421-7-373541
noga@savba.sk

Nooijen, Marcel,
University of Florida
Quantum Theory Project
343 Williamson Hall P.O. Box 118435
Gainesville FL 32611-8435
USA
Phone: 352-392-1597
Fax: 352-392-8722
nooijen@qtp.ufl.edu

Öhrn, Yngve
University of Florida
Quantum Theory Project
363 Williamson Hall P.O. Box 118435
Gainesville FL 32611-8435
USA
Phone: 352-392-1597
Fax: 352-392-8722
OHRN@QTP.UFL.EDU

Ornellas, Fernando, R.
University of Sao Paulo
Institute of Chemistry
Caixa Postal 20780
Sao Paulo 05599-970
BRAZIL
Phone: 55-11-818-3895
Fax: 55-11-815-5579
fromell@usp.br

Pahl, Felix
University of Cambridge
Dept. of Chemistry
Lensfield Road
Cambridge CB2 1EW
UK
Phone: 44-1223-336353
Fax: 44-1223-336362
felix@gmos.ch.cam.ac.uk

Pal, Sourav,
National Chemical Laboratory
Physical Chemistry Div.
Physical Chemistry Division Theoretical Chemistry Group
Pune Maharashtra 411008
INDIA
Phone: 91-212-336451
Fax: 91-212-330233
pal@ncl.ernet.in

Paldus, Josef,
University of Waterloo
Applied Mathematics Dept
M&C Building University Avenue
Waterloo Ontario N2L 3G1
CANADA
Phone: 519-888-4567
Fax: 519-746-4319
paldus@theochem.uwaterloo.ca

Perera, Ajith, S.
University of Florida
Quantum Theory Project
343 Williamson Hall P.O. Box 118435
Gainesville FL 32611-8435
USA
Phone: 352-392-1597
Fax: 352-392-8722
PERERA@QTP.UFL.EDU

Peris-Ripolles, Guillermo
Universitat Jaume I
Ciencies Experimentals
Box 224 Campus Ctra Borriol s/n
Castellon 12080
Spain
Phone: 34-64-345741
Fax: 34-64-345654
peris@nuvol.uji.es

Piecuch, Piotr
University of Toronto
Chemistry
80 St. George Street
Toronto Ontario M5S3H6
Canada
Phone: 416-978-3625
Fax: 416-978-7580
ppiecuch@chem.utoronto.ca

Pople, John
Northwestern University
Dept of Chemistry
2145 N. Sheridan Road
Evanston IL 60208-3113
USA
Phone: 847-491-3403
Fax: 847-491-7713
POPLE@LITHIUM.CHEM.NWU.EDU

Reinhardt, Peter
Université Paul Sabatier
IRSAMC
118 Route de Narbonne
Toulouse F-31062
France
Phone: 33-5-61556045
Fax: 33-5-61556065
reinh@irsamc1.ups-tlse.fr

Rizzo, Antonio
Consiglio Nazionale delle Ricerche
Instituto di Chimica Quantistica ed Energetica Molecolare
Via Risorgimento 35
Pisa I-56126
Italy
Phone: 39-50-918240
Fax: 39-50-502270
rizzo@indigo.icqem.pi.cnr.it

Rozyczko, Piotr, B.
University of Florida
Quantum Theory Project
345 Williamson Hall PO Box 118435
Gainesville FL 32611-8435
USA
Phone: 352-392-1597
Fax: 352-392-8722
ROZYCZKO@QTP.UFL.EDU

Sánchez de Merás, Alfredo, Manuel.
Universitat de València
Dept. de Química
Dr. Moliner 50
Burjassot (Valencia) 46100
Spain
Phone: 34-6-3983155
Fax: 34-6-3983156
sancheza@bohr.quifis.uv.es

Seldno, Hideo,
Analatom

540 Weddell Drive Suite 9
Sunnyvale CA 94089
USA
Phone: 408-734-9392
Fax: 408-734-8335
analatom@netcom.com

Semenyaka, Alex,
University of Florida
Quantum Theory Project
343 Williamson Hall, P.O. Box 118435
Gainesville FL 32611-8435
USA
Phone: 352-392-1597
Fax: 352-392-8722
SEMENYAKA@QTP.UFL.EDU

Shavitt, Isaiah,
Ohio State University
Chemistry Department
100 W. 18th Ave.
Columbus OH 43210-1185
USA
Phone: 614/292-1668
Fax: 614-292-1685
shavitt@mps.ohio-state.edu

Sherrill, Charles, David.
University of California at Berkeley
Department of Chemistry
Box 308
Berkeley CA 94720-1460
USA
Phone: 510-643-2935
Fax: 510-643-1255
sherrill@bastille.cchem.berkeley.edu

Stanton, John,
University of Texas at Austin
Department of Chemistry
Welch Hall
Austin TX 78712
USA
Phone: 512/471-5903
Fax: 512-471-8696
stanton@jfs1.cm.utexas.edu

Suhai, Sandor,
German Cancer Research Centre
Molecular Biophysics
Molecular Biophysics Group INF 280
Heidelberg 69120
GERMANY
Phone: 49/62-21422369
Fax: 49-6221-422333
S.Suhai@dkfz-heidelberg.de

Sun, Jun-Qiang,
University of Florida
Quantum Theory Project
386 Williamson Hall, P.O. Box 118435
Gainesville FL 32611-8435
USA
Phone: 352-392-1597
Fax: 352-392-8722
SUN@QTP.UFL.EDU

Sundholm, Dage,
University of Helsinki
Department of Chemistry
P.O. B 55
Helsinki SF FIN-00014
FINLAND
Phone: 358-9-19140176
Fax: 358-9-19140169
sundholm@chem.helsinki.fi

Szalay, Péter, G.
Eotvos Lorand University
Dept of Theor Chem
P O Box 32
Budapest H-1518
Hungary
Phone: 36-1-209-0555
Fax: 36-1-209-0602
szalay@theo.elte.hu

Szalewicz, Krzysztof,
University of Delaware
Dept. of Physics
Newark DE 19716
USA
Phone: 302-831-6579
Fax: 302-831-1637
szalewic@udel.edu

Trickey, Samuel, B.
University of Florida
Quantum Theory Project
364 Williamson Hall, P.O. Box 118435
Gainesville FL 32611-8435
USA
Phone: 352-392-1597
Fax: 352-392-8722
TRICKEY@QTP.UFL.EDU

Urban, Miroslav,
Comenius University
Physical Chemistry Department
Mlynska Dolina
Bratislava SK-84215
Slovakia
Phone: 421-7-796417
Fax: 421-7-729064
urban@fns.uniba.sk

Visscher, Lucas,
Odense University
Dept. of Chemistry
Campusvej 55
Odense DK-5230
Denmark
Phone: 45-7-65572568
Fax: 45-7-66158780
luuk@chem.ou.dk

Watts, John,
University of Florida
Quantum Theory Project
P.O. Box 118435, 367 Williamson Hall
Gainesville FL 32611-8435
USA
Phone: 352-392-1597
Fax: 352-392-8722
WATTS@QTP.UFL.EDU

Wilson, Kenneth
University of Florida
Quantum Theory Project
P O BOX 118435
Gainesville FL 32611-8435
USA
Phone: 352-392-1597
Fax: 352-392-8722
WILSON@QTP.UFL.EDU

Yau, Anthony
University of Florida
Chemistry
QTP
Gainesville FL 32611
USA
Phone: 352-392-7184
Fax: 352-392-8722
yau@qtp.ufl.edu

MOLECULAR PHYSICS, 1998, VOL. 94, NO. 1, 1

Introduction

The Coupled Cluster Theory Electron Correlation Workshop "Fifty Years of the Correlation Problem"

The Coupled Cluster Theory Electron Correlation Workshop "Fifty Years of the Correlation Problem" was held at Cedar Key, Florida, on 15–19 June 1997, to recognize the essential developments of one of the dominant topics in the quantum theory of atoms, molecules, and solids. The meeting served simultaneously as a satellite of the International Congress of Quantum Chemistry, held in Atlanta, Georgia, from 9–14 June 1997, and was the third in a series of coupled cluster workshops. The first convened at the Harvard–Smithsonian Center for Astrophysics in 1990 (Proceedings in *Theoretica Chimica Acta*, 1991, vol. 80, nos. 2–6) and the second at Bad Honnef, Germany, in 1994.

The instantaneous Coloumbic interactions among electrons that correlate their motion (the electron correlation problem) have been the focal point of *ab initio* quantum chemistry and physics for many years. Only with the proper inclusion of electron correlation in approximate solutions of the Schrödinger (or Dirac–Fock) equation is it possible to provide predictive accuracy for most properties of atoms and molecules. Such quantities include energetics (involving multiplets, dissociation pathways, and activation barriers), excited states and first- and second-order properties (like moments, field gradients, polarizabilities, and magnetic susceptibilities), and vibrational, electronic, EPR and NMR spectra, among others.

In extended systems such as polymers and solids, correlation effects are critical to properties like cohesive energies, energy bands, and particularly band gaps; other optical properties like exciton spectra or nonlinear optical behaviour; and collective phenomena as in conductivity and superconductivity. Without adequate inclusion of electron correlation, theory cannot be predictive.

About 50 years after the correlation problem had been clearly identified, we were in a position to report on the remarkable progress that has been made and to point the way to the future. These accomplishments have been achieved by a combination of critical formal and methodological developments in the theory, such as coupled cluster theory, many-body perturbation theory, and propagator methods, and in the configuration interaction methods coupled to the dramatic progress in computational power. Together, today, accurate applications to molecular many-electron systems are possible, with polymers, surfaces, and crystals on the horizon. This Proceedings reports on the progress presented at the meeting in 23 papers.

To achieve some historical perspective, several of the pioneer investigators who have made contributions to the correlation problem spoke at the meeting. This, in fact, enabled us to have representatives of the four scientific generations of investigators who have worked on the correlation problem. Some have contributed to this volume.

The meeting was attended by 88 scientists from 25 different countries. Thirty-seven invited presentations were made, augmented by 37 poster presentations. In a panel session, we addressed the timely topic of "With Density Functional Theory, Is there Any Future for *Ab Initio* Correlated Methods?" which generated much discussion.

We acknowledge the generous support of the US Army Research Office, Grant No. DAAG55-97-1-0136 (Dr Mikael Ciftan); the Air Force Office of Scientific Research, Grant No. F49620-97-1-0091 (Dr Michael Berman); the Office of Naval Research, Grant No. N00014-97-1-0320 (Dr Peter Reynolds and Dr Peter Schmidt); the IBM Corporation (Dr Jamie Coffin); and the Office of Research, Technology, and Graduate Education at the University of Florida (Dr Karen Holbrook). Dr Steve Gwaltney helped do *everything*, and I particularly appreciate his help plus that of my graduate students and postdocs, who were instrumental to the success of the meeting. I want to especially thank Mrs Grace Kiltie (my Program Assistant), Mrs Judy Parker (the Quantum Theory Project Administrative Assistant), and Ms Zeynep Tufecki for their essential help in arranging this meeting. We are appreciative of the cooperation of the editors and editorial offices of *Molecular Physics* in making this Proceedings volume possible.

RODNEY J. BARTLETT

University of Florida

Guest Editor

MOLECULAR PHYSICS, 1998, VOL. 94, NO. 1, 3–17

The history and evolution of configuration interaction

By ISAIAH SHAVITT

Department of Chemistry, Ohio State University, Columbus, OH 43210-1185, USA

The configuration interaction (CI) method dates back to the earliest days of quantum mechanics, and is the most straightforward and versatile approach for dealing with electron correlation. The earliest applications typically involved 2–10 terms, while modern molecular CI calculations often employ many millions of configuration state functions (CSFs). In addition to the enormous increase in computer power over the last fifty years, many theoretical developments have contributed to the evolution of the CI approach, including the development of efficient algorithmic tools for the various computational steps and the exploration and optimization of the choices of basis sets, orbitals, and the structure of the CI expansion. Among the milestones in these developments have been the introduction of efficient matrix eigenvalue methods, the introduction of multireference CI expansions, the formulation of various corrections and modifications to overcome the major fault of CI, its lack of extensivity, and particularly the introduction of direct CI, which greatly increased the length of accessible CI expansions by eliminating the need to store the Hamiltonian matrix. Unitary group and related methods have helped make direct CI calculations particularly efficient. Specialized computer programs for full CI calculations have become very efficient and are producing benchmark results which are extremely useful for evaluating other methodologies. Although it has lost ground to the very attractive coupled cluster methods, CI still has an important role to play in quantum chemistry.

1. Origins

Configuration interaction (CI) is the most straightforward and general approach for the treatment of electron correlation in atoms and molecules. If we interpret the term in a very broad sense, as applying to any linear expansion of the wavefunction in which the linear coefficients are determined by the Ritz variational approach [1], then the earliest *ab initio* CI calculations would probably be Kellner's 1927 calculations for He and Li^+ [2], using a four-term expansion in functions of the lengths of the two vectors from the nucleus to the electrons and of the angle between the vectors. A similar 11-term expansion for He was reported by Hylleraas in 1928 [3]. This latter paper included a calculation using a six-term expansion in products of radial functions of the two electrons, presumably the first *ab initio* CI calculation in a narrower sense, not involving interelectron coordinates. These were followed by new Hylleraas treatments of the He atom in 1929 and 1930 [4], using the interelectronic distance instead of the intervector angle as one of the coordinates, and the similar treatment of the H_2 molecule by James and Coolidge in 1933 [5]. The broad definition would also include some valence bond (VB) calculations, such as the 1933 'VB + ionic' treatment of H_2 by Weinbaum [6], which is equivalent to a minimal basis molecular orbital-based CI calculation, and the 1936 VB + ionic treatment of H_3 by Hirschfelder, Eyring, and Rosen [7]. However, in modern usage the name configuration interaction is applied only to linear expansions of the wavefunction in terms of Slater determinants or in terms of 'configuration state functions' (CSFs), which are spin- and symmetry-adapted linear combinations of Slater determinants. The rest of this review deals with CI in this restricted sense.

The term configuration interaction (CI) and its variations were introduced in atomic electronic structure theory to deal with electronic states which could not be characterized adequately by single-configuration wavefunctions, and implied perturbation of an electronic configuration by neighbouring configurations. Two key papers with the same title, 'The theory of complex spectra', provided the initial framework for the treatment of atomic electronic states. The first, a 1929 paper by Slater [8], introduced the Slater determinant and showed how to derive multiplet structures originating in given electron configurations. It also showed how to calculate some matrix elements between Slater determinants, and derived electronic term energies expressed in terms of radial integrals. The second paper, by Condon [9], appeared in 1930. It completed the derivation of the rules (now known as the Slater–Condon rules) for the calculation of Hamiltonian matrix elements between pairs of Slater determinants con-

0026-8976/98 $12·00

structed from a set of orthonormal orbitals, and extended Slater's treatment to include the 'interaction of neighbouring configurations'.

Early applications of the theory treated the Slater radial integrals as adjustable parameters, determining their values by least-squares fitting to reproduce spectroscopic line positions. Two 1933 papers of this type included the terms 'interaction of configurations' [10] and 'configuration interaction' [11] in their titles.

2. The early years

An early five-configuration *ab initio* CI calculation on H_2, using elliptical orbitals, was reported by Nagamiya [12] in 1936. A two-configuration CI calculation with numerically determined orbitals on the excited ^2P state of O^+, using the $2s^22p^3$ and $2p^5$ configurations, was reported by Hartree, Hartree and Swirles [13] in 1939. That work included the first *ab initio* MCSCF calculation, and compared the use of orbitals optimized specifically for the two-configuration wavefunction with the use of single-configuration SCF orbitals in the same two-configuration wavefunction. Hartree disliked the name configuration interaction because of its perturbation theory implications, and introduced the alternative name 'superposition of configurations'.

Before the introduction and wide-spread use of Gaussian-type (GTO) basis functions, *ab initio* calculations for polyatomic molecules were hampered by the difficulty of calculating multicentre integrals over Slater-type (STO) basis functions. Some π-electron CI calculations were carried out with integral approximations in the late forties and early fifties. A two-configuration calculation on several electronic states of ethylene was reported by Parr and Crawford [14] in 1948, and included a study of the variation in the energy with twisting of the CH_2 groups. A calculation on six π-electron states of benzene, using up to six CSFs per state and ignoring all multicentre integrals, was reported in 1950 by Craig [15]. A more elaborate treatment of benzene, this time using the Sklar approximation [16] for the multicentre integrals, covering 14 electronic states and using 3–12 CSFs per state, was reported later that year by Parr, Craig and Ross [17].

Fully *ab initio* CI calculations involving more than two electrons started appearing in increasing numbers in the fifties. In 1950 appeared the first of a series of papers by Boys developing general procedures for CI calculations and applying them to several atoms and molecules. The first paper [18] included the proposal for the use of Gaussian basis sets in molecular calculations. The second paper in this series [19] appeared in the same year, and reported a calculation on the ground state of the Be atom using 10 CSFs with a (3s1p) STO-basis. In 1952, following several methodological papers dealing mostly with procedures for vector coupling and matrix element calculations for atoms, appeared a paper by Bernal and Boys [20] reporting CI calculations on the ten-electron series Na^+, Ne, and F^-. This work used a quite respectable STO basis set, (5s4p1d), significantly larger than any that had been attempted up to that time, and included 17 CSFs. It was followed in 1953 by two papers by Boys reporting calculations on three electronic states of Be [21] using a (4s4p2d) basis and 7–13 CSFs per state, and calculations on three states of boron and five states of carbon [22] using a (4s4p1d) basis and 12–18 CSFs per state. Among other atomic CI calculations in the early fifties we note the calculations on He by Taylor and Parr [23] in 1952 and by Shull and Löwdin [24] in 1955. The latter paper used an expansion in terms of natural spin orbitals.

An early molecular CI calculation was the 1951 treatment of linear symmetric H_3 by Walsh and Matsen [25], who used a minimal STO basis and three of the four CSFs which can contribute to the ground state in this case. It was followed in 1953 by a calculation on HF with a minimal STO basis and 6 CSFs by Kastler [26], and a calculation on two states of the open-shell O_2 molecule by Meckler [27], using a minimal GTO basis and 9 12 CSFs. Meckler used a computer (the Whirlwind at Massachusetts Institute of Technology) for the solution of the matrix eigenvalue problem, but the rest of the work was done with desk calculators.

Another series of atomic CI calculations was reported by Boys and Price [28] in 1954. These calculations, on ground and excited states of Cl, Cl^-, S, and S^-, used a (6s5p2d) STO basis and 23–32 CSFs per state, included relativistic corrections, and obtained very good results for excitation energies and electron affinities. The electronic computer EDSAC was used for the calculation of the basis set integrals and the integral transformations.

Reports of molecular CI calculations started appearing in increasing numbers in the mid fifties. Among these was a minimal-STO-basis calculation on H_2O by Ellison and Shull [29] using three CSFs, and extended-STO-basis calculations on BH, H_2O and H_3 reported by Boys and co-workers [30] in 1956. These latter calculations were fully automated, using the EDSAC computer for symbolic manipulations and formula derivations as well as numerical computations. Several minimal-STO-basis CI calculations were reported in 1957 and 1958, including an NH_3 calculation by Kaplan [31] using 13 CSFs, a treatment of several states of O_2 and O_2^+ by Kotani and co-workers [32], full-valence CI calculations for ten electronic states of BH by Ohno [33], and a series of calculations for several states of CH, NH and OH by Krauss and Wehner [34], using 8–18 CSFs per state.

We close this survey of early CI calculations by mentioning the landmark calculation on three states of CH_2 by Foster and Boys, reported at the first Boulder conference on theoretical chemistry in 1959 and published in 1960 [35]. That calculation obtained bending potential energy curves for the $^3B_1$, $^1A_1$ and $^1B_1$ states, and was the first to show a bent ground-state geometry for this radical.

3. Infrastructure development

A 'conventional' CI calculation involves the following computational steps [36]:

(i) calculation of basis set integrals;
(ii) determination of orbitals, e.g., by an SCF calculation;
(iii) transformation of basis set integrals to orbital integrals;
(iv) calculation and storage of the Hamiltonian matrix elements;
(v) solution of the matrix eigenvalue problem for the desired state.

Also, procedures for spin- and symmetry-adaptation of the CSFs have to be chosen, and methods for the calculation of Hamiltonian matrix elements between the CSFs have to be implemented [36]. In addition, several choices need to be made for each calculation [36]:

(a) Choice of the basis set;
(b) choice of the type of orbital to use (e.g., SCF, MCSCF, or natural orbitals);
(c) choice of the configuration state functions (CSFs) to include in the CI expansion.

Before *ab initio* CI calculations could be carried out efficiently and routinely, effective algorithmic tools had to be developed for the computational steps, and the various choices had to be explored and optimized. We shall not discuss basis set integral calculation, since it is common to all algebraic *ab initio* methods, and shall touch upon only aspects of basis set choice which are particularly relevant to correlated calculations. Matrix element calculation will be considered only as part of the issues of spin and symmetry adaptation. The other choices and computational steps will be discussed in the next few subsections.

3.1. *Structure of the configuration interaction expansion*

In the early CI calculations, such as those discussed in the previous section [12–35], the number of CSFs included in the CI expansion was very small, and these CSFs were generally selected individually on the basis of physical considerations or by trial and error. More systematic choices became possible as computer power increased and theoretical methods improved.

The ideal CI calculation would be 'full CI' (FCI), in which the full many-electron function space of the appropriate spin and symmetry generated by the basis set is used in the wavefunction expansion. Such a calculation provides the most complete solution of the non-relativistic Schrödinger equation within that function space, but is rarely feasible, because the number of CSFs in FCI goes up factorially with the basis set size. Therefore in most applications it is necessary to truncate the CI expansion space in some way to make the calculation practical. Nevertheless, a substantial number of FCI calculations of progressively increasing size have been reported [37–49] and are extremely useful as benchmarks for the assessment of various correlation methods.

Most configuration interaction expansions can be classified as single reference (SRCI) or multireference (MRCI). In the first case, the expansion is based on one dominant CSF, usually the Hartree–Fock configuration constructed from the SCF orbitals, and includes CSFs on the basis of their 'excitation level', i.e., the number of electrons occupying orbitals which are empty in the Hartree–Fock configuration [50, 51]. For practical reasons, such calculations usually are limited to single and double excitations (CISD, or SR-CISD), though higher excitations have been included in some cases (see, e.g., Sherrill and Schaefer [52]). In the multireference case, the expansion is based on a set of 'reference configurations' [53–56], and again the most common approach is to limit the expansion to single and double excitations (MR-CISD), i.e., to CSFs which are no more than doubly excited with respect to at least one of the reference CSFs. In both single-reference and multireference expansions, excitations from inner-shell orbitals usually are omitted ('frozen-core CI'), since they contribute little to the description of chemical processes, and since a meaningful treatment of inner-shell correlation requires a greatly expanded basis set [57].

In early MRCI applications, very few reference CSFs were used, and these were chosen individually, on the basis of physical considerations, such as the proper description of dissociation or of a set of electronic states [56], or on the basis of their contributions to the wavefunction or energy, often obtained by perturbation estimates or iteratively in a series of CI calculations [53–55, 58, 59]. In later work more systematic approaches to reference configurations selection were used, mostly based on the idea of an 'active space', a set of orbitals having variable occupancy in the reference configurations. Typically, the active space is composed of the valence shell orbitals (corresponding to the molecular orbitals generated from the atomic valence orbitals in a minimal-basis calculation) or a

subset of them. The total orbital space may include all or some of the following subspaces:

(i) Frozen orbitals (usually inner-shell orbitals), which are doubly occupied in all CSFs;
(ii) inactive occupied orbitals, doubly occupied in all the reference CSFs but correlated in the MRCI expansion;
(iii) active orbitals, varying in occupancy between the reference CSFs;
(iv) virtual (excited) orbitals, unoccupied in any of the reference CSFs, but used in the MRCI expansion;
(v) discarded orbitals, usually of very high orbital energy, which are completely left out of the CI expansion.

A highly desirable, but not always practical, form of the reference space is the 'complete active space' (CAS) [60], which consists of a full CI expansion within the active orbitals. However, when all the valence orbitals are included in the active space [61], the CAS is often quite large and generates an impractically large number of CSFs in the MRCI expansion. Effective alternatives include the 'restricted active space' (RAS) [42, 62], in which occupancy restrictions are placed on various subsets of the active orbitals, and the GVB-type active space, generated from a generalized valence bond form of the wavefunction [63, 64].

The number of CSFs in the MRCI expansion sometimes is reduced by systematic restrictions, such as limitation to CSFs which have nonzero Hamiltonian matrix elements with at least one reference CSF (interacting-space limitation [55, 65]), or by individual selection methods. An MRCI calculation with a complete valence active space and all CSFs with up to one electron or up to two electrons in the virtual orbitals space is sometimes referred to as 'first-order CI' (FOCI) or 'second-order CI' (SOCI), respectively [52, 66], though these names are misleading, since this type of expansion does not consist of the set of terms that contributes to the corresponding order of the perturbation theory wavefunction or energy. Individual selection, in which CSFs are screened and selected on the basis of approximate energy contribution [20–22, 36, 51, 53, 54, 58, 59, 67, 68] (usually estimated by perturbation-based methods) were quite common in conventional CI, in which the Hamiltonian matrix was computed in a systematic order and stored before the eigenvalue computation. In the modern 'direct CI' approach, in which matrix elements are calculated as part of each iteration of the eigenvalue determination, particularly as used on vector computers, individual configuration selection usually is not employed, because it interferes with the smooth flow of the calculation.

3.2. *Spin adaptation*

A variety of approaches has been used for the construction of complete sets of S^2 eigenfunctions and for the calculation of Hamiltonian matrix elements between them. The principal approaches can be classified as follows.

Symmetric group methods, which were pioneered by Wigner [69], Weyl [70], Dirac [71], and Waller and Hartree [72], and developed further by Serber [73], Yamanouchi [74], Kotani *et al.* [75], Matsen [76], Ruedenberg [77], and others.
Projection operator methods (Löwdin [78]), including genealogical construction (see, e.g., Paunez [79]) and the use of 'Sanibel coefficients' (Manne [80], Smith and Harris [81]).
'Bonded functions', which are Rumer-like pairwise spin couplings [82], introduced in molecular CI calculations by Boys and Reeves (see Reeves [83]) and independently by Sutteliffe [84] and by Cooper and McWeeny [85].
Unitary group methods, introduced in quantum chemistry by Paldus [86] and adapted for efficient CI calculations by Shavitt [87].

The methods in most common use today are based on the unitary group approach or the related symmetric group approach [88], or else avoid spin adaptation and rely on expansions in terms of Slater determinants. However, it should be remembered that spin and symmetry adaptation are important not just for increased efficiency of the calculation, but also to ensure that the resulting wavefunction describes an electronic state of the desired multiplicity and symmetry type and is not contaminated by contributions of the wrong type.

3.3. *Spatial symmetry adaptation*

Symmetry adaptation is particularly important in atomic calculations. The use of full spin and spatial symmetry in atomic CI calculations can reduce the length of the CI expansion by orders of magnitude compared with expansions in Slater determinants, and is important in focusing the calculation on the desired electronic states and in fully characterizing these states. The process of CSF construction for atomic calculations has been called 'vector coupling', and was addressed in the early work on multiplet structure by Wigner [69, 89], Slater [8], and Condon [9], and later for *ab initio* CI calculations by Boys [90], Nesbet [91], Salmon and Ruedenberg [92], Bunge and Bunge [93], Sasaki [94], and Munch and Davidson [95], among others.

Symmetry adaptation is trivial in the case of molecules described by Abelian point-group symmetry. In such cases it is necessary only to use symmetry-adapted

orbitals in the construction of the CSFs, and to limit the CI expansion to terms of the desired overall symmetry. Taking advantage of non-Abelian point group symmetry in molecular CI calculations leads to significant complications, and is often eschewed, settling instead for the use of an Abelian subgroup of the full molecular symmetry group. A procedure for utilizing axial point group symmetry (primarily for C_{nv} and D_{nh}) using complex molecular orbitals was developed by Gershgorn and Shavitt [96] and implemented in a conventional CI program by Pipano and Shavitt [97], but was abandoned in later direct CI programs. Projection operator techniques have been developed for the general case (e.g., Wigner [69], Nesbet [98], Simons and Harriman [99]), but have not seen extensive use.

3.4. *Basis sets*

The basis set requirements of correlated calculations are much more demanding than those for SCF treatments. Here we shall focus only on basis set developments of particular interest for correlated treatments (for a recent review on Gaussian basis sets see Shavitt [100]).

A very important advance in basis set technology for high-level calculations was the introduction of 'generally contracted' Gaussian basis sets [101]. General contraction can produce significantly more efficient basis sets than the usual 'segmented' contraction, because generally contracted basis functions can be chosen to reproduce atomic Hartree–Fock orbitals or atomic natural orbitals, or other desired choices. Correlated calculations typically expend most of their computational effort in the steps following the basis set integrals evaluation and SCF or MCSCF calculation. Furthermore, the effort in the post-SCF stages increases more steeply with basis set size (typically with the sixth power of the number of basis functions) than does the integral evaluation and SCF effort (which is proportional at most to the fourth power). Therefore it is important to derive the maximum benefit from whatever number of contracted basis functions is used, e.g., by employing larger primitive Gaussian sets as well as general contraction, even at the cost of increased integral computation time.

Two types of generally contracted Gaussian basis set specifically designed for correlated calculations have been introduced in recent years. The first type is the atomic natural orbital (ANO) basis sets introduced by Almlöf and Taylor [102]. A particularly effective variation of this approach is the use of ANO basis sets generated by diagonalizing density matrices averaged over several electronic states of the atoms [103] including, in some cases, states of positive and negative ions [104, 105]. The other type are the 'correlation-consistent' polarized valence basis sets of Dunning and coworkers [106], denoted cc-pVxZ (x = D, T, Q, 5, 6 for double-, triple-, quadruple-, quintuple- and hextuple-zeta, respectively) and aug-cc-pVxZ (for basis sets augmented with diffuse functions). The cc basis sets are particularly useful for studying systematic trends with basis set enlargement, and facilitate extrapolation to the limit of a complete basis [107, 108].

It should be understood that basis sets designed for the treatment of valence–shell electron correlation cannot, in general, provide useful descriptions of core–core and core–valence correlation effects. Calculations attempting to correlate all electrons using such valence-type basis sets are not justified, and may even be harmful, since the fraction of core correlation contributions they recover is rather small and not meaningful [57]. Enlarged cc basis sets that include functions useful for the description of core–valence correlation, denoted cc-pCVxZ, have been added recently [109].

The ANO and cc basis sets provide very satisfactory solutions to the basis set problem, at least in situations in which large enough versions of these sets can be used. With the addition of the extrapolation capabilities it is now possible, in many cases, to distinguish errors due to basis set incompleteness from errors due to limitations of the correlation treatment.

3.5. *Orbital choices*

The configuration state functions in CI expansions are constructed from orbitals which are linear combinations of the basis functions. Most commonly in single-reference CI expansions these are the canonical SCF (Hartree–Fock) orbitals, both occupied and virtual, of the molecule in the electronic state being studied. In open-shell cases, restricted SCF orbitals typically are used, or sometimes orbitals of a closely related closed-shell state. (The use of different orbitals for α and β spins is rarely advisable in CI calculations.) A common choice in multireference CI expansions are orbitals obtained in corresponding MCSCF calculations.

In general, the results of a CI calculation are invariant to any linear transformation of a set of orbitals which are treated equivalently in the construction of the expansion. For example, in single-reference calculations which include all excitations of a given set of levels (e.g., all single and double excitations, CISD), separate linear transformations of the SCF-occupied and virtual orbitals do not affect the final wavefunction and energy. The same is true of frozen-core calculations with respect to separate linear transformations of the core, occupied valence, and virtual orbitals. The same is true also of multireference CI calculations using a complete-

active-space (CAS) reference space with respect to separate transformations of the inactive-occupied, active, and inactive-virtual orbitals. However, if some of the orbitals are to be discarded or frozen, or if individual CSFs are to be selected for inclusion in the CI expansion, then the choice of the orbital transformation can make a substantial difference [53, 110].

Most attempts to improve upon the SCF orbitals for use in CI calculations focus upon the virtual orbitals. The virtual canonical SCF orbitals are obtained as eigenfunctions of a Fock operator representing an N-electron potential, rather than the effective $(N-1)$-electron potential acting on the electrons in occupied orbitals. As a result, the lower-energy virtual orbitals tend to be relatively diffuse and not very effective for correlating the electrons in occupied orbitals [53]. In fact, most of the exact virtual Hartree–Fock orbitals (as would be obtained in numerical calculations) are continuum orbitals, representing a free electron in the field of the neutral molecule. Modified virtual orbitals obtained in an $(N-1)$-electron potential have been used by Kelly [111] and by Hunt and Goddard [112], and correspond more closely to SCF orbitals occupied in excited states. Other modifications to the virtual orbitals have been developed by Bender and Davidson [113], Huzinaga and Arnau [114], Whitten [115], Luken [116], Cooper and Pounder [117], Bauschlicher [118], Adamowicz and Bartlett [119], and others. Some approaches modified both the occupied and the virtual orbitals, as in Davidson's 'internally consistent' SCF orbitals [120].

An important class of orbital useful in CI calculations is natural orbitals (NOs) [121], usually obtained in a preliminary approximate calculation [122–124] or determined iteratively in a sequence of CI calculations [67]. An expansion in terms of NOs tends to be more compact, in the sense that fewer terms are needed for a given accuracy [110], but unless this property is exploited by orbital set truncation or CSF selection, little is gained. A particularly powerful application of natural orbitals ideas is the 'pair natural orbitals' (PNO) approach [125–129], applied most effectively in the 'self-consistent electron pair' (SCEP) method [127, 130].

Expansions in terms of localized orbitals [131–133] can lead also to compact wavefunctions [134, 135], particularly for larger molecules, though usually they entail giving up the use of spatial symmetry.

3.6. *Integral transformation*

An important step in a CI calculation (and in most correlated calculations) is the transformation of the one-electron and two-electron basis set integrals to corresponding integrals over the orbitals. While this step can be avoided or partially avoided in some correlated treatments [126, 130, 136, 137], generally it is simplest to formulate the Hamiltonian matrix element calculation in terms of fully transformed orbital integrals.

In the early work of Boys [19], Nesbet [138], and others, when basis sets were very small and computer storage was extremely limited, it was found most convenient to perform the transformation of the two-electron integrals in a two-stage process in which the computational effort was proportional to the sixth power of the basis set size. In later work the more efficient four-stage n^5 process was adopted [36, 139–141], and optimized procedures for its implementation were developed [142–145]. The assembly of the integral matrices prior to the transformation and their reordering between transformation steps were facilitated greatly by the bin sorting method of Yoshimine [146] (see also Bunge and Cisneros [147]).

An interesting variation of the treatment of the integral transformation step is due to Beebe and Linderberg [148] (see also Wilson [149]). Their approach, which is a form of singular-value decomposition, is based on Cholesky decomposition of the two-electron integrals matrix followed by truncation, and was designed to deal with problems of near linear dependence of the basis set and the limited precision of the computer arithmetic.

3.7. *Matrix eigenvalue problem*

Most Hamiltonian matrices that occur in CI calculations are sparse and diagonally dominant. As a result, iterative methods employing simple element-by-element updates based on perturbation theory [19, 150] usually are quite effective, at least for the lowest root. Important advantages of such methods are that they scale as the square of the matrix dimension (instead of the third power for direct methods), that the matrix is not modified, and that space in the computer central memory is required for only one or two vectors at a time. A generalization for several low roots, based on an improved 'optimal relaxation' algorithm involving minimization of the Rayleigh quotient [151], was introduced by Shavitt *et al.* [152]. A constraint of these methods is that they require the Hamiltonian matrix to be read in from external storage one row at a time, in sequence. This constraint creates no difficulties in conventional CI treatments, in which the Hamiltonian matrix elements are computed once, in the desired order, and stored on magnetic tape or disk.

An important new approach was introduced by Davidson [153] in 1975. In the spirit of the Lanczos method [154], the Davidson approach is based on an expansion of the desired eigenvector in an accumulating series of trial vectors but, unlike the Lanczos method, it exploits the diagonal dominance of the matrix by

generating the trial vectors by perturbation-based corrections. This method has two important advantages: it allows the calculation of higher roots without requiring the prior calculation of all lower roots, and it does not require that the matrix elements be provided in any particular order. This latter property, which is due to the fact that the principal computational step of the algorithm is simply the multiplication of the matrix into the current estimate of the eigenvector, is particularly important in facilitating direct CI calculations, in which the matrix elements are available in an order dictated by the processing order of the integrals or by related considerations. As a result, the Davidson method now is the standard method for the solution of the matrix eigenvalue problem in CI calculations.

The method of optimal relaxation (MOR) and the Davidson method have been reformulated also for the simultaneous calculation of several roots, resulting in the 'block MOR' [155, 156] and 'block Davidson' [157] methods. Other modifications of the Davidson method have been proposed [44, 158–165] (see also Davidson [166] and references therein).

4. The new age of big CI: direct CI

An extremely important development, which opened the way for very large CI calculations, was the introduction of direct CI by Roos and Siegbahn [167, 168]. The basic idea of direct CI is the avoidance of the formal, sequential calculation and storage of the Hamiltonian matrix, concentrating instead on the direct calculation of the product of the matrix into the current trial vector in the iterative procedure for the solution of the matrix eigenvalue problem. This product is calculated directly from the one- and two-electron integrals, using 'coupling coefficients' which specify the nonzero contributions of each integral to the matrix elements. At first glance this approach may appear to be counterproductive, since the matrix element contributions have to be recomputed in each iteration. However, most nonzero matrix elements have nonzero contributions from only one or two integrals, and the procedure lends itself to very efficient and streamlined operation, with few logical manipulations, resulting in a substantial net gain in speed over conventional CI. Furthermore, this method is extremely easy to adapt to vector computing. The avoidance of Hamiltonian matrix storage removes a significant barrier for very large CI calculations, and the efficiency of the direct CI approach has made such large calculations quite practical.

The original direct CI procedure was developed in a spin-adapted form for single-reference closed-shell CISD calculations, for which the determination of the coupling coefficients was quite easy [167]. Later [168] it was extended to SR-CISD expansions in a determinantal basis for any state and to full CI for three electrons. Subsequent extensions to full CI in a determinantal basis made possible the proliferation of benchmark full CI calculations [37–49], some of them employing several billion determinants [44, 46, 47]. Spin-adapted extensions for single-reference triplet states [169] and for multireference closed-shell cases limited to closed-shell reference CSFs [170] were reported also. The SCEP method [130] also can be considered a form of direct CI.

Generalization of direct CI in a spin-adapted CSF basis to any open-shell state and to multireference CI expansions became possible with the introduction of the unitary group approach [86] (UGA), particularly in its graphical form [87] (GUGA). Several computer programs applying the graphical unitary group approach [171–175] and variations based on the symmetric group [88] and other graphical schemes [176] or related ideas [137, 177] were developed, and together with the introduction of powerful supercomputers, these programs made possible MR-CISD calculations using millions of CSFs (e.g., Kedziora and Shavitt [178]). In recent years, the introduction of parallel computers and the adaptation of several computer programs to take full advantage of their capabilities have facilitated even larger CI calculations. For example, a parallel version of the Columbus program [179] has been used recently to carry out MR-CISD calculations with over two hundred million CSFs [180]. Parallel versions of full CI programs have been used in full CI calculations with over a billion determinants [47].

In comparing determinantal based CI calculations and spin-adapted expansions it is useful to note that in a full CI expansion for N electrons using n orbitals, ignoring spatial symmetry, the number of determinants exceeds the number of spin-adapted CSFs by a factor of

$$\frac{n_{\text{det}}}{n_{\text{CSF}}} = \frac{m+S+1}{2S+1}\left(1-\frac{m-S}{n+1}\right)$$

where $m = N/2$ and S is the total spin quantum number. This ratio is between four and five for most of the full CI calculations reported. For example, the FCI calculation on the Mg atom [44, 46], containing about 2.5 billion determinants in D_{2h} symmetry, corresponds to about half a billion spin-adapted CSFs.

Another important development in CI methodology is the introduction of 'contracted' CI methods, which gain increases in the scope of achievable MRCI calculations at the cost of reduced flexibility in the variational expansion and, therefore, some sacrifice in the energy compared with fully unconstrained expansions. Two different contraction approaches have been introduced, both aimed at reducing the number of independently varied coefficients and thus greatly reducing the size of

the matrix eigenvalue problem. The first, 'externally contracted' CI [181], is no longer in use today. It employs a perturbation procedure to fix the relative values of the coefficients in sets of CSFs that share the same internal (active-space) part.

In the more common 'internally contracted' CI [129, 182, 183] the multiconfigurational reference function, optimized in an MCSCF calculation, is treated as a single contracted reference configuration, and excited configurations are generated by the application of excitation operators to this contracted function. Each excited configuration is then a linear combination of many ordinary CSFs, with the linear coefficients fixed by the reference wavefunction. As a result, the number of independently varied coefficients is similar to the number of terms in a single-reference calculation. For given numbers of orbitals and electrons, the length of an uncontracted MR-CISD expansion is approximately proportional to the number of reference configurations. Therefore internal contraction can provide a drastic reduction in the length of the CI vector and allow the use of substantially larger reference spaces than would be practical in uncontracted calculations, making the use of complete valence active spaces more affordable. At the same time it should noted that the reduction in the computational effort is not as drastic as in the length of the CI vector, since the Hamiltonian matrix in contracted CI is not nearly as sparse as for uncontracted expansions.

Usually energy loss due to internal contraction, compared with uncontracted MRCI, is very small [184], and energy differences, such as dissociation energies, are reproduced well [108], but there are some exceptions [108], particularly in the vicinity of avoided crossings in potential energy curves and surfaces, for which the location of the avoided crossing may differ substantially between the reference MCSCF wavefunction and the corresponding MRCI wavefunction. A generalization which overcomes this problem by using more than one multiconfigurational reference function has been reported [185]. The power of the internally contracted CI method is demonstrated, for example, by a recent application to the calculation of a water molecule potential energy surface [186].

5. Strengths and weaknesses

The conceptual simplicity of the configuration interaction method is very appealing, and its variational nature is an important advantage, but its principal strength lies in its flexibility and generality. It can be applied straightforwardly to any electronic state, and can be spin- and symmetry-adapted relatively easily. Its multireference formulation is straightforward, and applicable readily to any type of reference space, complete or otherwise. Apart from the increased size, and therefore increased computational requirements, multireference CI is not notably more difficult than the single-reference form, and the ability to use incomplete active spaces can be employed to limit the computational requirements substantially. As a result, MRCI is usually the method of choice for dealing with non-dynamic electron correlation [187] (reflecting near degeneracies and related effects), including the treatment of bond breaking and potential energy surfaces [188]. In particular, the reference space can be chosen to minimize bias in the description of different regions of a potential energy surface.

The multireference capabilities of CI contrast with the situation in many-body perturbation theory (MBPT) and coupled cluster (CC) theory, for which multireference generalizations are substantially more difficult than their single-reference counterparts and for which the use of incomplete reference spaces introduces additional difficulties. Also, unlike multireference many-body methods, no problems of intruder states arise in MRCI.

The principal weakness of truncated configuration interaction is its lack of proper scaling with the size of the system. The proper scaling of a computational model, referred to as 'extensivity' or 'size extensivity' [189], is the main facet of the 'separability condition' [190, 191]. It can be related to its many-body diagrammatic representation, and is dependent on the absence of 'unlinked diagram' contributions in its energy expression (see, e.g., Paldus and Čížek [192], Bartlett and co-workers [189, 193], and Harris *et al.* [194]). In an extensive model such as MBPT or CC, in which the energy is expressed entirely in terms of linked diagrams, the energy of an assembly of non-interacting identical subsystems is proportional to the number of subsystems, and the energy of a uniform system, such as an electron gas, is proportional to its extent. It is obvious, for example, that the CISD energy of a collection of non-interacting helium atoms does not satisfy this requirement, since it provides the full CI energy for a single atom but not for more than one atom. In fact, the CISD energy of such a collection scales as the square root of the number of atoms as this number becomes large [191, 195, 196]. The lack of extensivity also affects the accuracy of computed ionization potentials and electron affinities, unless appropriate corrections are applied.

The energy contribution associated with an unlinked diagram consisting of k separate parts is proportional to the kth power of the size of the system, and therefore such contributions must cancel if extensivity is to be maintained. These unlinked diagram contributions do cancel for the exact (full CI) energy, as well as in each order of Rayleigh–Schrödinger perturbation theory and

at each excitation level of a coupled-cluster treatment. However, the unlinked diagram contributions at a given excitation level of CI are cancelled by contributions from other excitation levels, so that unlinked terms remain in a truncated CI energy, resulting in lack of extensivity.

Unlike the energy, which should be additively separable, the wavefunction should be multiplicatively separable [190], and its diagrammatic expansion contains disconnected (but not unlinked) diagrams.† Such diagrams represent disconnected clusters which describe simultaneous independent interactions in smaller clusters of electrons as products of lower-level connected clusters [191]. The most important of these terms are products of double excitations. It is the lack in CISD (but not in its coupled clusters counterpart, CCSD) of the disconnected quadruple excitation contributions deriving from products of double excitations which is its most serious defect, and is responsible for most of its deviation from extensivity. It is this disconnected quadruples contribution for which the various correction formulas for CISD try to compensate.

Another facet of the separability condition is 'size consistency' [136, 197]. A computational model is size consistent if, when applied to a molecule dissociated into two or more parts, the energy of the dissociated molecule, treated as one system, equals the sum of the energies of the subsystems computed by the same model. Again, truncated CI fails this test, and as a result, when it is applied naïvely, fails to provide satisfactory dissociation energies and some other energy differences. This deficiency can be reduced by the application of various corrections, as discussed in the next section. Satisfactory dissociation energies also can be obtained by treating the dissociated limit as a 'supermolecule', using the same type of CI expansion as for the bound system [198]. In fact, in multireference treatments, this supermolecule approach is the only consistent method for the calculation of dissociation energies and for the asymptotic regions of potential energy surfaces [178].

Extensivity and size consistency, although closely related, are not equivalent [189]. For example, a single-reference many-body correlation treatment built upon a closed-shell restricted Hartree–Fock reference function for a molecule is not size consistent with respect to dissociation into open-shell fragments, yet usually it satisfies the extensivity criterion because of its linked-diagram energy expression. On the other hand, multiconfigurational wavefunctions often can be constructed to be size consistent without being extensive.

Although the use of higher than doubly-excited CSFs in CI expansions is easy in principle, the exponential increase in the size of a CI expansion with the level of excitation usually makes such calculations impractical. Also, the extension of direct CI programs to handle higher excitation CSFs is complicated by the increased complexity of the coupling coefficients determination. As a result of this latter factor, most attempts to include higher excitations [52] or to implement full CI calculations [37–49] use a determinantal formulation.

The difficulty of extending the CI expansion to higher excitations is a serious shortcoming because of its very slow convergence. Unlike the situation in the many-body methods, the connected and disconnected cluster contributions to each excited CSF are inextricably combined in the CI formalism. Thus it is not possible to separate the disconnected cluster wavefunction contributions from the connected cluster contributions at the same overall excitation level. From the quadruple excitations level and up, the disconnected cluster contributions are much more important than the connected terms. Because these contributions are represented by different diagrams, they are separated in the many-body formalism, where the disconnected contributions are much easier to compute than the connected terms, and appear in lower orders of perturbation theory and lower CC excitation levels. As a result, quadruple and higher excitation terms are much more important in CI than in CC. For example, the major CI quadruple excitation contributions that are particularly important for extensivity are obtained in factorizable form at fourth order in MBPT, at relatively low cost, and are included as disconnected cluster terms (as products of double excitations) in the double excitation CC wavefunction [191, 199–204].

The use of a multireference CISD expansion can account for some of the most important contributions arising from higher excitations in single-reference models, but is not sufficient to offset the intrinsic limitation of the truncated CI approach. Furthermore, as previously noted, the length of a multireference CISD expansion is approximately proportional to the number of reference configurations, making the use of a theoretically desirable CAS reference space prohibitively expensive in many cases. While this difficulty can be reduced by the use of incomplete active spaces of various kinds [42, 62, 63, 178], such tactics are not entirely satisfactory, particularly in the treatment of potential energy surfaces.

† Some of the earlier literature does not distinguish properly between the terms 'unlinked' and 'disconnected'. An unlinked diagram contains separate *closed* parts. A disconnected, but linked diagram contains separate *open* parts, but no closed parts. Unlinked diagrams cancel in both the exact energy expression and the exact wavefunction; disconnected diagrams are proper constituents of the exact wavefunction (though they cancel in the coupled cluster *equations*).

6. Corrections and modifications

As discussed in the previous section, the principal defect of the configuration interaction method is the lack of extensivity and size consistency of truncated CI expansions. The various approaches that have been used to compensate for this deficiency fall into two classes: the first class applies *post hoc* corrections to CISD results, while the second modifies the CISD algorithm itself.

The *post hoc* corrections often are called 'quadruples corrections', because they attempt to account for the disconnected quadruple excitation contributions that are needed to cancel the unlinked diagram components in the CISD energy [203, 205]. They modify the CISD energy, but do not produce a corrected wavefunction or modify derived properties. The best known and most widely used of these are the Davidson correction [206] and its variations [196, 207]. The original Davidson formula tends to overestimate the magnitude of the missing disconnected quadruples contributions to the total energy [208], primarily because it ignores the problem of 'exclusion-principle-violating' (EPV) terms [203]. The modified corrections exacerbate the problem because they increase the magnitude of the correction. In fact, while the Davidson correction tends to overestimate the disconnected quadruples contribution, there is nothing in its formulation to account for other missing terms, such as connected triple excitation contributions, and therefore the corrected CISD energy usually lies above the full CI limit. However, such fortuitous and unsystematic cancellation of errors cannot be counted on reliably in the determination of binding energies and other energy differences.

A scale factor that sometimes has been applied to the Davidson corrections is $(N-2)/N$ [136, 209], where N is the number of electrons being correlated. It is designed to eliminate the correction entirely for a two-electron system (for which CISD is equivalent to full CI). A more recently proposed scale factor is $(N-2)(N-3)/[N(N-1)]$ [210], which eliminates the correction for both two-electron and three-electron systems.

While the Davidson correction was developed originally for single-reference CISD calculations, a straightforward generalization [209], without formal justification, has been applied widely to multireference expansions. Generally it has been successful (e.g., [39-41, 186, 209, 211]), but the name 'full CI correction' that sometimes has been applied to it [209] is not appropriate, since it is designed only to deal with one of the various types of contribution missing in an MR-CISD expansion. A more systematic multireference generalization of the Davidson correction was proposed by Jankowski *et al.* [212].

Another popular extensivity correction for SR-CISD is the Pople correction [136]. It was designed to produce exact energies for assemblies of non-interacting two-electron systems, and vanishes automatically for the two-electron case. The performance of two versions of the Davidson correction, with and without scaling, and of the Pople correction has been compared in calculations of binding energies of several complexes by Del Bene and co-workers [198]. Other interesting comparisons of several correction formulas were reported, for example, by Martin *et al.* [213].

The second type of approach for dealing with the extensivity defect of truncated CI involves modifications of the CI procedure itself. The modifications are based on electron-pair concepts [129, 130, 191, 199, 200, 214-216] deriving from coupled cluster ideas. Early attempts to treat pair correlations independently, in the form of the independent electron-pair approximation (IEPA) [191, 199, 200], were not very successful [126 128, 191, 217], and gave way to several versions of the coupled electron-pair approximation (CEPA) [127, 128, 191, 201, 218]. These versions range from CEPA(0) to CEPA(5) [219], depending mainly on the way they try to account for EPV diagram effects. The simplest version, CEPA(0), ignores the EPV problem entirely, and is known also as linearized coupled pair many-electron theory (LCPMET) [201] or the linearized coupled cluster method (LCCM), because it can be obtained by linearization of the coupled cluster doubles (CCD) or singles and doubles (CCSD) equations. The other versions are more complicated, and include in their formulas pair correlation energies obtained by summing sets of double excitation coefficients in the wavefunction expansion.

One limitation of the CEPA method and related approximations is that their energy expression is not obtained by a stationarity condition for an energy functional. While this feature is of no consequence for energy calculations, it is a disadvantage in the analytical calculation of energy derivatives. The alternative 'coupled pair functional' (CPF) [220] and 'modified CPF' (MCPF) [221] approximations obtain the energy by minimizing a modified energy functional, and have been tested in a number of molecular calculations [39-41].

The CEPA and CPF approximations were derived for single-reference treatments. A multireference generalization of LCCM was derived by Laidig *et al.* [222]. Multireference generalizations for several CEPA models were proposed by Fulde and Stoll [223]. A simplified form of CPF applicable to multireference treatments is the 'averaged coupled pair functional' (ACPF) of Gdanitz and Ahlrichs [224]. This approach uses a flexible functional form which can be varied to obtain a range

of approximations, including a multireference LCCM. One such variant of the functional, based on the Meissner scale factor idea [210], has been introduced recently under the name 'averaged quadratic coupled cluster' (AQCC) approximation [225]. A number of other variants have been proposed by Füsti-Molnár and Szalay [226], who provide interesting comparisons of several models. All these methods are at least approximately extensive in most applications. They maintain the functional stationarity feature of CPF, and thus are convenient in applications in which energy derivatives are to be calculated. The principal algorithmic effect of these various approximations is that they convert the matrix eigenvalue problem to a system of linear equations (for LCCM) or a system intermediate between an eigenvalue problem and a simultaneous equations problem. Comparisons of ACPF and LCCM results with other models in calculations of binding energies of several complexes have been reported [198].

Numerous other analyses and proposed correction formulas and modifications for dealing with the extensivity problem of CI have been published, and only a subset of them can be mentioned here [205, 227–241].

Finally, we mention the B_k approximation [242] (see Shavitt [243] and references therein), in which the CSFs are divided into a relatively small primary set and a much larger secondary set, and all off-diagonal matrix elements between pairs of secondary CSFs are neglected. It is not strictly an extensivity correction, but it has been used in some cases to estimate triple and quadruple excitation contributions on top of CISD [243].

7. Summary

Configuration interaction is a very versatile and powerful *ab initio* method. Aided by the remarkable advances in computers in the last few decades, it has developed and matured to a sophisticated level applicable to many problems and capable of providing useful answers to questions of physical and chemical interest. Although it suffers from some important limitations, notably lack of extensivity and slow convergence, and although it has been supplanted to a considerable extent by modern many-body methods, particularly coupled cluster theory, CI still has an important role to play in molecular electronic structure theory. This situation is likely to prevail at least until multireference coupled cluster methods become more standardized and accessible to the chemistry research community.

Modified CI approaches and configuration-based multireference perturbation theory can also be very useful in the arsenal of computational quantum chemistry methods.

References

[1] Ritz, W., 1909, *J. reine angew. Math.*, **135,** 1.
[2] Kellner, G. W., 1927, *Z. Phys.*, **44,** 91, 110.
[3] Hylleraas, E. A., 1928, *Z. Phys.*, **48,** 469.
[4] Hylleraas, E. A., 1929, *Z. Phys.*, **54,** 347; Hylleraas, E. A., and Undheim, B., 1930, *Z. Phys.*, **65,** 759.
[5] James, H. M., and Coolidge, A. S., 1933, *J. chem. Phys.*, **1,** 825.
[6] Weinbaum, S., 1933, *J. chem. Phys.*, **1,** 593.
[7] Hirschfelder, J., Eyring, H., and Rosen, N., 1936, *J. chem. Phys.*, **4,** 121.
[8] Slater, J. C., 1929, *Phys. Rev.*, **34,** 1293.
[9] Condon, E. U., 1930, *Phys. Rev.*, **36,** 1121.
[10] Bacher, R. F., 1933, *Phys. Rev.*, **43,** 264.
[11] Ufford, C. W., 1933, *Phys. Rev.*, **44,** 732.
[12] Nagamiya, T., 1936, *Proc. phys.-math. Soc. Jap.*, **18,** 497.
[13] Hartree, D. R., Hartree, W., and Swirles, B., 1939, *Phil. Trans. R. Soc. Lond. A*, **238,** 229.
[14] Parr, R. G., and Crawford, B. L., Jr., 1948, *J. chem. Phys.*, **16,** 526.
[15] Craig, D. P., 1950, *Proc. R. Soc. Lond. A*, **200,** 474.
[16] Sklar, A. L., 1939, *J. chem. Phys.*, **7,** 984.
[17] Parr, R. G., Craig, D. P., and Ross, I. G., 1950, *J. chem. Phys.*, **18,** 1561.
[18] Boys, S. F., 1950, *Proc. R. Soc. Lond. A*, **200,** 542.
[19] Boys, S. F., 1950, *Proc. R. Soc. Lond. A*, **201,** 125.
[20] Bernal, M. J. M., and Boys, S. F., 1952, *Phil. Trans. R. Soc. Lond. A*, **245,** 139.
[21] Boys, S. F., 1953, *Proc. R. Soc. Lond. A*, **217,** 136.
[22] Boys, S. F., 1953, *Proc. R. Soc. Lond. A*, **217,** 235.
[23] Taylor, G. R., and Parr, R. G., 1952, *Proc. Natn. Acad. Sci. USA*, **38,** 154.
[24] Shull, H., and Löwdin, P.-O., 1955, *J. chem. Phys.*, **23,** 1565.
[25] Walsh, J. M., and Matsen, F. A., 1951, *J. chem. Phys.*, **19,** 526.
[26] Kastler, D., 1953, *J. Chim. phys.*, **50,** 556.
[27] Meckler, A., 1953, *J. chem. Phys.*, **21,** 1750.
[28] Boys, S. F., and Price, V. E., 1954, *Phil. Trans. R. Soc. Lond. A*, **246,** 451.
[29] Ellison, F. O., and Shull, H., 1955, *J. chem. Phys.*, **23,** 2348.
[30] Boys, S. F., Cook, G. B., Reeves, C. M., and Shavitt, I., 1956, *Nature*, **178,** 1207.
[31] Kaplan, H., 1957, *J. chem. Phys.*, **26,** 1704.
[32] Kotani, M., Mizuno, Y., Kayama, K., and Ishiguro, E., 1957, *J. phys. Soc. Jap.*, **12,** 707.
[33] Ohno, K., 1957, *J. phys. Soc. Jap.*, **12,** 938.
[34] Krauss, M., and Wehner, J. F., 1958, *J. chem. Phys.*, **29,** 1287.
[35] Foster, J. M., and Boys, S. F., 1960, *Rev. mod. Phys.*, **32,** 305.
[36] Shavitt, I., 1977, *Methods of Electronic Structure Theory*, edited by H. F. Schaefer III (New York: Plenum), p. 189.
[37] Handy, N. C., 1980, *Chem. Phys. Lett.*, **74,** 280; Saxe, P., Schaefer, H. F., III, and Handy, N. C., 1981, *Chem. Phys. Lett.*, **79,** 202; Harrison, R. J., and Handy, N. C., 1983, *Chem. Phys. Lett.*, **95,** 386; **98,** 97.
[38] Knowles, P. J., and Handy, N. C., 1984, *Chem. Phys. Lett.*, **111,** 315; 1989, *J. chem. Phys.*, **91,** 2396; 1989, *Comput. Phys. Commun.*, **54,** 75; Knowles, P. J., 1989, *Chem. Phys. Lett.*, **155,** 513.

[39] Bauschlicher, C. W., Jr., Langhoff, S. R., Taylor, P. R., and Partridge, H., 1986, *Chem. Phys. Lett.*, **126**, 436; Bauschlicher, C. W., Jr., Langhoff, S. R., Taylor, P. R., Handy, N. C., and Knowles, P. J., 1986, *J. chem. Phys.*, **85**, 1469; Bauschlicher, C. W., Jr., Langhoff, S. R., Partridge, H., and Taylor, P. R., 1986, *J. chem. Phys.*, **85**, 3407.

[40] Bauschlicher, C. W., Jr., and Taylor, P. R., 1986, *J. chem. Phys.*, **85**, 2779, 6510; 1987, *J. chem. Phys.*, **86**, 858, 1420, 5600; 1987, *Theor. Chim. Acta*, **71**, 263.

[41] Bauschlicher, C. W., Jr., and Langhoff, S. R., 1987, *J. chem. Phys.*, **86**, 5595; **87**, 2919, 4665; 1988, *J. chem. Phys.*, **89**, 2116, 4246; Bauschlicher, C. W., Jr., Langhoff, S. R., and Taylor, P. R., *Adv. chem. Phys.*, **77**, 103.

[42] Olsen, J., Roos, B. O., Jørgensen, P., and Jensen, H. J. A., 1988, *J. chem. Phys.*, **89**, 2185.

[43] Zarrabian, S., Sarma, C. R., and Paldus, J., 1989, *Chem. Phys. Lett.*, **155**, 183; Harrison, R. J., and Zarrabian, S., 1989, *Chem. Phys. Lett.*, **158**, 393.

[44] Olsen, J., Jørgensen, P., and Simons, J., 1990, *Chem. Phys. Lett.*, **169**, 463.

[45] Bendazzoli, G. L., and Evangelisti, S., 1993, *J. chem. Phys.*, **98**, 3141; 1993, *Int. J. Quantum Chem. Symp.*, **27**, 287; Evangelisti, S., Bendazzoli, G. L., and Gagliardi, L., 1994, *Chem. Phys.*, **185**, 47; Evangelisti, S., and Bendazzoli, G. L., 1995, *Nuovo Cimento D*, **17**, 289.

[46] Mitrushenkov, A. O., 1994, *Chem. Phys. Lett.*, **217**, 559.

[47] Evangelisti, S., Bendazzoli, G. L., Ansaloni, R., and Rossi, E., 1995, *Chem. Phys. Lett.*, **233**, 353; Evangelisti, S., Bendazzoli, G. L., Ansaloni, R., Durì, F., and Rossi, E., 1996, *Chem. Phys. Lett.*, **252**, 437.

[48] Christiansen, O., Koch, H., Jørgensen, P., and Olsen, J., 1996, *Chem. Phys. Lett.*, **256**, 185.

[49] Olsen, J., Jørgensen, P., Koch, H., Balkova, A., and Bartlett, R. J., 1996, *J. chem. Phys.*, **104**, 8007.

[50] Nesbet, R. K., 1958, *Phys. Rev.*, **109**, 1632.

[51] Pipano, A., and Shavitt, I., 1968, *Int. J. Quantum Chem.*, **2**, 741.

[52] Sherrill, C. D., and Schaefer, H. F., III, 1996, *J. phys. Chem.*, **100**, 6069.

[53] Whitten, J. L., and Hackmeyer, M., 1969, *J. chem. Phys.*, **51**, 5584; Hackmeyer, M., and Whitten, J. L., 1971, *J. chem. Phys.*, **54**, 3739; Whitten, J. L., 1972, *J. chem. Phys.*, **56**, 5458.

[54] Peyerimhoff, S. D., and Buenker, R. J., 1972, *Chem. Phys. Lett.*, **16**, 235; Buenker, R. J., and Peyerimhoff, S. D., 1974, *Theor. Chim. Acta*, **35**, 33.

[55] McLean, A. D., and Liu, B., 1973, *J. chem. Phys.*, **58**, 1066; Bagus, P. S., Liu, B., McLean, A. D., and Yoshimine, M., 1973, *Computational Methods for Large Molecules and Localized States in Solids*, edited by F. Herman, A. D. McLean, and R. K. Nesbet (New York: Plenum), p. 87.

[56] Kahn, L. R., Hay, P. J., and Shavitt, I., 1974, *J. chem. Phys.*, **61**, 3530.

[57] Bauschlicher, C. W., Jr., Langhoff, S. R., and Taylor, P. R., 1988, *J. chem. Phys.*, **88**, 2540; Almlöf, J., DeLeeuw, B. J., Taylor, P. R., Bauschlicher, C. W., Jr., and Siegbahn, P., 1989, *Int. J. Quantum Chem. Symp.*, **23**, 345; Taylor, P. R., 1992, *Lecture Notes in Quantum Chemistry, Lecture Notes in Chemistry*, Vol. 58, edited by B. O. Roos (Berlin: Springer), p. 325.

[58] Nesbet, R. K., 1955, *Proc. R. Soc. Lond.* A, **230**, 312.

[59] Shavitt, I., 1984, *Advanced Theories and Computational Approaches to the Electronic Structure of Molecules*, edited by C. E. Dykstra (Dordrecht: Reidel), p. 185.

[60] Roos, B. O., Taylor, P. R., and Siegbahn, P. E. M., 1980, *Chem. Phys.*, **48**, 157; Roos, B. O., 1980, *Int. J. Quantum Chem. Symp.*, **14**, 175.

[61] Ruedenberg, K., Schmidt, M. W., Gilbert, M. M., and Elbert, S. T., 1982, *Chem. Phys.*, **71**, 41, 65.

[62] Malmqvist, P.-Å., Rendell, A., and Roos, B. O., 1990, *J. phys. Chem.*, **94**, 5477.

[63] Harding, L. B., and Goddard, W. A., III, 1975, *J. Am. chem. Soc.*, **97**, 6293; Dunning, T. H., Jr., Cartwright, D. C., Hunt, W. J., Hay, P. J., and Bobrowicz, F. W., 1976, *J. chem. Phys.*, **64**, 4755.

[64] Dunning, T. H., Jr., 1984, *Advanced Theories and Computational Approaches to the Electronic Structure of Molecules*, edited by C. E. Dykstra (Dordrecht: Reidel), p. 67.

[65] Bunge, A., 1970, *J. chem. Phys.*, **53**, 20.

[66] Schaefer, H. F., III, Klemm, R. A., and Harris, F. E., 1969, *Phys. Rev.*, **181**, 137; 1969, *J. chem. Phys.*, **51**, 4643.

[67] Bender, C. F., and Davidson, E. R., 1966, *J. phys. Chem.*, **70**, 2675; 1969, *Phys. Rev.*, **183**, 23.

[68] Raffenetti, R. C., Hsu, K., and Shavit, I., 1977, *Theor. Chim. Acta*, **45**, 33.

[69] Wigner, E., 1927, *Z. Phys.*, **40**, 492, 883; 1931, *Gruppentheorie und ihre Anwendung auf die Quantenmechanik der Atomspektren* (Braunschweig: Vieweg) English translation: 1959, *Group Theory and Its Application to the Quantum Mechanics of Atomic Spectra* (New York: Academic Press)

[70] Weyl, H., 1928, *Gruppentheorie und Quantenmechanik* (Leipzig: Hirzel) English translation: 1931, *The Theory of Groups and Quantum Mechanics* (London: Methuen)

[71] Dirac, P. A. M., 1929, *Proc. R. Soc. Lond. A*, **123**, 714.

[72] Waller, I., and Hartree, D. R., 1929, *Proc. R. Soc. Lond. A*, **124**, 119.

[73] Serber, R., 1934, *J. chem. Phys.*, **2**, 697; 1934, *Phys. Rev.*, **45**, 461.

[74] Yamanouchi, T., 1935, *Proc. phys.-math. Soc. Jap.*, **17**, 274; 1937, *Proc. phys.-math. Soc. Jap.*, **19**, 436.

[75] Kotani, M., Ohno, K., and Kayama, K., 1961, *Encyclopedia of Physics*, edited by S. Flügge (Berlin: Springer), Vol. 37/2, p. 1.

[76] Matsen, F. A., 1964, *Adv. Quantum Chem.*, **1**, 59.

[77] Ruedenberg, K., 1971, *Phys. Rev. Lett.*, **27**, 1105; Salmon, W. I., and Ruedenberg, K., 1972, *J. chem. Phys.*, **57**, 2776.

[78] Löwdin, P.-O., 1955, *Phys. Rev.*, **97**, 1509; 1956, *Adv. Phys.*, **5**, 1.

[79] Pauncz, R., 1967, *Alternant Molecular Orbital Method* (Philadelphia: Saunders); 1979, *Spin Eigenfunctions* (New York: Plenum).

[80] Manne, R., 1966, *Theor. Chim. Acta*, **6**, 116.

[81] Smith, V. H., and Harris, F. E., 1969, *J. math. Phys.*, **10**, 771.

[82] Heitler, W., and Rumer, G., 1931, *Z. Phys.*, **68**, 12.

[83] Reeves, C. M., 1957, Ph.D. Thesis, Cambridge University; 1966, *Commun. ACM*, **9**, 276.

[84] Sutcliffe, B. T., 1966, *J. chem. Phys.*, **45**, 235.

[85] COOPER, I. L., and MCWEENY, R., 1966, *J. chem. Phys.*, **45,** 226, 3484.
[86] PALDUS, J., 1974, *J. chem. Phys.*, **61,** 5321; 1976, *Theoretical Chemistry: Advances and Perspectives*, edited by H. Eyring and D. Henderson (New York: Academic Press), Vol. 2, p. 131.
[87] SHAVITT, I., 1977, *Int. J. Quantum Chem. Symp.*, **11,** 131; 1978, *Int. J. Quantum Chem. Symp.*, **12,** 5; 1981, *The Unitary Group, Lecture Notes in Chemistry* 22, edited by J. Hinze (Berlin: Springer), p. 51; 1988, *Mathematical Frontiers in Computational Chemical Physics*, edited by D. G. Truhlar (New York: Springer), p. 300.
[88] DUCH, W., and KARWOWSKI, J., 1979, *Theor. Chim. Acta*, **51,** 175; DUCH, W., 1980, *Theor. Chim. Acta*, **57,** 299.
[89] WIGNER, E., 1927, *Z. Phys.*, **43,** 624; **45,** 601.
[90] BOYS, S. F., 1951, *Proc. R. Soc. Lond. A*, **207,** 181, 197; 1952, *Phil. Trans. R. Soc. Lond. A*, **245,** 95; BERNAL, M. J. M., and BOYS, S. F., 1952, *Phil. Trans. R. Soc. Lond. A*, **245,** 116; BOYS, S. F., and SAHNI, R. C., 1954, *Phil. Trans. R. Soc. Lond. A*, **246,** 463.
[91] NESBET, R. K., 1961, *J. math. Phys.*, **2,** 701.
[92] SALMON, W. I., and RUEDENBERG, K., 1972, *J. chem. Phys.*, **57,** 2776.
[93] BUNGE, C. F., and BUNGE, A., 1973, *Int. J. Quantum Chem.*, **7,** 927.
[94] SASAKI, F., 1974, *Int. J. Quantum Chem.*, **8,** 605.
[95] MUNCH, D., and DAVIDSON, E. R., 1975, *J. chem. Phys.*, **63,** 980.
[96] GERSHGORN, Z., and SHAVITT, I., 1967, *Int. J. Quantum Chem. Symp.*, **1,** 403.
[97] PIPANO, A., and SHAVITT, I., 1968, unpublished work; PIPANO, A., GILMAN, R. R., BENDER, C. F., and SHAVITT, I., 1970, *Chem. Phys. Lett.*, **4,** 583; HAY, P. J., and SHAVITT, I., 1974, *J. chem. Phys.*, **60,** 2865.
[98] NESBET, R. K., 1958, *Ann. Phys.* (N.Y.), **3,** 397.
[99] SIMONS, J., and HARRIMAN, J. E., 1969, *J. chem. Phys.*, **51,** 296.
[100] SHAVITT, I., 1993, *Israel J. Chem.*, **33,** 357.
[101] RAFFENETTI, R. C., 1973, *J. chem. Phys.*, **58,** 4452.
[102] ALMLÖF, J., and TAYLOR, P. R., 1987, *J. chem. Phys.*, **86,** 4070; 1990, *J. chem. Phys.*, **92,** 551; 1991, *Adv. Quantum Chem.*, **22,** 301.
[103] BAUSCHLICHER, C. W., JR., 1987, *Chem. Phys. Lett.*, **142,** 71; BAUSCHLICHER, C. W., JR., and TAYLOR, P. R., 1993, *Theor. Chim. Acta*, **86,** 13.
[104] LANGHOFF, S. R., BAUSCHLICHER, C. W., JR., and TAYLOR, P. R., 1988, *J. chem. Phys.*, **88,** 5715; **89,** 7650.
[105] WIDMARK, P.-O., MALMQVIST, P.-Å., and ROOS, B. O., 1990, *Theor. Chim. Acta*, **77,** 291; WIDMARK, P.-O., PERSSON, B.-J., and ROOS, B. O., 1991, *Theor. Chim. Acta*, **79,** 419.
[106] DUNNING, T. H., JR., 1989, *J. chem. Phys.*, **90,** 1007; KENDALL, R. A., DUNNING, T. H., JR., and HARRISON, R. J., 1992, *J. chem. Phys.*, **96,** 6796; WOON, D. E., and DUNNING, T. H., JR., 1993, *J. chem. Phys.*, **98,** 1358; **99,** 3730; 1994, *J. chem. Phys.*, **100,** 2975.
[107] FELLER, D., 1992, *J. chem. Phys.*, **96,** 6104; 1993, *J. chem. Phys.*, **98,** 7059; WOON, D. E., and DUNNING, T. H., JR., 1993, *J. chem. Phys.*, **99,** 1914.,
[108] PETERSON, K. A., KENDALL, R. A., and DUNNING, T. H., JR., 1983, *J. chem. Phys..*, **99,** 1930, 9790.
[109] WOON, D. E., and DUNNING, T. H., JR., 1995, *J. chem. Phys.*, **103,** 4572.
[110] SHAVITT, I., ROSENBERG, B. J., and PALALIKIT, S., 1976, *Int. J. Quantum Chem. Symp.*, **10,** 33; 1977, *Int. J. Quantum Chem. Symp.*, **11,** 651.
[111] KELLY, H. P., 1964, *Phys. Rev.*, **136,** B896.
[112] HUNT, W. J., and GODDARD, W. A., III, 1969, *Chem. Phys. Lett.*, **3,** 414.
[113] BENDER, C. F., and DAVIDSON, E. R., 1967, *J. chem. Phys.*, **47,** 4972.
[114] HUZINAGA, S., and ARNAU, C., 1970, *Phys. Rev. A*, **1,** 1285; 1971, *J. chem. Phys.*, **54,** 1948.
[115] WHITTEN, J. L., 1972, *J. chem. Phys.*, **56,** 5458.
[116] LUKEN, W. L., 1979, *Chem. Phys.*, **40,** 301.
[117] COOPER, I. L., and POUNDER, N. M., 1979, *J. chem. Phys.*, **71,** 957.
[118] BAUSCHLICHER, C. W., JR., 1980, *J. chem. Phys.*, **72,** 880.
[119] ADAMOWICZ, L., and BARTLETT, R. J., 1987, *J. chem. Phys.*, **86,** 6314.
[120] DAVIDSON, E. R., 1972, *J. chem. Phys.*, **57,** 1999.
[121] LÖWDIN, P.-O., 1955, *Phys. Rev.*, **97,** 1474; LÖWDIN, P.-O., and SHULL, H., 1956, *Phys. Rev.*, **101,** 1730.
[122] HAY, P. J., 1973, *J. chem. Phys.*, **59,** 2468.
[123] SIU, A. K. Q., and HAYES, E. F., 1974, *J. chem. Phys.*, **61,** 37.
[124] JAFRI, J. A., and WHITTEN, J. L., 1977, *Theor. Chim. Acta*, **44,** 305.
[125] EDMISTON, C., and KRAUSS, M., 1966, *J. chem. Phys.*, **45,** 1833.
[126] MEYER, W., 1971, *Int. J. Quantum Chem. Symp.*, **5,** 341; 1973, *J. chem. Phys.*, **58,** 1017.
[127] MEYER, W., 1974, *Theor. Chim. Acta*, **35,** 277.
[128] AHLRICHS, R., LISCHKA, H., STAEMMLER, V., and KUTZELNIGG, W., 1975, *J. chem. Phys.*, **62,** 1225; AHLRICHS, R., DRIESSLER, F., LISCHKA, H., STAEMMLER, V., and KUTZELNIGG, W., 1975, *J. chem. Phys.*, **62,** 1235.
[129] MEYER, W., 1977, *Methods of Electronic Structure Theory*, edited by H. F. Schaefer III (New York: Plenum), p. 413.
[130] AHLRICHS, R., and DRIESSLER, F., 1975, *Theor. Chim. Acta*, **36,** 275; MEYER, W., 1976, *J. chem. Phys.*, **64,** 2901; DYKSTRA, C. E., SCHAEFER, H. F., III, and MEYER, W., 1976, *J. chem. Phys.*, **65,** 2740.
[131] LENNARD-JONES, J., and POPLE, J. A., 1950, *Proc. R. Soc. Lond. A*, **202,** 166.
[132] FOSTER, J. M., and BOYS, S. F., 1960, *Rev. mod. Phys.*, **32,** 300; BOYS, S. F., 1966, *Quantum Theory of Atoms, Molecules, and the Solid State*, edited by P.-O. Löwdin (New York: Academic Press), p. 253.
[133] EDMISTON, C., and RUEDENBERG, K., 1963, *Rev. mod. Phys.*, **35,** 457.
[134] WILHITE, D. L., and WHITTEN, J. L., 1973, *J. chem. Phys.*, **58,** 948.
[135] PULAY, P., 1983, *Chem. Phys. Lett.*, **100,** 151; SÆBØ, S., and PULAY, P., 1985, *Chem. Phys. Lett.*, **113,** 13.
[136] POPLE, J. A., SEEGER, R., and KRISHNAN, R., 1977, *Int. J. Quantum Chem. Symp.*, **11,** 149.
[137] SAUNDERS, V. R., and VAN LENTHE, J. H., 1983, *Molec. Phys.*, **48,** 923.
[138] NESBET, R. K., 1963, *Rev. mod. Phys.*, **35,** 552.
[139] TANG, K. C., and EDMISTON, C., 1970, *J. chem. Phys.*, **52,** 997.

[140] McLean, A. D., 1971, *Proceedings of the Conference on Potential Energy Surfaces in Chemistry*, edited by W. A. Lester Jr., Report RA-18, IBM Research Laboratory, San Jose, California, p. 87.
[141] Bender, C. F., 1972, *J. comput. Phys.*, **9**, 547.
[142] Elbert, S. T., 1973, Ph.D. Thesis, University of Washington.
[143] Diercksen, G. H. F., 1974, *Theor. Chim. Acta*, **33**, 1.
[144] Pendergast, P., and Fink, W. H., 1974, *J. comput. Phys.*, **14**, 286.
[145] Le Ruozo, H., Raseev, G., and Silvi, B., 1978, *Comput. Chem.*, **2**, 15.
[146] Yoshimine, M., 1973, *J. comput. Phys.*, **11**, 449.
[147] Bunge, C. F., and Cisneros, G., 1986, *Comput. Chem.*, **10**, 101, 109; Cisneros, G., Poulain, E., and Bunge, C. F., 1986, *Comput. Chem.*, **10**, 135.
[148] Beebe, N. H. F., and Linderberg, J., 1977, *Int. J. Quantum Chem.*, **12**, 683.
[149] Wilson, S., 1990, *Comput. Phys. Commun.*, **58**, 71.
[150] Cooper, J. L. B., 1948, *Quart. appl. Math.*, **6**, 179; Nesbet, R. K., 1965, *J. chem. Phys.*, **43**, 311; Shavitt, I., 1970, *J. comput. Phys.*, **6**, 124.
[151] Fadeev, D. K., and Fadeeva, V. N., 1963, *Computational Methods of Linear Algebra* (San Francisco: Freeman).
[152] Shavitt, I., Bender, C. F., Pipano, A., and Hosteny, R. P., 1973, *J. comput. Phys.*, **11**, 90.
[153] Davidson, E. R., 1975, *J. comput. Phys.*, **17**, 87.
[154] Lanczos, C., 1950, *J. Res. Natl. Bur. Stand.*, **45**, 255.
[155] Shavitt, I., 1977, *Reduction of I/O Costs and Improvement of Convergence in the Evaluation of Eigenvalues and Eigenvectors of Large Matrices in Configuration Interaction Calculations of Molecular Structure* (Report to the National Aeronautics and Space Administration), Battelle Columbus Laboratories, Columbus, Ohio.
[156] Raffenetti, R. C., 1979, *J. comput. Phys.*, **32**, 403.
[157] Liu, B., 1978, *Numerical Algorithms in Chemistry: Algebraic Methods*, edited by C. Moler and I. Shavitt, Report LBL-8158, Lawrence Berkeley Laboratory, Berkeley, California, p. 49.
[158] Wood, D. M., and Zunger, A., 1985, *J. Phys. A: Math. Gen.*, **18**, 1343.
[159] Morgan, R. B., and Scott, D. S., 1986, *SIAM J. sci. stat. Comput.*, **7**, 817.
[160] Bendazzoli, G. L., Evangelisti, S., and Palmieri, P., 1987, *Int. J. Quantum Chem.*, **31**, 663.
[161] Van Lenthe, J. H., and Pulay, P., 1990, *J. comput. Chem.*, **11**, 1164.
[162] Murray, C. W., Racine, S. C., and Davidson, E. R., 1992, *J. comput. Phys.*, **103**, 382.
[163] Bofill, J. M., and Anglada, J. M., 1994, *Chem. Phys.*, **183**, 19.
[164] Gadea, F. X., 1994, *Chem. Phys. Lett.*, **227**, 201.
[165] Van Dam, H. J. J., van Lenthe, J. H., Sleijpen, G. L. G., and van der Vorst, H. A., 1996, *J. comput. Chem.*, **17**, 267.
[166] Davidson, E. R., 1989, *Comput. Phys. Commun.*, **53**, 49.
[167] Roos, B., 1972, *Chem. Phys. Lett.*, **15**, 153.
[168] Roos, B. O., and Siegbahn, P. E. M., 1977, *Methods of Electronic Structure Theory*, edited by H. F. Schaefer III (New York: Plenum) p. 277.
[169] Lucchese, R. R., and Schaefer, H. F., III, 1978, *J. chem. Phys.*, **68**, 769.
[170] Roos, B. O., and Siegbahn, P. E. M., 1980, *Int. J. Quantum Chem.*, **17**, 485.
[171] Wetmore, R. W., and Segal, G. A., 1975, *Chem. Phys. Lett.*, **36**, 478; Segal, G. A., Wetmore, R. W., and Wolf, K., 1978, *Chem. Phys.*, **30**, 269.
[172] Brooks, B. R., and Schaefer, H. F., III, 1979, *J. chem. Phys.*, **70**, 5092; Brooks, B. R., Laidig, W. D., Saxe, P., Handy, N. C., and Schaefer, H. F., III, 1980, *Phys. Scripta*, **21**, 312; Saxe, P., Fox, D. J., Schaefer, H. F., III, and Handy, N. C., 1982, *J. chem. Phys.*, **77**, 5584.
[173] Siegbahn, P. E., 1979, *J. chem. Phys.*, **70**, 5391; 1980, *J. chem. Phys.*, **72**, 1647.
[174] Lischka, H., Shepard, R., Brown, F. B., and Shavitt, I., 1981, *Int. J. Quantum Chem. Symp.*, **15**, 91; Ahlrichs, R., Böhm, H.-J., Ehrhardt, C., Scharf, P., Schiffer, H., Lischka, H., and Schindler, M., 1985, *J. comput. Chem.*, **6**, 200; Shepard, R., Shavitt, I., Pitzer, R. M., Comeau, D. C., Pepper, M., Lischka, H., Szalay, P. G., Ahlrichs, R., Brown, F. B., and Zhao, J.-G., 1988, *Int. J. Quantum Chem. Symp.*, **22**, 149.
[175] Guldberg, A., Rettrup, S., Bendazzoli, G. L., and Palmieri, P., 1987, *Int. J. Quantum Chem. Symp.*, **21**, 513.
[176] Duch, W., 1986, *GRMS or Graphical Representation of Model Spaces* (Berlin: Springer).
[177] Siegbahn, P. E. M., 1984, *Chem. Phys. Lett.*, **109**, 417.
[178] Kedziora, G. S., and Shavitt, I., 1997, *J. chem. Phys.*, **106**, 8733.
[179] Schüler, M., Kovar, T., Lischka, H., Shepard, R., and Harrison, R. J., 1993, *Theor. Chim. Acta*, **84**, 489; Dachsel, H., Lischka, H., Shepard, R., Nieplocha, J., and Harrison, R. J., 1997, *J. comput. Chem.*, **18**, 430.
[180] Lischka, H., 1997, private communication.
[181] Siegbahn, P. E. M., 1977, *Chem. Phys.*, **25**, 197; 1983, *Int. J. Quantum Chem.*, **23**, 1869.
[182] Siegbahn, P. E. M., 1980, *Int. J. Quantum Chem.*, **18**, 1229.
[183] Werner, H.-J., and Reinsch, E.-A., 1982, *J. chem. Phys.*, **76**, 3144; Werner, H.-J., and Knowles, P. J., 1988, *J. chem. Phys.*, **89**, 5803.
[184] Werner, H.-J., 1987, *Adv. chem. Phys.*, **69**, 1.
[185] Knowles, P. J., and Werner, H.-J., 1992, *Theor. Chim. Acta*, **84**, 95.
[186] Partridge, H., and Schwenke, D. W., 1997, *J. chem. Phys.*, **106**, 4618.
[187] Mok, D. K. W., Neumann, R., and Handy, N. C., 1996, *J. phys. Chem.*, **100**, 6225.
[188] Brown, F. B., Shavitt, I., and Shepard, R., 1984, *Chem. Phys. Lett.*, **105**, 363.
[189] Bartlett, R. J., and Purvis, G. D., 1978, *Int. J. Quantum Chem.*, **14**, 561.
[190] Primas, H., 1965, *Modern Quantum Chemistry*, edited by O. Sinanoğlu (New York: Academic Press), Part II, p. 45.
[191] Kutzelnigg, W., 1977, *Methods of Electronic Structure Theory*, edited by H. F. Schaefer III (New York: Plenum), p. 129.
[192] Paldus, J., and Čížek, J., 1975, *Adv. Quantum Chem.*, **9**, 105.

[193] BARTLETT, R. J., 1981, *Ann. Rev. Phys. Chem.*, **32,** 359; KUCHARSKI, S. A., and BARTLETT, R. J., 1986, *Adv. Quantum Chem.*, **18,** 281.
[194] HARRIS, F. E., MONKHORST, H. J., and FREEMAN, D. L., 1992, *Algebraic and Diagrammatic Methods in Many-Fermion Theory* (New York: Oxford University Press).
[195] SASAKI, F., 1977, *Int. J. Quantum Chem. Symp.*, **11,** 125.
[196] DAVIDSON, E. R., and SILVER, D. W., 1977, *Chem. Phys. Lett.*, **52,** 403.
[197] POPLE, J. A., BINKLEY, J. S., and SEEGER, R., 1976, *Int. J. Quantum Chem. Symp.*, **10,** 1.
[198] DEL BENE, J. E., and SHAVITT, I., 1989, *Int. J. Quantum Chem. Symp.*, **23,** 445.; DEL BENE, J. E., STAHLBERG, E. A., and SHAVITT, I., 1990, *Int. J. Quantum Chem. Symp.*, **24,** 455.
[199] SINANOĞLU, O., 1961, *Proc. R. Soc. Lond.* A, **260,** 379; 1962, *J. chem. Phys.*, **36,** 706, 3198.
[200] NESBET, R. K., 1965, *Adv. chem. Phys.*, **9,** 321.
[201] ČÍŽEK, J., 1966, *J. chem. Phys.*, **45,** 4256; 1969, *Adv. chem. Phys.*, **14,** 35.
[202] HURLEY, A. C., 1976, *Electron Correlation in Small Molecules* (London: Academic Press).
[203] BARTLETT, R. J., and SHAVITT, I., 1977, *Int. J. Quantum Chem. Symp.*, **11,** 165; 1978, *Int. J. Quantum Chem. Symp.*, **12,** 543.
[204] BARTLETT, R. J., DYKSTRA, C. E., and PALDUS, J., 1984, *Advanced Theories and Compututational Approaches to the Electronic Structure of Molecules*, edited by C. E. Dykstra (Dordrecht: Reidel), p. 127.
[205] MEUNIER, A., LEVY, B., and BERTHIER, G., 1976, *Int. J. Quantum Chem.*, **10,** 1061.
[206] DAVIDSON, E. R., 1974, *The World of Quantum Chemistry*, edited by R. Daudel and B. Pullman (Dordrecht: Reidel), p. 17; LANGHOFF, S. R., and DAVIDSON, E. R., 1974, *Int. J. Quantum Chem.*, **8,** 61.
[207] SIEGBAHN, P. E. M., 1978, *Chem. Phys. Lett.*, **55,** 386.
[208] PALDUS, J., 1983, *New Horizons of Quantum Chemistry*, edited by P.-O. Löwdin and B. Pullman (Dordrecht: Reidel), p. 31.
[209] BURTON, P. G., BUENKER, R. J., BRUNA, P. J., and PEYERIMHOFF, S. D., 1983, *Chem. Phys. Lett.*, **95,** 379; PHILLIPS, R. A., BUENKER, R. J., BRUNA, P. J., and PEYERIMHOFF, S. D., 1984, *Chem. Phys.*, **84,** 11.
[210] MEISSNER, L., 1988, *Chem. Phys. Lett.*, **146,** 204.
[211] BUENKER, R. J., and PEYERIMHOFF, S. D., 1983, *New Horizons of Quantum Chemistry*, edited by P.-O. Löwdin and B. Pullman (Dordrecht: Reidel), p. 183.
[212] JANKOWSKI, K., MEISSNER, L., and WASILEWSKI, J., 1985, *Int. J. Quantum Chem.*, **28,** 931.
[213] MARTIN, J. M. L., FRANÇOIS, J. P., and GIJBELS, R., 1990, *Chem. Phys. Lett.*, **172,** 346, 354.
[214] HURLEY, A. C., LENNARD-JONES, J., and POPLE, J. A., 1953, *Proc. R. Soc. Lond.* A, **220,** 446.
[215] PARKS, J. M., and PARR, R. G., 1958, *J. chem. Phys.*, **28,** 335.
[216] SZÁSZ, L., 1960, *Z. Naturforsch.*, **15a,** 909; 1962, *Phys. Rev.*, **126,** 169; 1963, *Phys. Rev.*, **132,** 936; 1968, *J. chem. Phys.*, **49,** 679.
[217] NESBET, R. K., BARR, T. L., and DAVIDSON, E. R., 1969, *Chem. Phys. Lett.*, **4,** 203; BARR, T. L., and DAVIDSON, E. R., 1970, *Phys. Rev.* A, **1,** 644.
[218] KELLY, H. P., 1964, *Phys. Rev.*, **134,** A1450.
[219] KOCH, S., and KUTZELNIGG, W., 1981, *Theor. Chim. Acta*, **59,** 387.
[220] AHLRICHS, R., SCHARF, P., and EHRHARDT, C., 1985, *J. chem. Phys.*, **82,** 890; AHLRICHS, R., SCHARF, P., and JANKOWSKI, K., 1985, *Chem. Phys.*, **98,** 381.
[221] CHONG, D. P., and LANGHOFF, S. R., 1986, *J. chem. Phys.*, **84,** 5606.
[222] LAIDIG, W. D., and BARTLETT, R. J., 1984, *Chem. Phys. Lett.*, **104,** 424; LAIDIG, W. D., SAXE, P., and BARTLETT, R. J., 1987, *J. chem. Phys.*, **86,** 887.
[223] FULDE, P., and STOLL, H., 1992, *J. chem. Phys.*, **97,** 4185.
[224] GDANITZ, R. J., and AHLRICHS, R., 1988, *Chem. Phys. Lett.*, **143,** 413.
[225] SZALAY, P. G., and BARTLETT, R. J., 1995, *J. chem. Phys.*, **103,** 3600.
[226] FÜSTI-MOLNÁR, L., and SZALAY, P. G., 1996, *J. phys. Chem.*, **100,** 6288.
[227] STAMPER, J. G., 1968, *Theor. Chim. Acta*, **11,** 459.
[228] PRIME, S., and ROBB, M. A., 1975, *Chem. Phys. Lett.*, **35,** 86; PRIME, S., REES, C., and ROBB, M. A., 1981, *Molec. Phys.*, **44,** 173.
[229] KARLSTRÖM, G., 1977, *Theor. Chim. Acta*, **44,** 165.
[230] LUKEN, W. L., 1978, *Chem. Phys. Lett.*, **58,** 421.
[231] MEUNIER, A., and LEVY, B., 1979, *Int. J. Quantum Chem.*, **16,** 955.
[232] RUTTINK, P. J. A., 1981, *Chem. Phys. Lett.*, **79,** 253; RUTTINK, P. J. A., VAN LENTHE, J. H., ZWAANS, R., and GROENBOOM, G. C., 1991, *J. chem. Phys.*, **94,** 7212.
[233] BANERJEE, A., and SIMONS, J., 1981, *Int. J. Quantum Chem.*, **19,** 207; 1982, *J. chem. Phys.*, **76,** 4548.
[234] WENZEL, K. B., 1982, *J. Phys. B: atom. molec. Phys.*, **15,** 835.
[235] BRÄNDAS, E. J., COMBS, L. L., and CORREIA, N. S., 1982, *Int. J. Quantum Chem.*, **21,** 259; BRÄNDAS, E. J., BENDAZZOLI, G. L., and ORTOLANI, F., 1983, *Int. J. Quantum Chem. Symp.*, **17,** 321.
[236] PULAY, P., 1983, *Int. J. Quantum Chem. Symp.*, **17,** 257.
[237] TANAKA, K., and TERASHIMA, H., 1984, *Chem. Phys. Lett.*, **106,** 558; TANAKA, K., SAKAI, T., and TERASHIMA, H., 1989, *Theor. Chim. Acta*, **76,** 213; SAKAI, T., and TANAKA, K., 1993, *Theor. Chim. Acta*, **85,** 451.
[238] CAVE, R. J., and DAVIDSON, E. R., 1988, *J. chem. Phys.*, **88,** 5770; **89,** 6798; MURRAY, C., RACINE, S. C., and DAVIDSON, E. R., 1992, *Int. J. Quantum Chem.*, **42,** 273.
[239] HOFFMANN, M. R., and SIMONS, J., 1989, *J. chem. Phys.*, **90,** 3671.
[240] HEULLY, J.-L., and MALRIEU, J.-P., 1992, *Chem. Phys. Lett.*, **199,** 545; DAUDEY, J.-P., HEULLY, J.-L., and MALRIEU, J.-P., 1993, *J. Chem. Phys.*, **99,** 1240; MALRIEU, J.-P., DAUDEY, J.-P., and CABALLOL, R., 1994, *J. Chem. Phys.*, **101,** 8908.
[241] FINK, R., and STAEMMLER, V., 1993, *Theor. Chim. Acta*, **87,** 129.
[242] GERSHGORN, Z., and SHAVITT, I., 1968, *Int. J. Quantum Chem.*, **2,** 751.
[243] SHAVITT, I., 1992, *Chem. Phys. Lett.*, **192,** 135.

MOLECULAR PHYSICS, 1998, VOL. 94, NO. 1, 19–28

Electron correlation and quantum electrodynamics†

By INGVAR LINDGREN
Department of Physics, Chalmers University of Technology/Göteborg University,
S-412 96 Göteborg, Sweden

A review is given of the coupled-cluster approach for a multi-reference model space. Various schemes of normalization are discussed, particularly the hermitian formulation. Relativistic many-body schemes are analysed, starting from the no-virtual-pair approximation (NVPA). Effects beyond NVPA are discussed in the framework of QED, and in particular the QED effects on the electron correlation for He-like ions are analysed.

1. Introduction

Non-relativistic many-body procedures have been extensively used over the past 40 years and can now be regarded as well developed. The important *linked-diagram expansion* (LDE) was discovered by Brueckner and Goldstone [1] in the middle of the 1950s. The advent of LDE represented a great progress in the many-body procedure and is normally regarded as the starting point of *many-body perturbation theory* (MBPT). In the 1960s the procedure was further developed for open-shell systems by Brandow, Sandars, Kelly and others and later also for quasi-degenerate or general multi-reference model space [2]. In an order-by-order expansion, like LDE, however, the number of terms increases drastically with the order, and this has the consequence that the method becomes essentially intractable for open-shell systems beyond the third-order energy.

Instead of an order-by-order expansion it is often more efficient to treat certain effects—like one- and two-particle effects—to all orders in a recursive manner. A particularly useful version of such a procedure is the *coupled-cluster approach* (CCA), where the wavefunction (or wave operator) is expressed in exponential form. This approach was developed in nuclear physics by Coester and Kümmel [3] and introduced into quantum chemistry by Cizek in the 1960s [4]. It was first developed and applied to closed-shell systems [5] and in the 1970s extended to open-shell systems and general multi-reference model space [6].

The multi-reference CCA (MR-CCA) is a very clean procedure with many nice features. It satisfies the important *size-extensivity* criterion for the energy and also the *separability* or *size consistency* condition for the wavefunction [5 (b), 5 (c), 7]. In the MR-CCA it is—at least in principle—possible to include important mixing states into the model space, which will improve the accuracy and speed up the convergence of the iterations. However, the original formulation was limited to a *complete model space*. In practical applications such a space can be quite large, with the consequence that *intruder states* [8], destroying the convergence of the procedure, are very likely to appear.

A well-known classical example of the intruder problem is the Be atom. With the orbitals generated in the HF potential of the $1s^2$ the core, the configurations $1s^22s^2$ and $1s^22p^2$ are closely degenerate and strongly mixed. An extended model space with the two configurations contains two ^1S states, of which the upper one is very highly excited, in fact above the 2s ionization limit. This means that there is an infinite number of other ^1S states (from the $1s^22sns$ configurations) which will fall between the states originating from the model space. It was earlier observed that the standard CC procedure does not converge in this situation [9]. Later, it has been possible to circumvent the intruder problem in this special case by means of special tricks [10].

Normally, one is interested in only a limited number of states originating from a complete model space—usually some low-lying states—and it would then be desirable to work with a more limited model space in order to reduce the intruder problem. However, the CC procedures were until recently developed only for complete model spaces. For an incomplete model space the standard MR-CCA procedure with *intermediate normalization* (IN) generally leads to *disconnected* cluster operators and loss of size extensivity. It was first pointed out by Mukherjee and co-workers [11] that connectivity could be restored for very general incomplete model spaces by abandoning the IN. This opened up quite new possibilities and turned out to be one effective way of handling the intruder problem in MR-CCA.

Another way of handling the intruder problem is the *intermediate hamiltonian approach*, developed by

† Invited talk at the workshop '50 Years of the Correlation Problem', Cedar Key, Florida, 15–19 June 1997.

0026–8976/98 $12·00

Malrieu, Durand and others [12]. Here, only a few of the eigenstates of the effective hamiltonian correspond to real states. This may give sufficient freedom in constructing that hamiltonian so that the intruder problem could be avoided.

It is also possible to construct a '*state-specific*' procedure, which is size extensive, as recently demonstrated by Mukherjee and co-workers [13].

Relativistic many-body procedures were not developed until the 1980s. Relativistic SCF procedures (MCDF) were used already in the 1970s but based on a non-rigorous hamiltonian [14].

Breit had derived already around 1930 the relativistic corrections to the Coulomb interaction [15]. The original Breit interaction, however, could be used only in first order and was not suitable for many-body procedures. It was demonstrated by Brown and Ravenhall [16] in the early 1950s that a relativistic hamiltonian based upon the Coulomb interaction (with or without the Breit interaction) has eigenvalues that are not bound from below, due to the presence of the negative energy states. The problem with the Breit interaction was further emphasized by Bethe and Salpeter [17], and this did for a long time hamper the use of the Breit interaction in many-body applications.

It was demonstrated by Sucher in 1980 [18] that the problem with negative energy states could be avoided by the use of *projection operators*. This leads to the so-called *no-virtual-pair approximation* (NVPA). In this scheme it is perfectly legitimate to iterate also the Breit interaction to self-consistency. There are other effects ('*QED effects*') that are of the same order as the second-order Breit interaction, but the important point here is that the Breit interaction could be treated on the same footing as the Coulomb interaction without any fear of 'falling into the Dirac sea'.

Relativistic effects are intimately connected to *quantum electrodynamics* (QED), and an analysis of the relativistic many-body problem must by necessity start from QED. It turns out that such an analysis yields an interelectronic interaction that is *gauge dependent*. SCF calculations performed with the interactions derived using, for instance, the Coulomb and the Feynman gauges turned out to yield significantly different results, and this caused confusion for some time [19].

In order to resolve the problem with the interelectronic interaction, it is necessary to consider also the *two-photon exchange* between the electrons (see figure 4, section 3.2). It was then demonstrated that the gauge dependence could be explained to first order by the effects left out of the two-photon exchange [20]. For instance, the crossed-photon diagram, entirely left out in any many-body procedure developed so far, is an order of magnitude larger in the Feynman gauge than in the Coulomb gauge. In fact, the Coulomb gauge turns out to be the optimum gauge for many-body applications, and this gauge leads (in the no-retardation limit) exactly to the original Breit interaction.

The NVPA, based upon the Coulomb gauge with the Coulomb and the Breit interactions, is a very efficient computational procedure for atomic and molecular systems that are not highly charged. It has in recent years been applied by several groups, particularly to atomic problems [21].

The effects left out in NVPA are referred to as *QED effects*. These are of two kinds: (a) *non-radiative effects* (sometimes referred to as the Araki Sucher effect [22]) and (b) *radiative effects*. The former are caused by the negative energy states and the retardation effects left out in NVPA. The radiative effects are of Lamb-shift type and involve self energy and vacuum polarization.

For highly charged systems the single-electron Lamb shift can be comparable to the first-order Breit interaction. Since it is a single-particle effect, however, it has no effect upon the electron correlation. The non-radiative effects and the higher-order Lamb shift, on the other hand, do have such effects. This has recently been studied for He-like ions [23] and compared with experimental results [24]. The experimental accuracy is not yet sufficient for detecting the effects, but with only a moderate improvement of the accuracy a significant test will be possible. This will constitute an important test of QED (beyond first-order Lamb shift) at very strong fields.

In the present paper we shall in section 2 review some recent developments in the non-relativistic CC theory, particularly regarding incomplete model space and the hermitian formulation. Some new results will be reported. In section 3 we shall first analyse the gauge dependence of the electron–electron interaction in the NVPA, and finally the QED effects upon the electron–electron interaction will be discussed and some new results for He-like ions be reported.

2. Non-relativistic many-body theory

2.1. *Multi-reference model space*

As a background for the following treatment and for defining our notations, we will first briefly review the well-known non-relativistic many-body theory for a general multi-reference model space. We shall apply the Bloch formalism, which yields a transparent relation between different formulations [2(i)].

We start from the Schrödinger equation for a number of states (target states),

$$H\Psi^{(a)} = E^{(a)}\Psi^{(a)} \quad (a = 1, 2, \ldots, d), \tag{1}$$

where H is the hamiltonian and Ψ is the wavefunction of the system. The corresponding *zeroth-order wavefunctions* (ZOWF), $\Psi_0^{(a)}$, are confined to a *model space*, P, which might contain several zeroth-order energies (multi-reference model space). If the model space contains all possible occupancies of the valence orbitals, it is said to be *complete*, but the treatment here holds for a general, *incomplete* model space. (For a more extensive discussion about the incomplete-model-space problem, see e.g. the review by Lindgren and Mukherjee [11 (d)]).

We assume that a *wave operator* (W) transforms all ZOWF into the corresponding exact wavefunctions,

$$\Psi^{(a)} = \Omega\Psi_0^{(a)} \quad (a = 1, 2, \ldots, d). \tag{2}$$

The ZOWF are eigenfunctions of an *effective* or *model hamiltonian*, H_{eff}, with eigenvalues equal to the exact energies

$$H_{\text{eff}}\Psi_0^{(a)} = E^{(a)}\Psi_0^{(a)} \quad (a = 1, 2, \ldots, d). \tag{3}$$

The explicit form of this operator depends on the normalization scheme employed (see below).

For the following we shall partition the hamiltonian into an unperturbed hamiltonian, H_0, and a perturbation, V,

$$H = H_0 + V, \tag{4}$$

and we define a corresponding *effective interaction*, V_{eff}, by

$$V_{\text{eff}} = H_{\text{eff}} - PH_0P. \tag{5}$$

The wave operator satisfies the generalized Bloch equation [2 (g)–2 (i)]

$$[\Omega, H_0]P = (V\Omega - \Omega V_{\text{eff}})P, \tag{6}$$

where P is the projection operator of the model space. In *intermediate normalization* (IN) we have

$$\Psi_0^{(a)} = P\Psi^{(a)}; \quad P\Omega P = P;$$
$$H_{\text{eff}} = PH\Omega P \quad \text{and} \quad V_{\text{eff}} = PV\Omega P. \tag{7}$$

Other normalization schemes are discussed below.

2.2. *The linked-diagram expansion*

In the standard perturbation theory the wave operator is expanded order by order,

$$\Omega = \Omega^{(0)} + \Omega^{(1)} + \Omega^{(2)} + \cdots \tag{8}$$

[$X^{(0)} = 1$ in IN]. Inserting this expansion into the generalized Bloch equation (6) yields

$$[\Omega^{(n)}, H_0]P = (V\Omega - \Omega V_{\text{eff}})^{(n)}P. \tag{9}$$

This equation leads to the general Rayleigh–Schrödinger (RS) expansion for a multi-reference model space.

In the diagrammatic representation the RS expansion contains '*unlinked*' diagrams, i.e. diagrams with a disconnected, closed part. Such diagrams can be shown to cancel, which leads to the *linked-diagram expansion* (LDE) [1, 2]. The LDE can then be expressed by means of a 'modified Bloch equation'

$$[\Omega, H_0]P = (V\Omega - \Omega V_{\text{eff}})_{\text{linked}}P \tag{10}$$

with the order-by-order expansion

$$[\Omega^{(n)}, H_0]P = (V\Omega - \Omega V_{\text{eff}})^{(n)}_{\text{linked}}P. \tag{11}$$

This form of the perturbation theory is very convenient for generating the LDE. The term ΩV_{eff} represents the *folded* or *backwards* diagrams [2 (a), 2 (f)].

The order-by-order expansion is usually impractical beyond the third-order energy due to the large number of diagrams appearing. For many atomic and molecular systems, which are not highly charged, however, third order is often insufficient, and more efficient methods have been developed.

2.3. *The all-order and coupled-cluster approaches*

Instead of an order-by-order expansion (8) we separate the wave operator into zero-, one-, two-,... body terms, defined by means of second-quantization,

$$\Omega = \Omega_0 + \Omega_1 + \Omega_2 + \cdots = \Omega_0 + \sum_{i,j} x_j^i\{a_i^\dagger a_j\}$$
$$+ \tfrac{1}{2}\sum_{ijkl} x_{kl}^{ij}\{a_i^\dagger a_j^\dagger a_l a_k\} + \cdots. \tag{12}$$

Solving the corresponding partitions of the Bloch equation iteratively to self-consistency,

$$[\Omega_n, H_0]P = (V\Omega - \Omega V_{\text{eff}})_{n,\text{linked}}P, \tag{13}$$

is equivalent to treating the corresponding effects to *all orders of perturbation theory*.

In the LDE all energy or effective-hamiltonian diagrams are *connected*. The wave-operator expansion, on the other hand, also contains disconnected diagrams with open pieces. For a single-reference model space such diagrams factorize into an ordinary product of connected diagrams. This can be generalized to the *exponential Ansatz* or *coupled-cluster approach* (CCA) [3]

$$\Omega = \exp S = 1 + S + \frac{1}{2!}S^2 + \frac{1}{3!}S^3 \ldots, \tag{14}$$

where the '*cluster operator*' S is completely connected [4, 5].

For open-shell systems (multi-reference model space) the disconnected diagrams factorize into a normal-ordered rather than an ordinary product. This leads to

the *normal-ordered exponential Ansatz*, proposed independently by Lindgren [6(c)] and Ey [6(e)]

$$\Omega = \{\exp S\} = 1 + S + \frac{1}{2!}\{S^2\} + \frac{1}{3!}\{S^3\} \ldots . \quad (15)$$

The cluster operator is under general conditions completely connected also in this case and satisfies an equation, which is quite analogous to the wave-operator equations (6) and (10),

$$[S, H_0]P = (V\Omega - \Omega V_{\text{eff}})_{\text{conn}} P. \quad (16)$$

For the following we shall make the assumption of *valence universality*, which implies that the wave operator introduced above transforms the wave functions for all valence sectors, m, i.e. for all systems with one or several valence electrons removed or one or several valence holes filled (or any combination thereof). The Bloch cluster equation (16) is then extended to

$$[S, H_0]P^{(m)} = (V\Omega - \Omega V_{\text{eff}})_{\text{conn}} P^{(m)}, \quad (17)$$

for all sectors m. Here $P^{(m)}$ is the projections operator for the model space of the valence sector m. The assumption of valence universality makes the cluster operator uniquely defined by the Bloch-type equation, and it leads to connectivity, using general normalization schemes [11(c), 11(d)].

Expanding the cluster operator in analogy with the wave-operator (12) and truncating after the two-body term

$$S = S_1 + S_2 \quad (18)$$

leads to the frequently used CCSD approximation. The coupled one- and two-electron equations are in this approximation [2(i), 6(c)]

$$[S_1, H_0]P^{(m)} = \{V + VS + \tfrac{1}{2}VS_1^2 + VS_1S_2 + \cdots - S_1V_{\text{eff},1}\}_{1,\text{conn}} P^{(m)}, \quad (19a)$$

$$[S_2, H_0]P^{(m)} = \{V + VS + \tfrac{1}{2}VS_1^2 + VS_1S_2 + \tfrac{1}{2}VS_2^2 + \cdots - S_2V_{\text{eff},2} - \cdots\}_{2,\text{conn}} P^{(m)}. \quad (19b)$$

2.4. *Incomplete model space*

The most frequently used normalization scheme in many-body theory is the *intermediate normalization* (IN) (7), which works well for a complete model space. Such a model space, however, can in realistic applications be impractically large and may likely lead to *intruder states* [8], which destroy the convergence of the perturbation expansion.

In most cases only a limited number of states within a complete model space are of interest for the problem at hand. One way to avoid—or at least reduce—the intruder problem is then to restrict the model space, and work with an *incomplete model space*. In such a scheme, however, the connectivity or size extensivity cannot be guaranteed, when the IN is employed. It was first demonstrated by Mukherjee and co-workers [11] that connectivity and size extensivity can be generally restored for an incomplete model space by abandoning the IN.

Introducing the inverse of the wave operator, operating to the left on the model space, leads to

$$P^{(m)}\Omega^{-1}\Omega P^{(m)} = P^{(m)} \quad (20)$$

instead of the IN relation (7) $P^{(m)}\Omega P^{(m)} = P^{(m)}$. The effective hamiltonian then becomes

$$H_{\text{eff}}^{(m)} = P^{(m)}\Omega^{-1}H\Omega P^{(m)}. \quad (21)$$

In IN the effective interaction to be used in the CC Bloch equation (16) can be given an explicit form (6). This is not the case with a general normalization scheme. Instead, we have here to consider the Q as well as the P projections as coupled equations and solve them iteratively [11(d)],

$$Q^{(m)}[S, H_0]P^{(m)} = Q^{(m)}(V\Omega - \chi V_{\text{eff}})_{\text{conn}} P^{(m)} \quad (22a)$$

$$P^{(m)}[S, H_0]P^{(m)} = P^{(m)}(V\Omega - \Omega V_{\text{eff}})_{\text{conn}} P^{(m)} \quad (22b)$$

with $\chi = \Omega - 1$. From the P projection we get an implicit expression for the effective interaction

$$V_{\text{eff}}^{(m)} = P^{(m)}(V\Omega - \chi V_{\text{eff}}^{(m)} - [S, H_0])_{\text{conn}} P^{(m)}. \quad (23)$$

There are other ways of handling the intruder problem, such as the *intermediate-hamiltonian* (IH) formalism, introduced by Malrieu, Durand and co-workers [12]. Here, the effective hamiltonian is defined in such a way that it reproduces the exact energies only for a subgroup of the target states. With this technique one can utilize the larger model space with its good representation of the ZOWF and simultaneously to a large extent avoid the intruder problem. Other schemes are focusing on a single state of a multi-reference model space, *state-specific methods*, as recently analysed by Mukherjee and co-workers [13]. We shall not consider these schemes any further here, since they will be the subject of special talks later at this workshop.

2.5. *Hermitian formulation*

The IN (as well as several other schemes) also has the disadvantage that the effective hamiltonian is *non-hermitian*. Several hermitian schemes have been developed and applied in many-body theory [25]. We shall particularly consider the scheme of Jørgensen [26]. Here, the normalization condition is

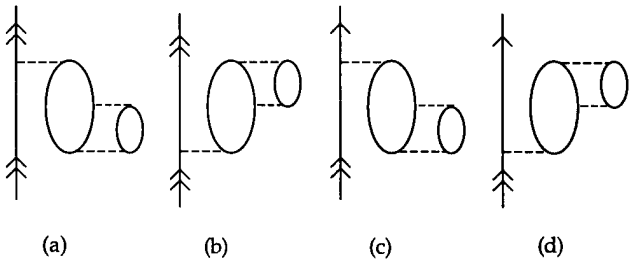

Figure 1. In the standard pair-correlation (CCSD) approach (19), the effective-operator diagram (*a*) would be generated in intermediate normalization but not the corresponding hermitian adjoint diagram (*b*). Similarly, the wave-operator diagram (*c*) would be included but not the analogous diagram (*d*), which involves a triple excitation. In the 'symmetrized' hermitian formulation (29) all these diagrams would be included in the CCSD approach.

$$P^{(m)} = P^{(m)}\Omega^{\dagger}\Omega P^{(m)}. \tag{24}$$

and the effective hamiltonian becomes

$$H_{\text{eff}}^{(m)} = P^{(m)}\Omega^{\dagger}H\Omega P^{(m)}, \tag{25}$$

which is manifestly hermitian. It has been shown by Lindgren [25 (d)] that connectivity is preserved in the CCA also in this scheme.

The non-hermiticity caused by IN leads to an asymmetry in the representation at a particular level, which can be illustrated by the diagrams in figure 1. In the CCSD procedure (19), where only single and double excitations are considered in the cluster operator (with no passive valence orbital), diagram (*a*) will be included but not its hermitian adjoint (*b*). The reason for this is that the corresponding wave-operator diagram (*d*) contains a triple excitation, before it is closed.

Even with the Jørgensen condition (24), however, non-hermiticity can be introduced by *truncations*. The general equation for the effective interaction (23) leads obviously with the Jørgensen condition to hermiticity, when *all* effects are included, but not necessarily so for a truncated expansion [25 (d)].

In order to improve hermiticity for truncated expansions, following the procedure of Lindgren in [25 (d)], we shall develop more symmetric expressions by operating on the CC Bloch equation (17) with $\Omega^{\dagger}$ from the left,

$$\Omega^{\dagger}[S, H_0]P^{(m)} = \Omega^{\dagger}(V\Omega - \Omega V_{\text{eff}}^{(m)})_{\text{conn}}P^{(m)}. \tag{26}$$

Using $\chi = \Omega - 1$, this leads to the P and Q projected equations

$$Q[S, H_0]P^{(m)} = Q(V\Omega - \Omega V_{\text{eff}}^{(m)} + \chi^{\dagger}(V\Omega - \Omega V_{\text{eff}}^{(m)} - [S, H_0]))_{\text{conn}}P^{(m)} \tag{27}$$

$$V_{\text{eff}}^{(m)} = P^{(m)}(V\Omega - \chi V_{\text{eff}}^{(m)} - [S, H_0] + \chi^{\dagger}(V\Omega - \Omega V_{\text{eff}}^{(m)} - [S, H_0]))_{\text{conn}}P^{(m)}. \tag{28}$$

The extra terms, compared to (22) and (23), vanish, when *all* effects are considered, but not necessarily so for truncated expansions. The extra terms may improve the hermiticity for truncated schemes, as will be illustrated below.

In the expressions (27) and (28) large cancellations occur between the terms of the right-hand side, and a more convenient way of expressing the relations is

$$Q[S, H_0]P^{(m)} = Q(V\Omega - \Omega V_{\text{eff}}^{(m)} + \chi^{\dagger}(V\Omega - \Omega V_{\text{eff}}^{(m)})_{+})_{\text{conn}}P^{(m)} \tag{29a}$$

$$V_{\text{eff}}^{(m)} = P^{(m)}(V\Omega - \chi V_{\text{eff}}^{(m)} - [S, H_0] + \chi^{\dagger}(V\Omega - \Omega V_{\text{eff}}^{(m)})_{+})_{\text{conn}}P^{(m)}, \tag{29b}$$

where the + sign represents effects with the intermediate state outside the approximation employed [25 (d)].

The extended expressions (29) reduce the non-hermiticity also with other normalizations, such as the IN. This can be illustrated by means of the diagrams in figure 1. Also with the extension terms the diagrams (*b*) and (*d*) will in the CCSD approximation be included in the effective hamiltonian and the wave operator, respectively. The importance of the hermitian extension terms was demonstrated in an early calculation on the sodium atom by Salomonson and Ynnerman [27].

The inclusion of the hermitian extension terms lead to a systematic extension of the CC equations. This is illustrated with the single-particle equation. In the case of a passive valence orbital it can be shown that the extended equations (29) in the IN lead to the complete *random-phase approximation* (RPA), with forward and backward loops, while the standard procedure only leads to the *Tamm-Dankoff approximation* (TDA) with only forward loops (see figure 2) [25 (d)].

The hermitized CC procedure has recently been applied by Salomonson *et al.* [28] in a calculation of the electron affinity of the Ca and Sr atoms. The binding of the last electron of the negative ion is here very delicate, and it is only recently that this quantity has been reliably measured [29]. The corresponding theoretical evaluation has also for a long time challenged the theo-

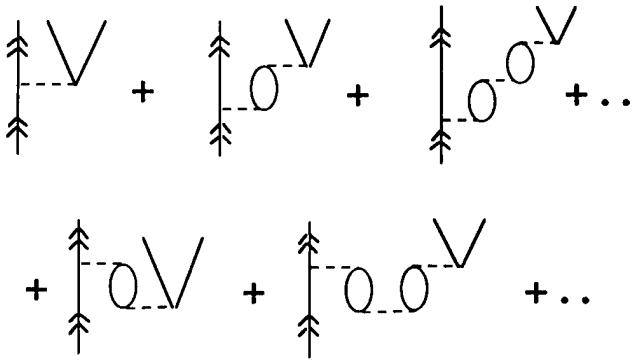

Figure 2. The diagram of the first row with forward loops only are generated in the single-electron approximation (with a passive valence orbital) in the standard CCA. The second-row diagrams with backward loops are generated by the extension terms in (29). This represents the complete *random-phase approximation* (RPA).

reticians [30]. The technique used by Salomonson *et al.* is based on the quasi-particle equation

$$h_{\mathrm{HF}}\varphi(\mathbf{r}) + \int \mathrm{d}^3 r \Sigma^*(\mathbf{r},\mathbf{r}',\varepsilon)\varphi(\mathbf{r}_1) = \varepsilon\varphi(\mathbf{r}) \qquad (30)$$

with an energy-dependent self-energy potential, $\Sigma^*(\mathbf{r},\mathbf{r}',\varepsilon)$, evaluated by means of the CC procedure,

$$\Sigma^*(\mathbf{r},\mathbf{r}',\varepsilon) = \langle \mathbf{r}'|P(V_2S_2 + V_2S_1 + S_1^\dagger V_2 + S_2^\dagger (V_2S_2)_+)_{1\varepsilon,\mathrm{conn}}P|\mathbf{r}\rangle. \qquad (31)$$

The rhs depends on the energy (ε) of the valence orbital, and equations (30) and (31) are iterated until self-consistency is reached. This procedure yields for the first time good agreement with the experimental results for Ca^- as well as Sr^- [28].

3. Relativistic many-body theory and QED

3.1. *No-virtual-pair approximation*

For relativistic many-body calculations a frequently used hamiltonian is the *Dirac–Coulomb hamiltonian*

$$H = \sum h_{\mathrm{D}} + \sum \frac{1}{r_{ij}}, \qquad (32)$$

where the single-electron Schrödinger hamiltonian, h_{S}, of the standard non-relativistic hamiltonian is replaced by the corresponding Dirac hamiltonian

$$h_{\mathrm{D}} = c\boldsymbol{\alpha}\cdot\mathbf{p} + \beta mc^2 - \frac{Z}{r} \qquad (33)$$

(using Hartree atomic units, $e = m = \hbar = 4\pi\varepsilon_0 = 1$). This hamiltonian has been used, for instance, for a long time in multi-configuration Dirac–Fock (MCDF) calculations [14] and to some extent also in relativistic MBPT calculations. The eigenvalues of this hamiltonian, however, are not bound from below, with the consequence that the eigenstates may dissolve into the negative continuum [16].

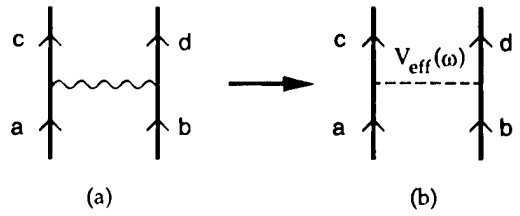

Figure 3. The exchange of a single photon between two electrons (*a*) is compared with an effective-potential interaction (*b*).

A more rigorous basis for relativistic many-body work is the *projected hamiltonian* [18]

$$H = \Lambda_+(\sum h_{\mathrm{D}} + \sum V_{ij})\Lambda_+, \qquad (34)$$

where Λ_+ is the projection operator for positive-energy states, which prevents the negative-energy states from entering into the wave function. This is the *no-(virtual-)pair approximation* (NVPA), in which virtual electron–positron pairs are not allowed in intermediate states.

With the form (34) of the Hamiltonian it is relatively straightforward to set up a relativistic CC procedure, following the non-relativistic procedure outlined in the previous section. This has been done by various groups during the last 5–8 years [21].

The form of the interelectronic potential, V_{ij}, can be derived from QED, but unfortunately it turns out that this depends on the gauge used, and it is not obvious which potential is the best to use in relativistic many-body theory. In the next section we shall analyse this problem by considering the one- and two-photon exchange between the electrons.

3.2. *One- and two-photon exchange*

We consider first the exchange of a single photon between the electrons, represented by the Feynman diagram in figure 3(*a*). We employ *bound-state QED* with the field operators

$$\Psi = \sum a_i\phi_i(x);\ \Psi^\dagger = \sum a_i^\dagger\phi_i^*(x) \qquad (35)$$

and the orbitals generated in the external (nuclear) field, $V(\mathbf{x})$, (Furry picture [31])

$$[c\boldsymbol{\alpha}\cdot\mathbf{p} + \beta mc^2 + V(\mathbf{x})]\phi(\mathbf{x}) = \varepsilon\phi(\mathbf{x}). \qquad (36)$$

The S-matrix for the single-photon exchange (figure 3(*a*)) then becomes

$$\langle cd|S^{(2)}|ab\rangle = -2\pi i\delta(\varepsilon_a + \varepsilon_b - \varepsilon_c - \varepsilon_d) \times \langle cd|a_1^\mu \alpha_2^\nu e^2 D_{F\nu\mu}(\mathbf{x}_2 - \mathbf{x}_1, \omega)|ab\rangle, \quad (37)$$

where $D_{F\nu\mu}(x_2 - x_1, \omega)$ is the Feynman photon propagator and $a^\mu = (1, -\mathbf{a})$ the Dirac operators in covariant form. The expression (37) can be compared with the corresponding expression for single potential scattering (figure 3 (*b*))

$$\langle cd|S^{(1)}|ab\rangle = -2\pi i\delta(\varepsilon_a + \varepsilon_b - \varepsilon_c - \varepsilon_d)\langle cd|V_{\text{eff}}(\omega)|ab\rangle, \quad (38)$$

which leads to the '*effective*' interaction potential

$$V_{\text{eff}}(\omega) = \alpha_1^\mu \alpha_2^\nu e^2 D_{F\nu\mu}(\mathbf{x}_2 - \mathbf{x}_1, \omega). \quad (39)$$

This potential is *energy dependent*, through the energy parameter ω, representing the energy transfer of the photon, and—as mentioned earlier—it is also *gauge dependent*.

We consider particularly two gauges, the *Feynman* and the *Coulomb* gauges. In these gauges the unretarded or frequency-independent part of the interaction becomes

$$V_{\text{eff}}^F(\omega = 0) = \frac{1}{r_{12}}(1 - \alpha_1 \cdot \alpha_2) \quad (40\,a)$$

$$V_{\text{eff}}^C(\omega = 0) = \frac{1}{r_{12}}\left(1 - \tfrac{1}{2}\alpha_1 \cdot \alpha_2 - \frac{(\alpha_1 \cdot \mathbf{r}_{12})(\alpha_2 \cdot \mathbf{r}_{12})}{2r_{12}^2}\right), \quad (40\,b)$$

known as the *Coulomb–Gaunt* and *Coulomb–Breit* interactions, respectively.

In principle, the results of QED are gauge independent in each order. Nevertheless, it has been found that the interactions derived with the two gauges (even with retardation included) lead to significantly different results, when used in SCF or MBPT calculations [19]. The single-photon exchange in QED, however, involves *energy conservation* (37), and the potential derived is therefore strictly valid only for evaluating the *first-order* energy contribution (in which case the two gauges yield identical results). When the potential is used iteratively in many-body procedures, on the other hand, gauge dependence appears. In order to analyse the gauge dependence, it is then necessary to consider the *two-photon exchange* (figure 4).

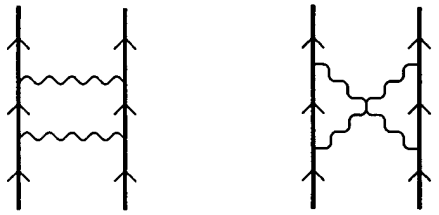

Figure 4. Two two-photon exchange between the electrons is represented by two Feynman diagrams, (*a*) the 'ladder' and (*b*) the 'crossed-photon' diagram.

In a many-body procedure, where a single-photon potential of the type (40) is used iteratively, the crossed-photon diagram is left out completely and the ladder diagram is only partly included. It can be shown that the parts left out are much more important in the Feynman gauge than in the Coulomb gauge. Therefore, the potential derived in the latter gauge yields more accurate results in a many-body procedure. In fact, the Coulomb-gauge potential leads to errors of the order of α^3 hartrees, while most other gauges would cause errors of the order of α^2 hartrees. This leads to the recommended *no-virtual-pair approximation* (NVPA)

$$H = \Lambda_+\left(\sum h_{\text{D}} + \sum\left(\frac{1}{r_{ij}} + B_{ij}\right)\right)\Lambda_+, \quad (41\,a)$$

where

$$B_{12} = -\frac{1}{2r_{12}}\left(\alpha_1 \cdot \alpha_2 + \frac{(\alpha_1 \cdot \mathbf{r}_{12})(\alpha_2 \cdot \mathbf{r}_{12})}{r_{12}^2}\right) \quad (41\,b)$$

is the Breit interaction (40 *b*), representing the first-order magnetic interaction and retardation of the (instantaneous) Coulomb interaction.

Table 1. Two-electron contribution to the ground-state energy of He-like ions. Comparison between theory and experiment (in eV).

Nuclear charge	MBPT			Non-radiative	Lamb shift	Total theory	Experimental
	First order	2nd	3rd				Marrs *et al.*
32	567.1	−5.22	0.02	0.03	−0.42	562.02 (10)	562.6 ± 1.6
54	1036.56	−7.04	0.03	0.16	−1.56	1028.15 (10)	1027.2 ± 3.5
66	1347.45 (1)	−8.59	0.03	0.36	−2.66	1336.59 (10)	1341.5 ± 4.3
74	1586.93 (2)	−9.91	0.04	0.55	−3.68	1573.93 (10)	1568.9 ± 15
83	1897.56 (4)	−11.77	0.04	0.86	−5.16	1881.5 (2)	1875 ± 14
92	2265.87 (10)	−14.16	0.05	1.28	−7.12	2245.9 (2)	

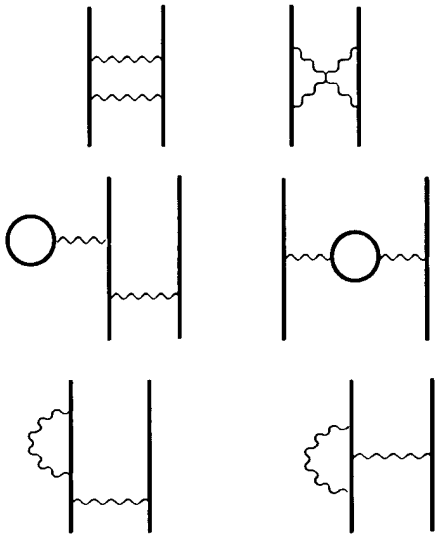

Figure 5. Feynman diagrams of the second-order two-electron contribution to the binding energy of He-like systems. The first line represents the many-body part and the non-radiative QED part, and the remaining lines the radiative contribution (screening of the Lamb shift).

The NVPA in the Coulomb gauge is nowadays the standard approximation for relativistic many-body calculations. It forms the basis for the modern versions of the MCDF procedures [19(a), 19(b), 32] and has been employed in MBPT and coupled-cluster calculations [21].

3.3. *QED effects*

The effects left out in the NVPA are defined as QED effects. They are of two types:

(a) *non-radiative effects*, i.e. effects of retardation and of negative-energy states,
(b) *radiative effects*, i.e. self-energy and vacuum-polarization or Lamb-shift effects.

In lowest order the QED effect on the electron–electron interaction is represented by the diagrams shown in figure 5. The non-radiative part, represented by the diagrams of the first row, have been evaluated for the ground state of He-like ions by Blundell *et al.* [23(a)] and by Lindgren *et al.* [23(b)]. The remaining diagrams represent the radiative part, involving vacuum polarization (second row) and self-energy (third row). This part has been estimated using various approximate schemes, and a full QED calculation has recently been performed by Persson *et al.* [23(c)]. The results are shown in table 1 together with the non-QED parts and compared with the experimental results from the Livermore–GSI collaboration [24].

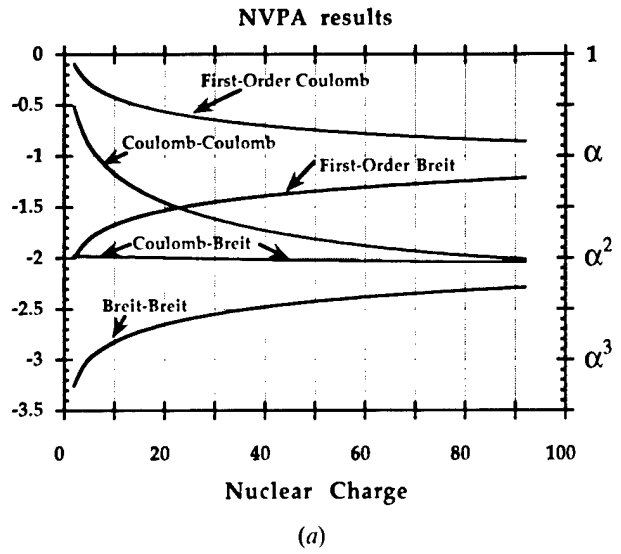

(*a*)

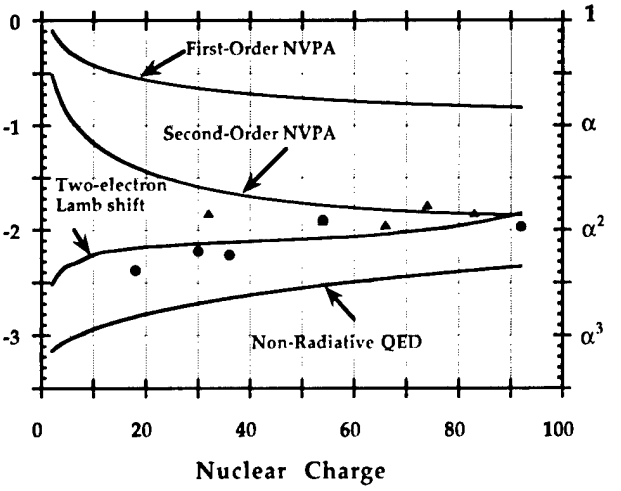

(*b*)

Figure 6. (*a*) The relative size of the first- and second-order contributions to the two-electron part of the binding energy for He-like ions in the no-virtual-pair approximation (NVPA). The contributions are related to the single-electron binding energy. The scale is logarithmic, one unit corresponding to a factor of $\alpha \approx 1/137$. (*b*) Same as figure 6(*a*), where the first- and second-order NVPA contributions are compared with the two-electron Lamb shift and non-radiative QED contributions. Note that for large Z the relative first-order contribution is of order α and all second-order effects of order α^2. Note that the QED effects are of the same order as the second-order NVPA contributions for highly charged ions. The dots represent the uncertainty in the experimental results, X-ray spectroscopy (circular) and electron binding energy (triangular) [33].

In figure 6(*a*) we have illustrated the first- and second-order non-QED or NVPA (41) contributions to the two-body part of the binding energy for the ground state of

He-like ions. The result is normalized to the single-electron binding energy, and the scale is logarithmic. Obviously, the Coulomb interaction dominates for light elements, but the Breit interaction becomes comparable to the second-order Coulomb interaction already around $Z=20$. The second-order relativistic effects, Coulomb–Breit and Breit–Breit contributions, are quite small for light elements but are of the same order as the second-order Coulomb interaction for heavy ions.

In figure 6(*b*) the corresponding NVPA and QED results are displayed. The second-order Lamb shift is for medium and highly charged ions comparable to the Coulomb–Breit contribution (see figure 6(*a*)), while the non-radiative contribution is considerably smaller and comparable with the Breit–Breit interaction. Note that all first-order contributions, including the first-order Lamb shift, for very highly charged ions are of the order of alpha times the one-electron binding energy, while all second-order effects are roughly another factor of alpha smaller.

In figure 6(*b*) also the uncertainty of the experimental results is indicated. This can be seen to be comparable to the two-electron Lamb shift, which means that this effect is now right on the verge of being detectable.

The experimental uncertainties deduced from X-ray measurements (fine-structure separations) are generally smaller than those deduced from measurements of the binding-energy. In order to compare fine structure results with theory, however, it is necessary to make the evaluations also for excited states. Such calculations have not yet been performed but are now in progress at our laboratory. One problem here is that the two p states, $p_{1/2}$ and $p_{3/2}$, are strongly mixed, and it will be necessary to work with an *extended model space* also for the QED calculations. However, the standard S-matrix procedure is based upon energy conservation (37) and can therefore be employed only for evaluating *diagonal* elements of the effective hamiltonian. Therefore, in order to be able to evaluate also non-diagonal elements, required for an extended model space, some modification of the formalism is required.

The author wishes to express his thanks to his co-workers, Ann-Marie Pendrill, Sten Salomonson, Hans Persson and Per Sunnergren, as well as to the Swedish Natural Science Research Council, The Knut and Alice Wallenberg and the Nobel Foundations for financial support.

References

[1] (a) BRUECKNER, K. A., 1955, *Phys. Rev.*, **100,** 36; (b) GOLDSTONE, J., 1957, *Proc. Roy. Soc.* (London), **A239,** 267.

[2] (a) BRANDOW, B. H., 1967, *Rev. Mod. Phys.*, **39,** 771; (b) BLOCH, C., 1958, *Nucl. Phys.*, **6,** 329; (c) BLOCH, C., 1958, *Nucl. Phys.*, **7,** 451; (d) KELLY, H. P., 1963, *Phys. Rev.*, **133,** 684; (e) KELLY, H. P., 1969, *Adv. Chem. Phys.*, **14,** 129; (f) SANDARS, P. G. H., 1969, *Adv. Chem. Phys.*, **14,** 365; (g) LINDGREN, I., 1974, *J. Phys.*, **B7,** 2441; (h) KVASNICKA, V., 1974, *Czech. J. Phys.*, **B24,** 605; 1977, *Adv. Chem.*, **36,** 345; (i) LINDGREN, I., and MORRISON, J., 1986, *Atomic Many-Body Theory*, 2nd edn (Berlin: Springer-Verlag).

[3] (a) HUBBARD, J., 1957, *Proc. Roy. Soc.* (London), **A240,** 539; (b) COESTER, F., 1958, *Nucl. Phys.*, **1,** 421; (c) COESTER, F., and KÜMMEL, H., 1960, *Nucl. Phys.*, **17,** 477.

[4] (a) CIZEK, J., 1966, *J. chem. Phys.*, **45,** 4256; CIZEK, J., 1969, *Adv. Chem. Phys.*, **14,** 35.

[5] (a) PALDUS, J., and CIZEK, J., 1975, *Adv. quant. Chem.*, **9,** 105; (b) BARTLETT, R. J., and PURVIS, G. D., 1978, *Int. J. quant. Chem.*, **14,** 561; (c) BARTLETT, R., 1981, *Ann. Rev. Phys. Chem.*, **32,** 359.

[6] (a) MUKHERJEE, D., MOITRA, R. K., and MUKHOPADHYAY, A., 1975, *Molec. Phys.*, **30,** 1861; (b) MUKHERJEE, D., MOITRA, R. K., and MUKHOPADHYAY, A., 1977, *Molec. Phys.*, **33,** 955; (c) LINDGREN, I., 1978, *Int. J. quant. Chem.*, **S12,** 33; (d) OFFERMANN, R., EY, W., and KÜMMEL, H., 1976, *Nucl. Phys.*, **A273,** 349; (e) EY, W., 1978, *Nucl. Phys.*, **A296,** 189; (f) JEZIORSKI, B., and MONKHORST, H. J., 1981, *Phys. Rev.*, **A24,** 1668; (g) HAQUE, A., and KALDOR, U., 1986, *Chem. Phys. Lett.*, **117,** 347.

[7] (a) PRIMAS, H., 1965, *Modern Quantum Chemistry*, edited by O. Sinanoglu (Academic Press), p. 45; (b) POPLE, J. A., BINKLEY, J. S., and SEEGER, R., 1976, *Int. J. quant. Chem.* **S10**, 1; (c) POPLE, J. A., BINKLEY, J. S., and SEEGER, R., 1976, *Int. J. quant. Chem.*, **14,** 545.

[8] (a) SCHUCAN, T. H., and WEIDENMÜLLER, H. A., 1972, *Ann. Phys.* (New York), **73,** 108; (b) SCHUCAN, T. H., AND WEIDENMÜLLER, H. A., 1973, *Ann. Phys.* (New York), **76,** 483; (c) HOSE, A., and KALDOR, U., 1979, *J. Phys.*, **B12,** 3827.

[9] (a) SALOMONSON, S., LINDGREN, I., and MÅRTENSSON, A.-M., 1980, *Phys. Scr.*, **21,** 351; (b) KALDOR, U., 1988, *Phys. Rev.*, **A38,** 6013.

[10] (a) JANKOWSKI, K., and MALINOWSKI, P., 1994, *J. Phys.*, **B27,** 829, 1287; (b) LINDROTH, E., and MÅRTENSSON-PENDRILL, A.-M., 1996, *Phys. Rev.*, **A53,** 3151.

[11] (a) MUKHERJEE, D., 1986, *Chem. Phys. Lett.*, **125,** 207; (b) MUKHERJEE, D., 1986, *Int. J. quant. Chem.*, **S20,** 409; (c) MUKHERJEE, D., and PAL, S., 1989, *Adv. quant. Chem.*, **20,** 291; (d) LINDGREN, I., and MUKHERJEE, D., 1987, *Phys. Rep.*, **151,** 93.

[12] (a) MALRIEU, J. P., DURAND, PH., and DAUDEY, J. P., 1985, *J. Phys.*, **A18,** 809; (b) DURAND, PH., and MALRIEU, J. P., 1987, *Adv. Chem. Phys.*, **67,** 321; (c) HEULLY, J.-L., and DAUDEY, J. P., 1988, *J. Chem. Phys.*, **88,** 1046; (d) EVANGELISTI, S., DURAND, PH., and HEULLY, J. L., 1991, *Phys. Rev.*, **A43,** 1258; (e) EVANGELISTI, S., DURAND. PH., and HEULLY, J. L., 1996, *Phys. Rev.*, **105,** 6887; (f) MALRIEU, J. P., DAUDEY, J. P., and CABALLOL, R., 1994, *J. chem. Phys.*, **101,** 8908; (g) MUKHOPADHYAY, B., DATTA, B., and MUKHERJEE, D., 1992, *Chem. Phys. Lett.*, **197,** 236.

[13] (a) DATTA, B., and MUKHERJEE, D., 1995, *Chem. Phys. Lett.*, **235,** 31; (b) MAHAPATRA, U.S., DATTA, B., BANDYOPADHYAY, B., and MUKHERJEE, D., 1997, *Adv.*

quant. Chem., **29** (in the press); (c) MAHAPATRA, U.S., DATTA, B., and MUKHERJEE, D., 1997, *Modern Ideas in Coupled-Cluster Methods*, edited by R. J. Bartlett (Singapore: World Scientific).

[14] (a) DESCLAUX, J. P., 1975, *Comput. Phys. Commun.*, **9**, 31; (b) GRANT, I. P., *et al.*, 1980, *Comput. Phys. Commun.*, **21**, 207.

[15] BREIT, G., 1928, *Nature*, **122**, 649.

[16] BROWN, G. E., and RAVENHALL, D. G., 1951, *Proc. Roy. Soc.* (London), **A208**, 552.

[17] BETHE, H. A., and SALPETER, E. E., 1957, *Quantum Mechanics of One- and Two-Electron Atoms* (Berlin: Springer-Verlag).

[18] SUCHER, J., 1980, *Phys. Rev.*, **A22**, 348.

[19] (a) GORCEIX, O., and INDELICATO, P., 1988, *Phys. Rev.*, **A37**, 1087; (b) GORCEIX, O., INDELICATO, P., and DESCLAUX, J. P., 1987, *J. Phys.*, **B20**, 639; (c) LINDROTH, E., and MÅRTENSSON-PENDRILL, A.-M., 1989, *Phys. Rev.*, **A39**, 3794.

[20] (a) SUCHER, J., 1988, *J. Phys.*, **B21**, L585; (b) LINDGREN, I., 1990, *J. Phys.*, **B23**, 1085; (c) CHIA-CHU CHEN, 1993, *J. Phys.*, **B26**, 599.

[21] (a) LINDROTH, E., 1988, *Phys. Rev.*, **A37**, 316; (b) JOHNSON, W. R., BLUNDELL, S. A., and SAPIRSTEIN, J., 1988, *Phys. Rev.*, **A37**, 307, 2764; (c) JOHNSON, W. R., BLUNDELL, S. A., and SAPIRSTEIN, J., 1990, *Phys. Rev.*, **A42**, 1087; (d) SALOMONSON, S., and ÖSTER, P., 1989, *Phys. Rev.*, **A40**, 5559; (e) ILYABAEV, E., and KALDOR, U., 1992, *J. chem. Phys.*, **97**, 8455; (f) ILYABAEV, E., and KALDOR, U., 1992, *Chem. Phys. Lett.*, **194**, 95; (g) ILYABAEV, E., and KALDOR, U., 1993, *Phys. Rev.*, **A47**, 137; (h) ELIAV, E., KALDOR, U., and ISHAKAWA, Y., *Phys. Rev.*, **A47**, 1724; (i) ELIAV, E., KALDOR, U., and ISHAKAWA, Y., 1996, *Phys. Rev. Lett.*, **77**, 5350; (j) VISSCHER, L. *et al.*, 1994, *Comp. Phys. Comm.*, 81, 120.

[22] (a) ARAKI, H., 1957, *Prog. Theor. Phys.*, **17**, 619; (b) SUCHER, J., 1957, *Phys. Rev.*, **109**, 1010; (c) SUCHER, J., PhD thesis, Columbia University (unpublished).

[23] (a) BLUNDELL, S., MOHR, P. J., JOHNSON, W. R., and SAPIRSTEIN, J., 1993, *Phys. Rev.*, **A48**, 2615; (b) LINDGREN, I., PERSSON, H., SALOMONSON, S., and LABZOWSKY, L., 1995, *Phys. Rev.*, **A51**, 1167; (c) PERSSON, H., SALOMONSON, S., SUNNERGREN, P,. and LINDGREN, I., 1996, *Phys. Rev. Lett.*, **76**, 204.

[24] MARRS, R. E., ELLIOTT, S. R., and STÖHLKER, TH., 1995, *Phys. Rev.*, **A52**, 3577.

[25] (a) DES CLOIZEAUZ, J., 1960, *Nucl. Phys.*, **20**, 321; (b) KVASNICKA, V., 1981, *Chem. Phys. Lett.*, **79**, 89; (c) PAL, S., PRASAD, M. D., and MUKHERJEE, D., 1984, *Theor. Chim. Acta*, **66**, 311; (d) LINDGREN, I., 1991, *J. Phys.*, **B24**, 1143; (e) BARTLETT, R. J., KUCHARSKI, A., and NOGA, J., 1989, *Chem. Phys. Lett.*, **155**, 133

[26] JORGENSEN, F., 1975, *Molec. Phys.*, **29**, 1137

[27] SALOMONSON, S., and YNNERMAN, A., 1991, *Phys. Rev.*, **A43**, 88.

[28] SALOMONSON, S., WARSTON, H., and LINDGREN, I., 1996, *Phys. Rev. Lett.*, **76**, 3092.

[29] (a) WALTER, C., and PETERSON, J., 1992, *Phys. Rev. Lett.*, **68**, 2281 (Ca); (b) NADEAU, M.-J.,*et al.*, 1992, *Phys. Rev.*, **A46**, R3588 (Ca); (c) PETRUNIN, V., *et al.*, 1996, *Phys. Rev. Lett.*, **76**, 744 (Ca); (d) BERKOVITS, D., *et al.*, 1995, *Phys. Rev. Lett.*, **75**, 414 (Sr).

[30] (a) FROESE-FISCHER, C., 1989, *Phys. Rev.*, **A39**, 963; (b) JOHNSON, W., SAPIRSTEIN, J., and BLUNDELL, S., 1989, *J. Phys.*, **B22**, 2341; (c) DUBZA, V., *et al.*, 1991, *Phys. Rev.*, **A44**, 2823.

[31] See, for instance, MANDL, F., and SHAW, G., 1984, *Quantum Field Theory* (New York: John Wiley and Sons).

[32] (a) QUINEY, H. M., GRANT, I. P., and WILSON, S., 1987, *J. Phys.*, **B20**, 1413; (b) QUINEY, H. M., GRANT, I. P., and WILSON, S., 1990, *J. Phys.*, **B23**, L271.

[33] PLANTE, D. R., JOHNSON, W. R., and SAPIRSTEIN, J., 1994, *Phys. Rev.*, **A49**, 3519.

MOLECULAR PHYSICS, 1998, VOL. 94, NO. 1, 29–39

Generalized maximum-overlap orbitals for multi-reference-state theories

By KAROL JANKOWSKI, KRZYSZTOF RUBINIEC and PIOTR STERNA
Institute of Physics, Nicholas Copernicus University, 87-100 Toruń, Poland

An attempt to generalize the maximum overlap or Brueckner orbitals, which are defined in the single-reference-state formulations of the many-electron theory, to the case of multi-reference-state approaches is made. The generalization is obtained by considering the orbitals that yield the maximum proximity of the subspace $\mathcal{M}$ spanned by the set of d exact wavefunctions considered in the MR method with the model space $\mathcal{M}_0$ spanned by d determinants providing approximations to these wavefunctions. The new orbitals are referred to as maximum-proximity orbitals (MPOs). The general problem of defining the distance between pairs of finite dimensional subspaces of the Hilbert space is shortly reviewed. To better understand the impact of the distance of the $\mathcal{M}_0$ and $\mathcal{M}$ spaces on MR-type approaches, model studies have been undertaken for the MBS H4 system, which offers the possibility of a simple parametrization of arbitrary symmetry-adapted orbital sets. Proximity indices of 13 standard quantum-chemical orbital sets are compared for various degrees of quasi-degeneracy of the states considered. It is demonstrated that the MPOs minimize the impact of singly-excited determinants on the structure of the wavefunctions. The MPOs are applied in calculations based on MR-CC approaches of valence-universal and state-universal types. Results superior to those for HF orbitals are obtained. The improvement is especially evident outside the strong quasi-degeneracy region.

1. Introduction

One-particle wavefunctions (orbitals) belong to the fundamental concepts of contemporary quantum theory of many-electron systems on two counts: First, orbitals are the building blocks of individual independent-particle models (IPM) which represent the basic approaches of the theory. The form of the one-particle functions reflects the physical or mathematical requirements imposed on the model. Second, the choice of the orbitals determines important details of the formal structure as well as the computational characteristics of most of the many-electron theories going beyond the independent-particle formulations, which in physical terms consists in a more complete description of the correlation of the relative movement of electrons.

For almost six decades the most important role has been played by the Hartree–Fock (HF) orbitals [1] which are defined by equations obtained when using the best-energy criterion for the wavefunction of the IPM. The corresponding HF picture is broadly considered to represent the most comprehensive independent-particle model. Various HF results are commonly used as reference points in studies of electron-correlation effects (see, e.g. [2, 3]). HF orbitals are also routinely employed for the formulation of the vast majority of methods for the description of these effects (for details, see [4, 5]).

Among the non-HF IPM approaches, considerable attention has been attracted by the model defined by the requirement that the determinantal wavefunction Φ corresponding to the exact wavefunction Ψ is such that

$$\|\Psi - \Phi\| = \min \quad \text{for } \|\Psi\| = \|\Phi\| = 1 \tag{1}$$

or, equivalently, that the overlap of these functions is maximum, i.e.

$$\langle \Phi | \Psi \rangle = \max. \tag{2}$$

The first explicit use of the condition (1) for the definition of the one-particle wavefunctions can be found in the work of Brenig [6] who was concerned with the problem of generalizing to finite nuclear systems Brueckner's self-consistent field approach formulated for infinitely extended nuclear matter in terms of two-particle reaction operators (see, e.g. [7]). The same author has also found that determinants Φ_a^r obtained by single substitutions of the single-particle functions φ_a from the set defining the optimum determinant Φ by an orbital φ_r orthogonal to any function of this set are orthogonal to the exact wavefunction, i.e.

$$\langle \Phi_a^r | \Psi \rangle = 0 \quad \text{for} \quad 0 \leq a \leq N < r, \tag{3}$$

where N is the number of particles.

As has been reminded by Paldus *et al.* [8], the idea of using condition (1) as a criterion of goodness of the IPM was actually put forward within the framework of

0026–8976/98 $12·00

many-electron theory prior to its nuclear-physics application. This was done by Laforgue (see, e.g. [9]) in an overlooked work based on the use of a so called *fonction d'erreur*, which corresponds to using condition (1). Broad attention of the quantum-chemical community to IPMs based on criteria of accuracy for the wavefunctions has been attracted by the work of Nesbet [10] who reformulated the configuration interaction (CI) approach in such a way that it resembles, as far as possible, Brueckner's formulation [7]. To achieve his aim he imposed on the orbital set the condition (3) which he called the 'Brueckner condition'. Notice that this condition eliminates the singly excited configurations from the CI expansion of the exact wavefunction. Further impetus to the work in this field was due to Löwdin [11], who assumed the best-overlap criterion (2) in his 'exact self-consistent theory'. Primas [12] has coined the names: Brueckner determinant for the best overlap determinant Φ_B satisfying conditions (1) and (2), and Brueckner orbitals (BO) for the corresponding maximum overlap orbitals. Interesting discussion of the relationships between the maximum-overlap IPM and other models can be found in the work by Kutzelnigg and Smith [13]. Paldus *et al.* [8] derived stability conditions for maximum-overlap independent-particle wavefunctions and applied them to the π-electronic model.

The main difference between the HF and Brueckner IPMs consists of the fact that, unlike the HF orbitals, the direct determination of the BOs requires the knowledge of the exact wavefunction. Therefore, there has been a rather general feeling that BOs are more of theoretical than of practical interest. They turned out to be especially useful in studies of the detailed structure of the terms of the wavefunction representing various correlation effects. However, over the years computational methods implying the use of BOs have been developed, e.g. Larsson [14] and Stolarczyk and Monkhorst [15] have proposed to obtain these orbitals from HF type equations modified by a 'correlation' potential. An interesting field of practical applications of BOs seems to be the coupled-cluster (CC) methods [16, 17]. Theoretical [15] and computational [18] coupled-cluster studies of the applicability of these orbitals have been performed by several groups. Recently several interesting coupled cluster type approaches based on the use of BOs have been put forward and applied (for reviews and references see [19]).

At the end of these remarks on the origin and significance of the maximum overlap IPM as well as of the BOs (or maximum overlap orbitals), we would like to emphasize that in all the theoretical and computational developments in this area considerations have focused on one state at a time, i.e. both the maximum overlap determinant Φ and the BOs are defined for a specific exact wavefunction Ψ. Moreover, one would expect that Φ is especially well suited for the representation of such wavefunctions Ψ which contain in their CI expansion a single dominant determinant. For the states corresponding to these wavefunctions the correlation effects, which are often referred to as dynamical [20], are well described in terms of single-reference-state (SR) methods of variational, perturbational and coupled-cluster type.

It is well known, however, that for a large class of states known as quasi-degenerate ones the CI-expansion of the wavefunction contains more than one important configuration. The description of the electron correlation effects in such states, which include important non-dynamical effects [20], by means of SR methods encounter various difficulties. These difficulties can be to a large extent overcome within the framework of multi-reference-state (MR) formulations of perturbational (for details and references, see, e.g., [21–24]) and CC-type (see [22, 25 28] and references therein) methods. Unlike SR-type methods, the MR ones are concerned with several states at the same time. In MR methods one starts with a model space $\mathcal{M}_0$ spanned by a set of Slater determinants Φ_i (d in number, say) and defines a wave operator, Ω, which generates a set of d exact normalized wavefunctions Ψ_i by acting upon d suitable linear combinations, $\Psi_i^{(0)}$ of the Φ_i determinants, i.e.

$$\Psi_i = \Omega \Psi_i^{(0)}, \quad (i = 1, 2, \ldots, d) \tag{4}$$

where

$$\Psi_i^{(0)} = \sum_{k=1}^{d} c_{ik} \Phi_k. \tag{5}$$

The space, $\mathcal{M}$ spanned by the d exact wavefunctions Ψ_i is referred to as target space [23]. The set of Φ_i is chosen such that it includes the dominant configurations of the states considered.

From an intuitive point of view, it seems that the degree of complexity in constructing the Ω operator depends on how much the model and target spaces are close to each other. Therefore, it might be useful to establish some quantitative description of the proximity of the subspaces involved. For a given $\mathcal{M}$ this proximity depends on the choice of determinants spanning $\mathcal{M}_0$ and the orbital sets used for their construction. Hence, if the structure of the determinants is fixed the distance is determined by the choice of orbital set, and it is possible to define orbitals that correspond to maximum proximity of the $\mathcal{M}_0$ and $\mathcal{M}$ spaces. These orbitals represent a generalization of the BOs discussed above, and become identical with the BOs for one-dimensional model and target spaces.

In this paper we present methods useful for a quantitative characterization of the proximity of model and target spaces employed in MR formulations. Next, we employ these methods to define generalizations to the MR case of the BOs (or maximum overlap orbitals), i.e. orbitals corresponding to the maximum proximity of the pairs of subspaces considered. To get a preliminary insight into the usefulness of the methods proposed, calculations have been performed for the H4 model [29]. This model consists of four hydrogen atoms arranged in a trapezoidal way that is fully determined by a single parameter. If this parameter approaches zero the wavefunctions corresponding to the two lowest energies reveal strong quasi-degeneracy (for details see [29]). The H4 model has been employed by several authors (for references see [30, 31]) for studying the performance of various SR and MR approaches. Since for this model one can specify arbitrary symmetry-adapted orbital sets by means of two parameters [32], the determination of the generalized BOs is a relatively simple task.

2. Distance between pairs of finite dimensional subspaces

A general method for characterizing the distance of pairs of d-dimensional subspaces of the Hilbert space was proposed by one of the present authors [33]. It is based on the following generalization of the theorem of Krejn, Krasnoselski, and Milman [34]:

Theorem: Let $\mathcal{M}$ and $\mathcal{M}_0$ be d-dimensional subspaces of the Hilbert space $\mathcal{H}$. There exist orthonormal basis sets $\{\psi_i\}_{i=1}^d$ and $\{\varphi_i\}_{i=1}^d$ in $\mathcal{M}$ and $\mathcal{M}_0$, respectively, such that

$$(\psi_i, \varphi_j) = M_i \delta_{ij} \quad (i,j = 1,2,\ldots,d). \tag{6}$$

and

$$[1 - \theta^2(\mathcal{M}, \mathcal{M}_0)]^{1/2} \leq M_i \leq 1 \quad (i = 1,2,\ldots,d). \tag{7}$$

The number $\theta(\mathcal{M}, \mathcal{M}_0) = \|P - P_0\|$ is called the gap of the subspaces $\mathcal{M}$ and $\mathcal{M}_0$ associated with the projection operators P and P_0, respectively.

The M_i values appearing in the theorem can be used to establish convenient means of precise description of a pair of subspaces of the Hilbert space.

Let us also notice that the M_i numbers are square roots of the eigenvalues of the following operators [33]

$$V_1 = PP_0P = (PP_0)(PP_0)^+, \tag{8}$$

$$V_2 = P_0PP_0 = (P_0P)(P_0P)^+ \tag{9}$$

i.e.

$$V_1\psi_i = M_i^2\psi_i \quad \text{and} \quad V_2\varphi_i = M_i^2\varphi_i \quad (i = 1,\ldots,d) \tag{10}$$

Let us assume that $\mathcal{M}$ and $\mathcal{M}_0$ are spanned by arbitrary orthonormal basis sets $\{\Psi_i\}_{i=1}^d$ and $\{\Phi_i\}_{i=1}^n$, respectively. If $\mathbf{M}$ denotes the mixed-overlap matrix defined as

$$(\mathbf{M})_{ij} = \langle \Phi_i | \Psi_j \rangle, \tag{11}$$

then the matrix representations of V_1 and V_2 are:

$$\mathbf{V}_1 = \mathbf{M}^+\mathbf{M} \quad \text{and} \quad \mathbf{V}_2 = \mathbf{M}\mathbf{M}^+, \tag{12}$$

i.e. M_i^2 can be obtained by diagonalizing the product of the mixed-overlap matrix and its Hermitian conjugate. Hence, to get the M_i numbers it is sufficient to know the $\mathbf{M}$ matrix for arbitrary orthogonal basis sets.

To provide further insight into the properties of the M_i numbers and the eigenfunctions of V_1 and V_2, we mention the following inequalities [33]: first, if the M_i numbers are arranged in non-increasing order, $M_i \geq M_{i+1}$, then for every s, $1 \leq s \leq d$, the following inequality holds:

$$\sum_{i=1}^{s} M_i \geq \sum_{i=1}^{s} |\mathbf{M}_{ii}|. \tag{13}$$

Second, for the eigenfunctions of V_1 and V_2 and arbitrary basis sets $\{\Psi_i\}_{i=1}^d$ and $\{\Phi_i\}_{i=1}^d$ in $\mathcal{M}$ and $\mathcal{M}_0$, respectively one has the inequality:

$$\sum_{i=1}^{d} \|\psi_i - \varphi_i\|^2 \leq \sum_{i=1}^{d} \|\Psi_i - \Phi_i\|^2. \tag{14}$$

This inequality states that in the case when a comparison of two subspaces is made by means of a least-squares-like study of the differences of their basis functions, a unique characterization can be obtained by utilizing the eigenfunctions of the V_1 and V_2 operators.

The following examples of using the M_i numbers for defining quantities useful in the characterization of the proximity of the subspaces $\mathcal{M}$ and $\mathcal{M}_0$ have been given in [33]:

(a) the whole set or suitably chosen subsets of the M_i numbers;

(b) the sum

$$T = \sum_{i=1}^{d} M_i; \tag{14a}$$

(c) the sum

$$D = \sum_{i=1}^{d} M_i^2; \tag{14b}$$

(d) the product

$$I = \prod_{i=1}^{d} M_i. \tag{14c}$$

For getting close subspaces, one should maximize the appropriate proximity measure. Notice that for one-dimensional subspaces, $d = 1$, all quantities (*a*)–(*d*),

lead to the same proximity criterium:

$$M_1 = \langle \Phi_1 | \Psi_1 \rangle = \text{maximum}. \tag{15}$$

A convenient global proximity measure is given by (14*b*) which represents the trace of the product $\mathbf{M}^+\mathbf{M}$ or $\mathbf{M}\mathbf{M}^+$, i.e.

$$D = \sum_{i=1}^{d} M_i^2 = \sum_{i=1}^{d} (\mathbf{M}^+\mathbf{M})_{ii} = \sum_{i,k} |\langle \Phi_k | \Psi_i \rangle|^2 \tag{16}$$

According to equation (7) $M_i^2 \leq 1$, hence $0 \leq D \leq d$. The upper bound is reached in the case of identical subspaces.

3. Proximity of model and target spaces in multi-reference-state methods

The methods of characterization of the distance between a pair of subspaces presented above can be conveniently applied within the framework of MR approaches. First, one may use proximity criteria to characterize a given model space from the point of view of its distance from the respective target space. Second, one may optimize the proximity of the model ($\mathcal{M}_0$) and target ($\mathcal{M}$) spaces by a proper choice of the orbital set. Notice that, according to (15) for one-dimensional model spaces, i.e. in the SR case, all maximum-proximity criteria are equivalent to the maximum-overlap condition (2) which can be used for defining the BOs. Hence, in the MR case, the orbital of the set for which maximum proximity of $\mathcal{M}_0$ and $\mathcal{M}$ is attained can be considered as generalizations of the maximum-overlap orbitals or BOs. We shall refer to these orbitals as *maximum proximity orbitals* (MPO). Notice that the detailed form of the MPOs depends on the proximity criterium chosen. We denote by Φ_i^{MPO} the determinants constructed from the MPOs. Then the set $\{\Phi_i^{\mathrm{MPO}}\}_{i=1}^{d}$ defining $\mathcal{M}_0$ can be considered as a generalization to the MR case of the Brueckner determinant Φ_{B} used in SR approaches. One might expect that the MPOs will play a similar role for MR-type theories as the BOs play for the SR ones.

In the present work we define the proximity of $\mathcal{M}_0$ and $\mathcal{M}$ using the index D defined by equation (14*b*). Hence the MPOs are obtained from the requirement

$$D = \max. \tag{17}$$

According to equation (16) this condition is equivalent to maximizing the sum of squares of the magnitudes of the elements mixed-overlap matrix defined by the sets $\{\Phi_i\}_{i=1}^{d}$ and $\{\Psi_i\}_{i=1}^{d}$.

In the SR approach for the determinant constructed from BOs condition (3) holds. Notice that this condition is equivalent to

$$c_a^r = 0 \quad \text{for} \quad 0 \leq a \leq N < r, \tag{18}$$

where c_a^r stand for the coefficients of singly-excited (with respect to reference determinant Φ) configurations of the exact wavefunction Ψ. Moreover, condition (18) holds for any normalization imposed on this function.

Bearing in mind that the MPOs correspond to the BOs in SR theories, one might expect that in the case of maximum proximity of $\mathcal{M}_0$ and $\mathcal{M}$ in MR approaches, the role of singly-excited configurations (represented in terms of MPOs) will be minimized. The specific form of the conditions fulfilled by the coefficients of singly excited configurations (with respect to the determinants spanning $\mathcal{M}_0$) depends on the form of the proximity criteria.

When formulating perturbation or CC methods of the SR-type it is convenient to impose on the exact wavefunction the intermediate normalization condition $\langle \Phi | \tilde{\Psi} \rangle = 1$, where $\tilde{\Psi}$—the intermediate-normalization equivalent of Ψ—is obtained by the simple renormalization procedure $\tilde{\Psi} = c_0^{-1}\Psi$ with c_0 the coefficient of the reference configuration in the FCI expansion of Ψ. From equation (17) it is clear that for the BOs the renormalized coefficients $\tilde{c}_a^r = c_0^{-1}c_a^r$ satisfy the equation $\tilde{c}_a^r = 0$. It is well known from the cluster analysis of the $\tilde{\Psi}$ function that the $\tilde{c}_a^r$ coefficients are equal to the one-body cluster amplitudes [17].

In the MR case the intermediate normalization condition is generalized in the following way [26]:

$$\langle \Phi_i | \tilde{\Psi}_k \rangle = \delta_{ik} \quad (i,k = 1,\ldots,d). \tag{19}$$

The renormalized functions $\tilde{\Psi}_k$ are obtained from their orthonormal counterparts Ψ_i as

$$\tilde{\Psi}_k = \sum_{l=1}^{d} [\mathbf{C}_0^{-1}]_{lk} \Psi_l \quad (k = 1,\ldots,d) \tag{20}$$

where $\mathbf{C}_0$ is the matrix of coefficients c_{jl} of the reference determinants in the Ψ_l functions, i.e.

$$\Psi_l = \sum_{j=1}^{d} c_{jl}\Phi_j + \chi_l, \tag{21}$$

where χ_l belongs to the orthogonal complement $\mathcal{M}_0^{\perp}$ of $\mathcal{M}_0$. Notice that the renormalized wavefunctions take the form

$$\tilde{\Psi}_k = \Phi_k + \tilde{\chi}_k \quad (k = 1,\ldots,d) \tag{22}$$

with $\tilde{\chi}_k \in \mathcal{M}_0^{\perp}$, and can be represented as [26, 35]

$$\tilde{\chi}_k = \sum_{a_1, r_1} \tilde{c}_{a_1}^{r_1}(k)(\Phi_k)_{a_1}^{r_1} + \ldots + \sum_{\substack{a_1 \ldots a_N \\ r_1 \ldots r_N}} \tilde{c}_{a_1\ldots a_N}^{r_1\ldots r_N}(k)(\Phi_k)_{a_1\ldots a_N}^{r_1\ldots r_N}, \tag{23}$$

where $(\Phi_k)_{a_1\ldots a_N}^{r_1\ldots r_N}$ denotes the determinant obtained from Φ_k by the replacement of the spin orbitals $a_1,\ldots,a_s$ by the spin orbitals $r_1,\ldots,r_s$. Let us mention that in MR

Table 1. Comparison of proximity indices for the $(\mathcal{M}_0, \mathcal{M})$ subspsaces corresponding to the $(1^1A_1, 2^1A_1)$-states and CI coefficients $(\tilde{c}_1^3, \tilde{c}_2^4)$ obtained for standard quantum-chemical orbitals and MPOs for the H4 model at $\alpha = 0.005$.

System	Orbitals		Proximity indices $(\times 10^6)^b$			CI coefficients	
	Type	Parameters[a]	D	M_1	M_2	$\lvert\tilde{c}_1^3\rvert$	$\lvert\tilde{c}_2^4\rvert$
$H4^{++}$	HF	1.034 0.973	−40	−1	−20	0.0022	0.0065
	Brueckner	1.031 0.975	−21	−4	−17	0.0015	0.0059
$H4^{+}$	HF($1a_1^2 2a_1$)	1.040 0.964	−134	1	−71	0.0036	0.0094
	HF($1a_1^2 2b_2$)	1.044 0.863	−167	3	−106	0.0047	0.0096
H4	HF	1.038 0.983	0	0	0	0.0036	0.0030
	Brueckner	1.053 0.973	−118	12	−74	0.0074	0.0060
	Natural	1.051 0.974	−101	11	−64	0.0069	0.0057
	HF($1a_1^2 2a_1^2$)	1.040 0.968	−96	4	−55	0.0037	0.0094
	MCSCF(1.0;0.0)[c]	1.088 0.948	−742	−30	−357	0.0160	0.0138
	MCSCF(0.6;0.4)[c]	1.045 0.978	−48	8	−33	0.0054	0.0045
	MCSCF(0.4;0.6)[c]	1.032 0.987	27	−9	23	0.0021	0.0018
	MCSCF(0.05;0.95)[c]	1.016 0.998	25	−49	63	0.0020	0.0014
	Kohn–Sham[d]	1.070 0.977	−239	2	−127	0.0121	0.0043
	Maximum proximity[e]	1.024 0.993	38	−26	47	0.0001	0.0001

[a] See equation (27). For each orbital x_a is listed above x_b.
[b] Relative to the indices for the HF orbitals: $D = 1.867\,522$, $M_1 = 0.974\,914$, $M_2 = 0.957\,635$.
[c] The weights given in parenthesis are defined in equation (29).
[d] Orbitals for the BLYP potential.
[e] Defined by condition (17).

approaches the intermediately normalized wavefunctions (22) are the basis for the cluster analysis of the set of exact wavefunctions [26, 35], e.g. the $\tilde{c}_a^r(k)$ coefficients are equal to one-body cluster amplitudes. For this reason, the renormalized form seems to be the most natural one also for MR perturbational approaches to the wavefunctions. Therefore, when studying the significance of the singly-excited configurations in the FCI form of the exact wavefunctions our attention will be focused on the renormalized coefficients $\tilde{c}_a^r(k)$.

Concluding this section, we observe that when using equations (16) and (21), condition (17) defining the MPOs can be re-expressed as

$$\sum_{j,l} |c_{jl}|^2 = \max. \qquad (24)$$

4. Results of pilot applications

4.1. *Model*

We shall present results of numerical studies for the H4 model [29] in which the trapezoidal arrangement of the four hydrogen atoms is fully specified by a single parameter α defining the angle $\phi = \alpha\pi$ if the nuclear separation between the nearest neighboring atoms is fixed (in our case at 2 au). Varying continuously the parameter α from 0 to 0.5, we proceed from a very strongly quasi-degenerate regime to an almost non-degenerate situation. Although the model system considered is relatively small, it is known to epitomize many of the essential difficulties encountered in quantum-chemical computations. The four MOs of the H4 MBS model are labelled according to their C_{2v} symmetry species. One has two orbitals of a_1 symmetry species, which

Table 2. Comparison of proximity indices for the $(\mathcal{M}_0, \mathcal{M})$ subspaces and CI coefficients obtained for standard quantum-chemical orbitals and MPOs for the H4 model at $\alpha = 0.5$.

			$(1^1A_1, 2^1A_1)$ states				$(1^1A_1, 3^1A_1)$ states			
	Orbitals		Proximity indices[b] ($\times 10^4$)			CI[d] coefficients	Proximity indices[c] ($\times 10^4$)			CI[d] coefficients
System	Type	Parameters[a]	D	M_1	M_2	$\lvert\tilde{c}_1^3\rvert \lvert\tilde{c}_2^4\rvert$	D	M_1	M_2	$\lvert\tilde{c}_1^3\rvert \lvert\tilde{c}_2^4\rvert$
$H4^{++}$	HF	3.354 0.786	−406	0	−348	0.3046 0.0561	191	12	132	0.0165 0.0473
	Brueckner	2.914 0.803	−320	2	−275	0.2777 0.0527	192	19	122	0.0393 0.0444
$H4^+$	HF($1a_1^2 2a_1$)	3.737 0.479	−539	37	−526	0.3178 0.1549	−115	−136	120	0.0083 0.1442
	HF($1a_1^2 2b_2$)	2.220 0.842	−155	3	−135	0.2195 0.0449	152	21	98	0.0897 0.0378
H4	HF	1.626 0.823	0	0	0	0.1426 0.0541	0	0	0	0.1598 0.0484
	Brueckner	1.683 0.793	−18	3	−20	0.1510 0.0620	15	3	8	0.1522 0.0560
	Natural	1.682 0.793	−18	3	−20	0.1509 0.0620	15	3	8	0.1523 0.0560
	HF($1a_1^2 2a_1^2$)	3.737 0.437	−574	29	−548	0.3168 0.1709	−190	−172	116	0.0095 0.1599
	MCSCF(1.0;0.0)[e]	1.897 0.727	−84	12	−90	0.1801 0.0796	54	4	37	0.1260 0.0728
	MCSCF(0.6;0.4)[e]	1.700 0.794	−33	5	−35	0.1537 0.0616	6	0	4	0.1498 0.0552
	MCSCF(0.4;0.6)[e]	1.535 0.862	24	−6	30	0.1281 0.0442	−35	−8	−16	0.1731 0.0390
	MCSCF(0.05;0.95)[e]	0.820 1.407	−118	7	211	0.0436 0.0669	−973	−300	−321	0.3403 0.0661
	Kohn–Sham[f]	2.006 0.699	−118	15	−124	0.1932 0.0874	62	1	48	0.1144 0.0801
	Maximum proximity[g]	1.167 0.965	76	−45	135	0.0542 0.0216	223	25	138	0.0081 0.0032

[a] See equation (27). For each orbital x_a is listed above x_b.
[b] Relative to the indices for the HF orbitals: $D = 1.3351$, $M_1 = 0.9860$, $M_2 = 0.6024$.
[c] Relative to the indices for the HF orbitals: $D = 1.3630$, $M_1 = 0.9862$, $M_2 = 0.6248$.
[d] Coefficients $|\tilde{c}_1^3|$ are listed above $|\tilde{c}_2^4|$.
[e] The weights given in parenthesis re defined in equation (29).
[f] Orbitals for the BLYP potential.
[g] Defined by the condition (17). Parameters for the $(1^1A_1, 3^1A_1)$ states: $x_a = 3.462$, $x_b = 0.953$.

can be written in terms of Gaussian functions χ_k, centred at atom k as

$$\varphi_i^a = c_i^a(\chi_1 + \chi_4) + d_i^a(\chi_2 + \chi_3) \quad (i = 1, 2) \qquad (25)$$

and two orbitals of b_2 symmetry species

$$\varphi_i^b = c_i^b(\chi_1 - \chi_4) + d_i^b(\chi_2 - \chi_3) \quad (i = 1, 2). \qquad (26)$$

We assume that $i = 1$ for the orbital corresponding to the lower expectation value of the one-electron Hamiltonian. Since we are concerned with the three lowest $^1A_1$ states, the nodeless φ_1^a orbital is included in all model-space determinants. The normalization and orthogonality conditions mean that for each symmetry species all four coefficients in equations (25) and (26) can be expressed in terms of a single parameter. For the reference functions employed in this work it is convenient to use the parameters

$$x_a = d_1^a/c_1^a \quad \text{and} \quad x_b = d_1^b/c_1^b \qquad (27)$$

for the a_1 and b_2 symmetry species, respectively. Varying these parameters in the range $(0, \infty)$ allows one to define a vast variety of orbital sets for the H4 model. It is convenient to represent every orbital set as a point on the (x_a, x_b)-plane.

Table 3. Proximity indices D and M_1 for the $(\mathcal{M}_0, \mathcal{M})$ subspaces and renormalized CI coefficients $(\tilde{c}_1^3, \tilde{c}_2^4)$ obtained for the MPOs and HF orbitals for various geometries of the H4 model.

		$(1^1A_1, 2^1A_1)$ states				$(1^1A_1, 3^1A_1)$ states			
α	Orbital type	Orbital parameters[a]	D	M_1	$\lvert\tilde{c}_1^3\rvert \lvert\tilde{c}_2^4\rvert$[b]	Orbital parameters	D	M_1	$\lvert\tilde{c}_1^3\rvert \lvert\tilde{c}_2^4\rvert$[b]
0.005	MPO	1.024 0.993	1.86756	0.97489	0.0001 0.0001	$4.265 \cdot 10^6$ 0.340	1.12275	0.98063	0.4983 0.1453
	HF	1.038 0.983	1.86752	0.97491	0.0036 0.0030	1.038 0.983	0.95089	0.97490	19.11 9.390
0.010	MPO	1.047 0.986	1.86406	0.97450	0.0002 0.0002	$2.948 \cdot 10^5$ 0.351	1.10636	0.98091	0.4888 0.1530
	HF	1.071 0.968	1.86394	0.97459	0.0061 0.0058	1.071 0.968	0.95150	0.97454	8.8828 1.8639
0.050	MPO	1.185 0.953	1.82225	0.97379	0.0020 0.0016	60.74 0.400	1.08133	0.98764	0.2346 0.0886
	HF	1.322 0.874	1.81982	0.97515	0.0300 0.0264	1.322 0.874	0.99041	0.97540	1.0012 0.4872
0.100	MPO	1.251 0.949	1.71685	0.97560	0.0073 0.0054	12.28 0.496	1.15902	0.99086	0.0437 0.0136
	HF	1.506 0.835	1.71164	0.97828	0.0536 0.0396	1.506 0.835	1.09749	0.97901	0.3741 0.1488
0.200	MPO	1.228 0.969	1.47979	0.97869	0.0275 0.0164	5.177 0.775	1.30807	0.98898	0.0024 0.0002
	HF	1.637 0.804	1.47157	0.98285	0.0993 0.0618	1.637 0.804	1.27640	0.98329	0.2050 0.0050
0.500	MPO	1.167 0.965	1.34270	0.98151	0.0542 0.0216	3.462 0.953	1.38532	0.98869	0.0081 0.0032
	HF	1.626 0.823	1.33505	0.98596	0.1426 0.0541	1.626 0.823	1.36302	0.98620	0.1598 0.0484

[a] See equation (27). For each orbital x_a is listed above x_b.
[b] $|\tilde{c}_1^3|$ is listed above $|\tilde{c}_2^4|$.

In this work we define the model space $\mathcal{M}_0$ as spanned by two determinants:

$$\Phi_1 = |\varphi_1^a \overline{\varphi}_1^a \varphi_1^b \overline{\varphi}_1^b| \quad \text{and} \quad \Phi_2 = |\varphi_1^a \overline{\varphi}_1^a \varphi_2^a \overline{\varphi}_2^a|. \tag{28}$$

The MPOs for $\mathcal{M}_0$ spanned by the determinants (28) consisting of orbitals defined by the x_a and x_b values can be easily obtained. Notice that for these orbitals the FCI coefficients are also functions of x_a and x_b, i.e. $c_{jl} = c_{jl}(x_a, x_b)$, and by value of (24) the condition defining the MPOs can be written as $D(x_a, x_b) = \max$. The maximum of $D(x_a, x_b)$ with respect to x_a and x_b has been found numerically using the downhill simplex method included in *Numerical Recipes* [36].

4.2. *Proximity of $\mathcal{M}_0$ and $\mathcal{M}$ for standard orbital sets*

To get an idea about the proximity of the model and target spaces $\mathcal{M}_0$ and $\mathcal{M}$ in calculations based on various orbitals, we have calculated the proximity parameters for several orbital sets employed so far in quantum-chemical calculations. A common feature of these orbitals is that they have been obtained as a result of some optimization procedure. We consider the HF orbitals for the $1a_1^2 1b_2^2$ and $1a_1^2 2a_1^2$ configurations, the 'exact' BOs obtained for the FCI function, the natural orbitals (NO) and the Kohn–Sham orbitals [37]. The BO, NO, and Kohn–Sham orbitals have been generated for the ground state by means of the GAUSSIAN 92 system of programs [38]. Moreover, we consider the MCSCF(w_1, w_2) orbitals which minimize the weighted sum

$$\overline{E} = w_1 E_1 + w_2 E_2 \tag{29}$$

of eigenvalues E_1 and E_2 (in increasing energy order) of the Hamiltonian matrix corresponding to the configurations $1a_1^2 1b_2^2$ and $1a_1^2 2a_1^2$ defining the multiconfigurational state. Notice that the MCSCF(1.0; 0.0) orbitals are just the standard MCSCF orbitals for the ground state. The MCSCF orbitals for (w_1, w_2) equal to (0.6; 0.4) and (0.4; 0.6) might be expected to provide a balanced description of both members of the pair of states considered. All MCSCF orbitals have been obtained by means of the GAMESS electronic structure

Table 4. Comparison of the proximity parameters, D, and differences of the VU-CCSDT[a] and FCI energies, δE_1 and δE_3, for the 1^1A_1 and 3^1A_1 states, respectively, calculated for the H4 model when using MPO and HF orbital sets.

	MPO				HF			
α	x_a, x_b[b]	D	δE_1	δE_3	x_a, x_b[b]	D	δE_1	δE_3
0.2	5.177 0.775	1.308	−4.641	15.60	1.637 0.804	1.276	−8.256	53.09
0.3	3.977 0.915	1.345	−2.090	12.79	1.642 0.812	1.320	−3.042	33.50
0.5	3.462 0.953	1.385	−1.266	13.53	1.626 0.823	1.363	−1.867	29.28

[a] For details see [40].
[b] Orbital parameters x_a are listed above x_b.

Table 5. Comparison of the proximity parameters, D, and differences of the SU-CCSD[a] and FCI energies, δE_1 and δE_2, for the 1^1A_1 and 2^1A_1 states, respectively, calculated for the H4 model when using MPO and HF orbital sets.

	MPO				HF			
α	x_a, x_b[b]	D	$\delta E_1, \delta E_2$[c]	S_1^3	x_a, x_b[b]	D	$\delta E_1, \delta E_2$[c]	S_1^3
0.005	1.024 0.993	1.867 56	0.035 0.005	2×10^{-4}	1.038 0.983	1.867 52	0.035 0.007	0.004
0.01	1.047 0.986	1.864 06	0.022 0.008	3×10^{-4}	1.071 0.968	1.863 94	0.020 0.021	0.006
0.05	1.185 0.953	1.822	0.008 −0.017	0.002	1.322 0.875	1.820	−0.045 0.051	0.030
0.1	1.251 0.949	1.717	−0.110 −0.678	0.007	1.506 0.835	1.712	−0.218 −0.685	0.054
0.2	1.228 0.969	1.480	−0.845 −3.824	0.027	1.637 0.804	1.472	−1.101 −4.440	0.100
0.5	1.167 0.965	1.343	−1.656 −6.073	0.052	1.626 0.823	1.335	−2.015 −7.093	0.141

[a] For details see [41].
[b] Orbital parameters x_a are listed above x_b.
[c] Energy differences δE_1 are listed above δE_2.

package [39]. In addition to the orbitals for H4, we have considered several orbitals defined for the $H4^{++}$ and $H4^{+}$ systems. The latter are in VU-type approaches the predecessors of the former system in the valence universal hierarchy [26].

The proximity indices obtained when using various standard orbital sets for defining $\mathcal{M}_0$ are compared with the indices obtained for the MPOs defined by equation (17). We have also calculated the renormalized coefficient $\tilde{c}_a^r(k)$ of the singly excited configurations in the FCI wavefunctions. Let us notice that for the $^1A_1$ states of our model there do not exist singly-excited determinants with respect the determinant Φ_2 defined in (28). Therefore, we may omit the index of the reference determinant in the coefficient and write $\tilde{c}_a^r$ instead of $\tilde{c}_a^r(1)$.

The orbitals discussed are obtained for two geometries of our model system defined by the following values of α: (a) $\alpha = 0.005$ corresponding to the strong quasi-degeneracy region, (b) $\alpha = 0.5$ corresponding to the weak quasi-degeneracy case.

The results of our calculations are collected in tables 1 and 2. In the former table one can see that in the strong quasi-degeneracy region from among the standard orbitals the MCSCF(0.05;0.95) ones entail the largest proximity of the $\mathcal{M}_0$ and $\mathcal{M}$ spaces. By far the smallest

proximity is attained for the MCSFC(1.0;0.0) orbitals. This situation is certainly related to the small value of M_2, which seems to be a consequence of the fact that for strong quasi-degeneracy the MCSCF(1.0;0.0) overestimates the role of the Φ_2 configuration, with respect to the Φ_1 one, in the description of the ground state. Notice that in the strong quasi-degeneracy region the Brueckner and natural orbitals generate $\mathcal{M}_0$ spaces of smaller overlap with $\mathcal{M}$ than the HF orbitals. Perusing the magnitudes of the CI coefficients one can see that they decrease with increasing proximity index D. These coefficients are extremely small for the MPOs.

In table 2 we compare the proximity indices and $\tilde{c}_a^r$ values obtained for the case of weak quasi-degeneracy. We consider the pairs of subspaces corresponding to the pairs of states (1^1A_1, 2^1A_1) and (1^1A_1, 3^1A_1). Notice that for these states the D values are rather close and are significantly smaller from their counterparts for the (1^1A_1, 2^1A_1) pair corresponding to $\alpha = 0.005$. This fact indicates that the MR description of the two former pairs of states based on the orbital sets considered is more difficult than for the latter one, which is in fact the case (see e.g. [30–32]). On the other hand, for $\alpha = 0.5$ one would expect that the MR description of both pairs will be of comparable quality, which has also been demonstrated (see e.g. [30–32]). One can see in the table that for the (1^1A_1, 2^1A_1) pair maximum proximity for standard orbitals is attained for the HF orbitals, whereas in the case of the (1^1A_1, 3^1A_1) pair for the HF orbitals of $H4^{++}$ and $H4^{+}$ and the BOs of $H4^{++}$. For the latter pair the D index is especially small for the MCSCF(0.05;0.95) orbitals, which is a consequence of the fact that, according to equation (29), these orbitals are determined from the requirement that the second energy be minimum, which results in a relatively better description of the 2^1A_1 state than the 3^1A_1 one. Comparing the magnitudes of the $\tilde{c}_a^r$ coefficients one can see again that for all but one orbital sets their magnitudes decrease with increasing proximity of the $\mathcal{M}_0$ and $\mathcal{M}$ spaces, and that the minimum participation of the singly excited determinants in the FCI function takes place for the MPOs.

To shed more light on the effectiveness of the MPOs in reducing the significance of singly-excited configurations in MR-type representations of the wavefunctions, we compare in table 3 the proximity indices and $\tilde{c}_a^r$ coefficients obtained for the MPOs determined for the pairs of states (1^1A_1, 2^1A_1) and (1^1A_1, 3^1A_1) with those obtained for HF orbitals. Let us recall that the $\tilde{c}_a^r$ coefficients correspond to one-body amplitudes in MR-CC methods. The results correspond to states of various degrees of quasi-degeneracy. For completeness, we have included in the table the results for the (1^1A_1, 3^1A_1) pair obtained in the strong quasi-degeneracy regime ($\alpha = 0.005, 0.050$) where the determinants (28) are inadequate for the description of this pair of states. It is apparent from the table that the magnitudes of the CI coefficients obtained for the MPOs are in all cases considerably smaller than for the HF orbitals. The reduction of these magnitudes is especially pronounced in the strong, quasi-degeneracy regime. When proceeding to the region of intermediate and weak quasi-degeneracy this reduction is less pronounced. One can also see from the table that in this region the reduction of the CI coefficients is much larger for the (1^1A_1, 3^1A_1) pair than for the (1^1A_1, 2^1A_1) one. Comparison of the M_1 values obtained for the MPOs and HF orbitals reveals that for the latter pair, proceeding from the HF orbitals to MPOs results in an increase of M_1, whereas for the former pair one can find the opposite situation. At present, we cannot give any convincing rationalization of this behaviour.

The results just discussed provide an indirect way of assessing the impact of using MPOs on the formal structure of the MR-CC description. Let us now present two examples of direct applications of MPOs in MR-CC approaches.

In table 4 we present the energies of the 1^1A_1 and 3^1A_1 states obtained when using the VU-CCSDT [26, 31] method based on the MPOs and HF orbital sets for such geometries of H4 for which the determinants (28) provide a reasonable model space. The MPOs are determined from the requirement of maximum proximity of the model and target spaces at the two-valence-electron level (for details see [40]). We note from the results of the table that when employing MPOs in the calculation instead of HF orbitals the magnitudes of the differences between VU-CCSDT and FCI energies, which represent the exact results, decrease. The improvement of the energies is especially pronounced for the 3^1A_1 state. Notice that the (x_a, x_b) parameters of the MPOs are significantly different from those of the corresponding HF orbitals and the other standard orbitals listed in table 1.

The second example concerns the direct applications of MPOs in calculations based on SU-CCSD methods. In table 5 we show the differences of the SU-CCSD and FCI energy for the 1^1A_1 and 2^1A_1 states obtained in an extensive study of the impact of the choice of orbital sets on the performance of SU-CC methods [41]. Orbital parameters and D values are also included. For comparison, we present the results for HF orbitals. One sees from the table that the energy differences δE_1 and δE_2 are considerably smaller for the MPOs than for the HF orbitals. The difference is larger for the weakly quasi-degenerate states (e.g. $\alpha = 0.5$), where the differences of the values of the overlap index D are larger. The only exception can be found for $\alpha = 0.005$ and 0.01 where

δE_1 is slightly smaller for the HF orbitals than for the MPO ones, whereas the opposite is true for δE_2. Notice, however, that for these α-values the D indices for the two orbital sets considered are very close indeed.

As may be seen in table 5 the S_1^3 amplitudes obtained for the MPOs are significantly smaller than for the HF orbitals, e.g. in the intermediate and weak quasi-degeneracy regions these amplitudes differ by one order of magnitude. It is also interesting to note that the magnitudes of the S_1^3 amplitudes obtained in the SU-CCSD calculation are very close to those of the $\tilde{c}_1^3$ coefficients of the FCI wavefunctions given in table 3. Since these coefficients are equal to the exact S_1^3 amplitudes, one can see that the approximations involved in the SU-CCSD approach have little effect on the one-body CC amplitudes considered.

5. Concluding remarks

In this work we make an attempt to generalize the maximum overlap orbitals or BOs, which are defined in the SR-state formulations of the many-electron theory, to the case of MR-state approaches that are concerned with several states at once. The subspace $\mathcal{M}$ spanned by the exact wavefunctions of these states is referred to as target space, whereas the subspace spanned by the independent-particle-model (i.e. determinantal) approximations to these wavefunctions is termed model space $\mathcal{M}_0$. It seems to us that a natural generalization of the BOs to the MR case is obtained by considering the orbitals that yield the maximum proximity of $\mathcal{M}$ and $\mathcal{M}_0$. These orbitals are referred to as maximum-proximity orbitals (MPOs). We have shortly reviewed the general problem of defining the distance between pairs of finite dimensional subspaces of the Hilbert space. Employing one of the possible proximity parameters, we have defined the set of MPOs. In an attempt to better understand the impact of the distance of the model and target space in MR-type approaches, model studies have been undertaken for the MBS H4 system [29]. This model offers the unique possibility of defining arbitrary symmetry-adapted orbitals in terms of two parameters x_a and x_b, which greatly alleviates the generation of MPOs.

It has been found that the differences of the proximity indices for $\mathcal{M}_0$ and $\mathcal{M}$ obtained for various standard quantum-chemical orbitals increase considerably when proceeding from the strong, quasi-degeneracy region to the intermediate, or weak, quasi-degeneracy ones. We have also calculated the renormalized coefficients $\tilde{c}_a^r$ of singly excited configurations in the FCI expansion of the wavefunctions considered. These coefficients are equal to one-body cluster amplitudes in full MR-CC theories. They also provide a characterization of the importance of singly-excited determinants for the description of the set of wavefunctions considered. Let us recall that in the SR case the use of BOs eliminated these determinants from the FCI expansion. The results of our calculations employing standard orbitals indicate that in almost all cases considered the magnitudes of $\tilde{c}_a^r$ decrease with increasing proximity. Exceptions are found for weakly quasi-degenerate states associated with relatively small differences of proximity indices. For all cases considered, it is found that for the MPOs the $\tilde{c}_a^r$ indices are considerably smaller than for the standard quantum-chemical orbitals, which indicates that the MPOs in fact minimize the impact of singly-excited determinants on the structure of the wavefunctions considered. Hence, the MPOs play in the MR-case a similar role as do the BOs in the SR approaches.

To directly study the impact of using the MPOs on the results of MR-CC methods, we have performed calculation based on the VU-CCSDT [26, 40] and SU-CCSD [28, 30] approaches. It has been found that in both cases the MPOs yield more accurate results than the HF orbitals. This is especially true outside the strong-quasi-degeneracy regime. Therefore, one might expect that by employing orbital sets similar to the MPOs it is possible to extend the range of state quasi-degeneracies for which individual MR-CC methods give highly accurate results.

In this work we have employed one of many possible criteria of proximity of the $\mathcal{M}_0$ and $\mathcal{M}$ spaces. The problem of finding proximity criteria better suited for the characterization of the subspaces encountered in many-electron theories is still an open one.

The results of this work seem to indicate that MPOs may play in MR-type approaches a similar role as do the BOs in the SR case. The MPOs can be used to set up standards for comparison of different methods, especially for the results dependent on the singly excited configurations. They also proved to be well suited for defining basis sets for MR-CC approaches applicable to states whose quasi-degeneracy is expected to vary in a relatively wide range.

The authors would like to thank the referee for providing them with [19 (b) (c)] and Dr Leszek Meissner for providing them with his SU-CCSD program.

References

[1] (a) HARTREE, D. R., 1928, *Proc. Cambridge Phil. Soc.*, **24**, 328; (b) FOCK, V., 1930, *Z. Phys.*, **61**, 126; (c) SLATER, J. C., 1930, *Phys. Rev.*, **35**, 1210.

[2] CARBO, R., and KLOBUKOWSKI, M., 1990, *Self-Consistent Field Theory and Applications* (Amsterdam: Elsevier).

[3] LAWLEY, K. P., 1987, *Ab Initio Methods in Quantum Chemistry* (New York: Wiley).

[4] URBAN, M., ČERNUŠAK, I., KELLÖ, V., and NOGA, J., 1987, *Methods in Computational Chemistry*, Vol. 1, edited by S. Wilson (New York: Plenum Press), p. 117.
[5] JANKOWSKI, K., 1987, *Methods in Computational Chemistry*, Vol. 1, edited by S. Wilson (New York: Plenum Press), p. 1; 1992, *ibid.*, Vol. 5, p. 1.
[6] BRENIG, W., 1957, *Nucl. Phys.*, **4,** 363.
[7] (a) BRUECKNER, K. A., and LEVINSON, C. A., 1955, *Phys. Rev.*, **97,** 1344; (b) BRUECKNER, K. A., and WADA, W., 1956, *Phys. Rev.*, **103,** 1008; (c) BETHE, H. A., *Phys. Rev.*, 1956, **102,** 1553.
[8] PALDUS, J., ČIŽEK, J., and KEATING, B. A., 1973, *Phys. Rev.* A, **8,** 640.
[9] LAFORGUE, A., 1955, *Cah. Phys.*, **9** (57-5), 23.
[10] NESBET, R. K., 1958, *Phys. Rev.*, **109,** 1632.
[11] LÖWDIN, P. O., 1962, *J. Math. Phys.*, **3,** 1171.
[12] PRIMAS, H., 1973, *Helv. Chim. Phys.*, **58,** 5049.
[13] (a) KUTZELNIGG. W., and SMITH, V., 1964, *J. chem. Phys.*, **41**; (b) SMITH, V., and KUTZELNIGG, W., 1968, *Ark. Fys.*, **38,** 309.
[14] LARSSON, S., 1973, *J. chem. Phys.*, **58,** 5049.
[15] STOLARCZYK, L. Z., and MONKHORST, H. J., 1984, *Int. J. quant. Chem.*, **S18,** 267.
[16] COESTER, F., and KÜMMEL, H., 1960, *Nucl. Phys.*, **7,** 477.
[17] (a) ČIŽEK, J., 1966, *J. chem. Phys.*, **45,** 4256; (b) ČIŽEK, J., and PALDUS, J., 1971, *Int. J. quant. Chem.*, **5,** 359.
[18] (a) CHILES, R. A., and DYKSTRA, C. E., 1981, *J. chem. Phys.*, **74,** 4544; (b) PURVIS III, G. D., and BARTLETT, R. J., 1982, *J. chem. Phys.*, **76,** 1910; (c) SCUSERIA, G. E., and SCHAEFER II, H. F., 1987, *Chem. Phys. Lett.*, **142,** 354.
[19] (a) KOBAYASHI, R., AMOS, R. D., and HANDY, N. C., 1994, *J. chem. Phys.*, **100,** 1375; (b) BARTLETT, R. J., 1995, *Modern Electronic Strucure Theory, Part II*, edited by D. R. Yarkony (Singapore: World Scientific), p. 1047; (c) SCUSERIA, G. E., and LEE, T., 1995, *Quantum Mechanical Structure Calculations with Chemical Accuracy*, edited by S. R. Langhoff (Dordrecht: Kluwer), p. 47.
[20] SINANĞLU, O., and BRUECKNER, K. A., 1970, *Three Approaches to Electron Correlation in Atoms* (New Haven: Yale University Press), p. 361.
[21] BRANDOW, B., 1967, *Rev. Mod. Phys.*, **39,** 771.
[22] LINDGREN, I., and MORRISON, J., 1968, *Atomic Many-Body Theory*, 2nd edition (New York: Springer), p. 260.
[23] DURAND, PH., and MALRIEU, J. P., 1987, *Ab Initio Methods in Quantum Chemistry*, edited by K. P. Lawley (New York: Wiley), p. 321.
[24] (a) HURTUBISE, V., and FREED, K. F., 1993, *Adv. Chem. Phys.*, **83,** 465; (b) FINLEY, J. P., and FREED, K. F., 1995, *J. chem. Phys.*, **102,** 1306; (c) FINLEY, J. P., CHAUDHURI, R. K., and FREED, K. F., 1995, *J. chem. Phys.*, **103,** 4990.
[25] (a) PALDUS, J., 1992, *Methods in Computational Molecular Physics*, edited by S. Wilson and G. F. H. Diercksen (New York: Plenum Press), p. 99; (b) PALDUS, J., 1992, *Relativistic and Correlation Effects in Molecules and Solids*, edited by G. L. Malli (New York: Plenum Press), p. 207.
[26] JEZIORSKI, B., and PALDUS, J., 1989, *J. chem. Phys.*, **90,** 2714.
[27] LINDGREN, I., 1978, *Int. J. quant. Chem.*, **S12,** 33.
[28] JEZIORSKI, B., and MONKHORST, H. J., 1981, *Phys. Rev.* A, **24,** 1668.
[29] JANKOWSKI, K., and PALDUS, J., 1980, *Int. J. quant. Chem.*, **17,** 1243.
[30] PALDUS, J., PIECUCH, P., PYLYPOV, L., and JEZIORSKI, B., 1993, *Phys. Rev.* A, **47,** 2738.
[31] (a) JANKOWSKI, K., PALDUS, J., GRABOWSKI, I., and KOWALSKI, K., 1992, *J. chem. Phys.*, **97,** 7600; (b) 1994, *ibid.*, **101,** 3085.
[32] JANKOWSKI, K., KOWALSKI, K., RUBINIEC, K., and WASILEWSKI, J., 1998, *Int. J. quant. Chem.* (in the press).
[33] JANKOWSKI. K., 1976, *Int. J. quant. Chem.*, **10,** 683.
[34] (a) KRASNOSELSKY, M. A., VAINIKKO, G. M., ZABEIKO, P. P., RUTICKY, JA. B., STECENKO, V. JA., 1969, *Approximate Solutions to Operator Equations* (Moskva: Nauka), in Russian; (b) KREJN, M. G., KRASNOSELSKY, M. A., and MILMAN, D. P., 1948, *Sbornik Trudov Instituta Matematiki An USSR*, No. 11, in Russian.
[35] JANKOWSKI, K., PALDUS, J., and WASILEWSKI, J., 1991, *J. chem. Phys.*, **95,** 3549.
[36] 1992, *Numerical Recipes in C: the Art of Computing* (Cambridge: Cambridge University Press) p. 408.
[37] KOHN W., and SHAM, L. J., 1965, *Phys.Rev.*, A, **140,** 1133.
[38] FRISCH, M. J., TRUCKS, G. W., HEAD-GORDON, M., GILL, P. M., WONG, M. W., FORESMAN, J. B., JOHNSON, B. G., SCHLEGEL, H. B., ROBB, M. A., REPLOGLE, E. S., GOMPERTS, R., ANDRES, J. L., RAGHAVACHARI, K., BINKLEY, J. S., GONZALES, C., MARTIN, R. L., FOX, D. J., DEFREES, D. J., BAKER, J., STEWART, J. J. P., and POPLE, J. A., 1992, GAUSSIAN 92, Revision E.2 (Pittsburgh: Gaussian, Inc.,).
[39] SCHMIDT, M. W., BALDRIGE, K. K., BOATZ, J. A., JENSEN, J. H., KOSEKI, J., GORDON, M. S., NGUYEN, K. A., WINDUS, T. L., and ELBERT, S. T., 1990, *QCPE Bull.*, **10,** 52.
[40] JANKOWSKI, K., GRYNIAKOW, J., and RUBINIEC, K., 1998, *Int. J. quant. Chem.* (in the press).
[41] JANKOWSKI, K., MEISSNER, L., and RUBINIEC, K., 1998, *Int. J. quant. Chem.* (in the press).

MOLECULAR PHYSICS, 1998, VOL. 94, NO. 1, 41–54

Unitary group based open-shell coupled cluster method with corrections for connected triexcited clusters. II. Applications

By XIANGZHU LI and JOSEF PALDUS†

Department of Applied Mathematics, University of Waterloo, Waterloo, Ontario, Canada N2L 3G1

The performance of several non-iterative, perturbative accounts of triply excited connected clusters in the unitary group based coupled cluster method with singles and doubles spanning the first order interacting space (UGA-CCSD(is)) is examined for a number of open shell systems. These approaches can account for genuine triples or only for the so-called pseudo-doubles. The latter case (CCSD{f}) represents an approximation to UGA-CCSD employing the full single and double excitation manifold (CCSD(f)), while the remaining approaches account for genuine triple excitations as well, and differ in the way in which they include singly excited clusters (CCSD{T}, CCSD[T] and CCSD(T) methods; see Li X. and Paldus J., 1998, *Int. J. quantum Chem.*, in the press). We explore the range of applicability of these approaches by considering both the equilibrium and stretched geometries for the systems involving one [OH], two [NH_2] or three [CH_3] single bonds, or one multiple bond [CN]. A sensitive test is provided by examining harmonic vibrational frequencies in both the ground and excited states of the isoelectronic homonuclear ions N_2^+ and C_2^-.

1. Introduction

The coupled cluster (CC) methods exploiting the unitary group approach (UGA) [1–4] are attractive techniques for studying open-shell (OS) systems. The singles and doubles (SD) approximation, even at the minimum interacting space (is) level, already provides useful and reliable results in various applications [5–7]. Higher order theories can be developed by accounting for higher order clusters, such as triples, in either iterative or non-iterative ways. In a preceding paper [8] (Part I), we outlined a non-iterative, perturbative account of triply excited connected clusters. This formalism enables us to estimate the contribution of pseudo-doubles (i.e. three body double excitations) and of genuine triples (three body triple excitations) to the total CCSD(is) energies as perturbative effects.

The first problem to explore is to examine how this approach accounts for pseudo-doubles (pDs), which are explicitly considered in our UGA-CCSD(f) method that employs the full SD space. We recall that pDs do not contribute directly to the energy, but only indirectly via their interaction with standard singles and doubles. Thus, instead of solving iteratively for pDs together with standard SDs when computing CCSD(f) energies, we first restrict the CCSD problem to the first order interacting space SDs, obtaining the CCSD(is) energy, which we subsequently correct for pDs using the perturbative type approach outlined in Part I [8] and referred to as CCSD{f}. We recall that although both CCSD(f) and CCSD(is) methods scale in the same way with the size of the basis set, since both Ds and pDs involve four inactive or external orbital labels, the latter method is several times more efficient since it uses a considerably smaller excited state manifold. Since the perturbative estimate of the pD energy contribution is non-iterative, the CCSD{f} approach requires the same effort as a single CCSD(f) iteration. It is thus worthwhile to compare the performance of the iterative CCSD(f) and non-iterative CCSD{f} methods.

The importance of connected triples for achieving highly reliable and quantitative results is nowadays generally recognized [9]. Nonetheless, the computational effort required by fully iterative CCSDT method prohibits its wider applications. Viable schemes accounting for connected triples in a non-iterative way and using converged CCSD amplitudes rely on perturbative approaches.

The most often used schemes in the spin–orbital or closed shell cases are the so-called CCSD(T) [10] and CCSD+T(CCSD) or CCSD[T] [11] methods, which generally provide excellent results in the vicinity of equilibrium geometries. For example, a series of benchmark calculations on spectroscopic constants by Dunning and

† Also at: Department of Chemistry and $(GWC)^2$—Waterloo Campus, University of Waterloo, Waterloo, Ontario, Canada N2L 3G1; presently at: Max-Planck-Institut für Astrophysik, Karl-Schwarzschild-Str. 1, 85740 Garching bei München, Germany.

0026–8976/98 $12·00

co-workers found that 'CCSD(T) performed very nearly as well as (internally contracted multireference configuration interaction) CMRCI at a much reduced computational expense' [12]. Unfortunately, all perturbative approaches eventually break down away from the equilibrium (cf. e.g. figure 4 of [13]).

In Part I of this series [8] we have formulated three versions of a triple correction scheme for UGA based CC approaches, differing in the account of the single triple interactions. These schemes are very similar to those proposed for the spin orbital based CC methods [10, 11], except that they employ spin-adapted UGA formalism. We also note that although we employ a different set of triple excitation operators (see Part I) than the one given in [4], both sets are mutually equivalent.

The account of triples via a non-iterative perturbative scheme is computationally affordable, but has its limitations. Of course, the first assumption for its use is that the CCSD method itself converges. In fact, the rate of convergence of the CCSD procedure is indicative of the quality of the perturbative estimate of triples: when CCSD performs well and provides highly accurate energies, the triple corrections are small and their perturbative estimate reliable. In the case of a poor performance of CCSD, the triple (and most likely higher) corrections are significant, and their perturbative treatment may not be satisfactory. This is invariably the case far away from the equilibrium geometries. With these restrictions in mind, we will explore the performance of three types of triple corrections by computing potential energy surfaces (PESs) and harmonic vibrational frequencies in representative systems.

In examining the effectiveness of perturbative pseudo-double and triple corrections, we thus first consider various bond breaking situations for simple OS doublet states, representing the ground or excited states of several radicals. To complement our earlier UGA-CCSD results [6], we examine the following radicals in order to model various bond breaking situations: OH, modelling the breaking of a single bond, NH_2 and CH_3 for the simultaneous breaking of two and three single bonds, respectively, and CN to study the stretching of a multiple bond. For these systems we have already explored [6] the performance of the interacting and full CCSD methods relative to the exact full CI (FCI) or highly accurate large scale limited CI benchmarks. In this study, we provide even larger limited CI benchmarks in cases where FCI is not available.

As a very sensitive test of the correct shape of the PES in the vicinity of the equilibrium geometry we also compute harmonic vibrational frequencies. In this case only small changes in the geometry and the total energy are involved, so that we can expect a good performance of our perturbative estimates. For example, when choosing as a step size in the bond distance the value of 0.005 Å, the corresponding energy changes are of the order of 10^{-4} au. Thus, a microhartree (10^{-6} hartree) error in the total energy could lead to a larger than $10\,cm^{-1}$ error in computed frequencies. In an earlier paper [7], we have carried out a systematic study of vibrational frequencies and equilibrium geometries in both ground and excited states of the first row diatomics using the UGA-CCSD method and 6-31G(d) basis sets. This study comprised 48 distinct electronic states (most of them open shells) of 9 diatomic hydrides and 18 diatomics, including both neutral and charged species, and employed different kinds of MOs. In all instances we found a very satisfactory agreement with the available experimental data, independently of whether the ground or excited states, high or low spin states, or the so-called 'well-behaved' or 'difficult' cases were involved. In this paper, we consider two isoelectronic systems, namely N_2^+ and C_2^-. In our earlier study we found the largest difference between the computed and experimental ω_e values for the $B^2\Sigma_u^+$ state of N_2^+. Moreover, the computation of vibrational frequencies for these multiply bonded systems provides us with a very sensitive test of the importance of pseudo-double and triple clusters.

Following a brief overview of the corrections for the connected triply excited clusters for the UGA based CCSD methods in section 2, we present and discuss the results of our calculations for the PESs of OH, NH_2, CH_3 and CN in section 3, and of the vibrational frequencies of N_2^+ and C_2^- in section 4. The final section 5 draws appropriate conclusions.

2. Method and computational details

To account perturbatively for pDs and triples in our UGA CCSD(is) approach, we employ the formalism outlined in Part I of this series [8]. Here we only recall that the required non-iterative corrections ΔE to the CCSD(is) energies have always the following general form

$$\Delta E(X) = -\sum_{K\in\Omega_K(X)}\sum_{I\in\Omega_I(X)}\sum_{J\in\Omega_J(X)} \Delta_K^{-1} t_I t_J H_{IK} H_{JK}\,, \tag{1}$$

where t_I designates CCSD(is) amplitudes, $H_{IK} = \langle\Phi_I|H|\Phi_K\rangle$ the corresponding CI matrix elements and Δ_I^{-1} the denominators given by the differences of the diagonal Fock matrix elements corresponding to the particle and hole states defining the configuration $|\Phi_I\rangle$. Thus, when $|\Phi_I\rangle \equiv |\Phi^{\nu_1\nu_2\cdots}_{\mu_1\mu_2\cdots}\rangle$, then $\Delta_I = (F^{\nu_1}_{\nu_1} - F^{\mu_1}_{\mu_1}) + (F^{\nu_2}_{\nu_2} - F^{\mu_2}_{\mu_2}) + \cdots$. The summation ranges $\Omega_I(X)$ then extend over appropriate configuration state functions,

Table 1. Summation ranges $\Omega_L(X)$ appearing in equation (1) for the non-iterative pseudo-double (pD) and triple (T) cluster corrections leading to the UGA-CCSDX methods.

Method	X	$\Omega_K(X)$	$\Omega_I(X)$	$\Omega_J(X)$
CCSD{f}	{f}	pD	SD(is)[a]	SD(is)
CCSD{T}	{T}	T	SD(is)	SD(is)
CCSD(T)	(T)	T	SD(is)	D(is)
CCSD[T]	[T]	T	D(is)[b]	D(is)

[a] SD(is): the first order interacting space singles and doubles.
[b] D(is): the first order interacting space doubles.

depending on the approximation designated by X. When accounting perturbatively for pD states ($X = \{f\}$), we obtain CCSD{f} energies, while the three approximations that we use to account for triples (and, automatically, for pDs) are designated as CCSD{T}, CCSD(T) and CCSD[T], with $X = \{T\}$, (T) and [T], respectively. The corresponding summation ranges for each case are summarized in table 1.

The required codes generating CI matrix elements H_{IJ} are based on our sequence of programs for an automated implementation of various UGA-CCSD methods, as described in [3]. We also use the GAMESS [14] package to carry out SCF and various limited CI or FCI computations for the sake of comparison, namely CISD(is) (CI interacting space singles and doubles), $CISD^+$ (the superscript '+' indicates that the wave function contains an unspecified number of higher than SD excited configurations, since UGA-CI cannot be efficiently truncated by the excitation order [14]), as well as $CISDT^+$, $CISDTQ^+$, etc.

For the $^2\Pi$ state of OH, the $^2A_1$ and $^2B_1$ states of NH_2, the $^2A_2''$ state of CH_3, and the $^2\Sigma^+$ and $^2\Pi$ states of CN, we employ the same basis sets as in our earlier study [6], namely a double-zeta (DZ) and a double-zeta plus polarization (DZP) bases. We refer to [6] for further details.

For the $^2\Pi$ state of the OH radical we use the equilibrium bond length $R_e = 1.832$ bohr. Calculations are performed for $R = R_e$, as well as for the three stretched geometries with the O–H internuclear separation $R = 1.25R_e$, $R = 1.5R_e$ and $R = 2R_e$. In the case of the $^2A_1$ and $^2B_1$ states of NH_2, we again consider equilibrium geometry, as well as distorted geometries with both N–H bonds stretched to $1.5R_e$ and $2R_e$, while the bond angle ∠HNH is kept unchanged. We also investigate a special geometry with the H–H bond distance equal to the H_2 equilibrium value and the N–H distance about twice the R_e value for NH_2. This geometry, denoted as N···H–H [15], models the dissociation of NH_2 into N and H_2. The Cartesian coordinates defining these geometries may be found in [15]. The geometry of CH_3 is assumed to have always the D_{3h} symmetry [16] with $R_e = 2.06$ bohr, although only the C_{2v} subgroup is exploited in actual CC and CI calculations. Computations are also performed for geometries in which all three C–H bonds are simultaneously stretched to $1.5R_e$ and $2R_e$. Finally, to examine the breaking of multiple bonds, we consider the $^2\Sigma^+$ and $^2\Pi$ states of CN, with experimental equilibrium bond lengths 1.1718 Å and 1.2333 Å [17], respectively. We perform calculations for both the R_e and $1.5R_e$ geometries.

For non-degenerate electronic states, we employ the ROHF orbitals in the same way as in [6]. A slightly different approach is used in the case of degenerate Π states (OH or CN). Due to the current implementation of perturbative corrections for triples, in which a simple Fock matrix for half-closed shell state is used, π orbital degeneracy is not enforced at the self-consistent field (SCF) level. Consequently, the resulting SCF π orbitals are non-degenerate, yielding lower SCF and correlated energies, and leading to a symmetry breaking at the SCF orbital level: we obtain b_1 and b_2 orbitals instead of π_x and π_y orbitals. This causes no problem at the correlated level, since the degeneracy of the total electronic state can be retained if different orbitals are used for different components of the degenerate state. For example, for the $^2\Pi$ state of CN, the SCF orbitals optimized for the configuration [(core) $1b_1^2\ 1b_2^1$], instead of [(core) $1\pi_x^2\ 1\pi_y^1$], have lower $1b_1$ orbital energy. However, if we use SCF orbitals optimized for the configuration [(core) $1b_1^2\ 1b_2^1$] for the $^2B_2$ state, and SCF orbitals optimized for the configuration [(core) $1b_2^2\ 1b_1^1$] for the $^2B_1$ state, then $^2B_1$ and $^2B_2$ become degenerate, i.e. we in fact obtain $^2\Pi_x$ and $^2\Pi_y$. Of course, in actual calculations, only one component needs to be considered.

When considering the vibrational frequencies of N_2^+ and C_2^-, we employ a 6-31G(d) basis set, as in our earlier work [7], as well as Sadlej's [5s3p2d] basis [18] (for N_2^+ only) and an atomic natural orbital (ANO) basis set [5s4p2d1f] of Widmark *et al.* [19]. The latter one is obtained from the ANO [6s5p3d2f] basis set [19] by deleting functions from the right hand side of the tables given in [19]. For both systems, we always employ the ROHF orbitals optimized for the state considered. Inner shell 1s correlation is not important for the equilibrium bond lengths and vibrational frequencies (e.g. they change ω_e by less than 10 cm^{-1}). However, to facilitate the comparison with other results, all electrons are correlated when using the 6-31G(d) basis. On the other hand, to simplify computations, we correlate only the valence electrons (i.e. two core 1s orbitals are kept frozen) when larger [5s3p2d] or ANO [5s4p2d1f] basis sets are used. The force constants, and thus the vibrational harmonic frequencies, are obtained by a twofold numerical differentiation of energies with the

step-size of 0.005 Å. Typical errors arising from the numerical differentiation using at least 5 points do not exceed a few wave numbers.

To avoid possible confusion when presenting our results, we briefly recall the acronyms for various methods and their features. CCSD(is) designates the CC method with interacting space singles and doubles, i.e. with those singly and doubly excited states that are produced by one- and two-electron promotion from the reference and have a non-vanishing CI matrix element with the reference. The CCSD(is) represents a basic method of the UGA-CC series, requiring the smallest computational effort and, consequently, is most often used. Thus, unless the confusion could arise, we simply refer to it as CCSD. When the full SD space is adopted and we solve for all singly and doubly excited cluster amplitudes, including pDs, the method is designated as CCSD(f), i.e. the UGA-CC method with the full SD space. The CCSD(f) calculations are several times more expensive than the CCSD(is) ones. For example, for a general high-spin state of total spin S, the CCSD(f) method requires about $(S+\frac{1}{2})(S+2)$-times as many amplitudes as CCSD(is). Moreover, the CCSD(f) codes are more extensive and complex than the CCSD(is) ones. It is thus advantageous to handle the pseudo-doubles perturbatively, and the resulting method is referred to as CCSD{f} [8]. The computation and assessment of the CCSD(f) and CCSD{f} energy differences is one of the goals of this paper.

The three different perturbative corrections for triples, having the general form

$$\Delta E = \sum_{K}^{T} \Delta_K^{-1} \langle \Psi_{CC}|V|\Phi_K\rangle\langle\Phi_K|V|\Psi_{CC}\rangle, \qquad (2)$$

where the linearized CC wave function is given as $|\Psi_{CC}\rangle = \sum_I t_I|\Phi_I\rangle$, with $\{|\Phi_I\rangle\}$ representing the interacting SD excited state manifold, lead to equation (1) and table 1. Since we always employ the converged CCSD(is) amplitudes when correcting for triples, we do not include the abbreviation 'is' in designating the corresponding CC methods. The different triple correction schemes depend on whether only doubly excited or both doubly and singly excited cluster amplitudes are employed. When both the bra and ket Ψ_{CC} are chosen to involve all the configurations contained in the interacting space for CCSD(is), we get the CCSD{T} approach. When both involve only doubles, we have the CCSD[T] scheme. Finally, when one Ψ_{CC} involves singles and another one does not, we get the CCSD(T) approach [8].

3. Potential energy surfaces for OH, NH_2, CH_3 and CN

We first consider PESs, or symmetric cuts of PESs, corresponding to a simultaneous breaking of one, two or three single bonds, as well as of a single multiple bond. The emphasis is on the difference between the CCSD(f) and CCSD{f} energies and on the performance of various corrections for triples. The merits of CCSD ('is' or 'f') over limited, low order CI (such as CISD) were examined in our earlier study [6], and will not be discussed here. To roughly assess the similarity in the shape of the computed cuts of the PESs, we use the so-called 'non-parallelism error' (NPE) defined as the difference between the maximal and minimal deviations of the total energy of a given method from FCI over the range of geometries considered.

3.1. *The OH radical*

We will start by considering the OH radical, representing a model for breaking of a single bond. The total energies for the degenerate $^2\Pi$ state of the OH radical, obtained with both DZ and DZP basis sets, are given in table 2. In our earlier study [6], the degeneracy of π MOs was enforced by using the C_{4v} symmetry. As already mentioned, only the C_{2v} subgroup is used in the present study, and the resulting symmetry breaking at the SCF level is not expected to cause any problems at the correlated level. As shown in table 2, very little difference is found at the CCSD(is) level when different MOs are used, even though the broken symmetry orbitals lead to a slightly lower energy that is closer to FCI. The difference between the CCSD(f) and CCSD{f} methods is found to be small, both reducing the CCSD(is) error by about a tenth of a millihartree (mhartree) at R_e and by about 2–3 mhartree at $2R_e$. This leads to better CCSD(f) and CCSD{f} potentials with the NPEs smaller than the CCSD(is) one by about 2–3 mhartree.

Considering next the performance of various T_3 correction schemes and using a larger DZP basis as an example, we see that all corrections overcorrect the FCI results. The absolute errors range from less than 0.5 mhartree at R_e and $1.5R_e$, to 2–5 mhartree at $2R_e$, which must be compared with the CCSD(is) errors ranging from 2–5 mhartree at R_e and $1.5R_e$ to almost 13 mhartree at $2R_e$. At R_e, the performance of the three correction schemes can be ordered as CCSD{T} > CCSD(T) > CCSD[T]. At $1.25R_e$–$1.5R_e$, the ordering becomes CCSD(T) > CCSD{T} > CCSD[T], while at $2R_e$ another ordering, namely CCSD(T) > CCSD[T] > CCSD{T}, applies. The performance of various T_3 corrections is better measured in terms of NPEs of the resulting PESs. For example, in the case of a DZP basis, the CCSD(is) and CCSD(f) NPEs are about 10

Table 2. Total energies, reported as $-(E+75)$ hartree, and energy differences relative to FCI, $\Delta E = E - E(\text{FCI})$, obtained with various methods using both DZ and DZP basis sets for the $^2\Pi$ state of OH at four internuclear separations $R = R_e, 1.25R_e, 1.5R_e$ and $2R_e$; $R_e = 1.832$ bohr. Non-parallelism errors[a] (NPEs, in mhartree) are given in the last row.

	$-(E+75)$/au				$\Delta E = E - E(\text{FCI})$/mhartree				
Method	R_e	$1.25R_e$	$1.5R_e$	$2R_e$	R_e	$1.25R_e$	$1.5R_e$	$2R_e$	NPE[a]
DZ [4s2p/2s] basis/C_{4v} symmetry									
CCSD(is)[b]	0.479 995	0.460 256	0.420 935	0.367 113	1.229	1.759	2.755	5.646	4.417
CCSD(f)[b]	0.480 042	0.460 347	0.421 176	0.369 150	1.182	1.668	2.514	3.609	2.427
DZ [4s2p/2s] basis/C_{2v} symmetry									
CCSD(is)	0.480 028	0.460 298	0.420 986	0.367 113	1.196	1.717	2.704	5.646	4.450
CCSD{f}	0.480 076	0.460 394	0.421 252	0.369 196	1.148	1.621	2.438	3.563	2.415
CCSD{T}	0.481 056	0.461 836	0.423 758	0.376 953	0.168	0.179	−0.068	−4.194	4.373
CCSD(T)	0.481 224	0.461 985	0.423 757	0.374 787	0.000	0.030	−0.067	−2.028	2.058
CCSD[T]	0.481 511	0.462 368	0.424 313	0.375 949	−0.287	−0.353	−0.623	−3.190	2.903
FCI	0.481 224	0.462 015	0.423 690	0.372 759	0.000	0.000	0.000	0.000	0.000
DZP [4s2p1d/2s1p] basis/C_{4v} symmetry									
CCSD(is)[b]	0.565 531	0.535 566	0.486 989	0.419 894	2.484	3.360	5.111	12.751	10.267
CCSD(f)[b]	0.565 659	0.535 784	0.487 482	0.422 908	2.356	3.142	4.618	9.737	7.381
DZP [4s2p1d/2s1p] basis/C_{2v} symmetry									
CCSD(is)	0.565 575	0.535 621	0.487 054	0.419 946	2.440	3.305	5.046	12.699	10.259
CCSD{f}	0.565 719	0.535 858	0.487 562	0.422 653	2.296	3.068	4.538	9.992	7.696
CCSD{T}	0.568 216	0.539 122	0.492 497	0.438 174	−0.201	−0.196	−0.397	−5.529	5.333
CCSD(T)	0.568 250	0.539 083	0.492 168	0.434 991	−0.235	−0.157	−0.068	−2.346	2.278
CCSD[T]	0.568 520	0.539 438	0.492 647	0.435 743	−0.505	−0.512	−0.547	−3.098	2.593
FCI	0.568 015	0.538 926	0.492 100	0.432 645	0.000	0.000	0.000	0.000	0.000

[a] The non-parallelism error (NPE) for a given potential is defined as the difference between the maximal and minimal deviation from the FCI potential.
[b] Reference [6].

and 7 mhartree, respectively. With (T) or [T] correction schemes these NPEs are reduced to about 2 mhartree (in absolute terms), even though the {T} correction gives a slightly larger NPE of about 5 mhartree. It should be noted, however, that the resulting PESs in the vicinity of the equilibrium geometry differ by an almost constant shift from the FCI PES. The NPEs for the region from R_e to $1.25R_e$ are 0.005 ($= -0.196 + 0.201$; see table 2), 0.078 and 0.007 mhartree for {T}, (T) and [T] corrections, respectively. These are considerably smaller than the NPEs obtained with the CCSD(is), (f) or {f} schemes in the same region, which range from 0.8 to 0.9 mhartree. This indicates that various T_3 corrections provide excellent results in the vicinity of the equilibrium geometry.

3.2. *The NH_2 radical*

We next consider the NH_2 radical, for which we explored both the $^2B_1$ ground state and the lowest excited, totally symmetric $^2A_1$ state. The total energies obtained for the $^2A_1$ and $^2B_1$ states of NH_2 with various CC methods using a DZ and a DZP basis sets are given in tables 3 and 4, respectively. The FCI results [15] are included for comparison. Consider first the $^2A_1$ state. We see that CCSD(f) provides a better approximation than CCSD ≡ CCSD(is), as does CCSD{f}. In fact, it makes very little difference whether we treat pseudo-doubles iteratively or non-iteratively: the differences between the CCSD(f) and CCSD{f} energies are 0, 0.044, 0.825, and −0.040 mhartree at the equilibrium, 50% stretched, 100% stretched, and N···H–H geometries, respectively. Similar situation is found with a DZP basis, the differences being, respectively, 0.010, 0.108, 0.493 and −0.018 mhartree. In the case of the $^2B_1$ state, we find similar results, except that with a DZ basis set neither CCSD(is) nor CCSD(f) converges at $2R_e$. Again, we find that the differences between the CCSD(f) and CCSD{f} energies are very small.

We next assess the performance of various corrections for triples. At the equilibrium geometry and for both the $^2A_1$ and $^2B_1$ states, the CCSD(is) errors are about 1.3 mhartree for a DZ and 3 mhartree for a DZP basis. The errors of all three T_3 correction schemes are less than 0.1 mhartree for a DZ basis and −0.5 mhartree for a DZP basis. Thus at R_e, all T_3 corrections are very similar. An almost identical performance of the

Table 3. Total energies, reported as $-(E+55)$ hartree, and energy differences relative to FCI, $\Delta E = E - E(\mathrm{FCI})$, obtained with various methods using both DZ and DZP basis sets for the $^2A_1$ state of NH_2 at the equilibrium and stretched geometries (see the text for details).

	$-(E+55)$ /au				$\Delta E = E - E(\mathrm{FCI})$ /mhartree				
Method	R_e	$1.5R_e$	$2R_e$	N···H_2	R_e	$1.5R_e$	$2R_e$	N···H_2	NPE[a]
DZ [4s2p/2s] basis									
CCSD(is)	0.602 126	0.444 781	0.339 515	0.454 784	1.278	5.065	16.251	7.335	14.973
CCSD(f)	0.602 203	0.445 157	0.341 375	0.454 892	1.201	4.689	14.391	7.227	13.190
CCSD{f}	0.602 203	0.445 201	0.342 200	0.454 852	1.201	4.645	13.566	7.267	12.365
CCSD{T}	0.603 254	0.449 709	0.353 871	0.459 355	0.150	0.137	1.895	2.764	2.627
CCSD(T)	0.603 297	0.449 550	0.352 876	0.459 328	0.107	0.296	2.890	2.791	2.783
CCSD[T]	0.603 437	0.449 825	0.354 716	0.459 344	−0.033	0.021	1.050	2.775	2.808
FCI[b]	0.603 404	0.449 846	0.355 766	0.462 119	0.000	0.000	0.000	0.000	0.000
DZP [4s2p1d/2s1p] basis									
CCSD(is)	0.685 728	0.509 736	0.389 703	0.523 390	3.034	7.878	25.430	12.691	22.396
CCSD(f)	0.685 946	0.510 310	0.393 984	0.523 540	2.816	7.304	21.149	12.541	18.333
CCSD{f}	0.685 956	0.510 418	0.394 477	0.523 522	2.806	7.196	20.656	12.559	17.850
CCSD{T}	0.689 067	0.517 670	0.412 087	0.531 885	−0.305	−0.056	3.046	4.196	4.501
CCSD(T)	0.688 956	0.517 370	0.409 885	0.531 738	−0.194	0.244	5.248	4.343	5.442
CCSD[T]	0.688 982	0.517 463	0.412 279	0.531 711	−0.220	0.151	2.854	4.370	4.590
ROHF CCSD[c]	0.685 713	0.509 696	0.390 892		3.049	7.918	24.241		21.192
ROHF CCSD(T)[c]	0.688 212	0.515 408	0.403 733		0.550	2.206	11.400		10.850
UHF CCSD(T)[c]	0.688 230	0.515 422	0.405 106		0.532	2.192	10.027		9.495
UHF CCSDT[c]	0.688 539	0.516 803	0.413 640		0.223	0.811	1.493		1.270
FCI[b]	0.688 762	0.517 614	0.415 133	0.536 081	0.000	0.000	0.000	0.000	0.000

[a] The non-parallelism error (NPE) is defined as the difference between the maximal and minimal deviation from FCI.
[b] Reference [15].
[c] Reference [9].

Table 4. Total energies, reported as $-(E+55)$ hartree, and energy differences relative to FCI, $\Delta E = E - E(\mathrm{FCI})$, obtained with various methods using both DZ and DZP basis sets for the $^2B_1$ state of NH_2 at the equilibrium and stretched geometries (see the text for details).

	$-(E+55)$ /au				$\Delta E = E - E(\mathrm{FCI})$ /mhartree				
Method	R_e	$1.5R_e$	$2R_e$	N···H_2	R_e	$1.5R_e$	$2R_e$	N···H_2	NPE
DZ [4s2p/2s] basis									
CCSD(is)	0.644 689	0.530 372	[a]	0.469 990	1.339	4.437		2.756	
CCSD(f)	0.644 826	0.530 886	[a]	0.470 077	1.202	3.923		2.669	
CCSD{f}	0.644 819	0.530 897		0.470 044	1.209	3.912		2.702	
CCSD{T}	0.646 024	0.536 085		0.472 425	0.004	−1.276		0.321	
CCSD(T)	0.646 024	0.535 754		0.472 421	0.004	−0.945		0.325	
CCSD[T]	0.646 113	0.536 185		0.472 488	−0.085	−1.376		0.258	
FCI[b]	0.646 028	0.534 809	0.449 427	0.472 746	0.000	0.000	0.000	0.000	
DZP [4s2p1d/2s1p] basis									
CCSD(is)	0.739 353	0.596 240	0.486 051	0.538 385	3.267	8.969	19.473	6.175	16.206
CCSD(f)	0.739 605	0.597 205	[a]	0.538 533	3.015	8.004		6.027	
CCSD{f}	0.739 609	0.597 152	0.494 238	0.538 515	3.011	8.057	11.286	6.045	8.275
CCSD{T}	0.743 160	0.606 831	0.526 134	0.543 559	−0.540	−1.622	−20.610	1.001	21.611
CCSD(T)	0.742 987	0.606 059	0.519 488	0.543 423	−0.367	−0.850	−13.964	1.137	15.101
CCSD[T]	0.742 994	0.606 389	0.521 051	0.543 441	−0.374	−1.180	−15.527	1.119	16.646
FCI[b]	0.742 620	0.605 209	0.505 524	0.544 560	0.000	0.000	0.000	0.000	0.000

[a] Not able to converge using the ROHF orbitals.
[b] Reference [15].

three different T_3 corrections is also found for the N···H–H geometries. They always provide a great improvement over CCSD(is), reducing its error from 7.3 to 2.8 mhartree ($^2A_1$/DZ), 12.7 to 4.3 mhartree ($^2A_1$/DZP), 2.8 to 0.3 mhartree ($^2B_1$/DZ) and 6.2 to 1.1 mhartree ($^2B_1$/DZP), with a very little difference between them. Once the bond is stretched to $1.5R_e$, the CCSD(is) errors are about 4–5 mhartree for DZ and 8–9 mhartree for DZP basis. When the T_3 corrections are applied, these errors are reduced to less than 0.3 mhartree for the $^2A_1$ state and both DZ and DZP basis sets. For the $^2B_1$ state, the CCSD{T}, CCSD(T) and CCSD[T] errors are −1.3, −0.9 and −1.4 mhartree for DZ, and −1.6, −0.9 and −1.2 mhartree for DZP basis, respectively. When the bonds are further stretched to $2R_e$, we face certain complications. For the $^2A_1$ state, the CCSD{T}, CCSD(T), and CCSD[T] schemes reduce the CCSD(is) errors relative to FCI from 16.3 mhartree to 1.9, 2.9 and 1.1 mhartree for a DZ basis, and from 25.4 mhartree to 3.0, 5.2 and 2.9 mhartree for a DZP basis, respectively. However, for the $^2B_1$ state and a DZP basis, the CCSD(is) error amounts to 19.4 mhartree, while the T_3 corrections grossly overshoot, with the errors amounting to −20.6, −14.0 and −15.5 mhartree for the {T}, (T), and [T] approximations, respectively. We may thus conclude that CCSD{T}, CCSD(T) and CCSD[T] give similar results for a moderate bond stretching of two single bonds. When these bonds are severely stretched, these methods may overcorrect. If they do not overcorrect, CCSD{T} and CCSD[T] yield similar and better energies than CCSD(T). When they do overcorrect, CCSD(T) may be better since it overcorrects less. In any case, we cannot expect these methods to work when we are far away from the equilibrium geometries, just as in CS cases.

The above described performance of various T_3 corrections can be better assessed using the NPEs of the resulting PESs. Consider, for example, the results obtained with a DZP basis set. For the $^2A_1$ state, the NPEs of various CCSD approximations are about 20 ± 2 mhartree. With T_3 corrections, these NPEs are reduced to about 5 ± 0.5 mhartree, i.e. they are nearly 75% smaller than those obtained with the CCSD(is), (f) or {f} methods. For near equilibrium geometries (from R_e to $1.5R_e$), the NPEs of various T_3 correction schemes are less than 0.5 mhartree in absolute terms, that is an order of magnitude smaller than the CCSD NPEs (which are about 4.4–4.8 mhartree) for the same region. The situation for the $^2B_1$ state is more complicated due to the convergency difficulties encountered at $2R_e$. Nonetheless, considering PESs between R_e and $1.5R_e$, the NPEs with triple corrections are less than 1.1 mhartree. In comparison, the CCSD(is), (f) and {f} NPEs are about 5–6 mhartree.

Both states of the DZP model of the NH_2 radical considered above were also extensively treated in [9] using various ROHF and UHF based CC approaches involving triples, including CCSDT. For the sake of easier comparison, we include in table 3 a few typical results from this reference for a DZP model of the $^2A_1$ state. Not surprisingly, the ROHF CCSD results [9] are very close to our UGA CCSD(is) ones. When triples are handled perturbatively, both the ROHF- and UHF-based results [9] (which are in fact very similar) are inferior to ours. Although we do not find much of a difference at the equilibrium geometry, already at $1.5R_e$ the (ROHF, UHF)-CCSD(T) errors are an order of magnitude larger than the UGA CCSD(T), [T] or {T} ones (2.2 mhartree versus at most 0.2 mhartree). At $2R_e$, these errors increase to about 10–11 mhartree [9], while those of the UGA-based perturbatively corrected triples are only 3–5 mhartree. Clearly, different formulations of triple corrections may lead to significant differences at severely stretched geometries.

As might be expected, the computationally demanding full UHF CCSDT method [9] performs better than any perturbatively based estimate at larger internuclear separations (NPE for the $^2A_1$ state is 1.270 mhartree). Surprisingly enough, this is not the case in the immediate neighbourhood of the equilibrium geometry (up to $1.5R_e$), where any of our estimates (i.e. CCSD(T), [T] or {T}) is better than the full UHF CCSDT.

The results in [9] for the $^2B_1$ state are much more complicated. For example, there are two UHF solutions, either of which can be employed as a reference. However, not all CC methods converge when these two UHF references are employed. For instance, CCSDT converges neither with ROHF nor with one of the UHF references. The spin contamination also appears to be much more serious in this case. For all these reasons we do not include these results [9] for the $^2B_1$ state in our tables and the interested reader is referred to the original paper for more details.

3.3. *The CH_3 radical*

We next consider a simultaneous breaking of three single bonds. Total energies obtained for the $^2A_2''$ state of the CH_3 radical, using CCSD plus various T_3 corrections are given in table 5. At the equilibrium geometry, the difference between the CCSD(f) and CCSD{f} energies is very small, both improving CCSD(is) by about 0.2–0.3 mhartree. Relative to the FCI values, the CCSD(is) energies deviate by about 1 mhartree for a DZ basis and by about 2.8 mhartree for a DZP basis.

Table 5. Total energies, reported as $-(E+39)$ hartree, as well as energy differences relative to FCI, $\Delta E = E - E(\mathrm{FCI})$, obtained with various methods using both DZ and DZP basis sets for the $^2A_2''$ state of CH_3 at the equilibrium ($R_{CH} = R_e = 2.06$ bohr) and stretched ($R_{CH} = 1.5R_e$ and $2R_e$) geometries.

	$-(E+39)$/au			$\Delta E = E - E(\mathrm{FCI})$/mhartree			
Method	R_e	$1.5R_e$	$2R_e$	R_e	$1.5R_e$	$2R_e$	NPE
DZ [4s2p/2s] basis							
CCSD(is)	0.643 420	0.423 891	0.228 724	1.253	6.773	34.292	33.039
CCSD(f)	0.643 593	0.425 060	0.232 434	1.080	5.604	30.582	29.502
CCSD{f}	0.643 576	0.424 927	0.231 340	1.097	5.737	31.676	30.579
CCSD{T}	0.644 750	0.431 121	0.269 606	−0.077	−0.457	−6.590	6.513
CCSD(T)	0.644 700	0.430 965	0.269 148	−0.027	−0.301	−6.132	6.105
CCSD[T]	0.644 718	0.431 404	0.269 784	−0.045	−0.740	−6.768	6.723
FCI	0.644 673	0.430 664	0.263 016	0.000	0.000	0.000	0.000
DZP [4s2p1d/2s1p] basis							
CCSD(is)	0.718 378	0.473 724	0.264 401	2.834	9.129	38.731	35.897
CCSD(f)	0.718 649	0.474 829	0.267 553	2.563	8.024	35.579	33.016
CCSD{f}	0.718 636	0.474 762	0.266 990	2.576	8.091	36.142	33.566
CCSD{T}	0.721 570	0.483 692	0.309 721	−0.358	−0.839	−6.589	6.231
CCSD(T)	0.721 392	0.483 261	0.308 951	−0.180	−0.408	−5.819	5.639
CCSD[T]	0.721 375	0.483 671	0.309 734	−0.163	−0.818	−6.602	6.439
ROHF CCSD[a]	0.718 363	0.474 010	0.265 810	2.849	8.843	37.322	34.473
ROHF CCSD(T)[a]	0.720 694	0.480 740	0.292 148	0.518	2.113	10.984	10.466
UHF CCSD(T)[a]	0.720 713	0.480 184	0.332 040	0.499	2.669	−28.908	29.407
ROHF CCSDT[a]	0.721 934	0.482 991	0.298 730	−0.722	−0.138	4.402	5.124
UHF CCSDT[a]	0.721 956	0.482 961	0.301 4	−0.744	−0.108	1.732	2.476
FCI[b]	0.721 212	0.482 853	0.303 132	0.000	0.000	0.000	0.000

[a] Reference [9].
[b] Reference [16].

These errors are reduced to less than −0.1 mhartree (DZ basis) and (−0.2)–(−0.4) mhartree (DZP basis) with all three T_3 corrections. When the three C–H bonds are stretched by 50%, CCSD(f) or CCSD{f} reduce the CCSD(is) errors (amounting to 6.8 mhartree for DZ and 9.1 mhartree for DZP basis) by about 1.1 mhartree with either basis set, while the T_3 corrected values are still less than −0.8 mhartree in error. The differences between the FCI and CCSD(is) energies are considerably larger at $2R_e$ (34.3 mhartree for DZ and 38.7 mhartree for DZP basis). Using the full SD space in CCSD(f) or CCSD{f} approaches, these errors are reduced by about 3–4 mhartree. The T_3 corrected values are about (−6)–(−7) mhartree in error at $2R_e$. It is again difficult to establish a definite ordering of the performance of T_3 corrections. At the equilibrium geometry, CCSD(T) and CCSD[T] give similar and better results than CCSD{T}, while at stretched ($1.5R_e$ and $2R_e$) geometries, CCSD{T} and CCSD[T] are similar and poorer than CCSD(T). This suggests that CCSD(T) performs best in most cases. Nonetheless, the differences between different T_3 correction schemes are less than 1 mhartree in all cases, so that this ordering is not very significant. In terms of the NPEs of the resulting PESs, we find again a substantial reduction from about 33–36 mhartree for various CCSD methods to about 6 ± 0.4 mhartree for the T_3 corrected methods. Also, the NPEs of T_3 corrected PESs in the vicinity of the equilibrium geometry are very small.

The CH_3 system was also examined in [9] using the same DZP basis set. For the sake of comparison, we included the ROHF-based CCSD, CCSD(T), and CCSDT results, as well as the UHF-based CCSD(T) and CCSDT results, in table 5. We see again that the ROHF CCSD results [9] are very close to those obtained with UGA CCSD(is). However, both perturbative CCSD(T) approaches [9], based on either the ROHF or the UHF reference, give much poorer results in this case than our UGA based triply corrected CCSD: NPEs for these results [9] are 10.466 and 29.407 mhartree (for the ROHF and UHF based CCSD(T), respectively), while those for UGA based approaches do not exceed 6.4 mhartree (see table 5). In fact the errors of perturbatively corrected methods at $2R_e$ seem to be very sensitive to the formulation employed. Thus, the ROHF-CCSD(T) error at $2R_e$ is 11 mhartree, while the UHF-CCSD(T) error has an opposite sign and equals −29 mhartree [9]. The errors of UGA based perturbative

Table 6. Total energies obtained with various methods using both DZ and DZP basis sets, reported as $-(E+92)$ hartree, for the $^2\Sigma^+$ state of CN at equilibrium ($R_e = 1.1718$ Å) and stretched ($R = 1.5R_e$) geometries.

	$-(E+92)$ /au		ΔE[a] /mhartree	
Method	R_e	$1.5R_e$	R_e	$1.5R_e$
DZ [4s2p] basis				
CCSD(is)	0.358 931	0.190 620	9.963	35.661
CCSD(f)	0.359 796	0.191 860	9.098	34.421
CCSD{f}	0.359 992	0.193 155	8.902	33.126
CCSD{T}	0.370 649	0.240 413	−1.755	−14.132
CCSD(T)	0.368 867	0.239 228	0.027	−12.947
CCSD[T]	0.373 971	0.280 212	−5.077	−53.931
CISDT$^+$	0.356 309	0.187 069	12.585	39.212
CISDTQ$^+$	0.367 643	0.218 131	1.251	8.150
nFCI[b]	0.368 894	0.226 281	0.000	0.000
DZP [4s2p1d] basis				
CCSD(is)	0.479 111	0.279 037	13.320	31.013
CCSD(f)	0.480 710	0.280 764	11.721	29.286
CCSD{f}	0.481 537	0.282 653	10.894	27.397
CCSD{T}	0.502 494	0.346 369	−10.063	−36.319
CCSD(T)	0.498 247	0.337 801	−5.816	−27.751
CCSD[T]	0.502 770	0.373 118	−10.339	−63.068
CISDT$^+$	0.471 554	0.272 978	20.877	37.072
CISDTQ$^+$	0.492 431	0.310 050	0.000	0.000

[a] ΔE is $E - E$(nFCI) and $E - E$(CISDTQ$^+$) in the case of DZ and DZP basis sets, respectively.
[b] nFCI ≡ (near FCI) = CISDTQQS$^+$.

approaches are around −6 mhartree, being roughly in the middle between the ROHF-CCSD(T) and UHF-CCSD(T) ones.

We can also compare our results with the full treatment of triples given in [9]. In this case the authors [9] obtained the CCSDT results with both the ROHF and UHF references. The latter result gives the smallest NPE (2.476 mhartree), about a factor of two smaller than the ROHF CCSDT NPE (5.124 mhartree), which is of the same order of magnitude as the NPEs of our perturbatively corrected results (ranging from 5.6 to 6.4 mhartree). This is very gratifying in view of the great difference between the computational demands of the approaches involved.

3.4. *The CN radical*

We have chosen the cyanide radical, CN, to examine the breaking of a multiple bond, in both its ground $^2\Sigma^+$ and excited $^2\Pi$ states. This is a demanding system since the correct description of its separated limit requires sixfold excitations. We thus examine only $R = R_e$ and $R = 1.5R_e$ geometries. Total energies obtained for the $^2\Sigma^+$ and $^2\Pi$ states of CN with the CCSD and various T_3 corrected methods, for both DZ and DZP basis sets,

Table 7. Total energies obtained with various methods using both DZ and DZP basis sets, reported as $-(E+92)$ hartree, for the $^2\Pi$ state of CN at the equilibrium ($R_e = 1.2333$ Å) and stretched ($R = 1.5R_e$) geometries.

	$-(E+92)$ /au		ΔE[a] /mhartree	
Method	R_e	$1.5R_e$	R_e	$1.5R_e$
DZ [4s2p] basis/C_{4v} symmetry				
CCSD(is)[b]	0.305 519	0.193 791	7.433	17.150
CCSD(f)[b]	0.305 653	0.199 093	7.299	11.848
DZ [4s2p] basis/C_{2v} symmetry				
CCSD(is)	0.305 702	0.193 423	7.250	17.518
CCSD{f}	0.305 869	0.199 290	7.083	11.651
CCSD{T}	0.312 093	0.249 456	0.859	−38.515
CCSD(T)	0.312 392	0.243 992	0.560	−33.051
CCSD[T]	0.313 424	0.280 037	−0.472	−69.096
CISDT$^+$	0.302 814	0.178 484	10.138	32.457
CISDTQ$^+$	0.312 250	0.202 114	0.702	8.827
nFCI[c]	0.312 952	0.210 941	0.000	0.000
DZP [4s2p1d] basis/C_{4v} symmetry				
CCSD(is)[b]	0.444 664	0.284 816	9.348	23.581
CCSD(f)[b]	0.445 036	0.289 096	8.976	19.301
DZP [4s2p1d] basis/C_{2v} symmetry				
CCSD(is)	0.444 778	0.284 628	9.234	23.769
CCSD{f}	0.445 278	0.289 996	8.734	18.401
CCSD{T}	0.456 133	0.352 342	−2.121	−43.945
CCSD(T)	0.455 943	0.352 343	−1.931	−43.946
CCSD[T]	0.456 675	0.362 780	−2.663	−54.383
CISDT$^+$	0.440 296	0.277 049	13.716	31.348
CISDTQ$^+$	0.454 012	0.308 397	0.000	0.000

[a] ΔE is $E - E$(nFCI) and $E - E$(CISDTQ$^+$) in the case of DZ and DZP basis sets, respectively.
[b] Reference [6].
[c] nFCI ≡ (near FCI) = CISDTQQS$^+$.

are given in tables 6 and 7. The FCI values are not available for either basis set. For a DZ basis, the largest CI we can carry out is CISDTQQS$^+$ with ∼420 000 configurations, which can be regarded as a 'near FCI' (nFCI) result. For a DZP basis, we performed CISDTQ$^+$ with ∼680 000 configurations. This gives us better benchmarks than those used in our previous study [6]. Nonetheless, CISDTQ$^+$ is still not a good enough benchmark for the CN radical. As we can see in the case of a DZ basis for the $^2\Sigma^+$ state, nFCI decreases the CISDTQ$^+$ energies by about 1 mhartree at R_e, and about 8 mhartree at $1.5R_e$. Similarly, for the $^2\Pi$ state, the nFCI energy is lower than the CISDTQ$^+$ by about 9 mhartree at $1.5R_e$.

For the $^2\Sigma^+$ state of CN at $R = R_e$, the CCSD(is) and CCSD(f) or CCSD{f} energy differences amount to about 1 and 1.5 mhartree for a DZ and a DZP basis sets, respectively. These differences moderately increase

to 1.3–2.6 mhartree for a DZ basis and to 1.7–2.6 mhartree for a DZP basis once the C–N bond is stretched by 50%, the CCSD{f} energies being about 1 mhartree better than the CCSD(f) ones. The actual CCSD(is), CCSD(f) and CCSD{f} energies lie between the CISDT$^+$ and CISDTQ$^+$ ones at both $R = R_e$ and $1.5R_e$. Relative to nFCI (DZ basis), the CCSD(is), CCSD(f) and CCSD{f} errors are about 10 mhartree at R_e and 36 mhartree at $1.5R_e$. However, as we have mentioned earlier, no proper benchmarks are available for our DZP basis, since the nFCI is already 8 mhartree lower than CISDTQ$^+$ at $1.5R_e$ for a DZ basis. Further, the inclusion of T_3 corrections significantly improves the results in most cases. At $R = R_e$ and a DZ basis, the CCSD{T}, CCSD(T) and CCSD[T] errors relative to nFCI are −1.8, 0.03 and −5.1 mhartree, respectively. Since nFCI is still not FCI, the actual CCSD(T) error will be larger and the overcorrection by CCSD{T} and CCSD[T] smaller. At $1.5R_e$, the CCSD{T}, CCSD(T) and CCSD[T] schemes overcorrect the nFCI result by 14.1, 12.9 and 53.9 mhartree. It is notable that the CCSD[T] error at $1.5R_e$ is quite large, while the performance of CCSD{T} and CCSD(T) is very similar. Although CCSD(T) may appear to give a slightly better result than CCSD{T}, the errors relative to the R_e energies moderately favour CCSD{T} (12.4 versus 13 mhartree). Nonetheless, lacking an appropriate benchmark, we cannot be certain if these observations are true for a larger basis as well. For example, in the case of a DZP basis, CCSD(T) appears to be better than CCSD{T}.

Finally, we consider the results for the degenerate $^2\Pi$ state, given in table 7. We observe again that the use of broken symmetry π MOs leads to only a small difference in the resulting CCSD(is) energies. Both CCSD(f) and CCSD{f} perform similarly, and the energy differences between CCSD(is) and CCSD(f) or CCSD{f} are much smaller than for the $^2\Sigma^+$ state at $R = R_e$ (0.1–0.2 and 0.3–0.5 mhartree for DZ and DZP bases, respectively), but increase much faster once the C–N bond is stretched: at $R = 1.5R_e$, these differences are 4.3–5.8 mhartree. At either geometry (R_e or $1.5R_e$), the CCSD(is), CCSD(f) and CCSD{f} energies lie between the CISDT$^+$ and CISDTQ$^+$ energies. Different T_3 corrections yield similar results at R_e: the absolute errors of the three corrections relative to nFCI are less than 1 mhartree for the DZ basis. They overshoot CISDTQ$^+$ by 2–3 mhartree in the case of a DZP basis, but those CI results may still be above FCI by 1–2 mhartree. At $1.5R_e$, T_3 corrections certainly overshoot by a sizeable amount: for a DZ basis, the CCSD{T}, CCSD(T), and CCSD[T] schemes overcorrect nFCI by 38.5, 33.1 and 69.1 mhartree respectively. This indicates that the T_3 correction schemes give worse results than the simple CCSD{f} or even CCSD(is) method when a multiple bond is severely stretched.

Table 8. Non-parallelism error (NPE, in mhartree) for the region ranging from R_e to $1.5R_e$ obtained with various methods using a DZP basis for OH, NH_2 and CH_3.

Method	OH($^2\Pi$)	NH_2($^2A_1$)	NH_2($^2B_1$)	CH_3($^2A_2''$)
CCSD(is)	2.606	4.844	5.702	6.295
CCSD(f)	2.262	4.488	4.989	5.461
CCSD{f}	2.242	4.390	5.046	5.515
CCSD{T}	0.201	0.249	1.082	0.481
CCSD(T)	0.167	0.438	0.483	0.238
CCSD[T]	0.042	0.371	0.806	0.655

3.5. *Performance in the vicinity of the equilibrium geometry*

We conclude this section by illustrating the performance of various T_3 corrections in the vicinity of the equilibrium geometry. We present in table 8 the non-parallelism errors of the resulting PESs for the region ranging from R_e to $1.5R_e$ for OH, NH_2 and CH_3. Only the results obtained with DZP basis sets are included. These data clearly show that the NPEs of various T_3 corrected schemes are about an order of magnitude smaller than those obtained with various CCSD approximations.

4. Harmonic vibrational frequencies of N_2^+ and C_2

We next address the computation of molecular harmonic vibrational frequencies, ω_e, which are known to provide a rather severe test of any method. Our earlier study [7] of 48 distinct electronic states of 9 diatomic hydrides and 18 diatomics, using the UGA-CCSD method and 6-31G(d) basis sets, nicely demonstrates the power of this method in reproducing experimental vibrational frequencies. For diatomic hydrides, for example, the mean absolute deviation in the bond length and harmonic frequencies amounted to 0.013 Å and 55 cm^{-1}, respectively. Similarly, for diatomics these average deviations were 0.012 Å and 73 cm^{-1}, respectively.

However, we also found several examples for which the difference between the computed and experimental ω_e values was considerably larger. For example, the largest difference between the computed and experimental ω_e values for diatomics, which amounts to 203 cm^{-1}, is found for the $B\,^2\Sigma_u^+$ state of N_2^+, a value almost three times the mean absolute deviation. Similarly, the difference between the computed and experimental ω_e for the $B\,^2\Sigma_u^+$ state of the isoelectronic C_2^- radical is 132 cm^{-1}, nearly twice the mean absolute deviation. Clearly, these two systems deserve a closer examination.

Table 9. Equilibrium bond lengths R_e (in Å) and harmonic vibrational frequencies ω_e (in cm^{-1}) of the ground and excited states of N_2^+ obtained with UGA CCSD(is) method and various basis sets. The differences are defined as $\Delta R_e = R_e(\text{cal.}) - R_e(\text{exp.})$ and $\Delta\omega_e = \omega_e(\text{cal.}) - \omega_e(\text{exp.})$.

State	Method	Basis	R_e /Å	ΔR_e /mÅ	ω_e /cm^{-1}	$\Delta\omega_e$ /cm^{-1}
$B\,^2\Sigma_u^+$	CCSD(is)	6-31G(d)	1.082	8	2623	203
		[5s3p2d][a]	1.084	10	2572	152
		ANO[b]	1.065	−9	2646	226
	Exp.[c]		1.074		2420	
$A\,^2\Pi_{ui}^+$	CCSD(is)	6-31G(d)	1.184	9	1988	84
		[5s3p2d][a]	1.191	16	1943	39
		ANO[b]	1.172	−3	1988	84
	Exp.[c]		1.175		1904	
$X\,^2\Sigma_g^+$	CCSD(is)	6-31G(d)	1.129	13	2267	60
		[5s3p2d][a]	1.133	17	2220	13
		ANO[b]	1.115	−1	2274	67
	Exp.[c]		1.116		2207	

[a] Reference [18].
[b] [5s4p2d1f] ANO basis from [19].
[c] Reference [17].

In order to find out whether these rather large discrepancies are due to the limitations of the basis sets employed or due to the approximations involved in the methods used, we first consider three states ($X\,^2\Sigma_g^+$, $A\,^2\Pi_{ui}$, $B\,^2\Sigma_u^+$) of N_2^+, using the interacting space UGA-CCSD method and three basis sets, namely a 6-31G(d) basis, a [5s3p2d] basis [18] and an atomic natural orbital (ANO) basis of the [5s4p2d1f] type [19]. The results are given in table 9. The [5s3p2d] basis yields slightly longer bond lengths and smaller frequencies (about 45–50 cm^{-1} smaller) than those obtained with the 6-31G(d) basis. The agreement with the experimental values is thus better by the same amounts. Even so, for the $B\,^2\Sigma_u^+$ state, the discrepancy amounts to 152 cm^{-1}. When using yet a better ANO basis set, a kind of a basis set that is highly versatile and gives generally very accurate results, the computed bond lengths are slightly shorter than the experimental ones, while the computed ω_e are roughly identical and even slightly poorer than those obtained with the 6-31G(d) basis. Clearly, use of a better basis set does not necessarily improve the computed frequencies and we must use better methods to reduce the discrepancies.

To calibrate the performance of various methods, we carried out a series of CI and CC calculations using a relatively small basis set for which the FCI results are available. Unfortunately, we do not have computational resources to carry out FCI calculations with the 6-31G(d) basis. Instead, we used a smaller DZV [3s2p] basis set [20], which yields the results given in table 10. We must emphasize, however, that due to the absence of polarization functions, these results are of a purely methodological value and cannot be used for a comparison with the experiment. We should also point out that the errors in computed ω_e relative to FCI found with a DZV basis cannot be used to infer the size of the errors for larger basis sets, particularly for the $B\,^2\Sigma_u^+$ state, since for larger basis sets the errors of any approximation relative to FCI will be smaller. This can be illustrated, for example, on the SCF method. For the $B\,^2\Sigma_u^+$ state, the ROHF ω_e is almost 1000 cm^{-1} larger than the FCI ω_e when using a DZV basis. We carried out a series of calculations using the SCF method with increasingly larger basis sets [21]. Our estimate for the ROHF ω_e in the basis set limit is 3090 cm^{-1}, 670 cm^{-1} larger than the experimental value (which should be equivalent to the FCI result in the basis set limit). Hence, the error in computed ROHF ω_e for the $B\,^2\Sigma_u^+$ state in the basis set limit is about 330 cm^{-1} smaller than the error with a DZV basis.

As shown in table 10, the errors of the SCF result with a DZV basis (relative to FCI) are very large, in particular for ω_e: these errors are 465, 737 and 997 cm^{-1} for the $X\,^2\Sigma_g^+$, $A\,^2\Pi_u$ and $B\,^2\Sigma_u^+$ states, respectively. The error for the $B\,^2\Sigma_u^+$ state is by far the largest. Even at the CISD level, the errors in ω_e remain sizeable, amounting to 212, 219 and 595 cm^{-1}, respectively. At the CISDT and CISDTQ levels, these errors are still about 200 and 100 cm^{-1}. These results clearly show the challenge in computing of vibrational frequencies. Turning our attention to the CC methods, the errors of the CCSD ω_e are 88, 118 and 348 cm^{-1} for the $X\,^2\Sigma_g^+$, $A\,^2\Pi_u$ and $B\,^2\Sigma_u^+$ states, respectively. This explains why the maximum error was found for the $B\,^2\Sigma_u^+$ state of N_2^+ in our earlier calculations [7]. When corrected perturbatively for pseudo-doubles (i.e. three-

Table 10. Equilibrium bond lengths R_e (in Å) and harmonic vibrational frequencies ω_e (in cm^{-1}) of the ground and excited states of N_2^+ obtained with DZV [3s2p] basis set and various methods. Differences from the FCI values are given in parentheses.

	$X\,^2\Sigma_g^+$		$A\,^2\Pi_u$		$B\,^2\Sigma_u^+$	
Method	R_e	ω_e	R_e	ω_e	R_e	ω_e
FCI	1.173	1948	1.249	1591	1.137	1991
SCF	1.115	2413	1.171	2328	1.055	2988
	(−58)	(465)	(−78)	(737)	(−82)	(997)
$CISD^+$	1.150	2160	1.223	1810	1.095	2586
	(−23)	(212)	(−26)	(219)	(−42)	(595)
$CISDT^+$	1.159	2100	1.229	1761	1.124	2170
	(−14)	(152)	(−20)	(170)	(−13)	(179)
$CISDTQ^+$	1.170	1981	1.246	1617	1.133	2051
	(−3)	(33)	(−3)	(26)	(−4)	(60)
CCSD(is)	1.163	2036	1.235	1709	1.113	2339
	(−10)	(88)	(−14)	(118)	(−24)	(348)
CCSD{f}	1.164	2033	1.236	1700	1.125	2094
	(−9)	(85)	(−13)	(109)	(−12)	(103)
CCSD{T}	1.174	1932	1.245	1622	1.137	1859
	(1)	(−16)	(−4)	(31)	(0)	(−132)
CCSD(T)	1.174	1930	1.246	1607	1.140	1811
	(1)	(−18)	(−3)	(16)	(3)	(−180)
CCSD[T]	1.177	1899	1.249	1580	1.145	1711
	(3)	(−49)	(0)	(−11)	(8)	(−280)

body double excitations), the CCSD{f} ω_e are slightly improved for the $X\,^2\Sigma_g^+$ and $A\,^2\Pi_u$ states, but change dramatically for the $B\,^2\Sigma_u^+$ state, reducing the error from 348 to 103 cm^{-1}. Thus, at the CCSD{f} level, the computed ω_e values are already better than the CISDT ones. The T_3 correction brings further improvement for the better behaving states $X\,^2\Sigma_g^+$ and $A\,^2\Pi_u$, where the absolute errors are now within 50 cm^{-1}, but not for the difficult $B\,^2\Sigma_u^+$ state, where the errors are −132, −180 and −280 cm^{-1} for the CCSD{T}, CCSD(T) and CCSD[T] correction schemes, respectively.

The results given in table 10 imply two interesting tendencies. First, for the states such as $X\,^2\Sigma_g^+$ and $A\,^2\Pi_u$, in which the T_3 clusters are of lesser importance, the T_3 corrections always improve the CCSD(is) result, while for difficult systems such as $B\,^2\Sigma_u^+$, in which triples play a significant role, the T_3 corrections are likely to be excessive and will thus lead to large negative errors. Second, the computed ω_e values are larger when singly excited states play a greater role in the correction, i.e. the computed ω_e's have an ordering $\omega_e^{CCSD\{T\}} > \omega_e^{CCSD(T)} > \omega_e^{CCSD[T]}$. Since the T_3 corrections have a tendency to overcorrect in difficult systems, this explains why CCSD{T} gives a better result than CCSD(T), which in turn is better than CCSD[T]. Finally, we must emphasize again that due to the lack of polarization functions, the above results are only of a qualitative methodological value. With large basis sets, these tendencies are likely to remain valid, while the absolute errors of any method with respect to FCI should be smaller.

In table 11 we finally present the computed equilibrium bond lengths R_e and vibrational frequencies ω_e for both N_2^+ and C_2^- in their ground and several excited states, obtained with the standard 6-31G(d) basis set. Although this basis set is only of a moderate size, it reproduces the frequencies exceptionally well, while producing slightly longer bond lengths. We see that CCSD{f} gives a significant improvement over the CCSD(is) method, reducing the errors from 203 to 131 cm^{-1} for the $B\,^2\Sigma_u^+$ state of N_2^+ and from 132 to 97 cm^{-1} for the $B\,^2\Sigma_u^+$ state of C_2^-. Of course, this improvement is less remarkable than in the case of a DZV [3s2p] basis. For the other well-behaved states, the correction due to pseudo-doubles makes little difference. The T_3 corrections give better results in most cases, particularly for the $B\,^2\Sigma_u^+$ state of both N_2^+ and C_2^-, bringing errors to within 100 cm^{-1}, although they are probably overcorrecting in several cases. Again, we find CCSD{T} to be better than CCSD(T), which is in turn better than CCSD[T].

Table 11. Equilibrium bond lengths R_e (in Å) and harmonic vibrational frequencies ω_e (in cm^{-1}) of the ground and excited states of N_2^+ and C_2^- obtained with 6-31G(d) basis and UGA CCSD(is) method with various triple corrections. The experimental values and the differences between the calculated values and experiment are also shown for easier comparison.

System	State	Method	R_e /Å	ΔR_e /mÅ	ω_e /cm^{-1}	$\Delta\omega_e$ /cm^{-1}
N_2^+	$B\,^2\Sigma_u^+$	CCSD(is)	1.082	8	2623	203
		CCSD{f}	1.085	11	2551	131
		CCSD{T}	1.098	24	2365	−55
		CCSD(T)	1.099	25	2349	−71
		CCSD[T]	1.102	28	2311	−109
		Exp.[a]	1.074		2420	
	$A\,^2\Pi_{ui}^+$	CCSD(is)	1.184	9	1988	84
		CCSD{f}	1.185	10	1980	76
		CCSD{T}	1.195	20	1881	−23
		CCSD(T)	1.196	21	1875	−29
		CCSD[T]	1.197	22	1859	−45
		Exp.[a]	1.175		1904	
	$X\,^2\Sigma_g^+$	CCSD(is)	1.129	13	2267	60
		CCSD{f}	1.130	14	2261	54
		CCSD{T}	1.141	25	2132	−75
		CCSD(T)	1.141	25	2135	−72
		CCSD[T]	1.143	27	2129	−78
		Exp.[a]	1.116		2207	
C_2^-	$B\,^2\Sigma_u^+$	CCSD(is)	1.228	5	2101	132
		CCSD{f}	1.232	9	2066	97
		CCSD{T}	1.245	22	1952	−17
		CCSD(T)	1.246	23	1942	−27
		CCSD[T]	1.248	25	1918	−51
		Exp.[a]	1.223		1969	
	$X\,^2\Sigma_g^+$	CCSD(is)	1.274	6	1854	73
		CCSD{f}	1.274	6	1850	69
		CCSD{T}	1.284	16	1785	4
		CCSD(T)	1.284	16	1785	4
		CCSD[T]	1.287	19	1770	−11
		Exp.[a]	1.268		1781	

[a] Reference [17].

5. Conclusions

We have examined the performance of non-iterative pseudo-double and triple corrections for both the equilibrium and highly stretched geometries, as well as for the calculations of vibrational frequencies. We focus on OS doublet states, representing the ground and excited states of many radicals. The following general observations can be made.

The CCSD{f} method always represents an improvement over CCSD(is). There is very little difference between the iterative CCSD(f) and non-iterative CCSD{f} energies, and the latter are in fact slightly closer to the FCI values. While CCSD(f) is computationally much more demanding than CCSD(is), CCSD{f} requires only marginally increased computational effort over that of CCSD(is). In fact, the computer time required by CCSD{f} is equal to that for CCSD(is) plus the time required for a single CCSD(f) iteration, which in turn is equal to the time required for a few more CCSD(is) iterations. In addition, the CCSD{f} codes are much simpler than the CCSD(f) ones. All these features make CCSD{f} the method of choice for many applications.

Various T_3 corrections provide excellent results in the vicinity of the equilibrium geometry and, in this region, the resulting potential energy surfaces show a much better parallelism to the FCI potential than do those obtained with various CCSD approximations. Often, the T_3 corrected methods also provide good results for systems with moderately stretched bonds.

Concerning the relative performance of approximations investigated in this paper, we find that various

T_3 corrected schemes perform differently in different situations and it is hard to conclude with certainty which one is better, even though it seems that CCSD{T} and CCSD(T) are to be favoured. The situation is particularly inconclusive when studying the bond breaking or stretching in OH, NH_2, CH_3 and CN. Taking an overall point of view, we observe that in 24 cases (involving different systems, different states, and different basis sets), CCSD(T) gives the best performance, while both CCSD{T} and CCSD[T] do so in only 8 cases. Regarding the vibrational frequencies, we observe the following general ordering of the computed frequencies: $\omega_e^{CCSD\{T\}} > \omega_e^{CCSD(T)} > \omega_e^{CCSD[T]}$. However, this ordering according to the size of the computed ω_e does not imply the quality of the performance of the individual T_3 corrections. For well-behaved systems, when the T_3 corrected values may still be above the FCI ones, CCSD(T) or CCSD[T] are likely to be the best. For the 'difficult' systems, where the T_3 corrections have a tendency to overcorrect, CCSD{T} is to be preferred over CCSD(T), which in turn is better than CCSD[T].

In general, any perturbative T_3 correcting scheme cannot be expected to perform satisfactorily far away from the equilibrium geometry. In order to extend the CC methodology to such highly quasidegenerate situations, while avoiding theoretically and computationally demanding multi-reference approaches, we currently examine the so-called externally corrected CCSD schemes [22], in which the higher than pair clusters are first obtained by the cluster analysis of some relatively simple, *a priori* available or easily accessible wave function, and are then subsequently used to correct the CCSD equations, thus effecting a more appropriate decoupling of the full CC chain of equations at the pair cluster level. The exploitation of this scheme in the UGA-CCSD(is) method was described in [23], and is applied to the same systems studied here in [24].

A continued support by the National Science and Engineering Research Council of Canada (J.P.) is gratefully acknowledged. The second author also gratefully acknowledges the Alexander von Humboldt Research Award as well as the hospitality of Professor G. H. F. Diercksen and the Max Planck Institute for Astrophysics in Garching during his visit.

References

[1] PALDUS, J, and LI., X., 1993, *Symmetries in Science VI*, edited by B. Gruber (New York: Plenum), pp. 573–591.

[2] LI, X, and PALDUS, J., 1993, *Int. J. quant. Chem., Symp.*, **27**, 269.

[3] LI, X., and PALDUS, J., 1994, *J. chem. Phys.*, **101**, 8812.

[4] JEZIORSKI, B., PALDUS, J., and JANKOWSKI, P., 1995, *Int. J. quant. Chem.*, **56**, 129.

[5] LI, X., PIECUCH, P., and PALDUS, J., 1994, *Chem. Phys. Lett.*, **224**, 267; PIECUCH, P., LI, X., and PALDUS, J., 1994, *Chem. Phys. Lett.*, **230**, 377; LI, X., and PALDUS, J., 1994, *Chem. Phys. Lett.*, **231**, 1; LI, X., and PALDUS, J., 1995, *J. chem. Phys.*, **102**, 2013; LI, X., and PALDUS, J., 1995, *J. chem. Phys.*, **102**, 8059; LI, X., and PALDUS, J., 1995, *J. chem. Phys.*, **103**, 1024; LI, X., and PALDUS, J., 1995, *J. chem. Phys.*, **103**, 6536; PALDUS, J, and LI, X., 1996, *Can. J. Chem.*, **74**, 918.

[6] LI, X., and PALDUS, J., 1995, *J. chem. Phys.*, **102**, 8897.

[7] LI, X., and PALDUS, J., 1996, *J. chem. Phys.*, **104**, 9555.

[8] LI, X., and PALDUS, J., 1997, *Int. J. quant. Chem.*, (in the press, referred to as Part I).

[9] WATTS, J. D., GAUSS, J., and BARTLETT, R. J., 1993, *J. chem. Phys.*, **98**, 8718.

[10] RAGHAVACHARI, K., TRUCKS, G. W., POPLE, J. A., and HEAD-GORDON, M., 1989, *Chem. Phys. Lett.*, **157**, 479.

[11] URBAN, M., NOGA, J., COLE, S. J., and BARTLETT, R. J., 1995, *Chem. Phys. Lett.*, **83**, 4041.

[12] WOON, D. E., and DUNNING, JR, T. H., 1994, *J. chem. Phys.*, **101**, 8877.

[13] PIECUCH, P., KONDO, A. E., ŠPIRKO, V., and PALDUS, J., 1996, *J. chem. Phys.*, **104**, 4699.

[14] SCHMIDT, M. W., BALDRIDGE, K. K., BOATZ, J. A., ELBERT, S. T., GORDON, M. S., JENSEN, J. H., KOSEKI, S., MATSUNAGA, N., NGUYEN, K. A., SU, S. J., WINDUS, T. L., together with DUPUIS, M., and MONTGOMERY, J. A., 1993, *J. comput. Chem.*, **14**, 1347.

[15] BAUSCHLICHER, C. W., LANGHOFF, S. R., TAYLOR, P. R., HANDY, N. C., and KNOWLES, P. J., 1986, *J. chem. Phys.*, **85**, 1469.

[16] BAUSCHLICHER, C. W., and TAYLOR, P. R., 1987, *J. chem. Phys.*, **86**, 5600.

[17] HUBER, K. P., and HERZBERG, G., 1979, *Molecular Spectra and Molecular Structure, Vol. 4: Constants of Diatomic Molecules* (New York: Van Nostrand and Reinhold).

[18] SADLEJ, A. J., 1988, *Coll. Czech. chem. Commun.*, **53**, 1995; 1991, *Theor. chim. Acta*, **79**, 123.

[19] WIDMARK, P. O., MALMQVIST, P. A., and ROOS, B. O., 1990, *Theor. chim. Acta*, **77**, 291.

[20] DUNNING, JR., T. H., and HAY, P. J., 1977, *Methods of Electronic Structure Theory*, edited by H. F. Schaeffer III (New York: Plenum Press), pp. 1–27.

[21] LI, X., and PALDUS, J., 1997, unpublished results.

[22] PALDUS, J., ČÍŽEK, J., and TAKAHASHI, M., 1984, *Phys. Rev. A*, **30**, 2193; PALDUS, J., and PLANELLES, J., 1994, *Theor. chim. Acta*, **89**, 13; PLANELLES, J., PALDUS, J., and LI, X., 1994, *Theor. chim. Acta*, **89**, 33, 59; PIECUCH, P., TOBOLA, R., and PALDUS, J., 1996, *Phys. Rev. A*, **54**, 1210; PERIS, G., PLANELLES, J., and PALDUS, J., 1997, *Int. J. quant. Chem.*, **62**, 137.

[23] LI, X., PERIS, G., PLANELLES, J., RAJADELL, F., and PALDUS, J., 1997, *J. chem. Phys.*, **107**, 90.

[24] PERIS, G., PLANELLES, J., LI, X., RAJADELL, F., and PALDUS, J., 1998, *Molec. Phys.*, **94**, 235.

MOLECULAR PHYSICS, 1998, VOL. 94, NO. 1, 55–64

Vibrational dependence of the dipole moment and radiative transition probabilities in the $X^1\Sigma^+$ state of HF: a linear-response coupled-cluster study

By PIOTR PIECUCH†, VLADIMIR ŠPIRKO‡, ANNE E. KONDO§ and JOSEF PALDUS¶

† Department of Chemistry, University of Toronto, 80 St. George Street, Toronto, Ontario, Canada M5S 3H6

‡ J. Heyrovský Institute of Physical Chemistry, Academy of Sciences of the Czech Republic, Dolejškova 3, 18223 Prague 8, Czech Republic

§ Department of Chemistry, University of Western Ontario, London, Ontario, Canada N6A 5B7

¶ Quantum Theory Group, Departments of Applied Mathematics and of Chemistry and $(GWC)^2$, Waterloo Campus, University of Waterloo, Waterloo, Ontario, Canada N2L 3G1

The recently developed orthogonally spin-adapted linear-response coupled-cluster theory with singly and doubly excited clusters (LRCCSD) has been applied to calculate the dipole moment function of HF. Using an accurate potential energy function derived from spectroscopic data and a dipole moment function obtained in LRCCSD calculations, the effective dipole moment values in individual vibrational states and the corresponding vibrational transition dipole moments have been determined over a wide range of values of vibrational quantum numbers. The calculated matrix elements of the dipole moment have been found to be in good agreement with the available experimental and theoretical data, indicating the suitability of the LRCCSD approach for such calculations.

1. Introduction

Molecular electric properties, including dipole moments, exhibit an appreciable dependence on nuclear geometry [1]. The knowledge of the corresponding property functions describing this dependence is essential for the understanding of the role of vibrational and rotational contributions to properties [2–16].

The dipole moment functions are particularly important in spectroscopy. They provide a basis for calculations of transition probability coefficients and radiative lifetimes involving rovibrational states [17], which are in turn essential for the determination of internal energy distributions in the products of chemical reactions and for the understanding of chemical laser performance, where overtone emission from the vibrationally excited molecules, including hydrogen fluoride, plays a central role [18].

The dipole moment function of hydrogen fluoride continues to be a topic of vigorous experimental and theoretical studies. Since the pioneering studies of Weiss [19] and Muenter and Klemperer [20], who used a molecular beam electric resonance method to determine the dipole moment of HF in the ground ($v = 0$) vibrational state, and Lovell and Herget [21], who used absorption spectroscopy to determine the off-diagonal matrix element of the dipole for the fundamental $1 \leftarrow 0$ transition, a number of experimental studies of the dipole moment function of HF have been reported in the literature [22–28]. All of them carefully analyse the vibrational dependence of the dipole moment of HF and the corresponding transition moments, which we designate as

$$\mu_z^{\text{eff}}(v'', J''; v', J') \equiv \langle v'', J''|\hat{\mu}_z|v', J'\rangle, \tag{1}$$

or

$$\mu_z^{\text{vib}}(v'', v') \equiv \mu_z^{\text{eff}}(v'', 0; v', 0), \tag{2}$$

if rotationless quantities are discussed. Here, $\hat{\mu}_z \equiv \mu_z(r)$ is the dipole moment function of HF (i.e. its non-vanishing z component along the internuclear axis), r designates the H–F internuclear separation, and $|v, J\rangle$ are the rovibrational (radial) wave functions. The dipole moment function, $\mu_z(r)$, is extracted from the spectroscopic data by representing it as a power series in the internuclear distance r around the equilibrium geometry $r = r_e$ and by performing mathematical analysis, which allows extrapolation of the results outside the range of internuclear distances covered by experi-

0026–8976/98 $12·00

ment [24, 28, 29]. The most extensive information about vibrational matrix elements of the HF dipole moment can be found in [24], where the authors measured the emission intensities for the fundamental through fifth overtone bands for all transitions from $v \leq 9$ for HF and $v \leq 12$ for DF.

The dipole moment function of HF has also been investigated theoretically. For example, Werner and Meyer [4] evaluated the vibrational $v = 0$ correction to the electronic dipole moment of HF using the coupled electron pair approximation (CEPA) and the configuration interaction (CI) methods. Similar electronic structure methods were used earlier by Meyer and Rosmus [3], who calculated the dipole moment function $\mu_z(r)$ over a wide range of r values and the selected vibrational matrix elements of the dipole, such as $\mu_z^{\text{vib}}(v, v)$, $v = 0, 1$, and $\mu_z^{\text{vib}}(0, v)$, $v = 1 - 3$. In a more recent study [5], Werner and Rosmus used CEPA and MCSCF (multiconfigurational self-consistent field) approaches to calculate $\mu_z(r)$, $\mu_z^{\text{vib}}(v, v)$, $v = 0 - 8$, $\mu_z^{\text{vib}}(0, v)$, $v = 1 - 5$, and $\mu_z^{\text{vib}}(v - k, v)$, $v = 2 - 8$, $k = 1, 2$. Both papers [3, 5] point out the importance of electron correlation and discuss difficulties in balancing the role of various electronic configurations in *ab initio* calculations of dipole moment functions. This is particularly evident at the MCSCF level, which does not account for the dynamic correlation effects. Earlier MCSCF studies of the dipole moment function of HF include the 2-configurational SCF calculation by Lie [30] and the 8-configurational MCSCF calculations by Krauss and Neuman [31] and Amos [32]. The most accurate study to date is the recent calculation of $\mu_z(r)$ and $\mu_z^{\text{vib}}(v'', v')$, $v', v'' = 0 - 20$ ($v = 19$ is the highest experimentally observed level [33]) by Zemke *et al.* [34], who used a multi-reference (MR) CI method with singles and doubles (MRCISD), CASSCF (complete active space SCF) orbitals, and a very large [6s5p3d2f/4s3p2d] atomic natural orbital (ANO) basis set consisting of 73 contracted functions. The authors used an approach, in which the *ab initio* MRCISD/CASSCF dipole moment function was combined with the potential function derived from the available spectroscopic data [33] by using the Rydberg–Klein–Rees (RKR) method [35]. A similar strategy was used by us in our recent studies of quadrupole moment functions of HF [15], N_2 [15], and NH_3 [16]. We use this combined RKR/*ab initio* approach in the present paper as well.

The purpose of the present work is the determination of the vibrationally averaged dipole moments $\mu_z^{\text{vib}}(v, v)$ and various transition moments $\mu_z^{\text{vib}}(v'', v')$ of the HF molecule, over a wide range of vibrational quantum numbers, using the dipole moment function obtained in the linear-response coupled-cluster (LRCC) calculations. Some representative values of $\mu_z(r)$ that we use in this paper were reported earlier in [36]. In generating $\mu_z(r)$, we use the LRCC formalism suggested by Monkhorst [37] and further developed and implemented by us [36, 38] using the orthogonally spin-adapted (OSA) formulation [39] of the single-reference (SR) CC theory [40]. Thus, the present study represents the next step in our exploration of the capabilities offered by the SRCC theory of molecular electronic structure, in particular, by the LRCC approach to molecular properties.

Let us mention that CC theory [40] offers several advantages that are important in the determination of property functions. Thanks to the use of the exponential ansatz for the wave function, CC theory describes bulk of correlation effects, even at a relatively low level of approximation, and, unlike limited CI, is size extensive. The latter feature is particularly essential, since the generation of property functions of the type discussed in this paper requires electronic structure data for geometries that are far away from the equilibrium one. In addition, the LRCC formalism allows one to define one-electron properties, such as $\mu_z(r)$, without resorting to the direct determination of the expectation value, e.g. $\langle \Psi | \mu_z(r) | \Psi \rangle / \langle \Psi | \Psi \rangle$, with the CC wave function $|\Psi\rangle$. This expression would be very difficult to handle at the CC level of theory (cf. [36, 38] for discussion). Instead, the components of LRCC multipole moments are defined as first derivatives of the energy of a molecule with respect to the field components, even though numerical differentiation as used in the finite-field approaches [41] is entirely eliminated from the procedure and all differentiations of energy are carried out analytically by solving linear systems of equations [36, 38]. This is crucial for the application discussed in this paper, since the finite-field approach becomes expensive if the entire property function is to be generated (at least a few values of the energy, converged to very high precision, would have to be calculated at each geometry). Moreover, the numerical differentiation of the energy with respect to field components may become unstable at stretched geometries due to significant reduction of the radius of convergence of the power series expansion describing the energy of a molecule in an electrostatic field [42] (see also [36]). The LRCC theory eliminates all those drawbacks of the finite-field and similar approaches and allows one to obtain highly accurate (5 decimal digits or more) and stable property values at any geometry and at relatively low cost. Unlike in the finite-field procedure, the precision of the LRCC property calculations can be easily increased if the fitting of property values to an analytic function so requires (calculations reported in this paper are based on a fitting of this type). The advantages of the OSA formulation of CC theory used in this study were discussed in a number of places [36, 38, 39].

Our primary goal is to compare the LRCC results for $\mu_z(r)$ and $\mu_z^{\text{vib}}(v'', v')$ with the earlier calculations of the dipole moment function of HF and experimental data. We demonstrate that LRCC theory is capable of producing high-quality spectroscopic data, including transition dipole moments for overtone bands, at relatively low cost.

The paper is organized as follows. In section 2, we outline the methodology and describe computational details. Section 3 describes and discusses the results, which are then summarized in section 4.

2. Synopsis of theory and computational details

According to equation (1), in order to calculate the rovibrationally averaged dipole moments $\mu_z^{\text{eff}}(v, J; v, J)$ and the corresponding transition dipole moments $\mu_z^{\text{eff}}(v'', J''; v', J')$, we must first generate the radial rovibrational wave functions $\psi_{v,J}(r) \equiv \langle r|v, J\rangle$. They are obtained using the procedure described in [15]. Let us thus only mention that we solve the eigenvalue problem for the radial Hamiltonian,

$$H = -\frac{\hbar^2}{2\mu}\frac{\mathrm{d}^2}{\mathrm{d}r^2} + V(r) + \frac{\hbar^2}{2\mu r^2}J(J+1), \qquad (3)$$

by numerical integration. We use a grid of 3000 values of r from the interval $[r_1, r_2]$ and follow the Numerov–Cooley procedure [43]. We assume the boundary conditions $\psi_{v,J}(r_1) = \psi_{v,J}(r_2) = 0$ and choose the interval $[r_1, r_2]$ to be large enough to provide energies of the highest evaluated rovibrational states with an accuracy better than 0.1 cm^{-1}. The potential energy function $V(r)$ that defines H is represented by the power series

$$V(r) = \sum_i F_i y^i, \qquad (4)$$

where the variable y is defined as

$$y = 1 - \exp[-a(r - r_e)]. \qquad (5)$$

The coefficients F_i (we use 10 terms in expansion (4)) and the parameters a and r_e are obtained by a least squares fit to the RKR potential, which for the HF molecule in the $X\,^1\Sigma^+$ state has been determined in [33].

Once the RKR radial wave functions $|v, J\rangle$ are available, we evaluate matrix elements $\mu_z^{\text{eff}}(v'', J''; v', J')$ by numerical integration (cf. [44]). Clearly, we have to find a suitable analytical representation of the dipole moment function $\mu_z(r)$, whose selected values are generated in *ab initio* LRCC calculations (see the discussion below). As in our earlier study of the quadrupole moment function of HF [15, 45], we represent $\mu_z(r)$ as a power series of the form

$$\mu_z(r) = \sum_i \mu_i y^i, \qquad (6)$$

Table 1. Parameters defining the dipole moment function $\mu_z(r)$ (cf. equation (6)) of HF obtained by the least squares fit of the LRCCSD data. The coefficients μ_i and the standard deviation of the fit, σ, are in ea_0 ($1ea_0 = 2.541\,766$ D).

Parameter	Parameter value
r_e/Å	0.924 212[a]
a/Å^{-1}	1.13
μ_0	0.703 661
μ_1	0.516 815
μ_2	0.240 628
μ_3	−0.430 194
μ_4	−2.213 088
μ_5	5.535 609
μ_6	12.872 106
μ_7	−42.060 172
μ_8	−17.398 065
μ_9	84.207 629
μ_{10}	−41.961 465
σ	0.002 4

[a] The equilibrium bond length in HF obtained in CCSD calculations [45].

where y is given by equation (5). Of course, a different value of a than the one used in equation (4) must be used in equation (6). The coefficients μ_i and the parameter a are obtained by a least squares fit to the LRCC values of $\mu_z(r)$. The final values of μ_i, a, and r_e corresponding to *ab initio* data generated in this study (cf. also [36]) are listed in table 1. We note that for the parameter r_e we simply use the equilibrium bond length in HF obtained in the CCSD (CC singles and doubles) calculations reported in [45]. The final numerical integration of the expression $\psi_{v'',J''}(r) \times \mu_z(r) \times \psi_{v',J'}(r)$ over r, which defines matrix elements $\mu_z^{\text{eff}}(v'', J''; v', J')$ (cf. equation (1)), is performed on the same grid of 3000 points used to generate the wave functions $\psi_{v,J}(r)$.

The LRCC calculations of $\mu_z(r)$ were performed using the CCSD approximation. This means that the zero-order cluster operators defining the wave function of HF in the absence of an electric field, and their first-order counterparts describing the response of the system to an applied electric field, were approximated by their singly and doubly excited components relative to the restricted Hartree–Fock (RHF) reference (see [36, 38] for details). The corresponding LRCCSD values of $\mu_z(r)$ used for the fitting (cf. table 1) and for the subsequent numerical evaluation of $\mu_z^{\text{eff}}(v'', J''; v', J')$ are listed in table 2 and compared with other results in figure 1. Differences between dipole moment values obtained in *ab initio* LRCCSD calculations and the corresponding values of the dipole resulting from the fit (6) are listed in table 2 as well.

Table 2. The LRCCSD values of the dipole moment of HF [z-component $\mu_z(r)$, in ea_0] used for the fitting according to equation (6) and differences between LRCCSD and fitted values (also in ea_0). The internuclear separation r is in bohr (1 bohr = 1 a_0 = 0.529 177 249 Å).

r	$\mu_z(r)$	LRCCSD − fit (6)
1.039 349	0.4938	0.0139
1.126 32	0.5176	−0.0055
1.299 6	0.5672	0.0037
1.5	0.6276	−0.0001
1.6	0.6585	−0.0000
1.732 8[a]	0.6995	0.0001
1.8	0.7200	−0.0002
1.95	0.7648	−0.0003
2.166	0.8246	0.0011
2.36	0.8707	0.0023
2.599 2	0.9123	0.0011
2.7	0.9230	−0.0002
2.83	0.9295	−0.0016
2.9	0.9293	−0.0020
3.032 4	0.9211	−0.0020
3.1	0.9129	−0.0015
3.21	0.8934	−0.0004
3.3	0.8720	0.0009
3.465 6	0.8204	0.0027
3.6	0.7683	0.0032
3.7	0.7248	0.0027
3.8	0.6784	0.0016
3.9	0.6300	−0.0003
4.0	0.5808	−0.0026
4.1	0.5318	−0.0050
4.2	0.4839	−0.0073
4.332	0.4236	−0.0098
5.198 4	0.1563	−0.0034
6.931 2	0.0269	0.0110
8.664	0.0102	0.0012
10.396 8	0.0083	−0.0031
12.129 6	0.0096	−0.0031

[a] The experimental equilibrium bond length.

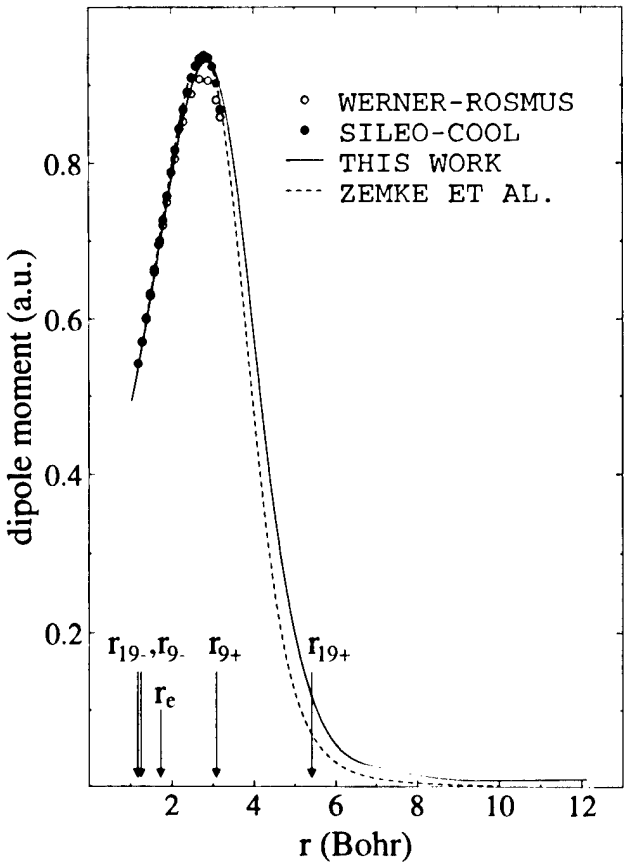

Figure 1. Dipole moment function, $\mu_z(r)$, of the HF molecule. The solid line represents our LRCCSD results, while the short-dashed line gives the MRCISD results of Zemke *et al.* [34]. The open circles represent the SCEP/CEPA values of Werner and Rosmus [5]. The experimentally derived values of Sileo and Cool [24] are represented by solid circles. The experimental equilibrium geometry and selected leftmost (rightmost) turning points for the RKR vibrational states $|r,0\rangle$ are designated by r_e and r_{r_+} (r_{r_+}), respectively. The interval $[r_{9^-}, r_{9^+}]$ represents the limited region of geometries for the Sileo Cool [24] and Werner Rosmus [5] results.

We converged the LRCCSD equations until 5–6 decimal figures for the dipole, and 4–5 decimal digits for the corresponding first-order cluster amplitudes, became stable in the iterative procedure.

As in our earlier LRCCSD calculations [15, 16, 36, 45], we used Sadlej's polarized [5s3p2d/3s2p] basis set [46], which is a medium size basis set of triple zeta plus two sets of polarization functions (TZ + 2P) quality, designed for calculations of electric properties (all 6 Cartesian components of the fluorine d functions were included). In consequence, several dipole moment values listed in table 2 are identical to their analogues reported in our earlier paper [36]. We added, however, several new points to the previously published list of nuclear geometries. As explained in the introduction, we used the OSA formulation of the LRCCSD theory described in detail in [36, 38], and the calculation was performed using our own computer codes [36, 38] (for a description of the corresponding SRCCSD codes, see [47]; for a description of the algorithm used to converge CC equations, see [48]). The only exceptions were generation of the RHF molecular orbitals (MOs) and transformation of one- and two-electron integrals from atomic orbital (AO) to MO basis, which we performed using GAMESS [49]. Our own codes, however, were used to calculate one-electron integrals involving the dipole moment operator.

In the initial SRCCSD calculations (needed to generate the zero-order cluster amplitudes for LRCCSD calculations) and in the LRCCSD calculations of the first-order cluster and dipole moment components, the lowest core MO was kept frozen. The SRCCSD equations were converged until 10 decimal digits for the

energy, and 9 decimal digits for the zero-order cluster amplitudes, stabilized (we could use less tight criteria, but the calculations were so fast that we could afford a slightly higher precision than required).

3. Results and discussion

The final results of this study are presented in tables 3–5. Table 3 lists the effective dipole moment values (cf. equation (2)) $\mu_z^{\text{vib}}(v) \equiv \mu_z^{\text{vib}}(v;v) = \mu_z^{\text{eff}}(v,0;v,0)$ in the vibrational states $|v,0\rangle$, $v = 0 - 19$ (recall that $v = 19$ is the highest experimentally observed vibrational level and the highest v value considered in the RKR study [33]) and the vibrationless value of the dipole, μ_e, calculated at the experimental equilibrium geometry. In addition, we list in this table the purely vibrational ($J = 0$) term values $G(v)$ corresponding to RKR (experimental) and CCSD electronic potentials $V(r)$, even though the only potential that we used in this study to generate $|v,J\rangle$ states is the RKR potential of Coxon and Hajigeorgiou [33]. Table 4 lists the vibrational transition moments (absolute values) $\mu_z^{\text{vib}}(v'',v')$ for the vibrational quantum number $v' \leq 9$, so that a comparison can be made with the experimental data of Sileo and Cool [24]. The remaining transition moments with $v' = 10 - 19$ are presented in table 5. In the latter case, we can only compare our results with the MRCISD/CASSCF calculations of Zemke *et al.* [34], who considered all transition moments with $v' \leq 20$. In presenting transition dipole moments, we focus on the fundamental ($\Delta v \equiv v'' - v' = -1$) and first overtone ($\Delta v = -2$) bands, even though we evaluated all transition moments with $v', v'' \leq 19$ (results not presented are

Table 3. The CCSD vibrational term values $G(v)$ relative to RKR (in cm^{-1}) and the vibrational dependence of the dipole moment of HF in the $X^1\Sigma^+$ state. A comparison of calculated (*ab initio*, theory) and experimental (exp) results. $\mu_z^{\text{vib}}(v)$ (in ea_0) designates diagonal matrix element $\mu_z^{\text{vib}}(v,v)$ (rotationless value; cf. equation (2)) and μ_e (also in ea_0) is the vibrationless dipole moment corresponding to the equilibrium geometry.

			$\mu_z^{\text{vib}}(v)$ (*ab initio*)				$\mu_z^{\text{vib}}(v)$ (exp)				
	$G(v)$			Werner and	Zemke	$\mu_z^{\text{vib}}(v)$ (theory/exp)	Sileo and	Bass	Muenter and	Gough	Barnes
v	RKR[a]	CCSD[b]	**LRCCSD**[c]	Rosmus[d]	*et al.*[e]	Ogilvie[f]	Cool[g]	*et al.*[h]	Klemperer[i]	*et al.*[j]	*et al.*[k]
0	2050.8	1	**0.7083**	0.7109	0.7174	0.7186	0.7156	0.718 621	0.718 605		
1	6012.2	3	**0.7256**	0.7278	0.7361	0.7372	0.7337	0.737 162		0.7365	
2	9801.6	8	**0.7423**	0.7444	0.7544	0.7553	0.7511	0.756 6			0.7548
3	13 423.6	15	**0.7584**	0.7601	0.7720	0.7728	0.7684				0.7717
4	16 882.4	25	**0.7740**	0.7751	0.7885	0.7893	0.7845				
5	20 181.8	38	**0.7888**	0.7888	0.8034		0.7994				
6	23 324.6	50	**0.8024**	0.8006	0.8163		0.8128				
7	26 313.1	61	**0.8143**	0.8109	0.8266		0.8238				
8	29 148.9	67	**0.8236**	0.8171	0.8335		0.8313				
9	31 832.4	66	**0.8296**		0.8361		0.8345				
10	34 362.9	57	**0.8315**		0.8335						
11	36 738.4	37	**0.8282**		0.8246						
12	38 954.9	3	**0.8187**		0.8079						
13	41 006.6	−46	**0.8014**		0.7819						
14	42 884.4	−116	**0.7747**		0.7446						
15	44 576.1	−212	**0.7361**		0.6937						
16	46 064.2	−345	**0.6819**		0.6263						
17	47 325.7	−527	**0.6061**		0.5383						
18	48 328.5	−779	**0.4980**		0.4239						
19	49 026.5	−1134	**0.3353**		0.2722						
μ_e			**0.6995**	0.7011	0.7080	0.7092	0.7066	0.709 38	0.706 8	0.7093	0.7090

[a] From [33]. The dissociation energy is $D_e = 49\,362 \pm 5\,\text{cm}^{-1}$ (see [34] and references therein).
[b] From [15]. The OSA CCSD calculation using the same basis set as employed in this study.
[c] Present work.
[d] From [5]. SCEP/CEPA calculation.
[e] From [34]. MRCISD/CASSCF calculation.
[f] From [29].
[g] From [24].
[h] From [27].
[i] From [20]. $v = 0$ and $J = 1$.
[j] From [25].
[k] From [28].

Table 4. Transition dipole moments $\mu_z^{\text{vib}}(v'', v')$ (absolute values, in ea_0) for the fundamental ($\Delta v \equiv v'' - v' = -1$) and first overtone ($\Delta v = -2$) bands of HF with the vibrational quantum number $v' \leq 9$. Results for the higher overtone bands include the off-diagonal matrix elements of the dipole moment with $v'' = 0$ and $v' = 3, 4$ (matrix elements with $v' > 4$ are smaller in absolute value than $10^{-4} ea_0$).

		Ab initio			Experiment					
v''	v'	**LRCCSD**[a]	Werner and Rosmus[b]	Zemke *et al.*[c]	Sileo and Cool[d]	Bass *et al.*[e]	Lovell and Herget[f]	Pine *et al.*[g]	Meredith[h]	Spellicy *et al.*[i]
0	1	**0.0377**	0.0370	0.0402	0.0388	0.0392	0.0388	0.0392		
0	2	**0.0050**	0.0049	0.0051	0.0050	0.0049			0.0049	
0	3	**0.0007**	0.0007	0.0007	0.0007	0.0006				0.0006
0	4	**0.0001**	0.0001	0.0002	0.0001	0.0001				
1	2	**0.0524**	0.0515	0.0562	0.0543					
2	3	**0.0629**	0.0618	0.0676	0.0653					
3	4	**0.0710**	0.0688	0.0760	0.0736					
4	5	**0.0772**	0.0736	0.0818	0.0795					
5	6	**0.0814**	0.0763	0.0851	0.0834					
6	7	**0.0836**	0.0759	0.0858	0.0846					
7	8	**0.0834**	0.0736	0.0833	0.0830					
8	9	**0.0802**		0.0775	0.0779					
1	3	**0.0090**	0.0088	0.0093	0.0090					
2	4	**0.0131**	0.0129	0.0137	0.0131					
3	5	**0.0173**	0.0174	0.0184	0.0176					
4	6	**0.0216**	0.0222	0.0236	0.0224					
5	7	**0.0263**	0.0273	0.0293	0.0276					
6	8	**0.0314**	0.0325	0.0354	0.0334					
7	9	**0.0370**		0.0420	0.0397					

[a] Present work.
[b] From [5]. SCEP/CEPA calculation.
[c] From [34]. MRCISD/CASSCF calculation.
[d] From [24].
[e] From [27].
[f] From [21].
[g] From [26].
[h] From [22].
[i] From [23].

available from us upon request). We also focus on the rotationless values. The results for the higher overtone bands that we report in this paper are limited to transition dipole moments with $v'' = 0$ and $|\Delta v| \leq 4$ (see table 4). As noted in [34], the fundamental and first overtone transition probabilities for emission are largest for $v' < 15$, so that $|\Delta v| \leq 2$ transition moments are representative of the entire set of $\mu_z^{\text{vib}}(v'', v')$ values. Moreover, the number of the available significant digits is largest for the transition dipole moments corresponding to $|\Delta v| \leq 2$ bands (we must realize that the number of decimal digits in the calculated transition dipole moments is determined by the accuracy of the computed dipole moment function). As a result, the comparison of the LRCCSD transition dipole moments obtained in this study with the results obtained by other authors is most meaningful for $|\Delta v| \leq 2$.

Before discussing the results collected in tables 3–5, let us notice that the LRCCSD dipole moment function is in a very good agreement with the dipole moment function derived from experiment by Sileo and Cool [24] (see figure 1). There is also an excellent agreement between the single-reference LRCCSD results reported here and very accurate *ab initio* results reported in [34], where the authors used a significantly more expensive multi-reference approach. The *ab initio* dipole moment function of Werner and Rosmus obtained using the SCEP/CEPA approach [5] is also quite good, but in worse agreement with experiment than our curve, particularly near the region where $\mu_z(r)$ approaches its maximum value. It must be emphasized that the basis set employed in our study is significantly smaller than the basis sets used by Werner and Rosmus [5] and Zemke *et al.* [34] (our basis set, in spite of the use of all Cartesian components of fluorine d functions, consists of only 35 orbitals, compared to 73 orbitals used in [34]). In particular, our basis set lacks fluorine f functions, which were included in the calculations reported in [5, 34].

For $r > 3.0$ bohr (1 bohr $= 1a_0 = 0.529\,177\,249$ Å), our results begin to deviate from the results reported

Table 5. Calculated transition dipole moments $\mu_z^{vib}(v'', v')$ (absolute values, in ea_0) for the fundamental ($\Delta v \equiv v'' - v' = -1$) and first overtone ($\Delta v = -2$) bands of HF with the vibrational quantum number $v' = 10 - 19$.

v''	v'	LRCCSD[a]	Zemke *et al.*[b]
9	10	**0.0736**	0.0678
10	11	**0.0632**	0.0536
11	12	**0.0485**	0.0346
12	13	**0.0290**	0.0102
13	14	**0.0044**	0.0197
14	15	**0.0253**	0.0547
15	16	**0.0598**	0.0935
16	17	**0.0976**	0.1325
17	18	**0.1341**	0.1638
18	19	**0.1549**	0.1682
8	10	**0.0431**	0.0489
9	11	**0.0495**	0.0558
10	12	**0.0558**	0.0624
11	13	**0.0614**	0.0678
12	14	**0.0651**	0.0709
13	15	**0.0656**	0.0697
14	16	**0.0606**	0.0614
15	17	**0.0471**	0.0424
16	18	**0.0215**	0.0090
17	19	**0.0181**	0.0362

[a] Present work.
[b] From [34]. MRCISD/CASSCF calculation.

in [34]. This deviation grows as r increases, even though the overall shape of both dipole moment functions is pretty much the same. In view of the observed differences between both dipole moment functions, we can expect that the quality of the effective dipole moments and the corresponding transition dipole moments obtained in this study will deteriorate for higher values of v (we assume that the MRCISD calculation reported by Zemke *et al.*, who used twice as large basis set and a multi-configurational reference space, is more accurate and can serve as a benchmark for us). We should expect a significant worsening of the LRCCSD results for $v > 9$, since the rightmost turning point corresponding to $v = 9$ RKR state, r_{9+}, and turning points corresponding to $v > 9$ states, are greater than 3.0 bohr (cf. figure 1, $r_{9+} = 3.0874$ bohr [33]). The fact that the LRCCSD dipole moment function does not seem to vanish asymptotically (as it obviously should [45] and as Zemke *et al.*'s MRCISD dipole moment function does [34]; cf. figure 1) is probably of slightly lesser significance, since the rightmost turning point corresponding to the highest vibrational level discussed here, i.e. $v = 19$, is in the region where both MRCISD [34] and LRCCSD dipole moments are still significantly positive (see figure 1; $r_{19+} = 5.4181$ bohr [33]). Moreover, the LRCCSD values of the dipole moment are very small for r approaching ∞ (for $r = 7r_e = 12.1296$ bohr, the LRCCSD dipole is less than 0.01 au; cf. table 2; 1 au= $1ea_0 = 2.541\,766$ D). In order for the LRCCSD dipole moment function to vanish asymptotically, we would either have to replace the RHF orbitals by the UHF ones or to use the RHF orbitals and include connected tri-excited clusters, at least of the so-called semi-internal type [50]. The connected tri-excited clusters are also needed to eliminate a small gap between the RHF-based CC and full CI potential energy curves of HF at infinite H–F separations [51].

In principle, the results in tables 3–5 confirm our expectations, although there are cases in which the LRCCSD approach performs better than we expected. For $v \leq 10 - 12$, differences between dipole moment mean values $\mu_z^{vib}(v)$ obtained in this study and $\mu_z^{vib}(v)$ values reported by Zemke *et al.* [34] are very small and do not exceed 1–2% (see table 3). These differences become much larger when $v > 12$ (they increase from 2.5% for $v = 13$ to 23.2% for $v = 19$). This is a clear indication of the failure of the closed-shell SRCCSD formalism at very large H–F separations and, to a lesser degree, of our fitting procedure, which was designed to produce best results primarily for lower v values. We note that the LRCCSD dipole moments are best reproduced by our fit (6) for 1.2 bohr $< r <$ 3.3 bohr (cf. table 2).

Our results for $\mu_z^{vib}(v)$ are comparable to those obtained by Werner and Rosmus [5] who, as mentioned above, used a larger basis set than the one employed here. There is, however, one feature which, we believe, makes our results somewhat better. Differences between the SCEP/CEPA values of $\mu_z^{vib}(v)$ reported in [5] and the corresponding experimental values of $\mu_z^{vib}(v)$ reported by Sileo and Cool [24] vary with v. They increase from 0.005 au for $v = 0$ to 0.014 au for $v = 8$. Similar differences formed with our $\mu_z^{vib}(v)$ values are practically independent of v, and for $v \leq 8$ we obtain an almost constant difference of ca. 0.008–0.010 au between our and Sileo and Cool's values of $\mu_z^{vib}(v)$. In that sense our results are very similar to the most accurate $\mu_z^{vib}(v)$ values reported in [34] (in which case, differences with experimental values reported by Sileo and Cool vary between 0.002 and 0.004 au), even though the accuracy of the experimental data reported by Sileo and Cool may not be sufficient to draw such conclusions [29]. As a matter of fact, the newer results reported by Ogilvie [29], who based his theoretical analysis of the dipole moment function of HF on more recent and more accurate experimental data (published, for example, in [26, 27]) differ from the results for $\mu_z^{vib}(v)$ reported by Sileo and Cool by 0.002–0.005 au. The same applies to the experimentally derived $\mu_z^{vib}(v)$ values reported in [27, 28]. The agreement between *ab initio* results reported

by Zemke *et al.* [34] and these newer $\mu_z^{vib}(v)$ values is most impressive. Our $\mu_z^{vib}(v)$ values differ from those resulting from Ogilvie's analysis of experimental data [29] by ca. 0.010–0.015 au (see table 3). It should be pointed out, however, that it would be surprising to obtain perfect agreement between experimental and *ab initio* values of $\mu_z^{vib}(v)$ on the basis of nonrelativistic *ab initio* calculations relying on the Born–Oppenheimer approximation, which is an approximation used in our and all earlier *ab initio* studies of the HF dipole moment function. We believe that a constant difference of ca. 0.008–0.010 au between our and Sileo and Cool's values of $\mu_z^{vib}(v)$ for $v \leq 8$ is caused primarily by the fact that the LRCCSD calculations reported in this paper underestimate the experimental value of the vibrationless dipole moment μ_e by 0.0071–0.0099 au. A much better agreement between the LRCCSD and experimental value of μ_e should be obtained with a larger basis set. The calculation by Zemke *et al.* [34] is more accurate in this respect, even though the question of what degree of accuracy can be achieved by using nonrelativistic Born–Oppenheimer theory remains.

The results in table 3 indicate that we can rely on the LRCCSD estimates of $\mu_z^{vib}(v)$ for $v \leq 10$–12. This is consistent with the ability of the closed-shell CCSD approach to describe the first 10–12 vibrational term values. The reliability of the CCSD procedure to accurately reproduce $G(v)$ values for $v \geq 13$ is questionable, as is the reliability of the LRCCSD data for $\mu_z^{vib}(v)$ obtained with Sadlej's basis set (cf. [15]).

A similar pattern is observed for the rotationless transition dipole moments $\mu_z^{vib}(v'', v')$, even though in this case the LRCCSD approach performs significantly better, which supports our observation that a small constant shift of our dipole moment function might be sufficient to improve the LRCCSD values of the diagonal matrix elements $\mu_z^{vib}(v)$ (a constant shift of the dipole moment function would not affect the off-diagonal $\mu_z^{vib}(v'', v')$ elements). The LRCCSD values of $\mu_z^{vib}(v'', v')$ are clearly superior when compared to the SCEP/CEPA results obtained by Werner and Rosmus [5]. For the fundamental ($\Delta v = v'' - v' = -1$) transitions with $v' \leq 9$, differences between LRCCSD and experimental [24] data do not exceed 2–4% and can be as small as 0.5%, a very impressive result (see table 4). The analogous $\mu_z^{vib}(v'', v')$ values reported by Werner and Rosmus [5] differ from the corresponding experimental values reported by Sileo and Cool [24] by 5–11%. A similar statement applies to $\mu_z^{vib}(v'', v')$ values characterizing first overtone bands. For $v' = 2$–4 (or $v'' = 0$–2), the agreement between the LRCCSD and experimental results is better than 10^{-4} au. However, the SCEP/CEPA results of Werner and Rosmus [5] become slightly better for $v' = 6$–8 (see table 4).

The quality of the LRCCSD results for the transition dipole moments with $v' \leq 9$ is comparable to the quality of the MRCISD results reported in [34], which we and many others regard as the most accurate *ab initio* calculations to date. In fact, our results for first overtone transitions seem to be noticeably better than those reported in [34], at least with respect to agreement with the data published by Sileo and Cool [24]. We do not think, however, that the same remark applies to our transition dipole moments with $v' \geq 10$ (see table 5). In this case, differences between our results and those reported by Zemke *et al.* [34] are quite large. Since we do not use the large basis set employed in [34] and since we only rely on a SR formalism and a simple CCSD approximation, our results are probably less reliable than those obtained by Zemke *et al.* We base this remark on the significant differences between the dipole moment functions reported in this study and in [34] for $r > r_{9+}$. Interestingly enough, in spite of the observed differences, both calculations lead to similar behaviour of the transition dipole moments for $v' \geq 10$. For example, the LRCCSD $|\mu_z^{vib}(v'', v')|$ values corresponding to fundamental ($\Delta v = -1$) bands, which we obtained in this study, decrease with increasing v' to reach the minimum for $v' = 14$. For $v' > 14$, they increase with v'. A similar pattern is observed in the calculations reported by Zemke *et al.* [34] (see table 5). The behaviour of the LRCCSD approach is even better when we look at the $|\mu_z^{vib}(v'', v')|$ values characterizing first overtone bands ($\Delta v = -2$ case). In this case, differences between our LRCCSD values and the corresponding values published in [34] do not exceed 12% and can be as small as 1%, as long as $10 \leq v' \leq 17$. In fact, the LRCCSD values of $|\mu_z^{vib}(v' - 2, v')|$ seem to display a somewhat more regular dependence on v' for $v' \geq 10$ than the MRCISD values published in [34] (cf. the $|\mu_z^{vib}(v' - 2, v')|$ values for $v' = 18$ in table 5).

We can certainly conclude that the overall performance of the LRCCSD approach is very good, in spite of its inherent SR nature and the absence of higher-than-bi-excited clusters in the formalism. Let us thus summarize the results.

4. Summary and concluding remarks

We used the recently developed OSA LRCCSD approach [36, 38] to study the dipole moment function of HF. The effective dipole moment values in individual vibrational states and the corresponding vibrational transition dipole moments were calculated. This was accomplished by combining the LRCCSD dipole moment function with the RKR potential function reported in [33]. All vibrational states included in the RKR study [33] were considered.

A comparison was made with earlier *ab initio* calculations, including the recent MRCISD study reported in [34] and the seminal study by Werner and Rosmus [5] who used the SCEP/CEPA approach. We also compared the LRCCSD results with the available experimental data, including the extensive data for $\mu_z^{\text{vib}}(v'', v')$ published by Sileo and Cool [24].

The overall behaviour of the LRCCSD formalism was found to be very good. The diagonal and off-diagonal matrix elements $\mu_z^{\text{vib}}(v'', v')$ resulting from LRCCSD calculations are excellent up to $v'', v' \leq 10$. They are more accurate than the SCEP/CEPA values [5] and comparable in accuracy to the values published in [34], in spite of the fact that we used only a medium-size basis set lacking fluorine f functions, which were present in the calculations reported in [5, 34]. We believe that we could obtain even better results, should we decided to test our method with a larger basis set. As shown in our earlier papers (cf. for example [36, 38]), the LRCCSD results have a tendency to systematically improve with the size and quality of the basis set. It would be interesting to examine the performance of LRCCSD approach using the basis set employed in [34]. This would allow us to determine whether an approximately constant 0.008–0.010 au difference between the diagonal matrix elements $\mu_z^{\text{vib}}(v)$ obtained in this study and their counterparts reported in [24] is primarily due to a slight inaccuracy in the calculated value of μ_e, as suggested in this paper.

The LRCCSD results for the matrix elements $\mu_z^{\text{vib}}(v'', v')$, characterizing the $X\,^1\Sigma^+$ state of HF, deteriorate when $v'', v' \geq 10$, even though some transition moments (e.g. for first overtone bands) turn out to be very good. This must be related to the absence of tri-excited cluster components in the LRCCSD formalism. They could be included by using, for example, the state-selective (SS) CCSD(T) method (SSCCSD method with semi-internal tri-excited clusters) of [52]. As shown in [50], inclusion of tri-excited cluster components improves the description of the dipole moment function of HF at very large internuclear separations.

The LRCC results reported in this paper are most encouraging. We plan to explore the potential of the LRCC theory further by studying other molecules and by analyzing the ro-vibrational dependence of higher-order properties, such as first and second hyperpolarizabilities β and γ.

Two of us (P.P.) and (J.P.) would like to thank the Organizers of the 'Coupled Cluster Theory and Electron Correlation' workshop (Cedar Key, Florida, 14–19 June 1997), particularly Professor Rodney J. Bartlett, for invitation to give talks, so that the results discussed in this paper could be presented. Financial support by the Organizers (J.P. and P.P.) and by Professor John C. Polanyi (P.P.) is gratefully acknowledged. Continued support by the Natural Sciences and Engineering Research Council of Canada (J.P.) is gratefully acknowledged as well. Finally, we would like to thank Professor Peter F. Bernath for drawing our attention to recent papers on spectroscopy of the HF molecule.

References

[1] Dykstra, C. E., 1988, *Ab Initio Calculation of the Structures and Properties of Molecules* (Amsterdam: Elsevier), Chap. 7.
[2] Dykstra, C. E., Liu, S.-Y., and Malik, D. J., 1990, *Adv. chem. Phys.*, **75,** 37.
[3] Meyer, W., and Rosmus, P., 1975, *J. chem. Phys.*, **63,** 2356.
[4] Werner, H.-J., and Meyer, W., 1976, *Molec. Phys.*, **31,** 855.
[5] Werner, H.-J., and Rosmus, P., 1980, *J. chem. Phys.*, **73,** 2319.
[6] Rosmus, P., and Werner, H.-J., 1982, *Molec. Phys.*, **47,** 661.
[7] Adamowicz, L., and Bartlett, R. J., 1986, *J. chem. Phys.*, **84,** 4988; 1987, ibid., **86,** 7250 (Erratum).
[8] Bishop, D. M., Pipin, J., and Silverman, J.N., 1986, *Molec. Phys.*, **59,** 165.
[9] Kirtman, B., and Bishop, D. M., 1990, *Chem. Phys. Lett.*, **175,** 601; Bishop, D. M., and Kirtman, B., 1991, *J. chem. Phys.*, **95,** 2646; 1992, ibid., **97,** 5255.
[10] Dykstra, C. E., and Malik, D. J., 1987, *J. chem. Phys.*, **87,** 2806; Augspurger, J. D., and Dykstra, C. E., 1992, *Chem. Phys. Lett.*, **189,** 303.
[11] Cohen, M. J., Willetts, A., Amos, R. D., and Handy, N. C., 1994, *J. chem. Phys.*, **100,** 4467.
[12] Archibong, E. F., and Thakkar, A. J., 1993, *Chem. Phys. Lett.*, **201,** 485; 1994, *J. chem. Phys.*, **100,** 7471.
[13] Whitehouse, D. B., and Buckingham, A. D., 1993, *Chem. Phys. Lett.*, **207,** 332.
[14] Bishop, D. M., 1990, *Rev. mod. Phys.*, **62,** 343.
[15] Špirko, V., Piecuch, P., Kondo, A. E., and Paldus, J., 1996, *J. chem. Phys.*, **104,** 4716.
[16] Piecuch, P., Špirko, V., and Paldus, J., 1996, *J. chem. Phys.*, **105,** 11068.
[17] Townes, C. H., and Schawlow, A. L., 1955, *Microwave Spectroscopy* (London: McGraw-Hill).
[18] Polanyi, J. C., 1961, *J. chem. Phys.*, **34,** 347; 1965, *Appl. Opt. Chem. Laser. Suppl.*, **2,** 109; 1971, *Appl. Optics*, **10,** 1717; Kasper, J. V. V., and Pimentel, G. C., 1965, *Phys. Rev. Lett.*, **14,** 352; Pimentel, G. C., 1966, *Sci. Am.*, **214,** 32; 1976, *Proceedings of the Robert A. Welch Foundation Conferences on Chemical Research*, edited by W. O. Milligan (Houston, Texas: Robert A. Welch Foundation), p. 73; 1976, *Handbook of Chemical Lasers*, edited by R. W. F. Gross and J. W. Bott (New York: Wiley); Miller, J., 1987, *AIP Conference Proceedings*, Vol. 160, *Advances in Laser Science II*, edited by M. Lapp, W. C. Stwalley, and G. A. Kenney-Wallace (New York: AIP Press), p. 10.
[19] Weiss, R., 1963, *Phys. Rev.*, **131,** 659.
[20] Muenter, J. S., and Klemperer, W., 1970, *J. chem. Phys.*, **52,** 6033.

[21] LOVELL, R. J., and HERGET, W. F., 1962, *J. opt. Soc. Am.*, **52,** 1374.
[22] MEREDITH, R. E., 1972, *J. quant. Spectrosc. radiat. Transfer*, **12,** 485.
[23] SPELLICY, R. L., MEREDITH, R. E., and SMITH, F. G., 1972, *J. chem. Phys.*, **57,** 5119.
[24] SILEO, R. N., and COOL, T. A., 1976, *J. chem. Phys.*, **65,** 117.
[25] GOUGH, T. E., MILLER, R. E., and SCOLES, G., 1981, *Faraday Discuss. Chem. Soc.*, **71,** 77.
[26] PINE, A. S., FRIED, A., and ELKINS, J. W., 1985, *J. molec. Spectrosc.*, **109,** 30.
[27] BASS, S. M., DELEON, R. L., and MUENTER, J. S., 1987, *J. chem. Phys.*, **86,** 4305.
[28] BARNES, J. A., GOUGH, T. E., and STOER, M., 1994, *Can. J. Chem.*, **72,** 499.
[29] OGILVIE, J. F., 1988, *J. Phys.* B, 21, 1663.
[30] LIE, G. C., 1974, *J. chem. Phys.*, **60,** 2991.
[31] KRAUSS, M., and NEUMAN, D., 1974, *Molec. Phys.*, **27,** 917.
[32] AMOS, R. D., 1978, *Molec. Phys.*, **35,** 1765.
[33] COXON, J. A., and HAJIGEORGIOU, P. G., 1990, *J. molec. Spectrosc.*, **142,** 254.
[34] ZEMKE, W. T., STWALLEY, W. C., LANGHOFF, S. R., VALDERRAMA, G. L., and BERRY, M. J., 1991, *J. chem. Phys.*, **95,** 7846.
[35] RYDBERG, R., 1931, *Z. Phys.*, **73,** 376; 1933, *ibid.*, **80,** 514; Klein, O., 1932, *ibid.*, **76,** 226; Rees, A. L. G., 1947, *Proc. phys. Soc.*, **59,** 998.
[36] KONDO, A. E., PIECUCH, P., and PALDUS, J., 1996, *J. chem. Phys.*, **104,** 8566.
[37] MONKHORST, H. J., 1977, *Int. J. quantum Chem. Symp.*, **11,** 421.
[38] KONDO, A. E., PIECUCH, P., and PALDUS, J., 1995, *J. chem. Phys.*, **102,** 6511.
[39] PALDUS, J., ADAMS, B., and ČÍŽEK, J., 1977, *Int. J. quantum Chem.*, **11,** 813; PALDUS, J., 1977, *J. chem. Phys.*, **67,** 303; ADAMS, B. G., and PALDUS, J., 1979, *Phys. Rev.* A, **20,** 1; PIECUCH, P., and PALDUS, J., 1989, *Int. J. quantum Chem.*, **36,** 429; 1990, *Theor. chim. Acta*, **78,** 65.
[40] COESTER, F., 1958, *Nucl. Phys.*, **7,** 421; COESTER, F., and KÜMMEL, H., 1960, *ibid.*, **17,** 477; ČÍŽEK, J., 1966, *J. chem. Phys.*, **45,** 4256; 1969, *Adv. chem. Phys.*, **14,** 35; ČÍŽEK, J., and PALDUS, J., 1971, *Int. J. quantum Chem.*, **5,** 359.
[41] COHEN, H. D., and ROOTHAAN, C. C. J., 1965, *J. chem. Phys.*, **43,** S34.
[42] PIECUCH, P., and PALDUS, J., 1997, *J. math. Chem.*, **21,** 51.
[43] COOLEY, J. W., 1961, *Math. Comp.*, **15,** 363.
[44] ŠPIRKO, V., and BLABLA, J., 1988, *J. molec. Spectrosc.*, **129,** 59.
[45] PIECUCH, P., KONDO, A. E., ŠPIRKO, V., and PALDUS, J., 1996, *J. chem. Phys.*, **104,** 4699.
[46] SADLEJ, A. J., 1988, *Coll. Czech. chem. Commun.*, **53,** 1995.
[47] PIECUCH, P., and PALDUS, J., 1994, *J. chem. Phys.*, **101,** 5875.
[48] PIECUCH, P., and ADAMOWICZ, L., 1994, *J. chem. Phys.*, **100,** 5857.
[49] The GAMESS system of programs by M. DUPUIS, D. SPANGLER, and J. J. WENDOLOSKI, 1980, National Resource for Computations in Chemistry, Software Catalog, University of California, Berkeley, CA, Program QG01; SCHMIDT, M. W., BALDRIDGE, K. K., BOATZ, J. A., ELBERT, S. T., GORDON, M. S., JENSEN, J. H., KOSEKI, S., MATSUNAGA, N., NGUYEN, K. A., SU, S. J., WINDUS, T. L., DUPUIS, M., and MONTGOMERY, J. A., 1993, *J. comput. Chem.*, **14,** 1347.
[50] GHOSE, K. B., PIECUCH, P., PAL, S., and ADAMOWICZ, L., 1996, *J. chem. Phys.*, **104,** 6582.
[51] GHOSE, K. B., PIECUCH, P., and ADAMOWICZ, L., 1995, *J. chem. Phys.*, **103,** 9331.
[52] OLIPHANT, N., and ADAMOWICZ, L., 1991, *J. chem. Phys.*, **94,** 1229; 1992, *ibid.*, **96,** 3739; 1993, *Int. Rev. phys. Chem.*, **12,** 339; PIECUCH, P., OLIPHANT, N., and ADAMOWICZ, L., 1993, *J. chem. Phys.*, **99,** 1875.

MOLECULAR PHYSICS, 1998, VOL. 94, NO. 1, 65–71

Almost variational coupled cluster theory

By WERNER KUTZELNIGG
Lehrstuhl für Theoretische Chemie, Ruhr-Universität Bochum,
D-44780 Bochum, Germany

The energy expectation value of coupled-cluster theory can be formulated as the sum of the energy expression of *traditional coupled-cluster* (TCC) theory plus a correction term. The latter is simplified if the stationarity conditions of TCC hold. It is then of $O(S^4)$, where S is the coupled-cluster amplitude. The leading error contribution agrees with the leading term of the difference between the TCC energy and the energy expression of *extended coupled-cluster* (ECC) theory. It is suggested to evaluate this routinely at the end of any TCC calculation as a check of the reliability of the latter. The error of the ECC energy expression with respect to an expectation value is of $O(S^6)$. The error of traditional CCSD with respect to an expectation value is not affected by the inclusion of triple excitations in CCSDT. Approximations to CCSDT are also discussed. A hierarchy of approximations starting from TCC and ending at *variational coupled-cluster* (VCC) theory, alternative to the previously proposed *improved coupled-cluster* (ICC) method is presented.

1. Introduction

A drawback of the otherwise so successful *traditional*† [1, 2] coupled-cluster (TCC) theory‡ [3–5] is that it is not variational. This means that the traditional coupled cluster energy E_{TCC} is *not an upper bound* to the exact energy, further that no hypervirial relations hold, which makes the calculation of properties somewhat non-trivial [6]. Variational variants of coupled cluster theory (VCC) have been known for some time, but they are so much more complicated that they have never been competitive. A comparison of various coupled-cluster (CC) approaches can be found in [1].

The coupled-cluster ansatz for the wave function of a closed-shell state, that to zeroth order can be approximated by a single Slater determinant Φ, is [7, 8]

$$\Psi = \exp(S)\Phi; \qquad S = S^{(k)} = S_1 + S_2 + \cdots S_k, \quad (1)$$

$$S_1 = S_a^i a_i^a; \qquad S_2 = S_{ab}^{ij} a_{ij}^{ab}, \ldots . \quad (2)$$

We choose Φ normalized to unity. Labels i,j,k refer to spin–orbitals occupied in Φ, a,b,c to virtual spin–orbitals. The a_i^a, a_{ij}^{ab} etc. are *excitation operators*, namely one-particle and two-particle operators, respectively. The corresponding *de-excitation operators* are a_a^i and a_{ab}^{ij}. The S_a^i etc. are the expansion coefficients (amplitudes) of S. The Einstein summation convention is implied [9] . We shall use the symbolic notation $\hat{a}_1, \hat{a}_2$ for any of the a_i^a or a_{ij}^{ab}, respectively, and correspondingly $\hat{a}_1^\dagger, \hat{a}_2^\dagger$ for the a_a^i or a_{ab}^{ij}; $\hat{a}$ and $\hat{a}^\dagger$ mean any $\hat{a}_k$ or $\hat{a}_k^\dagger$ for arbitrary excitation rank k.

In the earliest formulation of traditional coupled cluster theory (TCC) [7, 8] one inserts (1) into the Schrödinger equation and projects from the left by $\langle\Phi|$ or $\langle\Phi|\hat{a}^\dagger$ (this is often called the method of moments):

$$\langle\Phi|H\exp(S)|\Phi\rangle = E_{\mathrm{TCC}}\langle\Phi|\exp(S)|\Phi\rangle = E_{\mathrm{TCC}}, \quad (3)$$

$$\langle\Phi|\hat{a}^\dagger\hat{H}\exp(S)|\Phi\rangle = E_{\mathrm{TCC}}\langle\Phi|\hat{a}^\dagger\exp(S)|\Phi\rangle. \quad (4)$$

Note that $\langle\Phi|\exp(S) = \langle\Phi|$.

An alternative, but equivalent formulation [10] is now generally accepted. One constructs the Hamiltonian

$$L = \exp(-S)H\exp(S) = H + [H,S] + \tfrac{1}{2}[[H,S]S] + \ldots \quad (5)$$

obtained from H by means of a similarity transformation with $\exp(S)$. One then considers the Schrödinger equation for this transformed Hamiltonian (which is not hermitian)

$$L\Phi = \exp(-S)H\exp(S)\Phi = E_{\mathrm{TCC}}\Phi \quad (6)$$

and projects it to the left as in (3) and (4)

$$\langle\Phi|L|\Phi\rangle = E_{\mathrm{TCC}}, \quad (7)$$

$$\langle\Phi|\hat{a}^\dagger L|\Phi\rangle = 0, \quad (8)$$

with E_{TCC} the same in (3) and (7).

The operator L has the nice property that its

† The name *traditional coupled cluster* (TCC) has been coined in [1]. It appears preferable to the name *normal* CC, used by Arponen *et al.* [2], since to call something *normal* usually implies that it has some distinctive features, which are hardly recognized here.

‡ For an older review see [3], for more recent ones [4] and [5].

0026–8976/98 $12·00

Hausdorff expansion terminates at $O(S^4)$

$$L = H + [H,S] + \tfrac{1}{2}[[H,S],S] + \tfrac{1}{6}[[[H,S],S],S] + \tfrac{1}{24}[[[[H,S],S],S],S] = H + (HS)_c + \tfrac{1}{2}(HSS)_c + \tfrac{1}{6}(HSSS)_c + \tfrac{1}{24}(HSSSS)_c, \quad (9)$$

where c stands for *connected*. One uses here, of course, that that commutators are necessarily connected and that S on the left of H cannot connect with H. L as given by (9) is at most a $(4k-2)$-particle operator, more precisely a $(4k-2)$-fold excitation operator, with k defined via (1). Inserted into (7) and (8) the expansion (9) terminates even earlier.

The advantage of (7) and (8) over (3) and (4) is that in (8) E does not appear, and that from (8) it is more directly obvious that only connected terms are present.

TCC is exact, i.e. *equivalent to full CI* in the same one electron basis, *provided that* $S = S^{(n)}$ for an n-electron system. For $S = S^{(k)}$ with $k < n$ it is approximate (see later).

Equations (7) and (8) can be interpreted as conditions for stationarity of the *Arponen functional* [1, 2] with respect to variation of $\tilde{S}^\dagger$

$$F(S,\tilde{S}^\dagger) = \langle\Phi|(1+\tilde{S}^\dagger)L|\Phi\rangle \quad (10)$$

with $E = F(S,\tilde{S}^\dagger)$ at the stationary point.

The oldest form of variational coupled cluster theory (VCC) is based on the expectation value (see e.g. [3])

$$E = \frac{\langle\Phi|\exp(S^\dagger)H\exp(S)|\Phi\rangle}{\langle\Phi|\exp(S^\dagger)\exp(S)|\Phi\rangle} \quad (11)$$

that is then made stationary with respect to variations of S and $S^\dagger$. Not only are the stationarity conditions complicated coupled equations, even the evaluation of (11) is very tedious. In the power series expansion of $\exp(S)$ one has to go up to $(1/n!)S^n$ if S contains S_1, otherwise to $[(n/2)!]^{-1}S^{n/2}$.

An alternative to (11) is

$$E = \langle\Phi|\exp(S^\dagger)H\exp(S)|\Phi\rangle_L, \quad (12)$$

where L stands for linked. This means essentially connected, but including all exclusion-principle-violation (EPV) terms with repeated identical indices. This is essentially equivalent to

$$E = \langle\Phi|\exp(S^\dagger)H\exp(S)|\Phi\rangle \times [1 + (\langle\Phi|\exp(S^\dagger)\exp(S)|\Phi\rangle - 1)]^{-1} = \langle\Phi|\exp(S^\dagger)H\exp(S)|\Phi\rangle \times \{1 - (\langle\Phi|\exp(S^\dagger)\exp(S)|\Phi\rangle - 1) + (\langle\Phi|\exp(S^\dagger)\exp(S)|\Phi\rangle - 1)^2 + \cdots\} \quad (13)$$

after cancellation of disconnected terms. Both (12) and (13) have the disadvantage that the expansion in powers of S is infinite, and usually very slowly convergent [1, 3, 11]. As to a detailed discussion of expectation values for coupled-cluster wavefunctions see [12].

The aesthetically most appealing variational approach is unitary coupled cluster (UCC) theory [1, 3]. It is based on

$$E = \langle\Phi|\exp(-\sigma)H\exp(\sigma)|\Phi\rangle; \qquad \sigma = T - T^\dagger \quad (14)$$

with T expanded like S in (1) and (2). The transformed Hamiltonian $\exp(-\sigma)H\exp(\sigma)$ is unitary at variance with the non-unitary L defined by (5). Unfortunately the Hausdorff expansion of (14) in powers of σ does not break off and we have an infinite expansion as in (12) or (13), but a much faster converging one [1, 3].

To make VCC or UCC practically manageable it is recommened to truncate the expansion in powers of S or σ. This leads to variants like VCC-SD(l) [1], where l indicates the power of S at which one truncates. Then one loses either the upper bound property or the size-extensivity or possibly both. Truncating (13) or (14) at a finite order in S or σ preserves the size-extensivity, but does not yield an upper bound. Truncating (11) consistently in numerator and denominator yields an upper bound, but E is not size-extensive. There has also been some controversy on whether in truncating one should only care about orders of S (or σ) [1] or whether one should (in the spirit of perturbation theory) treat H_0 and V differently, including higher orders in powers of S together with H_0 than together with V [13]. There are arguments in favour of either choice.

Anyway the chances for VCC or UCC (full or truncated at some power of S) to beat TCC with respect to accuracy are very low, especially if one compares the cost performance ratio.

In this paper we start from the paradigm that TCC is rather good already, and we try to formulate a hierarchy of approximations of which TCC is the first step and which ends at VCC. Depending on the circumstances one may stop at any appropriate level in this hierarchy. When we refer to VCC we shall always mean that expectation values are evaluated exactly, with no truncation in powers of S—but, of course, with a truncated expansion of S at $S^{(k)}$.

A hierarchy of this kind has already been proposed in [1] under the name *improved coupled cluster* (ICC) in terms of an asymmetric expectation-value like expressions starting from

$$E = \frac{\langle\Phi|(1+S^\dagger)H\exp(S)|\Phi\rangle}{\langle\Phi|(1+S^\dagger)\exp(S)|\Phi\rangle} \quad (15)$$

via

$$E = \frac{\langle \Phi|(1 + S^\dagger + \frac{1}{2}S^{\dagger 2})H \exp(S)|\Phi\rangle}{\langle \Phi|(1 + S^\dagger + \frac{1}{2}S^{\dagger 2}) \exp(S)|\Phi\rangle} \tag{16}$$

ending at (11).

Here we consider an alternative hierarchy that passes by *extended coupled-cluster* (ECC) theory [2]. Both TCC and VCC are separable and hence size-extensive and expressible in terms of connected diagrams only. This does not necessarily hold for the steps in between, unless certain precautions are taken, about which we are not going to worry, since this is not necessary in the present context.

2. Relation of the variational coupled cluster (VCC) to the traditional coupled cluster (TCC) approach

We start from the expectation value (11), but we insert the identity $1 = \exp(S) \exp(-S)$.

$$E = \frac{\langle \Phi|XL|\Phi\rangle}{\langle \Phi|X|\Phi\rangle}, \tag{17}$$

$$X = \exp(S^\dagger) \exp(S), \tag{18}$$

with L defined by (5). Although XL is hermitian, one may choose an alternative in which the hermiticity is more directly manifest

$$E = \mathrm{Re}\,\frac{\langle \Phi|XL|\Phi\rangle}{\langle \Phi|X|\Phi\rangle} = \frac{\langle \Phi|XL + L^\dagger X|\Phi\rangle}{2\langle \Phi|X|\Phi\rangle} \tag{19}$$

We are led to VCC if we make (17) stationary with respect to variations of $S^\dagger$. The stationarity conditions are:

$$\langle \Phi|\delta S^\dagger X(L - \tilde{\lambda})|\Phi\rangle = 0. \tag{20}$$

It is much simpler to interpret (17) as an Arponen functional, with $X/\langle \Phi|X|\Phi\rangle = 1 + \tilde{S}$ and to make it stationary with respect to variations of X. Then one has to satisfy

$$\langle \Phi|\delta X(L - \lambda)|\Phi\rangle = 0, \tag{21}$$

where λ (like $\tilde{\lambda}$ in equation (20)) is a Lagrange multiplier. Equation (21) is, of course equivalent to the TCC equation (4) or (8). The expansion of (21) in powers of S terminates at $O(S^4)$ at variance with that of (20), where the termination depends on the particle number n.

If (21) holds for *all* de-excitation operators $\delta X = \hat{a}^\dagger$, it follows that

$$0 = \langle \Phi|X(L - \lambda)|\Phi\rangle \tag{22}$$

$$E = \frac{\langle \Phi|XL|\Phi\rangle}{\langle \Phi|X|\Phi\rangle} = \lambda = \langle \Phi|L|\Phi\rangle. \tag{23}$$

The Lagrange multiplier λ in (21) is then equal to the expectation value (17), which is the energy expression of TCC theory, and which is easily evaluated.

We only need those contributions to X, which do not vanish when applied to the left on Φ, i.e. which contain only de-excitation operators, conjugate to those in (2). We expand

$$\langle \Phi|X = \sum_k \langle \Phi|X_k^\dagger, \tag{24}$$

$$X_0^\dagger = X_0 = \langle \Phi|X|\Phi\rangle = 1 + [S_1^\dagger S_1 + (S_2^\dagger + \tfrac{1}{2}S_1^{\dagger 2}) \times (S_2 + \tfrac{1}{2}S_2^2)]_{fc} + \cdots \tag{25}$$

$$X_1^\dagger = S_1 + [(S_2^\dagger + \tfrac{1}{2}S_1^{\dagger 2})S_1]_{\mathrm{fc}} + [(S_3^\dagger + S_1^\dagger S_2^\dagger + \tfrac{1}{6}S_1^{\dagger 3})(S_2 + \tfrac{1}{2}S_1^2)]_{\mathrm{fc}} + \cdots = X_i a_a^i, \tag{26}$$

$$X_2^\dagger = S_2^\dagger + [(S_3^\dagger + S_1^\dagger S_2^\dagger + \tfrac{1}{6}S_1^{\dagger 3})S_1]_{\mathrm{fc}} + \cdots = X_{ij}^{ab} a_{ab}^{ij}. \tag{27}$$

Here fc means fully contracted, e.g.

$$(S_1^\dagger S_2)_{\mathrm{fc}} = S_k^c S_{ab}^{ij}(a_c^k a_{ij}^{ab})_{\mathrm{fc}} = S_i^a S_{ab}^{ij} a_j^b - S_i^b S_{ab}^{ij} a_j^a - S_j^a S_{ab}^{ij} a_i^b + S_j^b S_{ab}^{ij} a_i^a. \tag{28}$$

Not fully contracted parts (e.g. normal products of excitation and de-excitation operators) are neither pure excitation nor de-excitation operators and have either $\langle \Phi|X = 0$ or $X|\Phi\rangle = 0$. Note the difference between *contracted* and *connected*.

Let us now make *no assumptions* on fulfilled stationarity conditions and let us just assume that the wave function is of the form (1). The expectation value (11) or (17) can then always be rewritten as

$$E = \langle \Phi|L|\Phi\rangle + \frac{\langle \Phi|(X - X_0)L|\Phi\rangle}{X_0}, \tag{29}$$

$$\langle \Phi|(X - X_0) = \langle \Phi|\sum_{m=1}^{n} X_m^\dagger. \tag{30}$$

The second term on the right hand side of (29), which represents the error of $\langle \Phi|L|\Phi\rangle$ with respect to an expectation value, is simplified considerably, if stationarity conditions of the type (8) are satisfied. It would be ideal if (8) would hold for all $X_m^\dagger$ in the sum (30). Then the correction term would vanish and $\langle \Phi|L|\Phi\rangle$ would be equal to an expectation value. A necessary condition for this is that the number of conditions to be satisfied is not greater than the number of parameters to be determined.

This is, of course, the case for an untruncated expansion, i.e. for $S = S^{(n)}$ (n always means the number of particles) but not for $S = S^{(k)}$ with $k < n$. Let us now assume that $S = S^{(k)}$ and that S has been obtained from the condition that (21) is satisfied for $\delta X = a_m^\dagger$, $m = 1, 2, \ldots k$, i.e. from TCC. Then (30), when inserted

into (29), reduces to

$$\langle\Phi|(X - X_0) = \langle\Phi| \sum_{m=k+1}^{M} X_m^\dagger; \qquad M = \min(n, 4k-2). \tag{31}$$

At this point three stategies are possible.

(a) One evaluates the sum (31) in (29) exactly and obtains a rigorous upper bound to the energy, that will be slightly above the best variational energy. In fact (29) is an expectation value irrespective of any stationarity conditions satisfied. So if (31) holds, we can insert this into (29) and this will remain an expectation value, although it is, of course, not stationary with respect to variation of the $S^{(k)}$. This procedure is rather tedious, as already has been mentioned, since there is no automatic n-independent termination of the expansion in powers of S.

(b) One evaluates only the *leading term* of the correction and gets so an estimate of how far the TCC energy is off an upper bound and one is able to judge the quality of the TCC energy.

(c) One tries to find an alternative functional and the corresponding stationarity conditions, such that the error of this functional at the stationary point is smaller than that of TCC.

We illustrate the situation for two simple cases, namely for $S = S_2$, i.e. for CCD (CC with doubles) in section 3, and for $S = S^{(3)}$, i.e. CCSDT (CC with singles, doubles, and triples) in in section 4. We then come back to the general case in section 5.

3. Coupled-pair theory

Let us now consider that $S = S_2$, then

$$X_0 = 1 + (S^\dagger S + \tfrac{1}{4} S^{\dagger 2} S^2 + \tfrac{1}{36} S^{\dagger 3} S^3)_{\rm fc} + \cdots, \tag{32}$$

$$X_1^\dagger = X_3^\dagger = X_5^\dagger = \cdots = 0, \tag{33}$$

$$X_2^\dagger = S^\dagger + \tfrac{1}{2}(S^{\dagger 2} S)_{\rm fc} + \tfrac{1}{12}(S^{\dagger 3} S^2)_{\rm fc} + \cdots, \tag{34}$$

$$X_4^\dagger = \tfrac{1}{2} S^{\dagger 2} + \tfrac{1}{6}(S^{\dagger 3} S)_{\rm fc} + \tfrac{1}{48}(S^{\dagger 4} S^2)_{\rm fc} + \cdots, \tag{35}$$

$$X_6^\dagger = \tfrac{1}{6} S^{\dagger 3} + \tfrac{1}{24}(S^{\dagger 4} S)_{\rm fc} + \tfrac{1}{240}(S^{\dagger 5} S^2)_{\rm fc} + \cdots. \tag{36}$$

L is given by (9). This is at most a 6-particle operator, hence

$$\langle\Phi|\hat{a}_k^\dagger (L - \lambda)|\Phi\rangle = 0 \quad \text{for } k > 6. \tag{37}$$

Since $\delta X_1 = \delta X_3 = 0$, the conditions (21) that we want to satisfy in order to have a variational approach are

$$\langle\Phi|a_2^\dagger (L - \lambda)|\Phi\rangle = \langle\Phi|a_2^\dagger L|\Phi\rangle = 0, \tag{38}$$

$$\langle\Phi|a_4^\dagger (L - \lambda)|\Phi\rangle = \langle\Phi|a_4^\dagger L|\Phi\rangle = 0, \tag{39}$$

$$\langle\Phi|a_6^\dagger (L - \lambda)|\Phi\rangle = \langle\Phi|a_6^\dagger L|\Phi\rangle = 0. \tag{40}$$

It is obviously not possible to satisfy (38) to (40) simultaneously. In TCC one satisfies (38) which leads to a condition for the expansion coefficients of $S = S_2$. There is no more freedom left. Let us now compare the expectation value E given by (17) for this TCC wave function and the TCC energy λ given by (23). We have, starting from (17) and using (38)

$$E = \frac{\langle\Phi|(X_0 + X_2^\dagger + X_4^\dagger + X_6^\dagger)L|\Phi\rangle}{X_0}$$

$$= \langle\Phi|L|\Phi\rangle + \frac{\langle\Phi|(X_4^\dagger + X_6^\dagger)L|\Phi\rangle}{X_0}. \tag{41}$$

The deviation of the TCC energy from an upper bound is hence

$$\begin{aligned} X_0^{-1}\langle\Phi|X_4^\dagger L|\Phi\rangle &= X_0^{-1}\langle\Phi|(\tfrac{1}{2} S_2^{\dagger 2} + \tfrac{1}{6} S^{\dagger 3} S + \cdots)_{\rm fc} \\ &\quad \times (H + [H,S] + \tfrac{1}{2}[[H,S],S] + \cdots)|\Phi\rangle \\ &= X_0^{-1}\tfrac{1}{4}\langle\Phi|(S^{\dagger 2} + \tfrac{1}{6} S^{\dagger 3} S + \cdots)_{\rm fc} \\ &\quad \times [[H,S],S] + \cdots|\Phi\rangle \end{aligned} \tag{42}$$

plus a similar contribution due to $X_6^\dagger$. Note that H and $[H,S]$ have no 4-particle-excitation contributions and can hence not contract with $X_4^\dagger$. The correction term (42) is dominated by something of $O(S^4)$. The term involving $X_6^\dagger$ even starts with $O(S^7)$. The leading term of the *error* is obviously of $O(S^4)$, i.e. the TCC energy is correct to $O(S^3)$, which has, of course, been known before [1]. The leading contribution to the error

$$\tfrac{1}{4}\langle\Phi|S^{\dagger 2}[[H,S],S]|\Phi\rangle \tag{43}$$

is a measure of the quality of the TCC-D approach and should be evaluated routinely. The relevance of this correction term, although not derived as shown here, has also been realized previously [6, 14].

Alternatively to only satisfy (38) but to ignore (39) and (40) we can start from (41) and insert $X_4^\dagger$ and $X_6^\dagger$ explicitly, which is rather tedious since the expansion in powers of S does not terminate automatically.

In order to get a more accurate, but still simple, functional than that of TCC we can proceed in the following way. Rather than to require that (38) holds, which corresponds to minimizing the functional (S is implicit in L)

$$F_{\rm TCC}(S, S^\dagger) = \langle\Phi|(1 + S^\dagger)L|\Phi\rangle \tag{44}$$

with respect to variation of $S^\dagger$, we consider the functional

$$\begin{aligned} F_{\rm ECC}(S, S^\dagger) &= \langle\Phi|(1 + S^\dagger + \tfrac{1}{2} S^{\dagger 2} + \tfrac{1}{6} S^{\dagger 3})L|\Phi\rangle \\ &= \langle\Phi|\exp(S^\dagger)L|\Phi\rangle. \end{aligned} \tag{45}$$

The label ECC stands for *extended* [1, 2] coupled cluster. We make the functional (45) stationary with respect to

variation of $S^\dagger$, with the condition

$$\langle\Phi|a_2^\dagger(1+S^\dagger+\tfrac{1}{2}S^{\dagger 2})L|\Phi\rangle = \langle\Phi|a_2^\dagger \exp(S^\dagger)L|\Phi\rangle = 0 \tag{46}$$

which implies

$$\langle\Phi|(S^\dagger+S^{\dagger 2}+\tfrac{1}{2}S^{\dagger 3})L|\Phi\rangle = \langle\Phi|S^\dagger \exp(S^\dagger)L|\Phi\rangle = 0, \tag{47}$$

$$\lambda_{\mathrm{ECC}} = F_{\mathrm{ECC}}^{\mathrm{opt}}(S^\dagger) = \langle\Phi|(1+\tfrac{2}{3}S^\dagger+\tfrac{1}{6}S^{\dagger 2})L|\Phi\rangle, \tag{48}$$

where, of course, L is different from that discussed before, because S is different. We do not consider the conditions for stationarity with respect to variation of S.

As we shall demonstate in section 5 the leading term of the error is now of $O(S^6)$.

4. CCSDT theory

Let us now choose $S = S^{(3)} = S_1 + S_2 + S_3$, i.e. CCSDT. The expressions for the $X_k^\dagger$, generally given by (25) to (27) are no longer of the simple form (32) to (36) as for CCD theory. Nevertheless the first condition of the type (38) to (40) not satisfied at TCC-SDT level is (39) just as for TCC-D. The condition with highest m not satisfied automatically is that for $m = 4k-1 = 11$. The leading contribution to the error of TCC with respect to TCC is again that given by (43). This is not changed by the presence of S_1 and S_3. The inclusion of S_1 and S_3 *does not automatically improve* S_2. This is only achieved to a large extent if one includes S_4 and satisfies the corresponding stationarity conditions as well.

In TCC-SDT one does take care of the 'coupling' of S_2 to S_1 and S_3, but not to $S_2^{\dagger 2}$, which is probably no less important. The question arises whether it is really consistent to update S_2 'in the field of' S_3, if one does not at the same time update it 'in the field of' $S_2^{\dagger 2}$, for which ECC-SDT would be required. Applications of ECC in quantum chemistry have, so far, not been too successful [15].

In most approximate variants of TCC-SDT, as in CCSD(T) [16] or CCSD[T] [17], the stationarity condition, that involves $a_3^\dagger$, is not satisfied exactly. The error due to this approximation can, of course, be evaluated as

$$X_0^{-1}\langle\Phi|X_3^\dagger L|\Phi\rangle = X_0^{-1}\langle\Phi|(S_3^\dagger+\tfrac{1}{2}S_2^{\dagger 2}S_1+\cdots)_{\mathrm{fc}}([H,S] + \tfrac{1}{2}[[H,S],S]+\cdots)_{\mathrm{fc}}|\Phi\rangle. \tag{49}$$

It is probably a good check of the validity of these approximations, and by the way, also of so-called *quadratic CI* [18], to evaluate the leading term of the correction (49). To renounce on exact stationarity, but to estimate the correction to VCC might be a serious alternative to the standard procedure.

5. ECC as the next step in a coupled-cluster hierarchy, and beyond

Let us go back to the general case, and let us start again from the expectation value (17). We rewrite it as

$$E = \frac{\langle\Phi|\exp(S^\dagger)L|\Phi\rangle + \langle\Phi|[X]L|\Phi\rangle}{1+\langle\Phi|[X]|\Phi\rangle};$$

$$[X] = [\exp(S^\dagger), \exp(S)]. \tag{50}$$

If we now argue that $[X]$ is of $O(S^2)$, and hence smaller than the other terms, we can (noting that $\exp(-S^\dagger)|\Phi\rangle = |\Phi\rangle$) approximate E (50) by

$$E_{\mathrm{ECC}} = \langle\Phi|\exp(S^\dagger)L|\Phi\rangle = \langle\Phi|\exp(S^\dagger)L\exp(-S^\dagger)|\Phi\rangle = \langle\Phi|\tilde{L}|\Phi\rangle \tag{51}$$

and regard

$$\tilde{L} = \exp(S^\dagger)L\exp(-S^\dagger) = \exp(S^\dagger)\exp(-S)H\exp(S)\exp(-S^\dagger) \tag{52}$$

as a Hamiltonian to which two consecutive similarity transformations have been applied. Of course this can also be regarded as a single similarity transformation with $\exp(S)\exp(-S^\dagger)$. This is the basis of the extended coupled-cluster theory of Arponen and co-workers [2].† The transformed Hamiltonian (52) is still not hermitian, but closer to hermitian than is L.

Compare

$$L - L^\dagger = [H, S+S^\dagger] + O(S^2), \tag{53}$$

$$\tilde{L} - \tilde{L}^\dagger = [H,[S,S^\dagger]] + O(S^3). \tag{54}$$

To analyse the error of the ECC functional (51) we introduce the operator

$$\begin{aligned} Y &= \exp(S^\dagger)\exp(S)\exp(-S^\dagger) \\ &= 1 + \exp(S^\dagger)S\exp(-S^\dagger) \\ &\quad + \tfrac{1}{2}\exp(S^\dagger)S^2\exp(-S^\dagger)+\cdots \\ &= \exp(S) + [S^\dagger, \exp(S)] \\ &\quad + \tfrac{1}{2}[S^\dagger,[S^\dagger,\exp(S)]]+\cdots. \end{aligned} \tag{55}$$

Now we can reformulate the expectation value E as

$$E = \frac{\langle\Phi|Y\tilde{L}|\Phi\rangle}{\langle\Phi|Y|\Phi\rangle} = \langle\Phi|\tilde{L}|\Phi\rangle + \frac{\langle\Phi|(Y-Y_0)\tilde{L}|\Phi\rangle}{\langle\Phi|Y|\Phi\rangle} \tag{56}$$

† In the original reference to ECC [2] $S^\dagger$ is replaced by $\tilde{S}^\dagger$ with $\tilde{S}$ not necessarily equal to S. In fact, independent stationarity conditions for variation of S and $\tilde{S}^\dagger$ lead to different optimum $\tilde{S}$ and S. We consider here a simplified version, where $\tilde{S} = S$ is imposed and only stationarity with respect to variation of $S^\dagger$ is required.

with

$$Y_0 = \langle\Phi|Y|\Phi\rangle = X_0. \tag{57}$$

In analogy to (24) we can expand Y (applied to the left on Φ) as

$$\langle\Phi|Y = \sum_k \langle\Phi|Y_k^\dagger. \tag{58}$$

Stationarity condition for the ECC functional (51) with repect to variation of $S^\dagger$ is

$$\langle\Phi|a_m^\dagger \tilde{L}|\Phi\rangle = 0; \qquad m = 1,2,\ldots,k. \tag{59}$$

If we satisfy these conditions, i.e. determine the S_k from the ECC method†, the sum (58) in (56) can be replaced by

$$\langle\Phi|(Y - Y_0) = \langle\Phi| \sum_{m=k+1}^{M} Y_m^\dagger; \; M = \min(n, 4k-2). \tag{60}$$

To show that the error is now much smaller than for the S_k determined from the TCC method, we consider again the case of CCD, i.e. $S = S_2$. The counterpart of (32) to (36) is

$$Y_0 = X_0, \tag{61}$$

$$Y_1^\dagger = Y_3^\dagger = Y_5^\dagger = \cdots = 0, \tag{62}$$

$$Y_2^\dagger = \tfrac{1}{2}[S^\dagger,[S^\dagger,S]] + \tfrac{1}{12}[S^\dagger,[S^\dagger,[S^\dagger,S^2]]] + \cdots, \tag{63}$$

$$Y_4^\dagger = \tfrac{1}{6}[S^\dagger,[S^\dagger,[S^\dagger,S]]] + O(S^6), \tag{64}$$

$$Y_6^\dagger = \tfrac{1}{24}[S^\dagger,[S^\dagger,[S^\dagger,[S^\dagger,S]]]] + O(S^8). \tag{65}$$

The error of the ECC energy with respect to the VCC energy is dominated by

$$Y_0^{-1}\langle\Phi|Y_4^\dagger \tilde{L}|\Phi\rangle = \tfrac{1}{4}Y_0^{-1}\langle\Phi|(S^{\dagger 3}S)_{\rm fc}(HSS)_{\rm fc}|\Phi\rangle = O(S^6). \tag{66}$$

Compared to TCC the error with respect to VCC has been reduced by two orders in powers of S.

It is easy to see how one could go successively from ECC to VCC. Actually ECC is obtained from VCC by replacing Y by the first term in the second expression on the right hand side of (55), i.e. by 1. The next approximation would be to replace Y by

$$Y^{(1)} = 1 + \exp(S^\dagger) S \exp(-S^\dagger) \tag{67}$$

One would again 'win' two orders in S. Whether the so-defined hierarchy has any practical chances, remains to be seen. One should then also worry about size-consistency. As long as the potential of ECC has not been exploited, there is little interest in going beyond it.

† See footnote on page 69.

One should not forget that there is an alternative hierarchy from TCC to VCC via ICC (improved coupled-cluster) defined in [1], as mentioned at the end of section 1.

If we regard ECC as an important first step on the way from TCC to VCC, it may not really be necessary – in order to improve on TCC—to care for stationarity of the ECC functional. It may be sufficient to evaluate the ECC functional with S obtained from stationarity of the TCC functional. We can write

$$E_{\rm ECC} = E_{\rm TCC} + \tfrac{1}{2}\langle\Phi|(S^{\dagger 2} + \tfrac{1}{3}S^{\dagger 3} + \cdots)L|\Phi\rangle, \tag{68}$$

where we have taken care of the stationarity condition (8). It is not surprising that this agrees with the expression for the leading term of the error of $E_{\rm TCC}$ with respect to $E_{\rm VCC}$.

There is another way to relate ECC to VCC or rather to UCC, that we only sketch very briefly. We note that

$$\begin{aligned}\exp(S)\exp(-S^\dagger) &= \exp(S - S^\dagger + \tfrac{1}{2}[S^\dagger,S] \\ &\quad - \tfrac{1}{12}[[S^\dagger,S],S+S^\dagger] + O(S^4)) \\ &= \exp(S-S^\dagger)(1 + \tfrac{1}{2}[S^\dagger,S] + O(S^3))\end{aligned} \tag{69}$$

$$\begin{aligned}\exp(S^\dagger)\exp(-S) &= \exp(S^\dagger - S - \tfrac{1}{2}[S^\dagger,S] \\ &\quad + \tfrac{1}{12}[[S^\dagger,S],S+S^\dagger] + O(S^4)) \\ &= \exp(S^\dagger - S)(1 - \tfrac{1}{2}[S^\dagger,S] + O(S^3)).\end{aligned} \tag{70}$$

Hence $E_{\rm ECC}$ differs from a UCC-like energy expression by something of $O(S^2)$. The next step on the way from the double similarity transformation of ECC theory to the unitary transformation of UCC theory would be to replace the left hand side of (69) by

$$\exp(S)\exp(-S^\dagger)(1 - \tfrac{1}{2}[S^\dagger,S]) = \exp(S - S^\dagger) + O(S^3). \tag{71}$$

6. Conclusions

The traditional reluctance of the coupled-cluster community to care for a variational formulation of the theory is somewhat puzzling. The arguments currently put forward to justify this reluctance are:

(a) VCC calculations are so much more tedious than TCC ones, and TCC is already computationally very demanding, such that one can usually not afford more than just TCC. If one has not exhausted one's resources it is usually regarded as preferable to include higher S_m or to increase the basis rather than try to improve TCC calculations towards VCC. This is certainly valid as to routine calculations, but does not preclude benchmark studies. Surprisingly

enough TCC versus VCC calculations (untruncated in powers of S) have—to the author's knowledge—not even been performed at benchmark level. If one can do full CI one should certainly be able to do VCC-SD or VCC-SDT.

(b) $TCC^{(k)}$ is a member of a hierarchy that eventually becomes exact (i.e. equivalent to full CI) if one lets k go to n. In practice, however, one hardly goes beyond $k = 4$ or even $k = 3$. The convergence of the entire hierarchy has never been tested, neither at TCC nor at VCC level. All that exists are comparisons for $k = 2, 3, (4)$ with full CI. The present study indicates that the error of the TCC-SD energy with respect to an expectation value is not basically affected if one goes from CCSD to CCSDT. So even an improvement in this way is not necessarily a measure of the quality of the TCC-SD calculation.

There is a third argument that is usually not admitted so frankly:

(c) The non-variational behaviour of TCC can give rise to a fortunate and welcome error compensation and make the TCC energy closer to the full-CI counterpart than a VCC energy might be. In other words, the extra effort in going from TCC-SD to VCC-SD may not pay, in the sense that it may yield a poorer-looking, i.e. higher energy.

We have pointed out here that the energy change from TCC-SD to VCC-SD may contain important information on the reliabilty of the CC method in general, and that it deserves to be studied more than has been the case.

It is not the purpose of this paper to convince the CC community to switch from TCC to VCC, or at least to approximate VCC. Before one decides on such a change of paradigm one should first investigate to what extent TCC and VCC differ numerically. One will find this out if one evaluates more or less routinely the leading correction terms to TCC. If these turn out to be appreciable, e.g. if the the corrections to TCC-SD are of the same order of magnitude as the improvement due to inclusion of triple excitations in TCC-SDT, one has certainly to reconsider the matter.

Let us stress again that the standard argument that if CCSD is not good enough, one should go to CCSDT may need to be reconsidered. If TCC-SD is too far from its VCC-SD counterpart, this defect remains at the TCC-SDT level and only disappears if one goes to TCC-SDTQ.

Approximations to TCC-SDT such as CCSD(T) or CCSD[T] have so far mainly been proposed and discussed in terms of arguments from perturbation theory. The non-perturbative framework of this paper may offer an interesting alternative for finding balanced approximate treatments.

The author is indebted to D. Mukherjee and J. Noga for constructive comments.

References

[1] KUTZELNIGG, W., 1991, *Theoret. Chim. Acta*, **80,** 349.
[2] ARPONEN, J., 1983, *Ann. Phys.* (NY), **151,** 311; ARPONEN, J., BISHOP, R. F., and PAJANNE, E., 1987, *Phys. Rev.* A, **36,** 2519, 2539; Bishop, R. F., Arponen, J., and PAJANNE, E., 1989, *Aspects of Many-Body Effects in Molecules and Extended Systems*, edited by D. Mukherjee, Lecture Notes in Chemistry 50 (Berlin: Springer), p. 79; ARPONEN, J., 1997, *Phys. Rev.* A, **55,** 2686.
[3] KUTZELNIGG, W., 1977, *Modern Theoretical Chemistry*, Vol. 3a, edited by H. F. Schaeffer III (New York: Plenum).
[4] BARTLETT, R. J., 1989, *J. phys. Chem.*, **93,** 1697.
[5] BISHOP, R. F., and KÜMMEL, H., 1987, *Phys. Today*, **40,** 52; BISHOP, R. F., 1991, *Theoret. Chim. Acta*, **80,** 95.
[6] MONKHORST, H. J., 1977, *Int J. quantum Chem. Symp.*, **11,** 421.
[7] COESTER, C., and KÜMMEL, H., 1960, *Nucl. Phys.*, **17,** 4777.
[8] ČIŽEK, J., 1966, *J. chem. Phys.*, **45,** 4256;.
[9] KUTZELNIGG, W., 1982, *J. chem. Phys.*, **77,** 3081.
[10] KÜMMEL, H., and LÜHRMANN, H., 1972, *Nucl. Phys.* A, **191,** 525; *ibid.*, **194,** 225.
[11] PAL, S., PRASAD, M. D., and MUKHERJEE, D., 1983, *Theoret. Chim. Acta*, **62,** 523; PAL, S., 1990, *Phys. Rev.* A, **42,** 4358.
[12] JEZIORSKI, B., and MOSZYNSKI, R., 1993, *Int J. quantum Chem.*, **48,** 161.
[13] BARTLETT, R. J., and NOGA, J., 1988, *Chem. Phys. Lett.*, **150,** 29; WATTS, J. D., TRUCKS, B. W., and BARTLETT, R. J., 1989, *Chem. Phys. Lett.*, **157,** 359; NOGA, J., KUCHARSKI, S. A., and BARTLETT, R. J., 1989, *J. chem. Phys.* **90,** 3399.
[14] BARTLETT, R. J., WATTS, J. D., KUCHARSKI, S. A., and NOGA, J., 1990, *Chem. Phys. Lett.*, **165,** 513; KUCHARSKI, S. A., and BARTLETT, R. J., 1995, *Chem. Phys Lett.*, **237,** 264.
[15] KUCHARSKI, S. A., 1994, presented at the workshop on electron correlation at Smolenice, Slovakia.
[16] RAGHAVACHARI, K., TRUCKS, B. W., POPLE, J. A., and HEAD-GORDON, M., 1989, *Chem. Phys. Lett.*, **157,** 479.
[17] URBAN, M., NOGA, J., COLE, S. J., and BARTLETT, R. J., 1985, *J. chem. Phys.*, **83,** 404; NOGA, J., and KUTZELNIGG, W., 1994, *J. chem. Phys.*, **101,** 7738.
[18] POPLE, J. A., HEAD-GORDON, M., and RAGHAVACHARI, K., 1987, *J. chem. Phys.*, **87,** 5968.

MOLECULAR PHYSICS, 1998, VOL. 94, No. 1, 73–85

An *ab initio* coupled cluster theory of quantum spin lattices and their quantum critical behaviour

By R. F. BISHOP and D. J. J. FARNELL

Department of Physics, UMIST, University of Manchester Institute of Science and Technology, PO Box 88, Manchester M60 1QD, UK

Strongly interacting quantum spin–lattice models exhibit a wide variety of phases with diverse and subtle magnetic ordering properties. Their detailed description within a unified microscopic framework poses a real challenge for the many-body theorist. By specific application to the spin-$\frac{1}{2}$ anisotropic Heisenberg model on a square lattice, we show how the *ab initio* coupled cluster method, which has already been very successfully applied to a wide variety of quantum many-body and field-theoretic systems, may be very efficiently and systematically implemented for spin–lattice models. Results for such local properties as the ground-state energy and sublattice magnetization are thereby obtained which are on a par with those from the best of the available alternative methods. Furthermore, we demonstrate explicitly how the coupled cluster method now also provides an effective and fully microscopic tool to yield systematic and accurate estimates of the zero-temperature quantum phase transition boundaries between states of different quantum order, as well as of the critical behaviour of the system in the vicinity of the transition points.

1. Introduction

In recent years the *ab initio* techniques available for treating the properties of quantum-mechanical many-body systems at the fully microscopic level have become increasingly refined and accurate. The inexorable rise in the power of modern computers has also allowed the techniques to be applied to systems of ever-increasing complexity, whether these be larger or more complicated molecules or infinite systems with more subtle ordering properties.

One such method which stands to the fore in this regard is the coupled cluster method (CCM) [1–9]. The CCM, already very well known to the quantum chemistry community [2, 8], has also become widely recognized throughout the theoretical physics community as providing one of the most powerful, most widely applicable, and most accurate at attainable levels of practical implementation, of all available *ab initio* microscopic techniques of quantum many-body/field theory.

Despite the many achievements of the CCM and other techniques of modern quantum many-body theory (such as the method of correlated basis functions, which provides a systematic means of improving upon the variational results using such popular trial correlated wave functions as those used in Jastrow theory), the use of these techniques has been largely limited up until now to a local description of the properties of the system under consideration, rather than to its global behaviour. Thus, until very recently, most of these fully microscopic calculations had been restricted to calculations of such local properties as the ground-state energy, the excitation spectrum, and such other properties as the relevant order parameters and correlation functions. By contrast, very little progress had been made on using the *same* techniques to make contact at the microscopic level with the otherwise quite disparate corpus of work which relates to the study of phase transitions in infinite systems and to related (e.g. shape) transitions in finite systems. This situation is now beginning to change in fundamental ways, due largely to recent results obtained using the CCM which we describe in this article.

In order to set the scene for the results to be presented, we note that there are now many physical systems which are characterized by novel ground states which display *quantum order* in some regions of the relevant parameter space. Such regions are delimited by critical values which mark the respective *quantum phase transitions*. Very often, the critical phenomena displayed by the quantum systems differ profoundly from their corresponding classical counterparts (where they exist). The subtle correlated quantum-mechanical states usually cannot sensibly be viewed within the traditional language of Landau's theory of Fermi liquids, for example, or of other comparable phenomenological approaches which have been so useful in the past for so many conventional quantum many-body systems. Examples of systems or phenomena which fall into the unconventional (or novel) class include heavy fermions, the fractional quantum Hall effect, new quantum states in the condensed phases of helium, confinement/decon-

0026–8976/98 $12·00

finement phase transitions in gauge field theories, high-temperature superconductors and other strongly correlated electronic systems, and various phases of (antiferro)magnetic materials and low-dimensional quantum spin lattices.

The standard many-body techniques, such as perturbation theory, mean-field theories, and variational calculations, which have been successfully developed and applied for conventional systems, typically fail completely for these unconventional systems characterized by novel quantum order. One of the key challenges for modern quantum many-body theory is now to develop and exploit microscopic techniques which are capable of describing both these novel and the more conventional systems. A prime objective of our own recent work on quantum lattice systems [10–18] has been to show that at least one such modern technique, namely the CCM, is in fact already able to bridge these two classes of systems.

We note that the CCM has been applied over the last five or so years to a variety of lattice Hamiltonian systems [15, 16], including spin lattices of interest, for example, in magnetism [10–14, 19–26] and the solid phases of ^{3}He [19]; electron lattice models of interest, for example, in the cuprate high-temperature superconductors (e.g. the Hubbard model) [17, 27]; and lattice gauge theories, such as the Abelian $U(1)$ model [18] and the non-Abelian $SU(2)$ model [28]. In all cases the CCM may readily be implemented to high orders of approximation by the use of computer-algebraic techniques. Values for ground-state (and, increasingly, also excited-state) properties are thereby obtained which are fully competitive with those from other state-of-the-art calculations, including the much more computationally intensive quantum Monte Carlo techniques. What we now further demonstrate, by a specific application to the spin-$\frac{1}{2}$ anisotropic Heisenberg model on the two-dimensional (2D) square lattice, is that the CCM can also provide information on the quantum order and quantum criticality inherent in this model. We believe that this example illustrates how the CCM is now well placed to study in a very systematic and unbiased manner the quantum phase transitions of the novel non-Fermi-liquid systems discussed above.

In section 2 below we briefly describe the fundamentals of the CCM as it is applied to quantum spin lattices, and in section 3 we describe its application in detail to various phases of the 2D spin-$\frac{1}{2}$ XXZ (or anisotropic Heisenberg) model on a square lattice. The results are discussed in section 4, with special emphasis both on their accuracy and their ability to predict phase transitions and to describe the ensuing critical behaviour at the transition points. We conclude in section 5 with a discussion of possible extensions of the method and its potential for use with other systems which exhibit quantum phase transitions between states of different quantum order.

2. The CCM for quantum spin lattices

Although detailed descriptions of both the general CCM formalism [1–9] and its application to specific spin lattice models [10–14] have been given elsewhere, we highlight here such of the essential general ingredients as are required for present purposes. Our aim in this section is to be as general as possible.

In the so-called single-reference version of the normal (as opposed to the extended [5, 7]) variant of the CCM, to which we restrict ourselves here, we first require the choice of a suitable single model or reference state $|\Phi\rangle$, in terms of which a quantitative and systematic description of the many-body (i.e. in the present case, multi-spin) correlations or fluctuations may be given. We defer until later the important question of how to choose $|\Phi\rangle$ in practice, but simply recall now that it is required only to be a cyclic vector with respect to two well-defined Abelian subalgebras of multi-configurational creation operators $\{C_I^+\}$ and their Hermitian-adjoint destruction counterparts $\{C_I^- \equiv (C_I^+)^\dagger\}$. Thus, $|\Phi\rangle$ plays the role of a vacuum state with respect to a suitable set of (mutually commuting) many-body creation operators $\{C_I^+\}$,

$$C_I^-|\Phi\rangle = 0, \qquad \forall I \neq 0, \tag{1}$$

with $C_0^- \equiv I$, the identity operator. These operators are also complete in the many-body Hilbert (or Fock) space,

$$I = |\Phi\rangle\langle\Phi| + \sum_{I\neq 0} C_I^+|\Phi\rangle\langle\Phi|C_I^-. \tag{2}$$

The choice of the operators $\{C_I^+\}$ clearly depends on the choice of $|\Phi\rangle$, but for spin lattice problems in general C_I^+ will involve products of the basic $SU(2)$ spin operators $\{s_k^+, s_k^-, s_k^z\}$ on different lattice sites k, which obey the fundamental commutation relations,

$$[s_k^z, s_l^\pm] = \pm s_k^\pm \delta_{kl}; \qquad [s_k^+, s_l^-] = 2s_k^z\delta_{kl}, \tag{3}$$

where $s_k^\pm \equiv s_k^x \pm is_k^y$. The set-index I will thus generally incorporate the indices for a set of lattice sites. We discuss particular choices of $\{|\Phi\rangle, C_I^+\}$ in more detail below in the context of a specific example.

The exact ground-state energy eigenket and eigenbra vectors, $|\Psi\rangle$ and $\langle\tilde{\Psi}|$ respectively, of a many-body system described by a Hamiltonian H, satisfy the Schrödinger equations,

$$H|\Psi\rangle = E_g|\Psi\rangle; \qquad \langle\tilde{\Psi}|H = E_g\langle\tilde{\Psi}|. \tag{4}$$

We have introduced the tilde notation on the bra state, $\langle\tilde{\Psi}|$, to remind ourselves of the fact that although the *exact* $\langle\tilde{\Psi}|$ is self-evidently related to $|\Psi\rangle$ by Hermiticity, the CCM parametrizations of $|\Psi\rangle$ and $\langle\tilde{\Psi}|$ do not manifestly preserve this Hermiticity as explained below.

Furthermore, the tilde notation also serves to recall that even if the exact Hermiticity holds, $\langle\tilde{\Psi}|$ differs from $(|\Psi\rangle)^\dagger$ by a normalization constant, as discussed below.

The ket and bra states are now specified within the single-reference normal CCM as,

$$\begin{aligned} |\Psi\rangle &= \exp(S)|\Phi\rangle; \qquad S = \sum_{I\neq 0} \mathcal{S}_I C_I^+, \\ \langle\tilde{\Psi}| &= \langle\Phi|\tilde{S}\exp(-S); \qquad \tilde{S} = 1 + \sum_{I\neq 0} \tilde{\mathcal{S}}_I C_I^-, \end{aligned} \tag{5}$$

where the tilde notation on the operator $\tilde{S}$ is not intended to convey any direct mathematical relationship between $\tilde{S}$ and S. Rather, equation (5) *defines* the operators S and $\tilde{S}$. We note that the correlation operator S is decomposed entirely in terms of the multiconfigurational creation operators $\{C_I^+\}$, and similarly for $\tilde{S}$ in terms of the destruction operators $\{C_I^-\}$. We further note that although the manifest Hermiticity, $(\langle\tilde{\Psi}|)^\dagger = |\Psi\rangle/\langle\Psi|\Psi\rangle$, is lost, the intermediate normalization condition, $\langle\tilde{\Psi}|\Psi\rangle = \langle\Phi|\Psi\rangle = \langle\Phi|\Phi\rangle \equiv 1$ is imposed. Furthermore, the correlation coefficients $\{\mathcal{S}_I, \tilde{\mathcal{S}}_I\}$ are regarded as being independent variables, even though formally we have the relation,

$$\langle\Phi|\tilde{S} = \frac{\langle\Phi|\exp(S^\dagger)\exp(S)}{\langle\Phi|\exp(S^\dagger)\exp(S)|\Phi\rangle}. \tag{6}$$

In particular, the full set of coefficients $\{\mathcal{S}_I, \tilde{\mathcal{S}}_I\}$ provides a complete CCM description of the many-body ground state. For example, an arbitrary operator A has a ground-state expectation value,

$$\begin{aligned} \bar{A} &\equiv \langle\tilde{\Psi}|A|\Psi\rangle = \langle\Phi|\tilde{S}\exp(-S)A\exp(S)|\Phi\rangle \\ &= \bar{A}(\{\mathcal{S}_I, \tilde{\mathcal{S}}_I\}). \end{aligned} \tag{7}$$

We note that the specific parametrization of equation (5) for $\langle\tilde{\Psi}|$ is consistent with the Hellmann–Feynman theorem [5], even though it does not manifestly preserve the Hermiticity relation with $|\Psi\rangle$. Furthermore, and very importantly, this parametrization for $\langle\tilde{\Psi}|$ is actually derivable from the Hellmann–Feynman theorem if one chooses the specific functional form for the energy, $E_g = \langle\Phi|\exp(-S)H\exp(S)|\Phi\rangle$, which immediately follows from equations (4) and (5).

As is by now well known, the exponentiated form of the ground-state eigenket parametrization of equation (5) ensures both the proper counting of the *independent* fluctuations of excited multi-spin configurations (described by the set-index I) with respect to $|\Phi\rangle$, which are present in the exact ground state $|\Psi\rangle$, and the exact incorporation of the linked cluster theorem of Goldstone. The latter, in turn, guarantees the size-extensivity of all relevant physical quantities, and thus allows us to work in the CCM directly in the thermodynamic limit, $N \to \infty$, where N is the number of lattice spins.

By taking appropriate projections of the ground-state bra and ket Schrödinger equations (i.e. with states $C_I^+|\Phi\rangle$ and $\langle\Phi|C_I^-$, respectively), we obtain coupled sets of equations which may be solved to obtain the coefficients $\{\mathcal{S}_I\}$ and $\{\tilde{\mathcal{S}}_I\}$. Completely equivalently, the correlation coefficients $\{\mathcal{S}_I, \tilde{\mathcal{S}}_I\}$ may be determined variationally by requiring that the ground-state energy functional $\bar{H}(\{\mathcal{S}_I, \tilde{\mathcal{S}}_I\})$, defined as in equation (7), is stationary with respect to variations in each of the (independent) variables of the full set. The following coupled sets of equations are thereby easily derived,

$$\delta\bar{H}/\delta\tilde{\mathcal{S}}_I = 0 \Rightarrow \langle\Phi|C_I^-\exp(-S)H\exp(S)|\Phi\rangle = 0, \quad \forall I \neq 0; \tag{8}$$

$$\delta\bar{H}/\delta\mathcal{S}_I = 0 \Rightarrow \langle\Phi|\tilde{S}\exp(-S)[H, C_I^+]\exp(S)|\Phi\rangle = 0, \quad \forall I \neq 0. \tag{9}$$

Equation (8) also ensures that the ground-state energy at the stationary point has the simple form

$$E_g = E_g(\{\mathcal{S}_I\}) = \langle\Phi|\exp(-S)H\exp(S)|\Phi\rangle, \tag{10}$$

which also follows simply by projecting the ground-state ket equation (4) with $\langle\Phi|\exp(-S)$. We note that this bivariational formulation does *not*, however, lead to an upper bound for E_g when the summations over configurations $\{I\}$ in equation (5) for S and $\tilde{S}$ are truncated in specific approximations, since the exact Hermiticity between $|\Psi\rangle$ and $\langle\tilde{\Psi}|$ will thereby be lost. On the other hand, it is important to note that the Hellmann–Feynman theorem *is* preserved in all such approximations, and for many purposes this may be of greater usefulness than the variational bound on the energy.

Equation (8) clearly represents a coupled set of nonlinear multinomial equations for the c-number correlation coefficients $\{\mathcal{S}_I\}$. The well-known nested commutator expansion for the similarity-transformed Hamiltonian,

$$\begin{aligned} \hat{H} &\equiv \exp(-S)H\exp(S) \\ &= H + [H, S] + \frac{1}{2!}[[H, S], S] + \cdots, \end{aligned} \tag{11}$$

taken together with the fact that all of the individual components of S in the sum in equation (5) commute with one another, imply that each element of S in equation (5) is thus directly linked to the Hamiltonian in each of the non-vanishing terms in equation (11). Each of the coupled set of equations (8) is hence of linked cluster type. What is more, each of these equations is also of finite length when expanded using equation (11), since this otherwise infinite series will actually terminate at a finite order here, provided only that each term in the Hamiltonian H contains a finite number of single-site

spin operators, as is usually the case. The CCM parametrization thus leads in a very natural way to a workable scheme, which can also be efficiently implemented as described in more detail below. It is also important to realize that the similarity transformation lies at the heart of the CCM and is one of its most vital ingredients. It may be contrasted with its unitary transformation counterpart in a standard variational formulation in which the bra state $\langle\tilde{\Psi}|$ is manifestly taken as being proportional to the Hermitian adjoint of $|\Psi\rangle$, as in equation (6).

We turn now to the choice of $|\Phi\rangle$ and the operators $\{C_I^+\}$ for spin–lattice problems. To be specific we restrict ourselves henceforth to spin-$\frac{1}{2}$ quantum antiferromagnets in regions where the corresponding classical limit is described by a generalized Néel-like ordering in which all spins on each sublattice are separately aligned in the coordinates of a global spin quantization axis and corresponding global spin axes. In such cases it is a simple matter (and see section 3 for specific details in the case considered here) to introduce a different local quantization axis and spin coordinates on each sublattice, by a suitable rotation in spin space, so that the corresponding Néel-like state becomes a fully aligned ('ferromagnetic') state in the local axes. This 'ferromagnetic' state is chosen as the uncorrelated CCM model state, $|\Phi\rangle$, in which all spins point, say, along the respective negative z axis of the corresponding local frames,

$$|\Phi\rangle = \bigotimes_{i=1}^{N} |\downarrow\rangle_i; \text{in the local quantization axes.} \qquad (12)$$

Thus, in the local spin coordinates,

$$s_k^z|\Phi\rangle = -\tfrac{1}{2}|\Phi\rangle, \qquad (13)$$

for any arbitrary site k.

The correlation operator S of equation (5) may now be decomposed wholly in terms of sums of products of single spin-raising operators, s_k^+, again defined with respect to the local quantization axes. Thus, we may write,

$$\begin{aligned} S &= \sum_{i_1} \mathcal{S}_{i_1} s_{i_1}^+ + \sum_{i_1,i_2} \mathcal{S}_{i_1 i_2} s_{i_1}^+ s_{i_2}^+ + \cdots \\ &= \sum_{n=1}^{N} \sum_{i_1 \cdots i_n} \mathcal{S}_{i_1 \cdots i_n} s_{i_1}^+ \cdots s_{i_n}^+, \end{aligned} \qquad (14a)$$

where $\mathcal{S}_{i_1 i_2 \cdots i_n}$ are the corresponding (symmetric) spin-correlation coefficients specified by the sets of site indices $\{i_1, i_2, \cdots, i_n\}$ on the regular lattice under consideration. The corresponding expansion for the operator $\tilde{S}$ of equation (5) is given by

$$\tilde{S} = 1 + \sum_{n=1}^{N} \sum_{i_1 \cdots i_n} \tilde{\mathcal{S}}_{i_1 \cdots i_n} s_{i_1}^- \cdots s_{i_n}^-. \qquad (14b)$$

The coefficients $\{\mathcal{S}_{i_1 \cdots i_n}, \tilde{\mathcal{S}}_{i_1 \cdots i_n}; n = 1, 2, \ldots, N\}$ are thus what we denoted generically by the set $\{\mathcal{S}_I, \tilde{\mathcal{S}}_I\}$ previously. Equation (8) thus yields the specific set of coupled nonlinear CCM equations,

$$\langle\Phi| s_{i_1}^- s_{i_2}^- \cdots s_{i_n}^- \exp(-S) H \exp(S) |\Phi\rangle = 0, \qquad (15)$$

to determine the correlation coefficients $\{\mathcal{S}_{i_1 i_2 \cdots i_n}\}$.

We note that we may map the sets of coefficients $\{\mathcal{S}_{i_1 \cdots i_n}\}$ and $\{\tilde{\mathcal{S}}_{i_1 \cdots i_n}\}$ onto sets $\{\mathcal{X}_r\}$ and $\{\tilde{\mathcal{X}}_r\}$ respectively, where r labels the *independent* or fundamental configurations, i.e. only those that are inequivalent under the lattice symmetries (namely, translations, rotations, and reflections) of the Hamiltonian and under permutations of the indices. The sets $\{\mathcal{X}_r\}$ and $\{\tilde{\mathcal{X}}_r\}$ are thus defined to count the independent correlation coefficients associated with each fundamental configuration once and once only. Generally speaking there will be $N\nu_r(n_r)!$ equivalent configurations on the lattice associated with each fundamental configuration, where n_r is the number of sites in the rth configuration and $(n_r)!$ is the combinatorial factor associated with permutations of the n_r indices, the factor N arises from the translations, and the factor ν_r is the replication factor of the rth configuration associated with the point symmetry group (or sub-group) of transformations on the lattice which preserve the Hamiltonian. In particular, we need only to consider one of the $N\nu_r(n_r)!$ equivalent sets of equations (15) associated with each independent coefficient $\mathcal{X}_r$.

At this point we need to consider approximation schemes whereby the expansions of S and $\tilde{S}$ in equations (14a) and (14b) may be truncated to some finite or infinite subset of the full set of independent (fundamental) multi-spin configurations. The three most commonly employed schemes have been: (1) the SUBn scheme, in which all correlations involving only n or fewer spins are retained, but no further restriction is made concerning their spatial separation on the lattice; (2) the SUBn-m sub-approximation, in which all SUBn correlations spanning a range of no more than m adjacent lattice sites are retained; and (3) the localized LSUBm scheme, which retains all multi-spin correlations over all possible distinct locales on the lattice defined by m or fewer contiguous sites. For the results reported below we adopt only the LSUBm scheme here.

The practical implementation of the CCM thus now consists of first enumerating all distinct multi-spin correlation configurations retained in the selected approximation, and then generating the corresponding set of CCM equations. The first stage is essentially a problem in graph theory, whereas equation (15) shows that the second stage involves two distinct computational aspects

in the calculation of all possible non-zero contributions to the matrix element on the left-hand side of this equation. Thus, the first step is to calculate the similarity-transformed Hamiltonian, $\hat{H} = \exp(-S)H\exp(S)$, and hence $\hat{H}|\Phi\rangle$; while the second is to select those terms of $\hat{H}|\Phi\rangle$ which match exactly the string of spin-lowering operators represented by the set of site indices $\{i_1, i_2, \ldots, i_n\}$, and which hence give a non-zero overlap. Clearly, the former problem is intrinsically related to the non-commutative nature of quantum spin operators, and relies only on the algebraic relations of equation (3); while the latter problem is intrinsically related to the geometric properties of the spatial lattice under consideration, and is essentially a problem of pattern-matching. We have shown elsewhere [29] how each of the above stages may very efficiently be implemented computationally to very high orders, to yield a set of coupled CCM ket-state equations which may then be solved by standard Newton–Raphson techniques. The bra-state equations are also handled in an analogous fashion.

In the following section the power of the CCM is illustrated by application to the spin-$\frac{1}{2}$ anisotropic Heisenberg (or *XXZ*) model on an infinite 2D square lattice.

3. The spin-$\frac{1}{2}$ XXZ antiferromagnet on the 2D square lattice

3.1. *The Hamiltonian*

The *XXZ* Hamiltonian is specified in terms of global spin coordinates as follows,

$$H = \sum_{\langle i,j \rangle} [s_i^x s_j^x + s_i^y s_j^y + \Delta s_i^z s_j^z], \tag{16}$$

where the sum on $\langle i,j \rangle$ runs over all nearest-neighbour pairs and counts each pair once only. We note that on the 2D square lattice this model has no exact solution, unlike its 1D chain counterpart which has been shown to be exactly integrable (and hence solved) using the Bethe ansatz. The *XXZ* model appears to have at least three distinct regimes: an Ising-like phase for sufficiently large values of the anisotropy parameter Δ, which is characterized by non-zero Néel order wherein nearest-neighbour spins in the ground-state wave function align antiparallel along the z axis; a planar-like phase in which the spins in the ground-state wave function are believed to lie in the xy plane; and a ferromagnetic phase.

Barnes and his co-workers [30] have performed a Monte Carlo study of the 2D *XXZ* model on a square lattice. They observed that while the staggered magnetization is non-zero in the z direction for $\Delta > 1$, it appears to fall to zero below $\Delta = 1$. They conclude that there is a phase transition at or very near to the Heisenberg point $\Delta = 1$, exactly as in the 1D case. Kubo and Kishi [31] have also investigated the ground state of the 2D square lattice *XXZ* model by making use of exact sum rules. They found that the ground state possesses an off-diagonal long-range order similar to that of the *XY* model at small values of the anisotropy parameter, $0.0 < \Delta < 0.13$. They also found that for values $\Delta > 1.78$ the system possesses non-zero Ising-like long-range order. Finally, at $\Delta = -1$ there is a first-order phase transition to a ferromagnetic phase which exists for all $\Delta < -1$ for this model. Although there are no exact proofs available, it is widely believed that the model has a phase (or perhaps more than one phase) with planar-like order for $-1 < \Delta < 1$, and an Ising-like phase with Néel-like antiferromagnetic order along the z axis for $\Delta > 1$.

The isotropic Heisenberg point ($\Delta = 1$) is thus expected to be a critical point marking the transition between states of different quantum order. We shall use it here as a specific example to test the ability of the CCM to predict phase transitions and its potential to discuss the critical phenomena (e.g. the critical indices) at this point. For the sake of later comparisons we note that Runge [32] has performed the most accurate Monte Carlo simulations available up until now for the square-lattice spin-$\frac{1}{2}$ isotropic Heisenberg antiferromagnet. By performing simulations on lattices up to size 16×16, and by extrapolating to the infinite lattice limit, $N \to \infty$, he finds a value for the ground-state energy per spin of $E_g/N = -0.669\,34 \pm 0.000\,04$, and a value for the sublattice magnetization, M^+, which is $(61.5 \pm 0.5)\%$ of the classical value. By comparison, linear spin-wave theory (LSWT) [33] gives a value of $E_g/N = -0.658$ and a value for M^+ which is 60.6% of the classical value.

3.2. *Choice of CCM model state*

There is never a unique choice of model state $|\Phi\rangle$. Our choice should usually be guided by any physical insight available to us concerning the system or, more specifically, that particular phase of it which is under consideration. In the absence of any insight into the quantum many-body system one may sometimes be guided by the behaviour of the corresponding classical system. The *XXZ* model under consideration provides just such an illustrative example. Thus, for $\Delta > 1$ the *classical* Hamiltonian of equation (16) on the 2D square lattice (and, indeed, on any bipartite lattice) is minimized by a perfectly antiferromagnetically Néel-ordered state in the z direction, whereas for $-1 < \Delta < 1$ it is minimized by a correspondingly ordered state with spins antiferromagnetically aligned along any direction in the xy plane, say along the x axis. Thus, we see that even for the same spin model and lattice, different choices of model state may be preferable, depending

on the particular regime of parameter space in which we are interested. For present purposes we shall utilize both of these classical Néel states, namely the z-aligned Néel state and the x-aligned Néel state (with the latter henceforth denoted as the planar model state), for two separate sets of corresponding CCM calculations. In both cases we now set up different local sets of spin axes on both sublattices so that in the local coordinates all spins in both model states point in the negative z direction, as discussed above in section 2 (and see equation (12)).

For the z-aligned Néel state we simply perform a rotation of the axes of the up-pointing spins by 180° about the y axis, such that

$$s^x \rightarrow -s^x, \qquad s^y \rightarrow s^y, \qquad s^z \rightarrow -s^z. \tag{17}$$

The Hamiltonian of equation (16) may now be written in these local axes as

$$H^z = -\frac{1}{2}\sum_{\langle i,j\rangle}\left[s_i^+ s_j^+ + s_i^- s_j^- + 2\Delta s_i^z s_j^z\right], \tag{18}$$

where the superscript z on H^z reminds us that the Hamiltonian is written in the local spin coordinate axes appropriate to the z-aligned Néel model state.

In order to produce a 'ferromagnetic' model state, as in equation (12), for the planar model state in the local frames, we rotate the axes of the left-pointing spins (i.e. those pointing in the negative x direction) in the planar state by 90° about the y axis, and the axes of the corresponding right-pointing spins by −90° about the y axis. (Note that the positive z axis is defined here to point upwards and the positive x axis is defined to point rightwards.) Thus, the transformations of the local axes are described such that

$$s^x \rightarrow s^z, \qquad s^y \rightarrow s^y, \qquad s^z \rightarrow -s^x \tag{19}$$

for the left-pointing spins, and such that

$$s^x \rightarrow -s^z, \qquad s^y \rightarrow s^y, \qquad s^z \rightarrow s^x \tag{20}$$

for the right-pointing spins. The transformed Hamiltonian of equation (16) may now be written in these local axes as

$$H^{\mathrm{p}} = -\frac{1}{4}\sum_{\langle i,j\rangle}\left[(\Delta+1)(s_i^+ s_j^+ + s_i^- s_j^-) + (\Delta-1)(s_i^+ s_j^- + s_i^- s_j^+) + 4 s_i^z s_j^z\right], \tag{21}$$

where, again, the superscript p on H^{p} reminds us that the Hamiltonian is written in the local spin coordinate axes appropriate to the planar model state. It is important to recall that since the Hamiltonians H, H^z, and H^{p} of equations (16), (18), and (21) differ only by similarity transformations their eigenvalue spectra are identical.

3.3. *Enumeration of the independent correlation configurations*

The first step in the practical implementation of the CCM at the LSUBm level of approximation discussed in section 2 is to enumerate all of the distinct multi-spin configurations or correlated clusters, which we shall henceforth call *fundamental* configurations, $\{i_1, i_2, \ldots, i_n\}$ with $n < m$, which are retained at the LSUBm level. Only those configurations which cannot be obtained from one another using the lattice symmetries (namely, translations, rotations and reflections) shared by the Hamiltonian are to be counted as distinct. For the square lattice under consideration there are four rotational operations, (0°, 90°, 180°, 270°), and four reflections (along the x and y axes, and along the lines $y = \pm x$), which preserve the symmetries of both the lattice and the Hamiltonian. Each such fundamental configuration is associated with two single independent correlation coefficients $\mathcal{X}_r$ and $\tilde{\mathcal{X}}_r$ associated with the cluster operators S and $\tilde{S}$ respectively, as discussed in section 2. Each correlated cluster may be either a connected cluster of size m (also known as a 'lattice animal' or 'polyomino') or a connected or disconnected subset of it. We note that the enumeration of the number of lattice animals of size m on a regular lattice as m becomes large remains an open problem in combinatorial graph theory. However, efficient algorithms for their enumeration for $m \lesssim 20$ have been developed in such fields as cell growth and percolation theory.

We also note that although H^{p} and H^z are fully equivalent to one another, the number of fundamental LSUBm configurations at each level $m > 2$ is greater for H^{p} than for H^z due to other constraints which arise from symmetries of the Hamiltonian. Thus, firstly, we note that both H^{p} and H^z contain only even products of spin-flip operators (plus a single term containing two s^z operators). Repeated application of either Hamiltonian to the model state $|\Phi\rangle$ will thus only create states with an even number of spin flips with respect to it. Since the exact ground state may be obtained as a linear combination of states obtained by repeated application of the Hamiltonian to $|\Phi\rangle$, assuming only that $|\Phi\rangle$ is not orthogonal to the exact ground state, we may hence restrict ourselves to LSUBm fundamental configurations which contain an even number of spin flips, i.e. to coefficients $\mathcal{S}_{i_1 i_2 \cdots i_n}$ where n is even.

Secondly, we note that the number of fundamental configurations can be further reduced for H^z. Thus, H^z has the additional feature that when applied to $|\Phi\rangle$ it produces states with the same number of spin flips on both sublattices, and hence we can further restrict the fundamental configurations to those which preserve this feature. This symmetry is related to the fact that the original Hamiltonian, and hence also H^{p} and H^z, com-

mute with the z component of the total uniform magnetization, $s_T^z = \sum_i s_i^z$ (where s_i^z is defined with respect to the original global quantization axis, and the sum over the index i runs over all $N \to \infty$ lattice sites). However, whereas the z-aligned Néel model state is an eigenstate of s_T^z, the planar model state is not. Hence, for the z-aligned Néel model state one may explicitly conserve s_T^z (as zero for the antiferromagnetic sector) by restricting the fundamental configurations to those which produce no change in $s_T^z (= 0)$. We note the number of fundamental configurations up to the LSUB8 level of approximation for both model states in table 1. The actual calculations reported below are performed up to this level for H^z, but only up to LSUB6 level for H^{p} due to the increased number of fundamental configurations in the latter case.

We note also that H^{p} and H^z become identical at the Heisenberg point $\Delta = 1$. In the actual calculations this is reflected by the fact that the additional cluster correlation coefficients at a given LSUBm level included for H^{p} beyond those included for H^z become zero at this point, $\Delta \to 1^-$. Further details of the enumeration of the independent configurations is contained in [29].

3.4. *The CCM ket-state equations*

In order to evaluate the CCM ket-state equations (15), we first require the similarity-transformed Hamiltonians, $\hat{H}^z$ and $\hat{H}^{\mathrm{p}}$, defined as in equation (11). By making use of the fundamental $SU(2)$ commutation relations of equation (3) it is straightforward to show that after letting $\hat{H}^z$ act on $|\Phi\rangle$, as needed in equation (15), we have

$$\hat{H}^z|\Phi\rangle \equiv \exp(-S)H^z\exp(S)|\Phi\rangle = (\hat{H}_1^z + \hat{H}_2^z + \hat{H}_3^z)|\Phi\rangle, \tag{22}$$

where

$$\begin{aligned}\hat{H}_1^z = &-\frac{1}{2}\Delta\sum_{k\rho}(F_k^z F_m^z + G_{km}^z)s_k^+ s_m^+ \\ &-\frac{1}{4}\sum_{k\rho}[1 + (F_k^z)^2(F_m^z)^2 + 4F_k^z F_m^z G_{km}^z \\ &+ 2(G_{km}^z)^2]s_k^+ s_m^+,\end{aligned} \tag{23}$$

$$\begin{aligned}\hat{H}_2^z = &\frac{1}{4}\Delta\sum_{k\rho}(F_k^z s_k^+ + F_m^z s_m^+) \\ &+\frac{1}{4}\sum_{k\rho}(F_k^z F_m^z + 2G_{km}^z)(F_k^z s_k^+ + F_m^z s_m^+),\end{aligned} \tag{24}$$

$$\hat{H}_3^z = -\frac{1}{8}\sum_{k\rho}[\Delta + 2(F_k^z F_m^z + G_{km}^z)], \tag{25}$$

and where k runs over all lattice sites, and $m \equiv k + \rho$ such that ρ runs over all 4 nearest neighbours to k on the lattice. The operators F_k and G_{km} are defined generically as follows,

$$F_k \equiv \sum_{l=1}^{\infty} l \sum_{i_1 \cdots i_{l-1}} \mathcal{S}_{k i_1 \cdots i_{l-1}} s_{i_1}^+ \cdots s_{i_{l-1}}^+, \tag{26}$$

$$G_{km} \equiv \sum_{l=2}^{\infty} l(l-1) \sum_{i_1 \cdots i_{l-2}} \mathcal{S}_{km i_1 \cdots i_{l-2}} s_{i_1}^+ \cdots s_{i_{l-2}}^+, \tag{27}$$

and F_k^z and G_{km}^z are the particular cases where $\mathcal{S}_{i_1 \cdots i_n} \to \mathcal{S}_{i_1 \cdots i_n}^z$, namely the cluster correlation coefficients obtained by use of the present z-aligned Néel state and H^z. Equation (25) shows that the ground-state energy for the z-aligned Néel model state is simply given in terms of $x_1^z \equiv \mathcal{S}_{k,k+\rho}^z$, the nearest-neighbour two-body cluster correlation coefficient obtained by using H^z and the z-aligned Néel model state, as

$$\frac{E_{\mathrm{g}}}{N} = -\frac{1}{2}(4x_1^z + \Delta). \tag{28}$$

We note that $x_1^z \equiv \mathcal{S}_{k,k+\rho}^z$ is independent of k and ρ by the translational and rotational symmetries of the lattice.

The equivalent relations for $\hat{H}^{\mathrm{p}}$ are obtained as follows,

$$\hat{H}^{\mathrm{p}}|\Phi\rangle \equiv \exp(-S)H^{\mathrm{p}}\exp(S)|\Phi\rangle = (\hat{H}_1^{\mathrm{p}} + \hat{H}_2^{\mathrm{p}} + \hat{H}_3^{\mathrm{p}})|\Phi\rangle, \tag{29}$$

where

$$\begin{aligned}\hat{H}_1^{\mathrm{p}} = &\frac{1}{2}\sum_{k\rho}\Big\{-(F_k^{\mathrm{p}}F_m^{\mathrm{p}} + G_{km}^{\mathrm{p}}) + \frac{1}{4}(\Delta - 1) \\ &\times [(F_k^{\mathrm{p}})^2 + (F_m^{\mathrm{p}})^2]\Big\}s_k^+ s_m^+ \\ &-\frac{1}{8}(\Delta + 1)\sum_{k\rho}[1 + (F_k^{\mathrm{p}})^2(F_m^{\mathrm{p}})^2 + 4F_k^{\mathrm{p}}F_m^{\mathrm{p}}G_{km}^{\mathrm{p}} \\ &+ 2(G_{km}^{\mathrm{p}})^2]s_k^+ s_m^+,\end{aligned} \tag{30}$$

$$\begin{aligned}\hat{H}_2^{\mathrm{p}} = &\frac{1}{4}\sum_{k\rho}[F_k^{\mathrm{p}}s_k^+ + F_m^{\mathrm{p}}s_m^+ + \frac{1}{2}(1 - \Delta)(F_k^{\mathrm{p}}s_m^+ + F_m^{\mathrm{p}}s_k^+)] \\ &+\frac{1}{8}(\Delta + 1)\sum_{k\rho}(2G_{km}^{\mathrm{p}} + F_k^{\mathrm{p}}F_m^{\mathrm{p}})(F_k^{\mathrm{p}}s_k^+ + F_m^{\mathrm{p}}s_m^+),\end{aligned} \tag{31}$$

$$\hat{H}_3^{\mathrm{p}} = -\frac{1}{8}\sum_{k\rho}[1 + (\Delta + 1)(F_k^{\mathrm{p}}F_m^{\mathrm{p}} + G_{km}^{\mathrm{p}})]. \tag{32}$$

The operators F_k^{p} and G_{km}^{p} are again defined as in equations (26) and (27), but with the cluster correlation coefficients $\mathcal{S}_{i_1 \cdots i_n} \to \mathcal{S}_{i_1 \cdots i_n}^{\mathrm{p}}$ obtained by use of the present

planar model state and H^{P}. Equation (32) immediately yields,

$$\frac{E_{\mathrm{g}}}{N} = -\frac{1}{2}[2x_1^{\mathrm{P}}(\Delta + 1) + 1], \tag{33}$$

where $x_1^{\mathrm{P}} \equiv \mathcal{S}^{\mathrm{P}}_{k,k+\rho}$, the nearest-neighbour two-body cluster correlation coefficient obtained by using H^{P} and the planar model state.

In both cases the corresponding LSUBm equations are obtained by evaluating all non-zero contributions to equation (15). There is one such (coupled nonlinear) equation for every fundamental configuration retained, and hence N_{F} equations in N_{F} coefficients, for each level of approximation. The actual derivation of the ket-state equations from equation (15) and equations (22)–(25) or equations (29)–(32) is thus seen to reduce essentially to a pattern-matching exercise, and we describe elsewhere [29] its efficient computational implementation. The bra-state equations can also be derived in an analogous fashion.

4. Results

4.1. *Ground-state energy*

Results for the ground-state energy using the two model states are illustrated in figure 1 at the LSUB4 and LSUB6 levels of approximation, where they are compared with the Monte Carlo results of Barnes *et al.* [30]. The highest approximation that we have undertaken for the planar model state case is LSUB6, which contains 131 independent cluster configuration coefficients and which yields an energy per spin, $E_{\mathrm{g}}/N = -0.667\,00$ at the Heisenberg point ($\Delta = 1$). Due to the reduced number of independent configurations for the case of the z-aligned Néel model state we have also been

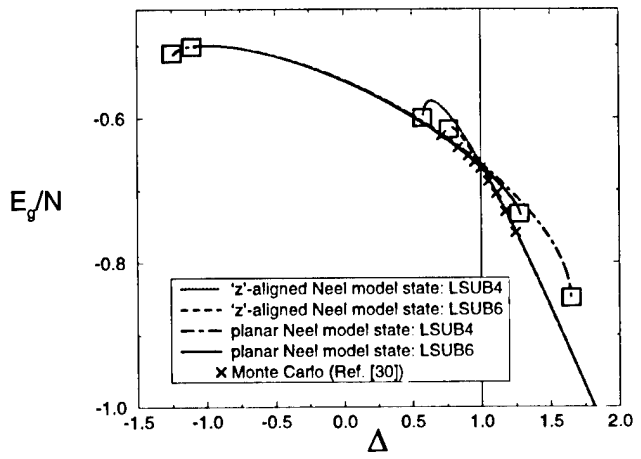

Figure 1. Results for the CCM ground-state energy of the spin-$\frac{1}{2}$ XXZ model on the 2D square lattice, using the LSUBm approximation with $m = 4, 6$ based on both the planar and z-aligned Néel model states, compared to the Monte Carlo results of [30]. LSUBm critical points, $\Delta_{\mathrm{F}}^{\mathrm{P}}$, $\Delta_{\mathrm{A}}^{\mathrm{P}}$ and Δ_{A}^{z}, are indicated by the boxes.

able to solve the higher LSUB8 approximation in this case. The 1287 coupled equations in this case yield a value of the energy per spin, $E_{\mathrm{g}}/N = -0.668\,17$ at $\Delta = 1$. The results for the Heisenberg model (which are identical using both model states for this case) are summarized in table 1, and ground-state energies are also shown in table 2 for a range of values of Δ, and for calculations using both model states as CCM reference states.

In order to compare our results with those cited in section 3.1 from other methods, we attempt a simple heuristic extrapolation of our LSUBm results to the limit $m \to \infty$ at the isotropic Heisenberg point ($\Delta = 1$). As has already been found elsewhere [11], our results seem to extrapolate well to their asymptotic value with a leading m-dependent correction that scales as m^{-2}. In this way we obtain an extrapolated value for the ground-state energy per spin of $E_{\mathrm{g}}/N = -0.669\,68$. This compares very well with the best Monte Carlo simulation value [32] of $-0.669\,34 \pm 0.000\,04$, and is very much more accurate, by comparison with this Monte Carlo value, than with the linear spin-wave theory (LSWT) result [33] of $E_{\mathrm{g}}/N = -0.658$.

Figure 1 and table 2 illustrate that at a given LSUBm level of approximation the CCM result for the ground-state energy using the z-aligned Néel model state lies lower than its counterpart using the planar model state for $\Delta > 1$, and vice versa for $\Delta < 1$. This result is precisely as would be expected classically, as discussed above in section 3.2, and it illustrates the power of being able to employ different CCM model states which are specifically geared to different possible phases. If we were simply to take that solution with the lower energy for each value of Δ (for which we note, however, that there is no real justification), we would infer that there is a phase transition at $\Delta = 1$ between a phase with Ising-like order at $\Delta > 1$ and a planar-like phase for $\Delta < 1$.

We note, furthermore, and much more importantly, that each separate calculation also yields evidence of such a phase transition. Thus, we find that beyond certain critical values, Δ_{c}, of the anisotropy parameter there exists no physically reasonable solution to the LSUBm CCM equations for $m \geqslant 4$, as is illustrated for the cases $m = 4, 6$ in figure 1. In previous work [11] we have related this characteristic breakdown of the CCM equations at certain critical points to actual phase transitions of the real system, and we explore this further in section 4.2 below. A useful means to detect phase transitions within the LSUBm scheme is to calculate the so-called anisotropy susceptibility, χ_{a},

$$\chi_{\mathrm{a}} \equiv -\frac{\partial^2(E_{\mathrm{g}}/N)}{\partial \Delta^2}. \tag{34}$$

Table 1. Results obtained for the spin-$\frac{1}{2}$ XXZ model on the 2D square lattice using CCM LSUBm approximations ($m = 2, 4, 6, 8$). N_F^p denotes the number of fundamental configurations for the planar model state, which are further decomposed in terms of connected and disconnected ones respectively, and N_F^z denotes the number of fundamental configurations for the z axis Néel model state. The ground-state energy per spin, E_g/N, and the sublattice magnetization, M^+, at the isotropic Heisenberg point ($\Delta = 1$) are shown, as well as extrapolated results in the limit $m \to \infty$. Various critical anisotropy parameters are also given. Δ_F^p and Δ_A^p indicate the LSUBm critical points for the planar model state corresponding to the ferromagnetic and antiferromagnetic phase transitions. Δ_A^z indicates the critical point for the z-axis Néel model state corresponding to the antiferromagnetic phase transition. Note that there are no terminating points in the LSUB2 approximation.

m	N_F^p	N_F^z	$\left.\frac{E_g}{N}\right\|_{\Delta=1}$	$M^+\|_{\Delta=1}$	Δ_F^p	Δ_A^p	Δ_A^z
2	1(1 + 0)	1(1 + 0)	−0.648 33	0.8414	—	—	—
4	10(6 + 4)	7(5 + 2)	−0.663 66	0.7648	−1.250	1.648	0.577
6	131(41 + 90)	75(29 + 46)	−0.667 00	0.7273	−1.084	1.286	0.7631
8	2793(410 + 2383)	1287(259 + 1028)	−0.668 17	0.7048	?	?	0.8429
∞	—	—	−0.669 68	0.62	−0.95	1.00	0.96 ± 0.04

Table 2. Results for the ground-state energy per spin of the 2D spin-$\frac{1}{2}$ XXZ model on the square lattice using both the planar and z-aligned Néel model states, compared with the Monte Carlo results of [30]. The '—' symbol indicates values of Δ which lie outside the range, defined by the Δ_F^p, Δ_A^p, and Δ_A^z critical points, in which there exists a physically reasonable solution to the LSUBm CCM equations for $m \geqslant 4$. The '**' symbol indicates points at which a Monte Carlo solution has not yet been determined.

	CCM results based on the planar Néel state				CCM results based on the z-aligned Néel state			
Δ	LSUB2	LSUB4	LSUB6	Monte Carlo	LSUB8	LSUB6	LSUB4	LSUB2
−1.0	−0.5	−0.5	−0.5	**	—	—	—	−0.8483
−0.5	−0.5103	−0.5145	−0.5151	**	—	—	—	−0.5885
0.0	−0.5403	−0.5473	−0.5483	**	—	—	—	−0.4472
0.5	−0.5874	−0.5959	−0.5975	**	—	—	—	−0.4885
0.714 29	−0.6120	−0.6222	−0.6242	−0.624	—	—	−0.5891	−0.5480
0.833 33	−0.6267	−0.6385	−0.6408	−0.641	—	−0.6199	−0.6116	−0.5875
0.90 909	−0.6364	−0.6496	−0.6523	−0.652	−0.6415	−0.6390	−0.6338	−0.6144
0.952 38	−0.6420	−0.6562	−0.6591	−0.661	−0.6535	−0.6518	−0.6477	−0.6304
1.0	−0.6483	−0.6637	−0.6670	−0.669	−0.6682	−0.6670	−0.6637	−0.6483
1.052 63	−0.6554	−0.6723	−0.6762	−0.687	−0.6856	−0.6848	−0.6821	−0.6686
1.111 11	−0.6634	−0.6823	−0.6871	−0.704	−0.7062	−0.7056	−0.7035	−0.6917
1.176 47	−0.6726	−0.6940	−0.7005	−0.729	−0.7303	−0.7298	−0.7282	−0.7180
1.25	−0.6830	−0.7082	−0.7189	−0.759	−0.7585	−0.7582	−0.7570	−0.7482
1.5	−0.7201	−0.7680	—	**	−0.8611	−0.8610	−0.8604	−0.8550
2.0	−0.8000	—	—	**	−1.0833	−1.0833	−1.0831	−1.0806

Since the CCM equations are known analytically, χ_a and all other derivatives may also be calculated *directly* (i.e. from analytic equations). We find that χ_a diverges at the critical points.

More specifically, we find that for the CCM calculations based on the planar model state χ_a diverges at critical values $\Delta_c = \Delta_F^p$ and Δ_A^p, corresponding to the ferromagnetic and antiferromagnetic phase transitions respectively, for all LSUBm approximations with $m > 2$. These results are illustrated in table 1, which also displays the single critical point at $\Delta_c = \Delta_A^z$ for the CCM calculations based on the z-aligned Néel model state, and which again corresponds to the antiferromagnetic phase transition. As one might hope, the position of the critical point Δ_F^p becomes closer to the true ferromagnetic phase transition at $\Delta = -1$ as the approximation level is increased. Also, both Δ_A^p and Δ_A^z appear to converge with increasing LSUBm index m, and for a given value of m always bound the point $\Delta = 1$ at which the true antiferromagnetic phase transition is believed (by symmetry arguments) to lie. We have shown elsewhere [11] how the corresponding SUB2-m

results for Δ_A^z seem to approach the full SUB2 value as m^{-2}, and the same rule fitted to the LSUBm results yields the corresponding predictions for the extrapolated antiferromagnetic point indicated in table 1, namely $\Delta_A^z \approx 0.96 \pm 0.04$, and $\Delta_A^p \approx 1.00$. Both predictions are compatible with each other and with the expected value $\Delta_A = 1$.

4.2. *Sublattice magnetization*

In order to discuss the phase transition further it is necessary to consider the degree of quantum order inherent in the CCM wave functions obtained at the various LSUBm levels of approximation, and based on both model states. The simplest such order parameter is the sublattice magnetization, $M^+ \equiv -2\langle s^z \rangle$, which is defined as the average over the entire lattice of s^z in the *local* (rotated) spin coordinates, or, equivalently over a single sublattice of the corresponding unrotated component of the spin in the original *global* coordinates. Thus, $M^+ = 1$ for both model states, with perfect antiferromagnetic alignment along the global z axis for the z-aligned state and along the global x axis for the planar state. Quantum fluctuations (i.e. multi-spin correlations) present in the exact interacting ground state are expected to reduce M^+ below unity. We would expect, *a priori*, that a phase transition would be marked by M^+ becoming zero (or, in an approximate calculation, singular) at some critical value of the coupling parameter, namely Δ for the present XXZ model.

By inserting the CCM parametrizations of equation (5) we find,

$$M^+ = -\frac{2}{N}\sum_{k=1}^{N}\langle\tilde{\Psi}|s_k^z|\Psi\rangle$$

$$= -\frac{2}{N}\sum_{k=1}^{N}\langle\Phi|\tilde{S}\exp(-S)s_k^z\exp(S)|\Phi\rangle, \qquad (35)$$

where s_k^z is in the local coordinates of each sublattice. In the notation of equation (26) we find

$$M^+ = 1 - \frac{2}{N}\sum_{k=1}^{N}\langle\Phi|\tilde{S}F_k s_k^+|\Phi\rangle$$

$$= 1 - \frac{2}{N}\sum_{n=1}^{\infty} n(n!)\sum_{i_1\cdots i_n}\tilde{\mathcal{S}}_{i_1\cdots i_n}\mathcal{S}_{i_1\cdots i_n}. \qquad (36)$$

The sum in equation (36) may be rewritten in terms of the independent correlation coefficients $\tilde{\mathcal{X}}_r$ and $\mathcal{X}_r$ associated with the N_F fundamental configurations of a given LSUBm approximation, which were introduced in section 2, to give the LSUBm estimate for M^+,

$$M^+ = 1 - 2\sum_{r=1}^{N_f} n_r(n_r!)^2\nu_r\tilde{\mathcal{X}}_r\mathcal{X}_r$$

$$= 1 - 2\sum_{r=1}^{N_f} n_r(n_r!)\tilde{x}_r x_r, \qquad (37)$$

where n_r is the number of spin flips with respect to $|\Phi\rangle$ for the rth fundamental configuration, and where we have introduced the notation $x_r \equiv \mathcal{X}_r$ and $\tilde{x}_r \equiv (n_r!)\nu_r\tilde{\mathcal{X}}_r$. For the square lattice considered here $\nu_r = 4$ or 8 for all allowed fundamental configurations.

Evaluation of the sublattice magnetization requires both the ket- and bra-state cluster correlation coefficients. We have described the computation of the ket-state coefficients in broad outline above. The bra-state coefficients are calculated similarly, by making use of the generic linear equations (9), once the ket-state coefficients are known. The actual procedure is straightforward, and is also described in more detail elsewhere [29].

Results for M^+ for the spin-$\frac{1}{2}$ 2D XXZ model on the square lattice using both CCM model states are shown in figure 2. Table 1 also summarizes the results at the isotropic Heisenberg point, $\Delta = 1$. We note again that the corresponding LSUBm results for M^+ at a given truncation level m are identical at $\Delta = 1$. We see clearly that over the entire range $-1 < \Delta < 1$ our results seem to converge well to a non-zero in-plane long-range order, with a non-zero planar sublattice magnetization, whereas for all $\Delta > 1$ we have comparable non-zero

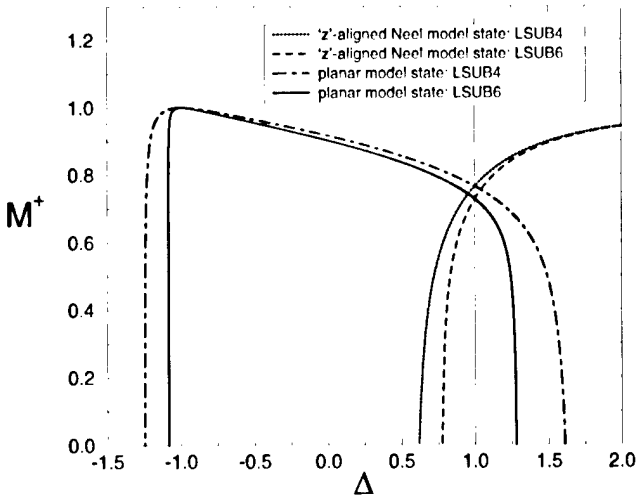

Figure 2. Results for the CCM sublattice magnetization M^+ of the spin-$\frac{1}{2}$ XXZ model on the 2D square lattice using the LSUBm approximation with $m = 4, 6$ based on both the planar and z-aligned Néel model states. The results indicate non-zero long-range order in the xy plane for $-1 < \Delta < 1$, and along the z axis for $\Delta > 1$.

long-range order along the spin z axis and a non-zero z component of sublattice magnetization.

We also note the divergence in M^+ near the critical points Δ_A^z and Δ_A^p, which strongly reinforces our interpretation of these points as reflecting a phase transition. As we approach one of these antiferromagnetic critical points for a given LSUBm approximation, we typically find that at least one of the CCM correlation coefficients x_r becomes very large, and hence M^+ diverges from equation (36).

We once again attempt a simple heuristic extrapolation of our LSUBm results for M^+ at the Heisenberg point ($\Delta = 1$) to the limit $m \to \infty$, in order to compare our results with those from other calculations. As has been found elsewhere [11] the results for M^+ extrapolate well to their asymptotic value with a leading correction that scales as m^{-1}. As shown in table 1 we thus obtain an extrapolated value, $M^+ = 0.62$. This compares extremely well with the best available Monte Carlo simulation value of Runge [32], $M^+ = 0.615 \pm 0.005$, and with the value $M^+ = 0.62 \pm 0.02$ from series expansion techniques [34].

4.3. *Critical properties*

We have demonstrated so far that CCM calculations using the LSUBm approximation scheme based on different model states are well able to describe both the Ising-like phase for $\Delta > 1$ and the planar-like phase for $-1 < \Delta < 1$ of the spin-$\frac{1}{2}$ 2D XXZ model on the square lattice. The results are not only extremely accurate for such quantities as the ground-state energy and sublattice magnetization as functions of Δ, but calculations based on each model state separately give accurate results for the critical values Δ_c which delimit the regime in Δ in which that model state is apposite. These critical values clearly mark (at the level of approximation considered) the physical phase boundaries. In this context it is natural to ask now whether our CCM formalism also has the power to predict the critical behaviour of the physical observables near such phase transitions, i.e. whether we can extract from the LSUBm results useful information on critical indices. We show below, by specific application to the same spin-$\frac{1}{2}$ square-lattice XXZ model, that this question can firmly be answered in the affirmative.

Thus, the critical index for the singular (non-analytic) term in E_g/N near an LSUBm critical point $\Delta_c(m)$ can first be obtained, for example, by direct examination of the anisotropy susceptibility, $\chi_a \equiv -\partial^2(E_g/N)/\partial\Delta^2$, of equation (34). For $m > 2$ we find,

$$\chi_a^m(\Delta) \longrightarrow \bar{\chi}_a^m |\Delta - \Delta_c(m)|^{-\alpha_0}; \qquad \Delta \to \Delta_c(m). \tag{38}$$

Direct calculation for the LSUBm approximations using both the z-aligned and planar Néel model states shows that for $m > 2$ we have $\alpha_0 \approx 1.500 \pm 0.005$. However, the prefactors $\bar{\chi}_a^m$ in equation (38) are themselves strongly dependent on the truncation index m. We may now use a variant of the so-called coherent anomaly method (CAM) of Suzuki [35], to extract further information. Thus, we attempt to fit $\bar{\chi}_a^m$ with the coherent anomaly form,

$$\bar{\chi}_a^m \longrightarrow K|\Delta_c(\infty) - \Delta_c(m)|^{\nu}; \qquad \Delta \to \Delta_c(\infty), \tag{39}$$

where K is a constant. Thus, as explained by Suzuki [35] one may intuit or prove that the exact $\chi_a(\Delta)$ has the critical form,

$$\chi_a(\Delta) \longrightarrow \kappa|\Delta - \Delta_c(\infty)|^{-\alpha_0+\nu}; \quad \Delta \to \Delta_c(\infty) \equiv \Delta_c, \tag{40}$$

where κ is a constant.

A CAM analysis along these lines of the LSUBm results based on the z-aligned Néel state gives $\nu \approx 1.25$ using the $\Delta_A^z(4)$ and $\Delta_A^z(6)$ data, and $\nu \approx 0.97$ using the $\Delta_A^z(6)$ and $\Delta_A^z(8)$ data. We thus obtain a singular term in E_g/N near Δ_A^z with a critical exponent $2 - \alpha_0 + \nu \approx 1.50$–$1.75$. This may be compared with the corresponding value of 3/2 for both the mean-field-like CCM SUB2 approximation (in which *all* 2-spin-flip correlation terms are retained, however far apart on the lattice) and linear spin-wave theory (LSWT). A corresponding analysis may also be carried out on the LSUBm results based on the planar model state near Δ_A^p. We again find $\alpha_0 \approx 1.500 \pm 0.005$ for both the LSUB4 and LSUB6 results, and a corresponding critical anomaly based on these of $\nu \approx 1.27$. We thus obtain a singular term in E_g/N near Δ_A^p with a critical exponent $2 - \alpha_0 + \nu \approx 1.77$. These preliminary data are clearly compatible with the hypothesis that the critical exponent in the energy is the same on both sides of the antiferromagnetic phase transition Δ_A.

Similar CAM analyses can also be performed for the ground-state energy near the corresponding ferromagnetic critical point Δ_F^p, and for such other properties as the sublattice magnetization M^+ near any of these critical points.

5. Conclusions

Our aim in the present paper has been to show that the well-known and much used coupled cluster method of microscopic quantum many-body theory may be used to great advantage to study quantum spin–lattice models at a level which includes the quantitative identification of zero-temperature quantum phase transition points between states of different magnetic ordering, and the various critical indices which describe their behaviour in the vicinity of these transitions. The CCM is now in the position of being virtually the only fully microscopic method available which can yield very ac-

curate results for both local ground-state properties and the global critical behaviour of these highly non-trivial systems.

We note that for spin–lattice models with nearest-neighbour interactions on bipartite lattices, such as the XXZ model considered here, quantum Monte Carlo results are also available. These are practicable for these models since the infamous 'minus-sign problem' which bedevils Monte Carlo simulations can be circumvented by mapping the models onto equivalent bosonic problems or, equivalently, by utilizing the Marshall sign rule [36] concerning the phase relations between the projection coefficients of the ground-state wave function onto a complete set of spin configurations. We have seen that our own CCM formalism can now be effectively implemented computationally to levels where the results are comparable in accuracy to the best Monte Carlo results for these cases.

By contrast, for *frustrated* models (e.g. models with both nearest-neighbour and next-nearest-neighbour interactions [12, 24, 25], or the same XXZ model considered here but on a 2D triangular lattice [13]) Monte Carlo simulations are much more difficult to implement (e.g. see [37] for the typical case of the isotropic spin-$\frac{1}{2}$ Heisenberg model on a triangular lattice). On the other hand, as we have shown elsewhere [12, 13, 24, 25], the CCM is no more difficult to implement, either in principle or in practice, for such frustrated systems. In particular, there is now a real hope that the CCM results can be used to guide more ambitious fixed-node-type Monte Carlo simulations of such systems, by providing better trial wave functions whose nodal surface structure can be taken from CCM LSUBm results.

Further extensions of our CCM formalism may also be envisaged. For example, LSUBm calculations on spin lattices where the spins have quantum number $s > \frac{1}{2}$ present no real difficulty [10(f)]. Thus, one merely generalizes to the case of 'multiple occupancy' of the sites $\{i_1, \ldots, i_n\}$ in the retained fundamental configurations, where each site can now be 'occupied' up to $2s$ times (i.e. since the spin-raising operator s_k^+ on site k can act on the 'ferromagnetic' model state $|\Phi\rangle$ in the local spin coordinates up to $2s$ times before it annihilates $|\Phi\rangle$). We are also hopeful that our general methodology can be applied to other unconventional (non-Fermi-liquid-type) systems of the sort discussed in section 1. Systems which seem particularly ripe for further application of the CCM techniques considered here include the valence-bond solids [24, 26] and lattice models with electronic degrees of freedom, such as the Hubbard model [17, 27].

Finally, we note that it would be of great interest to extend the CCM treatment of all of the above models, including the XXZ model considered here, to finite temperatures. One obvious way to do this would be to extend the formalism by utilizing the general framework of thermofield dynamics [38]. In the same context we also note that Mukherjee [39] and others have suggested alternative ways to extend the CCM to incorporate a thermal averaging procedure.

We thank J. B. Parkinson, Y. Xian, and C. Zeng for useful discussions. One of us (R.F.B.) also gratefully acknowledges a research grant from the Engineering and Physical Sciences Research Council (EPSRC) of Great Britain.

References

[1] Coester, F., 1958, *Nucl Phys.*, **7**, 421; Coester, F., and Kümmel, H., 1960, *ibid.*, **17**, 477.
[2] Čížek, J., 1966, *J. chem. Phys.*, **45**, 4256; 1969, *Adv. chem. Phys.*, **14**, 35.
[3] Bishop, R. F., and Lührmann, K. H., 1978, *Phys. Rev. B*, **17**, 3757.
[4] Kümmel, H., Lührmann, K. H., and Zabolitzky, J. G., 1978, *Phys. Rep.*, **36C**, 1.
[5] Arponen, J. S., 1983, *Ann. Phys.* (New York), **151**, 311.
[6] Bishop, R. F., and Kümmel, H., 1987, *Phys. Today*, **40**(3), 52.
[7] Arponen, J. S., Bishop, R. F., and Pajanne, E., 1987, *Phys. Rev. A*, **36**, 2519; 1987, *ibid.*, **36**, 2539; 1987, *Condensed Matter Theories*, Vol. 2, edited by P. Vashishta, R. K. Kalia and R. F. Bishop (New York: Plenum), p. 357.
[8] Bartlett, R. J., 1989, *J. phys. Chem.*, **93**, 1697.
[9] Bishop, R. F., 1991, *Theor. Chim. Acta*, **80**, 95.
[10] (a) Bishop, R. F., Parkinson, J. B., and Yang Xian, 1991, *Phys. Rev. B*, **43**, 13 782; (b) 1991, *ibid.*, **44**, 9425; (c) 1992, *ibid.*, **46**, 880; (d) 1991, *Theor. Chim. Acta*, **80**, 181; (e) 1992, *J. Phys.: Condens. Matter*, **4**, 5783; (f) 1993, *ibid.*, **5**, 9169.
[11] Bishop, R. F., Hale, R. G., and Xian, Y., 1994, *Phys. Rev. Lett.*, **73**, 3157.
[12] Farnell, D. J. J., and Parkinson, J. B., 1994, *J. Phys.: Condens. Matter*, **6**, 5521.
[13] (a) Zeng, C., Staples, I., and Bishop, R. F., 1995, *J. Phys.: Condens. Matter*, **7**, 9021; (b) 1996, *Phys. Rev. B*, **53**, 9168.
[14] Bishop, R. F., Farnell, D. J. J., and Parkinson, J. B., 1996, *J. Phys.: Condens. Matter*, **8**, 11 153.
[15] Bishop, R. F., and Xian, Y., 1994, *Condensed Matter Theories*, Vol. 9, edited by J. W. Clark, K. A. Shoaib and A. Sadiq (Commack, New York: Nova Science Publ.), p. 433.
[16] Bishop, R. F., 1995, *Recent Progress in Many-Body Theories*, Vol. 4, edited by E. Schachinger, H. Mitter and H. Sormann (New York: Plenum), p. 195.
[17] Bishop, R. F., Xian, Y., and Zeng, C., 1995, *Int. J. quantum Chem.*, **55**, 181.
[18] Bishop, R. F., and Xian, Y., 1993, *Acta Phys. Polonica B*, **24**, 541; Bishop, R. F., Kendall, A. S., Wong, L.Y., and Yang Xian, 1993, *Phys. Rev. D*, **48**, 887; Bishop, R. F., and Xian, Y., 1994, *Nucl. Phys. B (Proc. Suppl.)*, **34**, 808; Davidson, N. J. and Bishop, R. F.,

1995, *ibid.*, **42,** 817; BAKER, S. J., BISHOP, R. F. and DAVIDSON, N. J., 1997, *ibid.*, **53,** 834.
[19] ROGER, M., and HETHERINGTON, J. H., 1990, *Phys. Rev.* B, **41,** 200.
[20] LO, C. F., PANG, K. K., and WANG, Y. L., 1991, *J. Appl. Phys.*, **70,** 6080.
[21] HARRIS, F. E., 1993, *Phys. Rev.* B, **47,** 7903.
[22] CORNU, F., JOLICOEUR, TH., and LE GUILLOU, J. C., 1994, *Phys. Rev.* B, **49,** 9548.
[23] WONG, W. H., LO, C. F., and WANG, Y. L., 1994, *Phys. Rev.* B, **50,** 6126.
[24] XIAN, Y., 1994, *J. Phys.: Condens. Matter*, **6,** 5965.
[25] BURSILL, R., GEHRING, G. A., FARNELL, D. J. J., PARKINSON, J. B., XIANG, T., and ZENG, C., 1995, *J. Phys.: Condens. Matter*, **7,** 8605.
[26] XIAN, Y., 1995, *Condensed Matter Theories*, Vol. 10, edited by M. Casas, M. de Llano and A. Polls (Commack, New York: Nova Science Publ.), p. 541.
[27] ROGER, M., and HETHERINGTON, J. H., 1990, *Europhys. Lett.*, **11,** 255; LO, C. F., MANOUSAKIS, E., and WANG, Y. L., 1991, *Phys. Lett.* A, **156,** 42; PETIT, F., and ROGER, M., 1994, *Phys. Rev.* B, **49,** 3453.
[28] LLEWELLYN SMITH, C. H., and WATSON, N. J., 1993, *Phys. Lett.* B, **302,** 463.
[29] ZENG, C., FARNELL, D. J. J., and BISHOP, R. F., 1998, *J. statist. Phys.*, **90,** 327.
[30] BARNES, T., KOTCHAN, D., and SWANSON, E. S., 1989, *Phys. Rev.* B, **39,** 4357.
[31] KUBO, K., and KISHI, T., 1988, *Phys. Rev. Lett.*, **61,** 2585.
[32] RUNGE, K. J., 1992, *Phys. Rev.* B, **45,** 12292; 1992, *ibid.*, **45,** 7229.
[33] ANDERSON, P. W., 1952, *Phys. Rev.*, **86,** 694; OGUCHI, T., 1960, *ibid.*, **117,** 117.
[34] SINGH, R. R. P., 1989, *Phys. Rev.* B, **39,** 9760; SINGH, R. R. P., and HUSE, D. A., 1989, *ibid.*, **40,** 7247; ZHENG, W., OITMAA, J., and HAMER, C. J., 1991, *ibid.*, **43,** 8321.
[35] SUZUKI, M., 1986, *J. Phys. Soc.* (Japan), **55,** 4205.
[36] MARSHALL, W., 1955, *Proc. R. Soc.* (London) A, **232,** 48.
[37] BONINSEGNI, M., 1995, *Phys. Rev.* B, **52,** 5304.
[38] UMEZAWA, H., MATSUMOTO, H., and TACHIKI, M., 1982, *Thermo Field Dynamics and Condensed States* (Amsterdam: North-Holland); UMEZAWA, H., and YAMANAKA, Y., 1988, *Adv. Phys.*, **37,** 531.
[39] SANYAL, G., MANDAL, S. H., and MUKHERJEE, D., 1992, *Chem. Phys. Lett.*, **192,** 55.

MOLECULAR PHYSICS, 1998, VOL. 94, No. 1, 87–97

Electronic excitations and correlation effects in metals

By ADOLFO G. EGUILUZ† and WOLF-DIETER SCHÖNE

Department of Physics and Astronomy, The University of Tennessee, Knoxville, TN 37996-1200, USA and Solid State Division, Oak Ridge National Laboratory, Oak Ridge, TN 37831-6030, USA

Theoretical descriptions of the spectrum of electronic excitations in real metals have not yet reached a fully predictive, 'first-principles' stage. In this paper we begin by presenting brief highlights of recent progress made in the evaluation of dynamical electronic response in metals. A comparison between calculated and measured spectra—we use the loss spectra of Al and Cs as test cases—leads us to the conclusion that, even in 'weakly-correlated' metals, correlation effects beyond mean-field theory play an important role. Furthermore, the effects of the underlying band structure turn out to be significant. Calculations which incorporate the effects of *both* dynamical correlations and band structure from first principles are not yet available. As a first step towards such a goal, we outline a numerical algorithm for the self-consistent solution of the Dyson equation for the one-particle Green's function. The self-energy is evaluated within the shielded-interaction approximation of Baym and Kadanoff. Our method, which is fully conserving, is a finite-temperature scheme which determines the Green's function and the self-energy at the Matsubara frequencies on the imaginary axis. The analytic continuation to real frequencies is performed via Padé approximants. We present results for the homogeneous electron gas which exemplify the importance of many-body self-consistency.

1. Introduction

Most properties of metals are strongly influenced by the electron–electron interactions [1]. For example, these interactions are responsible for the existence of collective excitations, such as plasmons and spin waves; without exchange and correlation there would be no metallic cohesion, or magnetism in the 3d transition metals, etc.

The theoretical treatment of correlation has traditionally been restricted to 'simple models' which, by design, isolate some of the features of the problem which are deemed to be important. Now, approximations at two different levels are actually built into the models. First, a compromise is made in the description of the underlying band structure. In the jellium model, the band structure is simply ignored altogether—the electrons propagate in plane-wave states. This model has played a time-honoured role in the study of correlation in simple metals. In the opposite end we have the Hubbard model [2], which corresponds to a tight-binding description of the band structure, in which, e.g. the hybridization of sp and d orbitals at the Fermi surface is neglected. This model was originally proposed for the study of transition-metal magnetism, and has been much-invoked in recent years for the study of highly-correlated electrons (e.g. in the cuprate high-temperature superconductors).

† Corresponding author; e-mail: eguiluz@utk.edu.

Second, a 'model' or an approximation is introduced for the actual description of dynamical correlations. Thus, in the case of electronic excitations in jellium, the Coulomb interaction is often treated in a mean-field sense, such as the random-phase approximation (RPA) [1]. Short-range correlations are usually added on in simplified ways [3]. In the case of the Hubbard model, recent progress has been made in the treatment of correlation processes beyond mean-field theory. These include self-consistent diagrammatic approaches [4–6]—which, in fact, provide motivation for our work described below—and non-perturbative treatments of the Coulomb interaction via quantum Monte Carlo methods [6], and exact diagonalization of the Hamiltonian for small clusters [7]. However, the long-range aspects of the Coulomb interaction are typically ignored in these schemes, which allow the electrons to interact only when they encounter each other at a given atomic site with opposite spin projections.

Of course, if the compromise contained in the above models at the level of the band structure is considered to be unreasonable for the problem at hand, one still has available the powerful method of density functional theory (DFT), which has the great appeal that the electronic structure is dealt with in a very realistic way [8, 9]. However, in typical implementations of DFT the correlation problem is basically 'taken for granted', in the sense that one assumes the validity of the local-density approximation (LDA), or gradient corrections thereof.

0026–8976/98 $12·00

At the level of the LDA we rely on an available approximate solution of the correlation problem for electrons in jellium. While the DFT method has proved extremely successful over the last two decades [10–12], its realm is basically confined to ground state observables which are obtainable from a knowledge of the total energy of the system.

In the first part of this article we briefly discuss some key results of recent work on the spectrum of elementary excitations of sp-bonded metals such as Al and Cs [13, 14]. The theoretical work goes beyond the simple-model stage in the sense that the electrons are allowed to propagate in the 'actual' band structure of the metal [13–21] (the band structure is, of course, that obtained in the LDA). However, the treatment of correlation is still at the mean field level, and there is no attempt at self-consistency. Nonetheless, the fact that the band structure is dealt with realistically allows us to establish a useful interplay with the results of modern spectroscopic measurements on these systems [22, 23]. The end result is that we actually learn new physics and pose new questions. For example, it becomes clear that the effects of the band structure can be significant, even for these otherwise jellium-like systems [13–18, 20]. In particular, this interplay has led to the experimental determination of the so-called many-body local field factor of Al [23, 24]. This quantity condenses the effect of correlations beyond the RPA; its measured value [23] differs from theoretical predictions for wave vectors $q \sim 2k_F$, where k_F is the Fermi wave vector.

Thus, even for weakly-correlated, 'jellium-like' metals, a complete treatment of the excitation spectrum must include not only the effects of the band structure, but it must also incorporate the effects of correlation on the same footing. Little is known quantitatively about this joint problem beyond the description contained in the LDA.

In the case of semiconductors, a rather large volume of work has been devoted to a description of the impact of dynamical correlations on the fundamental band gap and quasi-particle energy-shifts of the one-electron band structure [25–29]. As is well known, the energy difference between the lowest unoccupied and the highest occupied Kohn–Sham eigenvalues deviates from the experimental value of the band gap by 50–100%. This problem has been addressed in recent years at the level of the so-called *GW* approximation [26–29], which yields results in apparent *quantitative* agreement with experiment. (We note that some of these calculations contain one or more *ad hoc* approximations—such as the neglect of the damping processes contained in the imaginary part of the self-energy, and the use of a plasmon-pole approximation; furthermore, the many-body requirement that the propagators must be dressed fully self-consistently with the self-energy has typically been neglected.) Recent calculations [30] have included the actual frequency dependence of the polarizability in the evaluation of the *GW* self-energy, with equal degree of success—as measured by agreement with the experimental band gap. Some work along similar lines has been performed for metals. For example, the self-energy effects in the occupied bandwidth of simple metals [31] and the exchange splitting of the magnetic bands of Ni [32] have been calculated; the agreement with experiment in this case is not as good as it is in the case of semiconductors.

With the above material as background and motivation, we move on to discuss ongoing work which constitutes a first step towards a realistic description of correlation in metals. We report results of a fully conserving solution of the Dyson equation for the one-particle Green's function within the shielded-interaction approximation [33]. That the solution is conserving means that it obeys important microscopic conservation laws [33, 34]; technically, the propagators are dressed self-consistently with the self-energy. We find that many-body self-consistency is important. We illustrate this conclusion with numerical results for the spectral function, the quasi-particle weight at the Fermi surface, and the density of states. Of course, the shielded-interaction approximation ignores additional correlation effects (e.g. renormalized vertices). More general self-energy functionals will be addressed elsewhere.

In this preliminary account of our method for the treatment of correlation in metals we confine the discussion to the homogeneous electron gas, or jellium model. However, our finite-temperature many-body techniques are applicable for realistic band structures. In fact, the calculations reported in this article correspond to an 'empty-lattice' treatment of the band structure, since we sample wave vector space over a discrete three-dimensional mesh. Calculations for actual metals are in progress.

Accurate results for the Green's function, polarizability, self-energy, etc., are obtained by the implementation of a procedure which efficiently minimizes the impact of the frequency cutoff in the evaluation of the Green's function for imaginary times. The polarizability for imaginary times is then obtained as a product of two Green's functions (in wave vector space we perform a convolution), and is subsequently fast-Fourier transformed to the Matsubara frequencies. The analytic continuation of the self-energy to real frequencies is performed via Padé approximants [35].

2. Dynamical response in real metals: a brief 'status report'

The latest generation of calculations of dynamical electronic response in metals has reached a new level of sophistication [13–21]. Indeed, it is now possible to account for the effects of the one-electron band structure (as produced by the LDA) in great detail. In conjunction with significant developments on the experimental front (greatly enhanced energy and momentum resolutions have become available; improved sample-preparation techniques have made possible the realization of experiments yielding much 'cleaner' data) the new theoretical algorithms allow us to delve into the physics of the excitations to a degree which was not possible until recently. As a result of this feedback between theory and experiment, new physical mechanisms are coming to the fore, as we sketch briefly next.

The comparison between measured and calculated cross sections for the inelastic scattering of, e.g. electrons and X-rays, can be conveniently formulated in terms of the dynamical structure factor [1]

$$S(\mathbf{q};\omega) = -2\hbar\Omega_N \mathrm{Im}\,\chi_{\mathbf{G}=0,\mathbf{G}'=0}(\mathbf{q};\omega), \qquad (1)$$

where χ is the dynamical density-response function. In the *ab initio* work performed so far [13–21], which is basically 'RPA-like', the response function is given by [24]

$$\chi = P^{(0)}\{1 - \nu(1-G)P^{(0)}\}^{-1}, \qquad (2)$$

where v is the bare Coulomb interaction. In equation (2) we have used symbolic notation; in the present discussion, aimed at simple metals, it should be thought of as a matrix equation in the Fourier representation which arises naturally in the scattering problem implicit in equation (1). In equation (2) we have introduced the many-body local-field factor $G(\mathbf{q};\omega)$ [24] which (following the early work of Hubbard) is defined such that it accounts for all the effects of exchange and short-range correlations [36]. The Fourier transform of the non-interacting polarizability $P^{(0)}$ entering equation (2) is given by the well-known formula

$$P^{(0)}_{\mathbf{G},\mathbf{G}'}(\mathbf{q};\omega) = \frac{1}{\Omega_N}\sum_{\mathbf{k}}^{BZ}\sum_{n,n'}\frac{f_{\mathbf{k},n} - f_{\mathbf{k}+\mathbf{q},n'}}{E_{\mathbf{k},n} - E_{\mathbf{k}+\mathbf{q},n'} + \hbar(\omega + i\eta)} \times \langle \mathbf{k}, n|e^{-i(\mathbf{q}+\mathbf{G})\cdot\hat{\mathbf{x}}}|\mathbf{k}+\mathbf{q}, n'\rangle \times \langle \mathbf{k}+\mathbf{q}, n'|e^{i(\mathbf{q}+\mathbf{G}')\cdot\hat{\mathbf{x}}}|\mathbf{k}, n\rangle, \qquad (3)$$

about which we will have more to say later on. (In equations (1) and (3) Ω_N denotes the volume of the periodically-repeated 'cluster' on whose sides we apply Born–von Karman periodic boundary conditions). Equations (1)–(3) form the basis of several recent studies. Here we shall only touch on two test cases, which have proved quite instructive.

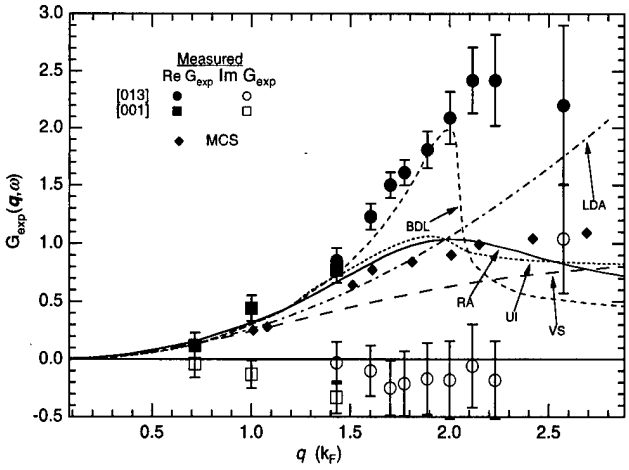

Figure 1. Measured many-body local field factor, $G(\mathbf{q};\omega)$, for Al [23]. The full (empty) symbols correspond to the real (imaginary) part of G, respectively. The local-field factors calculated (for jellium) in [38] (UI), [39] (RA), [40] (BDL), and [41] (MCS) are also shown, as is the corresponding LDA result.

2.1. *The many-body local-field factor of Al*

An enormous number of calculations of the many-body local field factor have been reported in the literature over the years. Most calculations refer to the static limit, in which the exchange-correlation hole—whose physics is accounted for by the presence of $G(\mathbf{q};\omega)$ in the response function given by equation (2)—is assumed to adjust instantaneously as its 'parent' electron propagates through the system.

The availability of *ab initio* results for the non-interacting polarizability $P^{(0)}_{\mathbf{G},\mathbf{G}'}(\mathbf{q};\omega)$ given by equation (3), computed for the LDA band structure, suggests that a *measurement* of the loss spectrum (which is basically given by $\mathrm{Im}\,\chi$, according to equation (1)), followed by an 'inversion' of the data, would lead to an experimental determination of $G(\mathbf{q};\omega)$ via equation (2) [13]. Because of error-propagation in the data inversion, both the experimental measurements and the calculated values of the polarizability must be of high quality. This procedure was implemented recently by Larson *et al.* [23], who performed measurements of $S(\mathbf{q};\omega)$ for Al over a large wave vector domain, with particular emphasis on the crucial regime $q \approx 2k_F$.

The experimental result for $G(\mathbf{q};\omega)$ is shown in figure 1. For illustration purposes, we compare the measured local-field factor with a small subset of the available theoretical results for this quantity (its zero-frequency limit) calculated for jellium with the average density of Al, $r_S = 2.07$; these are, the many-body results of

Vashishta and Singwi (VS) [37], Utsumi and Ichimaru (UI) [38], Richardson and Ashcroft (RA) [39], and Brosens, Devreese and Lemmens (BDL) [40], as well as the local-density approximation (LDA) [16], and the recent Quantum Monte Carlo simulations of Moroni, Ceperley and Senatore (MCS) [41]. (The experimentally-determined $G(\mathbf{q};\omega)$ turns out to be predominantly real, and largely frequency-independent, over a rather wide energy interval, $10 \leqslant \hbar\omega \leqslant 40$ eV; thus, the comparison with static local-field factors is reasonable, even if preliminary.)

Clearly, the theoretical values of the many-body local-field factor are in good agreement with experiment up to $q \approx 1.5k_F$. The data of Larson *et al.* [23] are also consistent with the plasmon dispersion relation calculated by Quong and Eguiluz [15] in a time-dependent extension of local-density functional theory (TDLDA). (That is, the local-field factor implicitly built into the dispersion relation of the Al plasmon obtained in [15] agrees with the measurements of Larson *et al.* [23] for the wave vectors for which the response of the electrons is predominantly collective.) However, for the larger wave vectors for which the electronic response is incoherent, in particular, for $q \to 2k_F$, the experimental $G(\mathbf{q};\omega)$ differs significantly from —*it becomes much larger than* — the theoretical predictions.

(Although, as seen in figure 1, the result of BDL [40] agrees closely with the measured $G(\mathbf{q};\omega)$ up to $q \approx 2k_F$, the significance of this agreement (which does not subsist beyond $2k_F$) is not obvious, since the calculations of BDL did not account for the screening of the exchange ladders. Furthermore, a dynamical $G(\mathbf{q};\omega)$ obtained by the same group [40] differs markedly from experiment.)

The above finding is indicative of the existence of significant many-body correlations in this prototype of 'simple and weakly-correlated metal' behaviour —and it highlights the fact that theory still does not have predictive power in the treatment of dynamical correlations in metals, particularly at large wave vectors. Additional work along similar lines [42] further reinforces the message that correlation must be tackled on the same footing with a realistic description of the underlying band structure, i.e. a simple model like jellium does not suffice. And neither does the simple LDA description of correlation, even if its adoption allows the use of realistic band structures.

2.2. *The plasmon dispersion relation in Cs*

The dispersion relation of the plasmon in the heavy alkali metal Cs, measured by vom Felde *et al.* [22] via high-resolution electron energy loss spectroscopy, is in *qualitative* disagreement with textbook physics [1]. The RPA for the density-response function, which corresponds to equation (2) with $G = 0$, is expected to be accurate in the small-wave vector limit, in which the bubble diagrams dominate the polarizability. This mean-field approximation yields a quadratic dispersion relation for small q's (of course, with positive curvature), in qualitative accord with experiments performed over the years for many sp-bonded elements —which, to a good extent, accounts for the popularity and usefulness of the RPA for these systems. However, in the case of Cs, the dispersion relation of the plasmon turns out to have a *negative slope* for small wave vectors [22]. Moreover, for large wave vectors the dispersion relation is quite flat, in sharp contrast with the strong dispersion predicted by available theories of correlation for electrons in jellium with the bulk density of Cs, $r_S = 5.6$.

The original interpretation of the experiment of vom Felde *et al.* [22] was that it provided a signature of the presence of strong electron –electron correlations. Since the restoring force for the plasmon is related to the compressibility of the electron gas, the negative dispersion appeared to raise the issue of the stability of the system —a possible scenario would be a tendency towards Wigner-crystal formation. Of course, since Cs has the lowest valence-electron density of all elemental metals, the question of the importance of correlation suggests itself *a priori*.

As we now know [14], short range correlations do play a role in the present problem, but the same is different from the initial conjecture [22]. Indeed, the negative slope of the plasmon dispersion in Cs has been shown to be a band-structure effect [18]. More specifically, this effect has been traced to the contribution to the polarizability $P^{(0)}_{\mathbf{G},\mathbf{G}'}(\mathbf{q};\omega)$ from one-electron transitions to a complex of final states which are nearly-degenerate with the plasmon energy (~3 eV) [14]. Since a pedagogical discussion of this effect has been given elsewhere [36], and in keeping with the theme of this article, we move on to sketch the way in which the effects of correlation are contained in the experimental data.

Figure 2 shows calculated dispersion curves for the Cs plasmon. It is significant that the polarizability given by equation (3) was obtained from an LDA band structure in which the 5p orbitals were treated as valence states. (To this end an *ab initio* pseudopotential was constructed for the ionic configuration 5p6, 6s0.7 [14].) The left panel of figure 2 shows the plasmon dispersion curve obtained from a scalar version of equation (2), in which we only keep the $\mathbf{G} = \mathbf{G}' = 0$ element of $P^{(0)}$. Such solution ignores the 'crystal local fields', i.e. the contribution to the screening from density fluctuations of wavelengths comparable with the lattice constant. For small q's the effect of the many-body local field, or 'vertex correction' $f_{xc} = -vG$, is negligible. This is as expected, since, as recalled above, in this limit the bubble diagrams dominate the response. The agreement

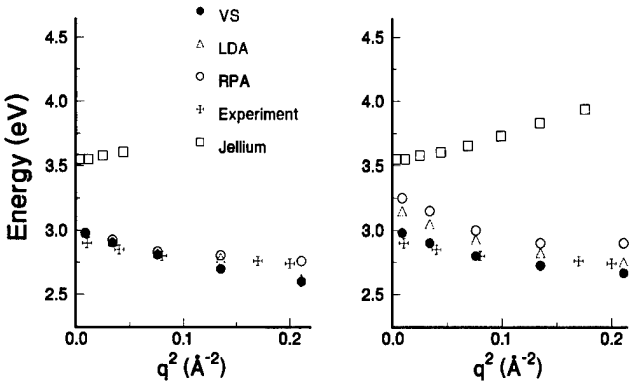

Figure 2. Plasmon dispersion relation in Cs for small wave vectors along the (110) direction [14]. The 5p semi-core states were treated as valence states. Right (left) panel includes (ignores) the crystal local fields. Theoretical curves are labelled by the vertex correction used in the respective calculation—see text.

with the experimental data shown in figure 2 is excellent—in fact, it is 'too good', as we indicate momentarily.

The very inclusion in the polarizability of spatially-localized orbitals—and these semicore states do contribute to the calculated plasmon dispersion for small wave vectors—immediately prompts the question of whether the crystal local fields can really be ignored. They cannot. Dispersion curves computed in the presence of the crystal local fields are shown on the right panel of figure 2. Three sets of calculations are actually represented (as was the case on the left panel), corresponding to different approximations for the treatment of the electron–electron correlations. These are, respectively: (i) RPA, for which $f_{xc} = 0$, (ii) TDLDA, for which $f_{xc} = \int d^3x \exp(-i\mathbf{q}\cdot\mathbf{x})\, dV_{xc}(\mathbf{x})/dn(\mathbf{x})$, where $V_{xc}(\mathbf{x})$ is the exchange-correlation potential obtained in the LDA ground-state calculation, and (iii) Vashishta-Singwi (VS), who obtained an approximate vertex function from a decoupling of the equation of motion for the electron–hole pair density-fluctuation operator [37] (this vertex was already considered in figure 1). It is quickly apparent that figure 2 (right panel) presents us with a surprise: *the calculated dispersion relation contains a sizable correlation effect for small wave vectors.*

The explanation of this result is as follows. The loss spectrum $S(\mathbf{q};\omega)$ (whose main peak defines the energy position of the plasmon for a given wave vector) is obtained upon inverting the matrix $(1-\nu(1-G)P^{(0)})^{-1}$. The inversion of this matrix gives rise to a 'feedback' between *large* wave vector arguments $\mathbf{q}+\mathbf{G}$ in $P^{(0)}$ and the *small* wave vector $\mathbf{q}$ of the plasmon (we recall that $P^{(0)}_{\mathbf{G},\mathbf{G}'}(\mathbf{q};\omega) \equiv P^{(0)}(\mathbf{q}+\mathbf{G}, \mathbf{q}+\mathbf{G}';\omega)$). At the level of the RPA this crystal local-field effect shifts the energy of the plasmon *upwards*. This is a purely kinetic-energy (or electron-gas pressure) effect. By contrast, the introduction of a vertex correction $f_{xc} = -\nu G$ in equation (2) induces a *downward* shift of ω_p; this is a physical consequence of the weakening of the screening due to the presence of an exchange-correlation hole about each screening electron. Note that the reason that this mechanism becomes operative for small q's is the feedback induced by the crystal local fields, which ultimately originates in the contribution from the localized semicore charge to the dynamical polarizability.

We emphasize that, while we are in the presence of a correlation effect for small wave vectors, the same is quite different from the initial assumptions about the origin of the negative plasmon dispersion in Cs [22]. This example illustrates again the importance of *ab initio* calculations of dynamical response. Without a realistic description of the effects of the band structure, the interpretation of the experimental data becomes clouded by built-in assumptions (or 'prejudices') stemming from simple model descriptions (e.g. electrons in jellium).

Note also that the above treatment of correlation, via 'off the shelf' many-body local field factors, is far less than 'fundamental'. The merit of the above procedure is simply that it illustrates the fact that both in the present problem, and in the case of the large-wave vector response of Al, correlation effects play a quantitatively important role. In both problems, an accurate, first-principles theory of dynamical correlations for electrons propagating in the actual band structure of the system has yet to be developed.

3. Back to the beginning: self-consistent solution of the Dyson equation

A rigorous formulation of the many-body problem of interacting electrons starts out from the Dyson equation for the one-particle Green's function [24, 33], which we write down as

$$G^{-1}(\mathbf{q};i\omega_n) = G_0^{-1}(\mathbf{q};i\omega_n) - \Sigma_{xc}(\mathbf{q};i\omega_n), \qquad (4)$$

where we have Fourier-transformed the space- and time-dependence of all quantities. We use the finite-temperature Matsubara formalism [24], in which the Green's function for imaginary-times is Fourier-analysed according to

$$G(\mathbf{q};i\omega_n) = \int_0^{\beta\hbar} d\tau \exp(i\omega_n\tau) G(\mathbf{q};\tau), \qquad (5)$$

where $\beta = 1/k_B T$ and $\omega_n = (2n+1)\pi/\beta\hbar$, n being an integer (positive, negative, or zero); for boson-like quantities, such as the polarizability introduced below, $\omega_n = 2n\pi/\beta\hbar$.

In equation (4) $G_0(\mathbf{q}; i\omega_n)$ denotes the Green's function for non-interacting electrons; the same is given by the equation

$$G_0(\mathbf{q}; i\omega_n) = \frac{1}{i\omega_n - \omega_{\mathbf{q}}}, \tag{6}$$

where the 'band energies' are given by the equation

$$\hbar\omega_{\mathbf{q}} = \hbar^2 q^2/2m - \mu, \tag{7}$$

μ being the chemical potential. In equation (4) we have also introduced the self-energy $\Sigma_{xc}(\mathbf{q}; i\omega_n)$, which can be thought of as (the Fourier transform of) the non-local, time-dependent 'potential' in which a 'real' (i.e. interacting) electron propagates. We emphasize that the notation employed in equations (4) and (6) is appropriate for a spatially-homogeneous medium (jellium), in which all physical quantities are scalars. Our notation also reflects the fact that, for the homogeneous electron gas, the 'tadpole' diagram [43] vanishes (this is why one-electron potentials—e.g. the Hartree potential, or the Kohn-Sham one-electron potential [9]—are not included in either the G_0 given by equation (6) or in Σ_{xc}, which here is entirely due to exchange and correlation. For electrons in a periodic crystal, the Dyson equation, equation (6), and equations (8) and (9) below, are replaced by matrix equations in either configuration space or in an appropriate basis spanning the Hilbert space of the system; also the tadpole must be accounted for. This more general case is discussed in a forthcoming publication [44].

A key point about equation (4) is that the self-energy is a functional of the Green's function G [33, 34]. Physically, this means that the particle whose propagation we follow contributes self-consistently to the dynamical 'potential' in which it moves. Mathematically, this means that equation (4) must be solved self-consistently, i.e. in a 'loop' which starts out from the computation of Σ_{xc} in terms of G_0, followed by a recomputation of the self-energy from an updated Green's function G obtained from equation (4), and so on, until convergence is achieved to a desired accuracy. As noted in the introduction, equation (4) has been solved self-consistently in recent years for Hubbard-like models with short range interactions [4, 5]. This self-consistency has traditionally been ignored for systems with long-range interactions. (A partial degree of self-consistency for electrons in jellium has been reported very recently [45, 46]; in the case of semiconductors, self-consistency in the search for the real part of the quasi-particle energies has also been implemented approximately [26, 27].)

We consider the simplest non-trivial self-energy functional which includes the effects of dynamical screening, namely the shielded-interaction approximation (SIA) of Baym and Kadanoff [33], in which

$$\Sigma_{xc}(\mathbf{q}; i\omega_m) = -\frac{1}{\hbar\Omega_N}\sum_{\mathbf{k}} \times \frac{1}{\beta\hbar}\sum_{i\omega_n} G(\mathbf{q}-\mathbf{k}; i\omega_m - i\omega_n) V_S(\mathbf{k}; i\omega_n), \tag{8}$$

where the shielded (or screened) Coulomb interaction V_S is given by

$$V_S(\mathbf{q}; i\omega_n) = \frac{\nu(\mathbf{q})}{1 - \nu(\mathbf{q})P(\mathbf{q}; i\omega_n)}, \tag{9}$$

in terms of the dynamical polarizability, which in the present approximation is of RPA form,

$$P(\mathbf{q}; \tau) = 2\sum_{\mathbf{k}} G(\mathbf{q}+\mathbf{k}; \tau) G(\mathbf{k}; -\tau). \tag{10}$$

Equations (4), (6), (8) (10) define a self-consistent problem, whose solution yields (implicitly) the self-energy as a functional of the Green's function, $\Sigma_{xc}[G]$, within the SIA. It should be recognized that *the diagram* for the SIA given by equation (8) corresponds to the GW or *screened-Hartree Fock* approximation for the self-energy [47, 48].

In equation (10) we have written down the polarizability for imaginary times, as this is the representation in which we actually calculate this function first. This may seem to be a roundabout way to proceed, in view of the fact that from the Dyson equation we obtain an update for $G(\mathbf{q}; i\omega_n)$, not $G(\mathbf{q}; \tau)$, and, furthermore, it is the Fourier transform of the polarizability, $P(\mathbf{q}; i\omega_n)$, which is required in the screened interaction given by equation (9). However, the direct evaluation of $P(\mathbf{q}; i\omega_n)$ as a frequency convolution of two G's (obtained by Fourier-transforming equation (10)) converges quite poorly as a function of the frequency cutoff which must necessarily be imposed [49]. Thus, we actually use equation (10) as it stands. Formally, we generate the Green's function for imaginary times via the inverse of equation (5), i.e.

$$G(\mathbf{q}; \tau) = \frac{1}{\beta\hbar}\sum_{i\omega_m} \exp(-i\omega_m\tau) G(\mathbf{q}; i\omega_m). \tag{11}$$

Unfortunately, a direct numerical evaluation of the frequency sum in equation (11) is not feasible [49] - this problem is traced to the slow $1/\omega$ decay of the Green's function for large frequencies [50]. We have solved this difficulty by implementing the following physically-motivated procedure. We add and subtract from the argument of the sum in equation (11) the Fock Green's function G_x, i.e. the Green's function which corresponds to a bare-exchange treatment of the electron–electron interactions: G_x is of the form of equation (6), except that the single-particle eigenvalues are shifted by a *frequency-independent* exchange self-energy $\Sigma_x(\mathbf{q})$. Since the energy-position of the pole of G_x is known, we

can evaluate its Fourier transform (equation (11)) in closed form. We then have that

$$G(\mathbf{q};\tau) = \frac{1}{\beta\hbar}\sum_{i\omega_m} \exp(-i\omega_m\tau)\{G(\mathbf{q};i\omega_m) - G_x(\mathbf{q};i\omega_m)\} - \exp[-(\omega_{\mathbf{q}} + \Sigma_x(\mathbf{q}))\tau] \times \left(1 - \frac{1}{\exp[\beta\hbar(\omega_{\mathbf{q}} + \Sigma_x(\mathbf{q}))] + 1}\right), \quad (12)$$

where the second term corresponds to the contribution from G_x. Of course, the sum in equation (12) is evaluated with a finite cutoff; however, since $G_x \approx G$ for large frequencies—physically, this is the case because correlation becomes inoperative at high excitation energies—this sum converges rapidly [49]. Equation (12) is central to our numerical algorithms. From the knowledge of $G(\mathbf{q};\tau)$ we obtain $P(\mathbf{q};\tau)$ according to equation (10), and the required Fourier coefficients $P(\mathbf{q};i\omega_n)$ are subsequently obtained via Fast-Fourier-transform techniques.

Finally, we note that the chemical potential μ (which was introduced into the above scheme through equations (6) and (7)) is not known *a priori*, since its value is affected by the electron–electron interactions (and the effect is not negligible, as our numerical results show). The renormalization of the chemical potential is self-consistently determined through the implicit equation

$$n = \frac{2}{\Omega_N}\sum_{\mathbf{k}}\frac{1}{\beta\hbar}\sum_{i\omega_m}\exp(i\omega_m\delta)G(\mathbf{k};i\omega_m|\mu), \quad (13)$$

where n is the electron density. Equation (13) is solved for each iteration of equation (4). The notation used in equation (13) is meant to emphasize the fact that the updated Green's function G depends on the current (updated) value of μ. Of course, as was the case with equation (11), we cannot solve equation (13) as it stands. Rather, we manipulate the right-hand-side of equation (13) in the same way as done above for equations (11) and (12)—this yields a rapidly converging sum over the Matsubara frequencies. Further details will be presented elsewhere [49].

It is instructive to note that, even at just the level of the evaluation of the polarizability, the present approach contains significant advantages relative to the conventional representation given by equation (3), which was the basis of the recent progress summarized earlier in this paper.† First, because of the pole structure

† We recall that equation (3) is obtained from equation (10) upon setting $G = G_0$ (this corresponds to the zeroth-order step in the iteration loop) which, by virtue of the simple pole structure of equation (6), makes possible a closed-form evaluation of the internal frequency convolution.

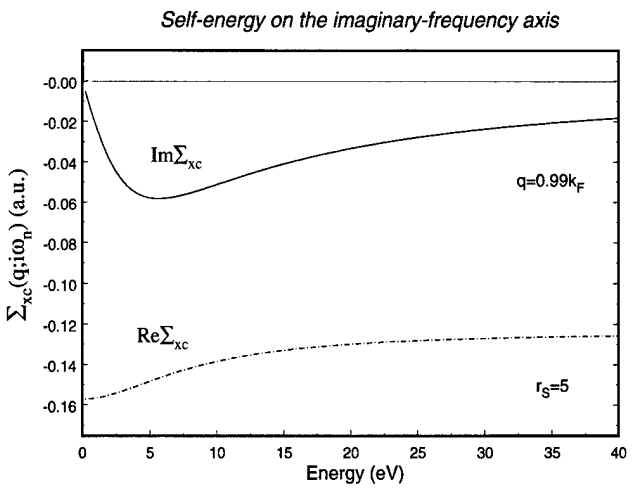

Figure 3. Electron self-energy $\Sigma_{xc}(\mathbf{q};i\omega_n)$ for $q = 0.99k_F$, plotted as function of the continuous variable $i\omega$. The figure refers to a first evaluation of the self-energy, i.e. $\Sigma_{xc} = \Sigma_{xc}[G_0]$, for $r_S = 5$.

of equation (3), an accurate sampling of the Brillouin zone typically requires substantially denser meshes than are required with the present method [49]; this is a major practical advantage, which should become even more relevant in the treatment of more elaborate self-energy functionals. Second, there is no direct generalization of equation (3) once the propagators are dressed by the self-energy (which is the case for all iterations of equation (4) beyond the zeroth order, $G = G_0$).

We turn next to a presentation of selected results obtained by the self-consistent implementation of the above scheme. We confine our discussion to the homogeneous electron gas, and consider the case $r_S = 5$; for this low-density 'metal' the effects of correlation are more easily visualized. All the results presented below correspond to a temperature $T = 800$ K. The restriction to the jellium model has the conceptual advantage that it allows us to isolate system-independent, or universal, features of the solution of equation (4), which, to a greater or lesser extent, should be relevant for all metals.

In figures 3 and 4 we show characteristic results for the self-energy, plotted as function of frequency, for a wave vector which lies very close to the Fermi surface. The fact that this wave vector does not equal k_F *exactly* may seem surprising. However, as a preamble to the implementation of our methods for real crystals [44], we have actually solved equation (4) over a discrete mesh of wave vectors, which are required to satisfy Born–von Karman periodic boundary conditions. Thus, in essence, we have performed 'empty lattice' calculations. (In order to facilitate the comparison with the case of potassium, discussed elsewhere [44], whose bulk density is comparable to the one used in the present

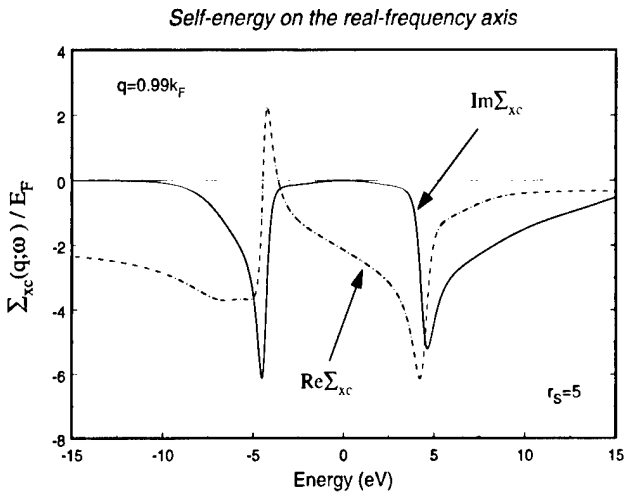

Figure 4. Analytic continuation of the electron self-energy of figure 3 to real frequencies. It is instructive to compare the sharp spectral features observed in this figure with the smooth frequency dependence shown in figure 3.

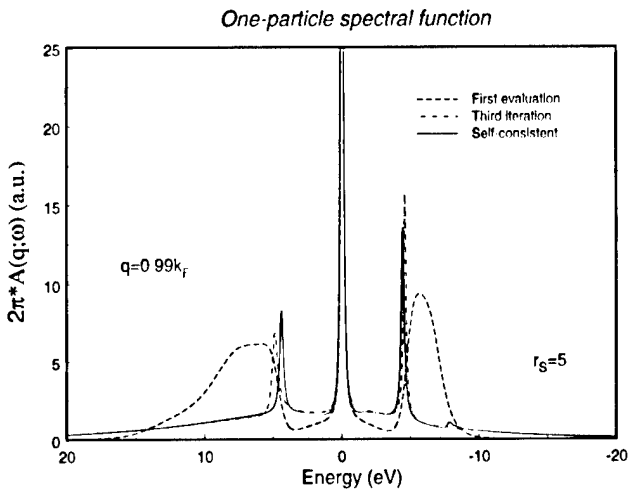

Figure 5. Spectral function for one-particle excitations, $A(\mathbf{q};\omega)$, for $q = 0.99k_F$. The figure shows the spectral function obtained from a first evaluation of the self-energy (dashed line), from the third iteration of the solution of equation (4) (dashed-dotted line), and from the self-consistent solution of equation (4) (solid line).

calculations, we have assumed a bcc Bravais lattice.) The wave vector $\mathbf{q} = 0.99k_F$ happens to be the closest one to the Fermi surface in our numerical mesh.

Now figures (3) and (4) refer to the initial evaluation of the self-energy in terms of the non-interacting Green's function G_0, i.e. $\Sigma_{xc}[G_0]$. This corresponds to the level of the calculation of the self-energy of the homogeneous electron gas reported over the years by many authors, starting from the pioneering work of Quinn and Ferrell [47], Hedin [48], and Lundqvist [51]. For the most part, such work has been carried out on the basis of the ground-state ($T = 0$ K) formalism, which yields all physical variables directly on the real-frequency axis. In our case, the data displayed in figure 4 were obtained from the data of figure 3 via Padé approximants [35]. Basically, the self-energy evaluated over the Matsubara frequencies is fitted to a ratio of polynomials (whose degree is typically of the order of 30, in the calculations reported herein); this allows us to 'stretch' the domain of definition of the self-energy elsewhere in the complex frequency plane. In particular, we can perform the analytic continuation to points just above the real axis (10 meV above the real axis, in the present calculations), and obtain the retarded self-energy shown in figure 4, which agrees well with previous work [48, 51, 52]. (A detailed discussion of the impact of various numerical parameters on the analytic continuation will be presented in [49].)

Figures 3 and 4 are meant to illustrate a point which provides strong motivation for the method we have implemented: While the self-energy is a smooth function of frequency on the imaginary axis, its analytic continuation has sharp structures on the real axis—due, in this case, to resonant coupling to the plasmon [51]. The same qualitative remark applies to all other dynamical quantities, including the polarizability. It is then rather self-suggestive that, as noted above for the particular case of the polarizability, our finite-temperature scheme lends itself to a more efficient sampling of the Brillouin zone than the ground-state methods (relatively coarse meshes yield accurate results [49]). Of course, in applications to simple metals, the use of a finite temperature method is not essential; rather, as just noted, we find it to be very practical. On the other hand, in the case of, e.g. magnetic response of transition metals, the temperature plays an essential physical role, which our method is designed to incorporate.

An important physical quantity related to the one-particle Green's function is the spectral function $A(\mathbf{q};\omega)$, which gives the probability that an added particle with momentum $\hbar\mathbf{q}$ will find an eigenstate of the interacting $(N+1)$-particle system with energy $\hbar\omega$ [24]. The one-particle spectral function is defined by the equation

$$A(\mathbf{q};\omega) = -\frac{1}{\pi}\,\mathrm{Im}\,G(\mathbf{q};\omega), \tag{14}$$

which we evaluate from the knowledge of the self-energy. Figure 5 shows the spectral function for the same wave vector considered in figure 4. The prominent quasi-particle peak at the Fermi surface (energies are measured from the chemical potential), and the well-known satellites which arise as a feedback of the plasmon resonance onto the one-particle spectrum, are clearly observed.

The main point about figure 5 is that it illustrates the impact of self-consistency in the solution of the Dyson equation. The dashed line corresponds to the evaluation of $A(\mathbf{q};\omega)$ from the knowledge of the self-energy obtained in terms of the non-interacting Green's function, i.e. $\Sigma_{xc}[G_0]$; this non-self-consistent result agrees well with previous calculations [48, 51, 52]. The dashed-dotted line is the spectral function obtained after three iterations through equation (4). It is apparent that the spectral weight of the satellites has been substantially reduced. Since the integrated spectral weight is controlled by the sum rule

$$\int_{-\infty}^{+\infty} d\omega\, A(\mathbf{q};\omega) = 1, \tag{15}$$

whose fulfilment is essential for the probability interpretation of the spectral function, the weight lost by the satellites must go to the quasi-particle—it does. Our numerical solution of equation (4) (its analytic continuation) fulfils equation (15) to within 0.1%. We note, in passing, that the first-frequency moment sum rule [51] is also fulfilled by our results (in this case, to within 1%); this clearly serves as a powerful check of the overall quality of our numerical solution of the Dyson equation. Finally, the solid line in figure 5 shows the spectral function for the converged, self-consistent, Green's function (which, on the scale of the figure, corresponds basically to the sixth iteration of the solution of equation (4)). Clearly, the trend noted above for the intermediate (third iteration) step holds all the way to convergence.

We can quantify the reduction in the weight of the satellite structure brought about by the self-consistency by noting the related increase in the weight of the quasi-particle state at the Fermi surface, Z_k [24]. The latter is given by the area under the central peak in figure 5; $Z_k = 1$ corresponds to a strict delta-function peak, which is only realized for the non-interacting system. For the three iteration steps considered in figure 5 we have, respectively, $Z_k = 0.60$—which reproduces the 'canonical' value reported by Hedin [48] for $r_S = 5$—, $Z_k = 0.73$, and $Z_k = 0.74$. Clearly, the effect of self-consistency is to make the quasi-particles more Sommerfeld-like.

It is also of interest to consider the density of one-particle states, defined by the equation

$$\rho(\omega) = \frac{2}{\Omega_N} \sum_{\mathbf{k}} A(\mathbf{k};\omega). \tag{16}$$

Now, because of the presence of sharp structures in $A(\mathbf{k};\omega)$ (while figure 5 displays the spectral function as a function of frequency, $A(\mathbf{k};\omega)$ also contains considerable structure as a function of wave vector), the sum

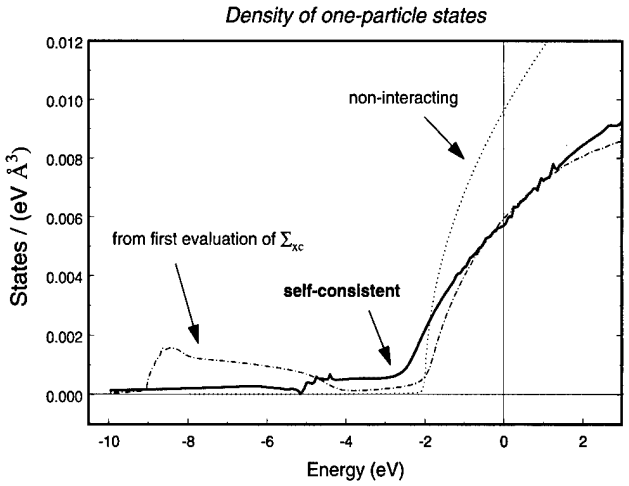

Figure 6. Density of one-particle states, $\rho(\omega)$, for $r_S = 5$. The figure shows the $\rho(\omega)$ which corresponds to a first evaluation of the self-energy, i.e. $\Sigma_{xc} = \Sigma_{xc}[G_0]$, and to the converged, self-consistent solution of equation (4). For reference, the $\rho(\omega)$ for non-interacting electrons is also shown.

required in equation (16) must be performed over a dense **k**-mesh—much denser than the one for which we need to solve equation (4) to obtain converged results for, e.g. the quasi-particle weight, or the chemical potential. This computational requirement was handled by performing a cubic-spline interpolation of the (real-ω) self-energy from the coarser **k**-mesh for which we solve the self-consistency problem to the denser **k**-mesh required by equation (16). (We would like to mention, in passing, that this procedure required an 'automated' use of Padé approximants for the entire mesh for which equation (4) was solved; fortunately, this caused no problems, despite the notorious 'instabilities' associated with Padé methods.)

The calculated density of states is shown in figure 6. The dashed-dotted line is the $\rho(\omega)$ which corresponds to the initial computation of the self-energy, $\Sigma_{xc}[G_0]$; this curve agrees well with Lundqvist's original *GW* results [51] (the slight rounding of features in the satellite structure compared to the corresponding curve in [51] is due to the analytic continuation via Padé). The solid line represents the converged result, obtained from the self-consistent result for spectral function shown in figure 5. For reference, in figure 6 we also show the density of states for non-interacting electrons. The large reduction of the weight of the satellite structure in $\rho(\omega)$ observed in figure 6 is consistent with the results for the spectral function, and the quasi-particle weight, discussed above.

A related feature of the calculated $\rho(\omega)$ needs to be addressed. This is the widening of the occupied bandwidth observed in figure 6 (note that the zero of energy is the renormalized chemical potential for the corre-

sponding solution of equation (4)). This result, which is intimately connected with the reduction in the weight of the satellites brought about by self-consistency, seems to be contrary to observation [53]; note, however, that there is no clear experimental evidence for the existence of intrinsic many-body satellites in simple metals. A related issue is the fact that, for small wave vectors, the renormalized polarizability P differs qualitatively from the bare polarizability $P^{(0)}$ for frequencies in the plasmon region; this question will be discussed in more detail elsewhere [49]. It is, of course, possible that the inclusion of vertex corrections—which at least to low order in perturbation theory have been shown to 'counteract' the effect of the self-energy insertions [54] –will alter the above results, yielding, for example, a reduction in the occupied bandwidth, and a concomitant increase in the weight of the satellites. We will explore more general self-energy functionals in future work. Nonetheless, our present results indicate that a self-consistent treatment of the interactions is required in order to obtain quantitatively reliable results.

W.-D. S. gratefully acknowledges a postdoctoral fellowship from the Deutsche Forschungsgemeinschaft. This work was supported by National Science Foundation Grant No. DMR-9634502 and the National Energy Research Supercomputer Center. Oak Ridge National Laboratory is managed by Lockheed Martin Energy Research Corp., for the Division of Materials Sciences, U.S. DOE under contract DE-AC05-96OR22464.

Note added in proof:—Higher resolution X-ray measurements and further analyses (in progress, [42]) indicate some reduction in the strength of the measured $G(\mathbf{q};\omega)$ near $2k_F$; however, $G(\mathbf{q};\omega)$ remains substantially above available theory.

References

[1] Pines, D., and Noziéres, P., 1966, *The Theory of Quantum Liquids*, Vol. 1 (New York: Benjamin).
[2] Hubbard, J., 1963, *Proc. Roy. Soc.* (London) A, **276**, 238; 1964, *ibid.*, **277**, 237; 1964, *ibid.*, **281**, 401.
[3] Zangwill, A., and Soven, P., 1980, *Phys. Rev.* A, **21**, 1561.
[4] Bickers, N. E., Scalapino, D. J., and White, S. R., 1989, *Phys. Rev. Lett.*, **62**, 961; Bickers, N. E., and White, S. R., 1991, *Phys. Rev.* B, **43**, 8044.
[5] Serene, J. W., and Hess, D. W., 1991, Phys. *Rev.* B, **44**, R3391; Deisz, J. J., Serene, J. W., and Hess, D. W., 1996, *Phys. Rev. Lett.*, **76**, 1312.
[6] Putz, R., Preuss, R., Muramatsu, A., and Hanke, W., 1996, *Phys. Rev.* B, **53**, 5133; Preuss, R., Hanke, W., and Von der Linden, W., 1995, *Phys. Rev. Lett.*, **75**, 1344.
[7] Dagotto, E., 1995, *Rev. mod. Phys.*, **66**, 763.
[8] Hohenberg, P., and Kohn, W., 1964, *Phys. Rev.*, **136**, B864.
[9] Kohn, W., and Sham, L. J., 1965, *Phys. Rev.*, **140**, A1133.
[10] Lundqvist, S., and March, N. H. (eds), 1983, *Theory of the Inhomogeneous Electron Gas* (New York: Plenum).
[11] Trickey, S. B. (ed.), 1990, *Density Functional Theory of Many-Fermion Systems* (New York: Academic).
[12] Gross, E. K. U., and Dreizler, R. M. (eds), 1994, *Density Functional Theory* (New York: Plenum); Dreizler, R. M., and Gross, E. K. U., 1990, *Density Functional Theory: An Approach to the Quantum Many-Body Problem* (Berlin: Springer-Verlag).
[13] Fleszar, A., Quong, A. A., and Eguiluz, A. G., 1995, *Phys. Rev. Lett.*, **74**, 590.
[14] Fleszar, A., Stumpf, R., and Eguiluz, A. G., 1997, *Phys. Rev.* B, **55**, 2068.
[15] Quong, A. A., and Eguiluz, A. G., 1993, *Phys. Rev. Lett.*, **70**, 3955.
[16] Maddocks, N. E., Godby, R. W., and Needs, R. J., 1994, *Europhys. Lett.*, **27**, 681.
[17] Maddocks, N. E., Godby, R. W., and Needs, R. J., 1994, *Phys. Rev.* B, **49**, R8502.
[18] Aryasetiawan, F., and Karlsson, K., 1994, *Phys. Rev. Lett.*, **73**, 1679.
[19] Aryasetiawan, F., and Gunnarsson, O., 1994, *Phys. Rev.* B, **49**, 16214.
[20] Eguiluz, A. G., Fleszar, A., and Gaspar, J., 1995, *Nucl. Instrum. Methods* B, **96**, 550.
[21] Lee, K. -H., and Chang, K. J., 1996, *Phys. Rev.* B, **54**, R8285.
[22] Vom Felde, Sprösser-Prou, A., J., and Fink, J., 1989, *Phys. Rev.* B, **40**, 10181.
[23] Larson, B. C., Tischler, J. Z., Isaacs, E. D., Zschack, P., Fleszar, A., and Eguiluz, A. G., 1996, *Phys. Rev. Lett.*, **77**, 1346.
[24] Mahan, G. D., 1990, *Many-Particle Physics*, 2nd edn (New York: Plenum).
[25] Strinati, G., Mattausch, H. J., and Hanke, W., 1982, *Phys. Rev.* B, **25**, 2867.
[26] Hybertsen, M., and Louie, S. G., 1986, *Phys. Rev.* B, **34**, 5390. For a review, see, Louie, S. G., 1994, *Surf. Sci.*, **299/300**, 346.
[27] Godby, R. W., Schlüter, M., and Sham, L. J., 1987, *Phys. Rev.* B, **35**, 4170.
[28] Bechstedt, F., Fiedler, M., Kress, C., and Del Sole, R., 1994, *Phys. Rev.* B, **49**, 7357; Del Sole, R., Reining, L., and Godby, R. W., 1994, *Phys. Rev.* B, **49**, 8024.
[29] Rohlfing, M., Krüger, P., and Pollmann, J., 1995, *Phys. Rev.* B, **52**, 1905.
[30] Rojas, H. N., Godby, R. W., and Needs, R. J., 1995, *Phys. Rev. Lett.*, **74**, 1827; Fleszar, A., and Hanke, W., 1997, *Phys. Rev.* B, **56**, 10228.
[31] Surh, M. P., Northrup, J. E., and Louie, S. G., 1988, *Phys. Rev.* B, **38**, 5976.
[32] Aryasetiawan, F., 1992, *Phys. Rev.* B, **46**, 13051.
[33] Baym, G., and Kadanoff, L. P.,1961, *Phys. Rev.*, **124**, 287.
[34] Baym, G., 1962, *Phys. Rev.*, **127**, 1391.
[35] Vidberg, H. J., and Serene, J. W., 1977, *J. Low Temp. Phys.*, **29**, 179.
[36] Eguiluz, A. G., 1996, *Int. J. quantum Chem.: Quantum Chem. Symp.*, **30**, 1457.
[37] Vashishta, P., and Singwi, K. S., 1972, *Phys. Rev.* B, **6**, 875.

[38] UTSUMI, K., and ICHIMARU, S., 1980, *Phys. Rev.* B, **22,** 5203; *ibid.,* 1981, **23,** 3291.
[39] RICHARDSON, C. F., and ASHCROFT, N. W., 1994, *Phys. Rev.* B, **50,** 8170.
[40] BROSENS, F., DEVREESE, J. T., and LEMMENS, L. F., 1980, *Phys. Rev.* B, **21,** 1363;. BROSENS, F., and DEVREESE, J. T., 1988, *Phys. Stat. Sol.* (B), **147,** 173.
[41] MORONI, S., CEPERLEY, D. M., and SENATORE, G., 1995, *Phys. Rev. Lett.*, **75,** 689.
[42] LARSON, B. C., TISCHLER, J. Z., FLESZAR, A., and EGUILUZ, A. G., to be published.
[43] MATTUCK, R. D., 1976, *A Guide to Feynman Diagrams in the Many-Body Problem*, 2nd edn (New York: Dover), p. 83.
[44] SCHÖNE, W.-D., GASPAR, J. A., and EGUILUZ, A. G., to be published.
[45] SHIRLEY, E. L., 1996, *Phys. Rev.* B, **54,** 7758.
[46] VON BARTH, U., and HOLM, B., 1996, *Phys. Rev.* B, **54,** 8411.
[47] QUINN, J. J., and FERRELL, R. F., 1958, *Phys. Rev.*, **112,** 812.
[48] HEDIN, L., 1965, *Phys. Rev.*, **139,** A796; HEDIN, L., and LUNDQVIST, S., 1969, *Solid State Physics*, Vol. 23, edited by H. Ehrenreich, F. Seitz and D. Turnbull (New York: Academic), p. 1.
[49] SCHÖNE, W.-D., and EGUILUZ, A. G., to be published.
[50] DEISZ, J. J., HESS, D. W., and SERENE, J. W., 1995, *Recent Progress in Many Body Theories,* Vol. 4, edited by E. Schachinger, H. Mitter and H. Sormann (New York: Plenum).
[51] LUNDQVIST, B. I., 1967, *Phys. Konden. Mater.*, **6,** 193; *ibid.*, 1967, **6,** 206; *ibid.*, 1968, **7,** 117.
[52] FROTA, H. O., and MAHAN, G. D., 1992, *Phys. Rev.* B, **45,** 6243.
[53] JENSEN, E, and PLUMMER, E. W., 1985, *Phys. Rev. Lett.*, **55,** 1912; LYO, I. W., and PLUMMER, E. W., 1988, *Phys. Rev. Lett.*, **60,** 1558.
[54] SERNELIUS, B. E., 1987, *Phys. Rev.* B, **36,** 1080.

MOLECULAR PHYSICS, 1998, VOL. 94, NO. 1, 99–104

Dissociative recombination: an electronic correlation problem

By JAN LINDERBERG
Department of Chemistry, Aarhus University, DK-8000 Aarhus C, Denmark

A recent application of propagator theory to very low-energy electron–molecule scattering provides information on the basic mechanisms in dissociative recombination. Current experiments in storage rings reveal that carbonium ions (CH_3^+) recombine and fragment into three parts equally often as into just two. An analysis of the possible resonances between free electron and bound electron states for the ions requires a detailed examination of the correlation effects plus the coupling to nuclear degrees of freedom, and thus is an ideal problem for the propagator approach.

1. Initial observations

Electronic correlation was a problem under intense scrutiny when I joined Per-Olov Löwdin and the Uppsala Quantum Chemistry Group in 1957. A preliminary exposure to the problem was provided by Löwdin's eight o'clock lectures in the Chemistry auditorium, where he gave a rapid tour of Hilbert space and its associated operator structures, followed by a description of the method of superposition of configurations, and it was overwhelming to be subjected to such a wealth of formalism presented at high speed and with meticulous blackboard management by an expert.

It was in August 1957 that my formal employment started. Löwdin had secured a contract with US Air Force Office of Scientific Research and was in a position to hire associates 'with an interest in numerical calculations'. I was given the month of August to absorb Schiff [1] and also Eyring, Walter and Kimball [2], after which it was time for Fock space. Löwdin was well aware of the development taking place in the mid-fifties with regard to the use of field theoretical approaches to the electron correlation problem in the electron gas. Feynman's path integral formulation of quantum mechanics [3], Bethe's approach to the elimination of certain infinities in quantum electrodynamics [4], and the Gell-Mann and Brueckner calculation for the electron gas [5] brought together an exciting alternative to the often awkward wavefunction and variational approach. Thus Löwdin directed me towards the method of second quantization through the Jordan–Wigner paper [6] and the thorough exposition by Fock [7]. The concepts of creation and annihilation operators for electrons, photons, and quanta of other kinds settled in my mind even though I had but marginal appreciation of their particular advantages and difficulties. It was then time to return to configuration space.

Löwdin's comprehensive review [8] of the correlation problem and the associated bibliographical survey [9] represent the state of knowledge at this time. It was appreciated that in the isoelectronic sequence including atomic helium and in molecular hydrogen there was a correlation energy of about 1 eV for a pair of electrons, whereas for the atomic ion Al^{+3} the pairs from the 2p-shell contributed some 2.4 eV each, when the relativistic corrections were allowed for [10]. The first fact was accounted for by the Hylleraas perturbation expansion in powers of the inverse nuclear charge [11]. Open shell degeneracies in the atomic systems with four or more electrons led Shull and myself to the conclusion that the constant correlation energy per pair of electrons was not a general feature [12], and that the failure of the Hartree–Fock approximation to accommodate near degeneracies leads to correlation energies increasing linearly with the nuclear charge.

Multitudinous experiences with Hilbert, Fock, and configuration spaces allowed me to go to Florida as a space scientist [13] in 1960. There I was once more brought in contact with the field theoretical approach to the many-electron problem through the lectures by Stig Lundqvist [14] at the first Winter Institute at the Quantum Theory Project. Such was the impact of Lundqvist's presentation that I became convinced that here was an area where progress could be made towards the correlation problem in general. I was assigned the problem 'cohesive properties of some rare gas crystals' upon my return to Uppsala in the fall of 1961. Löwdin proposed that I should base my study on the evaluation of the expression

0026–8976/98 $12·00

$$E = \left\langle \Phi_0 \middle| H + H\frac{P}{E-H}H \middle| \Phi_0 \right\rangle$$

with the zero-order wavefunction Φ_0 being the closed shell state formed from the free atom SCF orbitals. Overlaps should be dealt with according to the expansion method [15] pioneered in 1948. The reduced resolvent in the second term was to be constructed from the orthogonal complement represented by the projection operator P and some means to solve for the inverse operator. A principal part of the correlation energy for a molecular crystal is the so-called dispersion energy, which is associated with the van der Waals interaction. It is derived conveniently from the frequency dependent polarizability [16] as formulated for the extended system by means of the dielectric formulation. My first understanding of this approach and its application came from Nozières and Pines [17] and gave the incentive to pursue this further [18]. Response functions, propagators, and/or Green functions became part of my theoretical arsenal and proved to be the vehicles that allowed me to address the thesis problem effectively [19], and which opened the way towards my very rewarding collaboration with Yngve Öhrn.

2. Propagators

Use of Green functions was coming to the fore in many-electron theory in the late fifties. A proper historical account would far exceed the space at my disposal and I will concentrate on some events of particular significance to the development as I see it. Hubbard gave a thorough treatment of the homogenous electron gas [20] which utilized the propagator and self-energy concept elegantly and effectively. This development gave renewed interest in earlier work by Lindhard [21], who had calculated the dielectric response function for an electron gas in the Hartree approximation. Lindhard's function describes the plasmon excitations that are prominent features for extended systems, and provides a good estimate of the correlation energy through the dielectric formulation [17]. Translational symmetry was an essential simplification in the development, and the transcription of the theory to reduced symmetries proved to be something of a struggle. Ehrenreich and Cohen [22] and Goldstone and Gottfried [23] gave the proper form of the equations for the linearized time-dependent form of the Hartree–Fock theory originally put forward by Dirac [24]. The first molecular application was given by Ball and McLachlan [25] with a calculation for a two-electron, two-orbital model.

Hubbard [26] published in 1963 the first in a series of papers where he addressed the problem of itinerant versus localized magnetism. He suggested the Hamiltonian form that has carried his name since then. It is a form with great similarities to the then well established model for the electronic properties of conjugated systems by Pariser and Parr [27] and by Pople [28]. Yngve Öhrn and I embarked on a project to adapt and develop the Green function approach within the Hubbard model. We could build on the work by Coulson for the Hückel model [29, 30] and enjoyed some initial success [31, 32].

Stig Lundqvist and Lars Hedin spearheaded other approaches towards the determination of propagators in electronic systems. Hedin introduced a Coulomb-hole-screened-exchange approximation [33] which has a number of attractive features such as long range polarization contributions to the self-energy. There have been only a few applications of this scheme [34]. The difficulties associated with the construction of consistent approximations beyond the self-consistent field are considerable, and the appearance of the Hohenberg and Kohn [35] paper seemed to drain away the interest from the functional analysis formulation of the dynamic treatment.

Algebraic methods are more direct for molecular applications based on localized representations in terms of atomic orbitals. Various equation-of-motion calculations were favoured in the late sixties, with or without reference to propagators or response functions. A step forward came about when it was realized that some *ad hoc* decouplings employed in the truncation of hierarchies of propagator equations could be justified by means of systematic calculations of matrix elements in an operator algebra. Öhrn and I contributed to this by suggesting a procedure that could be made self-consistent and include a certain amount of correlation [36]. Further developments along this line were soon forthcoming [37], and the superoperator approach seems to reign supreme today [38].

Propagators carry information on relative energies between many-electron states through their spectral representations. The electron propagator has been used extensively to study the binding energies of photoelectrons [39] and to determine electron affinities [40]. It has been useful also in the study of coupling to nuclear displacements and spins [41]. The total electronic energy of a system can be derived from the electron propagator. A difficulty occurs when the approximation method is such that certain sum rules are violated. The result is an ambiguity where two formally equivalent expressions give different results. It is often not possible to conclude which of the alternative ground state energy expressions is variationally acceptable [42]. Similar complications are associated also with the polarization propagator [43]. The search for additional conditions continues, but partial results have been established [44, 45].

A particularly important sum rule is satisfied by certain approximations to the polarization propagator. It holds that the dipole length and dipole velocity forms of the oscillator strength for an electronic transition are equal, even in the linearized time-dependent Hartree–Fock or random phase approximation, provided that the operator truncations do not violate the basic quantum mechanical commutation rule. Such truncations can themselves be consistent at some level of approximation, as discussed some time ago [46, 47].

3. Dissociative recombination

ASTRID, the Aarhus STorage RIng in Denmark, has been used to study electron collisions with molecular ions at very low energies. The ions are circulating in the ring and electrons are injected parallel to the beam of ions at the same velocity. Recombination to neutral molecules or radicals takes place and results in dissociation when the surplus energy is disposed of. It was found that carbonium and oxonium ions fragmented into three parts equally often as into two. This rather unexpected result requires a somewhat detailed study of the electronic process, and it is interpreted here as a correlation effect.

A simple approach towards a characterization of the relevant electronic states in the recombination process is offered by the electron propagator equations. It is of concern to examine possible resonances in the electron scattering process, and thus to examine the nature of the poles of the electron propagator. We use the standard notation [48, 49] to define the Green functions in terms of electron annihilation $\{a_r\}$ and creation $\{a_s^\dagger\}$ operators. Thus we define

$$G_{rs}(E) \equiv \langle\langle a_r; a_s^\dagger\rangle\rangle_E \tag{1}$$

in the energy representation, where r and s relate to elements of a basis of spin orbitals. The equation of motion [49] obtains as

$$EG_{rs}(E) \equiv \langle [a_r; a_s^\dagger]_+\rangle + \langle\langle [a_r, H]; a_s^\dagger\rangle\rangle_E, \tag{2}$$

where H denotes the Hamiltonian of the system. Presently the treatment is restricted to an electronic Hamiltonian (no other degrees of freedom are considered) of the form [49]

$$H = \sum h_{rs} a_r^\dagger a_s + \tfrac{1}{2}\sum (pq|rs) a_r^\dagger a_p^\dagger a_q a_s, \tag{3}$$

and the average values involved in definition (1) and in the expectation values are evaluated for a reference state chosen as the Hartree–Fock ground state. The particular molecular ions under scrutiny have closed shell ground states, well separated from excited states. A basis of canonical, normalized, Hartree–Fock spin orbitals is chosen so that

$$[a_r, a_s^\dagger]_+ = \delta_{rs}, \langle a_s^\dagger a_r\rangle = n_r\delta_{rs}, \langle [[a_r, H], a_s^\dagger]_+\rangle = \varepsilon_r\delta_{rs}, \tag{4}$$

with occupation numbers n_r equal to zero or one for virtual or occupied spin orbitals, respectively. The residual operator $[a_r, H] - \varepsilon_r a_r$ is orthogonal to the primary operators in the sense expressed in equation (4) and is expressible in terms of an auxiliary set of operators as

$$\begin{aligned}[a_r, H] - \varepsilon_r a_r &= \sum \langle [[a_r, H] - \varepsilon_r a_r, a_s^\dagger a_q^\dagger a_p]_+\rangle a_p^\dagger a_q a_s \\ &= \sum \{(pq|rs) - (ps|rq)\} a_p^\dagger a_q a_s\end{aligned}$$

$$\begin{aligned}&\langle [a_p^\dagger a_q a_s, a_{s'}^\dagger, a_{q'}^\dagger, a_{p'}]_+\rangle \\ &\qquad = \delta_{pp'}\begin{vmatrix}\delta_{qq'} & \delta_{qs'} \\ \delta_{sq'} & \delta_{ss'}\end{vmatrix}(n_q - n_p)(n_s - n_p).\end{aligned} \tag{5}$$

Only distinct operators are included in the sum. It is clear that a chain of equations will result from iterations of the basic form (2), where increasingly complex operator products will appear. The truncation procedure suggested in 1967 [36] requires the calculation of the expectation values such as

$$\begin{aligned}&\langle [[a_p^\dagger a_q a_s, H], a_{s'}^\dagger a_{q'}^\dagger a_{p'}]_+\rangle \\ &\quad = (\varepsilon_q + \varepsilon_s - \varepsilon_p)\langle [a_p^\dagger a_q a_s, a_{s'}^\dagger a_{q'}^\dagger a_{p'}]_+\rangle \\ &\qquad + \delta_{pp'}\{(ss'|qq') - (sq'|qs')\} \\ &\qquad + \delta_{qq'}\{(sp|p's') - (ss'|p'p)\} \\ &\qquad + \delta_{ss'}\{(qp|p'q') - (qq'|p'p)\} \\ &\qquad - \delta_{sq'}\{(qp|p's') - (qs'|p'p)\} \\ &\qquad - \delta_{qs'}\{(sp|p'q') - (sq'|p'p)\},\end{aligned} \tag{6}$$

for $n_p = n_{p'} = 1$, $n_q = n_{q'} = n_s = n_{s'} = 0$. A simple interpretation of this expression is offered by the ordinary rules for matrix elements between configurations of two electrons and one hole relative to the reference Hartree–Fock ground state.

The *superoperator* [37, 50] formulation provides a matrix representation where the auxiliary set of operators form a column vector $\mathbf{h}$, a unit metric matrix is given as

$$\langle [\mathbf{h}, \mathbf{h}^\dagger]_+\rangle = \mathbf{I}_h, \tag{7}$$

and a general dynamic matrix as

$$\langle [[\mathbf{h}, H], \mathbf{h}^\dagger]_+\rangle = \mathbf{H}_h. \tag{8}$$

An approximate Green function equation is obtained as

$$(E - \varepsilon_r)G_{rs}(E) \equiv \delta_{rs} + \sum M_{rp}(E)G_{ps}(E)$$

with

$$M_{rp}(E) = \langle [[a_r, H], \mathbf{h}^\dagger]_+\rangle \{E\mathbf{I}_h - \mathbf{H}_h\}^{-1} \langle [[\mathbf{h}, H], a_p^\dagger]_+\rangle. \tag{9}$$

The poles of the Green function represent energy levels of states where an electron has been added or removed from the reference state [49]. A certain inconsistency is related to the development. Expectation values calculated from Green function (9) are not the same as those used to construct the equation. Forms like expression (9) have been used with advantage for numerous problems [39–41], and for resonances it has proved useful in the dilatation transformation method [51].

Presently the aim is to interpret the possible nature of transitions from free electron states at near zero energy to bound states. Thus we are looking for the coupling in the Green function between the free and the bound states. We examine a simple approximation to the self-energy where only a single intermediate state is used:

$$M_{rp}(E) = c_r \frac{1}{E-\alpha} c_p^*, \tag{10}$$

so that the solution to the Green function equation is

$$G_{rs}(E) = \frac{\delta_{rs}}{E-\varepsilon_r} + \frac{1}{E-\varepsilon_r} T_{rs}(E) \frac{1}{E-\varepsilon_s}, \tag{11}$$

with the elements of the T-matrix given by the equations

$$T_{rs}(E) = c_r \frac{1}{E-\hat{\alpha}(E)} c_s^*, \qquad \hat{\alpha}(E) = \alpha + \sum \frac{|c_r|^2}{E-\varepsilon_r}. \tag{12}$$

The previous discussion indicates that the structure of the self-energy is related closely to the spectrum of two electrons and one hole and to the one-electron and two-hole configurations of the reference system. We consider the former case and use the diagonal form of expression (6) to write, as an estimate for the parameter α,

$$\begin{aligned}\alpha &= \varepsilon_q + \varepsilon_s - \varepsilon_p + (ss|qq) - (sq|qs) + (sp|ps) \\ &\quad - (ss|pp) + (qp|pq) - (qq|pp) \\ &= \{\varepsilon_q - \varepsilon_p - (qq|pp)\} + \varepsilon_s + (ss|qq) - (ss|pp) \\ &\quad + (sp|ps) + (qp|pq) - (sq|qs).\end{aligned} \tag{13}$$

The second form indicates that the first term expresses an approximation to a triplet state excitation energy from the reference, the next is the added electron energy, corrected by the next terms for change in the Coulomb interaction, and the last three together express the exchange contributions. A proper spin analysis to pure doublet states will modify these slightly. Similarly, we estimate the amplitudes as

$$c_r = (pq|rs) - (ps|rq) \equiv \int dx\, u_r^*(x) f_{p,qs}(x) \tag{14}$$

from form (5) and the implication of a single intermediate state.

Equation (11) demonstrates that the total cross-section for electron scattering in a state r derives the imaginary part of the T-matrix according to the optical theorem [51]. This depends on the imaginary part of $\hat{\alpha}(E)$ which is the principal value integral over the basic spectrum and involves the spectral density function of the Hartree Fock approximation propagator. Various methods have been designed to construct a continuous spectrum from a finite basis set Hartree Fock approximation [51]. The precise argument is not significant in the following. It is observed here that for a bound state characterized as (p, qs) the amplitude function $f_{p,qs}$ is decaying exponentially towards a large distance from the system. Thus we expect the numerically largest amplitudes c_r for the low energy part of the free spectrum. A large scattering cross-section requires that the real part of $\hat{\alpha}(E)$ equals E. The conclusion of these considerations is that a substantial recombination rate occurs when there is a bound electronic state of the kind introduced above close in energy. This argument does not invoke energy transfer to nuclear modes of motion.

An example of dissociative recombination according to the argument presented here is given by the carbonium ion CH_3^+. Orbital energies have been obtained for the equilibrium geometry, D_{3h} symmetry, as well as the lowest triplet excitation energies. These results are listed in table 1, where the numbers show that it is reasonable to assume that there is a two-electron, one-hole state available to absorb a low energy free electron, and that it involves a hole in a degenerate e′-type orbital.

Table 1. Orbital energies and triplet excitation energies, with symmetry notation for the carbonium ion CH_3^+ at the equilibrium D_{3h} conformation with the C—H bond length 1.092 a_0. Calculations were performed with the suite of programs created by T. Helgaker, H. J. Aa. Jensen, P. Jørgensen, J. Olsen, H. Ågren, K. L. Bak, V. Bakken, P. Dahle, H. Heiberg, D. Jonsson, R. Kobayashi, H. Koch, K. V. Mikkelsen, P. Norman, K. Ruud, P. R. Taylor, and O. Vahtras: 'ABACUS, a second-order MCSCF molecular property program', using a moderately large basis set.

	Orbital symmetry				Triplet symmetry	
	a_1'	e'	a_2''	a_1'	$^3E''$	$^3A''$
Energy	$-1.275\,E_h$	$-0.949\,E_h$	$-0.284\,E_h$	$-0.130\,E_h$	$0.191\,E_h$	$0.336\,E_h$

The energy of the neutral bound states can be estimated from the required integrals to be at $-0.023\,E_h$ and at $0.074\,E_h$ for the $[(1e')^3(1a_2'')^2]^2E'$ and the $[(1e')^3(1a_2'')(3a_{1'})]^2E''$, respectively. Thus it is clear that there are states of this nature in near resonance with free electron states at very low energy. Symmetry requirements from the coupling elements of equation (14) show that it will be the p wave component for the free electron that can generate transitions to the $^2E'$ state while the d wave is required for the $^2E''$ state. It is to be expected that the first will give rise to the largest transition probability.

According to the Jahn–Teller theorem there cannot be a stable degenerate state under regular D_{3h} geometry, and it follows that there will be a distortion of the nuclear framework upon the recombination of the free electron and the ion. The two spatial components of the E′ state will split under E′ type nuclear displacements. There are two kinds of these, stretch and bend modes, and the calculations show that a combination of these gives the largest gradient on the triplet surface. Infinitesimal distortions give equal and opposite energy shifts for the two components, while finite distortions have second-order contributions and differentiate the two. Preliminary calculations show that the most effective distortion for lowering the energy is a superposition of some 25% stretch and 75% bend and that it involves the lengthening of one C—H bond and the decrease of the opposite HCH angle. The opposite distortion which shortens a C—H bond and opens up the opposite HCH angle provides a somewhat smaller decrease in energy for the same magnitude displacement.

Measurements of the propensity of the various fragment channels in dissociative recombination of carbonium ions [52] show that some 30% of the total appears as $C + H_2 + H$, while 16% comes as $CH + H + H$. The remainder is found as $CH + H_2$ (14%) and $CH_2 + H$ (40%). The processes seem to follow the pattern that the favoured motion of distortion splits off one hydrogen and continues to fragment almost half of the time into $C + H_2$. Alternatively, H_2 is separated and it dissociates with a probability of about 0.5. These suggestions should be corroborated by more detailed calculations on the motions on the triplet energy hypersurfaces.

4. Conclusion

Electronic correlation problems have been studied since the inception of quantum mechanics but the theme, '50 years of the electronic correlation problem', was an inspiration for me to review the development as I have experienced it during the last forty years. The particular emphasis that I give propagator theory derives from the very direct relation between the concept and the observable features. Wavefunction and state vector concepts dominate the chemical applications of quantum theory, though the applications in condensed matter theory presents a more balanced picture. Traditional objections to approximations in the calculation of Green functions derive from the lack of certification of N-representability [53] and the variational principle for the ground state energy. The latter deficiency is shared with the currently flourishing development of the method of coupled clusters [54]. Combined use of response function ideas and coupled cluster type representations has provided possibilities for accurate determinations of molecular properties.

Many manifestations of electronic correlation phenomena do not require large scale numerical calculations for their interpretation. The example of the fragmentation of carbonium ions upon dissociative recombination illustrates well that the coupling between a free electron state and an excited state causes substantial changes in the properties of an electronic system. These are identified readily through a low order approach to the electron propagator form.

It is a pleasure to thank Professor Rodney J. Bartlett for the invitation and the opportunity to give a presentation. My mentor, Professor P. O. Löwdin, deserves my thanks for the introduction to the correlation problem and continued inspiration and support. It has been of great benefit to have the inspiration and support of Professor S. O. Lundqvist, long time personal friendship and collaboration with Professor Yngve Öhrn, as well stimulation and challenge by Poul Jørgensen and Jens Oddershede. I am grateful to Asger Halkier and Mark Roberson for calculations related to dissociative recombination and to Professor Torkild Andersen for giving the direction to this phenomenon.

References

[1] SCHIFF, L. I., 1955, *Quantum Mechanics*, 2nd Edn (New York: McGraw-Hill).
[2] EYRING, H., WALTER, J., and KIMBALL, G. E., 1944, *Quantum Chemistry* (New York: Wiley).
[3] FEYNMAN, R. P., 1948, *Rev. mod. Phys.*, **20**, 367.
[4] BETHE, H. A., 1947, *Phys. Rev.*, **72**, 339.
[5] GELL-MANN, M., and BRUECKNER, K. A., 1957, *Phys. Rev.*, **106**, 364.
[6] JORDAN, P., and WIGNER, E. P., 1928, *Z. Physik*, **47**, 631.
[7] FOCK, V., 1932, *Z. Phys.*, **75**, 622.
[8] LÖWDIN, P. O., 1959, *Adv. chem. Phys.*, **2**, 207.
[9] YOSHIZUMI, H., 1959, *Adv. chem. Phys.*, **2**, 323.
[10] FRÖMAN, A., 1958, *Phys. Rev.*, **112**, 870.
[11] HYLLERAAS, E. A., 1930, *Z. Phys.*, **65**, 209.
[12] LINDERBERG, J., and SHULL, H., 1960, *J. molec. Spectrosc.*, **5**, 1.

[13] 'Karlskogabo rymdforskare i Amerika', headline in *Karlskoga Tidning*, 8 February 1960.
[14] LUNDQVIST, S. O., 1960, *The Field-theoretical Approach to the Many-electron Problem* (notes by Lars Hedin), Technical Note, Uppsala, Sweden.
[15] LÖWDIN, P. O., 1948, '*A Theoretical Investigation into some Properties of Ionic Crystals*, thesis (Uppsala: Almqvist & Wiksells).
[16] CASIMIR, H. B. G., and POLDER, D., 1948, *Phys. Rev.*, **73,** 360.
[17] NOZIÈRES, P., and PINES, D., 1958, *Nuovo Cimento*, **9,** 470.
[18] LINDERBERG, J., 1962, *Phys. Lett.*, **1,** 272.
[19] LINDERBERG, J., 1964, *Ark. Fys.*, **26,** 323; 1964, *Acta Universitatis Upsaliensis* (Abstracts of Uppsala Dissertations in Science) **40,** 1.
[20] HUBBARD, J., 1957, *Proc. R. Soc. Lond.* A, **240,** 539.
[21] LINDHARD, J., 1954, *Kgl. Danske Videnskab. Selskab. Mat.-Fys. Medd.*, **28,** No. 8.
[22] EHRENREICH, H., and COHEN, M. H., 1959, *Phys. Rev.*, **115,** 786.
[23] GOLDSTONE, J., and GOTTFRIED, K., 1959, *Nuovo Cimento*, **13,** 849.
[24] DIRAC, P. A. M., 1930, *Proc. Cambridge phil. Soc.*, **26,** 376.
[25] BALL, M. A., and MCLACHLAN, A. D., 1964, *Molec. Phys.*, **7,** 501; *Rev. mod. Phys.*, **36,** 844.
[26] HUBBARD, J., 1963, *Proc. R. Soc. Lond.* A, **276,** 238.
[27] PARISER, R., and PARR, R. G., 1953, *J. chem. Phys.*, **21,** 466, 767.
[28] POPLE, J. A., 1953, *Trans Faraday Soc.*, **42,** 1375.
[29] COULSON, C. A., 1940, *Proc. Cambridge phil. Soc.*, **40,** 201.
[30] COULSON, C. A., and LONGUET-HIGGINS, H. C., 1947, *Proc. R. Soc. Lond.* A, **191,** 39; **192,** 16; 1948, *Proc. R. Soc. Lond.* A, **193,** 447,456; **195,** 188.
[31] LINDERBERG, J., and ÖHRN, Y., 1965, *Proc. R. Soc. Lond.* A, **285,** 445.
[32] ÖHRN, Y., and LINDERBERG, J., 1965, *Phys. Rev.* A, **139,** 1063.
[33] HEDIN, L. T., 1965, *Phys. Rev.* A, **139,** 796.
[34] HEDIN, L. T., and LUNDQVIST, S. O., 1969, *Solid State Phys.*, **23,** 1.
[35] HOHENBERG, P., and KOHN, W., 1964, *Phys. Rev.* B, **136,** 864.
[36] LINDERBERG, J., and ÖHRN, Y., 1967, *Chem. Phys. Lett.*, **1,** 295.
[37] GOSCINSKI, O., and LUKMAN, B., 1970, *Chem. Phys. Lett.*, **7,** 573.
[38] BEENEN, J., and EDWARDS, D. M., 1995, *Phys. Rev.* B, **52,** 13636.
[39] LONGO, R., CHAMPAGNE, B., and ÖHRN, Y., 1995, *Theoret. chim. Acta*, **90,** 397 for a survey.
[40] SIMONS, J., 1978, *Theoretical Chemistry: Advances and Perspectives*, Vol. 3 (Academic Press).
[41] ORTIZ, J. V., 1992, *Int. J. Quantum Chem*, **S26,** 1.
[42] LINDERBERG, J., and ÖHRN, Y., 1973, *Propagators in Quantum Chemistry* (London: Academic Press), p. 111.
[43] LINDERBERG, J., 1980, *Physica Scripta*, **21,** 373.
[44] LINDERBERG, J., and ÖHRN, Y., 1977, *Int. J. Quantum Chem.*, **12,** 161.
[45] ÖHRN, Y., and LINDERBERG, J., 1979, *Int. J. Quantum Chem.*, **15,** 343.
[46] LINDERBERG, J., 1967, *Chem. Phys. Lett.*, **1,** 39.
[47] SEAMANS, L., and LINDERBERG, J., 1974, *Int. J. Quantum Chem.*, **8,** 925.
[48] ZUBAREV, D. N., 1960, *Usp. Fiz. Nauk*, **71,** 71; English translation, *Sov. Phys. Uspekhi*, 1960, **3,** 320.
[49] [42] Chap. 5
[50] See also LÖWDIN, P. O., 1996, *Adv. Quantum Chem.*, **27,** 371.
[51] MISHRA, M. K., and MEDIKERI, M. N., 1996, *Adv. Quantum Chem.*, **27,** 223.
[52] VEJBY, L., private communication.
[53] See, e.g., COLEMAN, A. J., 1963, *Rev. mod. Phys.*, **35,** 668.
[54] CIZEK, J., 1966, *J. chem. Phys.*, **45,** 4256.

MOLECULAR PHYSICS, 1998, VOL. 94, NO. 1, 105–119

Explicitly correlated coupled cluster calculations of the dissociation energies and barriers to concerted hydrogen exchange of $(HF)_n$ oligomers ($n = 2, 3, 4, 5$)

By WIM KLOPPER†‡, MARTIN QUACK‡ and MARTIN A. SUHM‡§

† Department of Chemistry, University of Oslo, PO Box 1033 Blindern, N-0315 Oslo, Norway

‡ Laboratorium für Physikalische Chemie der ETH Zürich (Zentrum), CH-8092 Zürich, Switzerland

The electronic dissociation energies and barriers to concerted hydrogen exchange of $(HF)_n$ oligomers with $n = 2, \ldots, 5$ are computed by means of a many-body decomposition of the total electronic energy. The one- and two-body terms are obtained from explicitly correlated coupled cluster calculations including singles, doubles, and a perturbative triples correction (CCSD(T)-R12), in a large Gaussian basis set consisting of 276 contracted atomic functions. The three-body term is computed at the conventional CCSD(T) level in a basis set containing 228 functions. The four- and five-body terms are obtained from explicitly correlated second-order perturbation theory calculations (MP2-R12), using basis sets with 305 (tetramer) and 380 (pentamer) functions. Since the many-body terms are computed using the same basis set (i.e. the basis of the largest fragment) for all fragments and subfragments, our calculations implicitly include a counterpoise correction. The results of the calculations are compared with semi-empirical one-, two-, and three-body potentials, and new best estimates of the electronic dissociation energies and barriers are inferred. For $(HF)_2$, $(HF)_3$, $(HF)_4$, and $(HF)_5$, respectively, we obtain for the electronic dissociation energies into monomers 19.1(2), 64(2), 116(3) and 158(4) kJ mol^{-1}, and for the electronic barriers to concerted hydrogen exchange 175(10), 85(10), 60(10) and 65(10) kJ mol^{-1}. The results are shown to be consistent with NMR line broadening data within the framework of transition state theory.

1. Introduction

The thermodynamics and kinetics of the fundamental processes of hydrogen bond dynamics in hydrogen bonded clusters are of wide ranging importance in chemistry, physics and biology. The first step in our theoretical understanding of such processes is provided by a good characterization of the most important parts of the electronic potential hypersurfaces for such systems [1], prototypes being clearly $(HF)_n$. These clusters show rearrangements of the three basic types, illustrated here for the dimer [2, 3]:

(i) Hydrogen bond dissociation

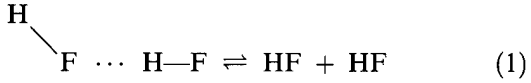

(1)

(ii) Hydrogen bond switching or concerted exchange between bonding and free positions

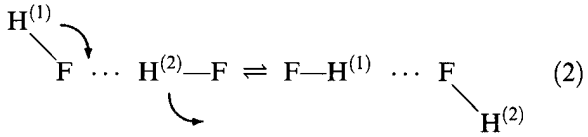

(2)

(iii) Concerted hydrogen exchange between binding sites

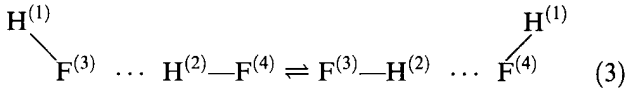

(3)

These processes being exemplified here for the dimer occur in a similar fashion also for larger complexes $(HF)_n$ with $n \geqslant 3$. Whereas at least for the dimer $(HF)_2$ there is considerable experimental and theoretical work available for the first two processes (i) and (ii), little is known about process (iii), and much less is known in general about all three processes in the larger clusters $(HF)_{n \geqslant 3}$ (see [1] and references cited therein). Some initial theoretical work to fill this gap has been carried out recently [4]. It is the aim of the present investigation to provide a more detailed *ab initio* investigation of the important properties of the electronic potential, particularly for the processes (i)

§ Present address: Institut für Physikalische Chemie, Universität Göttingen, Tammannstr. 6, D-37077 Göttingen, Germany.

and (iii) which are perhaps competitive in the larger clusters $(HF)_n$. In essence we aim for the highest possible level of electronic structure calculation which is currently practical for the $(HF)_n$ system. These results should thus provide a benchmark for simpler theoretical approaches and should also be useful for testing and improving empirical potential hypersurfaces for the larger clusters, somewhat similar in spirit to our investigation on $(HF)_2$ [5].

Cohesion in molecular solids and liquids is often described as a superposition of all individual molecular *pair* interactions, thus neglecting any cooperative effects. For electrostatic forces represented by the Coulomb law between point particles, this would be rigorously true. Given the success of electrostatic models for hydrogen bonding [6], pairwise additive approaches may therefore seem to be quite appropriate for this important class of intermolecular interactions. Hydrogen fluoride (HF) provides an interesting test case. Its charge distribution is highly polar and very compact, with only ten strongly bound electrons and a correspondingly small polarizability. Since important cooperative interaction mechanisms are proportional to the polarizability [7] (induction) or even to its cube [8] (dispersion), one might expect the pairwise additive approximation to be excellent for clusters of this molecule. The opposite is true. Upon aggregation, the molecular charge distribution is significantly distorted. As a consequence, the FH···F bond geometry, energetics, and dynamics vary over a wide range with increasing cluster size [4, 9–19]. Rather than trying to interpret these changes in terms of mechanistic contributions to the hydrogen bond, such as exchange or covalent terms, we will adopt the more formal approach of many-body decomposition. Regarding HF as the building block, we will evaluate which fraction of the total interaction energy can be reduced to pairs, triples, etc. of these molecular units.

A further reason to study hydrogen fluoride is that clusters of four to seven molecules are more abundant in the vapour phase of HF than in any other known gaseous hydrogen bonded system [18] under ordinary pressure and temperature conditions. A remarkable feature of this vapour phase is the coalescence of the ^1H–^{19}F spin–spin coupling doublet in NMR spectra down to the lowest pressures that have been investigated [20, 21]. This means that beyond rapid cluster dissociation/association processes, there must be an exchange of hydrogen atoms among the fluorine atoms [12, 22] on a microsecond or even shorter timescale [21]. Given the large dissociation energy of monomeric HF (D_e = 590.5 kJ mol^{-1}), more efficient paths have to be present in the clusters. It is now well established by theoretical calculations [4, 12, 19, 22–25] that these pathways involve a concerted cyclic hydrogen exchange, represented schematically as

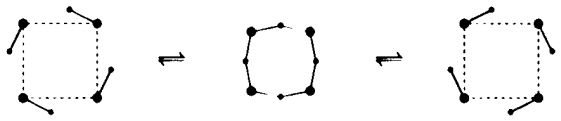
(4)

for the cyclic HF tetramer. The key quantities for an understanding of these thermodynamic and kinetic anomalies of the HF vapour are cluster dissociation energies D_e and hydrogen exchange barriers ΔE as a function of size. The main objective of the present study is to compute these quantities by means of a many-body decomposition of the total interaction energy. An optimal coverage of electron correlation contributions in these extended hydrogen bond systems is achieved by using different electronic structure approaches for the various k-body terms in the spirit of [16, 26].

2. Computational details

2.1. *Geometries*

In the present study, we apply a many-body decomposition of the total electronic energy of the HF oligomers [15] and employ different levels of *ab initio* theory and one-particle basis sets to compute the individual many-body terms. The use of a variety of computational methods is a key ingredient of our approach, and there is no fundamental difficulty in computing analytical first and second derivatives of the total energy with respect to the nuclear replacements, as these derivatives can be evaluated separately for each energy that contributes to a given many-body term. Thus, at least in principle, it is straightforward to optimize the geometries or, if desired, to compute the harmonic vibrational frequencies at such a mixed level of theory. At present, however, we have at our disposal neither the computational tools to carry out these optimizations nor, more importantly, the computing resources to do so at the very high levels of calculation that are applied in the present study. Therefore, due to the technical limitations, we concentrate on the computation of the total electronic energy of the HF oligomers at *fixed geometries*. These geometries are sketched in figure 1, and the corresponding geometrical parameters are given in table 1. The geometries correspond to the 'best estimates' derived by Maerker *et al.* [1, 4], except for the minimum energy structure of the trimer, which is taken from table 2 of [1]. This exception was made because the trimer structure of [1] has already served as a point of reference in previous *ab initio* investigations by Tschumper *et al.* [27]. The difference between the two trimer structures of [4] and [1] is so small that it is irrelevant for the purpose of the present study. The structure of [1] is

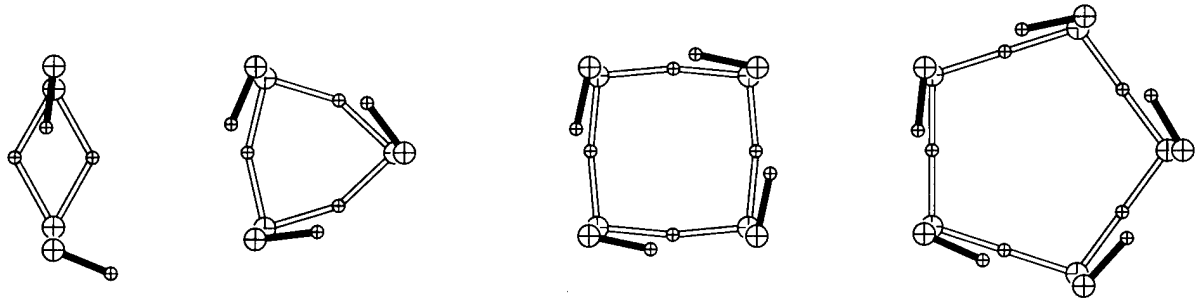

Figure 1. Superimposed representation of the minimum energy structure (upper) and the concerted hydrogen exchange saddle point structure (lower) of the cyclic $(HF)_n$ oligomers ($n = 2, \ldots, 5$). The corresponding geometrical parameters [1, 4] were kept fixed in the present study and are given in table 1.

Table 1. Geometrical parameters of the $(HF)_n$ oligomers. All parameters were kept fixed in the present study. Given are the F–F internuclear separation and the H–F bond length and H–F–F bond angle of the H atom engaged in the hydrogen bond. For the dimer, the H–F bond length and H–F–F bond angle of the 'free' H atom are given in parentheses.

n	Symmetry	R_{FF}/pm	R_{HF}/pm	∠HFF/°
(a) Minimum energy structures				
1	$C_{\infty v}$		91.7	
2	C_s	273.5	92.3 (92.0)	7 (68)
3	C_{3h}	257	93.3	23
4	C_{4h}	251	94.4	12
5	C_{5h}	248	94.8	6
(b) Concerted hydrogen exchange saddle points				
2	D_{2h}	206	118	
3	D_{3h}	224	115	
4	D_{4h}	226	113.5	
5	D_{5h}	226	113	

based on semi-empirical one-, two-, and three-body potentials, and is supposed to be rather accurate. Based on the semi-empirical potential energy hypersurface, harmonic vibrational frequencies have been computed [1], and a detailed comparison with corresponding *ab initio* CCSD(T) results is found in [27].

2.2. *Many-body decomposition*

The quantity $E^n(k)$, with $k \leqslant n$, is defined as the total (adiabatic) electronic and internuclear energy of the $(HF)_k$ fragment of the oligomer $(HF)_n$ for a given, fixed nuclear structure. This energy is obtained from an *ab initio* calculation of the fragment, taking as nuclear coordinates the positions of the nuclei in the $(HF)_n$ oligomer. In terms of these fragment energies, a many-body decomposition of the total energy can be carried out in the usual manner (cf. [1]). Due to the high point group symmetry of the $(HF)_n$ structures in the present study, the oligomers contain many equivalent fragments, and the m-body contributions can be expressed in terms of relatively few fragment energies $E^n(k)$, with $k \leqslant m$. The final expressions are displayed in table 2. Throughout the present study, all fragment energies $E^n(k)$ that contribute to the m-body term V_m of the oligomer $(HF)_n$ were computed employing the same basis set for all fragments $(HF)_k$ with $k = 1, \ldots, m$. The basis set used corresponds to the basis of the $(HF)_m$ fragment itself or of the whole $(HF)_n$ oligomer. Any difference between these two choices will vanish in the limit of an infinite basis. Thus, the counterpoise procedure [28] is incorporated automatically in all our calculations, and in the present study, we report only counterpoise corrected m-body terms. The basis sets used for the computation of a many-body term V_m are denoted as $(HF)_l$-'basis', where $l \geqslant m$ and 'basis' is either DZP, T/Q, or Q/5 (cf. section 2.4).

The high symmetry of the oligomers cannot be exploited when the calculations are carried out in a basis set of a fragment smaller than the oligomer itself. For example, when the three-body term V_3 of the pentamer is computed using for all calculations the basis set of the trimer fragment of interest, the three calculations of the monomer units within the trimer fragment are no longer equivalent because the one-particle basis set is different for the three monomer units. This also applies to the calculation of the dimer fragments within the trimer fragment, and thus, the determination of a three-body term of the pentamer involves seven electronic structure calculations when the trimer fragment basis set is used (1 trimer, 3 dimer, and 3 monomer calculations). Using the whole pentamer basis set, the number of calculations is only four (1 trimer, 2 dimer, and 1 monomer calculations).

We emphasize that a meaningful discussion of many-body contributions to cluster interaction energies

Table 2. Many-body decomposition of the total electronic energy of $(HF)_n$ oligomers in terms of many-body contributions V_m, where $E^n(k)$ is the energy of the $(HF)_k$ fragment in the geometry of the $(HF)_n$ oligomer. For the geometries considered in the present study, the dimer contains two different HF monomer fragments (hydrogen bond donor and acceptor, denoted as 1 and 1′), the tetramer contains two different $(HF)_2$ fragments, denoted as 2 and 2′, and the pentamer contains two different $(HF)_2$ as well as two different $(HF)_3$ fragments, denoted as 2/2′ and 3/3′, respectively. The k' fragments refer to structures where one monomer unit is not neighbouring the other monomer unit(s). See also figure 1 of [1].

n	V_m
2	$V_1 = E^2(1) + E^2(1') - 2E^1(1)$
	$V_2 = E^2(2) - E^2(1) - E^2(1')$
3	$V_1 = 3[E^3(1) - E^1(1)]$
	$V_2 = 3[E^3(2) - 2E^3(1)]$
	$V_3 = E^3(3) - 3E^3(2) + 3E^3(1)$
4	$V_1 = 4[E^4(1) - E^1(1)]$
	$V_2 = 4[E^4(2) - 2E^4(1)]$
	$V_2' = 2[E^4(2') - 2E^4(1)]$
	$V_3 = 4[E^4(3) - 2E^4(2) - E^4(2') + 3E^4(1)]$
	$V_4 = E^4(4) - 4E^4(3) + 4E^4(2) + 2E^4(2') - 4E^4(1)$
5	$V_1 = 5[E^5(1) - E^1(1)]$
	$V_2 = 5[E^5(2) - 2E^5(1)]$
	$V_2' = 5[E^5(2') - 2E^5(1)]$
	$V_3 = 5[E^5(3) - 2E^5(2) - E^5(2') + 3E^5(1)]$
	$V_3' = 5[E^5(3') - E^5(2) - 2E^5(2') + 3E^5(1)]$
	$V_4 = 5[E^5(4) - 2E^5(3) - 2E^5(3') + 3E^5(2) + 3E^5(2') - 4E^5(1)]$
	$V_5 = E^5(5) - 5E^5(4) + 5E^5(3) + 5E^5(3') - 5E^5(2) - 5E^5(2') + 5E^5(1)$

requires realistic and uniform geometries due to the strong dependence of these contributions on the cluster structure. Comparison of dimer-derived geometries [29] or among different minimum structures for various electronic structure levels [30] are less useful.

Finally, the many-body decomposition of the total electronic energy of the oligomers is not completely straightforward for the concerted hydrogen exchange saddle points. In these structures, the monomer fragments lose their identity. Nevertheless, we decompose the energies in the same manner as for the equilibrium structures. This would not be a problem, if the structure is displaced infinitesimally from the symmetric structure, anyway.

2.3. *Electronic structure calculations*

The main objective of the present work is to compute the electronic dissociation energies D_e and the barriers to concerted hydrogen exchange ΔE as close as technically possible to the limit of a complete one-particle basis set, preferably to the highest level of electronic structure calculations that is currently available and affordable.

For the one- and two-body terms, we employ the CCSD(T)-R12 method. This method is identical to the usual CCSD(T) model, but exploits many-electron basis functions that depend explicitly on the interelectronic coordinates r_{ij}. In contrast to the CCSD(T)-R12 method, conventional *ab initio* calculations employ many-electron basis functions that consist of (antisymmetrized) products of one-electron orbitals. The explicitly r_{ij}-dependent basis functions solve the interelectronic cusp problem, and yield a significantly improved convergence to the limit of a complete one-particle basis set for the computed energy. The CCSD(T)-R12 theory, as developed by Noga, Klopper and Kutzelnigg [31–34], has been applied very recently in the framework of benchmark coupled cluster calculations of the ten-electron systems CH_5^+ [35] and H_2O [36], demonstrating its great potential with respect to the quantitatively accurate computation of absolute energies.

For the three-body terms, we employ the *conventional* CCSD(T) method, that is, without explicit r_{ij}-dependence. Using an aug-cc-pVTZ/aug-cc-pVQZ-type basis set, these calculations represent presumably the most accurate level of *ab initio* theory that can be applied today for the computation of the three-body terms.

Finally, for the four- and five-body terms, we employ explicitly correlated second-order Møller Plesset perturbation theory (MP2-R12) using the same aug-cc-pVTZ/aug-cc-pVQZ-type basis set.

The 1s core orbitals of the F atoms were not correlated in any of the electron correlation treatments applied in the present work. This is in contrast to previous MP2/DZP calculations, where the core orbitals were included [16].

The SCF calculations of all fragments up to the pentamer were performed with the SORE program [37] on the Cray Origin 2000 of the University of Bergen. Subsequently, this program was run on the NEC SX-4 supercomputer of the Swiss Center for Scientific Computing (CSCS/SCSC) to provide the corresponding MP2 and MP2-R12 second-order correlation energies. The CCSD(T)-R12 calculations of the monomer and dimer fragments were carried out with the DIRCCR12-95 program [38] on the IBM RS/6000 workstations cluster of the University of Oslo. The conventional CCSD(T) calculations using the T/Q basis set (see section 2.4) of the dimer and trimer fragments were performed with the Gaussian 94 program [39] on the NEC SX-4 of the CSCS/SCSC computing centre. The corresponding calculations of the monomer fragments as well as all calculation with the DZP basis set were obtained with the same program on the DEC 8400 5/300 Alpha servers of the ETH Zürich (C^4 project).

2.4. *Basis sets*

Three basis sets have been used in the present study. The first basis set is the DZP basis set that was used in previous calculations of the three-body potential of $(HF)_n$ clusters [1, 16]. These calculations led to the HF3BG potential, which is an anaytical fit to about 3000 counterpoise corrected MP2/DZP points, without further adjustments [1].

The second basis set is the aug-cc-pV(T/Q)Z basis set (abbreviated as T/Q) that was used in previous calculations of the two-body potential [5]. Employing this basis set, counterpoise corrected MP2-R12 calculations were performed for 3284 points on the six-dimensional hypersurface of the HF dimer. Applying empirical adjustments, the analytical two-body potentials SC-2.9 and SO-3 were derived [5, 40].

The third basis set has been constructed for the present CCSD(T)-R12 study. It is denoted as aug-cc-pV(Q/5)Z basis (abbreviated as Q/5), and has been constructed in analogy with the T/Q basis. The Q/5 basis set for the F atom is 15s9p4d3f2g contracted to 10s7p4d3f2g. The s- and p-type primitive functions were taken from the aug-cc-pV5Z basis and contracted to 10s7p by the segmented contraction scheme (6111111111) for s and (3111111) for p, using the contraction coefficients of the innermost aug-cc-pV5Z orbitals. The 4d3f2g polarization functions were taken from the aug-cc-pVQZ basis. The Q/5 basis set for the H atom is 9s4p3d2f contracted to 7s4p3d2f. The s-type primitive functions were taken from the aug-cc-pV5Z basis and contracted to 7s by the segmented contraction scheme (3111111). The 4p3d2f set was taken from the aug-cc-pVQZ basis.

For completeness, the exponents and contraction coefficients of the three basis sets are given in table 3. All the parameters of the aug-cc-pVXZ (X = T, Q, 5) basis sets [41–43] were downloaded from the EMSL basis set database [44]. Only the pure spherical harmonic components of the basis functions (5d, 7f and 9g) were used in the calculations carried out in the course of the present work. Note that in our previous MP2/DZP calculations, six d-components were used [16].

As noted before, the fragment basis sets are denoted as $(HF)_l$-'basis'. For example, the $(HF)_3$-DZP basis set contains 60, the $(HF)_3$-T/Q basis set contains 228, the $(HF)_2$-Q/5 basis set contains 276, and the $(HF)_5$-T/Q basis set contains 380 basis functions.

3. Results

Table 4 displays the computed many-body decomposition of the total energy of the $(HF)_n$ oligomers for the minimum energy structures (a) and the concerted hydrogen exchange saddle points (b). This table collects our most accurate results, which are compared with the semi-empirical one- and two-body potentials [40] and the analytical fit (HF3BG) to the MP2/DZP-level three-body terms [16].

The CCSD(T)-R12/HF-Q/5 calculations of the one-body or monomer relaxation [45, 46] term agree excellently with the generalized Pöschl–Teller (GPT) monomer potential [40]. For the minimum energy structures, the difference between the *ab initio* computations and the GPT values is not larger than 0.05 kJ mol^{-1} per HF monomer fragment, and for the saddle points, this difference is not larger than 0.1 kJ mol^{-1} per fragment. It is very satisfactory to find that the CCSD(T)-R12 calculations describe the monomer potential so accurately, especially in view of the substantial HF bond elongation (by 20–25%) in the saddle point stuctures.

Concerning the two-body term, it is apparent that the semi-empirical SO-3 potential cannot be used to describe the two-body term of the saddle point structures. The very short FF distances in these structures lie outside the range of distances where the potential is valid. In contrast, the two-body terms V_2' for the interaction between two non-neighbouring monomer fragments as present in the tetramer and pentamer agree well with the *ab initio* calculations, as do the SO-3 values for the minimum energy structures. Comparison of the MP2-R12, CCSD(T)-R12 and SO-3 results for V_2 in table 4, part (a) suggests that the empirical modification of the SO-3 potential relative to the raw MP2-R12 *ab initio* potential is generally a refinement in the vicinity of the minimum energy structures. In conclusion, the SO-3 potential can be employed to describe the minimum energy structures, but not the saddle points. For the dimer the range of validity is expected to extend to about 100 kJ mol^{-1} above the minimum, still far below the exchange saddle point in this case. For the higher oligomers, the range of validity is restricted to even smaller *total* energies for some hydrogen exchange configurations.

Similar conclusions can be inferred from the comparison of the three-body terms. The HF3BG fit [16] of the MP2/DZP calculations fails for the saddle point structures, as no configurations near these structures had been incorporated into the fitting procedure. This is due to fundamental limitations of the current analytical V_2, V_3 expressions for situations where chemical bonds and hydrogen bonds are of comparable length [1]. In fact, the analytical surfaces are by design too repulsive in this situation, so that adiabatic symmetrization schemes [1, 47] can in principle be applied for refinement. In contrast, the inaccuracy of the HF3BG fit for the relatively small V_3' three-body term (where one monomer fragment is not neighbouring the other two) of the minimum energy structure of $(HF)_5$ is within the expected error bars of the analytical fit (which has a rms deviation of 1.8 kJ mol^{-1}, to be multiplied by 5 due to

Table 3. Gaussian basis sets used in the present study. ζ is the exponent of the basis function and c is the coefficient of the segmented contraction of the normalized primitive Gaussians.

	s		p		d	f	g
	ζ	c	ζ	c	ζ	ζ	ζ
			DZP				
Fluorine	9 994.790	0.002 017	44.355 50	0.020 868	1.200 000		
	1 506.030	0.015 295	10.082 00	0.130 092			
	350.269 0	0.073 110	2.995 900	0.396 219			
	104.053 0	0.246 420	0.938 300	0.620 368			
	34.843 20	0.612 593	0.273 300				
	4.368 800	0.242 489					
	12.216 40						
	1.207 800						
	0.363 400						
			T/Q				
	74 530.00	0.000 095	80.390 00	0.006 347	3.107 000	1.917 000	
	111 70.00	0.000 738	18.630 00	0.044 204	0.855 000	0.724 000	
	2 543.000	0.003 858	5.694 000	0.168 514	0.292 000		
	721.000 0	0.015 926	1.953 000				
	235.900 0	0.054 289	0.670 200				
	85.600 00	0.149 513	0.216 600				
	33.550 00		0.065 680				
	13.930 00						
	5.915 000						
	1.843 000						
	0.712 400						
	0.263 700						
	0.085 940						
			Q/5				
	211 400.0	0.000 026	241.900 0	0.001 002	5.014 000	3.562 000	2.376 000
	31 660.00	0.000 201	57.170 00	0.008 054	1.725 000	1.148 000	0.924 000
	7 202.000	0.001 056	18.130 00	0.038 048	0.586 000	0.460 000	
	2 040.000	0.004 432	6.624 000		0.207 000		
	666.400 0	0.015 766	2.622 000				
	242.000 0	0.048 112	1.057 000				
	95.530 00		0.417 600				
	40.230 0		0.157 400				
	17.720 00		0.055 000				
	8.005 000						
	3.538 000						
	1.458 000						
	0.588 700						
	0.232 400						
	0.080 600						
			DZP				
Hydrogen	19.240 60	0.032 828	1.000 000				
	2.899 200	0.231 208					
	0.653 400	0.817 238					
	0.177 600						
			T/Q				
	82.640 00	0.002 006	1.407 000		1.057 000		
	12.410 00	0.015 343	0.388 000		0.247 000		
	2.824 000	0.075 579	0.102 000				
	0.797 700						
	0.258 100						
	0.089 890						
	0.023 630						
			Q/5				
	402.000 0	0.000 279	2.292 000		2.062 000	1.397 000	
	60.240 00	0.002 165	0.838 000		0.662 000	0.360 000	
	13.730 00	0.011 201	0.292 000		0.190 000		
	3.905 000		0.084 800				
	1.283 000						
	0.465 500						
	0.181 100						
	0.072 790						
	0.020 700						

Table 4. Computed and semi-empirical m-body contributions V_m to the electronic dissociation energy for minimum (a) and saddle point structures (b) with respect to fragmentation of $(HF)_n$ oligomers into separate monomers. The two- and three-body terms are decomposed into two contributions: V_2/V_3 from structures with neighbouring monomer units, and V_2'/V_3' from structures where one of the monomer units is not neighbouring the other(s). All energies are given in kJ mol^{-1}.

V_m	$n=2$	$n=3$	$n=4$	$n=5$	Method	Basis[a]
(a) Minimum energy structures						
V_1	0.11	2.07	7.79	12.75	CCSD(T)-R12	HF-Q/5
	0.13	2.17	7.98	13.02	GPT[b]	
V_2	−19.07	−50.21	−64.21	−70.99	CCSD(T)-R12	$(HF)_2$-Q/5
	−19.21	−51.66	−66.89	−74.96	SO-3[c]	
	−18.22	−46.74	−60.25	−66.63	MP2-R12	$(HF)_n$-T/Q
V_2'			−14.47	−26.09	CCSD(T)-R12	$(HF)_2$-Q/5
			−16.06	−26.24	SO-3[c]	
			−15.17	−26.09	MP2-R12	$(HF)_n$-T/Q
V_3		−14.66	−38.98	−52.02	CCSD(T)	$(HF)_3$-T/Q
		−14.98	−36.86	−53.39	HF3BG[d]	
V_3'				−10.53	CCSD(T)	$(HF)_3$-T/Q
				−4.95	HF3BG[d]	
V_4			−3.60	−8.43	MP2-R12	$(HF)_n$-T/Q
V_5				−0.66	MP2-R12	$(HF)_n$-T/Q
(b) Concerted hydrogen exchange saddle points						
V_1	225.80	282.22	339.56	409.35	CCSD(T)-R12	HF-Q/5
	225.59	282.27	339.78	409.68	GPT[b]	
V_2	−66.72	−31.28	−8.66	13.65	CCSD(T)-R12	$(HF)_2$-Q/5
	101.08	12.53	21.02	48.37	SO-3[c]	
	−72.02	−40.08	−17.90	2.73	MP2-R12	$(HF)_n$-T/Q
V_2'			−35.21	−55.99	CCSD(T)-R12	$(HF)_2$-Q/5
			−32.64	−51.29	SO-3[c]	
			−36.12	−57.77	MP2-R12	$(HF)_n$-T/Q
V_3		−226.35	−310.39	−318.95	CCSD(T)	$(HF)_3$-T/Q
		−105.28	−263.72	−313.62	HF3BG[d]	
V_3'				−58.31	CCSD(T)	$(HF)_3$-T/Q
				−25.92	HF3BG[d]	
V_4			−35.05	−75.08	MP2-R12	$(HF)_n$-T/Q
V_5				−0.54	MP2-R12	$(HF)_n$-T/Q

[a] The notation $(HF)_n$-'basis' indicates that the particular m-body term is obtained from a series of calculations of different fragments that all use the composite basis set of the whole $(HF)_n$ oligomer, centred as its coordinates.
[b] Generalized Pöschl–Teller oscillator [5, 40].
[c] Semi-empirical pair potential [5, 40].
[d] Three-body term fitted to MP2/DZP results [16].

the fivefold occurrence of the *same* three-body interaction in V_3' of $(HF)_5$).

To gain insight into the basis set effects, second-order correlation effects, and higher-order correlation effects on the three-, four-, and five-body terms, we have computed these many-body terms using the DZP and T/Q basis sets in the framework of the SCF, MP2, and CCSD(T) methods. The results of these calculations are collected in table 5, and can be used to assess the accuracy or reliability of the three- and higher-body terms in table 4.

For the three-body term of the tetramer and pentamer, we have employed either the basis set of the trimer fragment of interest for all the calculations of this particular fragment and subfragments (denoted as $(HF)_3$-DZP or -T/Q), or the basis set of the whole $(HF)_n$ oligomer (denoted as $(HF)_n$-DZP or -T/Q). For the T/Q basis set, the differences between the results obtained with the $(HF)_3$- and $(HF)_n$-type basis sets are very small, with a maximum for the saddle points of *ca.* 0.4 kJ mol^{-1} at the MP2 level, but for the DZP basis set, we observe relatively large differences, up to

Table 5. Comparison of three-, four-, and five-body contributions obtained from different methods and basis sets. The term V_3' denotes the three-body contribution from a structure where one monomer unit is not neighbouring the other two units. All energies are given in kJ mol^{-1}.

Method	Basis[a]	$n=3$ V_3	$n=4$ V_3	$n=4$ V_4	$n=5$ V_3	$n=5$ V_3'	$n=5$ V_4	$n=5$ V_5
(a) Minimum energy structures								
SCF	$(HF)_3$-DZP	−13.48	−37.39		−52.05	−9.47		
MP2	$(HF)_3$-DZP	−14.49	−39.04		−53.77	−9.52		
CCSD(T)	$(HF)_3$-DZP	−14.44	−38.98		−53.85	−9.46		
SCF	$(HF)_n$-DZP	−13.48	−38.83	−2.72	−52.60	−10.30	−6.56	−0.40
MP2	$(HF)_n$-DZP	−14.49	−40.30	−3.22	−54.67	−10.76	−7.71	−0.54
CCSD(T)	$(HF)_n$-DZP	−14.44	−40.27	−3.32	−54.78	−10.68	−7.87	−0.57
SCF	$(HF)_3$-T/Q	−14.43	−38.79		−52.09	−10.60		
MP2	$(HF)_3$-T/Q	−14.86	−39.18		−51.90	−10.66		
CCSD(T)	$(HF)_3$-T/Q	−14.66	−38.98		−52.02	−10.53		
SCF	$(HF)_n$-T/Q	−14.43	−38.83	−3.16	−52.12	−10.63	−7.44	−0.51
MP2	$(HF)_n$-T/Q	−14.86	−39.24	−3.63	−51.96	−10.73	−8.50	−0.66
MP2-R12	$(HF)_n$-T/Q	−14.83	−39.17	−3.60	−51.89	−10.73	−8.43	−0.66
(b) Concerted hydrogen exchange saddle points								
SCF	$(HF)_3$-DZP	−239.05	−324.86		−343.64	−57.79		
MP2	$(HF)_3$-DZP	−237.18	−322.06		−335.87	−55.91		
CCSD(T)	$(HF)_3$-DZP	−244.72	−330.15		−344.10	−56.02		
SCF	$(HF)_n$-DZP	−239.05	−330.74	−32.66	−347.73	−62.14	−68.31	0.11
MP2	$(HF)_n$-DZP	−237.18	−331.08	−34.68	−342.75	−62.45	−77.61	1.19
CCSD(T)	$(HF)_n$-DZP	−244.72	−339.43	−36.26	−351.16	−62.45	−81.64	1.60
SCF	$(HF)_3$-T/Q	−230.08	−315.66		−329.05	−60.18		
MP2	$(HF)_3$-T/Q	−219.80	−302.98		−310.82	−58.36		
CCSD(T)	$(HF)_3$-T/Q	−226.35	−310.39		−318.95	−58.31		
SCF	$(HF)_n$-T/Q	−230.08	−315.82	−33.42	−329.21	−60.29	−68.37	−0.93
MP2	$(HF)_n$-T/Q	−219.80	−303.38	−35.37	−311.24	−58.65	−75.93	−0.51
MP2-R12	$(HF)_n$-T/Q	−218.69	−302.35	−35.05	−310.56	−58.63	−75.08	−0.54

[a] The notation $(HF)_3$-'basis' indicates that the three-body term is obtained from calculations using the basis set of the corresponding $(HF)_3$ fragment that is part of the $(HF)_n$ oligomer.

1.3 kJ mol^{-1} for the minimum energy structures and up to ≈10 kJ mol^{-1} for the saddle points.

A comparison of the DZP and T/Q results reveals that the four- and five-body terms are not very sensitive to the quality of the basis set, neither for the minimum energy structures, nor for the saddle points. The effects are of the order of 1–2 kJ mol^{-1}. This is in sharp contrast to the three-body term, in particular for the saddle point structures. For these structures, for example, the CCSD(T) values obtained from the two different basis sets differ by as much as 20–30 kJ mol^{-1}.

The difference between the MP2 and CCSD(T) values is very small for the many-body terms of the minimum energy structures. For the saddle point structures, however, the magnitude of the V_3 terms increases by as much as 7–8 kJ mol^{-1} from MP2 to CCSD(T). Interestingly, exactly the same increase due to higher-order correlation effects is observed for both basis sets, indicating that this effect is not very basis set dependent. A moderate increase in magnitude with higher order correlation contributions is also found for the V_4 terms.

Based on the above observations, we conclude the following: first, the three-body terms of the minimum energy structures computed at the CCSD(T)/$(HF)_3$-T/Q level are accurate to within 1 kJ mol^{-1}, or perhaps 2 kJ mol^{-1} for the pentamer. Second, noting the small difference between the MP2 and CCSD(T) results for the four- and five-body terms of the minimum energy structures at the DZP level, we conclude that the MP2-R12/$(HF)_n$-T/Q values are our most accurate four- and five-body terms, probably to within 1 kJ mol^{-1}. Third, the accuracy of the three-body terms of the saddle point structures remains quite uncertain. It appears that these terms, which are up to an order of magnitude larger than the pair attractions, are the most critical contributions. Owing to their uncertainty, we will not be able to reduce the error bars on our previous best estimates of the barrier to concerted hydrogen exchange significantly below 10 kJ mol^{-1} [4].

Table 6. Electronic dissociation energies and barriers to concerted hydrogen exchange of cyclic $(HF)_n$ oligomers ($n = 2, \ldots, 5$). All energies in kJ mol^{-1}. The dissociation energies in the upper part of the table refer to fragmentation into monomers. Stepwise dissociation energies can be obtained as the difference between adjacent D_e values and are explained and shown in figure 2. The values in brackets [...] do not include the four- and five-body terms and correspond to relaxed geometries in the respective potential.

(a) Electronic dissociation energy				
SQSBDE|HF3BG [3, 16, 48]	18.7	61.3	[113.6]	[152.9]
GPT|SC-2.9|HF3BG [1]	19.1	64.3	[111.6]	[147.0]
GPT|SO-3|HF3BG	19.1	64.5	[112.0]	[147.4]
B3LYP/6-311 + +G(3df, 3pd) [4]	20.2	66.3	125.6	173.5
MP2/6-311 + +G(3df, 3pd) [4]	20.7	64.7	121.7	168.1
MP2/[8s6p2d/6s3p] [16]		60.9		
MP2/aug-cc-pV(T/Q)Z[a]	18.8	61.4	114.6	158.1
	17.8[b]	58.3[b]	108.6[b]	149.0[b]
CCSD(T)/aug-cc-pV(T/Q)Z[a]	19.2	62.8		
	18.2[b]	59.8[b]		
CPF/[3s2p1d/3s1p] [23]	20.8	64.6	120.8	
CCSD(T)/[4s3p2d1f/3s2p1d] [24]		60.2		
'QCISD(T)/6-311+G(3df, 2p)' [49]	20.5	65.8		
CCSD(T)/TZ2P(f, d) [50]	19.8			
CCSD(T)/TZ2P(f, d) [27]	20.7	67.9		
CCSD(T)/aug-cc-pVQZ [51]	19.7			
	18.8[b]			
CCSD(T)/aug-cc-pVTZ [52]		66.2		
		60.1[b]		
Extrapolated CCSD(T) limit [51]	19.2			
D_e (*ab initio*),[c] present work[b]	19.0	62.8	113.5	156.0
D_e (semi-empirical),[d] present work[b]	19.1	64.2	117.6	159.8
Previous best estimate [1, 4, 5]	19.1(2)	63(3)	117(4)	161(5)
New estimate, present work	19.1(2)	64(2)	116(3)	158(4)
(b) Barrier to concerted hydrogen exchange				
B3LYP/6-311 + +G(3df, 3pd) [4]	157.8	69.6	43.6	40.8
MP2/6-311 + +G(3df, 3pd) [19]	167.4	78.2	53.1	52.7
MP2/aug-cc-pV(T/Q)Z[a]	169.1	77.3	51.6	52.9
	173.7[b]	85.2[b]	61.4[b]	64.3[b]
CCSD(T)/aug-cc-pV(T/Q)Z[a]	176.8	84.6		
	180.9[b]	91.9[b]		
CPF/[3s2p1d/3s1p] [23]	185	86.6	61.9	
CCSD(T)/[4s3p2d1f/3s2p1d] [24]		75.3		
CCSD(T)/aug-cc-pVTZ [52]		81.9		
'QCISD(T)/6-311+G(3df, 2p)' [49]	186.4	95.4		
CCSD(T)/6-311 + G** [4]		102.0	75.8	
ΔE (*ab initio*),[e] present work[b]	178.0	87.4	63.7	70.1
Previous best estimate [1, 4, 5]	170(10)	80(10)	55(10)	50(10)
New estimate, present work	175(10)	85(10)	60(10)	65(10)

[a] With respect to the fixed geometries of table 1.

[b] Corrected for the BSSE by the counterpoise procedure.

[c] D_e (*ab initio*) $= -(V_{1,2,2'}$[CCSD(T)-R12/$(HF)_{1,2}$-Q/5] $+ V_{3,3'}$[CCSD(T)/$(HF)_3$-T/Q] $+ V_{4,5}$[MP2-R12/$(HF)_n$-T/Q]).

[d] D_e (semi-empirical) $= -(V_1$[GPT] $+ V_{2,2'}$[SO-3] $+ V_{3,3'}$[CCSD(T)/$(HF)_3$-T/Q] $+V_{4,5}$[MP2-R12/$(HF)_n$-T/Q]).

[e] $\Delta E = \Delta V_{1,2,2'}$[CCSD(T)-R12/$(HF)_{1,2}$-Q/5] $+ \Delta V_{3,3'}$[CCSD(T)/$(HF)_3$-T/Q] $+\Delta V_{4,5}$[MP2-R12/$(HF)_n$-T/Q].

4. Discussion

4.1. *Dissociation energies*

Our final results for the potential energies of the relevant high energy stationary points with respect to global minima are displayed in table 6. The electronic dissociation energies (D_e) computed in the present study are compared with other *ab initio* calculations and with our previous best estimates of $D_e = 19.1(2)\,kJ\,mol^{-1}$ for the dimer, $D_e = 63(3)\,kJ\,mol^{-1}$ for the trimer, $D_e = 117(4)\,kJ\,mol^{-1}$ for the tetramer, and $D_e = 161(5)\,kJ\,mol^{-1}$ for the pentamer [1, 4].

Concerning the HF dimer, there is little doubt that the value obtained from the analytical GPT|SO-3 potential is very close (i.e. within $0.2\,kJ\,mol^{-1}$) to the true electronic dissociation energy. Our GPT|SO-3 value is consistent with the CCSD(T) limit of $19.2\,kJ\,mol^{-1}$ extrapolated by Peterson and Dunning [51] and with the corresponding CCSD(T)-R12/$(HF)_2$-Q/5 value of $19.0\,kJ\,mol^{-1}$. With respect to the *ab initio* calculations we note that it is crucial to employ the counterpoise procedure to avoid spurious BSSE effects. The *un*corrected *ab initio* calculations in table 6 yield a much too large D_e ranging from 19.7 to $20.8\,kJ\,mol^{-1}$. Considering the BSSE, it is worth noting that the two almost identical CCSD(T)/TZ2P(f,d) calculations of [50] and [27] differ by as much as $0.9\,kJ\,mol^{-1}$ for D_e. This difference is mainly due to the calculations of [50] having been performed in a basis set that included all Cartesian components of the basis functions (6d, 10f), whereas the calculations of [27] employed only the spherical harmonic components (5d, 7f). It appears that the BSSE due to the spherical harmonic basis set ($\approx 2.5\,kJ\,mol^{-1}$) is roughly $1\,kJ\,mol^{-1}$ larger than for the basis set with Cartesian components ($\approx 1.5\,kJ\,mol^{-1}$). In view of the BSSE, we also note that the counterpoise correction for the aug-cc-pVQZ basis set amounts to $1.0\,kJ\,mol^{-1}$ [51]. Thus, the *corrected* CCSD(T)/aug-cc-pVQZ result is $D_e = 18.8\,kJ\,mol^{-1}$, about $0.3\,kJ\,mol^{-1}$ below the estimated limit [51]. These findings confirm that BSSE and other basis set incompleteness effects remains a challenge for traditional correlated treatments of hydrogen bonded systems [53].

For the HF trimer, we have computed an electronic dissociation energy of D_e (*ab initio*) $= 62.8\,kJ\,mol^{-1}$. As the magnitude of the computed two-body interaction is about $1.5\,kJ\,mol^{-1}$ smaller than the value obtained from the SO-3 potential (cf. table 4, part (a)), the computed value might be too low by a similar amount. We may safely assume that the *ab initio* computed dissociation energy represents a *lower bound* to the true limit, not only for the trimer, but also for the other oligomers, including the dimer. Thus, assuming that the CCSD(T)-R12/$(HF)_2$-Q/5 level of theory still underestimates the magnitude of the pair interaction by a few per cent, we obtain a very realistic value of D_e(semi-empirical) $= 64.2\,kJ\,mol^{-1}$ by replacing the CCSD(T)-R12/$(HF)_2$-Q/5 one- and two-body terms by the GPT|SO-3 potential. In any case, both results are well within the uncertainty of the previous best estimate of $D_e = 63 \pm 3\,kJ\,mol^{-1}$. From the present calculations, we infer a new estimate of $D_e = 64 \pm 2\,kJ\,mol^{-1}$, which is only a small change with respect to our previous estimate. This value is also in good agreement with an unpublished geometry minimization at CCSD(T)/aug-cc-pVTZ level [52], which yields $60.1\,kJ\,mol^{-1}$ with and $66.2\,kJ\,mol^{-1}$ without counterpoise correction. Based partly on a fortuitous cancellation of the BSSE and (other) basis set truncation errors, the results of the other *ab initio* calculations displayed in table 6 are close to our new estimate. Only the CCSD(T) value of 60.2 $kJ\,mol^{-1}$ obtained by Kormonicki *et al.* [24] is surprisingly low. These authors employed a [4s3p2d1f/3s2p1d] basis set of atomic natural orbitals (ANO). If we were to correct their value for the BSSE by means of the counterpoise correction, the dissociation energy would be reduced further, notably by more than $6\,kJ\,mol^{-1}$ [24]. Thus, the corresponding counterpoise corrected CCSD(T)/[4s3p2d1f/3s2p1d] value would be in error by about $10\,kJ\,mol^{-1}$ or roughly 20%. As already anticipated by Komornicki *et al.*, this large error is presumably due to the lack of an appropriate augmentation of the ANO basis set.

Our previous estimates of the dissociation energies of the HF tetramer ($117(4)\,kJ\,mol^{-1}$) and pentamer ($161(5)\,kJ\,mol^{-1}$) are well confirmed by the present caculations (113.5–117.6 and 156.0–159.9 $kJ\,mol^{-1}$, respectively), and there is little reason to revise these estimates. Nevertheless, we infer new estimates of 116(3) for the tetramer and $158(4)\,kJ\,mol^{-1}$ for the pentamer. Again, previous *ab initio* calculations [4, 23] yielded too large dissociation energies. The contribution of four- and five-body terms to the binding energy of $(HF)_4$ and $(HF)_5$ is notable, but smaller than (and opposed to) the contribution from monomer non-rigidity (V_1).

If we take a best estimate of the anharmonic zero point energy difference between $(HF)_4$ and 4 HF of about $29(2)\,kJ\,mol^{-1}$ [16] and combine this with the experimental bounds for dissociation of a single HF from $(HF)_4$ ($\Delta D_0 = 42$–$43\,kJ\,mol^{-1}$) [18], for dissociation of a single HF from $(HF)_3$ ($\Delta D_0 = 29$–$32\,kJ\,mol^{-1}$) [54], and for dissociation of $(HF)_2$ ($D_0 = 12.70(2)\,kJ\,mol^{-1}$) [55], all in the sense of equation (1), we obtain $D_e((HF)_4) \approx 111$ to $119\,kJ\,mol^{-1}$, fully consistent with the present theoretical result. The new results support our previous conjecture [56] that $(HF)_4$ should be stable with respect to dissociation upon HF stretching fundamental excitation, rendering

a reinterpretation [56, 57] of recent predissociation-scattering experiments [58] quite likely.

4.2. *Barriers to concerted hydrogen exchange*

The computation of the barriers has proven to be significantly more difficult than the calculation of the dissociation energies. In fact, it is not possible to identify individual monomer fragments in the saddle point structures, and many-body decompositions and counterpoise corrections are not well defined. In any case, however, it is guaranteed that the procedure adopted in the present work will lead to the correct answers when the *ab initio* methods and basis sets are subsequently improved. Moreover, we are convinced that the calculations of the present work provide results that are as close to the true barriers as is achievable today from a computational point of view.

For the dimer and trimer, the computed barriers (178.0 and 87.4 kJ mol^{-1}, respectively) are 7–8 kJ mol^{-1} higher than our previous estimates. This is a satisfactory agreement in view of the large error bars of 10 kJ mol^{-1}, which result from the very slow and counterpropagating convergence of this quantity with basis size and electronic structure level [4]. Thus, our best estimates for the barrier are coincidentally close to earlier DZP MP2 predictions [4, 16], while improvement of the basis set or the correlation treatment alone would lead to larger discrepancies. For the trimer, an unpublished full CCSD(T)/aug-cc-pVTZ saddle point optimization [52] confirms our structure assumption and yields a BSSE uncorrected barrier of 81.9 kJ mol^{-1} (table 6).

More pronounced changes in the same direction are obtained for the tetramer and in particular for the pentamer. We find considerably larger barriers for these oligomers than anticipated in our earlier investigations. Note that there is a sizeable correlation contribution even for the four- and five-body terms. This contribution is not fully captured at MP2 level, but we can estimate the higher order effects from the DZP results. Thus, in the present study, we find that the tetramer may have a slightly lower barrier to concerted hydrogen exchange than the pentamer. There are only a few *ab initio* calculations available for comparison. Liedl *et al.* [19] and Maerker *et al.* [4] have performed MP2 and density functional calculations using a 6-311++ G(3df, 3pd) basis set, but the barriers computed with this basis set suffer from noticeable basis set limitations, as expected [4]. To illustrate the order of magnitude of the basis set effects, we include in table 6 our MP2 results obtained with the T/Q basis set, which is roughly comparable with the 6-311++G(3df, 3pd) basis set, even if it is slightly larger. For the dissociation energies, we observe counterpoise corrections of 6.0 kJ mol^{-1} for the tetramer and 9.1 kJ mol^{-1} for the pentamer. Due to the much shorter FF distances in the saddle point structures, we expect a larger BSSE for these structures than for the minimum energy structures. Indeed, the corresponding counterpoise corrections for the saddle points—assuming that they can be computed in the usual manner—are 15.8 and 20.5 kJ mol^{-1}, respectively. Thus, the barriers are increased by as much as 9.8 and 11.4 kJ mol^{-1} by the counterpoise correction. At this point, of course, we do not consider changes in the geometries due to the BSSE, but without doubt, a correction of *ca.* 10 kJ mol^{-1} is a reasonable estimate for the order of magnitude of the 6-311++G(3df, 3pd)-related BSSE at the MP2 level. Figures 2 and 3 provide a summary of various energies computed here, in a suitable graphical representation.

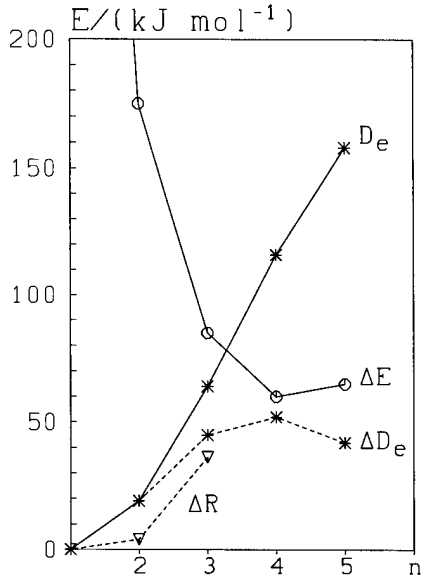

Figure 2. Dissociation energy ($D_e(n)$, stars, full line) for fragmentation of $(HF)_n$ into n HF molecules, hydrogen bond dissociation energy of $(HF)_n$ into $(HF)_{n-1}$ and HF ($\Delta D_e(n) = D_e(n) - D_e(n-1)$, stars, dashed line), energy barrier ($\Delta E(n)$, circles, full line) for the concerted hydrogen exchange between binding sites (see equation (4)), and energy barrier ($\Delta R(n)$, triangles, dashed line) for hydrogen bond switching (see equation (2)), all as a function of cluster size n. Beyond $n = 3$, the simultaneous hydrogen exchange in the cluster becomes more facile than complete cluster dissociation into monomers, but dissociation of a *single* HF from the cluster requires less or comparable energy. Asymptotically, for large ring clusters, both $D_e(n)$ and $\Delta E(n)$ should become proportional to n, whereas $\Delta D_e(n)$ will approach a finite, constant value.

Despite the current uncertainty of the electronic barriers, an analysis of the unimolecular isomerization process in terms of simple transition state theory is useful [4]. In this framework, the thermal rate constant $k_{(3)}(T)$ corresponding to the process of equation (3) is

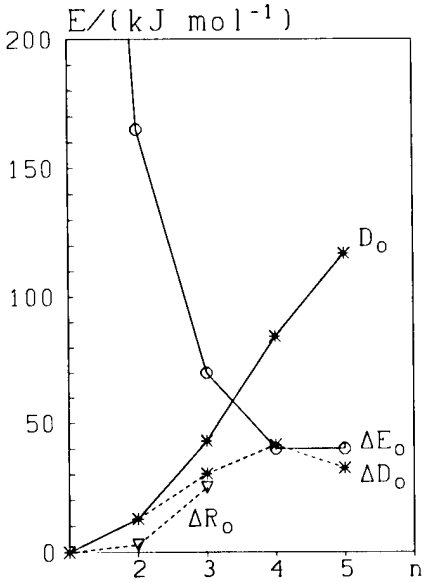

Figure 3. As figure 2, but now including zero point energy contributions to the dissociation energy into monomers (D_0), to the dissociation energy of a single monomer (ΔD_0), to the barrier for hydrogen transfer (ΔE_0, estimated harmonically) and to the barrier for hydrogen bond switching (ΔR_0, estimated harmonically, see, however [59], where the harmonic approximation for this quantity was shown to be poor).

given by

$$k_{(3)}(T) = \frac{kT}{h}\frac{q^{\ddagger}_{\mathrm{int}}}{q_{\mathrm{int}}}\exp(-\Delta E_0/RT). \qquad (5)$$

The ratio of internal partition functions $q_{\mathrm{int}} = q_{\mathrm{vib}}q_{\mathrm{rot}}/\sigma$ between the D_{nh} transition state (‡, symmetry number $\sigma^{\ddagger} = 2n$) and the C_{nh} ground state (without superscript, $\sigma = n$) can be estimated in the harmonic approximation from *ab initio* calculations. For the experimentally relevant temperature range of 250–330 K, $q^{\ddagger}_{\mathrm{int}}/q_{\mathrm{int}}$ is found to be 0.04 ± 0.02 for the tetramer and 0.02 ± 0.01 for the pentamer, based on MP2 DZP [16], B3LYP and BHHLYP calculations [4]. A more significant uncertainty is inherent in the zero-point energy corrected transition state barriers, which we estimate to be $\Delta E_0 = 40 \pm 10\,\mathrm{kJ\,mol^{-1}}$ for both the tetramer and the pentamer of HF (figure 3). These estimates are based on the best available electronic barriers derived in this work together with harmonic zero-point energy contributions at MP2 DZP [16] and density functional levels [4], which agree within ±10%.

Very little is known experimentally about these concerted hydrogen exchange barriers in cyclic HF clusters. From the absence of a spin–spin coupling doublet in the vapour NMR spectra, Mackor *et al.* [21] concluded within the framework of simple transition state theory (neglecting differences in the partition functions for the

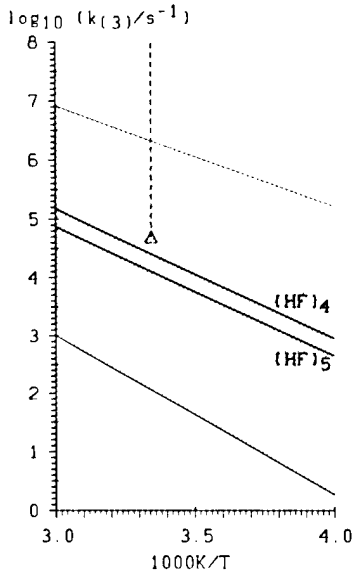

Figure 4. Decadic logarithm of the unimolecular hydrogen transfer rate $k_{(3)}$ in HF tetramers and pentamers from transition state theory without tunnelling (thick lines, the hatched region marks the theoretical uncertainty, which is dominated by the error bar for the barriers) as a function of reciprocal temperature $1/T$. For comparison, an experimental *lower* bound obtained in the gas phase at 299 K (independent of pressure) [21] is shown (triangle, the lower bound character is marked with dashes). Tunnelling will increase the rate by allowing transmission coefficients $\gamma_a > 0$ on each channel for energies $E \leqslant E_0$ (and $\leqslant$ channel maxima) but will also lead to a contribution decreasing the rate because of $\gamma_a < 1$ for $E \geqslant E_0$ (and $\geqslant$ channel maxima), say, in the framework of the adiabatic channel model [61]. Recent calculations by Loerting *et al.* [25(b)] seem to indicate tunnelling corrections of about two orders of magnitude.

D_{nh} and C_{nh} structures) that $\Delta E_0 < 48\,\mathrm{kJ\,mol^{-1}}$. Given the small ratio of D_{nh} to C_{nh} partition functions for $(HF)_4$ and $(HF)_5$ (*vide supra*), this upper bound is probably overestimated [4], although quantum tunnelling [25] may in part compensate for the partition function contribution even at room temperature [60] and anharmonic contributions represent a sizeable additional uncertainty [59]. Figure 4 compares experimental [21] and theoretical (equation (5)) results for the thermal rate constant $k_{(3)}(T)$. It is seen that the tetramer and the pentamer exhibit quite comparable exchange rates, which are close to the experimental lower bound of the gas phase rate at 299 K [21], namely $5 \times 10^4\,\mathrm{s^{-1}}$. Both larger [4] and smaller clusters will contribute much less to the exchange rate (see figure 3). Given the progress in NMR spectroscopy over the last three decades [62, 63], our results suggest that a reinvestigation of the vapour NMR spectra at lower temperatures (and pressures) might permit a detailed characterization of the spin

coupling doublet coalescence. This would provide important experimental information on this prototypical hydrogen transfer process and on the subsequent cluster dissociation kinetics. As shown in figures 2 and 3, the latter two processes have similar activation energies for $(HF)_n$ (with $n = 4$ and 5). Hydrogen exchange in collisional complexes between HF oligomers ($2 < n < 5$) and HF molecules is thus already feasible at low collisional energies without quantum tunnelling contributions [25]. At very low vapour pressures, the collision process itself may become rate limiting, thus allowing for a study of the cluster association/dissociation kinetics. This might be feasible with modern high-field NMR spectrometers but is also within reach of current IR spectroscopic methods.

Two restrictions apply to our prediction of a microsecond or only slightly faster timescale for the loss of monomer integrity in clustered HF vapour at moderately low temperatures. (a) There could be sizeable quantum tunnelling [64] corrections to the transition state rate. A recent investigation [25] does not seem to support rate enhancements over many orders of magnitude for the temperatures and cluster sizes considered here, although large-curvature corrections seem to contribute about two orders of magnitude [25 (b)]. The current uncertainty in the exchange barrier height ($\pm 10\,\mathrm{kJ\,mol^{-1}}$) may still dominate the overall uncertainty in the exchange rate, but in contrast to tunnelling contributions, it can increase or decrease the rate. Clearly, tunnelling is not efficient enough to lead to easily detectable splittings in the IR spectra [57], but a nanosecond exchange timescale would not be excluded by current experimental evidence. (b) There might be other tunnelling pathways with even lower barriers present in larger clusters, e.g. via ionic intermediates [49]. Strictly speaking, the existence of such competitive pathways cannot be rigorously excluded, although the enormous three-body enhancement (see table 4, part (b)) of the concerted process renders competitive non-concerted mechanisms rather unlikely. The fact that NMR spin-doublet coalescence can be suppressed in carefully neutralized *liquid* HF [21] would also tend to exclude such pathways.

In this context, one should note that hydrogen bond switching processes such as the well-characterized donor–acceptor hydrogen bond exchange (equation (2)) in the dimer [2, 59, 65] fully conserve monomer integrity. In figures 2 and 3, the barriers for these processes are given for the dimer and for the trimer [1], as obtained for the SO-3 potential energy hypersurface in combination with the HF3BG three-body potential. The barriers (ΔR) lie below the lowest dissociation thresholds (ΔD) for $(HF)_n$ with $n = 2$ and 3 but may in principle be larger for $n \geqslant 4$. However, one should note that *sequential* single monomer dissociation and association pathways for hydrogen bond switching are almost barrierless on the association side [16,18], in particular including zero-point energy. Therefore, a likely hydrogen bond switching scenario for larger ring clusters is the formation of the next smaller ring with a monomer loosely attached to it [18, 56, 66]. These attached monomers have a high peripheral mobility and can insert into the ring at another position, after which the next monomer can go to the periphery, etc. Such a *sequential* mechanism for hydrogen bond switching is unlikely to have a barrier ΔR significantly above the lowest dissociation threshold ΔD. In contrast, *concerted* hydrogen bond rearrangements tend to be become disfavoured for larger rings due to the strengthening of the hydrogen bond. Finally, there is obviously more than one result of concerted rearrangements for $n > 3$, giving rise to different saddle points. These will be studied in more detail elsewhere together with several dozens of local cluster minima which we have characterized on the analytical potentials for $n = 4$–8 [16].

5. Conclusion

The potential hypersurfaces for hydrogen bonded systems govern some of the most important chemical processes, from inorganic vapour condensation and evaporation phenomena to biochemical DNA replication reactions and dynamics of enzymes. The cooperative nature of hydrogen bonding presents a substantial challenge to high level quantum chemistry approaches due to their unfavourable scaling with the number of atoms involved. Quantitative insights have been obtained here for the simple and well studied prototype system $(HF)_n$ through judicious decomposition into separately calculated many-body contributions. An important result is the rapid decline of n-body contributions with increasing n *after* the three-body term, whereas two- and three-body terms are both essential for a description of the hydrogen bond in larger HF clusters. The detailed convergence pattern naturally depends on the investigated quantities, the geometries and the required accuracy. For a cluster of size $n > 3$, there will usually be special conformations for which even the highest (i.e. n-body) term is important, but in general these conformations will not be relevant for the hydrogen bond dynamics. Truncation after the three-body term is often found to be satisfactory for the hydrogen bond geometry and energetics, while hydrogen transfer barriers and some vibrational frequencies demand four-body contributions as well.

From $(HF)_2$ to $(HF)_5$, the electronic binding energy per hydrogen bond increases by 65%, the contribution of the pair potential to the hydrogen bond falls from 100 to about 60%, the three-body contribution rises from 0

to 40% and the concerted hydrogen exchange barrier per hydrogen drops to about 15% of its value in $(HF)_2$. Inclusion of zero-point energy further enhances some of the changes. The failure of density functional methods to describe the hydrogen exchange process turns out to be even more pronounced than expected. Further refinements on the cluster binding energies should include an explicit geometry optimization. The present results support previous IR spectroscopic analyses [56] and suggest that state of the art NMR gas phase studies should be able to quantitatively analyse the hydrogen exchange dynamics, whereas other types of kinetics studies would also be useful to investigate exchange processes in various mixed isotopomers $[(HF)_n(DF)_m]$, etc.

We would like to thank M. Borer, J. Brunson, C. Moor-Häberling, and U. Röthlisberger for the excellent and unbureaucratic support of our quantum chemical calculations, and T. Helgaker, K. R. Liedl, H. H. Limbach and H. F. Schaefer III for discussions and comments on the manuscript as well as the permission to cite from the unpublished work of [52]. We gratefully acknowledge generous allocations of computing resources by the Competence Centre of Computational Chemistry (C^4 project) in Zürich, the Centro Svizzero di Calcolo Scientifico (CSCS/SCSC) in Manno, Switzerland, and the computer centres of the University of Oslo and the University of Bergen. Our research is supported by the Schweizerischer Nationalfonds and by the Norwegian Research Council (Supercomputer Programme Grant No. NN2694K).

References

[1] Quack, M., and Suhm, M. A., 1997, *Conceptual Perspectives in Quantum Chemistry, Conceptual Trends in Quantum Chemistry*, Vol. III, edited by J.-L. Calais and E. S. Kryachko (Dordrecht: Kluwer), pp. 415–463.

[2] Puttkamer, K. v., and Quack, M., 1989, *Chem. Phys.*, **139,** 31.

[3] Quack, M., and Suhm, M. A., 1991, *J. chem. Phys.*, **95,** 28.

[4] Maerker, C., von Ragué Schleyer, P., Liedl, K. R., Ha, T.-K., Quack, M., and Suhm, M. A., 1997, *J. comput. Chem.*, **18,** 1695. There is a misprint in the eighth line before the end of the Conclusions in this paper, where it should read 20 to 40 kJ mol^{-1}, of course.

[5] Klopper, W., Quack, M., and Suhm, M. A., 1996, *Chem. Phys. Lett.*, **261,** 35.

[6] Price, S. L., 1997, *Molecular Interactions –From van der Waals to Strongly Bound Complexes*, edited by S. Scheiner (New York: Wiley), Chap. 9, pp. 297–333.

[7] Rigby, M., Smith, E. B., Wakeham, W. A., and Maitland, G. C., 1986, *The Forces Between Molecules* (Oxford: Clarendon Press).

[8] Axilrod, B. M., and Teller, E., 1943, *J. chem. Phys.*, **11,** 299.

[9] Del Bene, J. E., and Pople, J. A., 1971, *J. chem. Phys.*, **55,** 2296.

[10] Clark, J. H., Emsley, J., Jones, D. J., and Overill, R. E., 1981, *J. chem. Soc. Dalton Trans.*, 1219.

[11] Karpfen, A., Beyer, A., Schuster, P., 1983, *Chem. Phys. Lett.*, **102,** 289.

[12] Gaw, J. F., Yamaguchi, Y., Vincent, M. A., and Schaefer III, H. F., 1984, *J. Am. Chem. Soc.*, **106,** 3133.

[13] Liu, S., Michael, D. W., Dykstra, C. E., and Lisy, J. M., 1986, *J. chem. Phys.*, **84,** 5032.

[14] Latajka, Z., and Scheiner, S., 1988, *Chem. Phys.*, **122,** 413.

[15] Chałasiński, G., Cybulski, S. M., Szczęśniak, M. M., and Scheiner, S., 1989, *J. chem. Phys.*, **91,** 7048.

[16] Quack, M., Stohner, J., and Suhm, M. A., 1993, *J. molec. Struct.*, **294,** 33, and to be published.

[17] Chałasiński, G., and Szczęśniak, M. M., 1994, *Chem. Rev.*, **94,** 1723.

[18] Suhm, M. A., 1995, *Ber. Bunsenges. Phys. Chem.*, **99,** 1159.

[19] Liedl, K. R., Kroemer, R. T., and Rode, B. M., 1995, *Chem. Phys. Lett.*, **246,** 455.

[20] Hindermann, D. K., and Cornwell, C. D., 1968, *J. chem. Phys.*, **48,** 2017.

[21] Mackor, E. L., MacLean, C., and Hilbers, C. W., 1968, *Recl. Trav. Chim.*, **87,** 655.

[22] Heidrich, D., Köhler, H. J., and Volkmann, D., 1985, *Int. J. quant. Chem.*, **27,** 781.

[23] Karpfen, A., 1990, *Int. J. quantum Chem. (Quant. Chem. Symp.)*, **24,** 129.

[24] Komornicki, A., Dixon, D. A., and Taylor, P. R., 1992, *J. chem. Phys.*, **96,** 2920.

[25] (a) Liedl, K. R., Sekušak, S., Kroemer, R. T., and Rode, B. M., 1997, *J. phys. Chem.* A, **101,** 4707; (b) Loerting, T., Liedl, K. R., and Rode, B. M., 1998, *J. Am. Chem. Soc.* (in the press).

[26] Pedulla, J. M., Vila, F., and Jordan, K. D., 1996, *J. chem. Phys.*, **105,** 11091.

[27] Tschumper, G. S., Yamaguchi, Y., and Schaefer III, H. F., 1997, *J. chem. Phys.*, **106,** 9627.

[28] v. Duijneveldt, F. B., 1997, *Molecular Interactions – From van der Waals to Strongly Bound Complexes*, edited by S. Scheiner (New York: Wiley), Chap. 3, pp. 81–104.

[29] Tachikawa, M., and Iguchi, K., 1994, *J. chem. Phys.*, **101,** 3062.

[30] Xantheas, S. S., 1994, *J. chem. Phys.*, **100,** 7523.

[31] Noga, J., Kutzelnigg, W., and Klopper, W., 1992, *Chem. Phys. Lett.*, **199,** 497.

[32] Noga, J,, and Kutzelnigg, W., 1994, *J. chem. Phys.*, **101,** 7738.

[33] Noga, J., Klopper, W., and Kutzelnigg, W., 1997, *Recent Advances in Coupled-Cluster Theory*, Recent Advances in Computational Chemistry, Vol. III, edited by R. J. Bartlett (Singapore: World Scientific Publishers), pp. 1–48.

[34] Klopper, W., and Noga, J., 1995, *J. chem. Phys.*, **103,** 6127.

[35] Müller, H., Kutzelnigg, W., Noga, J., and Klopper, W., 1997, *J. chem. Phys.*, **106,** 1863.

[36] Helgaker, T., Klopper, W., Koch, H., and Noga, J., 1997, *J. chem. Phys.*, **106,** 9639.

[37] Klopper, W., 1991, SORE program.

[38] Noga, J., and Klopper, W., 1995, DIRCCR12 program.

[39] FRISCH, M. J., TRUCKS, G. W., SCHLEGEL, H. B., GILL, P. M. W., JOHNSON, B. G., ROBB, M. A., CHEESEMAN, J. R., KEITH, T., PETERSSON, G. A., MONTGOMERY, J. A., RAGHAVACHARI, K., AL-LAHAM, M. A., ZAKRZEWSKI, V. G., ORTIZ, J. V., FORESMAN, J. B., CIOSLOWSKI, J., STEFANOV, B. B., NANAYAKKARA, A., CHALLACOMBE, M., PENG, C. Y., AYALA, P. Y., CHEN, W., WONG, M. W., ANDRES, J. L., REPLOGLE, E. S., GOMPERTS, R., MARTIN, R. L., FOX, D. J., BINKLEY, J. S., DEFREES, D. J., BAKER, J., STEWART, J. P., HEAD-GORDON, M., GONZALES, C., and POPLE. J. A., 1995, Gaussian94, Revisions C.3 and D.2 (Pittsburgh, PA: Gaussian Inc).

[40] KLOPPER, W., QUACK, M., and SUHM, M. A., 1998, *J. chem. Phys.* (submitted).

[41] DUNNING JR, T. H., 1989, *J. chem. Phys.*, **90,** 1007.

[42] KENDALL, R. A., DUNNING JR, T. H., and HARRISON, R. J., 1992, *J. chem. Phys.*, **96,** 6796.

[43] DUNNING JR, T. H., unpublished.

[44] The aug-cc-pVXZ basis sets (X = T, Q, 5) were obtained from the Extensible Computational Chemistry Environment Basis Set Database, Version 1.0, as developed and distributed by the Molecular Science Computing Facility, Environmental and Molecular Sciences Laboratory which is part of the Pacific Northwest Laboratory, PO Box 999, Richland, Washington 99352, USA, and funded by the US Department of Energy. The Pacific Northwest Laboratory is a multi-program laboratory operated by Battelle Memorial Institute for the US Department of Energy under contract DE-AC06-76RLO 1830. Contact David Feller, Karen Schuchardt, or Don Jones for further information.

[45] MAYER, I., and SURJAN, P. R., 1992, *Chem. Phys. Lett.*, **191,** 497.

[46] XANTHEAS, S. S., 1996, *J. chem. Phys.*, **104,** 8821.

[47] CHANG, Y.-T., and MILLER, W. H., 1990, *J. chem. Phys.*, **94,** 5884.

[48] QUACK, M., and SUHM, M. A., 1996, *Theor. Chim. Acta*, **93,** 61.

[49] HEIDRICH, D., VAN EIKEMA HOMMES, N. J. R., and VON RAGUÉ SCHLEYER, P., 1993, *J. Comput. Chem.*, **14,** 1149.

[50] COLLINS, C. L., MORIHASHI, K., YAMAGUCHI, Y., and SCHAEFER III, H. F., 1995, *J. chem. Phys.*, **103,** 6051.

[51] PETERSON, K. A., and DUNNING JR, T. H., 1995, *J. chem. Phys.*, **102,** 2032.

[52] LIEDL, K. R., XANTHEAS, S. S., RODE, B. M., and DUNNING, Jr., T. H. J., 1997, private communication.

[53] NOVOA, J. J., PLANAS, M., and WHANGBO, M.-H., 1994, *Chem. Phys. Lett.*, **225,** 240.

[54] SUHM, M. A., and NESBITT, D. J.,1995, *Chem. Soc. Rev.*, **24,** 45.

[55] MILLER, R. E., 1990, *Acc. Chem. Res.*, **23,** 10.

[56] LUCKHAUS, D., QUACK, M., SCHMITT, U., and SUHM, M. A., 1995, *Ber. Bunsenges. Phys. Chem.*, **99,** 457.

[57] QUACK, M., SCHMITT, U., and SUHM, M. A., 1997, *Chem. Phys. Lett.*, **269,** 29.

[58] HUISKEN, F., KALOUDIS, M., KULCKE, A., LAUSH, C., and LISY, J. M., 1995, *J. chem. Phys.*, **103,** 5366.

[59] QUACK, M., and SUHM, M. A., 1991, *Chem. Phys. Lett.*, **183,** 187.

[60] STÖCKLI, A., MEIER, B. H., KREIS, R., MEYER, R., and ERNST, R. R., 1990, *J. chem. Phys.*, **93,** 1502.

[61] QUACK, M., and TROE, J., 1998, *Encyclopedia of Computational Chemistry* (New York: Wiley) (in the press). See also QUACK, M., and TROE, J., 1981, *Theor. Chem. Adv. Pesp.*, **6B,** 199.

[62] LIMBACH, H. H., SCHERER, G., MESCHEDE, L., AGUILAR-PARRILLA, F., WEHRLE, B., BRAUN, J., HOELGER, C., BENEDICT, H., BUNTKOWSKY, G., FEHLHAMMER, W. P., ELGUERO, J., SMITH, J. A. S., and CHAUDRET, B.,1994, *AIP Conference Proceedings (298): Ultrafast Reaction Dynamics and Solvent Effects* , Part III, edited by Y. Gauduel and P. J. Rossky (American Institute of Physics), pp. 225–239.

[63] ERNST, R. R., BODENHAUSEN, G., and WOKAUN, A., 1987, 1994, *Principles of Nuclear Magnetic Resonance in One and Two Dimensions* (Oxford: Clarendon Press).

[64] DRUKKER, K., and HAMMES-SCHIFFER, S., 1997, *J. chem. Phys.*, **107,** 363.

[65] DYKE, T. R., HOWARD, B. J., and KLEMPERER, W., 1972, *J. chem. Phys.*, **56,** 2442.

[66] HUISKEN, F., TARAKANOVA, E. G., VIGASIN, A. A., and YUKHNEVICH, G. V., 1995, *Chem. Phys. Lett.*, **245,** 319.

MOLECULAR PHYSICS, 1998, VOL. 94, NO. 1, 121–125

Adiabatic electron affinities of PF_5 and SF_6: a coupled-cluster study

By GENNADY L. GUTSEV† and RODNEY J. BARTLETT
Quantum Theory Project, PO Box 118435, University of Florida, Gainesville, FL 32611, USA

Adiabatic electron affinities ($E_{ea,ad}$) of the PF_5 and SF_6 molecules, notoriously difficult for modern density-functional-based methods, are computed at the coupled-cluster method with all singles and doubles and non-iterative inclusion of triple excitations (CCSD(T)) level with rather large basis sets. Our CCSD(T) estimates of 1.02 and 0.92 eV for the $E_{ea,ad}$ of PF_5 and SF_6, respectively, are in good agreement with the corresponding experimental values of 0.75 ± 0.15 and 1.0 ± 0.1 eV. The computed vertical detachment energy of 3.13 eV of the SF_6^- anion is to be compared to the experimental value of 3.16 eV.

1. Introduction

The SF_6 molecule is a well-known electron scavenger [1] and finds a wide range of technological applications [2]. Much experimental and theoretical effort has been expended towards the evaluation of the adiabatic electron affinity ($E_{ea,ad}$) [2, 3] of the SF_6 molecule and the vertical detachment energy (E_{vd}) of the SF_6^- anion [4, 5].

The experimental $E_{ea,ad}$ of SF_6 has been measured to be 1.0 ± 0.1 eV [6–9], which is in fortuitously good agreement with the first *ab initio* estimate of 1.03 eV obtained at the self-consistent field (SCF) level with a rather small basis set [10]. Further extensions of the basis have resulted in disagreement with the experiment, since the SF_6^- anion has been found [11] to be unstable by −0.36 eV with respect to the neutral parent.

Moreover, the octahedral configuration of SF_6^- presents a transition state on the potential energy surface obtained at the SCF/6-31 + G(d) level [12], according to the results of the vibrational analysis. Other calculations performed with different bases and levels of theory [13–18] have shown a rather wide range of computed values for the $E_{ea,ad}$ of SF_6 (for comparison of different results see [19]).

Unexpectedly, the local spin density (LSD) approximation with gradient corrections [20] led to an overestimated value of 3.44 eV [16] for the $E_{ea,ad}$ of SF_6, although this approximation generally provides rather reliable estimates of molecular $E_{ea,ad}$'s [21, 22]. Such a failure has stimulated some detailed studies [19, 23] of the dependence of the computed $E_{ea,ad}$ of SF_6 with modern density-functional-theory (DFT) exchange-correlation potentials and basis sets. The $E_{ea,ad}$ of SF_6 has been found to exhibit unusually strong variations (from 6.15 to 1.38 eV) [19] depending upon the basis and exchange-correlation functionals used in calculations. The best estimates of 1.61 eV [23] and 1.38 eV [19] have been obtained without any zero point energy (ZPE) corrections whose inclusion would further increase the discrepancy with experiment.

Phosphorus pentafluoride is widely used as an intercalant and a dopant [24, 25] because of its electron-acceptor properties. The first theoretical study [27] performed with the X_α method has provided an estimate of 0.6 eV for the $E_{ea,ad}$ of PF_5, which is in nice agreement with the recently obtained experimental value of 0.75 ± 0.15 [26]. However, the LSD approach with Becke's gradient corrections [28] has provided an overestimated value (by ≈ 1 eV) of the $E_{ea,ad}$ of PF_5. In order to test if there is an improvement when using recently introduced (DFT) schemes, Tschumper *et al.* [29] have performed a series of calculations with different bases and exchange-correlation functionals incorporated into the GAUSSIAN92/DFT program system and has obtained values ranging from 0.94 to 1.66 eV.

Since the infinite-order coupled-cluster method with all singles and doubles and non-iterative inclusion of triple excitations (CCSD(T)) appears to be reliable in estimating the $E_{ea,ad}$'s of complicated systems [30, 31], it is interesting to perform an evaluation of the $E_{ea,ad}$'s of the SF_6 and PF_5 molecules at the CCSD(T) level with reasonably large basis sets.

2. Computational details

The present calculations have been performed with the ACES II suite of programs [32] at the (CCSD(T)) [33–35] and HFDFT [36–39] levels of theory. The latter differs from most Kohn–Sham self-consistent DFT calculations in that a HF density is first obtained and then inserted in a DFT functional like BLYP or B3LYP to provide an estimate of the correlation correction.

† Also at: Institute of Chemical Physics at Chernogolovka of the Russian Academy of Sciences, Chernogolovka, Moscow Region 142432, Russian Federation.

0026–8976/98 $12·00

Table 1. Geometrical parameters and total energies of SF_6 and SF_6^- along with vibrational frequencies calculated at the MBPT(2) level with a 6-311 + G(2df) set on sulphur and 6-311 + (2d) sets on fluorines[a] together with the experimental data for SF_6. Total energies (E_{tot}) are in hartrees, bond lengths are in A, vibrational frequencies are in cm^{-1}, and the zero-point energies (Z) are in kcal mol^{-1}.

Level	Species	R_e(S–F)	$2S + 1$[b]	CCSD(T) E_{tot}
CCSD(T)/6-311 + G(2df)[c]	SF_6	1.5651[d]	1.0	−996.036 302
CCSD(T)/6-311 + G(3df)		1.5651[e]	1.0	−996.396 350
CCSD(T)/6-311 + G(2df)[c]	SF_6^-	1.7167	2.004	−996.065 358
CCSD(T)/6-311 + G(3df)		1.7167[e]	2.004	−996.423 113

Mode	SF_6			SF_6^-
	This work	Experiment [43]	Experiment [45]	This work
$\omega(t_{2u})$	346	344	347	237
$\omega(t_{2g})$	519	522	524	336
$\omega(t_{1u})$	611	614	614	306
$\omega(t_g)$	655	639	643	447
$\omega(a_{1g})$	779	769	775	626
$\omega(t_{1u})$	965	940	939	722
Z	13.46	13.31	13.35	9.05

[a] Optimized bond lengths at this level are 1.5721 and 1.7164 for SF_6 and SF_6^-, respectively.
[b] For evaluation of spin see [42].
[c] With 10 frozen core MOs.
[d] Experimental R_e(S–F) = 1.564 and 1.5622(7), see [43] and [44], respectively.
[e] Optimized at the preceding level.

Several basis sets have been employed, namely, 6-311 + G(2d), 6-311 + G(2df), and 6-311 + G(3df) [40] for SF_6 and SF_6^-. For PF_5 and PF_5^- we employed combined bases: 6-311 + (2d) at fluorines and 6-311 + G(3d) at P as well as Dunning's correlation-consistent augmented PVTZ basis set at fluorines and a PVTZ basis at P [41]. These bases will be referred to as 6-311 + (2d)* and PVTZ*, correspondingly. The optimizations were carried out until the RMS gradients fall below the threshold value of 0.1×10^{-3}.

The adiabatic electron affinity ($E_{ea,ad}$) measures the energy gain due to the attachment of an additional electron and is defined as the difference in the total energies of the anion and parent ground states. Within the Born Oppenheimer approximation, one can define the $E_{ea,ad}$ as

$$E_{ea,ad} = E_{tot}(N, R_e) + Z_N - E_{tot}(A, R_e^-) - Z_A$$
$$= \Delta E_{el} + \Delta E_{nuc}, \quad (1)$$

where R_e and R_e^- denote the equilibrium geometrical configurations of the neutral molecule (N) and the anion (A), respectively. The zero-point vibrational energies (Z) can be estimated within the harmonic approximation.

The vertical detachment energy (E_{vd}) of an anion is the minimal energy required for a sudden detachment of an extra electron. It can be defined as the difference in the total energies of the anion and its parent at the equilibrium geometry of the anion

$$E_{vd} = E_{tot}(N, R_e^-) + Z_N - E_{tot}(A, R_e^-) - Z_A$$
$$= \Delta E_{el} + \Delta E_{nuc}. \quad (2)$$

Since the geometry changes due to the attachment of an additional electron are generally moderate, one can use the Z's estimated for the neutral ground states, i.e. to use the same ΔE_{nuc} as in equation (1).

3. Results and discussions

Optimizations of the SF_6 and SF_6^- bond lengths within O_h symmetry constraints have been performed at the CCSD(T)/6-311 + G(2df) level with 10 frozen core MOs on a Cray-C90. Frequencies are calculated at a lower MBPT(2) level with a 6-311 + G(2df) set on sulphur and the 6-311 + (2d) sets on fluorines. Comparison of the results of our computations with the experimental data known for the SF_6 molecule presented in table 1 shows very good agreement. As can be seen from tables 4 and 11 of [19], the bond lengths in both SF_6 and SF_6^- depend strongly on exchange-correlation functionals and basis sets used in DFT calculations and make changes up to 0.2 Å. At the highest DFT level of theory (B3 + Perdew Wang gradient corrections and a

Table 2. Adiabatic electron affinity of SF_6 calculated according to equation (1) and the vertical detachment energies (E_{vd}) of SF_6^- calculated according to equation (2) with $\Delta Z = 0.19$ eV (from table 1) at the CCSD(T)/6-311+G(2df) optimized geometry. All values are in eV.

	$E_{ea,ad}$		E_{vd}	
Level	6-311+G(2df)	6-311+G(3df)[a]	6-311+G(2df)	6-311+G(3df)
HF	−0.76	−0.97	2.91	2.84
MBPT(2)	1.02	0.98	3.04	3.17
CCSD	0.68	0.58	3.07	3.16
CCSD+T[b]	1.04	0.98	3.04	3.14
CCSD(T)	0.965	0.92	3.03	3.13
Exp.	1.0 ± 0.1[c]		3.16[d]	

[a] HFDFT results (corrected at the $\Delta Z = 0.19$) with this basis and the CCSD(T)/6-311+(2d) bond lengths are 0.92, 1.70, 2.57, and 1.94 for the X_α, LDA, BLYP, and B3LYP exchange-correlation functionals, respectively.
[b] CCSD+T means the CCSD + T(CCSD) method [34].
[c] See reference [7].
[d] See reference [5].

Table 3. Results of calculations for PF_5 and PF_5^- performed with the Dunning PVTZ* and 6-311+(2d)* basis sets. Geometries are optimized at the MBPT(2) level and the CCSD(T) total energies are computed at the MBPT(2) equilibrium geometries. Total energies (E_{tot}) are in hartrees, bond lengths are in Å, bond angles are in degrees, frequencies are in cm^{-1}, Z's are in kcal mol^{-1}, intensities (available at the MBPT(2)/PVTZ+ level only) are in km mol^{-1}.

Basis	Species	R_{ax}(P–F)	R_{eq}(P–F)	$\angle F_{ax}PF_{eq}^{\circ}$	$\langle 2S+1^b \rangle$	CCSD(T) E_{tot}
PVDZ*	PF_5	1.6185	1.5858	90.0°	1.0	−839.323 084
6-311+(2d)*	PF_5	1.5857	1.5468	90.0°	1.0	−839.837 878
Experiment[a]	PF_5	1.576	1.530	90.0°	—	—
PVDZ*	PF_5^-	1.6485	1.7081	90.60°	2.005	−839.375 105
6-311+(2d)*	PF_5^-	1.6101	1.6670	90.96°	2.000	−839.872 389

	PF_5			PF_5^-	
Mode	PVTZ*	6-311+(2d)*	Mode	PVTZ*	6-311+(2d)*
$\omega(e')$	163[0.2]	175	$\omega(b_2)$	207[0.0]	226
$\omega(e'')$	460[0.0]	507	$\omega(e)$	285[0.01]	315
$\omega(e')$	489[41]	531	$\omega(b_1)$	368[0.0]	407
$\omega(a_2'')$	526[50]	568	$\omega(e)$	435[1.3]	474
$\omega(a_1')$	657[0.0]	637	$\omega(a_1)$	478[31]	493
$\omega(a_1')$	767[0.0]	800	$\omega(b_2)$	514[0.0]	514
$\omega(a_2'')$	970[416]	949	$\omega(a_1)$	568[8]	560
$\omega(e')$	1005[270]	1011	$\omega(e)$	758[555]	746
—	—	—	$\omega(a_1)$	803[177]	808
Z	10.22	10.58		8.43	8.69

[a] See references [46–48].
[b] For evaluation of spin see [42].

specially fitted basis set consisting of 406 functions) [19], the bond lengths are close to those obtained in the present work, however, their vibrational frequencies are in rather poor agreement with experiment, e.g. the deviation attains 104 cm^{-1} for the lowest $\omega(t_{1u})$ mode.

Table 2 presents the $E_{ea,ad}$ of SF_6 and the E_{vd} of SF_6^- computed at the CCSD(T) optimized geometries. The $E_{ea,ad}$ is negative at the HF level, which reflects the importance of correlation contributions. At the CCSD(T)/6-311+G(2df) optimized geometry, the MBPT(2), CCSD(T), and CCSD(T) levels provide estimates of the $E_{ea,ad}$ and E_{vd}, which are in nice agree-

Table 4. Adiabatic electron affinity of PF_5 calculated according to equation (1) and the vertical detachment energies (E_{vd}) of PF_5^- calculated according to equation (2) with $\Delta Z = 0.08$ eV (from table 3) at the geometries and with the basis sets described in table 3. All values are in eV.

	$E_{ea,ad}$		E_{vd}	
Level	PVTZ*	6-311 + (2d)*[a]	PVTZ*	6-311 + (2d)*[a]
HF	0.93	0.46	3.34	3.55
MBPT(2)	1.43	1.00	2.99	3.21
CCSD	1.45	0.99	3.14	3.37
CCSD + T[b]	1.52	1.03	3.02	3.21
CCSD(T)	1.50	1.02	3.04	3.25
Experiment[c]	0.75± 0.15		—	

[a] HFDFT results (corrected for $\Delta Z = 0.08$) with this basis and HFDFT(BLYP)/6-311 + (2d)* bond lengths are 0.25, 1.21, 1.33, and 1.34 for X_α, LDA, BLYP, and B3LYP, respectively.

[b] CCSD + T means the CCSD + T(CCSD) method [34].

[c] See reference [26]

ment with experiment. The results of our HFDFT calculations at the CCSD(T)/6-311 + G(2df) optimized geometry are presented in a footnote of table 2. Surprisingly, the simplest X_α approach provides an $E_{ea,ad}$ matching the $E_{ea,ad}$ value obtained at the CCSD(T) level. The HFDFT(B3LYP) approach gives an $E_{ea,ad}$ almost twice as large.

Having one fluorine atom fewer, the PF_5 molecule is more difficult for computations because of the lower C_s computational symmetry. Therefore, the geometry optimizations and computations of vibrational frequencies have been performed with smaller basis sets (PVTZ* and 6-311 + (2d)*) at the MBPT(2) level of theory and the total energies have been recomputed at the CCSD(T) level. As is seen from table 3, the PVTZ* basis provides rather poor bond lengths compared to the experimental values, and the 6-311 + (2d) basis makes a significant improvement in the calculated bond lengths. A similar strong dependence of the bond lengths on basis sets in both PF_5 and PF_5^- has been observed in the HFDFT calculations as well [29]. Only the lowest vibrational frequencies are presented in [29], namely, 149 cm^{-1} for PF_5 and 177 cm^{-1} for PF_5^-. These values have to be compared to our values of 175 and 226 cm^{-1}, respectively.

A similar dependence on the basis set has been found for the $E_{ea,ad}$ of PF_5 as well [29]. As is seen from table 4, the PVTZ* value of the $E_{ea,ad}$ appears to be overestimated by more than 0.5 eV, whereas the CCSD(T)/6-311 + (2d) $E_{ea,ad}$ value is close to the upper limit of the experimental estimate of 0.75 ± 0.15 [26] A footnote to table 4 shows the results of our HFDFT/6-311 + (2d) calculations of the $E_{ea,ad}$ of PF_5. The B3LYP level provides a somewhat overestimated value for the $E_{ea,ad}$ of PF_5, however, the discrepancy with the CCSD(T) value seems to be smaller than in the case of SF_6.

4. Conclusion

The CCSD(T) approach is shown to be reliable in estimating the adiabatic electron affinity of the SF_6 molecule with reasonably large basis sets, which is a difficult case for DFT-based approaches. Our computed value of 0.92 eV is in nice agreement with the experimental value of 1.0 ± 0.1 eV. The vertical detachment energy of SF_6^- has been measured to be 3.16 eV in very good accord with our computed value of 3.13 eV.

The PF_5 molecule presents a less 'pathological' case for DFT-based approaches, which overestimate the $E_{ea,ad}$ of PF_5 to a lesser extent than in the case of SF_6. Our value of 1.02 eV obtained at the CCSD(T)/6-311 + (2d) level should be compared to the recently obtained experimental value of 0.75 ± 0.15 eV.

This work was supported by the Office of Naval Research Grant number N00014-95-1-0614 and in part by a grant of HPC time from the DoD HPC Center.

References

[1] Foltin, M., Rauth, T., and Märk, T. D., 1992, *Int. J. Mass Spectrom. Ion Proc.*, **116**, 273.

[2] Christophorou, L. G. (editor), 1984, *Electron Molecule Interactions and Their Applications* (New York: Academic Press).

[3] Compton, R. N., Reinhardt, P. W., and Cooper, C. D., 1978, *J. chem. Phys.*, **68**, 2023.

[4] Mock, R. S., and Grimsrud, E. P., 1991, *Chem. Phys. Lett.*, **184**, 99.

[5] Datkos, P. G., Carter, J. G., and Christophorou, L. G., 1995, *Chem. Phys. Lett.*, **239**, 38.

[6] Streit, G. E., 1981, *J. chem. Phys.*, **77**, 826.

[7] GRIMSRUD, E. P., CHOWDHURY, S., and KEBARLE, P., 1985, *J. chem. Phys.* **83,** 1059.
[8] CHEN, E. C. M., SHUIE, L.-R., D'SA, E. D., BATTEN, C. F., and WENTWORTH, W. E., 1988, *J. chem. Phys.*, **88,** 4711.
[9] MILLER, A. E. S., MILLER, T. M., VIGGANO, A. A., MORRIS, R. A., VAN DOREN, J. M., ARNOLD, S. T., and PAULSON, J. F., 1995, *J. chem. Phys.*, **102,** 8865.
[10] HAY, P. J., 1982, *J. chem. Phys.*, **76,** 502.
[11] KLOBUKOWSKI, M., BARANDIARÁN, Z., SEIJO, L., and HUZINAGA, S., 1987, *J. chem. Phys.*, **86,** 1637.
[12] GUTSEV, G. L., unpublished results.
[13] BORING, M., 1977, *Chem. Phys. Lett.*, **46,** 242.
[14] TANG, R., and CALLAWAY, J., 1986, *J. chem. Phys.*, **84,** 6854.
[15] MIYOSHI, E., SAKAI, Y., and MIYOSHI, S., 1988, *J. chem. Phys.*, **88,** 1470.
[16] GUTSEV, G. L., 1992, *Int. J. Mass Spectrom. Ion Proc.*, **115,** 185.
[17] RICHMAN, K. W., and BANERJEE, A., 1993, *Int. J. quantum Chem.*, **S27,** 759.
[18] CHENG, Y.-S., CHEN, Y.-J., NG, C. Y., CHIU, S.-W., and LI, W.-K., 1995, *J. Am. chem. Soc.*, **117,** 9725.
[19] KLOBUKOWSKI, M., DIERCKSEN, G. H. F., and GARCÍA DE LA VEGA, J. M., 1997, *Adv. chem. Phys.*, **28,** 189.
[20] BECKE, A. D., 1988, *J. chem. Phys.* **88,** 1053.
[21] ZIEGLER, T., and GUTSEV, G. L., 1992, *J. comput. Chem.*, **13,** 70.
[22] GILL, P. M. W., JOHNSON, B. G., POPLE, J. A., and FRISH, M. J., 1992, *Chem. Phys. Lett.*, **197,** 499.
[23] KING, R. A., GALBRAITH, J. M., and SCHAEFER III, H. F., 1996, *J. phys. Chem.*, **100,** 6061.
[24] BARTLETT, N., and MCQUILLAN, B. W., 1982, *Intercalation Chemistry* (New York: Academic Press).
[25] CHIEN, J. C. W., 1984, *Polyacetylene: Chemistry, Physics, and Material Science* (Orlando, FL: Academic Press).
[26] MILLER, T. M., MILLER, A. E. S., VIGGANO, A. A., MORRIS, R. A. PAULSON, J. F., 1994, *J. chem. Phys.*, **100,** 7200.
[27] GUTSEV, G. L., BOLDYREV, A. I., and OVCHINNIKOV, A. A., 1988, *Russ. J. phys. Chem.*, **62,** 168.
[28] GUTSEV, G. L., 1993 , *J. chem. Phys.*, **98,** 444.
[29] TSCHUMPER, G. S., FERMANN, J. T., and SCHAEFER III, H. F., 1996, *J. chem. Phys.*, **104,** 3676.
[30] GUTSEV, G. L., and BARTLETT, R. J., 1996, *J. chem. Phys.*, **105,** 8765.
[31] GUTSEV, G. L., and BARTLETT, R. J., 1997, *Chem. Phys. Lett.*, **265,** 12.
[32] ACES II is a program product of the Quantum Theory Project, University of Florida. STANTON, J. F., GAUSS, J., WATTS, J. D., NOOIJEN, M., OLIPHANT, N., PERERA, S. A., SZALAY, P. G., LAUDERDALE, W. J., GWALTNEY, S. R., BECK, S., BALKOVA, A., BERNHOLDT, D. E., BAECK, K.-K., ROZYCZKO, P., SEKINO, H., HUBER, C., and BARTLETT, R. J. Integral packages included are VMOL (ALMLÖF, J., and TAYLOR, P. R.), VPROPS (TAYLOR, P. R.), and ABACUS (HELGAKER, H. J., JENSEN, A. A., JORGENSEN, P., and TAYLOR, P. R.).
[33] PURVIS III, G. D., and BARTLETT, R. J., 1982, *J. chem. Phys.*, **76,** 1910.
[34] URBAN, M., NOGA, J., COLE, S. J., and BARTLETT, R. J., 1985, *J. chem. Phys.*, **83,** 4041.
[35] BARTLETT, R. J., WATTS, J. D., KUCHARSKI, S. A., and NOGA, J., 1990, *Chem. Phys. Lett.*, **165,** 513.
[36] CLEMENTI, E., and CHAKRAVORTY, S. J., 1990, *J. chem. Phys.*, **93,** 2591.
[37] GILL, P. M. W., JOHNSON, B. G., and POPLE, J. A., 1992, *Int. J. quantum Chem. Symp.*, **26,** 319.
[38] OLIPHANT, N., and BARTLETT, R. J., 1994, *J. chem. Phys.*, **100,** 6550.
[39] SEKINO, H., OLIPHANT, N., and BARTLETT, R. J., 1994, *J. chem. Phys.*, **101,** 7788.
[40] FRISH, M. J., POPLE, J. A., and BINKLEY, J. S., 1984, *J. chem. Phys.*, **80,** 3265.
[41] WOON, D. E., and DUNNING, T. H., JR., 1993, *J. chem. Phys.*, **98,** 1358.
[42] PURVIS III, G. D., SEKINO, H., and BARTLETT, R. J., 1988, *Col. Czech. Chem. Commun.*, **53,** 2203.
[43] HERZBERG, G., 1966, *Molecular Spectra and Molecular Structure. III. Electronic Spectra and Electronic Structure of Polyatomic Molecules* (Princeton: Van Nostrand).
[44] MILLER, B. R., and FINK, M., 1981, *J. chem. Phys.*, **75,** 5326.
[45] NAKAMOTO, N., 1986, *Infrared and raman Spectra of Inorganic and Coordination Compounds* (New York: Wiley).
[46] HANSEN, K. W., and BARTELL, L. S., 1965, *Inorg. Chem.*, **4,** 1775.
[47] SPIRIDONOV, V. P., ISCHENKO, A. A., and IVASHKEVICH, L. S., 1981, *J. molec. Struct.*, **140,** 79.
[48] KURIMURA, H., YAMAMOTO, S., EGAWA, T., and KUCHITSU, K., 1986, *J. molec. Struct.*, **140,** 79.

MOLECULAR PHYSICS, 1998, VOL. 94, NO. 1, 127–138

Characterization of shape and Auger resonances using the dilated one electron propagator method

By MANOJ K. MISHRA, MILAN N. MEDIKERI, ARUN VENKATNATHAN and S. MAHALAKSHMI

Department of Chemistry, Indian Institute of Technology, Bombay, Powai, Mumbai 400 076, India

Some representative results from applications of the second order, diagonal 2ph-TDA and quasi-particle decouplings of the biorthogonal dilated electron propagator based on a complex scaled bivariational SCF to the investigation of ^2P Mg^-, $^2B_{2g}C_2H_4^-$ shape and ^2S $(1s^{-1})$ Be^+ Auger resonances are presented. These results demonstrate the effectiveness of the dilated electron propagator in calculation of energies and widths as also in unravelling of the mechanistic details of resonance formation and decay. The Feynman–Dyson amplitudes are shown to effectively isolate the LUMO as the resonant orbital.

1. Introduction

The electron propagator theory [1, 2] has provided an effective route to the calculation of electron detachment [3–6] and attachment [7, 8] energies and is well established as a powerful tool for the correlated treatment of electronic structure [9] and dynamics [10–12]. The dilated electron propagator [13] where electronic coordinates have been scaled by a complex scaling [14–16] factor ($\eta = \alpha \exp(i\theta)$) has emerged as a convenient method for the direct calculation of energies and width of shape resonances in electron–atom [17–23] and electron–molecule scattering [24–26].

The spectral representation of the matrix-dilated electron propagator

$$G_{sr}(E) = \lim_{\varepsilon \to 0^+} \sum_s \left[\frac{\langle {}^N_o \mid a_s \mid {}^{N+1}_s \rangle \langle {}^{N+1}_s \mid a_r^\dagger \mid {}^{N+1}_o \rangle}{E - (E_s^{N+1} - E_o^N) + i\varepsilon} + \frac{\langle {}^N_o \mid a_r^\dagger \mid {}^{N-1}_s \rangle \langle {}^{N-1}_s \mid a_s \mid {}^N_o \rangle}{E - (E_o^N - E_s^{N-1}) + i\varepsilon} \right] \quad (1)$$

provides for the simultaneous calculation of both the energy (real part) and width (twice the imaginary part) of electron detachment Auger $(E_0^N - E_n^{N-1})$ and electron attachment shape resonances $(E_n^{N+1} - E_0^N)$ from its appropriate poles. The pole structure of the dilated electron propagator has been discussed in detail elsewhere [17, 18, 27] but it is obvious from (1) that since resonant eigenvalues $(E_r - i\Gamma/2)$ have a negative imaginary part to account for their finite lifetime [28, 29] and the target ground state energy E_0^N is completely real, the poles corresponding to the Auger resonances will have a positive imaginary part and their trajectory as a function of variations in the scaling parameter α or θ will move in the first quadrant of the complex energy plane. The complex poles in the first quadrant displaying quasi-stability with respect to variations in η have therefore been associated with Auger resonances [27, 30, 31]. The quasi-stable complex poles in the fourth quadrant of the complex energy plane are similarly associated with electron attachment $(E_S^{N+1} - E_0^N)$ shape resonances.

The metastable nature of resonances affords considerable interaction between the target and the decaying electron and reliable treatment of resonances calls for the incorporation of higher order or renormalized decouplings in the construction of the dilated electron propagator. Considerable experience with the real propagator calculations has shown that the diagonal and full 2ph-TDA decouplings being infinite order renormalized summation of the most important ring and ladder diagrams, offer enhanced level of correlation in the treatment of ionization energies and electron affinities [3, 5, 6] and the diagonal 2ph-TDA has been routinely utilized as an economic means to improve upon the second order decoupling.

To attend to all these concerns and afford greater correlation with effective economy in the treatment of resonances, we have recently grafted the diagonal 2ph-TDA [23, 32] , second order and quasi-particle decouplings [33] on the dilated electron propagator technique as well. The results of our methodological developments and their applications to atomic and molecular shape and Auger resonances have been reviewed in detail recently [34]. It is our purpose in this paper to offer a brief summary of the method and some illustrative results which demonstrate its effectiveness.

0026–8976/98 $12·00

The rest of the paper is organized as follows. In the following section we collect the main equations. Section 3 presents some demonstrative results from our calculations on ^{2}P Mg$^-$, $^2B_{2g}C_2H_4^-$ and ^{2}S ($1s^{-1}$) Be$^+$ Auger resonances. A brief assessment of the strengths and shortcomings of the present level of development in this area concludes this paper.

2. Method

The Dyson equation for the bi-orthogonal matrix electron propagator $\mathbf{G}(\eta, E)$ may be expressed as [19]

$$\mathbf{G}^{-1}(\eta, E) = \mathbf{G}_0^{-1}(\eta, E) - \mathbf{\Sigma}(\eta, E), \tag{2}$$

where $\mathbf{G}_0(\eta, E)$ is the zeroth order propagator for the uncorrelated electron motion, here chosen as given by the bi-variational self-consistent field (SCF) approximation [35–39]. The self energy $\mathbf{\Sigma}(\eta, E)$ matrix contains the relaxation and correlation effects.

Solution of the bi-variational SCF equations for the N-electron ground state yields a set of occupied and unoccupied spin orbitals. In terms of these spin orbitals the matrix elements of $\mathbf{G}_0^{-1}(\eta, E)$ are

$$(\mathbf{G}_0^{-1}(\eta, E))_{ij} = (E - \varepsilon_i)\delta_{ij}, \tag{3}$$

where ε_i is the orbital energy corresponding to spin orbital i. Through the second order of electron interaction, the elements of the self-energy matrix are

$$\Sigma_{ij}^2(\eta, E) = \frac{1}{2}\sum_{k,\ell,m} N_{k\ell m}\frac{\langle ik \parallel \ell m\rangle\langle \ell m \parallel jk\rangle}{(E + \varepsilon_k - \varepsilon_\ell - \varepsilon_m)}, \tag{4}$$

where

$$N_{k\ell m} = \langle n_k\rangle - \langle n_k\rangle\langle n_\ell\rangle - \langle n_k\rangle\langle n_m\rangle + \langle n_\ell\rangle\langle n_m\rangle \tag{5}$$

with $\langle n_k\rangle$ being the occupation number for the kth spin orbital and the antisymmetric two-electron integral

$$\langle ij \parallel kl\rangle = \eta^{-1}\int \psi_i(1)\psi_j(2)\,[(1 - P_{12})/r_{12}] \times \psi_k(1)\psi_l(2)\,\mathrm{d}x_1\,\mathrm{d}x_2. \tag{6}$$

The lack of complex conjugation stems from the bi-orthogonal set of orbitals resulting from bi-variational SCF being complex conjugate of each other [35]. For the diagonal 2ph-TDA [3, 5, 6] decoupling of the dilated electron propagator [23]

$$\Sigma_{ij}^{2\mathrm{ph-TDA}}(\eta, E) = \frac{1}{2}\sum_{k,\ell,m} N_{k\ell m}\frac{\langle ik \parallel \ell m\rangle\langle \ell m \parallel jk\rangle}{(E + \varepsilon_k - \varepsilon_\ell - \varepsilon_m) - \Delta}, \tag{7}$$

where

$$\Delta = \tfrac{1}{2}\langle m\ell \parallel m\ell\rangle(1 - \langle n_m\rangle - \langle n_\ell\rangle) - \langle km \parallel km\rangle(\langle n_k\rangle - \langle n_m\rangle) - \langle k\ell \parallel k\ell\rangle(\langle n_k\rangle - \langle n_\ell\rangle). \tag{8}$$

The usual dilated electron propagator calculations proceed by iterative diagonalization of

$$\mathbf{L}(\eta, \mathbf{E}) = \varepsilon + \mathbf{\Sigma}(\eta, E) \tag{9}$$

where ε is the diagonal matrix of orbital energies and $\mathbf{\Sigma}$ is the self energy matrix. The propagator pole $\mathcal{E}$ is obtained by repeated diagonalizations such that one of the eigenvalues $\{\mathcal{E}_n(\eta, E)\}$ of $\mathbf{L}(\eta, \mathbf{E})$ fulfils the condition $\mathbf{E} = \mathcal{E}_n(\eta, E)$ [18]. The quasi-particle approximation for dilated electron propagator results from a diagonal approximation to the self-energy matrix $\mathbf{\Sigma}(\eta, E)$ with poles of the dilated electron propagator given by

$$E(\eta) = \varepsilon_i + \Sigma_{ii}(\eta, E) \tag{10}$$

which are determined iteratively beginning with $E = \varepsilon_i$ and Σ_{ii} may correspond to any perturbative (Σ^2) or renormalized decoupling like $\Sigma^{2\mathrm{ph\ TDA}}$.

3. Results and discussion

We have applied the different decouplings of the dilated electron propagator in the investigation of ^{2}P Be$^-$, ^{2}P Mg$^-$, ^{2}P Ca$^-$, $^2\Pi$ CO$^-$, $^2\Pi_g N_2^-$, $^2B_{2g}C_2H_4^-$ and ^{2}S ($1s^{-1}$) Be$^+$ Auger resonances. The findings from our applications to these atomic and molecular resonances have been presented in detail elsewhere [34]. The results from e-Mg ^{2}P, e-C_2H_4 $^2B_{2g}$ shape and ($1s^{-1}$) Be$^+$ Auger have offered some new insights about the strengths and weaknesses of our methods for the treatment of resonances and are briefly summarized in the following subsections.

3.1. *e-Mg ^{2}P shape resonance*

While the ^{2}P Be$^-$ shape resonance has served as the most popular test case [18 20, 30, 36], due to the toxic nature of Be, there are no experimental results for this system. The ^{2}P shape resonance in e-Mg scattering is well characterized [40] and the extensive literature on this resonance utilizing many different theoretical techniques [22, 41–45] makes it an excellent arbiter of the efficacy of different theoretical techniques for the treatment of resonances.

The resonant θ trajectories from different decouplings for the e-Mg ^{2}P shape resonance are plotted in figures 1 and 2. Though the complex scaling theorems prescribe total invariance to further changes in the complex scaling parameter, once the resonance has been uncovered, in finite basis set calculations only a quasi-stability is observed. The real part of the pole at the point of quasi-stability is associated with the resonance energy and the imaginary part with the half width ($\Gamma/2$) The results obtained for e-Mg scattering are presented in table 1. While the calculated values for the energy and the width are in excellent agreement with the experimental results, the real merit of our work stems from

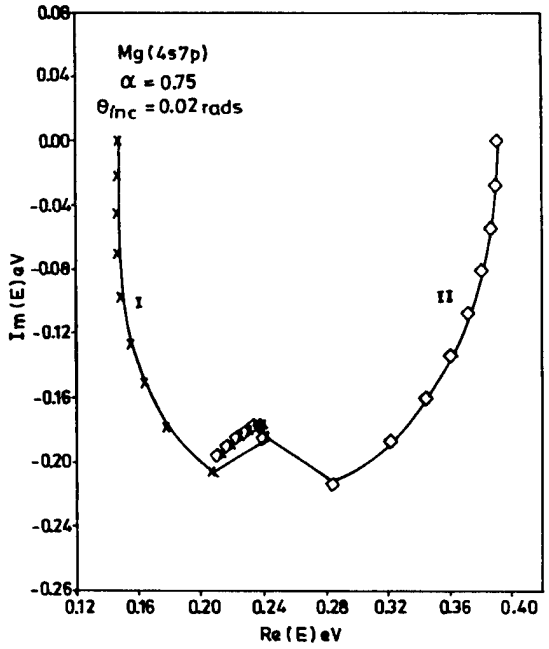

Figure 1. Theta trajectories for the e-Mg ^{2}P shape resonance from the second order (Σ^2) decoupling of the dilated electron propagator, using 4s,7p basis set.

Table 1. Energy and width of the ^{2}P shape resonances in e-Mg scattering.

Method/Reference	Energy/eV	Width/eV
Experiment [40]	0.15	0.13
Static exchange phase shift [42]	0.46	1.37
Static exchange plus polarizability [42] phase shift	0.16	0.24
Static exchange phase shift [43]	0.46	1.53
Static exchange plus polarizability [43] phase shift	0.14	0.24
Static exchange cross section [43]	0.91	2.30
Static exchange plus polarizability [43] cross-section	0.19	0.30
CI [44]	0.20	0.23
S-matrix pole (X_α) [46, 47]	0.08	0.17
Complex ΔSCF [48]	0.51	0.54
Dilated electron propagator based on real SCF [22]	0.14	0.13
Second order bi-orthogonal dilated electron propagator [33]	0.15	0.13
Diagonal 2ph-TDA bi-orthogonal dilated electron propagator [33]	0.15	0.13

the light it sheds on the parallelisms [22, 48–51] between the complex scaling and the stabilization method [50, 52, 53] for the treatment of resonances. A notable feature of the stabilization method is that at the point of optimal stabilization of the resonant root there is an avoided crossing with another nearly degenerate root which descends from above and replaces the stabilized root when further changes in the stabilization parameter (number of configurations as in [19] or scale parameter α as in [40, 44, 45, 48, 49, 54]) are effected.

The details of the stabilization method, especially, the superseding of a previously resonant root by a non-reso-

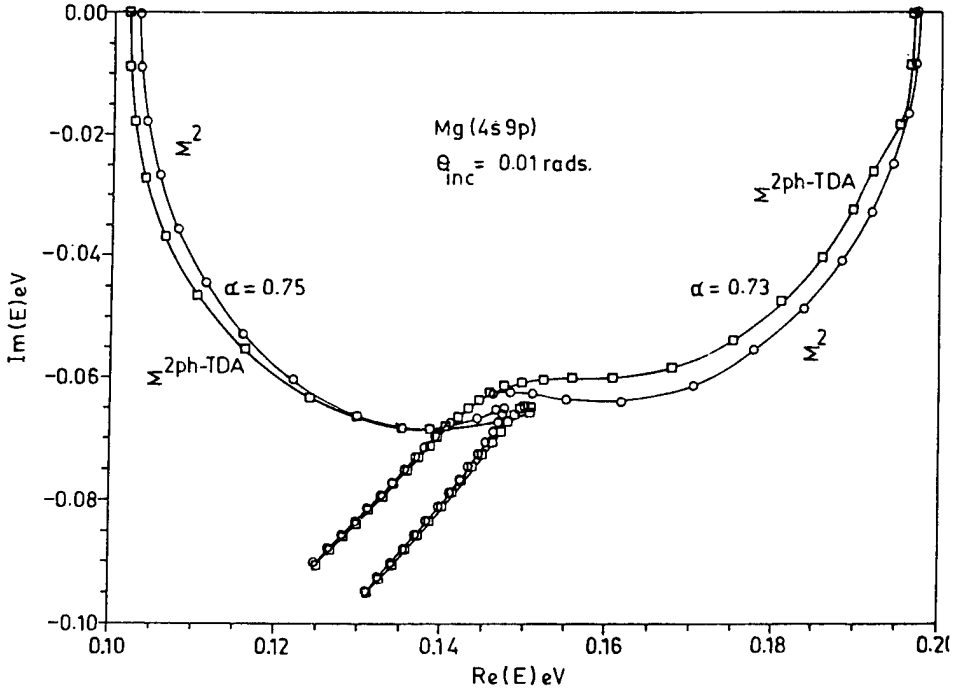

Figure 2. Theta trajectories for the e-Mg ^{2}P shape resonance from the second order (Σ^2) and diagonal 2ph-TDA ($\Sigma^{2ph-TDA}$) decouplings of the dilated electron propagator, using 4s,9p basis set.

nant root may be likened to the behaviour of rotated scattering roots neighbouring a resonance in the complex E plane. If through enough rotation, a scattering root passes by the resonance, it will uncover the neighbouring resonance and lose its previous scattering character. Our trajectories from figures 1 and 2 demonstrate this feature. It is worthwhile to note that the roots portrayed in figures 1 and 2 approach the same resonance from the opposite directions and that root II starts out as a typical scattering root. The pair of roots depicted in figure 1 have entirely different orbital genealogy initially and are described by a different linear combination of the SCF orbitals. This feature persists until the root II of figure 1, for example, has been rotated through $\theta = 0{\cdot}16$ rad at which stage this root changes to one portrayed by root I. Thereafter the two are identical. The presence of more than one resonant root is a basic feature of all bi-orthogonal dilated electron propagator calculations for e-Mg pa scattering with different basis sets [27, 33]. All of these roots show substantial contributions from more than one orbital (even for $\theta = 0{\cdot}0$ rad). This is understandable, since if the resonance is to be described as a wave packet localized by the polarization and centrifugal potentials induced in the target, the packet is made up of not just one wave but from all those with energies falling within the width of the so-called packet centre [50, 55]. As such, orbital bases of the kind employed here with nearly degenerate orbital energies in close proximity to the resonance energy will give rise to different roots describing different parts of the wave packet whose width is determined by the width of the widest root. Normal scattering roots *à la* complex scaling will emerge only when the poles of G are sought outside this energy region. The optimal results from different bases for the e-Mg ^{2}P shape resonances are in excellent agreement with the experimental results for the ^{2}P shape resonance in e-Mg scattering, which along with the results from other calculations are collected in table 1.

Due to the non-hermiticity of the complex scaled Hamiltonian, there is no orthonormality among the orbitals themselves, but there exists a bi-orthonormality $\int(\psi_i^*(r,\theta,\phi))^*\psi_j(r,\theta,\phi)\,d\tau = \delta_{ij}$ between the orbitals and their complex conjugate obtained from the bi-variational SCF procedure [37, 39, 49] and a plot of $4\pi r^2|\psi^2(r)|$ furnishes an appropriate measure of the magnitude of the radial charge density at distance r from the nucleus. For ease of differentiation between the radial charge density plots from the zeroth (bi-variational SCF orbital) and higher order (second order/diagonal 2ph-TDA) Feynman–Dyson (FD) amplitudes, even though only the radial part of ψ (orbital) or χ (FD amplitude) is plotted, we retain the symbol for the full orbital/FD amplitude.The factors affecting the formation and decay of shape resonances are examined by plotting the radial charge density [56] using the Feynman–Dyson Amplitudes (FDAs) corresponding to the resonant poles identified earlier [19, 20, 23, 27, 33] in figures 3–5.

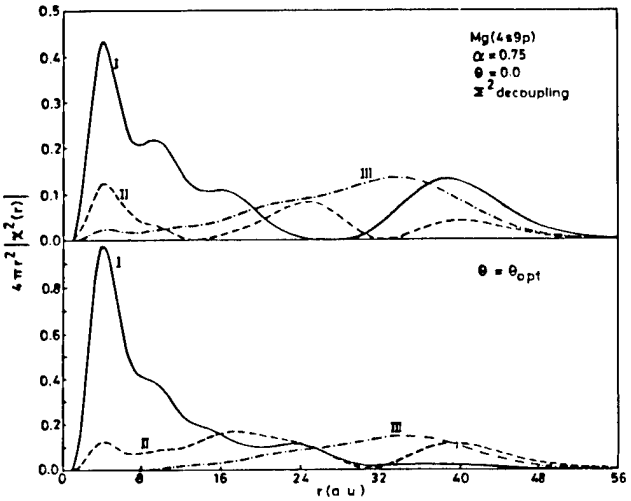

Figure 3. Radial charge density plot for the resonant FD amplitude in e-Mg scattering. For α = 0.75 considered here, only the root labelled I is resonant. The role of optimal theta (θ_{opt} = 0.12 rad) in accumulation of electron density near the nucleus is evident.

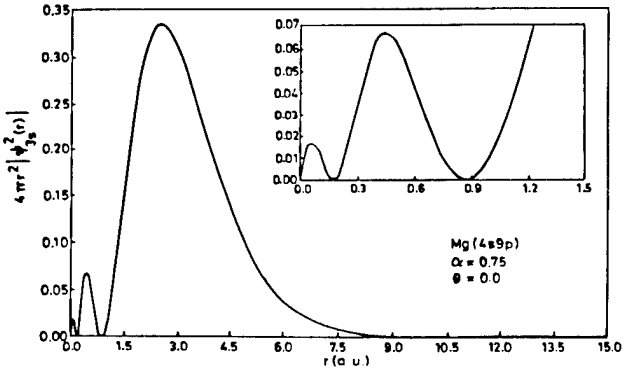

Figure 4. Radial charge density plot for the 3s orbital in Mg. The r_{max} is at 2·55 au.

The maximum in the radial charge density (r_{max}) for the outermost valence orbital for each target atom is taken as a rough guide for the radial extent of that atom and the extent of penetration of the impinging electron may be established by determining the r_{max} for the electron density plot from the corresponding resonant FDA. To account for any effect of the deviation of α_{opt} from 1.0 on the localization of the impinging electron, the valence orbital for Mg is also plotted at the same α_{opt} value as that for which the pole corresponding to the *resonant* orbital/FD amplitude shows the requisite quasi-stability [20, 23, 27, 33, 57]. The number of

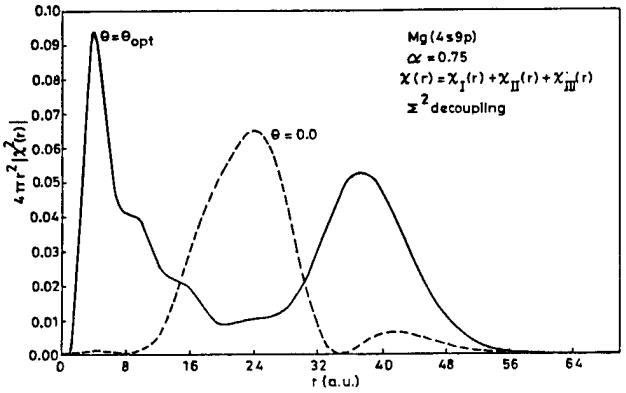

Figure 5. A plot of the charge density obtained from a linear combination of all the resonant amplitudes in e-Mg scattering with $\chi(r) = \chi_I(r) + \chi_{II}(r) + \chi_{III}(r)$, where the individual amplitudes are considered to describe different parts of the same resonant wave packet. The nodal pattern for $\theta = 0.0$ favours its identification as the lowest 3p-type unoccupied orbital of Mg. The role of optimal theta ($\theta_{opt} = 0.12$ rad) in shifting the electron density near the nucleus is clearly seen.

nodes in the radial charge density plots for the resonant FD amplitudes reveal the principal quantum number of the p-type target orbital/FD amplitude involved in the resonance formation. The difference between the radial charge densities from the uncorrelated zeroth order orbital and the correlated (second order/diagonal 2ph-TDA) FD amplitude(s) may be used to investigate the effect of correlation/relaxation in the formation and decay of shape resonances. Similarly, the role of the complex scaling parameter may be investigated by examining the difference between radial charge densities from orbital/FD amplitudes calculated for $\theta = 0{\cdot}0$ and $\theta = \theta_{opt}$. The results for the magnesium atomic system investigated in this fashion are discussed below.

For the ^2P shape resonance in e-Mg scattering, no orbital energy has the requisite theta trajectory to classify it as a resonant orbital [57] and even at the level of second order and diagonal 2ph-TDA decouplings, there are three different roots which fall within the width of this resonance [33, 57] becoming resonant for different values of the radial scale factor α. The corresponding FDAs have large mixing components from different orbitals. All these features have been taken to indicate that the three roots describe various parts of the same resonant wave packet [57]. The root which becomes resonant at $\alpha = 0{\cdot}75$ (root I) is seen to have a large charge density near the nucleus in figure 3, where the role of the optimal θ in enhancing the charge density near the nucleus is clearly seen. The charge densities from other resonant roots peak far away from the nucleus providing a mechanism for decay, i.e. the three roots seem to act in tandem to achieve metastability. None of the roots has a nodal pattern in the charge density plot which has any semblance with that expected for a conventional p-type orbital and buttresses an earlier conjecture about a lack of single orbital picture for this resonance [57]. In view of the competing demands in the formation and decay of metastable resonances, root I may be taken to provide for formation and the other two roots for the decay of the shape resonance. A comparison of figures 3 and 4 once again establishes that the charge density distribution does permit the captured electron to be localized close to the r_{max} for the valence 3s orbital.

The basis set employed here is the (4s9p) Mg basis used earlier for calculation of ^2P shape resonance energy and width by Donnelly and Simons [18] and Mishra *et al.* [57]. Among many basis sets used in these investigations, we have selected the results from the (4s9p) basis since this gives resonance energy and width in almost complete agreement with the experimental results [40].

Since all the three resonant roots fall within the width of the same resonance, in figure 5 we display a plot of charge density from the linear combination $\chi(r) = \chi_I(r) + \chi_{II}(r) + \chi_{III}(r)$ where the subscripts label the resonant roots identified in figure 3. Surprisingly, for $\theta = 0{\cdot}0$, the resultant radial charge density plot is indeed characteristic of a 3p type orbital (the lowest p-type orbital)! The accumulation of charge density near the nucleus, as also shown at large r values for θ_{opt} in figure 5, indicates large correlation and relaxation effects in the formation and decay of this shape resonance. This also elucidates the critical role of the complex scale parameter in catering to the inherently contradictory demands of metastability, requiring a route for both the formation and decay of these resonances.

3.2. *e-C_2H_4 $^2B_{2g}$ shape resonance*

The HOMO–LUMO based reactivity theories are at the heart of mechanistic pictures in organic chemistry [58] and the simplest prototypical representative with well established pictures of HOMO and LUMO is the ethylene molecule for which Hückel theory calculations are routine in characterizing its frontier orbitals. While qualitative correlations abound [59, 60], a rigorous quantitative investigation of this simple prototypical polyatomic molecule is specially significant [61, 62] and results from our own calculations are discussed below.

The resonant θ-trajectories from different decouplings are plotted in figure 6. The energy and the width for this resonance from different decouplings and those obtained by experiment and other methods are collected in table 2. That there is a cross-systemic validity to our explanations is made clear by figure 6 where just like in the case of N_2 and CO [34], the decouplings devoid of

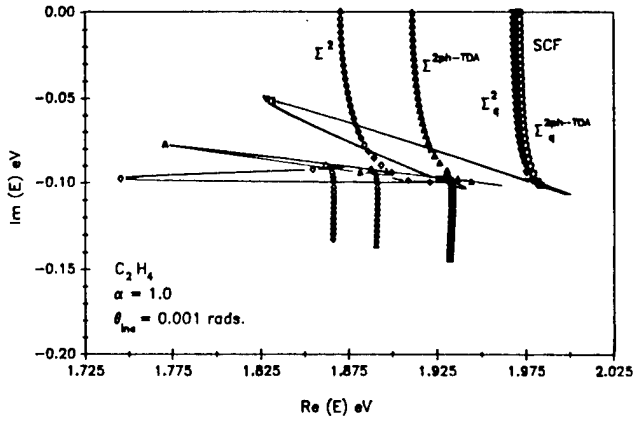

Figure 6. Resonant trajectories from different decouplings for C_2H_4. The lowering of LUMO energy by the decouplings incorporating orbital relaxation (Σ^2 *and* $\Sigma^{2ph\text{-}TDA}$) is seen for this system as well.

Table 2. Energy and width of the $^2B_{2g}$ $C_2H_4^-$ shape resonance.

Method/Reference	Energy/eV	Width/eV
Experiment [58]	1.78	0.70
Complex Kohn [63]	1.84	0.46
Second order dilated electron propagator (real SCF) [26]	1.71	0.08
Zeroth order, quasi-particle second order and quasi-particle diagonal 2ph-TDA bi-orthogonal dilated electron propagator [61]	1.93	0.19
Second order bi-orthogonal dilated electron propagator [61]	1.86	0.18
Diagonal 2ph-TDA bi-orthogonal dilated electron propagator [61]	1.89	0.18

orbital relaxation ($\Sigma^0, \Sigma_q^2, \Sigma_q^{2ph\text{-}TDA}$) clump together and maximum lowering of the HOMO–LUMO gap is offered by the second order self energy approximation. The resonance energy from different decouplings is quite reasonable but the calculated widths are much narrower.

While both HOMO and LUMO are well defined in approximate parametric SCF theories like the Hückel and the extended Hückel methods, in the *ab initio* SCF method used routinely now, only the occupied orbitals are invariant and well defined. The orbital energies and amplitudes for all the unoccupied orbitals are arbitrarily dependent on the underlying basis and with basis-set saturation, the LUMO orbital energy may be brought arbitrarily close to zero. The concept of LUMO in reactivity theories is thus made deficient in rigour and an additional mechanism for an unequivocal identification of the LUMO becomes necessary. Extensive success in the analysis of molecular shape resonance data through a qualitative correlation between the *resonant* orbital in which the impinging electron is temporarily trapped [59, 60] and the LUMO of the target molecule leaves little doubt that such an association is well founded. This intuitive notion may be investigated through identification and portrayal of the resonant orbital by using the FDAs as correlated orbitals as done earlier for Mg. The resonant poles for C_2H_4 have already been identified in figure 6.

The resonant FDAs for C_2H_4 are plotted in figure 7. The FDA from the Σ^2 decoupling on the real line has been plotted in figure 7 (*a*). This displays the familiar nodal pattern of the π^* LUMO of the ethylene molecule. Those from the Σ^0, and $\Sigma^{2ph\text{-}TDA}$ have identical features and we explore the role of correlation by plotting the difference between resonant FDAs from the Σ^2 and Σ^0 decouplings in figure 7 (*b*). In the case of C_2H_4 the reduction of antibonding nature of the π^* LUMO through depletion of small amounts of probability amplitude away from the C–H σ bond region and its accumulation near the C–C bond seems to be the major contribution from the correlated decouplings.

That the major role perhaps is that of relaxation is indicated by figure 7 (*c*) where the real part of the resonant FDA from the Σ^2 decoupling for $\theta = \theta_{opt}$ has been plotted. The most striking feature is that the optimal value of the complex scaling parameter has turned it into a diffuse anionic orbital preparing it for the metastable electron attachment.

Differences in the description of the $^2B_{2g}$ $C_2H_4^-$ shape resonance by the Σ^2 and the Σ^0 decouplings may be probed by plotting the difference between the values of the resonant FDAs from these decouplings. These results show that the major effect of correlation and relaxation incorporated by the Σ^2 and $\Sigma^{2ph\text{-}TDA}$ decouplings is through greater diffusion of both the real and imaginary parts of the resonant amplitude. Although the imaginary part of the resonant FDA is two orders of magnitude smaller than the real part and is not depicted here, it is responsible for accumulation of electron amplitude in the internuclear region. The complex scaling and correlation effects again seem to act in tandem to turn an antibonding LUMO for $\theta = 0.0$ into a diffuse anionic orbital for $\theta = \theta_{opt}$.

3.3. ^2S *Auger resonance*

As discussed earlier, the spectral representation of the matrix dilated electron propagator provides for the simultaneous calculation of the energy (real part) and the width (twice the imaginary part) of electron detachment Auger ($E_0^N - E_s^{N-1}(\eta)$) resonances as well. For Auger resonances, since resonant eigenvalues ($E_r - i\Gamma/2$) have a negative imaginary part to account for their finite lifetime [28, 64, 65] and the target ground

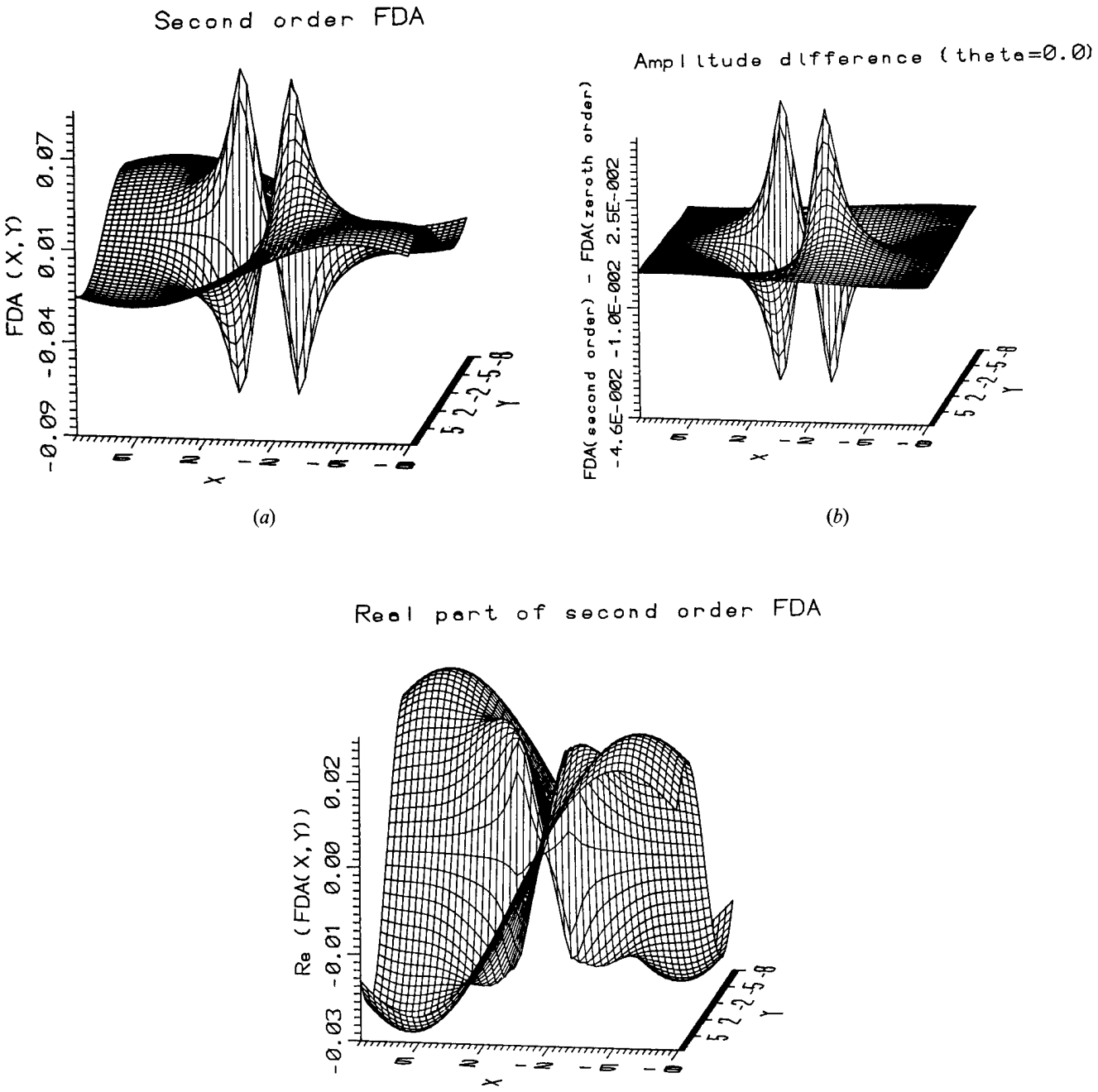

Figure 7. (*a*) Resonant FDA from the Σ^2 decoupling for the C_2H_4 molecule on the real line ($\theta = 0.0$). (*b*) Difference between the resonant FDAs from the Σ^2 and the Σ^0 decouplings for C_2H_4 on the real line. The real part of the diffuse resonant FDA at $\theta = \theta_{opt}$ is plotted in (*c*).

state energy E_0^N is completely real, the poles will have a positive imaginary part and their trajectory as a function of variations in the scaling parameter α or θ will move in the first quadrant of the complex energy plane and the complex poles in the first quadrant displaying quasi-stability with respect to variations in η may be associated with Auger resonances [27, 30]. Application of the second order, diagonal 2ph-TDA and quasi-particle decouplings to the treatment of electron detachment ($1s^{-1}$) Auger resonance in Be^+ therefore offers a complementary test for the comparative effectiveness of these decouplings of the dilated electron propagator.

Results from our calculations [31] using various decouplings of the dilated electron propagator discussed

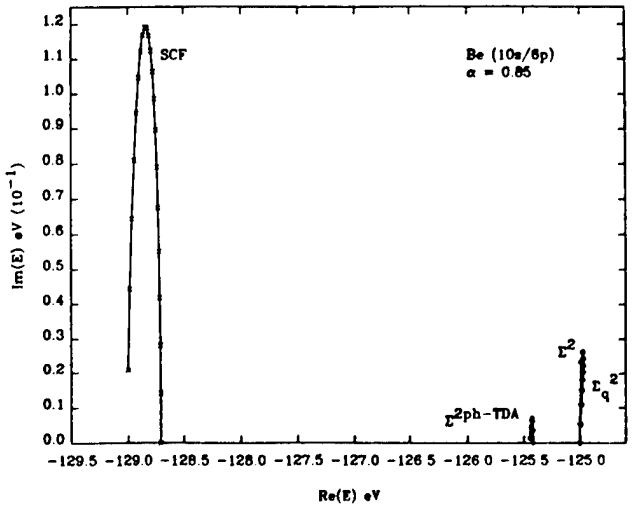

Figure 8. Theta trajectories for the Be^+ ($1s^{-1}$) Auger pole from the zeroth (bi-variational SCF), second order (Σ^2), quasi-particle second order (Σ_q^2), diagonal 2ph-TDA ($\Sigma^{2ph-TDA}$) and quasi-particle diagonal 2ph-TDA ($\Sigma_q^{2ph-TDA}$) decouplings of the dilated electron propagator. The disparity between the theta trajectories for the SCF and propagator poles makes apparent the magnitude of correlation and relaxation effects attending the Auger resonance formation.

Table 3. Energy and width of the Be^+ ($1s^{-1}$) ^2S Auger resonance.

Method/Reference	Energy/eV	Width/eV
Experiment [66, 67]	123.63	—
Many body perturbation theory [68]	—	0.09
Electron propagator with siegert boundary condition [27]	125.47	0.02
Second order dilated electron propagator [30]	124.98	0.05
quasi-particle second order dilated electron propagator [31]	124.98	0.05
Diagonal 2ph-TDA dilated electron propagator [31]	125.43	0.02
quasi-particle diagonal 2ph-TDA dilated electron propagator [31]	127.90	0.54
Zeroth order dilated electron propagator [31]	128.80	0.24

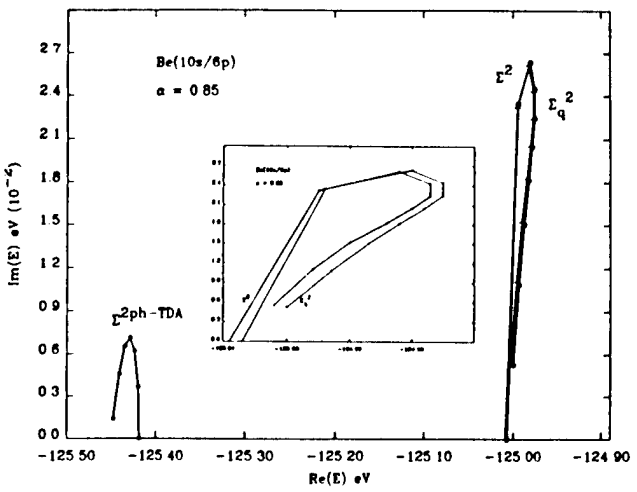

Figure 9. Same as figure 8 but without the zeroth order decoupling. The diagonal 2ph-TDA results predict higher energy and smaller width for the Auger resonance. A magnified version of the second order (Σ^2), and the quasi-particle second order (Σ_q^2) trajectories is displayed in the inset.

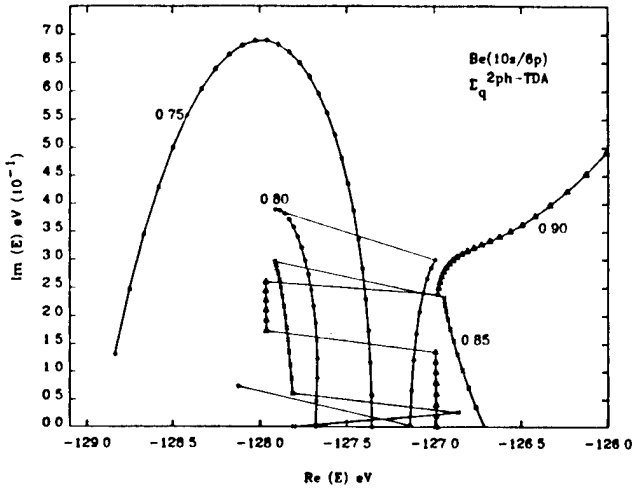

Figure 10. θ trajectories for different values of α for the quasi-particle diagonal 2ph-TDA ($\Sigma_q^{2ph\ TDA}$) decoupling. Because of multiple points of quasi-stability for many trajectories, the quasi-stable value of the resonant pole is elicited from the corresponding α trajectory in figure 11.

earlier are portrayed in figures 8 and 9. The marked disparity between the theta trajectories for the uncorrelated SCF and propagator poles makes apparent the magnitude of correlation and relaxation effects attending the Auger resonance formation. From figure 9 it is seen that the diagonal 2ph-TDA approximation predicts higher energy and smaller width (longer lifetime) for the Be^+ ($1s^{-1}$) ^2S Auger resonance. The choice of basis set and the optimal α value (0.85) are those from an earlier study [27]. The theta trajectories for the quasi-particle diagonal 2ph-TDA for this optimal alpha shows multiple inflection points and cusps and therefore theta trajectories for other nearby alpha values have also been plotted in figure 10.

Because of multiple regions of quasi-stability in many of these trajectories, the quasi-stable value of the Auger pole for this decoupling has been elicited from the alpha trajectory for $\theta = 0{\cdot}17$ rad, the angle for which there is a clear stability in the only regular trajectory ($\alpha = 0{\cdot}75$) from this decoupling. The theta trajectories for other α values also display some stability for $\theta_{opt} = 0{\cdot}17$ rad in

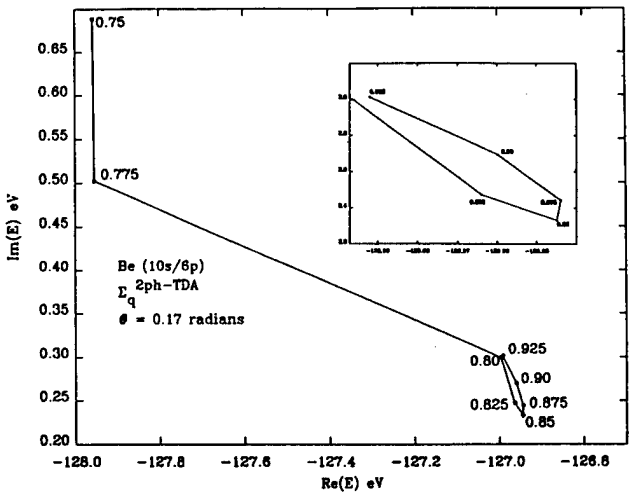

Figure 11. α trajectory for $\theta = 0{\cdot}17$ rad for the quasi-particle diagonal 2ph-TDA ($\Sigma_q^{2ph-TDA}$) decoupling. The distances narrow as $\alpha = 0.85$ is approached and then increase again. The quasi-stable value of the pole at this alpha value is therefore taken to be the best estimate of the energy and width of the Auger resonance from this decoupling.

the sense of more rapid decrease in ΔE as a function of the same uniform $\Delta\theta$ stepsize (i.e. numerical stability at least to first order). This alpha trajectory for the quasi-particle 2ph-TDA decoupling is displayed in figure 11 where the distances narrow as we approach $\alpha = 0.85$ and then increase again. This quasi-stable value in the alpha trajectory has been taken as the best estimate of the resonant Auger pole from this decoupling [31]. The values for the energies and widths of the Be^+ $(1s^{-1})$ ^2S Auger resonance from these calculations along with experimental and other theoretical results are collected in table 3.

It is clear from figures 8–11 and table 3 that results from both the the diagonal 2ph-TDA and quasi-particle diagonal 2ph-TDA seem to move away from the second order results towards those from the uncorrelated zeroth order bi-variational SCF calculations. Instead of being an improvement on the second order results, they deviate even more from the experimental [66, 67] and other more reliable theoretical calculations [69]. This behaviour of the diagonal 2ph-TDA where they offer little or no improvement on the second order results has also been observed in our molecular shape resonance calculations [23, 29, 33, 61]. The Auger decay is a correlated event and its description at the SCF level is not meaningful, and the energy and widths from bi-variational SCF are included only to assist in assessing the role of correlation and relaxation in the characterization of the Auger resonance, as well as to highlight the relatively poor quality of diagonal and quasi-particle diagonal 2ph-TDA results for this case.

The diagonal 2ph-TDA is an appealing approximation for reasons mentioned earlier and discussed in much greater detail elsewhere [5, 6]. However, it is also well known that though it is consistent up to second order, it is incomplete in third and higher orders. This has led to a somewhat mixed result where the diagonal 2ph-TDA does not always offer an improvement over second order results. The imbalance is compounded by the use of an uncorrelated reference state since many important third and higher order diagrams which should have been non-zero become zero in such calculations [3]. This imbalance has been noted by von Niessen *et al.* [6] and Öhrn and Born [5] have reviewed this with many numerical examples. A similar imbalance in the diagonal 2ph-TDA approximation even in the case of dilated electron propagator calculations is also seen and therefore care must be exercised in its use. This imbalance in the diagonal 2ph-TDA approximation seems to be aggravated by the quasi-particle approximation to this decoupling. The problem with quasi-particle diagonal 2ph-TDA could be again due to the inconsistent way in which non-diagonal diagrams which contribute to both the initial (2p-h term) and final (2h-p term) state correlations are excluded. This seems to lead, in this case, to a requirement of large rotation pushing the resonant pole higher into the complex energy plane thereby increasing its width in this approximation. The ADC(3) type consistent extended 2ph-TDA decouplings offer obvious advantages but are much more computationally demanding.

4. Concluding remarks

Our basic purpose in this brief review is to summarize some representative results from our attempts to harness the electron propagator theory for the investigation of electron-scattering and Auger resonances. The bi-orthogonal approach to the construction of the dilated electron propagator does lead to the same formulae as in the case of the unscaled real propagator and all the approximations from the real electron propagator formalism may be implemented using the formal and computational strategies adopted earlier [5, 6, 70, 71]. The use of a bi-variational SCF permits easy apportioning of relaxation and correlation contributions in the formation of shape resonances. Relaxation effects seem to be the most important in the formation and decay of atomic shape resonances, since there is no resonant root for Mg at the bi-variational SCF level and the values obtained for Be and Ca from the zeroth order approximation (bi-variational SCF) are much larger than that from second order and diagonal 2ph-TDA self energy approximations [34] .

The use of a complex scaled electron propagator for the treatment of molecular resonances [24–26] has shown extreme sensitivity to even minor variations in the scaling parameter, making the search for the resonant root much more demanding. We have speculated earlier [14, 15, 72, 73] that this may be due to the second order self energy approximation being employed in the investigation [24–26]. Later results, however, show that not much improvement may be had by employing the somewhat more demanding diagonal 2ph-TDA approximation. Molecular shape resonances are critically dependent on orbital mixing and quasi-particle approximations offer little improvement to the description obtained at the level of the bi-variational SCF itself. Maximum lowering of the HOMO–LUMO gap through the lowering of the antibonding nature of the LUMO is offered by the second order decoupling and the more demanding diagonal 2ph-TDA decoupling does not seem to be worth the extra effort involved in the computation of the denominator shift Δ in equation (7). Also, clear isolation of a single virtual orbital of the p/π-type from the whole manifold of all unoccupied orbitals, both for the ^{2}P e-Mg and the $^2B_{2g}$ e-C_2H_4 scattering shape resonances lends credence to the unoccupied orbital based mechanistic picture of shape resonances [52, 59, 60].

The orbital picture is at the core of quantum-chemical thinking [74] and a rigorous probe of this picture is clearly desirable. Although an orbital picture of resonance formation has persisted for long [59, 60] in the absence of a simple and unequivocal mechanism to identify the resonant orbital, its portrayal had not been possible earlier. Examination of radial charge density plots from resonant orbitals and Feynman–Dyson amplitudes for the ^{2}P shape resonances in e-Mg scattering has provided a preliminary outline with mixed results. The dominant features do point to the resonant orbital being the lowest p-type orbital, albeit with strong input from other orbitals in the same symmetry block. The competing demands of initial penetration and final decay are best served by a higher p-type orbital near the top and narrow end of the centrifugal barrier. On the other hand, temporary binding will be facilitated by the lower energy orbital(s) at the deeper and wider end of the barrier. These inherently contradictory attributes for the formation and decay preclude a simple orbital picture for the metastable states. In fact, the complex structure in charge density plots indicates that description of resonances will be extremely sensitive to the coordinate space span of the primitive basic set. The prevalent basis sets are biased in favour of occupied orbitals and our results emphasize the need for incorporation of GTOs which will provide sufficient flexibility to be able to cater for the competing demands of resonance formation and decay.

The complex scaling parameter is seen to play a critical role in providing a mechanism for the accumulation of electron density close to the target nucleus. The extensive correlation effects witnessed in the stabilization of shape resonances seems to indicate that the orbital picture for even the simplest of shape resonances investigated here needs to be interpreted judiciously. Optimal complex scaling is seen to turn the compact C_2H_4 LUMO on the real line into an anionic diffuse orbital preparing it for metastable electron attachment. That these trends persist for diverse systems like N_2 [34], CO [34] and C_2H_4 molecules generates faith in the ability of the bi-orthogonal dilated electron propagator to unmask molecular shape resonances and to unfold descriptive insights with cross-systemic validity.

Some limitations of the results obtained so far need sharper focus and the first and foremost is the inadequacy of the basis sets devoid of d-functions which might have assisted in a better description of the polarization effects. The initial applications with emphasis on complementary analysis of the molecular shape resonances through the hitherto unexplored resonant FDAs which alone can furnish mechanistic insights has necessitated the expediency of utilizing computationally convenient basis sets with proven effectiveness in the unmasking of these resonances. However, study of the basis set effects needs urgent and comprehensive attention. Furthermore, while the calculated energies are plausible, the calculated widths for all molecular resonances explored with the dilated electron propagator are much narrower than the experimental width for all the systems investigated here. The experimental widths have been obtained by fitting the cross-section data using empirical optical potential [75]. The larger experimental widths have been contested [76] as being due to the inadequacy of the empirical optical potential. The narrowness of the widths calculated using the dilated electron propagator technique may also be due to insufficiency of the primitive basis sets and/or the amount of correlation and relaxation incorporated by the decouplings employed here. The need for a comprehensive study of the basis set effects has been stressed earlier and an incorporation of the higher order decouplings like the third order, quasi-fourth order [9, 77] or balanced renormalized decouplings such as the algebraic diagrammatic construction (ADC(3)) [6] is an obvious extension of this technique.

The single equilibrium bond length calculation for molecules also needs to be extended by allowing bond-stretching and calculating $\mathcal{E}_{res}(R) = \frac{1}{2}k^2_{res}(R)$ as a function of the bond length R. One could then employ the Chandra [78, 79] approximation $E^{N+1}_{res}(R) =$

$E_0^N(R) + \frac{1}{2}k_{res}^2(R)$ in conjunction with semi-classical/quantal wave packet dynamics [80] on this complex $E_{res}^{N+1}(R)$ to unravel the vibrational structure in attending electron attachment resonances without having to employ empirical optical potentials.

All in all, the bi-orthogonal dilated electron propagator offers a simple extension of the real electron propagator technique and with the incorporation of higher order decouplings like the Σ^3, Σ_q^4 ADC(3) etc. and suitably large and flexible basis sets should offer same power and effectiveness in the treatment of metastable anions and cations as done by its real counterpart for stable bound systems. An effort along these lines is underway in our group.

We gratefully acknowledge the support from the Department of Science and Technology, India.

References

[1] LINDERBERG, J., and ÖHRN, Y., 1973, *Propagators in Quantum Chemistry* (New York: Academic Press).

[2] JÖRGENSEN, P., and SIMONS, J., 1981., *Second Quantization Based Methods in Quantum Chemistry* (New York: Academic Press).

[3] CEDERBAUM, L. S., and DOMCKE, W., 1977, *Adv. chem. Phys.*, **36,** 205.

[4] HERMAN, M. F., FREED, K. F., and YEAGER, D. L., 1981, *Adv. chem. Phys.*, **48,** 1.

[5] ÖHRN, Y., and BORN, G., 1981, *Adv. quantum Chem.*, **13,** 1.

[6] VON NIESSEN, W., SCHIRMER, J., and CEDERBAUM, L. S., 1984, *Computer Phys. Rep.*, **1,** 57.

[7] SIMONS, J., 1977, *Ann. Rev. phys. Chem.*, **28,** 15.

[8] SIMONS, J., 1978, *Theoretical Chemistry: Advances and Perspectives* (New York: Academic Press).

[9] ORTIZ, J. V., 1992, *Chem. phys. Lett.*, **199,** 530.

[10] MEYER, H.-D., 1989, *Phys. Rev.* A, **40,** 5605.

[11] MEYER, H.-D., PAL, S., and RISS, U. V., 1992, *Phys. Rev.* A, **46,** 186.

[12] CEDERBAUM, L. S., 1990, *Int. J. quant. Chem.*, **S24,** 393.

[13] MISHRA. M., 1989, *Lecture Notes in Quantum Chemistry*, Vol. 50 (Berlin: Springer-Verlag), p. 233.

[14] JUNKER, B. R., 1982, *Adv. at. molec. Phys.*, **18,** 207.

[15] REINHARDT, W. P., 1982, *Ann. Rev. phys. Chem.*, **33,** 223.

[16] HO, Y. K., 1983, *Phys. Rep.*, **99,** 2.

[17] WINKLER, P., 1979, *Z. Phys.* A, **291,** 199.

[18] DONNELLY, R. A., and SIMONS, J., 1980, *J. chem. Phys.*, **73,** 2858.

[19] MISHRA, M., FROELICH, P., and ÖHRN, Y., 1981, *Chem. Phys. Lett.*, **81,** 339.

[20] MISHRA, M., GOSCINSKI, O., and ÖHRN, Y., 1983, *J. chem. Phys.*, **79,** 5494.

[21] WINKLER, P., YARIS, R., and LOVETT, R., 1981, *Phys. Rev.* A, **23,** 1787.

[22] DONNELLY, R. A., 1982, *J. chem. Phys.*, **75,** 5414.

[23] MEDIKERI, M. N., and MISHRA, M. K., 1993, *Chem. Phys. Letts.*, **211,** 607.

[24] DONNELLY, R. A., 1982, *Int. J. quant. Chem.*, **S16,** 653.

[25] DONNELLY, R. A., 1985, *Int. J. quant. Chem.*, **S19,** 337.

[26] DONNELLY, R. A., 1986, *J. chem. Phys.*, **84,** 6200.

[27] MISHRA, M., GOSCINSKI, O., and ÖHRN, Y., 1983, *J. chem. Phys.*, **79,** 5505.

[28] DAS, A., and MELISSINOS, A. C., 1986, *Quantum Mechanics* (New York: Gordon and Breach), p. 534.

[29] MEDIKERI, M. N., and MISHRA, M. K., 1994, *Int. J. quant. Chem.*, **S28,** 29.

[30] PALMQUIST, M., ALTICK, P. L., RITCHER, J., WINKLER, J., and YARIS, R., 1981, *Phys. Rev.* A, **23,** 1795.

[31] MEDIKERI, M. N., and MISHRA, M. K., 1994, *Proc. Ind. Acad. Sci., Chem. Sci.*, **106,** 111.

[32] MEDIKERI, M. N., MISHRA, M. K., 1994, *J. chem. Phys.*, **100,** 2044.

[33] MEDIKERI, M. N., NAIR, J., and MISHRA, M. K., 1993, *J. chem. Phys.*, **99,** 1869.

[34] MISHRA, M. K., and MEDIKERI, M. N., 1996, *Adv. quantum Chem.*, **27,** 223.

[35] MISHRA, M., and ÖHRN, Y., 1981, *Phys. Lett.* A, 81, 4.

[36] MCCURDY, C. W., RESCIGNO, T. N., DAVIDSON, E. R., and LAUDERDALE, J. G., 1980, *J. chem. Phys.*, **73,** 3268.

[37] FROELICH, P., and LÖWDIN, P. O., 1983, *J. math. Phys.*, **24,** 89.

[38] LÖWDIN, P. O., FROELICH, P., and MISHRA, M., 1989, *Adv. quant. Chem.*, **20,** 185.

[39] LÖWDIN, P. O., FROELICH, P., and MISHRA, M., 1989, *Int. J. quant. Chem.*, **2,** 867.

[40] BURROW, P. D., MICHEDJA, J. A., and COMER, J., 1976, *J. Phys.* B, **9,** 3255.

[41] MCCURDY, C. W., LAUDERDALE, J. G., and MOWREY, R. C., 1981, *J. chem. Phys.*, **75,** 1835.

[42] KURTZ, H. A., and ÖHRN, Y., 1979, *Phys. Rev.* A, **19,** 43.

[43] KURTZ, H. A., and JORDAN, K., 1981, *J. Phys.* B, **14,** 4361.

[44] HAZI, A. U., 1978, *J. Phys.* B, **11,** L259.

[45] HUNT, J., and MOISEIWITSCH, B. L., 1970, *J. Phys.* B, **3,** 892.

[46] KRYLSTEDT, P., RITTBY, M., ELANDER, N., and BRÄNDAS, E. J., 1987, *J. Phys.* B, **20,** 1295.

[47] KRYLSTEDT, P., ELANDER, N., and BRÄNDAS, E. J., 1988, *J. Phys.* B, **21,** 3969.

[48] MOISEYEV, N., and WEINHOLD, F., 1978, *Int. J. quant. Chem.*, **14,** 727.

[49] SIMONS, J., 1981, *J. chem. Phys.*, **75,** 2465.

[50] HAZI, A. U., and TAYLOR, H. S., 1970, *Phys. Rev.* A, **1,** 1109.

[51] THOMPSON, T. C., and TRUHLAR, D. G., 1982, *Chem. Phys. Lett.*, **92,** 71.

[52] TAYLOR, H. S., 1970, *Adv. chem. Phys.*, **18,** 91.

[53] BRÄNDAS, E. J., and FROEHLICH, P., 1977, *Phys. Rev.* A, **16,** 2207.

[54] MCCURDY, C. W., and MCNUTT, J. F., 1983, *Chem. Phys. Lett.*, **94,** 306.

[55] TAYLOR, H. S., and HAZI, A. U., 1976, *Phys. Rev.* A, **14,** 2071.

[56] SLATER, J. C., 1968, *Quantum Theory of Matter* (New York: McGraw-Hill), p. 122.

[57] MISHRA, M., KURTZ, H. A., GOSCINSKI, O., and ÖHRN, Y., 1983, *J. chem. Phys.*, **79,** 1896.

[58] WALKER, I. C., STAMATOVIC, A., and WONG, S. F., 1978, *J. chem. Phys.*, **69,** 5532; BURROW, P. D., and JORDAN, K. D., 1975, *Chem. Phys. Lett.*, **36,** 594.
[59] JORDAN, K. D., and BURROW, P. D., 1978, *Acc. Chem. Res.*, **11,** 341; JORDAN, K. D., and BURROW, P. D., 1987, *Chem. Rev.*, **87,** 557.
[60] SIMONS, J., and JORDAN, K. D., 1987, *Chem. Rev.*, 87, 535.
[61] MEDIKERI, M. N., and MISHRA, M. K., 1995, *J. chem. Phys.*, **103,** 676.
[62] MEDIKERI, M. N., and MISHRA, M. K., 1995, *Chem. Phys. Lett.*, **246,** 26.
[63] SCHNEIDER, B. I., RESCIGNO, T. N., LENGSFIELD, B. H., and MCCURDY, C. W., 1991, *Phys. Rev. Lett.*, **66,** 2728.
[64] GAMOW G., 1931, *Constitution of Atomic Nuclei and Radioactivity* (Oxford: Oxford University Press).
[65] DIRAC P. A. M., 1927, *Proc. Roy. Soc.* (London) A, **14,** 243; see also DIRAC P. A. M., 1958, *The Principles of Quantum Mechanics*, (Oxford: Clarendon Press). p. 201.
[66] BISGARD, P., BRUCH, R. D., FATRUP, B., and RODBRO, M., 1978, *Phys. Scr.*, **17,** 49.
[67] RODBRO, M., BRUCH, R., and BISGARD, P., 1979, *J. Phys.* B, **12,** 2413.
[68] KELLY, H. P., 1974, *Phys. Rev.* A, **9,** 1582.
[69] KELLY, H. P., 1975, *Phys. Rev.* A, **11,** 556.
[70] HERMAN, M. F., FREED, K. F., and YEAGER, D. L., 1981, *Adv. chem. Phys.*, **48,** 1.
[71] ORTIZ, J. V., 1991, *J. chem. Phys.*, **94,** 6064.
[72] MCCURDY, C. W., 1979, *Electron-Molecule and Photon-Molecule Collisions* (New York: Plenum).
[73] SIMON, B., 1978, *Int. J. quant. Chem.*, **14,** 529.
[74] SIMONS, J., 1991, *J. phys. Chem.*, **95,** 1017.
[75] HERZENBERG, A., 1968, *J. Phys.* B, **1,** 548; BIRTWHISTLE, D. T., and HERZENBERG, A., 1971, *J. Phys.* B, **4,** 53.
[76] CHAO, J. S.-Y., FALCETTA, M. F., and JORDAN, K. D., 1990, *J. chem. Phys.*, **93,** 1125.
[77] ORTIZ, J. V., 1990, *Int. J. quant. Chem.*, **24,** 585.
[78] CHANDRA, N., 1977, *Phys. Rev.* A, **16,** 801.
[79] CHANDRA, N., and TEMKIN, A., 1976, *Phys. Rev.* A., **13,** 188.
[80] MCCURDY, C. W., and TURNER, J. L., 1983, *J. chem. Phys.*, **78,** 6773.

MOLECULAR PHYSICS, 1998, VOL. 94, NO. 1, 139–145

The hidden facet of the $C^3\Pi$ state of SO

By FERNANDO R. ORNELLAS and ANTONIO CARLOS BORIN
Instituto de Química, Universidade de São Paulo, Caixa Postal 26077, São Paulo, SP 05599-970, Brazil

Reliable evidence is presented which shows that the $C^3\Pi$ state of SO, previously thought to be mostly repulsive, does in fact have a relatively deep potential. As a result of an avoided crossing around $3.9\,a_0$, this state does have, for large internuclear distances, the repulsive nature experimentalists have agreed upon, and which has somehow been incorrectly extended to shorter distances; its supposed repulsive nature may have discouraged theoreticians from exploring excited states other than $A^3\Pi$, $B^3\Sigma^-$, and $^3\Delta$. As a consequence of the findings of this work, all existing experimental data on the excited states of $B^3\Sigma^-$ and part of $A^3\Pi$ will necessarily have to be reanalysed to properly take into account the perturbations caused by these new $^3\Pi$ states and other lower lying $^3\Sigma^+$ and $^3\Delta$ states on the spectra of SO. The theoretical predictions of this work were based on a state averaged complete active space self-consistent/internally contracted multireference configuration interaction (CASSCF/CMRCI) calculation using averaged natural orbitals expanded in terms of the cc-pVQZ set of atomic functions. The following spectroscopic constants characterizing these new states have been found: $R_e = 3.177\,a_0$, $T_e = 5.46$ eV, $\Delta G(\nu + 1/2) = 704, 681, 655, 634, 616, 607$ and $622\,cm^{-1}$ ($\nu = 0 - 6$), $\omega_e = 747\,cm^{-1}$, $\omega_e x_e = 21.06\,cm^{-1}$, $\omega_e y_e = 1.114\,cm^{-1}$, $R_{max} = 3.914\,a_0$, $E_{max} = 0.64$ eV for what we now call the $C^3\Pi$; and $R_e = 3.883\,a_0$, $T_e = 6.15$ eV, $\Delta G(\nu + 1/2) = 817, 752, 641$ and $152\,cm^{-1}$ ($\nu = 0 - 3$), $\omega_e = 838\,cm^{-1}$, $\omega_e x_e = -2.04\,cm^{-1}$, $\omega_e y_e = -7.702\,cm^{-1}$, $R_{max} = 4.394\,a_0$, $E_{max} = 0.42$ eV, for what we now call the $C'^3\Pi$ state. The very anharmonic nature of the latter state is obviously manifested in the vibrational constants.

1. Introduction

The molecular radical SO is a species of considerable chemical and physical interest. In interstellar chemistry [1], its role in the formation of molecular clouds is a subject of current research [2], as well as its participation in the photochemistry of sulphur compounds on Jupiter [3] and on the atmosphere of its satellites [4]. For the Earth atmosphere and troposphere, as a member of a class of sulphur oxides, its role in the acid rain cycle [5] is also an issue of global environmental interest. Spectroscopically, SO can be used as a monitoring species in the photodissociation [6–12] or combustion [13] of more complex sulphur-containing molecules, and also as a lasing system [14–17].

Experimentally, a considerable amount of spectroscopic data has been accumulated for the ground state ($X^3\Sigma^-$), and excited ($A^3\Pi, B^3\Sigma^-$) states [18–27]. Evidence for an excited $^3\Delta$ state has also been put forward by Tevault and Smardzewiski [28] and Colin [29]. Singlet states have also been characterized in investigations carried out by Colin [21] ($b^1\Sigma^+$), Lee and Pimentel [30] ($c^1\Sigma^-, a^1\Delta$), Barnes *et al.* [31] ($a^1\Delta$), and Burkholder *et al.* ($a^1\Delta$).

The analysis of perturbations in the $B^3\Sigma^- \leftrightarrow X^3\Sigma^-$ band system carried out by Martin [24] early in 1932 led that author to propose the existence of a nearly totally repulsive $C^3\Pi$ state crossing the state $B^3\Sigma^-$ close to $\nu' = 3$ and $\nu' = 15$. Although Abadie and Herman [32] have derived approximate constants for the perturbing state, Colin [20] stresses that there has been no definitive conformation that it is in fact a $^3\Pi$ state. We note, however, that an implicit assumption of the existence of a repulsive $^3\Pi$ state has been propagated from one investigation to another.

On the theoretical side, the number of accurate studies on this system has been surprisingly small [33–39], and, with the exception of the early work of Swope *et al.* [39], it has been limited to the investigation of only a few states. A less rigorous pseudopotential investigation by Dixon *et al.* [40] has described twenty one electronic states of the SO molecule.

Recently, Fülscher *et al.* [33] have described both the $X^3\Sigma^-$ and $A^3\Pi$ states and computed the radiative lifetimes of the $A^3\Pi$ state at a high level of correlation treatment. In this work, we have followed a similar approach but have used a larger active space and a more extended atomic basis set, since we wanted to explore other electronic states dissociating into excited state atoms.

Following a common procedure in our investigations of extracting from the Hamiltonian matrix the eigen-

0026–8976/98 $12·00

values associated with most of the states correlating with the first dissociation channel, and a few others correlating with higher lying dissociation channels, we have been surprised by the fact that the potential energy curves obtained in this calculation revealed a completely new picture of the $^3\Pi$ states which had been unsuspected in any of the previous experimental and theoretical studies.

This new finding invalidates several arguments used in the analysis of perturbations observed in transitions from both $A\,^3\Pi$ and $B\,^3\Sigma^-$ states and discussed in previous experimental works, and calls for a reanalysis and a reassessment of the existing experimental data on the states $A\,^3\Pi$, $B\,^3\Sigma^-$, and $C\,^3\Pi$. In view of this new evidence, our main purpose in this work is to present a highly accurate theoretical characterization of this new state thus providing reliable data that cannot only shed new light on the analysis of the existing experimental data but also provide new insights into the rich and complex spectroscopy of the SO molecule.

2. Methodology

Direct application of the Wigner–Witmer rules [41] shows that correlating with the first dissociation channel, $S(^3P_g) + O(^3P_g)$, the following molecular states $\Sigma^+(2)$, Σ^-, $\Pi(2)$, and Δ, with singlet, triplet and quintet multiplicities, are theoretically realizable; for the second dissociation channel, the allowed symmetries are: Σ^+, $\Sigma^-(2)$, $\Pi(3)$, $\Delta(2)$ and Φ. Considering now the region for which experimental data are available, it is clear that if one wants to describe these states within the C_{2v} point group symmetry representations, it more than suffices to calculate the first four eigenvalues of the $A_1(\Sigma^+, \Delta)$, and $A_2(\Sigma^-, \Delta)$ symmetries, and three eigenvalues of the B_1 symmetry; for the singlet states, two of each A_1 and A_2 symmetries and only one of the B_1 symmetry are needed in fact to be extracted from the hamiltonian matrix.

Concerning the atomic basis sets used in the present investigation, our choice has been the correlation-consistent polarized-valence quadruple-zeta (cc-pVQZ) basis functions developed by Dunning and collaborators [42, 43], symbolized as (12s, 6p, 3d, 2f, 1g)/[5s, 4p, 3d, 2f, 1g] for oxygen, and (16s, 11p, 3d, 2f, 1g)/[6s, 5p, 3d, 2f, 1g] for sulphur. The total number of contracted functions amounts to 114 and, as implicit in their definition, spherical gaussians are used in all calculations.

In the construction of the *n*-particle basis, we have employed a set of natural orbitals generated through the diagonalization of a state-averaged density matrix. The state-averaging process involved first a complete active space self-consistent field (CASSCF) calculation in which twelve electrons were distributed in ten active orbitals, denoted (4330) in C_{2v} point group symmetry; this space includes the 2s (3s) and 2p (3p) valence orbitals, respectively, plus one correlating orbital in each of the b_1 and b_2 symmetries. Core (1s) and inner-shell (S 2s and 2p) orbitals were kept doubly occupied in all calculations. In this process, a common set of molecular orbitals was constructed by optimizing an average energy which included the four lowest states of each A_1 and A_2 representations, and three of the B_1 and B_2 representations, with equal weights for all states [44, 45]. The CASSCF calculation generated sets of configuration state functions of dimensions 5154(A_1), 5196(A_2), and 5220(B_1).

To account for the dynamic correlation effects, a new set of reference configurations was constructed by selecting all those occupations from the CASSCF wave function which gave rise to at least one configuration state function (CSF) with a coefficient greater than 0.025 in absolute magnitude; next all single and double excitations were generated from this new reference set. The choice of this threshold has been amply demonstrated by Taylor [46], and also by Partridge *et al.* [47], to yield very reliable results. To make this study viable, we have made use of the internally contracted multireference configuration interaction (CMRCI) [48, 49] approach as implemented in the Molpro-96 suite of programs [50], which reduced the dimension of the CSF space from about 10–14 million terms to less than a million.

Vibrational energies and wavefunctions were computed with the 'intensity' program [51] based on the Numerov Cooley numerical solution of the radial Schrödinger equation. Spectroscopic constants were obtained by standard fitting procedures [41, 52–57].

3. Results and discussion

Total energies for the two lowest $^3\Pi$ states correlating with the first dissociation channel, $S(^3P) + O(^3P)$, and for a third $^3\Pi$ state correlating with the fragments of the second dissociation channel, $S(^1D) + O(^3P)$, are collected in table 1; the corresponding potential energy curves are displayed in figure 1. For the sake of completeness, we have also displayed in figure 1 the potential energy curves of other triplet states of relevance to the present discussion. Concerning the energies, it is worth pointing out that they have been corrected for quadruple excitations using Langhoff and Davidson's method [58]. As already pointed out by Fülscher *et al.* [33], this correction turns out to be important, specially for the $A\,^3\Pi$ state because of the very shallow minimum of its potential energy function. Spectroscopic constants are collected in table 2.

As to the whole manifold of low-lying singlet and triplet states, we note that a thorough discussion of most of the singlet and triplet states correlating with

Table 1. Energies (in au) for the lowest-lying $^3\Pi$ states of the SO molecule. The energies are given relative to −472.0 au. Distances are given in bohr.

R	$A^3\Pi$	$C^3\Pi$	$C'^3\Pi$	R	$A^3\Pi$	$C^3\Pi$	$C'^3\Pi$
2.20	−0.446 876	−0.335 712	−0.201 119	3.25	−0.675 189	−0.651 729	−0.585 388
2.25	−0.490 083	−0.386 291	−0.247 851	3.30	−0.675 152	−0.650 646	−0.591 106
2.30	−0.525 962	−0.429 517	−0.285 682	3.40	−0.674 753	−0.647 875	−0.600 970
2.35	−0.558 179	−0.469 215	−0.323 146	3.50	−0.673 725	−0.644 321	−0.609 064
2.40	−0.581 286	−0.500 122	−0.348 823	3.60	−0.672 487	−0.640 606	−0.615 683
2.50	−0.619 722	−0.552 687	−0.389 741	3.70	−0.670 941	−0.636 569	−0.621 122
2.60	−0.642 669	−0.588 815	−0.433 413	3.80	−0.669 244	−0.632 591	−0.625 454
2.65	−0.650 819	−0.602 757	−0.454 016	3.90	−0.667 086	−0.628 778	−0.627 335
2.70	−0.656 779	−0.614 108	−0.471 651	3.95	−0.666 013	−0.629 590	−0.625 906
2.75	−0.661 612	−0.623 606	−0.487 759	4.00	−0.664 912	−0.631 612	−0.623 501
2.80	−0.665 367	−0.631 481	−0.502 364	4.10	−0.662 496	−0.635 141	−0.621 445
2.85	−0.668 225	−0.637 332	−0.515 488	4.20	−0.660 304	−0.637 806	−0.616 317
2.90	−0.670 379	−0.642 127	−0.527 416	4.50	−0.656 981	−0.645 250	−0.614 394
2.95	−0.671 880	−0.645 722	−0.538 166	5.00	−0.657 554	−0.652 652	−0.615 452
3.00	−0.673 041	−0.648 490	−0.547 948	6.00	−0.660 162	−0.668 638	−0.616 686
3.10	−0.674 501	−0.651 472	−0.565 021	7.00	−0.660 517	−0.653 389	−0.618 963
3.15	−0.674 902	−0.652 068	−0.572 333	8.00	−0.660 328	−0.653 219	−0.618 701
3.20	−0.675 127	−0.652 016	−0.579 104				

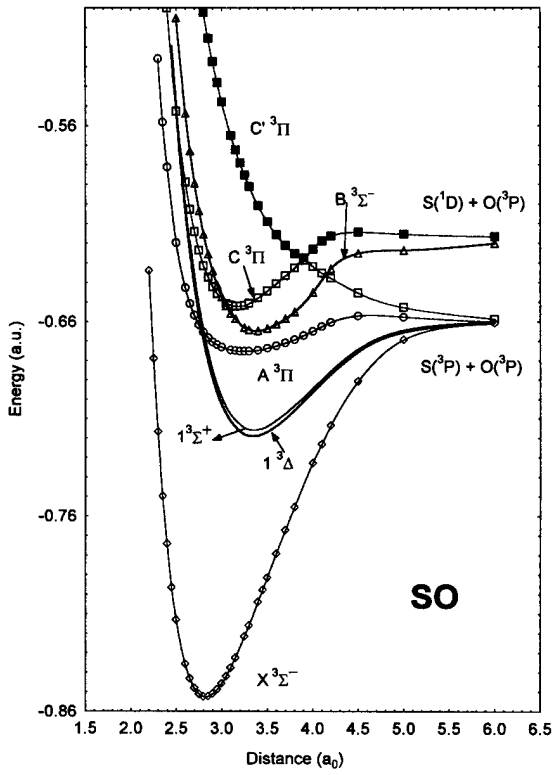

Figure 1. Potential energy curves for selected states of the SO molecule.

the first and second dissociating channels of the SO molecule will appear in a forthcoming paper. In this work, as already pointed out, our main focus is to provide a reliable description of the as yet unknown facet of the $C^3\Pi$ state which can be of help in the reinterpretation of existing data on the emission and absorption spectra of the SO molecule.

Table 2. Spectroscopic constants for the low-lying $^3\Pi$ states of SO. Unless otherwise indicated, all constants are given in cm^{-1}.

	$A^3\Pi$			$C^3\Pi$	$C'^3\Pi$
	This work	[33]	Experiment	This work	This work
R_e/a_0	3.249	3.214	3.041	3.177	3.883
T_e/eV	4.83	4.85	4.77	5.46	6.15
$\Delta G(1/2)$	372	344	416	704	817
$\Delta G(3/2)$	374	360	407	681	752
$\Delta G(5/2)$	374	369	404	655	641
$\Delta G(7/2)$	373	–	401	634	152
$\Delta G(9/2)$	371	–	397	616	–
$\Delta G(11/2)$	370	–	392	607	–
$\Delta G(13/2)$	369	–	382	622	–
$\Delta G(15/2)$	368	–	338	–	–
ω_e	371	332	413	747	838
$\omega_e x_e$	1.06	6.4	1.6	21.06	−2.04
$\omega_e y_e$	−0.129	–	–	1.114	−7.702

Before describing the new features of the $C^3\Pi$ state, and discussing its implications, a few comments on the experimental evidence leading to its proposal are worth making. The evidence is mostly inferred from the analysis of perturbations in some emission and absorption bands of the $B^3\Sigma^- \leftrightarrow X^3\Sigma^-$ transition. Martin [24] was the first to report an abrupt termination of the bands $0\text{–}\nu''$, $1\text{–}\nu''$, $2\text{–}\nu''$, and $3\text{–}\nu''$ at the rotational levels $N' = 66$, 53, 39, and 6, respectively, which have been

interpreted as a clear indication of a predissociation. Also, the increasing diffuseness in bands for $\nu' > 8$ and which reaches its maximum at $\nu' = 14$ and 15 are taken again as an indication of the setting of a second predissociation. Also, of relevance to our discussion is a strong vibrational perturbation near $\nu' = 16$, and small displacements of several other levels, specially $\nu' = 3$, 7 and 11. The 7–0 band, in particular, presents a triple head, assumed as probably due to an anomalously large splitting of the three components of the upper state. From the emission data involving the levels $\nu' = 0$–3, the existence of a very shallow well ($\approx 1600\,\text{cm}^{-1}$) with a minimum at $\approx 7.5\,a_0$ was inferred by Martin as characteristic of this perturbing $^3\Pi$ state. As to the second predissociation of the $B\,^3\Sigma^-$ state near $\nu' = 14$ and 15, it is supposed to be due to an avoided crossing of the $B\,^3\Sigma^-$ state now with the repulsive part of a higher lying $^3\Sigma^-$ state. Summarizing these data, an almost totally repulsive potential energy curve crossing the $B\,^3\Sigma^-$ state at $\nu' = 3$ and 15 has been used in the literature as characteristic of the $C\,^3\Pi$ [14].

As clearly depicted in figure 1, the new theoretical data on the $C\,^3\Pi$ state reported in this work does not support the above interpretation of perturbation effects in some of the bands of the $B\,^3\Sigma^-$ state, and the above description inferred for the $C\,^3\Pi$ state. This study reveals the existence of another bound $^3\Pi$ state with an equilibrium internuclear distance of $3.177\,a_0$ lying at 5.46 eV (T_e) above the ground state and correlating diabatically with the second dissociation channel; also another higher lying $^3\Pi$ state ($T_e = 6.15$ eV) which correlates diabatically with the first dissociation channel was found to have a repulsive nature for distances shorter than $\sim 3.9\,a_0$. At this point, an avoided crossing between these two states changes their characters and gives rise to a hump in the lower state with a maximum energy of 0.64 eV relative to its bottom. As a consequence of this avoided crossing, the minimum of the lower lying $^3\Pi$ state turns out to be located at 0.09 eV above its adiabatic dissociation limit, and a new minimum at $3.883\,a_0$ arises for the higher-lying $^3\Pi$ state; for this latter state a small hump of 0.42 eV relative to the bottom of the well was computed. Solution of the radial Schrödinger equation for these new bound states allowed us to predict the existence of at least eight and five vibrational states for the lower and higher of these $^3\Pi$ states, respectively.

Concerning the new features of the $^3\Pi$ states, it is worth calling attention to the sharpness of the avoided crossing between the C and C′ states with an energy splitting of 0.002 251 au. In this region, the adiabatic electronic wavefunctions change character in a rather sharp and drastic manner, and as a consequence, one expects a strongly peaked coupling matrix element between the adiabatic states near the internuclear distance where the diabatic curves cross. As discussed by Lefebvre-Brion and Field [59], a sharply peaked change in the coupling function is an indication of a preference for a diabatic picture of the dynamics of the system.

As a consequence of the strong coupling between the states, radiationless transitions between the adiabatic states are likely to occur. In fact, by making use of the Landau–Zener [60] expression and the approximations defined in [61], a rough estimate of 80% was obtained for the transition probability between the adiabatic states. It is well known that radiationless transitions lead to a decrease in the lifetime of a given level, and in the absence of any other relevant effect, the linewidth of transitions to that level are expected to increase.

To better analyse the various crossings of the potential energy curves, we have redrawn in figure 2 a rescaled version of figure 1 in which only the curves of the states $A\,^3\Pi$, $B\,^3\Sigma^-$, and the two new $^3\Pi$ states are shown. Also, to provide a more accurate relative position of the vibrational levels, we have rescaled our theoretical T_e values to match the experimental ones. We note that our prediction of T_e for the $B\,^3\Sigma^-$ state is underestimated by $423\,\text{cm}^{-1}$, whereas that for the $A\,^3\Pi$ state is overestimated by $475\,\text{cm}^{-1}$; the new $^3\Pi$ states have been rescaled similarly to the $A\,^3\Pi$ state. With this rescaling, one can notice that the setting of the continuum in the $A\,^3\Pi$ occurs just above vibrational level 1 of the $B\,^3\Sigma^-$ state. A closer look at the positions of the vibrational levels of

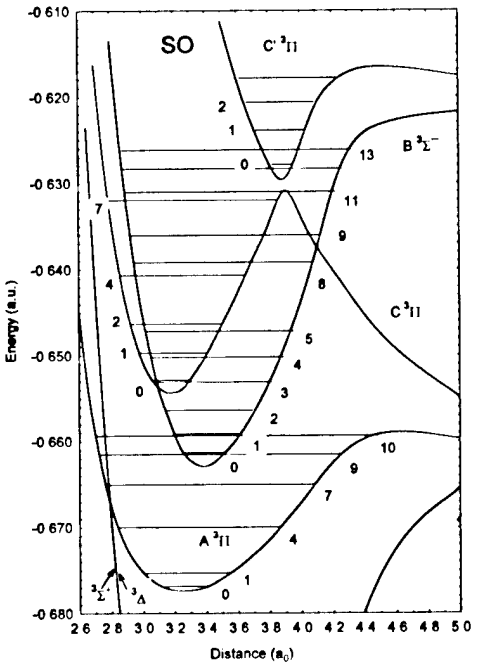

Figure 2. Amplified view of the potential energy curves for selected states of the SO molecule, including calculated vibrational levels.

the $B^3\Sigma^-$ state shows, however, that the crossing with the $C^3\Pi$ state occurs between levels 8 and 9, and not at $\nu' = 3$, as experimentally inferred. Similarly, the experimentally supposed crossing of the repulsive sides of both $C^3\Pi$ and $B^3\Sigma^-$ states does not in fact occur at $\nu' = 15$, but just below $\nu' = 0$. Clearly, these findings urge for other arguments in the explanation of these perturbative effects in the spectra.

On the basis of this new picture, the increasing diffuseness in bands for $\nu' > 8$ of the $B^3\Sigma^-$ state arises not only because of the crossing of this state by the external repulsive side of the $C^3\Pi$ state between levels 8 and 9, but certainly are also reflecting the strong interaction between the upper lying $^3\Pi$ states. Note that for $\nu' > 10$, these vibrational levels lie in the continuum of the new $C^3\Pi$ state and a predissociation of type I as discussed by Herzberg [41] is also likely to occur. The type of predissociation observed here is illustrative of a heterogeneous perturbation, and an increase in diffuseness is expected to occur with increasing N values, as well as a shift of the dissociation limit to higher energy values.

If the experimental spectra are really an indication of predissociation, how can one account for a mechanism of predissociation of the levels 0, 1, 2 and 3 of the $B^3\Sigma^-$ state? Apparently, one alternative involves a possible favourable overlap of some rotationally excited states of these low-lying vibrational levels with the continuum of the A state. However, as discussed by Herzberg [41] in the case of the $^2\Pi$ states of the NO molecule, the present situation is a typical one where quite low Franck–Condon factors would be expected to occur. A rough estimate of this expectation has been carried out by computing the Franck–Condon factors between the pairs of levels 0–9 and 1–10 of the A and B states for several combinations of the rotational quantum number which turned out to be practically zero. The other possible alternative to consider basically assumes that the experimental data are not actually reflecting a predissociation but rather a heterogeneous rotational perturbation by the new bound $C^3\Pi$ state on $B^3\Sigma^-$ close to $3.1\,a_0$. We recall that an abrupt termination of the bands $0\text{–}\nu'$, $1\text{–}\nu'$, $2\text{–}\nu'$, and $3\text{–}\nu'$ occur at the rotational levels $N' = 66$, 53, 39 and 6, respectively. Guided by these numbers, we computed the location of the rotational states, relative to the bottom of the B state potential, which could most closely reproduce the observed rotational quantum numbers. Our results, 65(2344), 53(2361), 39(2370) and 15(2364), where the numbers in parentheses are the energies in cm^{-1} relative to the bottom of the well, clearly indicate the existence of four vibro-rotational states within $20\,cm^{-1}$ of each other which are directly affected by the curve crossing close to $3.1\,a_0$. On the basis of these data, we are strongly inclined to accept this latter alternative as providing a more viable mechanism to explain the diffuseness in the spectra.

We also note that there is no mention of a $(9\text{–}\nu'')$ or a $(10\text{–}\nu'')$ band in Colin's [20] investigation of the A–X transition, but in this case, besides the expected low Franck–Condon factors, an additional effect contributes to the diffuseness of the lines, and it has to do with a predissociation by rotation (Herzberg's case III) which is expected to increase with increasing rotational quantum number. A further point to note in these potential energy curves is the close proximity of some vibrational levels of the $B^3\Sigma^-$ state to those of the $C^3\Pi$ state. An unambiguous experimental determination of these states is clearly needed.

In the case of the (7–0) band of the $B^3\Sigma^- - X^3\Sigma^-$ transition, which is reported to have a triple head, what one may be observing is in fact a transition from levels 3 and 4 of $C^3\Pi$ and 7 of $B^3\Sigma^-$. We recall that the three $\Delta G(\nu + 1/2)$ values approximately inferred for $\nu = 7$ differ by as much as $62\,cm^{-1}$. Additionally, if one takes into account that transitions from the new $C^3\Pi$ state can also be composed of three subbands, the band system in this region of the spectrum will certainly present a rather complex appearance.

Although a characterization of all low-lying singlets and triplets of SO will be presented in detail in a forthcoming paper, we can ,however, anticipate some points of relevance to the present study. We first recall that Colin [20] reports an anomalous behaviour on both extremities of his observed A–X spectrum, and notes that for $\nu' = 2$, 3 and 4, the $\Delta G(\nu + 1/2)$ values are quite regular. If we look closely at figure 2, we can note that the $A^3\Pi$ state curve is crossed by the $^3\Delta$ and $^3\Sigma^+$ states near $\nu' = 5$, which might be acting as perturbing states. The supposed existence of a nearby singlet perturbing the $A^3\Pi$ state has also been considered by some investigators. We note, however, that our calculation has found a $^1\Sigma^-$ state lower in energy than the $A^3\Pi$, but with a potential energy curve running almost parallel to that of the $^3\Delta$ state and displaced a little bit to shorter internuclear distances.

Concerning the characterization of the $A^3\Pi$ state, one important point still deserves some attention. The equilibrium distance predicted by Fülscher *et al.* [33] ($3.214\,a_0$) and that computed in this work ($3.249\,a_0$) differ from experiment by about $0.2\,a_0$, a result unexpectedly too large for this level of correlation treatment. For the ground state, theory and experiment differ by less than about $0.02\,a_0$, and for the $B^3\Sigma^-$ state the difference amounts to $0.04\,a_0$. Another indicator of the existence of difficulties in the characterization of this state, either theoretically or experimentally, is reflected in the values of $\Delta G(1/2)$, $\Delta G(3/2)$ and $\Delta G(5/2)$.

Experimentally, they are reported to be 416, 406 and 404 cm^{-1}; theoretically, Fülscher *et al.* obtained 344, 360 and 369 cm^{-1}, whereas in this study our values turned out to be 372, 374 and 374 cm^{-1}. Although our results represent an improvement over that of [33], the errors in ΔG are significantly larger than the ones for the ground state (14, 12 and 12 cm^{-1}). Clearly, this issue needs further investigation, but these differences do not affect the results and discussion we have presented for the new $^3\Pi$ states.

4. Conclusion

This work has provided reliable spectroscopic data which predict the existence of new bound $^3\Pi$ states in the spectra of the SO molecule. It invalidates previous inferences made by experimentalists in the interpretation of perturbations of various bands in the spectra of the $B\,^3\Sigma^- - X\,^3\Sigma^-$ transition. It is our hope that it cannot only guide spectroscopists in the analysis of the complex spectra of this molecule, but also motivates new theoretical and experimental investigations on this system.

The provision of computational facilities at the Laboratório de Computação Científica Avançada (LCCA) da Universidade de São Paulo is deeply acknowledged, as well as the continuous academic support of the Conselho Nacinal de Desenvolvimento Científico e Tecnológico (CNPq) and Fundação de Amparo à Pesquisa do Estado de São Paulo (FAPESP).

References

[1] Duley, W. W., and Williams, D. W., 1984, *Interstellar Chemistry* (New York: Academic Press).
[2] Turner, B. E., 1995, *Astrophys. J.*, **455**, 556.
[3] Moses, J. I., Allen, M., and Gladstone, G. R., 1995, *Geophys. Res. Lett.*, **22**, 1597; 1995, *ibid.*, **22**, 1601.
[4] Lellouch, E., Strobel, D. F., Belton, M. J. S., Summers, M. E., Paubert, G., and Moreno, R., 1996, *Astrophys. J.*, **459**, L107.
[5] Wayne, R. P., 1991, *Chemistry of the Atmospheres* (Oxford: Oxford Science Publications/Clarendon Press).
[6] Becker, S., Braatz, C., Lindner, J., and Tiemann, E., 1995, *Chem. Phys.*, **196**, 275.
[7] Thelen, M.-A., and Huber, J. R., 1995, *Chem. Phys. Lett.*, **236**, 558.
[8] Wu, F., Chen, X., and Weiner, B. R., 1995, *J. phys. Chem.*, **99**, 17380.
[9] Ebata, T., Nakazawa, O., and Ito, M., 1988, *Chem. Phys. Lett.*, **143**, 31.
[10] Kanamori, H., Butler, J. E., Kawaguchi, K., Yamada, C., and Hirota, E., 1985, *J. chem. Phys.*, **83**, 611.
[11] Felder, P., Effenhauser, C. S., Haas, B. M., and Huber, J. R., 1988, *Chem. Phys. Lett.*, **148**, 417.
[12] Kawasaki, M., and Sato, H., 1987, *Chem. Phys. Lett.*, **139**, 585.
[13] Gaydon, A. G., 1948, *Spectroscopy and Combustion Theory* (London: Chapman & Hall), p. 213.
[14] Miller, H. C., Yamasaki, K., Smedley, J. E., and Leone, S. R., 1991, *Chem. Phys. Lett.*, **181**, 250.
[15] Clyne, M. A. A., and Liddy, J. P., 1982, *J. Chem. Soc. Faraday Trans. II*, **78**, 1127.
[16] Cao, D. Z., and Setser, D. W., 1988, *J. phys. Chem.*, **92**, 1169.
[17] Lo, G., Beaman, R., and Setser, D. W., 1988, *Chem. Phys. Lett.*, **149**, 384.
[18] Kanamori, H., Butler, J. E., Kawaguchi, K., Yamada, C., and Hirota, E., 1985, *J. molec. Spectrosc.*, **113**, 262.
[19] Burkholder, J. B., Lovejoy, E. R., Hammera, P. D., and Howard, C. J., 1987, *J. molec. Spectrosc.*, **124**, 379.
[20] Colin, R., 1969, *Can. J. Phys.*, **47**, 979.
[21] Colin, R., 1968, *Can. J. Phys.*, **47**, 1539.
[22] McGarvey, J. J., and McGrath, W. D., 1963, *Proc. Roy. Soc.* (London), Ser. A, **278**, 490.
[23] Norrish, R. G., and Oldershaw, G. A., 1959, *Proc. Roy. Soc.* (London), Ser. A, **249**, 498.
[24] Martin, E. V., 1932, *Phys. Rev.*, **41**, 167.
[25] Clyne, M. A. A., and McDermid, I. S., 1979, *J. Chem. Soc. Faraday Trans. II*, **75**, 905.
[26] Clyne, M. A. A., and Tennyson, P. H., 1986, *J. Chem. Soc. Faraday Trans. II*, **82**, 1315.
[27] Hebert, G. R., and Hodder, R. V., 1974, *J. Phys.*, **B7**, 2244.
[28] Tevault, D. E., and Smardzewski, R. R., 1978, *J. chem. Phys.*, **69**, 3182.
[29] Colin, R., 1982, *J. Chem. Soc. Faraday Trans. II*, **78**, 1139.
[30] Lee, Y.-P., and Pimentel, G. C., 1978, *J. chem. Phys.*, **69**, 3063.
[31] Barnes, I., Becker, K. H., and Fink, E. H., 1979, *Chem. Phys. Lett.*, **67**, 310.
[32] Abadie, D., and Herman, L., 1963, *J. Quant. Spectrosc. Radiative Transfer*, **4**, 195.
[33] Fülscher, M. P., Jaszunski, M., Roos, B., and Kraemer, W. P., 1992, *J. chem. Phys.*, **96**, 504.
[34] Peterson, K. A., and Woods, R. C., 1990, *J. chem. Phys.*, **93**, 1876.
[35] Jin, S., and Schaefer, H. F., 1990, *J. chem. Phys.*, **93**, 1799.
[36] Klotz, R., Marian, C. M., Peyerimhoff, S. D., Hess, B. A., and Buenker, R. J., 1984, *Chem. Phys.*, **89**, 223.
[37] Klotz, R., Marian, C. M., Peyerimhoff, S. D., Hess, B. A., and Buenker, R. J., 1983, *Chem. Phys.*, **76**, 367.
[38] Theodorakopoulos, G., Peyerimhoff, S. D., and Buenker, R., 1981, *Chem. Phys. Lett.*, **81**, 413.
[39] Swope, W. C., Lee, Y.-P., and Schaefer, H. F., 1979, *J. chem. Phys.*, **71**, 3761.
[40] Dixon, R. N., Tasker, P. W., and Balint-Kurti, G.-G., 1977, *Molec. Phys.*, **34**, 1455.
[41] Herzberg, G., 1950, *Molecular Spectra and Molecular Structure*, Vol. I, *Spectra of Diatomic Molecules* (New York: Van Nostrand Reinhold).
[42] Dunning, H., 1989, *J. chem. Phys.*, **90**, 1007.
[43] Woon, D. E., and Dunning, T. H., 1993, *J. chem. Phys.*, **98**, 1358.
[44] Werner, H.-J., and Knowles, P. J., 1985, *J. chem. Phys.*, **82**, 5053.
[45] Knowles, P. J., and Werner, H.-J., 1985, *Chem. Phys. Lett.*, **115**, 259.

MOLECULAR PHYSICS, 1998, VOL. 94, NO. 1, 147–155

Calculational and conceptual study of cyano derivatives of diborane and their iso-analogues

By IVAN CERNUSAK†‡§ and JOEL F. LIEBMAN‡

† Department of Physical Chemistry, Faculty of Science, Comenius University, Mlynská dolina, SK-84215 Bratislava, Slovakia

‡ Department of Chemistry and Biochemistry, University of Maryland Baltimore County, 1000 Hilltop Circle, Baltimore, MD 21250, USA

We present the prediction of the MBPT(2)/DZP structures, CCSD + T(CCSD)/DZP and CCSD + T(CCSD)/cc-PVTZ energetics for 1,1-dicyanodiborane, *trans*-1,2-dicyanodiborane and μ,μ(C,C)-dicyanodiborane as well as for the diisocyano counterparts. The molecules with three-centre-two-electron (3c2e) bonds exhibit higher thermodynamic stability with respect to the H_2BCN or H_2BNC monomers than the μ,μ-isomers (cyano bridging) which are significantly less stable. Another possible reaction channel comprising the exchange reaction $B_2H_6 + 2HCN \rightarrow C_2H_4B_2N_2 + 2H_2$ exhibits even more enhanced differences between 1,1-, 1,2- and μ,μ(C,C) isomers, respectively, and related isocyano molecules. The effects of electron correlation are analysed for complexation reactions, isomer ordering and for various CN/NC isomerization reactions. Bonding analysis in terms of SCF and MBPT(2) bond orders is presented. Possible candidates for BNC-polymer modeling are also suggested on the basis of these molecular calculations.

1. Introduction

In the course of other work [1] on cyclic and chain dimers of H_2BCN we have suggested also the other possible structure (**1a**) corresponding to $C_2H_4B_2N_2$ isomer with non-classical, i.e. 3c2e boron bonds [2]. However, this is only one of several conceivable isomers of cyanoborane dimer. Depending on the position of the CN-group and/or the arrangement of carbon and nitrogen atoms one can consider also other isomers of $C_2H_4B_2N_2$: (H_b denotes bridging, H_t terminal hydrogen atom, respectively) **1b**, **2a**, **2b**.

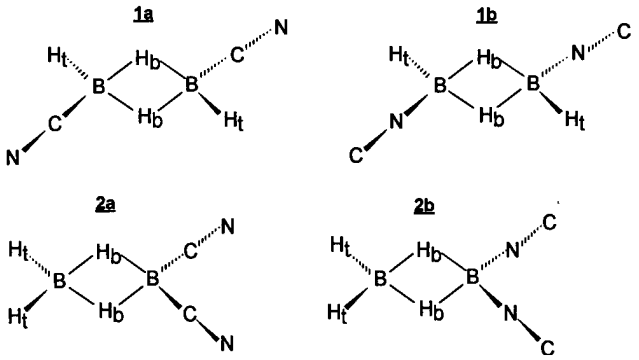

Of course, there could be even more isomers of cyanoborane dimer than selected in this paper (e.g. *cis*-1,2-dicyanodiborane). However, we are primarily interested in extreme cases for which one can observe the effect of the substituent on the isomers ordering, their thermodynamic stability and, eventually, B–B bonding.

The geometry of the B–C–N and B–N–C linkage in the cyano-bridged dimers is an interesting feature. One would expect these to be linear by the 'textbook' tenets of VSEPR and relatedly, in the absence of any constraints, one would expect linear B–C–N–B (and B–N–C–B) units as well. By the rules of geometry, both B–C–N–B (and B–N–C–B units) cannot be linear and form a six-membered ring. (The sum of the internal angles of planar hexagon equals 720° and so the local C–B–C, C–B–N and N–B–N angles would have to be 0°, an obvious impossibility.) Furthermore, we recognize these $C_2H_4B_2N_2$ species as isolectronic to the unreasonably strained cyclohexa-1,4-diyne

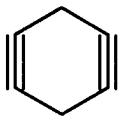

and so the B–C–N–B units must contain bent B–C–N and/or B–N–C subunits. If the local C–B–C, C–B–N and N–B–N angles were roughly tetrahedral, i.e. *ca.* 109°, then the remaining angles would have to equal *ca.* 125°. Alternatively, one can form species with 4-membered B–C–B–C or B-N–B–N rings with concomitantly exocyclic –N and –C, respectively. Given other

§ Author for correspondence.

long-known heteroatom bridged diboranes with 4-membered rings, we chose in this study to include also these latter small ring alternatives (**3a** and **3b**).

3a

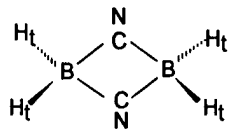

3b

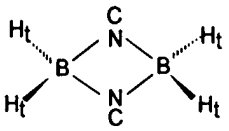

For the sake of comparison of present isomers with our previous study [1] we include in our tables also the non-planar ring 1,4-diaza-2,5-diboracyclohexadiene (**4**) (for simplicity, we intentionally avoid drawing of multiple bonds).

4

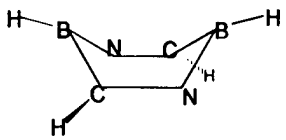

Since CN is an electron withdrawing substituent, its position can significantly reduce the electron density between boron atoms (i.e. affect the B–B bonding), alter the 3c2e-bonding network and, consequently, influence the stability of the resulting isomer. An interesting aspect of the relative dimerization energies of H_2BCN and H_2BNC when compared to the parent BH_3 refers to the description of B_2H_6 as a self-donoracceptor complex of two BH_3's. That is [3], the first BH_3 donates from one of its B–H σ bonds into the vacant π orbital of the second BH_3, while the BH bond of the second BH_3 donates into the π orbital of the first one. By replacing one non-bridging H by CN or NC the donating power of the B–H σ bond is expected to decrease because these groups are electron withdrawing. However, the accepting power of the borane is expected to increase for the same reason. It is therefore not obvious what is the ordering of the relative dimerization energies of BH_3, H_2BCN and H_2BNC.

We anticipate that some of these isomers can serve as good starting points for the models of BNC polymers, either acyclic or containing four-membered rings (similar to, e.g. polyaminosquaranines [4]). Depending on the arrangement of B, C and N atoms and on the presence of a suitable substituent one can tune up the electric properties of such a polymer with the aim of obtaining the most favoured band gap, comparable with that of polyacetylene or polyaminosquaranine.

2. Methods and computational details

Since one of the goals of this paper is to compare the new results for cyanoborane dimers with our preceding study, we have adopted the same computational strategy as in [1]. Therefore, the full details of the computational procedure will not be repeated here. Briefly, it consists of geometry optimizations at the level of second-order many-body perturbation theory, MBPT(2) [5, 6] and the harmonic frequencies calculation for each stationary point to confirm the minimum on the potential energy surface, followed by the evaluation of reaction energies using the single-point higher-level coupled cluster (CC) calculations [7–11]. Both MBPT(2) geometries and the CC single-point energies, CCSD (coupled cluster with singles and doubles) [8] and CCSD + T(CCSD) (CCSD with non-iterative triple-excitation correction) [9], have been obtained from the ACES-II program [12]. In the single point MBPT(2) and coupled-cluster calculations the inner- as well as the corresponding outer-shell orbitals for heavy atoms were left uncorrelated. We note that we have also calculated the CCSD(T) energies (the approximation which adds to CCSD + T(CCSD) one fifth-order term) [10, 11] but the energy differences were negligible, so we will present only CCSD + T(CCSD) data.

In order to analyse the changes in 3c2e-network introduced by substituents (and thus compare diborane with our isomers), we have calculated also the overlap populations and bond orders [13] from MBPT(2) first-order wavefunction. The GAMESS [14] program system was used in these calculations.

Three Gaussian basis sets were used. For the preliminary optimizations and initial guess of the hessians the DZ basis was selected [15]. Final geometry tuning and the single-point CC calculations were performed with the DZP basis set [16 (a)]. To compare the performance of DZP basis set and to describe better the (possible) intricacies of higher order dynamic correlation effects in relative energies, namely, in the isomers ordering and the formation from cyanoborane monomers, we have repeated the single-point coupled cluster calculations for H_2BCN, H_2BNC, **1a**, **1b**, **2a**, **2b**, **3a**, **3b** with the cc-PVTZ basis set [16 (b)].

3. Results and discussion

The optimal MBPT(2)/DZP geometry parameters for $C_2H_4B_2N_2$ molecules are listed in table 1 (full description of Z-matrices for ACES-II as well as the geometries of subsystems are available from I.C. upon request). The overlap populations and bond orders for BB, BH_t, and BH_b bonds in the 3c2e network are collected in table 2. Total and relative energies are in tables 3–6. All the data obtained with cc-PVTZ basis set are in italics in tables 3–6. The effects of electron correlation and basis set on

Table 1. Geometries of $C_2H_4B_2N_2$ isomers and related subsystems (bond lengths in Å, angles in degrees).

1a (C_{2h}): BB = 1.7748, BH_t = 1.1872, BH_b = 1.3272, BC = 1.5537, CN = 1.1890, BH_bB = 83.92, $\angle H_bBH_t$ = 109.53, $\angle H_tBC$ = 121.51, $\angle BCN$ = 179.10

1b (C_{2h}): BB = 1.7836, BH_t = 1.1863, BH_b = 1.3314, BN = 1.4582, NC = 1.1972, $\angle BH_bB$ = 84.11, $\angle H_bBH_t$ = 109.81, $\angle H_tBN$ = 121.52, $\angle BNC$ = 178.58

2a (C_{2v}): BB = 1.7770, BH_t = 1.1877, BH_b = 1.3383, $B'H_b$ = 1.3174 (B′ is bound to CN), BC = 1.5556, CN = 1.1893, $\angle B'H_bB$ = 84.00, $\angle H_bBH_t$ = 107.84, $\angle CBC$ = 118.58, $\angle BCN$ = 179.79

2b (C_{2v}): BB = 1.7753, BH_t = 1.1875, BH_b = 1.3201, $B'H_b$ = 1.3401 (B′ is bound to NC), BN = 1.4567, NC = 1.1978, $\angle B'H_bB$ = 83.72, $\angle H_bBH_t$ = 107.29, $\angle NBN$ = 118.01, $\angle BNC$ = 179.93

3a (D_{2h}): BB = 2.0063, BH = 1.1897, BC = 1.7050, CN = 1.1880, $\angle HBH$ = 125.84, $\angle CBC$ = 107.92, $\angle HBC$ = 105.54, $\angle BCN$ = 143.96, $\angle HBCN$ = 67.54

3b (D_{2h}): BB = 2.2455, BH = 1.1889, BN = 1.6437, NC = 1.2096, $\angle HBH$ = 124.13, $\angle NBN$ = 93.83, $\angle HBN$ = 108.66, $\angle BNC$ = 136.92, $\angle HBNC$ = 68.83

Table 2. MBPT(2)/DZP overlap populations (*S*) and bond orders [Mayer] (*BO*) for selected bonds[a].

molecule	B–B	*S*	*BO*	$B–H_t$	*S*	*BO*	$B–H_b$	*S*	*BO*
B_2H_6	1.781	0.268	0.585	1.192	0.856	0.971	1.323	0.398	0.465
1a	1.775	0.232	0.587	1.187	0.828	0.983	1.327	0.374	0.450
1b	1.783	0.203	0.543	1.186	0.800	0.934	1.331	0.344	0.453
2a	1.777	0.197	0.554	1.188	0.824	0.950	1.338	0.422	0.460
							1.317	*0.280*	*0.440*
2b	1.775	0.180	0.508	1.188	0.830	0.954	1.320	0.452	0.497
							1.340	*0.185*	*0.399*
3a	2.006	0.198	0.268	1.190	0.822	0.923			
3b	2.246	0.101	0.098	1.189	0.796	0.931			

[a] Data for B-H_b in italics refer to B bound to cyano/isocyano group (cf. B′ in table 1).

isomer ordering and on various CN/NC isomerization reactions are depicted in figures 1–4.

The nature of 3c2e double bridges in diborane and systems isoelectronic with B_2H_6 was the subject of studies done recently by Trinquier *et al.* [17]. Their main conclusion for B_2H_6 is that each BH_bB bridge is halfway between an allyl-like cation with two electrons in three orbitals in BH and HB bindings and cyclopropenyl-like (aromatic) cation with almost equivalent BH, HB, BB interactions [18]. Let us analyse briefly our results in terms of Mullikan overlap populations and Mayer bond orders. Presumably, Trinquier *et al.*'s results imply that one can expect the bond orders for the bridges to be approximately half of those for the terminal BH bonds.

Our MBPT(2)/DZP B-B bond lengths for H-bridged isomers lie between 1.77–1.78 Å, very close to 1.781 Å, which is the MBPT(2)/DZP B–B bond length in diborane. Note that it is longer by 0.018 Å than the experimental value, 1.763 Å [19], but MBPT(2)/DZP is known to overshoot slightly the bond lengths for the first-row atoms [20]. Thus the B–B bond itself is not a very sensitive measure of the substituent effect in this case. The Mullikan B–B overlap populations correlate loosely with the bond orders and, in general, show decrease of electron density from **1a** to **2b**. The strongest electron 'pumping' towards CN/NC groups occurs in 1,1-position and CN isomers are slightly less electron withdrawing than NC ones. This is reflected also by non-equivalent $B–H_b$ bonds in the $B–H_b–B$ bridges (last three columns in table 2). In **2b**, both bond order and overlap population are lower for the $B–H_b$ bond adjacent to B attached to the isocyano group than the corresponding indices in **2a** (B attached to the cyano group). On the other hand, they are almost identical for 'normal' $B–H_t$ bond. It seems that these simple bond indices are fairly sensitive to small $B–H_b–B$ bond-length fluctuations introduced by the cyano/isocyano-substituents.

To summarize a bit, the 3c2e bonding spreads over the whole BH_bH_bB four-membered ring and is fairly stable (insensitive to change) also for substituted species. The geometrical changes in $B–H_b–B$ bonding introduced by the CN groups are small, approximately ±0.015 Å with respect to B_2H_6. However, putting CN (or NC) *into* this ring in place of bridging hydrogens destroys the BB bonding almost completely. It would be also interesting to have only one CN/NC group in the

Table 3. Total energies (in hartrees) and ZPV corrections (in kJ mol^{-1}). Rows in italics refer to cc-PVTZ basis set.

	-SCF	-MBPT(2)	-CCSD	-CCSD + T(CCSD)	ZPV
1a	236.328532	237.085591	237.117646	237.152273	167.1
	236.372317	*237.285757*	*237.304598*	*237.356366*	—
1b	236.335293	237.055457	237.100372	237.134090	168.0
	236.378764	*237.251812*	*237.284286*	*237.333242*	
2a	236.323959	237.083200	237.114458	237.149371	166.5
	236.367496	*237.283401*	*237.301310*	*237.353432*	
2b	236.334969	237.055808	237.100406	237.134380	166.9
	236.378110	*237.252321*	*237.284427*	*237.333658*	
3a	236.267162	237.035659	237.079918	237.124473	161.9
	236.308729	*237.233383*	*237.249529*	*237.305773*	
3b	236.298457	237.013052	237.073159	237.110082	160.1
	236.340211	*237.205596*	*237.241233*	*237.290254*	
4[a]	236.347257	237.071432	237.113627	237.149339	176.3
$HB(CN)_2$	209.905944	210.539854	210.554260	210.585039	74.1
$HB(NC)_2$	209.929713	210.517057	210.545125	210.574127	74.6
H_2BCN[a]	118.161428	118.520515	118.539986	118.556109	73.7
	118.177118	*118.613775*	*118.627744*	*118.651411*	—
H_2BNC[a]	118.167339	118.512309	118.537689	118.553419	74.3
	118.186461	*118.604451*	*118.624592*	*118.646978*	—
HCN	92.883142	93.172389	93.179790	93.192439	41.3
	92.901051	*93.251236*	*93.253723*	*93.273391*	—
HNC	92.870418	93.143342	93.157007	93.169589	41.5
	92.887916	*93.222801*	*93.231481*	*93.250417*	—
B_2H_6	52.820091	53.037072	53.081420	53.087563	168.5
	52.834917	*53.096664*	*53.133661*	*53.143225*	—
BH_3	26.393117	26.485964	26.509800	26.511221	70.3
H_2	1.130983	1.158418	1.166716	1.166716	27.4
	1.132968	*1.164644*	*1.172332*	*1.172332*	—

[a] Taken from [1].

Table 4. Formation (kJ mol^{-1}) of dicyanodiborane isomers via exchange reactions (data in italics refer to cc-PVTZ basis set):

$$B_2H_6 + 2HCN \rightarrow C_2H_4B_2N_2 + 2H_2 \qquad (\underline{1a}, \underline{2a}, \underline{3a})$$

$$B_2H_6 + 2HNC \rightarrow C_2H_4B_2N_2 + 2H_2 \qquad (\underline{1b}, \underline{2b}, \underline{3b})$$

	(1a)	(1b)	(2a)	(2b)	(3a)	(3b)
SCF	−10.8	−95.4	1.2	−94.5	150.3	68.1
	−3.2	*−89.1*	*9.4*	*−87.4*	*163.7*	*81.1*
MBPT(2)	−54.0	−127.4	−47.7	−128.4	77.1	136.4
	−41.8	*−102.0*	*−35.6*	*−103.3*	*95.7*	*168.7*
CCSD	*−26.5*	*−100.7*	*−18.1*	*−100.8*	*72.6*	*90.3*
	−21.4	*−84.9*	*−12.8*	*−85.2*	*123.2*	*145.0*
CCSD + T(CCSD)	−34.8	−107.1	−27.2	−107.8	38.2	75.9
	−28.9	*−88.9*	*−21.2*	*−90.0*	*103.9*	*144.6*
ΔZPV	−29.2	−28.7	−29.8	−29.9	−34.4	−36.2
ΔH_{298K}	−55.1	−129.9	−48.3	−129.5	13.2	50.3

$-BH_bCNB-$ ring but respective molecule was beyond the scope of the present paper. We will postpone this question to our next paper [21], together with the harmonic vibrational spectra of the present molecules. Another interesting feature is the influence of the CN/NC position in **1a**, **1b**, **2a**, **2b** on the geometry BH_bB bridge. Nitrogen has higher electronegativity than carbon and this is manifested in the slight decrease of bond orders in the 3c2e moiety, most visible for the non-equivalent BH_b bonds in **2a**/**2b** isomers (tables 1 and 2).

Table 5. Formation of $C_2H_4B_2N_2$ isomers from two cyanoborane (**4**, **1a**, **3a**) or two isocyanoborane (**1b**, **3b**) molecules. Data in italics refer to cc-PVTZ basis set. For comparison, $2BH_3 \rightarrow B_2H_6$ complexation energies are given in the last column.

	4	**1a**	**1b**	**3a**	**3b**	B_2H_6[a]
SCF	−64.1	−14.9	−1.6	146.2	95.1	−88.9
	—	*−47.5*	*−15.3*	*119.5*	*85.9*	—
MBPT(2)	−79.8	−117.0	−81.0	14.1	30.4	−171.0
	—	*−152.8*	*−112.7*	*−15.3*	*8.7*	—
CCSD	−88.4	−98.9	−65.6	0.1	5.8	−162.3
	—	*−128.9*	*−92.2*	*15.6*	*20.9*	—
CCSD+T(CCSD	−97.5	−105.2	−71.6	−32.2	−8.5	−171.0
	—	*−140.6*	*−103.1*	*−7.7*	*9.7*	—
ΔZPV	28.8	19.7	19.5	14.4	11.6	27.9
ΔH_{298K}	−79.5	−90.7	−57.1	−22.4	1.8	−150.9

[a] Experimental enthalpy of complexation (−146 ÷ −167), other recent theoretical values are −156.5 (CCSD+T(CCSD)/6−311G**), −148.1 (CCSD+T(CCSD)/DZP) [33], −165.7 (MBPT(4)/6−311G++(3d,f;3p,d) [32] and −166.9 kJ/mol (B3LYP/TZ2Pf) [34].

Table 6. Formation of 1,1-isomers (**2a**, **2b**) from BH_3 and $HB(CN)_2$/$HB(NC)_2$.

	2a	**2b**
SCF	−65.4	−31.9
MBPT(2)	−150.7	−138.6
CCSD	−132.3	−119.4
CCSD+T(CCSD)	−139.4	−128.7
ZPV	22.1	22.0
ΔH_{298K}	−122.9	−112.3

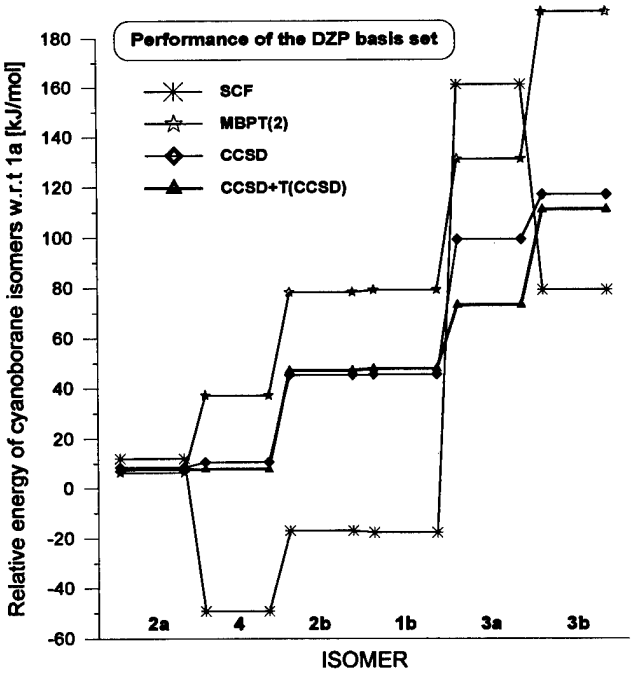

Figure 1. Relative energies of $C_2H_4B_2N_2$ isomers with respect to *trans*-1,2-dicyanodiborane (DZP basis set). The isomers are sorted according to the order of CCSD+T(CCSD) energies (diagram with the thick line).

We now will attempt to rationalize the relative cyano/isocyano isomer stabilities. It appears that electropositive substituents aid the isocyano form, RNC, over the cyano form RCN. For example, it is known that ionic cyanides show effectively spherical or isotropic anion behaviour suggesting the two isomers are of comparable stability [22]. Likewise, LiCN is well known to be a floppy molecule [23] and indeed the LiNC isocyano form is more stable than the cyano one, LiCN. The calculations [24] (including ours) show HCN with the much more moderate electropositive hydrogen is some 60 kJ mol^{-1} more stable than HNC. This is in very good agreement with 66 kJ mol^{-1} obtained from ICR experiments [25]. Explosion calorimetry experiments show CH_3CN to be 99 kJ mol^{-1} more stable than CH_3NC [26], a finding consistent with the higher electronegativity of C than H [27]. The electronegativity of B (cf. BH_2) is somewhat less than H and so we expect the H_2BCN/H_2BNC enthalpy of formation difference to be less than the 60 kJ mol^{-1} for H. Our calculations corroborate this and suggest the difference is now reduced to 6.4 kJ mol^{-1}. What about the case of 1,2-boranediyl derivatives, i.e. those of $-HB(H)_2BH-$? If the two cyano groups do not interact, then one might think the cyano/isocyano difference would be the same as its BH_2 monomer. *A fortiori*, because the two boron species lack vacant π orbitals we expect the NC to even more strongly gain stability.

The only complication is whether the two CN groups electronically interfere with each other. Consider the case of the dicyanoethylene, NCCH=CHCN, which

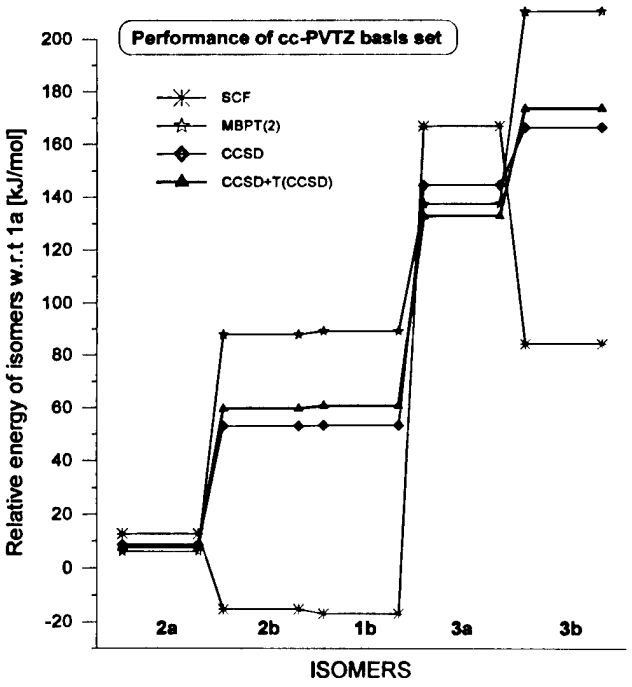

Figure 2. Relative energies of $C_2H_4B_2N_2$ isomers with respect to *trans*-1,2-dicyanodiborane (cc-PVTZ basis set).

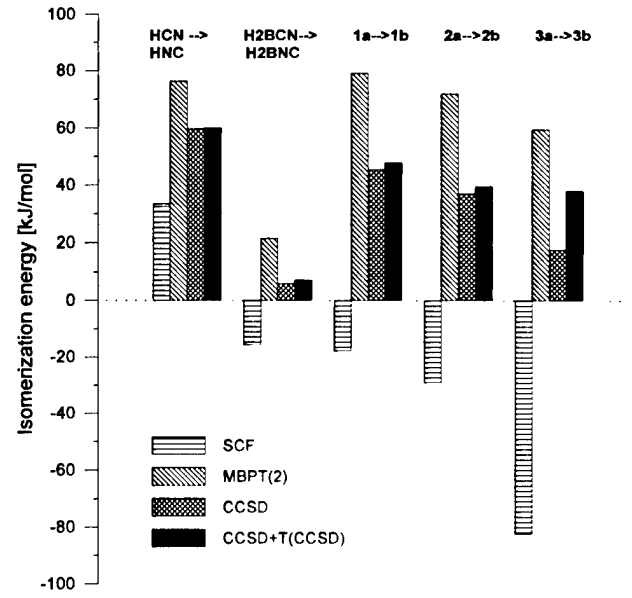

Figure 3. CN/NC-isomerization energies of various $C_2H_4B_2N_2$ systems (DZP basis set). HCN/HNC and H_2BCN/H_2BNC isomerizations are presented for comparison.

(like our choice of dicyanodiborane to which it is isoelectronic) has the two cyano groups *trans* and so there is no steric interaction. If the cyano groups were electronically innocuous, then we would expect the isodesmic reaction

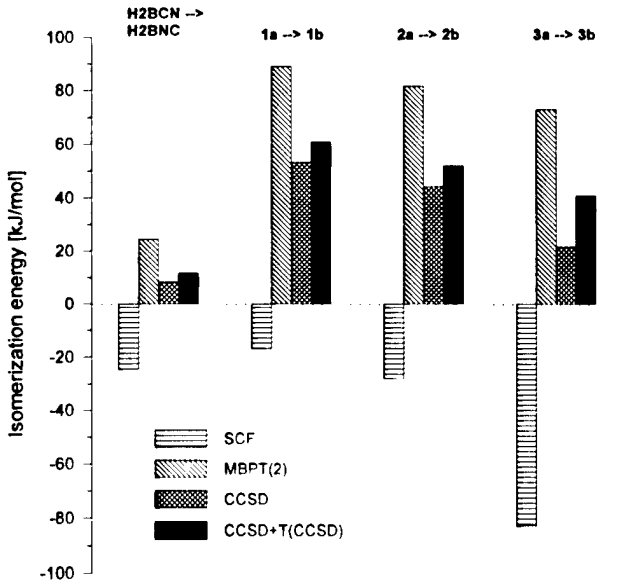

Figure 4. CN/NC-isomerization energies of various $C_2H_4B_2N_2$ systems (cc-PVTZ basis set). H_2BCN/H_2BNC isomerization is presented for comparison.

$$2CH_2{=}CHCN \rightarrow NCCH{=}CHCN + C_2H_4 \qquad (1)$$

to be thermoneutral –indeed, the related methyl reaction

$$2CH_2{=}CHCH_3 \rightarrow CH_3CH{=}CHCH_3 + C_2H_4 \qquad (2)$$

is thermoneutral to within 1 kJ mol^{-1} using enthalpies of formation from our standard thermochemical archive [28]. From data in this same source, we find reaction (1) is exothermic by 20 kJ mol^{-1} or some 10 kJ mol^{-1} per cyano. The dicyanodiborane is expected to have a smaller cyano/cyano interaction because the C–C distance in the dicyanoolefin is *ca.* 1.33 Å while the corresponding distance in the diborane is calculated to be *ca.* 1.78 Å. We thus deduce that the cyano/isocyano difference for the 1,2-disubstituted diborane should be less than 15 kJ mol^{-1} (per cyano) and indeed, the difference is -25 kJ mol^{-1} for DZP basis set and -30 kJ mol^{-1} for cc-PVTZ one (figures 1 and 2).

What then about the 1,1-boranediyl derivatives with

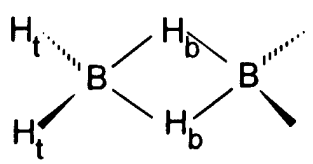

The effect of one cyano group on the other is expected to be much larger here; said differently, the group electro-

negativity of $H_2B(H)_2B(CN)$ may well be larger than BH_2. To illustrate the destabilizing effect of one cyano on the other, we should like to consider isodesmic reactions involving 1,1-dicyanoethylene. However, the desired enthalpy of formation of this latter organic substance is absent. One approach is to consider the isodesmic reaction

$$2CH_3CN \rightarrow CH_2(CN)_2 + CH_4 \quad (3)$$

Accepting the heat of formation of the monocyano compound from [29] this reaction is seen to be endothermic by 45 kJ mol^{-1} while the corresponding methyl reaction

$$2CH_3CH_3 \rightarrow CH_2(CH_3)_2 + CH_4 \quad (4)$$

is exothermic by 11 kJ mol^{-1}. Alternatively, consider the isodesmic reactions

$$CH_2{=}CHCN + NCCH{=}CHCN \rightarrow NCCH{=}C(CN)_2 + C_2H_4 \quad (5)$$

$$CH_2{=}CHCH_3 + CH_3CH{=}CHCH_3 \rightarrow CH_3CH{=}C(CH_3)_2 + C_2H_4 \quad (6)$$

The first reaction is endothermic by yet another 54 kJ mol^{-1}, while the second is again thermoneutral to within 1 kJ mol^{-1}. From either set of isodesmic reactions ((3) and (4), or (5) and (6)), we conclude that the two cyano groups more seriously interact in the 1,1-isomer than in the 1,2-isomer. We would thus expect to preferably favour the cyano isomer over that for the 1,2-case although we cannot say whether the 1,1-dicyano isomer will be preferred over the isocyano isomer. Our calculations show that the cyano compounds (**1a**, **2a**, **3a**) now, in fact, are more stable than their isocyano counterparts (**1b**, **2b**, **3b**) by 20–25 kJ mol^{-1} per cyano group for DZP and 20–30 kJ mol^{-1} for cc-PVTZ basis sets.

Let us proceed through electron correlation effects in the energetic features of the various $C_2H_4B_2N_2$ forms. First of all, we will analyse briefly the resulting CCSD wave function of all the studied isomers in terms of the largest T_1 and T_2 amplitudes to indicate possible importance of the non-dynamical correlation effects. T_1 amplitudes lie below |0.05| for all systems and both basis sets. The T_2 amplitudes are small for all hydrogen-bridged isomers, not exceeding 0.05 in absolute value, for both DZP and cc-PVTZ basis sets. The largest T_2 amplitudes for cyano/isocyano-bridged dimers are slightly higher in DZP (−0.1602 and −0.086 08) but still fairly low in cc-PVTZ basis set (−0.069 54 and −0.044 67). Thus, the single-reference CC approach is sufficient for the present isomers.

The formation of **1a**, **1b**, **2a**, and **2b** from diborane and HCN is predicted to be an exothermic process with moderate to large stabilizing correlation effects. Triple-excitation contribution plays marginal role here. The most exothermic is the reaction leading to **1b**, giving approximately −110 kJ mol^{-1} (based on ΔH_{298K}) per one B–N bond (or −64 kJ mol^{-1} at MBPT(2)). These quantities nicely bracket the result for $-N_3$ substitution calculated by Benard *et al.* [30], their MBPT(2)/6-31 + G* reaction heat for the experimentally observed process [31] $B_2H_6 + 4HN_3 \rightarrow (N_3)_2B(H)_2B(N_3)_2 + 4H_2$ is −306.9 kJ mol^{-1} which gives −76.7 kJ mol^{-1} per one B–N bond. Note that the tetra-azidodiborane is similar to our system **1b** via B–N bonding. The reactions leading to **3a** and **3b** isomers are endothermic and electron correlation is slightly destabilizing for **3b**. For these processes, MBPT(2) (compared to CC data) is quite irregular and thus unreliable. The extension of the basis to cc-PVTZ set reduces the exothermicity of these reactions by 6 kJ mol^{-1} (for **1a** and **2a**), 18 kJ mol^{-1} (for **1b** and **2b**) and increases endothermicity for **3a** and **3b** by 66 and 69 kJ mol^{-1}, respectively (CCSD + T(CCSD) energies).

Data in table 5 monitor the changes in dimerization energies (with respect to B_2H_6) introduced by substitution, **1a** being the most stable isomer for DZP basis set. First, let us mention the estimate of the experimental dimerization energy of diborane (−146 to −167 kJ mol^{-1}) suggested by Page *et al.* [32], which matches quite well with our ΔH_{298K}, as well as the previous theoretical results [32–34]. This gives additional credibility to the highest computational level used in our calculations. The order of dimerization energies from table 5 is as follows: $BH_3 > H_2BCN > H_2BNC$. Thus, the donating power of the BH σ bond and the accepting power of the borane are almost balanced in **1a** (cf. section 1), while the lower dimerization energy of **1b** signals that the decrease in the donating power of BH prevails over the (weaker) increase of the accepting power of the borane. The electron correlation contributes significantly to the stabilization of $C_2H_4B_2N_2$ (the trend already noticed in [1]), however, in 3c2e systems the correlation effects seem to be even more important and, in the complexation of **1a**, **1b**, **3a** and **3b**, the role of triples is by no means negligible. Though μ,μ(C,C)-dicyanodiborane and its iso-cyano analogue are less stable than 1,1- or 1,2-isomers, the planarity of their BCBC (BNBN) rings and the presence of π system makes them attractive targets for future polymer simulations. The formation of 1,1-isomers (**2a**, **2b**) from BH_3 and $HB(CN)_2/HB(NC)_2$ (table 6) is also exothermic and exhibits similar trends but the role of triples is very small. Interestingly, although the SCF complexation energy of **1b** is almost zero, the corresponding ΔH_{298K} is competitive with that of B_2H_6, the stability of **1b** is attributed exclusively to correlation contribution (note that MBPT(2) is just half of CCSD + T(CCSD) result).

While the cc-PVTZ dimerization energies are lower for **1a** (by 35 kJ mol^{-1}) and **1b** (by 32 kJ mol^{-1}), they are higher for **3a** (by 25 kJ mol^{-1}) and **3b** (by 18.5 kJ mol^{-1}).

The ordering of individual isomers (figure 1) reveals few additional features of the electron correlation effects. While the SCF pattern exhibits significant irregularities compared to the best levels of the theory, the MBPT(2) one indicates quite uniform overshooting with some serious quantitative deviations from the more elaborated CCSD and CCSD + T(CCSD) levels. The differences between CCSD and CCSD + T(CCSD) ordering are less significant but still above the assumed threshold of chemical accuracy, indicating importance of the triples. The ordering of isomers obtained with DZP and more polarized and diffuse cc-PVTZ basis set shows basically the same pattern (figures 1 and 2). The correlation effects are negligible for the change in the *position* of cyano/isocyano group (i.e. 1,1- or 1,2- in **1a**, **2a**, **1b**, and **2b**), while the change in the NC/CN bonding (or insertion to μ,μ- position, **3a** and **3b**) is accompanied with larger ones. The results obtained with cc-PVTZ basis indicate that the improvement in the wavefunction has almost no effect on SCF relative energies, little effect on MBPT(2) ones, but is accompanied by a moderate destabilizing effect (+60 kJ mol^{-1}) of higher order excitations for **3a** and **3b** with respect to **1a**.

Finally, let us comment on the correlation effects that can be observed in the CN/NC isomerizations (figures 3 and 4). In the DZP basis set, the HCN/HNC isomerization the SCF is at least qualitatively correct (although it amounts approximately to one half of the total reaction energy) but this is not the case for $H_2BCN \Leftrightarrow H_2BNC$ reaction. The **1a**/**1b** process is optically similar to $HCN \Leftrightarrow HNC$, except that the signs are reversed and the MBPT(2) fails very badly to fit into the pattern. In the remaining two isomerizations **2a**/**2b** and **3a**/**3b** the correlation contributions destabilize NC isomers in a similar way. From the present results, it follows that for the boranes the SCF approximation erroneously favours the NC isomers, while the correlation reverts this order, the corresponding effects are regular and relatively large, ranging from +60 to +120 kJ mol^{-1}. The extension of the basis set has little (destabilizing) effect on the isomerization energies, we can see that the cc-PVTZ results are almost identical with DZP ones.

4. Conclusions

In this study we have predicted some properties of a few new hypothetical $C_2H_4B_2N_2$ isomers. Although the calculations utilize moderate level of theory (CCSD + T(CCSD)/DZP and CCSD + T(CCSD)/cc-PVTZ), we consider it to be sufficient for our goals, since the primary aim of this study was to investigate the *trends* within the group of substituted boranes. They are sound for both basis sets. The most stable isomer appears to be *trans*-1,2-dicyanodiborane which exhibits some structural and energetic similarities with B_2H_6. The substitution of H_t by CN (or NC) in B_2H_6 (in terms of bond orders) results in weakening of the double bridge 'through-space' interactions, while the substitution of H_b practically destroys the B B bonding. However, the respective μ,μ-isomers posses the planar 4-membered ring with –CN (–NC) exocyclic group (π system) which makes them interesting for further investigations and/or polymer simulations. For the DZP basis set we have found strong and stabilizing effect of electron correlation (in some cases is comparable or even larger than SCF reaction energy) in the formation of the 3c2e-molecules and also strong and destabilizing correlation effects for the isomerizations. In accord with our previous studies [1] the performance of MBPT(2) for this type of molecules was found to be very poor. The use of the more flexible cc-PVTZ basis yielded a smaller effect of electron correlation in exchange reactions (table 4) and confirmed large correlation effects in dimerization reactions (table 5), the ordering of the present isomers and CN/NC isomerizations are less basis set sensitive.

I.C. would like to thank the Fulbright Commission (Slovakia) and CIES (Washington) for the Fulbright fellowship in the academic year 1996/97 that allowed him to become a visiting professor at the University of Maryland Baltimore County with J.F.L, the Fulbright Faculty Associate. We are grateful to the University Computing Services –UMBC and Computer Centre of Faculty of Sciences, Comenius University, Bratislava for computer time. Part of this project was supported by the Slovak Grant Agency, grant no. 1/4227/97.

References

[1] Cernusak, I., Urban, M., Stanton, J. F., and Bartlett, R. J., 1994, *J. phys. Chem.*, **98**, 8653; 1992, *J. Am. chem. Soc.* **114**, 10955.
[2] Lipscomb, W. N., 1993, *Boron Hydrides* (New York, Amsterdam: W. A. Benjamin, Inc.).
[3] Dixon, D. A., Peppenberg, I. M., and Lipscomb, W. N., *J. Amer. chem. Soc.*, **96**, 1325.
[4] Brocks, G., 1995, *J. chem. Phys.*, **102**, 2522.
[5] Bartlett, R. J., 1989, *J. phys. Chem.*, **93**, 1697.
[6] Bartlett, R. J., Stanton, J. F., and Watts, J. D., 1991, *Advances in Molecular Vibrations and Dynamics*; Vol.18 (Greenwich, CT: JAI Press, Inc.), pp. 139 167; Salter, E. A., Trucks, G. W., and Bartlett, R. J., 1989, *J. chem. Phys.*, **90**, 1752; Gauss, J., Stanton, J. F., and Bartlett R. J., 1991, *J. chem. Phys.*, **95**, 2623.
[7] Cizek, J., 1966, *J. chem. Phys.*, **45**, 4256; 1969, *Adv. chem. Phys.*, **14**, 35.
[8] Purvis, G. D., and Bartlett, R. J., 1982, *J. chem. Phys.*, **76**, 1910.

[9] URBAN, M., NOGA, J., COLE, S. J., and BARTLETT, R. J., 1985, *J. chem. Phys.*, **83,** 4041.
[10] BARTLETT, R. J., WATTS, J. D., KUCHARSKI, S. A., and NOGA, J., 1990, *Chem. Phys. Lett.*, **165,** 513.
[11] RAGHAVACHARI, K., TRUCKS, G. W., POPLE, J. A., and HEAD-GORDON, M., 1989, *Chem. Phys. Lett.*, **157,** 479.
[12] Advanced Concepts in Electronic Structure (ACES II): an *ab initio* program system for performing MBPT/CC calculations, including analytical gradients, methods for excited states, and a number of other unique methods, Authors: STANTON, J. F, GAUSS, J., WATTS, J. D., LAUDERDALE, W. J., and BARTLETT, R. J., Quantum Theory Project, University of Florida, Gainesville, FL, 1991. Basis sets were obtained from the Extensible Computational Chemistry Environment Basis Set Database, Version 1.0, as developed and distributed by the Molecular Science Computing Facility, Environmental and Molecular Sciences Laboratory which is part of the Pacific Northwest Laboratory, PO Box 999, Richland, Washington 99352, USA, and funded by the US Department of Energy. The Pacific Northwest Laboratory is a multi-program laboratory operated by Battelle Memorial Institute for the U.S. Department of Energy under contract DE-AC06-76RLO 1830. Contact David Feller, Karen Schuchardt, or Don Jones for further information.
[13] MAYER, I., 1983, *Chem. Phys. Lett.*, **97,** 270; 1985, *Chem. Phys. Lett.*, **117,** 396; 1985, *Theoret. Chim. Acta*, **67,** 315; 1986, *Int. J. quantum Chem.*, **29,** 73; 1986, *Int. J. quantum Chem.*, **29,** 477.
[14] SCHMIDT, M. W., BALDRIDGE, K. K., BOATZ, J. A., ELBERT, S. T., GORDON, M. S., JENSEN, J. H., KOSEKI, S., MATSUNAGA, N., NGUYEN, K. A., SU, S. J., WINDUS, T. L., DUPUIS, M., and MONTGOMERY, J. A., 1993, *J. comput. Chem.*, **14,** 1347.
[15] DUNNING, JR, T. H., 1970, *J. chem. Phys.*, **53,** 2823.
[16] (a) REDMON, L. T., PURVIS, G. D., and BARTLETT, R. J., 1979, *J. Amer. chem. Soc.*, **101,** 2856; (b) DUNNING, JR, T. H., 1989, *J. chem. Phys.*, **90,** 1007.
[17] TRINQUIER, G., MALRIEU, J.-P., and GARCIA-CUESTA, I., 1991, *J. Amer. chem. Soc.*, **113,** 6465; Trinquier, G., and MALRIEU, J.-P., 1991, *J. Amer. chem. Soc.*, **113,** 8634.
[18] DE KOCK, R. L., and BOSMA, W. B., 1988, *J. chem. Educ.*, **65,** 194.
[19] HARMONY, M. D., LAURIE, V. W., KUCZKOWSKI, R. L., SCHWENDEMAN, R. H., RAMSAY, D. A., LOVAS, F. J., LAFFERTY, W. J., and MAKI, A. G., 1979, *J. phys. chem. Ref. Data*, **8,** 619.
[20] URBAN, M., CERNUSAK, I., KELLO, V., and NOGA, J., 1987, *Methods in Computational Chemistry*, Vol.1, edited by S. Wilson (New York, Plenum Press).
[21] CERNUSAK, I., and LIEBMAN, J. F., in preparation.
[22] MEOT-NER (MAUTNER), M., CYBULSKI, S. M., SCHEINER, S., and LIEBMAN, J. F., 1988, *J. phys. Chem.*, **92,** 2738.
[23] DORIGO, A., SCHLEYER, P. V. R., and HOBZA, P., 1994, *J. Comput. Chem.*, **15,** 322; MAKAREWICZ, J., and HA, T.-K., 1994, *J. molec. Structure THEOCHEM*, **121,** 149; ADAMOWICZ, L., and FRUM, C. I., 1989, *Chem. Phys. Lett.*, **157,** 496.
[24] FANG, W.-H., LIU, R.-Z., and YOU, X.-Z., 1994, *Chem. Phys. Lett.*, **226,** 453; ABASHKIN, Y., and RUSSO, N., 1994, *J. chem. Phys.*, **100,** 4477; KOBAYASHI, R., AMOS, R. D., and HANDY, N. C., 1994, *J. chem. Phys.*, **100,** 1375; STANTON, J. F., and GAUSS, J., 1994, *J. chem. Phys.*, **100,** 4695.
[25] PAU , C. F., and HEHRE, W. J., 1982, *J. phys. Chem.*, **86,** 321.
[26] BAGHAL-VAYJOOEE, M. H., COLLISTER, J. L., and PRITCHARD, H. O., 1977, *Can. J. chem.*, **55,** 2634.
[27] POPPINGER, D., and RADOM, L., 1977, *J. Amer. chem. Soc.*, **99,** 7806.
[28] PEDLEY, J. B., NAYLOR, R. D., and KIRBY, S. P., 1986, *Thermochemical Data of Organic Compounds*, 2nd edition (New York: Chapman & Hall).
[29] AN, X. W., and MANSSON, M., 1983, *J. Chem. Thermodyn.*, **15,** 287.
[30] BENARD, D. J., BOEHMER, E., MICHELS, H. H., and MONTGOMERY, JR, J. A., 1994, *J. phys. Chem.*, **98,** 8952.
[31] WIBERG, E., and MICHAUD, H., 1954, *Z. Naturforsch*, **9B,** 497.
[32] PAGE, M., ADAMS, G. F., BINKLEY, J. S., and MELIUS, C. F., 1987, *J. phys. Chem.*, **91,** 2675.
[33] STANTON, J. F., BARTLETT, R. J., and LIPSCOMB, W. N., 1987, *Chem. Phys. Lett.*, **138,** 525.
[34] BARONE, V., ORLANDINI, L., and ADAMO, C., 1994, *J. phys. Chem.*, **98,** 13 185.

MOLECULAR PHYSICS, 1998, VOL. 94, NO. 1, 157–171

A state-specific multi-reference coupled cluster formalism with molecular applications

By U. S. MAHAPATRA, B. DATTA and D. MUKHERJEE†
Department of Physical Chemistry, Indian Association for the Cultivation of Science, Calcutta 700032, India

We present in this paper a state-specific coupled cluster method based on a reference function composed of determinants spanning a complete active space (CAS). The method treats all the reference determinants on the same footing and is hence expected to provide a uniform description over a wide range of molecular geometries. The combining coefficients are determined by diagonalizing an effective operator in the CAS and are thus completely flexible, and not constrained to pre-assigned values. The method uses a separate cluster operator for exciting to virtual functions from each reference determinant. The linear dependence implicit in this choice of cluster operators is eliminated by invoking suitable sufficiency conditions. The choice is dictated to ensure size-extensivity. The use of a CAS also guarantees size-consistency. Illustrative applications to the H_8 model system and ground state potential curve for Li_2 indicate both the accuracy of the method and its ability to bypass intruders.

1. Introduction

The coupled cluster (CC) approach has turned out over the last two decades as one of the most powerful theoretical tools for treating electron correlation for small to medium-sized molecules to a high accuracy. The exponential representation of the wave-operator provides in a powerful and efficient manner the desirable property of size-extensivity [1] (and often size-consistency [2]) of the computed energies. The most extensively used version of the CC approach is the single-reference coupled cluster method (SRCC) [2–5] which is ideally suited to describe closed-shell states. With the advent of more and more powerful computers in the last decade, the SRCC method has emerged as a predictive tool for high precision calculations for closed-shell states around equilibrium geometry—evolving from the truncation scheme employing single- and double-cluster operators (CCSD scheme) [6], to the more elaborate approximate [7] or exact inclusion of triples [8, 9] or even full inclusion of quadruples [10]. The SRCC method has thus steadily grown in power and degree of sophistication over the years. As a routine tool, the CCSD with an approximate inclusion of triples [7] provides satisfactory energies. The performance of the SRCC becomes poorer, however, for even the closed-shell states which are away from the equilibrium geometry, as one obtains in the dissociative or curve-crossing regions. In both these situations, there are functions which tend to become quasi-degenerate with the reference function. The three- and higher-body cluster operators then become very prominent and the truncation schemes at low cluster-ranks become progressively inaccurate with the increase of the degree of quasi-degeneracy. In addition, many excited or ionic states of molecules possess pronounced multi-reference character. This motivated a search for multi-reference coupled cluster (MRCC) methods.

Most of the early MRCC formulations were inspired by the formal developments of multi-reference many-body perturbation theory (MRMBPT) [11] and were based on the concept of effective hamiltonians. The reference determinants comprising the so-called model space provide the starting reference functions written as their combinations. Over the last two decades there have appeared in the literature several variants of MRCC theories, which can be broadly classified into two categories. One of them, now known as the valence-universal CC methods, uses a single wave-operator to describe not only the functions generated from the parent model space with a given number of occupancies but also from all the functions of model spaces with fewer valence occupancies [12–16]. If the functions generated from a model space of fixed valence occupancy are considered, the MRCC methods are said to belong to the valence-specific variety [17–22]. The valence-universal methods are more suited to study spectroscopic energy differences such as excitation energy, ionization potential or electron affinity etc., while the valence-specific methods are more suited to study several excited states of a molecule simultaneously, or for computing potential energy surfaces (PES). In both versions, size-extensivity is guaranteed by choosing the model space to

† Author for correspondence.

0026–8976/98 $12·00

be complete. Although there were some initial doubts, it was found possible to maintain size-extensivity even for incomplete model spaces, provided one chooses the normalization of the wave-operator and the attendant decoupling conditions for it in an appropriate manner [23]. MRCC formulations starting from incomplete model spaces for both valence-universal [23–26] and valence-specific [27, 28] categories have appeared in the literature. For some recent reviews, we refer to [29–32].

A serious limitation of the effective hamiltonian-based many-body methods is the appearance of intruder states [33, 34]. Methods with complete model space almost always suffer from convergence problems because of intruders. With incomplete model spaces, intruders are somewhat less threatening. They can, in fact, be almost completely avoided for states computed at fixed nuclear geometries or around a limited area of the PES, as at the dissociation region and real or avoided crossings [26, 29–32]. The main stumbling block for a divergence-free performance of MRCC methods for studying PES seems to be the inability to discern a unique as well as a stable model space throughout the entire region of the PES, for there are different intruders in the different regions of the PES [35]. This is the reason behind the widespread interest in recent years to formulate state-specific MRCC formulations which focus on only one specific state of interest, rather than generating many states in a blanket manner from an effective hamiltonian, some of which may be poorly described by the chosen model space. If one could abandon the requirement that all the roots of the effective hamiltonian are the eigenvalues of the parent hamiltonian, then one can exploit this to advantage for generating only those roots as the eigenvalues of H which are untrammeled by intruders and not impose the constraint that the other roots, affected by intruders, are eigenvalues of H.

Such a possibility was first exploited by Kirtman [36], who partitioned the model space into a main and an intermediate buffer subspace. The intermediate subspace interacts strongly with intruders while the main subspace does not. The functions of the main model space are allowed to mix with the functions of the orthogonal virtual complement via the wave operator but those in the intermediate subspace are allowed to remain uncorrelated. This strategy avoids intruders. This was generalized by Malrieu *et al.* [37], who provided a systematic method of 'intermediate hamiltonians' using the above partitioning concept. They also put forward a general scheme for determining the pseudo-wave operator which generates the eigenvalues of H for functions dominated by the reference determinants of the main model space. Unlike Kirtman [36], Malrieu *et al.* [37] allowed the intermediate functions to mix with the virtuals, but not as dictated by Bloch equation. This mixing was brought in only to enhance the convergence of the pseudo-wave operator contribution for the main roots (which are eigenvalues of H). Other roots are arbitrary. Although the preliminary results were encouraging, the formalisms were not size-extensive. Some later variants [38–40] also had the same limitations.

Size-extensive intermediate hamiltonians in the coupled cluster framework were systematically developed in our group [41, 42]. These formulations essentially made use of projectors to ensure that the equations determining the main roots are consistent with Schrödinger equations for these roots, while those for the extraneous roots have shifts in the definition of unperturbed energies for the intermediate reference determinants to avoid intruders. Koch [43] also proposed a many-body version of an intermediate hamiltonian using shifts for the intermediate functions, but could not prove size-extensivity of his formulation. Another size-extensive formulation was proposed by Datta *et al.* [44] by transcribing the MRCC equations into CI-like pseudo-eigenvalue equations in the union space of the model determinants and the virtuals reached by the cluster operators. The roots of the dressed hamiltonian defined in this union space then generate both the roots of the hamiltonians targeted by the MRCC formalism and the 'excited' roots as extraneous roots. With suitable root-homing procedures, the method obviates the convergence difficulty of the traditional MRCC formulations. This same strategy was also exploited by Malrieu *et al.* [39] in their dressed-CI formulation of intermediate hamiltonians.

There is a formal difficulty in a straightforward development of a state-specific MRCC formalism. If the cluster operators are chosen to excite from all the reference determinants to all the virtual functions, there are redundancies in the cluster operators [29]. Two strategies have been put forward to resolve this 'redundancy problem'. In one, the linearly dependent cluster operators are excluded. In the other, they are deliberately retained and auxiliary equations to determine them are supplied as sufficiency conditions. Approximate state-specific versions using the first strategy were suggested by several authors [45–47] who avoided the redundancy problem by a pre-selection of the cluster operators. This, however, raises the question of the uniqueness of the choice, since powers of cluster operators would generate different multiply excited virtual functions depending on the selection. For an early discussion of this aspect, we refer to [29]. Recently Meller *et al.* [48] proposed a cluster expansion approach to generate a specific state, starting with a multi-determinantal reference function. They used all the possible excitations from the model to

the virtual determinants in their cluster operator. The redundancy in the cluster amplitudes was eliminated by postulating reasonable sufficiency conditions, hence this method uses the second strategy. These authors also showed the size-consistency of their formulation using localized representation of the orbitals. Since they discussed only the leading terms of their working equations, it is difficult to discern how a manifestly size-extensive general formulation would emerge from their sufficiency conditions. Datta and Mukherjee [49] and Sinha Mahapatra *et al.* [50] suggested two versions of an explicitly size-extensive state-specific MRCC theory via the use of sufficiency conditions which amounted to separation of dynamical and non-dynamical correlation effects. There is a pre-eminence of one reference determinant in this formulation which defines the dynamic correlation, and in this sense the method is not tailored to treat the more general cases where the importance of the reference determinants change drastically over the entire region of the PES. Very recently, we have developed another state-specific MRCC theory [51], where all the reference determinants are treated on the same footing. Appropriate sufficiency conditions were posited with an eye to a strict maintenance of size-extensivity. Unlike the conditions used by Meller *et al* [48], the conditions used by us guarantee size-extensivity in a natural and transparent manner. In all these MRCC formulations, an essential step is the setting up of an eigenvalue equation for generating the combining coefficients via the diagonalization of an effective operator. The combining coefficients are thus completely flexible and not constrained to remain fixed at some pre-assigned values. We want to call this type of state-specific formulation as using a 'decontracted' or 'relaxed coefficients' mode of description.

There is an alternative mode of description, proposed long ago by Silverstone and Sinanoglu [52], where a multi-reference cluster expansion is performed from a combination of functions. Virtual functions were added to the reference functions by a cluster expansion with respect to each reference determinant. The prior fixing of the combining coefficients in this formulation confers a 'contracted' or 'frozen coefficients' description to the full function generated by the cluster expansion. Silverstone and Sinanoglu overcame the problem of redundancy by postulating what is called the anonymous parentage approximation. This imposed severe unphysical restrictions to the working equations and the method was not very successful. An essential modification of this approach in the perturbative context was suggested by several workers where either the redundancy is eliminated by the Gram–Schmidt [53, 54] procedure or the components of the wave operator are obtained by projecting only on the distinct virtual functions [55, 56]. We should also mention in this context that several MR versions of coupled electron pair theories also use a frozen description of the coefficients of the reference function [57–59].

An MRCC formulation of the 'frozen coefficients' variety was proposed recently by Mukherjee [60–62]. He developed the notion of normal ordering and the associated reordering theorem with respect to the entire multi-determinant function, and postulated an exponential type of wave-operator in this new normal order to generate the full function. The cluster operators in this formulation were also defined with respect to the entire reference function. This method may be rightly viewed as one specific coupled cluster type realization of the perturbative versions of [53, 54]. We have discussed in [51] the relative efficacies of this method *vis-à-vis* the 'relaxed coefficients' theory. An alternative way to look at the reordering problem, along with a pedagogic presentation of the background, was suggested by Kutzelnigg and Mukherjee [63].

We want to present in this paper the first molecular applications of the MRCC theory formulated in [51]. In section 2, we will give a self-contained exposition of the method. This will serve both to introduce the relevant concepts and notations and also to provide a perspective regarding the relation of the method with other allied formulations. Section 3 will discuss the algorithmic considerations and truncation schemes needed for implementing the method, as well as the pilot results. Section 4 will contain the concluding remarks.

2. A state-specific coupled cluster theory with a relaxed reference function

The formulation of a state-specific coupled cluster theory that we are going to describe would utilize a relaxed description of the multi-determinantal reference function. This implies that the combining coefficients of the reference determinants constituting the reference function would not be fixed at some pre-determined values, but would be iteratively updated along with the cluster amplitudes themselves. We shall start with a set of reference determinants which ensure a proper dissociation of a molecular state into appropriate fragments. Several physically motivated choices of such reference functions are possible, depending on the degree of elaborateness incorporated in the reference description. The most common choices are (a) a complete active space (CAS) reference function, of either a simple CI form (a CAS-CI) or of the more elaborate CAS-based multi-configuration self-consistent field (CAS-SCF) variety, (b) a CI or a MCSCF function on a quasi-complete active space (QCAS), a convenient incomplete active space respecting size-extensivity of its energy, studied by Lindgren [64] and others [23, 25, 28], or

(c) a strongly orthogonal generalized valence-bond (SO-GVB) function. Following the traditional convention of quasi-degenerate many-body nomenclature, we shall term the doubly filled orbitals as inactive 'core' orbitals, the partially filled occupied ones as active 'valence' orbitals and the virtual orbitals not contained in the reference function as inactive 'particle' orbitals. We shall designate the core orbitals by the Greek indices $\alpha,\beta,\ldots$ etc, the valence orbitals by English letters u, v, w, ... etc, and the virtuals by p, q, r,...etc. Arbitrary orbitals will be denoted by $a,b,\ldots$ etc. In all three choices for the model space mentioned above, the energy obtained from the reference function is size-extensive, and the functions support dissociation of the molecular state into fragments describable by orbitals obtained by a localizing transformation of the 'core' orbitals and the 'valence' orbitals onto the fragment components. Consequently, in all three choices, a cluster expansion decomposition of the combining coefficients of the reference determinants always leads to *connected* clusters. This property would turn out to be very crucial for guaranteeing both size-extensivity [1] and size-consistency [2] of our formulation. Considerable simplification is achieved in our formalism when the reference space is complete and we shall develop the present formulation with this choice (i.e. choice (a)). Formulations with more restricted choices for the reference space (i.e. of the types (b) and (c)) will form the topic of a future communication.

A CAS-CI or a CAS-SCF type of reference function ψ_0 can be expressed as a combination of reference determinants ϕ_μ's

$$\psi_0 = \sum_\mu c_\mu \phi_\mu, \tag{1}$$

where the set $\{\phi_\mu\}$ contains all the determinants of the CAS space. As we emphasized earlier, the combining coefficients for such a function can be generically represented in terms of a cluster expansion involving connected cluster amplitudes, using any ϕ_μ acting as the pivotal function for effecting the cluster expansion:

$$c_\nu/c_\mu = \langle\phi_\nu|\exp(\sigma_\mu)|\phi_\mu\rangle. \tag{2}$$

ψ_0 can thus be written in terms of the pivotal function as

$$\psi_0 = \exp(\sigma_\mu)\phi_\mu c_\mu, \tag{3}$$

The clusters σ_μ in equation (3) are manifestly connected. The operators in σ_μ involve excitation from the active orbitals of ϕ_μ to all other active orbitals defining the determinants ϕ_ν, with $\nu \neq \mu$. σ_μ's may thus be looked upon as 'internal' cluster operators.

In our formulation, we shall generate the exact function ψ as a cluster expansion in the manner advocated by Silverstone and Sinanoglu [52] but, unlike in their formulation, we shall allow our coefficients c_μ to relax to their exact values as a result of the mixing of the virtual functions. Transcribed into the many-body language, this amounts to the use of a separate exponential operator for each ϕ_μ, with 'external' cluster operators T_μ exciting from the corresponding ϕ_μ's to all the virtual determinants. Thus, we shall posit the following *Ansatz* for ψ:

$$\psi = \sum_\mu \exp(T^\mu)\phi_\mu c_\mu. \tag{4}$$

T^μ involves annihilation operators which delete electrons from ϕ_μ and creation operators for orbitals generating virtual determinants. There is no need to use 'spectator' orbitals. Also, we exclude from T^μ all such operators whose action on ϕ_μ is trivially zero. This implies that we exclude from T^μ all such operators which try to either excite from active orbitals not occupied in ϕ_μ, or excite into active orbitals already occupied in ϕ_μ. Such a cluster expansion representation is also reminiscent of the effective hamiltonian based multi-root approach of Jeziorski and Monkhorst [17], who used this same cluster expansion to convert all the N reference functions that can be constructed from the N reference determinants. In our state-specific formulation, we shall confine our attention to just the function of our interest, namely ψ, as in equation (4). This same Ansatz has also been used recently in a state-specific context by Meller *et al.* [48]. Since each T^μ excites to all the virtual functions from ϕ_μ, we necessarily encounter *redundancy* of the cluster amplitudes. As explained in section 1, we shall resolve the redundancy by invoking sufficiency conditions which would be physically appealing and would guarantee extensivity of the cluster amplitudes in a natural manner.

Since each ϕ_μ has different sets of active orbitals, any specific core-to-particle excitation would lead to a *different* virtual determinant from each ϕ_μ. It then follows that the cluster operators of the form $\langle pq\cdots|t^\mu|\alpha\beta\cdots\rangle a_p^\dagger a_q^\dagger \cdots a_\beta a_\alpha$, inducing core to particle excitations are all *linearly independent*. This is however not so for excitations involving active orbitals. For example, if two determinants ϕ_μ and ϕ_ν differ by a set of active orbitals, excitations from these sets in ϕ_μ and ϕ_ν to a common set of particle orbitals would generate the same virtual determinant. Thus, we would encounter redundancy only for the cluster operators involving active orbitals, and would need to take care of the redundancy only for such cluster operators. We will invoke suitable sufficiency conditions to resolve the redundancy problem.

ψ satisfies the Schrödinger equation with the eigenvalue E:

$$H\psi = H\sum_\mu \exp(T^\mu)\phi_\mu c_\mu = E\psi. \tag{5}$$

The coefficients c_μ for a CAS-CI or a CAS-SCF based ψ

can be determined by projecting equation (5) onto the reference determinants:

$$\sum_{\nu}\langle\phi_\mu|H\exp(T^\nu)|\phi_\nu\rangle c_\nu = Ec_\mu. \tag{6}$$

Evaluation of the matrix elements of $H\exp(T^\nu)$ between ϕ_μ and ϕ_ν, is particularly convenient if we rewrite H in normal order with respect to ϕ_ν as vacuum. This simplification of computation of matrix elements was first used in the context of perturbation theory by Hose and Kaldor [65]. This was carried over to MRCC by Jeziorski and Monkhorst [17] and has since then been exploited by many workers [18, 27, 28]. Since T^ν has only excitations out of ϕ_ν, it has only hole–particle creation operators defined with respect to ϕ_ν and consequently $\exp(T^\nu)$ is in *normal order* with respect to ϕ_ν. Using Wick's theorem, we then find

$$H\exp(T^\nu) = \{\overline{H\exp(T^\nu)}\exp(T^\nu)\}_\nu \tag{7}$$

$$= \exp(T^\nu)\{\overline{H\exp(T^\nu)}\}_\nu. \tag{8}$$

The connected entity $\{\overline{H\exp(T^\nu)}\}_\nu$ denotes all terms obtained by joining the operators in H with those of T^ν. The notation $\{\cdots\}_\nu$ signifies that the operator inside the curly bracket has been written in normal order with respect to ϕ_ν as the vacuum. Equation (8) follows from equation (7) because T^ν has no annihilation operators in the hole–particle form and hence can be taken out of the normal ordered term of equation (7) from the left. Since T^ν always excites ϕ_ν to the virtual manifold, it follows that, for a CAS-CI or a CAS-SCF type of reference function ψ_0,

$$\langle\phi_\mu|H\exp(T^\nu)|\phi_\nu\rangle = \langle\phi_\mu|\{\overline{H\exp(T^\nu)}\}_\nu|\phi_\nu\rangle. \tag{9}$$

From now on, we shall denote the above matrix-element by the symbol $\tilde{H}_{\mu\nu}$. $\tilde{H}_{\mu\nu}$ is clearly a connected term if the operator T^ν is connected. We shall prove later the connectivity of T^ν's.

Using equations (6) and (9), the equation determining the eigenvalue E is given by

$$\sum_{\nu}\tilde{H}_{\mu\nu}c_\nu = Ec_\mu. \tag{10}$$

To generate the equations determining the cluster amplitudes, we rewrite equation (5) in normal order, taking each ϕ_μ as the vacuum, and evaluate $H\exp(T^\mu)$. Using equations (7) and (8), we then obtain

$$\sum_{\mu}\exp(T^\mu)\{\overline{H\exp(T^\mu)}\}_\mu|\phi_\mu\rangle c_\mu = E\sum_{\mu}\exp(T^\mu)|\phi_\mu\rangle c_\mu. \tag{11}$$

Inserting the resolution of identity

$$I = Q + P = \sum_{I}|\chi_I\rangle\langle\chi_I| + \sum_{\mu}|\phi_\mu\rangle\langle\phi_\mu| \tag{12}$$

in equation (11), where Q is the projector onto the virtual space spanned by the set $\{\chi_I\}$, the sum $\sum_\mu|\phi_\mu\rangle\langle\phi_\mu|$ is the projector P onto the space of reference determinants, and using equation (9), we find that

$$\sum_{\mu}\exp(T^\mu)Q\{\overline{H\exp(T^\mu)}\}_\mu|\phi_\mu\rangle c_\mu + \sum_{\mu,\nu}\exp(T^\mu)|\phi_\nu\rangle\tilde{H}_{\nu\mu}c_\mu = E\sum_{\mu}\exp(T^\mu)|\phi_\mu\rangle c_\mu. \tag{13}$$

Due to the presence of linearly dependent cluster amplitudes, equation (13) would generate an insufficient number of equations for determining all the cluster amplitudes. This under-determinedness was recognized earlier by several workers. The most relevant among them in the present context are the works of Meller *et al.* [48] and Mahapatra *et al.* [50] who used various sufficiency conditions for generating the cluster amplitudes in their development of state-specific MRCC formalisms. Although explictly demonstrated only for the leading terms, the conditions used by Meller *et al.* [48] amount to equating the Q-projection of the right- and left-hand sides of equation (12) for each μ. These then produced as many equations as the number of cluster amplitudes. Mahapatra *et al.* [50] adopted an alternative strategy of separating the dynamical from the non-dynamical correlation effects, and used a single vacuum for generating the cluster equations. While it is difficult to discern from [48] what form the working equations will take for the complete expansion, Mahapatra *et al.* [50] spell out the general structure of their working equations. In either case, however, a general proof of the connectivity of the cluster operators as well as of the energy E is somewhat awkward. This has prompted us to look for simpler and more convenient sufficiency conditions.

We have developed in [51] precisely such a set of alternative sufficiency conditions for which the proof of the extensivity of the theory is particularly transparent, and in this sense, is more natural. We give below a succinct summary of these conditions and the aspects of size-extensivity implied by them.

In order to arrive at the sufficiency conditions, we interchange the dummy indices μ and ν in the second term on the right side of equation (13):

$$\sum_{\mu}\exp(T^\mu)Q\{\overline{H\exp(T^\mu)}\}_\mu|\phi_\mu\rangle c_\mu + \sum_{\mu,\nu}\exp(T^\nu)|\phi_\mu\rangle\tilde{H}_{\mu\nu}c_\nu = E\sum_{\mu}\exp(T^\mu)|\phi_\mu\rangle c_\mu. \tag{14}$$

We note that, instead of using the traditional form of the resolution of identity of equation (12), we can invoke a completely equivalent expression of the form

$$I = \exp(T'')[Q + P]\exp(-T''). \tag{15}$$

In this resolution our projection manifold consists of the set $\{\langle\chi_I|\exp(-T'')\}$ and $\{\langle\phi_\lambda|\exp(-T'') \equiv \langle\phi_\lambda|\}$ which has exactly the same number of functions $\{\langle\chi_I|\}$, $\{\langle\phi_\lambda|\}$, and are linearly independent and complete. They are, however non-orthogonal, whose dual bra vectors has been chosen as a bi-orthogonal complement with the sets $\exp(T'')\{|\chi_I\rangle\}$ and $\exp(T'')\{|\phi_\lambda\rangle\}$. We also note that for each μ there is a corresponding resolution of identity. Using this new resolution of identity, we can write equation (14) as

$$\sum_\mu \exp(T'')[Q + P]\exp(-T'')\exp(T'')Q\{\overline{H\exp(T'')}\}_\mu|\phi_\mu\rangle c_\mu + \sum_{\mu\nu}\exp(T'')[Q + P]\exp(-T'')\exp(T')|\phi_\mu\rangle\tilde{H}_{\mu\nu}c_\nu = E\sum_\mu \exp(T'')[Q + P]\exp(-T'')\exp(T'')|\phi_\mu\rangle c_\mu. \tag{16}$$

We now posit the *sufficiency conditions* that the terms in equation (16) containing $\exp(T'')Q$ for each μ are equal:

$$\exp(T'')Q\{\overline{H\exp(T'')}\}_\mu|\phi_\mu\rangle c_\mu + \sum_\nu \exp(T'')Q\exp(-T'')\exp(T')|\phi_\mu\rangle\tilde{H}_{\mu\nu}c_\nu = 0. \tag{17}$$

Using the form $Q = \sum_I |\chi_I\rangle\langle\chi_I|$ and the linear independence of each $\langle\chi_I|$, we then deduce that

$$\langle\chi_I|\{\overline{H\exp(T'')}\}_\mu|\phi_\mu\rangle c_\mu + \sum_\nu\langle\chi_I|\exp(-T'')\exp(T')|\phi_\mu\rangle\tilde{H}_{\mu\nu}c_\nu = 0 \quad \forall\, I, \mu. \tag{18}$$

The above set, equation (18) are our stipulated working equations for determining the cluster amplitudes of T''. It is straightforward to verify that the remaining part of equation (14), containing P, would also be equal and would generate equation (10), which indicates the consistency of our sufficiency conditions with respect to equation (10).

We now prove the connectedness of the cluster amplitudes from equation (18). The matrix elements $\langle\chi_I|\{\overline{H\exp(T'')}\}_\mu|\phi_\mu\rangle$ and $\tilde{H}_{\mu\nu}$ are connected entities joining H and $\exp(T'')$ by construction and are extensive quantities if T'' itself is connected. If we now multiply equation (18) through by c_μ^{-1} and use the explicit cluster representation for c_ν from equation (2), we get

$$\langle\chi_I|\{\overline{H\exp(T'')}\}_\mu|\phi_\mu\rangle + \sum_\nu\langle\chi_I|\exp(-T'')\exp(T')|\phi_\mu\rangle \times \tilde{H}_{\mu\nu}\langle\phi_\nu|\exp(\sigma_\mu)|\phi_\mu\rangle = 0. \tag{19}$$

$\tilde{H}_{\mu\nu}$ depends explicitly on the indices of all the active orbitals which distinguish ϕ_ν and ϕ_μ. This is because the operator $\{\overline{H\exp(T')}\}_\nu$ in $\tilde{H}_{\mu\nu}$ causes a transition from ϕ_ν to ϕ_μ. Since $\langle\phi_\nu|\exp(\sigma_\mu)|\phi_\mu\rangle$ also depends explicitly on the indices of all the active orbitals distinguishing ϕ_ν and ϕ_μ, each σ_μ contributing to $\langle\phi_\nu|\exp(\sigma_\mu)|\phi_\mu\rangle$ has at least one active orbital distinguishing ϕ_μ and ϕ_ν. Since each σ_μ is a connected operator because ψ_0 is a CAS-type function, it implies also that $\tilde{H}_{\mu\nu}\langle\phi_\nu|\exp(\sigma_\mu)|\phi_\mu\rangle$ is then a connected quantity if $\tilde{H}_{\mu\nu}$ is connected. The proof of the connectivity will be complete, if we can show that the entire second term in equation (19) is connected.

An apparent complication in proving the extensivity of a many body formalism using multiple vacua was first recognized by Jeziorski and Monkhorst [17] and since then by others [27, 28]. The complication lies in discerning the connectedness of composites which are not joined explicitly by creation/annihilation operators. Connectedness, if any, of such composites has thus to be inferred by noting whether the *amplitudes* of the operators comprising the composite have common orbital labels or not. Thus, when using many-body formalism employing multiple vacua, we have to take care not only of the labels of creation/annihilation operators explicitly appearing in the components of a composite, but also of the functional dependence of the amplitudes of the operators of the components on the various orbitals. This complication of proving the size-extensivity exists in our present formalism also, as will be apparent as we progress.

To continue, we focus on the the second term of equation (19) and rewrite the product $\exp(-T'')\exp(T')$ using the Baker–Campbell–Hausdorf formula:

$$\exp(-T'')\exp(T') = \exp[(T' - T'') + \tfrac{1}{2}[T', T''] + \tfrac{1}{12}[[T', T''], T''] - \tfrac{1}{12}[[T', T''], T'] + \cdots]. \tag{20}$$

Apart from the difference $(T' - T'')$, all other entities in the exponential on the right-hand side of equation (20) appear as commutators. Since the commutators $[T', T'']$ are non-vanishing only when one of the T's in the pair in (T', T'') has some creation operators of active orbitals and the other has the corresponding annihilation operators, they must involve the active orbitals which distinguish the determinants ϕ_μ and ϕ_ν; for in one operator in the pair (T', T'') these belong to the occupied set

(appearing in the annihilation operator) and in the other, to the unoccupied set (appearing in the creation operator). To make this point clear, we take an illustration. Let us consider the case where ϕ_μ and ϕ_ν have two active orbitals (u,v) and (u,x) respectively. For components of T^μ and T^ν of the types $\langle pq|t^\mu|u\alpha\rangle\ a_p^\dagger a_q^\dagger a_\alpha a_u$ and $\langle rs|t^\nu|u\beta\rangle\ a_r^\dagger a_s^\dagger a_\beta a_u$, a_u always appear as annihilation operator since this is occupied in both ϕ_μ and ϕ_ν and thus these terms commute. On the other hand, the components of T^μ and T^ν of the types $\langle px|t^\mu|\alpha u\rangle a_p^\dagger a_x^\dagger a_u a_\alpha$ and $\langle pq|t^\nu|\alpha x\rangle a_p^\dagger a_q^\dagger a_x a_\alpha$ do not commute since the orbital x is occupied in ϕ_ν but unoccupied in ϕ_μ. There is thus $a_x^\dagger$ in the T^μ component but a_x in T^ν. Hence all the terms from the expansion of the exponential on the right-hand side of equation (20) involving commutators will have at least some active orbital labels distinguishing ϕ_ν and ϕ_μ, and thus will have common orbitals with $\tilde{H}_{\mu\nu}\langle\phi_\nu|\exp(\sigma_\mu)|\phi_\mu\rangle$ appearing in equation (19)—the latter being explicitly labelled by *all* the active orbitals distinguishing ϕ_ν and ϕ_μ.

But T^ν and T^μ in general may involve creation/annihilation operators for active orbitals common to both ϕ_ν and ϕ_μ; or they may not even involve any active orbitals at all. Thus the individual terms from the expansion of the exponential involving powers of the difference $(T^\nu - T^\mu)$ multiplying $\tilde{H}_{\mu\nu}\langle\phi_\nu|\exp(\sigma_\mu)|\phi_\mu\rangle$ may not involve common orbital labels in their creation/annihilation operators and one may imagine that this would lead to disconnected terms. To see whether they are really so, we have to focus now on the functional dependence of the amplitudes of T_μ and T_ν on the labels on the various active orbitals. In fact, we prove now that, although, the individual terms such as $T^\nu\tilde{H}_{\mu\nu}\langle\phi_\nu|\exp(\sigma_\mu)|\phi_\mu\rangle$ etc. may be disconnected, the amplitude part of *the difference* $(T^\nu - T^\mu)$, such as powers of $(T^\nu - T^\mu)$ have functional dependence on active orbitals which are common with $\tilde{H}_{\mu\nu}\langle\phi_\nu|\exp(\sigma_\mu)|\phi_\mu\rangle$ and hence are connected.

We have to consider two possibilities: (a) the case when both T^ν and T^μ can excite from ϕ_μ to the given χ_l, and (b) when T^μ can excite from ϕ_μ, but there is no T^ν with the same orbital labels. This comes about because the active orbitals involved are such that T^ν with these labels acting on ϕ_ν gives zero. For the possibility (a), the proof follows from the fact that T^μ and T^ν in the exact, untruncated, formulation are treated on the same footing, and hence their amplitudes should have the same functional form, differing in their explicit dependence only on the labels of active orbitals present in ϕ_μ and ϕ_ν. Hence on taking the difference, the expression for the difference of the amplitudes of $(T^\nu - T^\mu)$ have only those terms surviving which are different for T^ν and T^μ, i.e. those involve active orbitals present in ϕ_ν and ϕ_μ. Thus $(T^\nu - T^\mu)$ depends functionally on some active orbitals distinguishing ϕ_ν and ϕ_μ and hence products of powers of $(T^\nu - T^\mu)$ with $\tilde{H}_{\mu\nu}\langle\phi_\nu|\exp(\sigma_\mu)|\phi_\mu\rangle$ have common orbital labels and hence are connected. For the possibility (b), the active orbitals involved in T^μ exciting to χ_l from ϕ_μ must be such that it is not possible to induce this excitation on ϕ_ν. This happens when their role of being occupied and unoccupied in ϕ_μ is reversed in ϕ_ν. In this case, creation/annihilation operators involving the active orbitals in T^μ itself will have some active orbitals distinguishing ϕ_μ and ϕ_ν. The powers of the difference $(T^\mu - T^\nu)$ multiplied to $\tilde{H}_{\mu\nu}\langle\phi_\nu|\exp(\sigma_\mu)|\phi_\mu\rangle$ will then again be a connected entity.

It thus follows from equation (19) that there exists one set of solutions for T^μ's where all the cluster amplitudes are connected. Hence $\tilde{H}_{\mu\nu}$'s are also connected. Since the reference determinants span a CAS, it also follows that the energy obtained as the eigenvalue of equation (10) is also size extensive. Since the CAS spanned by the reference determinants is invariant under localizing transformations separately among the holes and active orbitals, the extensivity of the energy also implies correct separation into fragments generated from the active orbitals, and hence size-consistency.

Let us now note carefully that our proof rested on the assumed exactness of the formulation, i.e. we have made no truncation in our equations. In practice, we shall invoke some truncation scheme for the cluster operators. Also, the series in equation (20) involving the difference of T^μ and T^ν and their commutators has to be truncated after some powers. For our proof to go through, even for truncated versions, there should be essentially separate sets $\{\chi_l^\mu\}$ for projections for the equation for T^μ. The functions $\{\chi_l\}$ now have an implicit μ-dependence in the sense that they are the virtual functions reached by the components of T^μ from ϕ_μ. Moreover, once a given χ_l is generated by a T^μ operator of a given rank in a truncation scheme, it is essential to include this excitation in all T^ν's—provided that such excitations acting on ϕ_ν's are non-zero. This is automatically guaranteed if we truncate the cluster operators at a given rank, and truncate the powers of the difference $(T^\mu - T^\nu)$ after any given power. We shall come back to this aspect once again in section 3.2.

We should also mention here that in practice we will solve equation (18) for the cluster amplitudes. The transcription of equation (18) to equation (19) is only for the purpose of proving the connectedness of the clusters. We shall never need to use σ_μ's anywhere for the actual application of our formalism, and all the ϕ_μ's are treated on the same footing.

Let us note that in solving the equations for the cluster amplitudes, equation (18), the knowledge of the coefficients c_μ's is required. The two sets are thus

coupled. In section 3, we shall discuss practical iteration algorithms for efficient solutions of the coupled MRCC equations. From the very mode of formulation of the theory, it is clear that the combining coefficients are iteratively updated to their values they should have in exact state ψ, and hence our formulation provides completely flexible relaxed coefficients. The development, however, has the additional advantage that we are not obliged to change the combining coefficients if we do not deem it to be necessary. In the illustrative applications of our formalism, we shall study the relative efficacies of both the frozen and relaxed modes of description.

We conclude this section with some comments pertaining to the related formulations of Meller *et al.* [48] and Mahapatra *et al.* [50] which were mentioned earlier. The method of Meller *et al.* uses the equality of Q-projections of equation (13) for each μ as sufficiency conditions. This seems like the most straightforward sufficiency conditions to be invoked, but the proof of the connectivity of T^{μ}'s becomes quite laborious and has not been shown for the general case. They show the size-consistency of their formulation only under certain approximations. Mahapatra *et al.* [50] posit another type of sufficiency condition, which follows from the assumption that the total energy E is a sum of dynamical (E_d) and non-dynamical (E_{nd}) correlation energies. There is a pivotal function with respect to which the dynamical correlation is defined. The dynamical correlation energy stems from the virtual functions which are reached by cluster operators acting on the pivotal function. The cluster operators acting on the other reference determinants generate contributions to the non-dynamical correlation energies. The sufficiency conditions in [50] are thus different from those in [48]. In contrast, the present development follows from a rearranged form of equation (13). We have shown that the resulting working equations lead to connected cluster amplitudes T^{μ} in a rather straightforward manner for the general case. The entire exercise hinges on the connectedness of $\exp(-T^{\mu})\exp(T^{\nu})|\phi_{\mu}\rangle\tilde{H}_{\mu\nu}\langle\phi_{\nu}|\exp(\sigma_{\mu})|\phi_{\mu}\rangle$. Since we also use multiple vacua to represent the wave-operator, there are no spectator orbitals.

Recently Adamowicz and his co-workers [66, 67] suggested a state-specific formulation where a special role is played by one reference determinant which is more dominant than the rest. The entire cluster expansion is performed with respect to this determinant. The non-dynamical correlation is brought into the formulation by including in the cluster operator three- and four-body terms with at least one active orbital different from those present in the dominant determinant. Their results are encouraging. There is also a closely related formulation by Stolarczyk [68]. Since all the cluster operators are defined with respect to a pivotal determinant, these formulations are not really based on an MRCC approach. Moreover, the presence of three- and four-body operators makes the organization of the equations rather complex. Our present formulation does not warrant the presence of a dominant determinant in the reference function. In this sense it is more general and involves fewer sets of diagrams to achieve similar accuracy.

3. Numerical implementation and truncation schemes

3.1. *Algorithmic considerations*

The MRCC formulation described above contains two different sets of variables, T^{μ}'s for all μ, and the coefficients c_{μ}. These variables appear in a coupled manner, as is evident in equation (18). A careful organizing strategy for their solution is essential for an efficient implementation of the method. After several trials, we have found that the following scheme provides a fast convergent and stable mode of solution. The solution is carried out in a nested iterative loop. In the outer loop, the coefficients c_{μ} are updated by solving the eigenvalue problem, equation (10). *It is imperative* to home to the desired root, since the correct choice of the relative signs of the mixing coefficients is essential to ensure convergence of the global iteration scheme. With the current set of the coefficients, we enter the inner loop where the cluster amplitudes T^{μ} are determined. Since a simultaneous updating of all the amplitudes for all μ would require very large computer memory, we initiate the inner loop to update each set $\{T^{\mu}\}$ for a fixed μ, keeping the rest of the amplitudes $\{T^{\nu}\}$, $\nu \neq \mu$, frozen. The inner loop runs over all μ's until converged amplitudes for all μ's are obtained. The amplitudes are then used to construct the matrix of $\tilde{H}$ defined in equation (9). The updating of the coefficients c_{μ} begins by moving out to the outer loop. The iteration is initiated by diagonalizing the Hamiltonian matrix in the space of reference determinants. In the first loop of the inner iteration, we start with all the amplitudes initialized to zero. We use the preconditioned conjugate gradient method of [69], which is equivalent to the method of [70], for solving the nonlinear equations for the amplitudes. The contributions from the frozen T^{ν} amplitudes, $\nu \neq \mu$, in the equations are incorporated by clubbing them to the constant terms, while the quadratic and higher powers of T^{μ} are added to the linear term to achieve an efficient quasi-linearization.

As emphasized in section 2, the advantage of the present MRCC formulation is in the flexibility of using the method in either a frozen or a relaxed mode for the coefficient of the reference determinants. The algorithm proposed above pertains to the decontracted mode. For the contracted mode, we initiate the iteration by diagonalizing the matrix of H in the reference space, and

keep these values frozen throughout the iteration process. Thus in this case the outer iteration loop is not operative.

3.2. *Truncation scheme for the cluster operators*

In our applications, we shall invoke a CCSD truncation scheme. This is the least elaborate truncation scheme which possesses most of the important features of correlation. As we have indicated in section 2, while proving the size-extensivity of our formalism, the connectedness of the composite $\exp(-T^{\mu})\exp(T^{\nu})|\phi_{\mu}\rangle\tilde{H}_{\mu\nu}$ was crucial to prove the size-extensivity of the formalism. This implies that if there is one operator in a particular T^{μ} exciting from a ϕ_{μ} to a χ_l, the corresponding excitation must be included in all T^{ν}'s, $\nu \neq \mu$ unless the action of this component of T^{ν} on ϕ_{ν} is zero. As we emphasized in section 2, this is achieved in any truncation scheme where all cluster operators up to a given excitation rank are included.

The MRCCSD equations generally involve high powers of cluster operators in the term containing $\langle\chi_l|\exp(-T^{\mu})\exp(T^{\nu}|\phi_{\mu}\rangle\tilde{H}_{\mu\nu}$ in equation (18). We have truncated this term after the quadratic power in the applications reported in this paper. This truncation scheme for the molecules studied by us seem to be quite accurate, as will be evidenced by the benchmark results.

3.3. *Results and discussions*

As illustrative numerical applications of our MRCC method, we have studied two molecules at various geometries which typically display quasi-degeneracy of two determinants at one point but progressive loss of quasi-degeneracy as the geometery changes. One is the model H_8 system and the other is the Li_2 molecule in the ground state over a wide range of internuclear separation. In both the systems studied by us, there are two active orbitals which respectively remain doubly occupied in the two determinants which become quasi-degenerate at one point. Since these two orbitals belong to different symmetries, the two-dimensional space spanned by these two determinants is a CAS. As mentioned in section 3, we use an SD-truncation of the cluster operators.

3.3.1. *The H_8 model system*

This has been widely studied by several workers [22, 71–74] using both an effective hamiltonian-based MRCC method and other SR-based state-specific theories. Two sets of H_2 molecules with H–H bond length fixed at 2.0 au are placed perpendicular to each other but parallelly in each set as shown in figure 1. One parallely oriented pair is shifted away from each other symmetrically from the most symmetric arrangement where the degeneracy is encountered. The distortion is usually

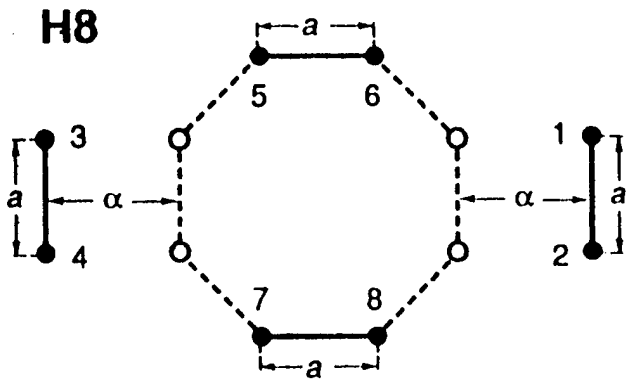

Figure 1. The geometrical arrangement of the four H_2 molecules in the H_8 model problem.

characterized by a parameter α which is just the shift from the most symmetrical arrangement. The larger range of α corresponding to non-degeneracy of the reference determinants and the possibility of encountering intruders for the higher lying determinants. The molecule possesses D_{2h} symmetry at all the values of α. At the degenerate point the fourth and fifth orbitals tend to become degenerate. We take as our active space the two determinants where these two orbitals are doubly filled. Since these orbitals belong to different symmetries, this two-dimensionsal model space is a CAS.

We have performed two sets of calculations on H_8, taking the minimal basis on each H. In one set, SCF orbitals of the determinant $a_g^2 b_{3u}^2 b_{2u}^2 a_g^2$ are used to generate all the determinants. Both contracted and decontracted MRCC results are displayed in table 1, which also lists the SCF energies, the SR-CCSD results. The benchmark full CI (FCI) results are also shown for assessing the performance of the various methods. The results with the 'relaxed coefficients' are generally closer to the FCI values and always lie below them. The description with 'relaxed coefficients' are higher in energy as compared to the FCI result. The SR-CCSD works quite well in the non-degenerate regions, though—as expected—its performance goes down around the quasi-degenerate region ($\alpha < 0.1$).

In another set of calculations, we have used the CAS-SCF orbitals obtained from the CAS-SCF calculation on the two-determinant active space, consisting of the determinants $a_g^2 b_{3u}^2 b_{2u}^2 a_g^2$ and $a_g^2 b_{3u}^2 b_{2u}^2 b_{1g}^2$. The second determinant becomes quasi-degenerate with the first one around $\alpha < 0.1$. The results of calculations are displayed in table 2, and the trend of the results is very different. Here, although the starting energy of the function ψ_0 is lower, the overall correlation effect after the virtuals are brought in is not necessarily more pronunced. Moreover, the results are now more sensitive on the relaxation of the coefficients c_{μ}. This is presum-

Table 1. Comparison of the SRCCSD and SSMRCC ground state energies of H_8 with the FCI results. All entries in au. SCF orbitals are used.

α	SCF	SRCCSD	SSMRCC (frozen)	SSMRCC (relaxed)	FCI
0.0001	−4.065562	−4.199764	−4.203496	−4.206361	−4.204803
0.001	−4.065828	−4.199880	−4.203465	−4.206444	−4.204886
0.003	−4.066418	−4.200143	−4.203850	−4.206836	−4.205075
0.01	−4.068474	−4.201095	−4.204373	−4.207545	−4.205769
0.03	−4.074276	−4.204081	−4.206349	−4.210337	−4.208036
0.06	−4.082780	−4.209146	−4.209955	−4.213558	−4.212169
0.08	−4.088316	−4.212815	−4.213155	−4.216389	−4.215336
0.10	−4.093745	−4.216648	−4.216640	−4.219924	−4.218763

Basis and geometry: 1985, *Int. J. quantum Chem.*, **28**, 931. $a = 2.0$ au.

Table 2. Comparison of the SSMRCC ground state energies of H_8 with the FCI results. All entries in au. CAS-SCF orbitals are used.

α	CAS-SCF	SSMRCC (frozen)	SSMRCC (relaxed)	FCI
0.0001	−4.082773	−4.207991	−4.206407	−4.204803
0.001	−4.082831	−4.208015	−4.206427	−4.204886
0.003	−4.082973	−4.208178	−4.206633	−4.205075
0.01	−4.083624	−4.208242	−4.206921	−4.205769
0.03	−4.086493	−4.209255	−4.210288	−4.208036
0.06	−4.092300	−4.211601	−4.214243	−4.212169
0.08	−4.096630	−4.214225	−4.217165	−4.215336
0.10	−4.101131	−4.217343	−4.220310	−4.218763

Basis and geometry: 1985, *Int. J. quantum Chem.*, **28**, 931. $a = 2.0$ au.

ably due to the optimization of both the orbitals and the coefficients in the CAS-SCF function which tends to attach more weight to the less important of the two active determinants. Inclusion of the virtual determinants should lead to scaling down of its importance in a relaxed description, which is not possible when the coefficients are frozen. We surmise that the use of CAS-SCF orbitals may not necessarily be the best starting point, but more studies are necessary to get a definite picture.

In figures 2 and 3 we give a plot of the difference energies for both the contracted and decontracted descriptions with respect to the FCI results for the SCF and CAS-SCF case, respectively. In both the set of calculations, the results are very encouraging, leading credence to the performance of the MRCC method.

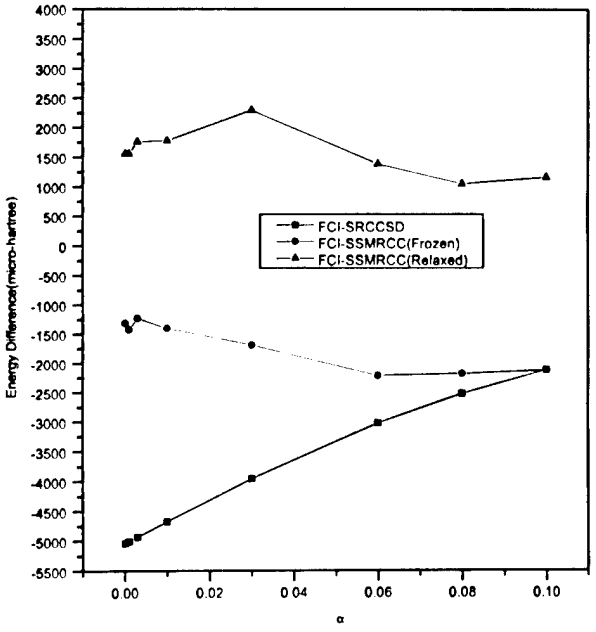

Figure 2. The differences of the SSMRCC energies with respect to the FCI values plotted against α. SCF orbitals have been used.

3.3.2. *The Li_2 ground-state potential curve*

This serves as a natural test-case for studying the efficacy of a state-specific theory. There is a wealth of low-lying excited states at different regions of the internuclear separation R. Especially around the equilibrium geometery, there exists several low-lying excited states

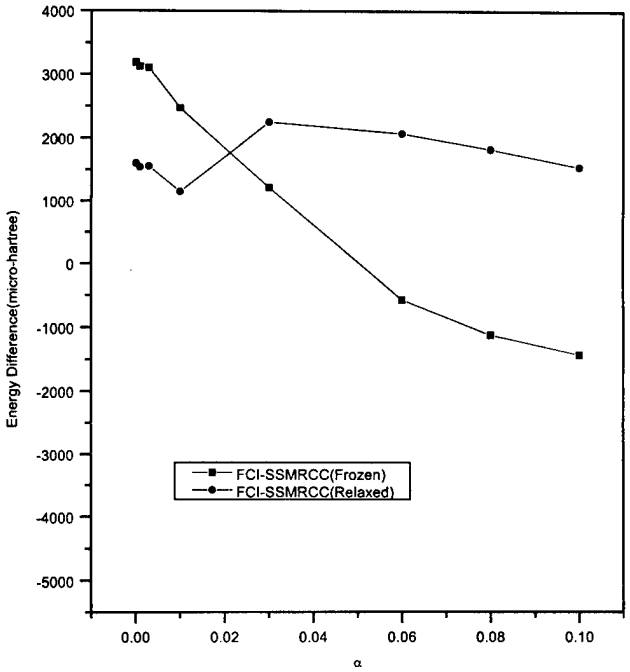

Figure 3. The differences of the SSMRCC energies with respect to the FCI values plotted against α. CAS-SCF orbitals have been used.

which tend to mix strongly with the active $2\sigma_\mu$-orbital which lies much higher than the other active counterpart, the $2\sigma_g$ orbital. $1\sigma_g^2\, 1\sigma_u^2\, 2\sigma_g^2$ and $1\sigma_g^2 1\sigma_u^2\, 1\sigma_u^2$ are the two reference determinants in the active space. Around $R = 9.0$ au, there are avoided crossings which should affect a smooth performance of a state-specific method unless it is very accurate. Beyond $R = 11.0$ au, the two active orbitals $2\sigma_g$ and $2\sigma_u$ tend to become prominently quasi-degenerate.

We have chosen a 6-311G** basis on each Li with an additional cartesian d function (exponent = 0.2) to study the potential curve. The same basis had been used earlier by Krishnan *et al.* [75]. Since FCI results for the potential curve for this basis is not available, we have performed a CISDTQ for providing a benchmark. Again we have performed our calculations with two sets of orbitals: SCF orbitals from the $1\sigma_g^2\, 1\sigma_u^2\, 2\sigma_g^2$ determinant, and the CAS-SCF orbitals for the two-determinant ground state. Again it is observed that the effect of decontraction is more pronunced for the CAS-SCF orbitals than for the SCF orbitals. A comparison with the CISDTQ results indicates that the numerical performance of the relaxed version of MRCC version is very good and it succeeds quite well to avoid intruders.

Results for both frozen and relaxed versions of MRCC are listed in tables 3 and 4 for the SCF and CAS-SCF starting functions, respectively. We have also performed an SRCCSD calculation for both functions and listed it alongwith the SCF values and the CISDTQ results in the table. A comparison shows that in both cases the relaxed description works better, being closer to the CISDTQ values than the frozen one. For the CAS-SCF case, the values are closer to the CISDTQ results. As expected, the SRCCSD performs quite well for the smaller values of R where no intruders are present but falls short at the near degenerate positions.

In figures 4 and 5 we have plotted the PES for the ground state of Li_2 for the SCF and CAS-SCF cases, respectively. The results obtained by the CAS-SCF calculation were found to be closer to the CISDTQ values

Table 3. Comparison of the SSMRCC ground state energies for Li_2 with various methods. All entries in au. SCF orbitals are used.

R	SCF	SRCCSD	SSMRCC (frozen)	SSMRCC (relaxed)	CISDTQ
3.5	−14.826445	−14.895177	−14.895075	−14.895177	−14.895765
4.0	−14.851662	−14.917176	−14.917080	−14.917178	−14.917659
4.5	−14.864822	−14.927754	−14.927719	−14.927793	−14.928159
5.0	−14.869984	−14.930968	−14.930884	−14.930973	−14.931332
5.1696	−14.870482	−14.930938	−14.930901	−14.930981	−14.931294
5.5	−14.870147	−14.929756	−14.929672	−14.929768	−14.930105
6.0	−14.867314	−14.926089	−14.926065	−14.926163	−14.926447
7.0	−14.857338	−14.916214	−14.916106	−14.916290	−14.916656
8.0	−14.845660	−14.907197	−14.907029	−14.907382	−14.907812
9.0	−14.834456	−14.900914	−14.900766	−14.901337	−14.901762
10.0	−14.824495	−14.897231	−14.897138	−14.897879	−14.898314
11.0	−14.815949	−14.895311	−14.895328	−14.896140	−14.896573
12.0	−14.808740	−14.894351	−14.894422	−14.895229	−14.895743
16.0	−14.790017	−14.893387	−14.893964	−14.894513	−14.894989

Basis: 6-311G** and a cartesian d function (=0.2).

Table 4. Comparison of the SSMRCC ground state energies for Li_2 with various methods. All entries in au. CAS–SCF orbitals are used.

R	CAS-SCF	SRCCSD	SSMRCC (frozen)	SSMRCC (relaxed)	CISDTQ
3.5	−14.833801	−14.895149	−14.893313	−14.895209	−14.895764
4.0	−14.858778	−14.917176	−14.915743	−14.917273	−14.917659
4.5	−14.872463	−14.927755	−14.926467	−14.927861	−14.928159
5.0	−14.878710	−14.930969	−14.929616	−14.931023	−14.931332
5.1696	−14.879686	−14.930938	−14.929586	−14.930995	−14.931294
5.5	−14.880438	−14.929756	−14.928399	−14.929825	−14.930105
6.0	−14.879633	−14.926087	−14.924795	−14.926204	−14.926447
7.0	−14.875097	−14.916209	−14.915093	−14.916441	−14.916656
8.0	−14.870507	−14.907191	−14.906550	−14.907553	−14.907813
9.0	−14.867406	−14.900895	−14.900924	−14.901517	−14.901763
10.0	−14.865694	−14.897205	−14.897780	−14.898080	−14.898315
11.0	−14.864857	−14.895276	−14.896164	−14.896316	−14.896575
12.0	−14.864478	−14.894288	−14.895370	−14.895457	−14.895745
16.0	−14.864211	−14.893306	−14.894642	−14.894706	−14.894991

Basis: 6-311G** and a cartesian d function (=0.2).

than those obtained by the SCF starting function. It is seen that around the equilibrium geometry, the contracted description with the CAS-SCF orbitals is somewhat poorer, presumably again due to the enhanced importance of the $2\sigma^2$ configuration in the reference CAS-SCF function. Around this internuclear distance, the effect of relaxation of the coefficients is more pronounced with the CAS-SCF orbitals than with the SCF orbitals. As can be seen from the plot, our present MRCC method obviates the problem of intruders effectively in the region of avoided crossing as mentioned earlier.

In figures 6 and 7 we again give a plot of the difference energies for the contracted and decontracted description, with respect to the CISDTQ values, for the SCF and CAS-SCF starting functions respectively to see the efficacy of our present formulation. To get a feeling for the efficiency of the present MRCC theory we also plot the difference energies for the SRCCSD with respect to the CISDTQ values. The performance of the SRCCSD, as is expected, becomes increasingly poorer with increasing internuclear distance.

4. Summary

We have presented in this paper a state-selective multi-reference coupled cluster approach which resolves the intruder problem in a manifestly size-extensive manner. The formalism uses a CAS-CI or a CAS-SCF function as the reference function ψ_0, and uses a relaxed mode of description in the sense that the combining

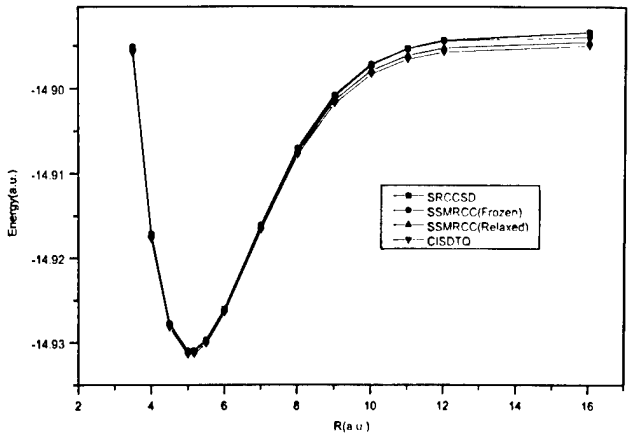

Figure 4. SSMRCC results plotted against R for Li_2. SCF orbitals are used. SRCCSD and CISDTQ results are also plotted for comparison.

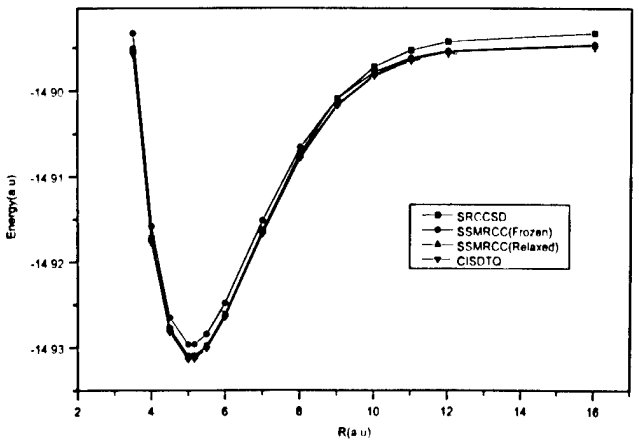

Figure 5. SSMRCC results plotted against R for Li_2. CAS-SCF orbitals are used. SRCCSD and CISDTQ results are also plotted for comparison.

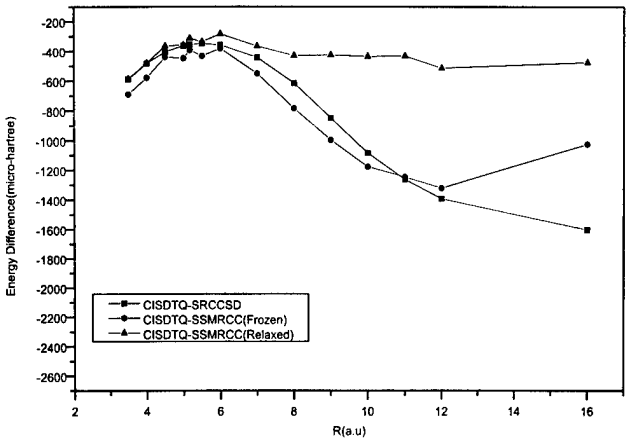

Figure 6. The differences of the SSMRCC energies with respect to the CISDTQ values plotted against R. SCF orbitals have been used.

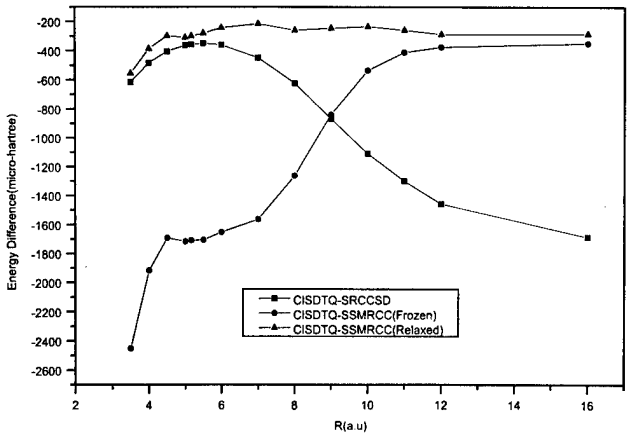

Figure 7. The differences of the SSMRCC energies with respect to the CISDTQ values plotted against R. CAS-SCF orbitals have been used.

coefficients c_μ of the reference determinants ϕ_μ comprising ψ_0 are iteratively relaxed—eventually leading to the fully relaxed values of the coefficients in the exact ψ. The method is flexible in the sense that we can use it also in a frozen mode, where we deliberately do not update the combining coefficients of ϕ_μ's forming ψ_0.

In our formulation, we retain the linearly dependent (redundant) cluster amplitudes in the wave operator, but invoke suitable sufficiency conditions which not only provide the extra equations needed for their determination but also ensure in a natural manner that the cluster amplitudes are manifestly connected. The method treats all the reference determinants on the same footing and is thus well suited to describing wide ranges of molecular geometry. Preliminary numerical applications to the model H_8 system and the ground state Li_2 potential curve clearly demonstrate the accuracy of the method as well as its ability to avoid intruders.

The authors thank the UGC (New Delhi) for providing financial support. The computations have been carried out on the HP-715/80 donated by the Alexander von Humboldt foundation. D. M. thanks the S. N. Bose National Centre for Basic Sciences for conferring on him an honorary Professorship. This article is dedicated to Dipak Chakrabarty of I. I. T.(Bombay) on the happy occasion of his 60th birthday.

References

[1] Bartlett, R. J., and Purvis, G. D., 1978, *Int. J. quantum Chem.*, **14,** 561.

[2] Pople, J. A., Binkley, J. S., and Seeger, R., 1976, *Int. J. quantum Chem.*, **S10,** 1.

[3] Coester, F., 1958, *Nucl. Phys.*, **1,** 421; Coester, F, and Kümmel, H., 1960, *Nucl. Phys.*, **17,** 477.

[4] Čížek, J., 1966, *J. chem. Phys.*, **45,** 4256; Čížek, J., 1969, *Adv. chem. Phys.*, **14,** 35; Čížek, J., and Paldus, J., 1971, *Int. J. quantum Chem.*, **5,** 359.

[5] Bartlett, R. J., 1981, *Ann. Rev. phys. Chem.*, **32,** 359; Bartlett, R. J., 1995, *Modern Electronic Structure Theory*, Part II, edited by D. A. Yarkony (Singapore: World Scientific).

[6] Purvis, G. D., and Bartlett, R. J., 1982, *J. chem. Phys.*, **76,** 1910,.

[7] Paldus, J., Čížek, J., and Shavitt, I., 1972, *Phys. Rev.* A **5,** 50; Kvasnicka, V., 1982, *Phys. Rev.* A, **25,** 671; Lee, Y. S., and Bartlett, R. J., 1984, *J. chem. Phys.*, **80,** 4371; Urban, M., Noga, J., Cole, S. J., and Bartlett, R. J., 1985, *J. chem. Phys.*, **83,** 4041; Raghavachari, K., Trucks, G. W., Pople, J. A., and Head-Gordon, M., 1989, *Chem. Phys. Lett.*, **157,** 479.

[8] Noga, J., and Bartlett, R. J., 1987, *J. chem. Phys.*, **86,** 7041; Sosa, C., Noga, J., and Bartlett, R. J., 1988, *J. chem. Phys.*, **88,** 5974; Kucharski, S. A., and Bartlett, R. J., 1991, *Theo. Chim. Acta*, **80,** 387.

[9] Scuseria, G. E., and Schaefer III, H. F., 1988, *Chem. Phys. Lett.*, **152,** 382.

[10] Kucharski, S. A., and Bartlett, R. J., 1992, *J. chem. Phys.*, **97,** 4282; Bartlett, R. J., Watts, J. D., Kucharski, S. A., and Noga, J., 1990, *Chem. Phys. Lett.*, **165,** 513; Oliphant, N., and Adamowicz, L., 1991, *J. chem. Phys.*, **95,** 6645.

[11] Brandow, B. H., 1967, *Rev. mod. Phys.*, **39,** 771; Lindgren, I., 1974, *J. Phys.*, **B7,** 2441.

[12] Mukherjee, D., Moitra, R. K., and Mukhopadhyay, A., 1975, *Molec. Phys.*, **30,** 1861; 1977, *ibid.* **33,** 955; Haque, A., and Mukherjee, D., 1984, *J. chem. Phys.*, **80,** 5058.

[13] Lindgren, I., 1978, *Int. J. quantum Chem.*, **S12,** 33.

[14] Offerman, R., Ey, W., and Kümmel, H., 1976, *Nucl. Phys.*, **A273,** 349; Offerman, R., 1976, *Nucl. Phys.*, **A273,** 368; Ey, W., 1978, *Nucl. Phys.*, **A296,** 189.

[15] Kutzelnigg, W., 1982, *J. chem. Phys.*, **77,** 3081.

[16] Haque, A., and Kaldor, U., 1985, *Chem. Phys. Lett.*, **117,** 347; Kaldor, U., 1987, *J. chem. Phys.*, **87,** 467; Hughes, S. R., and Kaldor, U., 1992, *Chem. Phys. Lett.*, **194,** 99.

[17] JEZIORSKI, B., and MONKHORST, H. J., 1981, *Phys. Rev.* A, **24,** 1668.
[18] JEZIORSKI, B., and PALDUS, J., 1988, *J. chem. Phys.*, **88,** 5673.
[19] MEISSNER, L., JANKOWSKI, K., and WASILEWSKI, J., 1988, *Int. J. quantum Chem.*, **34,** 535.
[20] PALDUS, L., PYLYPOW, J., and JEZIORSKI, B., 1989, *Many Body Methods in Quantum Chemistry, Lecture Notes in Chemistry*, Vol. 52, edited by U. Kaldor (Berlin: Springer Verlag); PIECUCH, P., and PALDUS, J., 1992, *Theo. Chim. Acta*, **83,** 69.
[21] BALKOVÁ, A., KUCHARSKI, S. A., MEISSNER, L., and BARTLETT, R. J., 1991, *Theo. Chim. Acta*, **80,** 335.
[22] KUCHARSKI, S. A., BALKOVÁ, A., SZALAY, P. G., and BARTLETT, R. J., 1992, *J. chem. Phys.*, **97,** 4289.
[23] MUKHERJEE, D., 1986, *Chem. Phys. Lett.*, **125,** 207; MUKHERJEE, D., 1986, *Int. J. quantum. Chem.*, **S20,** 409.
[24] SINHA, D., MUKHOPADHYAY, S. K., and MUKHERJEE, D., 1986, *Chem. Phys. Lett.*, **129,** 369.
[25] KUTZELNIGG, W., MUKHERJEE, D., and KOCH, S., 1987, *J. chem. Phys.*, **87,** 5902; MUKHERJEE, D., KUTZELNIGG, W., and KOCH, S., 1987, *J. chem. Phys.*, **87,** 5911; KOCH, S., and MUKHERJEE, D., 1988, *Chem. Phys. Lett.*, **145,** 321.
[26] PAL, S., RITTBY, M., BARTLETT, R. J., SINHA, D., and MUKHERJEE, D., 1988, *J. chem. Phys.*, **88,** 4357; PAL, S., RITTBY, M., BARTLETT, R. J., SINHA, D., and MUKHERJEE, D., 1987, *Chem. Phys. Lett.*, **137,** 273.
[27] MUKHOPADHYAY, D., and MUKHERJEE, D., 1989, *Chem. Phys. Lett.*, **163,** 171; MUKHOPADHYAY, D., and MUKHERJEE, D., 1991, *Chem. Phys. Lett.*, **177,** 441; MUKHOPADHYAY, D., and MUKHERJEE, D., 1992, *Applied Many-Body Methods in Spectroscopy and Electronic Structure*, edited by D. Mukherjee (New York: Plenum Press); MUKHERJEE, D., and ZAITSEVSKII, A., 1995, *Chem. Phys. Lett.*, **233,** 605.
[28] MEISSNER, L., KUCHARSKI, S., and BARTLETT, R. J., 1989, *J. chem. Phys.*, **91,** 6187; MEISSNER, L., and BARTLETT, R. J., 1990, *J. chem. Phys.*, **92,** 561.
[29] MUKHERJEE, D., and PAL, S., 1989, *Adv. quantum Chem.*, **20,** 292 and references therein.
[30] LINDGREN, I., and MUKHERJEE, D., 1987, *Phys. Rep.*, **151,** 93.
[31] PALDUS, J., 1992, *Methods in Computational Molecular Physics*, edited by S. Wilson and G. H. F. Diercksen (New York: Plenum Press).
[32] BARTLETT, R. J., 1989, *J. phys. Chem.*, **93,** 1697.
[33] SCHUCAN, T. H., and WEIDENMÜLLER, H. A., 1972, *Ann. Phys.*, **73,** 108.
[34] HOSE, G., and KALDOR, U., 1982, *J. phys. Chem.*, **86,** 2133.
[35] KALDOR, U., 1990, *Chem. Phys.*, **140,** 1; Koch, S., 1989, *Lecture Notes in Chemistry*, Vol. 50, edited by D. Mukherjee (Berlin: Springer-Verlag).
[36] KIRTMAN, B., 1981, *J. chem. Phys.*, **75,** 798.
[37] MALRIEU, J. P., DURAND, PH., and DAUDEY, J. P., 1985, *J. Phys. A Math. Gen.*, **18,** 809; HEULLY, J. L., and DAUDEY, J. P., 1988, *J. chem. Phys.*, **88,** 1046.
[38] MALRIEU, J. P., DAUDEY, J. P., and CABALLOL, R., 1994, *J. chem. Phys.*, **101,** 8908.
[39] MALRIEU, J. P., HEULLY, J. L., and ZAITSEVSKII, A., 1995, *Theo. Chim. Acta*, **90,** 167.
[40] NEBOT-GIL, I., SANCHEZ-MARIN, J., MALRIEU, J. P., HEULLY, J. L., and MAYNAU, D., 1995, *J. chem. Phys.*, **103,** 2576; HEULLY, J. L., MALRIEU, J. P., and ZAITSEVSKII, A., 1996, *J. chem. Phys.*, **105,** 6887.
[41] MUKHOPADHYAY, D., DATTA, B., and MUKHERJEE, D., 1992, *Chem. Phys. Lett.*, **197,** 236.
[42] SINHA, D., MUKHOPADHYAY, S., CHAUDHURI, R., and MUKHERJEE, D., 1989, *Chem. Phys. Lett.*, **154,** 544; CHAUDHURI, R., MUKHOPADHYAY, D., and MUKHERJEE, D., 1989, *Chem. Phys. Lett.*, **162,** 389.
[43] KOCH, S., 1991, *Theo. Chim. Acta*, **81,** 169.
[44] DATTA, B., CHAUDHURI, R., and MUKHERJEE, D. 1996, *J. molec. Structure* (Theochem), **361,** 21.
[45] LAIDIG, W. D., and BARTLETT, R. J., 1984, *Chem. Phys. Lett.*, **104,** 424.
[46] BANERJEE, A., and SIMONS, J., 1981, *Int. J. quantum Chem.*, **19,** 207; BANERJEE, A., and SIMONS, J., 1982, *J. chem. Phys.*, **76,** 4548.
[47] HOFFMANN, M. R., and SIMONS, J., 1988, *J. chem. Phys.*, **88,** 993.
[48] MELLER, J., MALRIEU, J. P., and CABALLOL, R., 1996, *J. chem. Phys.*, **104,** 4068.
[49] DATTA, B., and MUKHERJEE, D., 1995, *Chem. Phys. Lett.*, **235,** 31.
[50] SINHA MAHAPATRA, U., DATTA, B., and MUKHERJEE, D., 1997, *Modern Ideas in Coupled-Cluster Methods*, edited by R. J. Bartlett (Singapore: World Scientific).
[51] SINHA MAHAPATRA, U., DATTA, B., BANDYOPADHYAY, B., and MUKHERJEE, D., 1997, *Advances in Quantum Chemistry*, edited by D. Hanstorp and H. Persson (San Diego: Academic Press Inc.) (in the press).
[52] SILVERSTONE, H. J., and SINANOGLU, O., 1966, *J. chem. Phys.*, **44,** 1899, 3608.
[53] ANDERSSON, K., MALMQUIST, P., and ROOS, B. O., 1992, *J. chem. Phys.*, **96,** 1218.
[54] MURPHY, R. B., and MESSMER, R. P., 1992, *J. chem. Phys.*, **97,** 4170.
[55] HIRAO, K., 1992, *Chem. Phys. Lett.*, **190,** 374.
[56] HIRAO, K., 1992, *Int. J. quantum Chem.*, **S26,** 517.
[57] TANAKA, K., SAKAI, T., and TERASHIMA, H., 1989, *Theo. Chim. Acta*, **76,** 213; SAKAI, T., and TANAKA, K., 1993, *Theo. Chim. Acta*, **85,** 451.
[58] GDANITZ, R. J., and AHLRICHS, R., 1988, *Chem. Phys. Lett.*, **143,** 413.
[59] CAVE, R. J., and DAVIDSON, E. R., 1988, *J. chem. Phys.*, **89,** 6798; 1988, *ibid.*, **88,** 5770; SAKAI, T, and TANAKA, K., 1993, *Theo. Chim. Acta*, **85,** 451.
[60] MUKHERJEE, D., *Recent Progress in Many Body Theories*, Vol. 4, edited by E. Schachinger, H. Mitter and H. Sormann (New York: Plenum Press).
[61] MUKHERJEE, D., 1997, *Chem. Phys. Lett.*, **274** , 561.
[62] MUKHERJEE, D., *Chem. Phys. Lett.* (submitted).
[63] KUTZELNIGG, W., and MUKHERJEE, D., 1997, *J. chem. Phys.*, **107,** 432.
[64] LINDGREN, I., 1985, *Phys. Scripta*, **32,** 291; LINDGREN, I., 1985, *Phys. Scripta*, **32,** 611.
[65] HOSE, G., and KALDOR, U., 1979, *J. Phys.* B, **12,** 3827.
[66] OLIPHANT, N., and ADAMOWICZ, L., 1991, *J. chem. Phys.*, **94,** 1229; OLIPHANT, N., and ADAMOWICZ, L., 1992, *J. chem. Phys.*, **96,** 3739.
[67] PIECUCH, P., OLIPHANT, N., and ADAMOWICZ, L., 1993, *J. chem. Phys.*, **99,** 1875; BASU-GHOSE, K., PIECUCH, P., and ADAMOWICZ, L., 1995, *J. chem. Phys.*, **103,** 24.
[68] STOLARCZYK, L. Z., 1994, *Chem. Phys. Lett.*, **217,** 1.
[69] WORMER, P. E. S., VISSER, F., and PALDUS, J., 1982, *J. Comp. Phys.*, **48,** 23.

[70] PURVIS, G. D., and BARTLETT, R. J., 1981, *J. chem. Phys.*, **75,** 1284.
[71] JANKOWSKI, K., MEISSNER, L., and WASILEWSKI, J., 1985, *Inter. J. quantum. Chem.*, **28,** 931.
[72] PIECUCH, P., and ADAMOWICZ, L., 1994, *Chem. Phys. Lett.*, **221,** 121.
[73] LI, X., and PALDUS, J., 1995, *J. chem. Phys.*, **103,** 1024.
[74] PALDUS, J., WORMER, P. E. S., and BÉNARD, M., 1988, *Coll. Czech. Chem. Comm.*, **53,** 1919.
[75] KRISHNAN, R., BINKLEY, J. S., SEEGER, R., and POPLE, J. A., 1980, *J. chem. Phys.*, **72,** 650.

MOLECULAR PHYSICS, 1998, VOL. 94, NO. 1, 173–179

Single-root multireference Brillouin–Wigner coupled-cluster theory. Rotational barrier of the N_2H_2 molecule

By PAVEL MACH, JOZEF MÁŠIK, JÁN URBAN and IVAN HUBAČ

Department of Chemical Physics, Faculty of Mathematics and Physics, Comenius University, 842 15 Bratislava, Slovakia

Recently developed single-root multireference Brillouin–Wigner coupled-cluster (MR BWCC) theory, which deals with one state at a time while employing a multiconfigurational reference wave function, is applied to study the rotational barrier of the N_2H_2 molecule. The method represents a brand new coupled-cluster (CC) approach to quasi-degenerate problems which combines merits of two approaches: the single-reference CC method in a nondegenerate case and the Hilbert space MR CC method in quasi-degenerate case. The method is able to switch itself from a nondegenerate to a fully degenerate case in a continuous manner, thus providing smooth potential energy surfaces. Moreover, in contrast to the Hilbert space MR CC theory, it does not contain the so-called coupling terms and in a highly nondegenerate case it reduces to a standard single-reference CC method. In order to better judge the abilities of our new approach, we study the rotation barrier of the N_2H_2 molecule at the CCSD level and the results are compared with the single-reference CCSD and Hilbert space MR CCSD methods. The rotation of the N_2H_2 molecule from a *trans*- to *cis*-conformer represents a typical two-state problem in which the weights of reference configurations can change from 0 to 1 in a continuous manner and, in contrast to the H_4 models, it represents a real system.

1. Introduction

In the past two decades, the single-reference coupled-cluster (CC) method, based on the exponential expansion of the wave function, has become one of the most efficient and reliable methods to account for electron correlation in the closed-shell nondegenerate ground states of atoms and molecules [1–9]. Nevertheless, its extension to a multireference case, that is necessary when handling quasi-degenerate or general open-shell systems, has proven by no means an unambiguous and easy task. Existing multireference coupled-cluster (MR CC) methods can be roughly divided into two groups; namely the valence universal or Fock space approach which employs a single (valence universal) exponential wave operator [10–21] and the state universal or Hilbert space approach based on the exponential ansatz of Jeziorski and Monkhorst [22] who represent the wave operator as a superposition of exponential operators, one for each configuration spanning the reference space.

One of the main reasons why existing MR CC methods as well as related multireference Rayleigh–Schrödinger many-body perturbation theory (MR MBPT) cannot be considered as standard or routine methods is the occurrence of intruder states or, in general, convergence problems. As is well known, both MR MBPT/CC theories are built on the concept of the effective Hamiltonian, introduced by Bloch [23], that acts in a relatively small model or reference space and provides us with energies of several states at the same time as its eigenvalues. In order to warrant size-extensivity, both theories prefer the complete model space formulations; however, too large model spaces are more likely to be plagued by intruder states and even singularities may appear on the potential energy surfaces. This situation is more pronounced for MR MBPT where the use of various shifting techniques at the level of the zeroth-order Hamiltonian becomes necessary in order to get rid of singularities. To date, the bulk of the MR MBPT applications exploits an averaging of orbital energies in the active space as proposed by Freed and co-workers; see for example [24]. Such a shifting technique does not destroy size-extensivity and is denoted as a forced degeneracy partitioning. On the other hand, in the case of the MR CC methods, one has to solve a system of nonlinear equations which may be cumbersome to converge; especially when the model space does not contain all the necessary configurations to describe all states. Thus, a worsened description of one state due to the insufficient reference space may worsen the convergence of other states or even destroy the convergence at all.

Therefore, instead of a simultaneous treatment of several states within existing MR CC approaches based on the Bloch theory (referred to as 'multi-root' approaches in the next section) it is highly desirable to develop such alternative methods which would aim at one state while employing a multiconfigurational reference and

assuming that the size-extensivity is not significantly violated. These approaches are often denoted as one-state or state-selective or state-specific or single-root methods. The first state-selective CC methods were proposed by Harris [25], Paldus *et al.* [26] and Nakatsuji and Hirao [27]. The next group is based on the multiconfigurational self-consistent-field (MC SCF) wave function see [28–33], and, finally, we should mention a size-extensive, spin-free open-shell CC theory based on the unitary group approach (UGA) formalism developed by Li and Paldus [34] and successfully applied to several open-shell systems, see e.g. [35]. Needless to say, a great deal of state-selective CC methods are not size-extensive which seems to be an inevitable price paid for their conceptual simplicity [36].

In our recent articles [36, 37] we formulated the multireference Brillouin–Wigner coupled-cluster (MR BWCC) theory, which deals with one state while employing a multiconfigurational reference wave function. We start from the multireference Brillouin–Wigner perturbation theory (MR BWPT) and construct a state-specific wave operator expressed in terms of the Brillouin–Wigner resolvent; however, instead of a perturbative treatment, we exploit an exponential ansatz for the state-specific wave operator. Such an approach is denoted as a single-root MR BWCC method. Using the Hilbert space approach to the wave operator, the single-root MR BWCC method has several advantages over the existing 'multi-root' Hilbert space MR CC approaches: (i) it does not contain the so-called coupling terms, (ii) equations for cluster amplitudes do not mix various sets of amplitudes and (iii) it is relatively very simple; all necessary diagrams are already present in the standard single-reference CC theory (iv) in a highly non-degenerate case the method reduces to the standard single-reference CC method. On the other hand, the method is not fully size-extensive due to the fact that it does not work with a 'genuine' Bloch equation for the wave operator. The size-extensivity of this method will be the subject of further work.

In the single-reference case, the BWCC theory was shown to be fully equivalent to the standard CC theory [38–40]. Although the single-reference BWCC theory does not employ the Baker–Campbell–Hausdorff (BCH) formula, it is a size-extensive method since the disconnected diagrams are cancelled out by the iterative procedure. The single-root MR BWCC method does not have such an analogy within the standard MR CC theories due to the fact that it works with a state-specific wave operator in the Brillouin–Wigner form explicitly dependent on one exact energy. In this regard, the single-root MR BWCC method represents a brand new approach.

So far, we have applied our single-root MR BWCC method to the ground state and first excited state of the trapezoidal H4 model system using a two-determinant model space spanned by two closed-shell type configurations at the level of the CCSD approximation; i.e. the CC method truncated at the single and double excitation level [37]. In the case of the ground state, the method provides the best approximation to the FCI energies of all tested multireference methods with a balanced description in the quasi-degenerate and nondegenerate regions. Moreover, it does not suffer from intruder states. Further, we applied this method to the ground state of the F_2 molecule exploiting a two-determinant model space [41]. We found that the single-root MR BWCCSD is devoid of the intruder state problem and provides a balanced description of the potential energy curve with a correct shape over the whole region of internuclear distances.

Another important class of reactions which should be treated by multireference methods are processes in which the crossing of occupied and unoccupied orbitals of different symmetries occurs. The simplest example of these processes, which are forbidden according to the Woodward–Hoffman rules, are rotations around the double bond in ethylene or in the N_2H_2 (1,2-diimide) molecule. The diimide (1,2-diazene) molecule has been the subject of various experimental and theoretical studies; see e.g. [42–44]. Theoretical studies were mostly focused on studying the relative energies of *trans*- and *cis*- isomers and the isomerization pathways. The N_2H_2 molecule is metastable relative to dissociation to N_2 and H_2 by about 60 kcal mol^{-1}. For this reason, diimide is widely used as a reagent in stereospecific hydrogenation of double bond. The mechanism of hydrogenation requires isomerization from the more stable *trans*-conformer to *cis*-conformer, which is believed to be the rate determining step. Since our ambition is not to find an exact rotation barrier, but to compare our single-root MR BWCC method with standard single-reference and MR CC methods, we use a scarce double zeta (DZ) basis set. Likewise, no geometry optimization is carried out.

The rigid rotation of the N_2H_2 molecule represents a typical two-state problem in which the weights of reference configurations can change from 0 to 1 in a continuous manner and, in contrast to the previously studied H4 model, it represents a real system. Needless to say, the true *trans–cis* isomerization path for the N_2H_2 molecule is not via double bond rotation but as in-plane inversion or via partial dissociation into a N_2H radical [45]. Using different theoretical methods it was found that the double bond rotation is not favourable isomerization pathway since the energy barrier about 67 kcal mol^{-1} is too high [45].

2. Single-root formulation of the MR BWPT

As is usual in perturbation theory, let us assume that the exact Hamiltonian H can be split into two parts, namely

$$H = H_0 + V, \tag{1}$$

where H_0 is a zeroth-order Hamiltonian and V is a perturbation. Our task is to find a solution of the Schrödinger equation for the exact Hamiltonian H

$$H\Psi_\alpha = \mathcal{E}_\alpha \Psi_\alpha, \tag{2}$$

while we know the solution of the characteristic problem for the zeroth-order Hamiltonian H_0

$$H_0 \Phi_\mu = E_\mu \Phi_\mu. \tag{3}$$

In general, we do not need to know the whole energy spectrum, but we are interested in several low lying states. To this end, let us assume that we are interested in one state, say, for simplicity, the ground state Ψ_0 and let us further assume that the most important contributions to this state are provided by d configurations Φ_μ represented by Slater determinants in a spin–orbital form. Given dominant configurations span the so-called model or reference space. To simplify our derivation, we use Greek indices α, β to denote exact wave functions, indices μ, ν for configurations spanning the model space and the Latin index q for configurations from the complementary space. If we separate the complete configuration space into the d-dimensional model space P and its orthogonal complement Q, the projection operator associated with the model space will have the form

$$P = \sum_{\mu=1}^{d} |\Phi_\mu\rangle\langle\Phi_\mu| = \sum_{\mu\in P} |\Phi_\mu\rangle\langle\Phi_\mu|. \tag{4}$$

Within the multireference BWPT [46], the exact wave function Ψ_0 can be expanded in the Brillouin–Wigner (BW) perturbation series as follows

$$\Psi_0 = (1 + B_0V + B_0VB_0V + \ldots)\,\Psi_0^P, \tag{5}$$

where Ψ_0^P is a projection of the exact wave function onto the model space

$$\Psi_0^P = P\Psi_0\,. \tag{6}$$

B_0 is the BW type of propagator

$$B_0 = \sum_{q\in Q} \frac{|\Phi_q\rangle\langle\Phi_q|}{\mathcal{E}_0 - E_q} \tag{7}$$

and $\mathcal{E}_0$ is the exact energy of the ground state. If we introduce a new operator $\tilde{\Omega}$, acting on states from the model space, in the following way

$$\tilde{\Omega} = 1 + B_0V + B_0VB_0V + \ldots \tag{8}$$

the exact wave function (5) can be expressed in the form

$$\Psi_0 = \tilde{\Omega}\,(P\Psi_0) = \tilde{\Omega}\,\Psi_0^P, \tag{9}$$

which implies that the operator $\tilde{\Omega}$ has the property of a wave operator (it transforms the projection of the exact wave function into the exact wave function). However, it should be stressed that our wave operator $\tilde{\Omega}$ is a 'state-specific' or 'single-root' wave operator since it converts just one projected wave function into the corresponding exact wave function in contrast to the so-called Bloch wave operator [23] that transforms several projected wave functions Ψ_α^P into corresponding exact states. So, in order to avoid any confusion with the Bloch wave operator, we use a tilde for our state-specific wave operator. As is well known, the Bloch wave operator obeys the so-called Bloch equation [23, 46–49]. From definition (8) it is immediately seen that our wave operator $\tilde{\Omega}$ obeys the operator equation

$$\tilde{\Omega} = 1 + B_0V\tilde{\Omega} \tag{10}$$

that may be viewed as an analogue of the Bloch equation for the state-specific wave operator.

The 'effective' Hamiltonian $\tilde{H}_{\text{eff}}$, which acts within the model space, is defined in the same way as in the Bloch theories, i.e.

$$\tilde{H}_{\text{eff}} = PH\tilde{\Omega}P\,. \tag{11}$$

Employing equation (9), we get

$$\tilde{H}_{\text{eff}}\Psi_0^P = PH\Psi_0 = \mathcal{E}_0\Psi_0^P \tag{12}$$

which implies that the exact energy of the ground state is obtained as one of the eigenvalues (roots) of the effective Hamiltonian and, likewise, the projected wave function Ψ_0^P is obtained as one of the eigenvectors of $\tilde{H}_{\text{eff}}$. The remaining eigenvalues and eigenvectors are uniquely determined by a definition of the state-specific wave operator (8), even though they do not represent any physical meaningful solution. While in both 'multi-root' as well as 'single-root' approaches the effective Hamiltonian acts within the same d-dimensional reference space, within the Bloch or 'multi-root' approach all roots of the effective Hamiltonian are physically meaningful in contrast to the 'single-root' approach where just one root has physical meaning. This is why we prefer the notation 'multi-root' and 'single-root' approaches in order to better distinguish between them. In addition, using the name 'single-root' we would like to emphasize the fact that the weights of the model space configurations are not *a priori* fixed as is often done in the case of prediagonalization based MR techniques.

In order to obtain the wave operator $\tilde{\Omega}$ in a form suitable for practical calculations, we project equation (10) onto configurations from the Q and P

subspaces which brings us a system of equations for $\mu = 1, 2, \ldots, d$

$$\mathcal{E}_0 \langle \Phi_q | \tilde{\Omega} | \Phi_\mu \rangle = \langle \Phi_q | H \tilde{\Omega} | \Phi_\mu \rangle \tag{13}$$

that can be viewed as a matrix analogue of the Bloch equation for the single-root wave operator. In contrast to multi-root theories, such a system of equations is dependent on the exact energy of interest and must be solved simultaneously with the eigenvalue problem for the effective Hamiltonian.

3. Single-root MR BWCC theory—Hilbert space approach

So far, we have specified the wave operator $\tilde{\Omega}$ in the Brillouin–Wigner form. If we adopt an exponential ansatz for the wave operator $\tilde{\Omega}$, we can speak about the single-root MR BWCC theory. The simplest way to accomplish the idea of an exponential expansion is to exploit the Hilbert space exponential ansatz of Jeziorski and Monkhorst [22]

$$\tilde{\Omega} = \sum_{\mu \in P} \exp\,(T^{\prime\prime}) | \Phi_\mu \rangle \langle \Phi_\mu | \,, \tag{14}$$

where $T^{\prime\prime}$ is a cluster operator defined with respect to the μth configuration involving, in general, one-body ($T_1^{\prime\prime}$), two-body ($T_2^{\prime\prime}$) up to the N-body ($T_N^{\prime\prime}$) cluster components

$$T^{\prime\prime} = T_1^{\prime\prime} + T_2^{\prime\prime} + \ldots + T_N^{\prime\prime} \tag{15}$$

with N being the total number of electrons. We limit ourselves to a complete model space formulation which implies that amplitudes corresponding to internal excitations (i.e. excitations within the model space) are equal to zero. Using the Hamiltonian in the normal-ordered-product form, i.e.

$$H = \langle \Phi_\mu | H | \Phi_\mu \rangle + H_N(\mu) = H_{\mu\mu} + H_N(\mu) \tag{16}$$

the matrix elements of the effective Hamiltonian (11) can be expressed in the form

$$\tilde{H}_{\nu\mu}^{\text{eff}} = \langle \Phi_\nu | H \tilde{\Omega} | \Phi_\mu \rangle = H_{\mu\mu} \delta_{\nu\mu} + \langle \Phi_\nu | H_N(\mu) \exp\,(T^{\prime\prime}) | \Phi_\mu \rangle, \tag{17}$$

where the μth configuration plays the role of a Fermi vacuum. Diagonalization of the effective Hamiltonian provides us with several eigenvalues; the lowest one is taken as a new exact energy $\mathcal{E}_0$, while the remaining ones are thrown away. As concerns cluster amplitudes, substituting the exponential ansatz (14) into equation (13), we get a system of equations

$$(\mathcal{E}_0 - H_{\mu\mu}) \langle \Phi_q | \exp\,(T^{\prime\prime}) | \Phi_\mu \rangle = \langle \Phi_q | H_N(\mu) \exp\,(T^{\prime\prime}) | \Phi_\mu \rangle \tag{18}$$

that can be used for the calculation of cluster amplitudes in the single-root MR BWCC theory. We recall that we did not use the BCH formula! As one can see, these equations do not mix various sets of cluster amplitudes (i.e. amplitudes belonging to various reference configurations) and the coupling among them is provided indirectly through the exact energy $\mathcal{E}_0$. Within the single-root MR BWCCSD approximation (i.e. with the cluster operators $T^{\prime\prime}$ being approximated by their singly and doubly excited cluster components), the singly excited amplitudes in a spin-orbital form are given by [37]

$$(\mathcal{E}_0 - \tilde{H}_{\mu\mu}^{\text{eff}})\, t_I^A(\mu) = \langle \Phi_I^A(\mu) | H_N(\mu) \exp\,(T^{\prime\prime}) | \Phi_\mu \rangle_C, \tag{19}$$

where the subscript C denotes a connected part. In general, for the doubly excited amplitudes we can write [37]

$$\begin{aligned}(\mathcal{E}_0 - \tilde{H}_{\mu\mu}^{\text{eff}})(t_{IJ}^{AB} + t_I^A t_J^B - t_J^A t_I^B)_\mu \\ = \langle \Phi_{IJ}^{AB}(\mu) | H_N(\mu) \exp\,(T^{\prime\prime}) | \Phi_\mu \rangle_C \\ + \mathcal{P}_{IJ} \mathcal{P}_{AB} \left[t_I^A(\mu) \langle \Phi_J^B(\mu) | H_N(\mu) \exp\,(T^{\prime\prime}) | \Phi_\mu \rangle_C \right]\end{aligned} \tag{20}$$

where $\mathcal{P}_{IJ}$ is an antisymmerization operator with respect to its indices. The computational cost of the method scales as the number of reference determinants times the cost of one single-reference CCSD calculation. For a special case of a two-determinant model space, corresponding to two active orbitals of different symmetry, the above equation simplifies to

$$\begin{aligned}(\mathcal{E}_0 - \tilde{H}_{\mu\mu}^{\text{eff}})\, t_{IJ}^{AB}(\mu) = \langle \Phi_{IJ}^{AB}(\mu) | H_N(\mu) \exp\,(T^{\prime\prime}) | \Phi_\mu \rangle_C \\ + (\mathcal{E}_0 - \tilde{H}_{\mu\mu}^{\text{eff}})(t_I^A t_J^B - t_J^A t_I^B)_\mu.\end{aligned} \tag{21}$$

The principal property of the single-root MR BWCC method is its ability of a continuous transition between the single-reference and multireference approaches. In a nondegenerate case the coupling between the reference configurations is weak which implies that the off-diagonal elements of $\tilde{H}_{\text{eff}}$ are negligible and the difference $(\mathcal{E}_0 - \tilde{H}_{\mu\mu}^{\text{eff}})$ vanishes for the ground state configuration Φ_μ. Thus equations (19) and (21) reduce to the standard nondegenerate CCSD equations for the ground state. As the quasi-degeneracy increases, the coupling between the reference configurations is getting large and these equations switch to a multireference regime.

4. Results and discussion

In order to better judge abilities of our single-root MR BWCC method, we study the rotational barrier of the N_2H_2 molecule at the CCSD level and the results are compared with the single-reference CCSD and Hilbert space MR CCSD methods. Rotation of the N_2H_2 molecule from a *trans*- to *cis*-conformer represents a typical

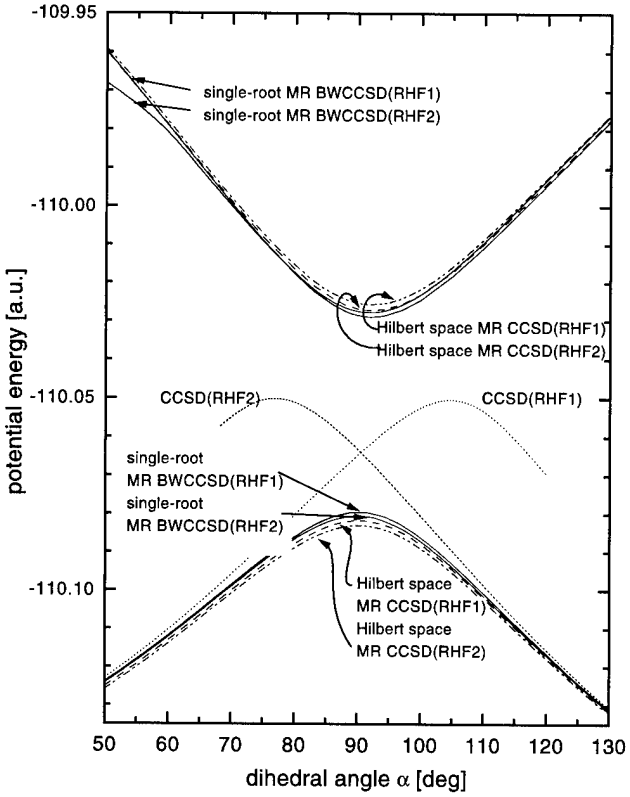

Figure 1. Potential energy curves for the ground and first biexcited states for the rigid rotation of the N_2H_2 molecule obtained by various coupled-cluster methods.

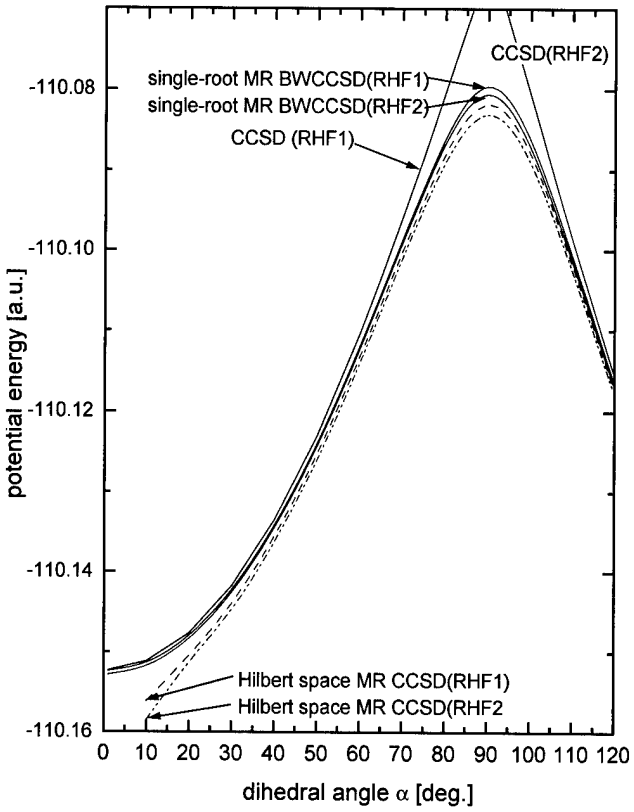

Figure 2. Close-up view of the rotational barrier for the N_2H_2 molecule obtained by various coupled-cluster methods. Note different behaviour for the Hilbert space MR CCSD and single-root MR BWCCSD methods in the nondegenerate region around the *cis*-conformer (dihedral angle = 0°).

two-state problem in which the weights of reference configurations can change from 0 to 1 in a continuous manner. In order to obtain a qualitatively correct potential energy curve, two closed-shell-type configurations have to be included in the reference space: the first configuration is a ground state for the *cis*-conformer (dihedral angle = 0°) and the second one is a ground state for the *trans*-conformer (dihedral angle = 180°). The ground state configuration for the *cis*-conformer represents a doubly excited configuration with respect to the ground state for the *trans*-conformer and vice versa.

Since the main goal of this article is to compare the behaviour of the single-root MR BWCCSD method with standard CC approaches, we confine ourselves to a scarce Gaussian (9s,5p) basis set contracted to [4s,3p] according to Dunning [50]. We employ a fixed geometry for the molecule; i.e. remaining internal coordinates are fixed at the values: r_{NN} = 2.573 bohr, r_{NH} = 1.930 bohr and θ_{HNN} = 106.2°. These values were optimized at the CASSCF level (two electrons in two orbitals) for a twisted (90°) conformation.

Molecular orbitals are taken from the restricted Hartree–Fock (RHF) calculations for the ground state. It is very interesting that two RHF solutions are possible over the whole range of dihedral angles. The first one, denoted as a RHF1 solution, represents a ground state for dihedral angles from 0° to 95°. Using the C_2 point group, the highest occupied molecular orbital (HOMO) has the B symmetry while the lowest unoccupied molecular orbital (LUMO) has the A symmetry. The second solution, denoted as a RHF2 solution, represents a ground state for dihedral angles from 95° to 180° with HOMO of the A symmetry and LUMO of the B symmetry. We performed calculations for both sets of molecular orbitals and they are distinguished by the presence of the suffix RHF1 or RHF2 behind the name of the method.

In figure 1, we present potential energy curves for the ground state obtained by the single-reference CCSD, Hilbert space MR CCSD and single-root MR BWCCSD methods as well as potential energy curves for the first bi-excited state. For a better distinction, we plot potential energy curves for dihedral angles from 50° to 130°. A detailed view of the ground state

(from 0° to 120°) is shown in figure 2. The model space consists of two closed-shell-type configurations and corresponds to the active orbital space spanned by two active orbitals: HOMO and LUMO. In view of a different spacial symmetry of active orbitals the model space is complete and one can exploit equation (21) for doubly excited cluster amplitudes. For a twisted conformation (about 90°) we observe a configurational degeneracy; that means the weights of both configurations become equal. The orbital HOMO–LUMO degeneracy is not observed, even though the orbital degeneracy alone is of less concern in the CC approaches.

As one can see, differences between the use of RHF1 and RHF2 orbitals are almost negligible and not substantial for the behaviour of the method. As expected, the single-reference CCSD method provides a reliable description of the ground state in the nondegenerate region (in the case of the RHF1 orbitals from 0° to 70°), but completely fails in regions where the ground state configuration is no longer a dominant configuration.

The Hilbert space MR CCSD method gives the correct shape of the potential energy barrier almost over the whole range of the dihedral angles, but fails in a highly nondegenerate region (in the proximity of 0° and 180°). Such a failure of the Hilbert space MR CCSD method is very often and may be attributed to the model space deficiency. Even though our model space contains all relevant configurations to describe the ground state, it may not be sufficient for the excited state. One must keep in mind that both states are treated simultaneously, so the insufficient description of one state (due to the reference space or truncation of the cluster operator) may worsen the convergence of the other state or even, alone, destroy the convergence. Probably, this explains why the Hilbert space MR CC method is not used to calculate potential energy surfaces and, on the other hand, why it is useful to develop such approaches which would aim at one state.

The single-root MR BWCCSD method provides us with a smooth potential energy barrier of correct shape for all dihedral angles. In the nondegenerate region, the single-root MR BWCCSD potential energy curve becomes identical (flows together) with the single-reference CCSD one, while in the quasi-degenerate region it approaches the Hilbert space MR CCSD curve. It is worth mentioning that the single-root MR BWCCSD and Hilbert space MR CCSD approximations do not become identical even in the case of a full configuration degeneracy since they work with different wave operators. Nevertheless, their difference can serve as a rough estimate of the size-extensivity error of our method. We see, that it is rather small (at least in this case).

For completeness, we also performed the single-root MR BWCCSD calculations for the excited state (see figure 1). It is remarkable that the differences from the Hilbert space MR CCSD method in the quasi-degenerate region are comparable with those observed for the ground state; so the single-root MR BWCC method can also be successfully applied to excited states; even though, in general, we are not able to exclude convergence difficulties. One can thus conclude that the single-root MR BWCC method appears as a viable and promising approach and should deserve our attention.

This work was supported by the grant 1/1334/94 of the Slovak Grant Agency and the COST Action D3 project.

References

[1] COESTER, F., 1958, *Nucl. Phys.*, **7**, 421; COESTER, F., and KÜMMEL, H., 1960, *Nucl. Phys.*, **17**, 477.

[2] ČÍŽEK, J., 1966, *J. chem. Phys.*, **45**, 4256; 1969, *Adv. chem. Phys.*, **14**, 35.

[3] ČÍŽEK, J., and PALDUS, J., 1971, *Int. J. quantum Chem.*, **5**, 359.

[4] PALDUS, J., ČÍŽEK, J., and SHAVITT, I., 1972, *Phys. Rev. A*, **5**, 50.

[5] PALDUS, J., 1992, *Methods in Computational Molecular Physics*, NATO ASI Series, edited by S. Wilson and G. H. F. Diercksen (New York: Plenum), pp. 99 194; 1994, *Relativistic and Correlation Effects in Molecules and Solids*, NATO ASI Series, edited by G. L. Malli (New York Plenum), pp. 207–282.

[6] BARTLETT, R. J., 1981, *Ann. Rev. phys. Chem.*, **32**, 359; 1989, *J. chem. Phys.*, **93**, 1697.

[7] BARTLETT, R. J., DYKSTRA, C. E., and PALDUS, J., 1984, *Advanced Theories and Computational Approaches for the Electronic Structure of Molecules*, edited by C. E. Dykstra (Dordrect: Reidel), pp. 127–159.

[8] JANKOWSKI, K., 1987, *Methods in Computational Chemistry*, Vol. 1, edited by S. Wilson (New York: Plenum), pp. 1–116; URBAN, M., ČERNUŠÁK, I., KELLÖ, V, and NOGA, J., *ibid.*, pp. 117–250.

[9] WILSON, S., 1984, *Electron Correlation in Molecules* (Oxford: Clarendon).

[10] COESTER, F., 1966, *Lectures in Theoretical Physics*, Vol. 11B, edited by K. T. Mahanthappa and W. E. Brittin (New York: Gordon and Breach), pp. 157–186.

[11] MUKHERJEE, D., MOITRA, R. K., and MUKHOPADHYAY, A., 1975, *Pramana*, **4**, 247; 1975, *Molec. Phys.*, **30**, 1861; 1977, *Molec. Phys.*, **33**, 955; HAQUE , A., and MUKHERJEE, D., 1984, *J. chem. Phys.*, **80**, 5058.

[12] OFFERMANN, R., EY, W., and KÜMMEL, H., 1976, *Nucl. Phys. A*, **273**, 349; OFFERMANN, R., 1976, *Nucl. Phys. A*, **273**, 368; EY, W., 1978, *Nucl. Phys. A*, **296**, 189.

[13] LINDGREN, I., 1978, *Int. J. quantum Chem. Symp.*, **12**, 33.

[14] STOLARCZYK, L. Z., and MONKHORST, H. J., 1985, *Phys. Rev.* A, **32,** 725; 1985, *ibid.* 743; 1988, *Phys. Rev.* A, **37,** 1908; 1988, *ibid.* 1926.
[15] KUTZELNIGG, W., 1984, *J. chem. Phys.*, **80,** 822.
[16] HAQUE, A., and KALDOR, U., 1985, *Chem. Phys. Lett.*, **117,** 347; 1985, *Chem. Phys. Lett.*, **120,** 261; 1986, *Int. J. quantum Chem.*, **29,** 425.
[17] KALDOR, U., 1987, *J. chem. Phys.*, **87,** 467; 1991, *Theor. Chim. Acta*, **80,** 427 and references therein.
[18] LINDGREN, I., and MUKHERJEE, D., 1987, *Phys. Rep.*, **151,** 93.
[19] MUKHERJEE, D., and PAL, S., 1989, *Adv. quantum Chem.*, **20,** 292 and references therein.
[20] MEISSNER, L., 1995, *J. chem. Phys.*, **103,** 8014; 1996, *Chem. Phys. Lett.*, **255,** 244.
[21] NOOIJEN, M., and BARTLETT, R. J., 1996, *J. chem. Phys.*, **104,** 2652; NOOIJEN, M., 1996, *J. chem. Phys.*, **104,** 2638.
[22] JEZIORSKI, B., and MONKHORST, H. J., 1981, *Phys. Rev.* A, **24,** 1668.
[23] BLOCH, C., 1958, *Nucl. Phys.*, **6,** 329.
[24] FREED, K. F., 1989, *Many-Body Methods in Quantum Chemistry, Lecture Notes in Chemistry*, Vol. 52, edited by U. Kaldor (Berlin: Springer), pp. 1–21 and references therein; FINLEY, J. P., CHAUDHURI, R. K., and FREED, K. F., 1995, *J. chem. Phys.*, **103,** 4990; 1996, *Phys. Rev.* A, **54,** 343.
[25] HARRIS, E. F., 1977, *Int. J. quantum Chem. Symp.*, **11,** 403.
[26] PALDUS, J., ČÍŽEK, J., SAUTE, M., and LAFORGUE, A., 1978, *Phys. Rev.* A, **17,** 805; SAUTE, M., PALDUS, J., and ČÍŽEK, J., 1979, *Int. J. quantum Chem.*, **15,** 463.
[27] NAKATSUJI, M., and HIRAO, K., 1978, *J. chem. Phys.*, **68,** 2053; 1978, *ibid.* 4279; NAKATSUJI, M., 1978, *Chem. Phys. Lett.*, **59,** 362; 1979, *Chem. Phys. Lett.*, **67,** 329; 1983, *Int. J. quantum Chem. Symp.*, **17,** 241 and references therein.
[28] BANERJEE, A., and SIMONS, J., 1981, *Int. J. quantum Chem.*, **19,** 207; 1982, *J. chem. Phys.*, **76,** 4548; 1983, *Chem. Phys.*, **81,** 297; 1984, *Chem. Phys.*, **87,** 215.
[29] BAKER, H., and ROBB, M. A., 1983, *Molec. Phys.*, **50,** 1077.
[30] TAKANA, R., and TERASHIMA, H., 1984, *Chem. Phys. Lett.*, **106,** 558.
[31] LAIDIG, W. D., and BARTLETT, R. J., 1984, *Chem. Phys. Lett.*, **104,** 424.
[32] LAIDIG, W. D., SAXE, P., and BARTLETT, R. J., 1987, *J. chem. Phys.*, **86,** 887.
[33] HOFFMANN, M. R., and SIMONS, J., 1988, *J. chem. Phys.*, **88,** 993.
[34] PALDUS, J., and LI, X., 1993, *Symmetries in Science* VI, edited by B. Gruber (New York: Plenum), pp. 573–591; LI, X., and PALDUS, J., 1993, *Int. J. quantum Chem. Symp.*, **27,** 269; 1994, *J. chem. Phys.*, **101,** 8812; JEZIORSKI, B., PALDUS, J., and JANKOWSKI, P., 1995, *Int. J. quantum Chem.*, **56,** 129.
[35] LI, X., and PALDUS, J., 1995, *J. chem. Phys.*, **102,** 2013; 1995, *ibid.*, **102,** 8059; 1995, *ibid.*, **103,** 1024; 1995, *ibid.*, **103,** 6536.
[36] MÁŠIK, J., and HUBAČ, I., 1997, *Quantum Systems in Chemistry and Physics: Trends in Methods and Applications*, edited by R. McWeeny, J. Maruani, Y. G. Smeyers, and S. WILSON (Dordrecht: Kluwer Academic Publishers.
[37] MÁŠIK, J., and HUBAČ, I., 1998, *Adv. Quant. Chem.* (in the press).
[38] HUBAČ, I., and NEOGRÁDY, P., 1994, *Phys. Rev.* A, **50,** 4558.
[39] HUBAČ, I., 1996, *New Methods in Quantum Theory*, NATO ASI Series, edited by C. A. Tsipis, V. S. Popov, D. R. Herschbach, and J. S. Avery (Dordrecht: Kluwer), pp. 183–202.
[40] MÁŠIK, J., and HUBAČ, I., 1997, *Coll. Czech. Chem. Commun.*, **62,** 829.
[41] MÁŠIK, J., MACH, P., and HUBAČ, I., 1998, *J. chem. Phys.* (in the press).
[42] WHITELEGG, D., and WOOLLEY, R. G., 1990, *J. molec. Struct. (Theochem)*, **209,** 23.
[43] KIM, K., SHAVITT, I., and DEL BENE, J. E., 1992, *J. chem. Phys.*, **96,** 7573.
[44] CIMIRAGLIA, R., and HOFMANN, H.-J., 1994, *Chem. Phys. Lett.*, **217,** 431.
[45] JENSEN, H. J. A., JÖRGENSEN, P., and HELGAKER, T., 1986, *J. chem. Phys.*, **85,** 3917.
[46] LINDGREN, I., 1974, *J. Phys.* B, **7,** 2441.
[47] KVASNIČKA, V., 1974, *Czech. J. Phys.* B, **24,** 605.
[48] KVASNIČKA, V., 1977, *Czech. J. Phys.* B, **27,** 599; 1977, *Adv. chem. Phys.*, **36,** 345.
[49] LINDGREN, I., 1978, *Int. J. quantum Chem. Symp.*, **12,** 33.
[50] DUNNING, T. H., 1970, *J. chem. Phys.*, **53,** 2823.

MOLECULAR PHYSICS, 1998, VOL. 94, NO. 1, 181–187

The relativistic coupled-cluster method: transition energies of bismuth and eka-bismuth

By EPHRAIM ELIAV, UZI KALDOR
School of Chemistry, Tel Aviv University, 69978 Tel Aviv, Israel

and YASUYUKI ISHIKAWA
Department of Chemistry, University of Puerto Rico, PO Box 23346, San Juan, Puerto Rico 00931–3346, USA

The relativistic coupled-cluster method, which incorporates relativistic terms through second order in the fine-structure constant α and correlation effects summed to all orders of the one- and two-electron excitations, is described. An application to the transition energies of bismuth and eka-bismuth (element 115) is described. A large basis (34s26p20d14f9g6h4i) is used to solve the Dirac–Fock–Breit equations, and the external 37 electrons of each atom are then correlated. Good agreement with experimental values is obtained for Bi, with an average error of 0.05 eV. Two bound states are predicted for the Bi^- anion. The trend of transition energies upon going from Bi to eka-bismuth shows a relative stabilization of the $p_{1/2}$ orbital and destabilization of $p_{3/2}$ in the heavier element, by 1.5–1.9 eV per electron.

1. Introduction

The structure and chemistry of a light atom or molecule may be investigated by means of the pertinent Schrödinger equation. This equation may be solved to a good approximation by the methods of modern quantum chemistry. Relativistic effects are not very large for the first few rows of the periodic table. When knowledge of these is required, e.g. to understand the fine structure of atomic spectra, they may be calculated by perturbation theory [1]. This approach is not satisfactory for heavier atoms, where relativistic effects become too large for perturbative treatment, changing significantly even such fundamental properties of the atom as the order of orbitals. The Schrödinger equation must then be supplanted by an appropriate relativistic wave equation such as Dirac–Coulomb or Dirac–Coulomb–Breit. Approximate one-electron solutions to these equations may be obtained by the self-consistent-field procedure. The resulting Dirac–Fock or Dirac–Fock–Breit functions are conceptually similar to the familiar Hartree–Fock functions; the Hartree–Fock orbitals are replaced, however, by four-component vectors. Correlation is no less important in the relativistic regime than it is for the lighter elements, and may be included in a similar manner.

Methodology for high-accuracy calculations of systems with heavy and super-heavy elements is described here. The no-virtual-pair Dirac–Coulomb–Breit Hamiltonian, which is correct to second order in the fine-structure constant α, provides the framework of the method. Correlation is treated by the coupled cluster (CC) approach. The relativistic coupled-cluster (RCC) method is applied to bismuth and eka-bismuth; the main properties of interest are transition energies (ionization potentials, excitation energies, electron affinities).

2. Methodology

2.1. *The relativistic Hamiltonian*

The relativistic many-electron Hamiltonian cannot be written in closed form; it may be derived perturbatively from quantum electrodynamics [2]. The simplest form is the Dirac–Coulomb (DC) Hamiltonian, where the non-relativistic one-electron terms in the Schrödinger equation are replaced by the one-electron Dirac operator h_D,

$$H_{DC} = \sum_i h_D(i) + \sum_{i<j} 1/r_{ij}\,, \tag{1}$$

with

$$h_D = c\boldsymbol{\alpha}\cdot\mathbf{p} + \beta c^2 + V_{nuc}\,. \tag{2}$$

$\boldsymbol{\alpha}$ and β are the four-dimensional Dirac matrices, and V_{nuc} is the nuclear attraction operator, with the nucleus modelled as a point or finite-size charge. Only the one-electron terms in the DC Hamiltonian include relativistic effects, and the two-electron repulsion remains in the non-relativistic form. The lowest-order correction to the two-electron repulsion is the Breit [3] operator

$$B_{12} = -\tfrac{1}{2}[\boldsymbol{\alpha}_1\cdot\boldsymbol{\alpha}_2 + (\boldsymbol{\alpha}_1\cdot\mathbf{r}_{12})\cdot(\boldsymbol{\alpha}_2\cdot\mathbf{r}_{12})/r_{12}^2]/r_{12}\,, \tag{3}$$

yielding the Dirac–Coulomb–Breit (DCB) Hamiltonian

0026–8976/98 $12·00

$$H_{\mathrm{DCB}} = \sum_i h_{\mathrm{D}}(i) + \sum_{i<j}(1/r_{ij} + B_{ij}). \tag{4}$$

All equations are in atomic units.

Neither the DC nor the DCB Hamiltonians are appropriate starting points for accurate many-body calculations. The reason is the admixture of the negative-energy eigenstates of the Dirac Hamiltonian by the two-body terms in an erroneous way [4, 5]. The no-virtual-pair approximation [6, 7] is invoked to correct this problem: the negative-energy states are eliminated by the projection operator Λ^+, leading to the projected Hamiltonians

$$H^+_{\mathrm{DC}} = \Lambda^+ H_{\mathrm{DC}} \Lambda^+ \tag{5}$$

or

$$H^+_{\mathrm{DCB}} = \Lambda^+ H_{\mathrm{DCB}} \Lambda^+ . \tag{6}$$

H^+_{DCB} is correct to second order in the fine-structure constant α, and is expected to be highly accurate for all neutral and weakly-ionized atoms [8]. Higher quantum electrodynamic (QED) terms are required for strongly-ionized species. A comprehensive discussion of higher QED effects and other aspects of relativistic atomic physics may be found in the proceedings of the 1988 Santa Barbara program [9].

2.2. *The one-electron equation*

The no-pair DCB Hamiltonian (6) is used as a starting point for variational or many-body relativistic calculations [10]. The procedure is similar to the non-relativistic case, with the Hartree–Fock orbitals replaced by the four-component Dirac–Fock–Breit (DFB) functions. The spherical symmetry of atoms leads to the separation of the one-electron equation into radial and spin-angular parts [11]. The radial four-vector has the so-called large component $P_{n\kappa}$ in the upper two places and the small component $Q_{n\kappa}$ in the lower two. The quantum number κ (with $|\kappa| = j + 1/2$) comes from the spin-angular equation, and n is the principal quantum number, which counts the solutions of the radial equation with the same κ. Defining

$$\phi_{n\kappa} = \begin{pmatrix} cP_{n\kappa}(r) \\ Q_{n\kappa}(r) \end{pmatrix}, \tag{7}$$

the DFB equation has the form

$$F_\kappa \phi_{n\kappa} = \varepsilon_{n\kappa} \phi_{n\kappa} , \tag{8}$$

where the one-electron DFB operator F_κ is [12–16]

$$F_\kappa = \begin{pmatrix} V_{\mathrm{nuc}} + U^{\mathrm{LL}} & c\Pi_\kappa + U^{\mathrm{LS}} \\ s\Pi^+_\kappa + U^{\mathrm{SL}} & V_{\mathrm{nuc}} + U^{\mathrm{SS}} - 2c^2 \end{pmatrix}, \tag{9}$$

with

$$\Pi_\kappa = -\mathrm{d}/\mathrm{d}r + \kappa/r \tag{10}$$

and

$$\Pi^+_\kappa = \mathrm{d}/\mathrm{d}r + \kappa/r . \tag{11}$$

V_{nuc} is the nuclear attraction potential. In the uniform charge distribution model used here, the charge of a nucleus of atomic mass A is distributed uniformly over a sphere with radius $R = 2.2677 \times 10^{-5} A^{-1/3}$. The nuclear potential for a nucleus with charge Z is then

$$V_{\mathrm{nuc}} = \begin{cases} -Z/r & \text{for } r > R \\ -(Z/2R)(3 - r^2/R^2) & \text{for } r \leqslant R . \end{cases} \tag{12}$$

The terms U^{LL} etc. represent the one-body mean-field potential, which approximates the two-electron interaction in the Hamiltonian, as is the practice in SCF schemes. In the DFB equations this interaction includes the Breit term (3) in addition to the electron repulsion $1/r_{ij}$.

The radial functions $P_{n\kappa}(r)$ and $Q_{n\kappa}(r)$ may be obtained by numerical integration [17, 18] or by expansion in a basis [19]. Since the Dirac Hamiltonian is not bound from below, failure to observe correct boundary conditions leads to 'variational collapse' [20–27], where admixture of negative-energy solutions may yield energies much below experimental. To avoid this failure, the basis sets used for expanding the large and small components must maintain 'kinetic balance' [24, 25]. In the non-relativistic limit ($c \to \infty$), the small component is related to the large component by [20]

$$Q_{n\kappa}(r) = (2c)^{-1} \Pi^+_\kappa P_{n\kappa}(r) , \tag{13}$$

where Π^+_κ is defined in (11). The simplest way to obtain kinetic balance is to derive the small-component basis functions from those used to span the large component by

$$\chi^{\mathrm{S}}_{\kappa j} = \Pi^+_\kappa \chi^{\mathrm{L}}_{\kappa j} . \tag{14}$$

Ishikawa and co-workers [16, 23] have shown that G-spinors, with functions spanned in Gaussian-type functions (GTF) chosen according to (14), satisfy the kinetic balance for finite c values if the nucleus is modelled as a uniformly-charged sphere.

2.3. *The Fock-space coupled-cluster method*

The coupled-cluster method is well-known by now, and only a brief account of aspects relevant to our applications is given here.

The Dirac–Coulomb–Breit Hamiltonian H^+_{DCB} may be rewritten in second-quantized form [6, 16] in terms of normal-ordered products of spinor creation and annihilation operators $\{r^+ s\}$ and $\{r^+ s^+ ut\}$,

$$H = H^{+}_{\mathrm{DCB}} - \langle 0|H^{+}_{\mathrm{DCB}}|0\rangle$$

$$= \sum_{rs} f_{rs}\{r^{+}s\} + \frac{1}{4}\sum_{rstu}\langle rs||tu\rangle\{r^{+}s^{+}ut\}, \qquad (15)$$

where

$$\langle rs||tu\rangle = \langle rs|tu\rangle - \langle rs|ut\rangle \qquad (16)$$

and

$$\langle rs|tu\rangle = \int d\mathbf{x}_1 d\mathbf{x}_2 \Psi^{*}_{r}(\mathbf{x}_1)\Psi^{*}_{s}(\mathbf{x}_2)(r_{12}^{-1} + B_{12})\Psi_{t}(\mathbf{x}_1)\psi_{u}(\mathbf{x}_2). \qquad (17)$$

Here f_{rs} and $\langle rs||tu\rangle$ are, respectively, elements of one-electron Dirac–Fock and antisymmetrized two-electron Coulomb–Breit interaction matrices over Dirac four-component spinors. The effect of the projection operators Λ^{+} is now taken over by the normal ordering, denoted by the curly braces in (15), which requires annihilation operators to be moved to the right of creation operators as if all anticommutation relations vanish. The Fermi level is set at the top of the highest occupied positive-energy state, and the negative-energy states are ignored.

By adopting the no-pair approximation, a natural and straightforward extension of the non-relativistic open-shell CC theory emerges. The multireference valence-universal Fock-space coupled-cluster approach is employed [28], which defines and calculates an effective Hamiltonian in a low-dimensional model (or P) space, with eigenvalues approximating some desirable eigenvalues of the physical Hamiltonian. The effective Hamiltonian has the form [29]

$$H_{\mathrm{eff}} = PH\Omega P \qquad (18)$$

where Ω is the normal-ordered wave operator,

$$\Omega = \{\exp(S)\}. \qquad (19)$$

The Fock-space approach starts from a reference state (closed-shell in our applications, but other single-determinant functions may also be used), correlates it, then adds and/or removes electrons one at a time, recorrelating the whole system at each stage. The sector (m, n) of the Fock space includes all states obtained from the reference determinant by removing m electrons from designated occupied orbitals, called valence holes, and adding n electrons in designated virtual orbitals, called valence particles. The practical limit is $m + n \leqslant 2$, although higher sectors have also been tried [30]. The excitation operator is partitioned into sector operators

$$S = \sum_{m\geqslant 0}\sum_{n\geqslant 0} S^{(m,n)}. \qquad (20)$$

This partitioning allows for partial decoupling of the open-shell CC equations. The equations for the (m, n) sector involve only S elements from sectors (k, l) with $k \leqslant m$ and $l \leqslant n$, so that the very large system of coupled nonlinear equations is separated into smaller subsystems, which are solved consecutively: first, the equations for $S^{(0,0)}$ are iterated to convergence; the $S^{(1,0)}$ (or $S^{(0,1)}$) equations are then solved using the known $S^{(0,0)}$, and so on. This separation, which does not involve any approximation, reduces the computational effort significantly. The effective Hamiltonian (18) is also partitioned by sectors. An important advantage of the method is the simultaneous calculation of a large number of states.

Each sector excitation operator is, in the usual way, a sum of virtual excitations of one, two,..., electrons,

$$S^{(m,n)} = \sum_{l} S^{(m,n)}_{l}, \qquad (21)$$

with l going, in principle, to the total number of electrons. In practice, l has to be truncated. The level of truncation reflects the quality of the approximation, i.e. the extent to which the complementary Q space is taken into account in the evaluation of the effective Hamiltonian. In the applications described below the series (21) is truncated at $l=2$. The resulting CCSD (coupled cluster with single and double excitations) scheme involves the fully self-consistent, iterative calculation of all one- and two-body virtual excitation amplitudes and sums all diagrams with these excitations to infinite order. As negative-energy states are excluded from the Q space, the diagrammatic summations in the CC equations are carried out only within the subspace of the positive-energy branch of the DF spectrum.

The H_{eff} diagrams may be separated into core and valence parts,

$$H_{\mathrm{eff}} = H^{\mathrm{core}}_{\mathrm{eff}} + H^{\mathrm{val}}_{\mathrm{eff}}, \qquad (22)$$

where the first term on the right-hand side consists of diagrams without any external (valence) lines and describes core electron correlation. The eigenvalues of $H^{\mathrm{val}}_{\mathrm{eff}}$ will then give directly the transition energies from the reference state, with correlation effects included for both initial and final states. The physical significance of these energies depends on the nature of the model space. Thus, electron affinities may be calculated by constructing a model space with valence particles only [$(0,n)$ sectors, $n > 0$], ionization potentials are given using valence holes [$(n, 0)$ sectors, $n > 0$], and both valence types are required to describe excitations out of the reference state [(m, n) sectors, $m, n > 0$].

3. Application to atoms

Different ways of implementing the relativistic coupled cluster (RCC) method are known. A numerical procedure for solving the pair equation has been developed by Lindgren and co-workers [31] and applied to

two-electron atomic systems [32]. Other approaches use discrete basis sets of local or global functions. This makes the application of the projection operators onto the positive-energy space much easier than in the numerical scheme; one simply ignores the negative-energy branch of the one-electron spectrum. A technique based on local splines was developed by Blundell and co-workers [33], while the Göteborg group introduced another type of local basis, obtained by discretizing the radial space [34]. The first relativistic coupled cluster calculation in a global basis [35] appeared in 1990, but was limited to s orbitals only, both in the occupied and virtual space. A more general and sustained implementation started two years later, with pilot calculations for light atoms in closed-shell [36] and open-shell [37] states. The method has since been applied to many heavy atoms, where relativistic effects are crucial to the correct description of atomic structure. Calculated properties include ionization potentials, excitation energies, electron affinities, fine-structure splittings, and for superheavy elements—the nature of the ground state. The additivity of relativistic and correlation effects was also studied. Systems investigated include the gold atom [38], few-electron ions [39], the alkali-metal atoms Li–Fr [40], the Xe atom [41], the f^2 shells of Pr^{3+} and U^{4+} [42], the ytterbium [43], lutetium [43], mercury [44], barium [45], radium [45], and thallium [46] atoms, and the superheavy elements lawrencium [43], rutherfordium [47], 111 [48], 112 [44], 113 [46], and 118 [49]. Applications to bismuth and eka-bismuth (element 115) are described below.

The spherical symmetry of atoms, which leads to angular decomposition of the wave function and coupled-cluster equations, is used at both the Dirac–Fock–Breit [16] and RCC [38, 40] stages of the calculation. The energy integrals and CC amplitudes which appear in the Goldstone-type diagrams defining the CC equations are decomposed in terms of vector-coupling coefficients, expressed by angular-momentum diagrams, and reduced Coulomb–Breit or **S** matrix elements, respectively. The reduced equations for single and double excitation amplitudes are derived using the Jucys–Levinson–Vanagas theorem [29] and solved iteratively. This technique makes possible the use of large basis sets with high l values, as a basis orbital gives rise to two functions at most, with $j = l \pm 1/2$, whereas in Cartesian coordinates the number of functions increases rapidly with l. Typically we go up to h ($l = 5$) or i ($l = 6$) orbitals. To account for core-polarization effects, which may be important for many systems, we correlate at least the two outer shells, usually 20–40 electrons. Finally, uncontracted Gaussians are used, since contraction leads to problems in satisfying kinetic balance and correctly representing the small components. On the other hand, it has been found that high-energy virtual orbitals have little effect on the transition energies we calculate, since these orbitals have nodes in the inner regions of the atom and correlate mostly the inner-shell electrons, which we do not correlate anyway. These virtual orbitals, with energies above 80 or 100 hartree, are therefore eliminated from the RCC calculation.

Bismuth is the heaviest non-radioactive element. Few theoretical investigations of its spectrum have been published. Keller *et al.* [50] calculated properties of all group 15 elements, including eka-bismuth, by the Dirac–Fock–Slater (DFS) method; the ionization potentials of Bi had errors of ~1 eV. Rose *et al.* [51] obtained multi-configuration Dirac–Fock (MCDF) excitation energies in the $6p^3$ manifold of Bi, with an accuracy of 0.15–0.4 eV. Bieron *et al.* [52] added configuration interaction to calculate oscillator strength for some transitions in Bi^+. Dzuba *et al.* [53] calculated transition energies within the Bi $6p^3$ configuration by relativistic many-body perturbation theory.

The Fock-space scheme used to obtain states of bismuth and its ions started from Bi^+. The spin–orbit splitting of the 6p orbitals is sufficiently large to make the $6s^2 6p_{1/2}^2$ ground state of Bi^+ a closed shell. Electrons were added in the $6p_{3/2}$ orbital to obtain the ionization potential and electron affinity of Bi, or removed from the 6s and $6p_{1/2}$ orbitals to yield states of Bi^{2+} and Bi^{3+}; excited states of Bi^+ were calculated by both adding and removing one electron from the reference state:

$$\begin{aligned} \mathrm{Bi}^+(0,0) \rightarrow \mathrm{Bi}(0,1) &\rightarrow \mathrm{Bi}^-(0,2) \\ &\rightarrow \mathrm{Bi}^{2+}(1,0) \rightarrow \mathrm{Bi}^{3+}(2,0) \\ &\rightarrow \mathrm{Bi}^{+*}(1,1). \end{aligned} \tag{23}$$

A similar scheme was used for eka-bismuth.

The universal basis set of Malli *et al.* [54] is employed. It consists of Gaussian-type orbitals, with exponents given by the geometric series

$$\zeta_n = \alpha \times \beta^{(n-1)}, \qquad \alpha = 106\,111\,395.371\,615,$$
$$\beta = 0.486\,752\,256\,286. \tag{24}$$

The basis included 34 s functions ($n = 1$–34), 26 p ($n = 9$–34), 20 d ($n = 13$–32), 14 f ($n = 17$–30), 9 g ($n = 21$–29), 6 h ($n = 24$–29), and 4 i orbitals ($n = 25$–28). The orbitals were left uncontracted. Virtual orbitals with energies higher than 80 hartree were omitted. The atomic masses taken were 208.980 for Bi and 277 for eka-bismuth. The external 36 electrons were correlated ($4f^{14}5s^25p^85d^{10}6s^26p^2$ in the case of Bi^+, corresponding shells for $E115^+$). All computations were carried out at Tel Aviv University.

Table 1. Transition energies of Bi and its ions (eV).

	Transition	Experiment [55, 56]	RCC	+ Breit
Bi IP:	$6p_{1/2}^2 6p_{3/2}\ ^4S_{3/2} \rightarrow 6p_{1/2}^2\ ^3P_0$	7.289	7.183	7.183
Bi EA:	$6p_{1/2}^2 6p_{3/2}\ ^4S_{3/2} \rightarrow 6p_{1/2}^2 6p_{3/2}^2\ ^3P_2$	0.95	1.031	1.034
	$\rightarrow 6p_{1/2}^2 6p_{3/2}^2\ ^3P_0$		0.179	0.180
Bi^+ IP:	$6p_{1/2}^2\ ^3P_0 \rightarrow 6p_{1/2}\ ^2P_{1/2}$	16.688	16.684	16.655
Bi^+ EE:	$6p_{1/2}^2\ ^3P_0 \rightarrow 6p_{1/2}6p_{3/2}\ ^3P_1$	1.652	1.692	1.672
	$\rightarrow 6p_{1/2}6p_{3/2}\ ^3P_2$	2.111	2.153	2.133
Bi^{2+} IP:	$6s^2 6p_{1/2},\ ^2P_{1/2} \rightarrow 6s^2\ ^1S_0$	25.563	25.562	25.570
Bi^{3+} EE:	$6s^2\ ^1S_0 \rightarrow 6s6p_{1/2}\ ^3P_0$	8.798	8.762	8.781
	$\rightarrow 6s6p_{1/2}\ ^3P_1$	9.414	9.493	9.510

Table 2. Transition energies of eka-bismuth (element 115) and its ions (eV).

	Transition	RCC	+ Breit	Reference [50]
E115 IP:	$7p_{1/2}^2 7p_{3/2}\ ^4S_{3/2} \rightarrow 7p_{1/2}^2\ ^3P_0$	5.579	5.583	5.2
E115 EA:	$7p_{1/2}^2 7p_{3/2}\ ^4S_{3/2} \rightarrow 7p_{1/2}^2 7p_{3/2}^2\ ^3P_2$	0.383	0.378	
$E115^+$ IP:	$7p_{1/2}^2 \rightarrow 7p_{1/2}\ ^2P_{1/2}$	18.232	18.168	18.1
$E115^+$ EE:	$7p_{1/2}^2\ ^3P_0 \rightarrow 7p_{1/2}7p_{3/2}\ ^3P_1$	5.252	5.194	5.6
	$\rightarrow 7p_{1/2}7p_{3/2}\ ^3P_2$	5.663	5.605	
$E115^{2+}$ IP:	$7s^2 7p_{1/2} \rightarrow 7s^2\ ^1S_0$	27.542	27.456	27.4
$E115^{3+}$ EE:	$7s^2\ ^1S_0 \rightarrow 7s7p_{1/2}\ ^3P_0$	10.264	10.294	
	$\rightarrow 7s7p_{1/2}\ ^3P_1$	11.205	11.232	

4. Results and discussion

The calculated ionization potentials (IP), electron affinities (EA), and excitation energies (EE) of the bismuth atom and cations are presented in table 1. As in previous cases, good agreement with experiment [55, 56] is obtained, with an average error of 0.05 eV and a maximum error of 0.1 eV. Inclusion of the Breit term has little effect on the transition energies. Of particular interest is the prediction of more than one bound state of the anion. The lowest electronic configuration of Bi^-, $6p_{1/2}^2 6p_{3/2}^2$, yields two states with j values of 0 and 2; both are bound. These states correspond in LS coupling to $^3P_0$ and $^3P_2$; the $^3P_1$ state, on the other hand, can only be obtained from the excited $6p_{1/2}6p_{3/2}^3$ configuration. The $^3P_2$ state in isoelectronic polonium is 0.93 eV above the ground $^3P_0$ state, close to the Bi^- calculated value of 0.85 eV. The Po $^3P_1$ excitation energy is 2.09 eV, so the corresponding Bi^- state is not expected to be bound.

Results for eka-bismuth (element 115) are shown in table 2. Differences relative to bismuth can be assigned to the stronger binding of $7p_{1/2}$ and weaker binding of $7p_{3/2}$ compared to 6p analogues. The first IP of eka-bismuth, representing the ionization of a $p_{3/2}$ electron, is lower by 1.6 eV than the corresponding Bi IP; the IPs for the first and second $p_{1/2}$ electrons are *higher* by 1.5 and 1.9 eV than for the lighter atom. A similar trend is observed in the excitation energies. Finally, it should be noted that the empirically corrected Dirac–Fock–Slater values of Keller *et al.* [50] are in reasonable agreement with our data.

5. Summary and conclusion

The relativistic coupled-cluster method includes simultaneously relativistic terms through second order in the fine-structure constant α and correlation effects summed to all orders of the one- and two-electron excitations. In atomic systems, where spherical symmetry allows the use of large basis sets, the method makes possible calculation of large numbers of heavy-atom states with unprecedented accuracy, and gives reliable predictions for superheavy elements. The largest remaining source of error is probably the omission of triple virtual excitations. The method is applied here to bismuth and eka-bismuth (element 115). Comparison with experimental values for Bi shows good agreement, within 0.1 eV, with an average error of 0.05 eV. The trend of transition energies upon going from Bi to eka-bismuth shows a relative stabilization of the $p_{1/2}$ orbital and destabilization of $p_{3/2}$ in the heavier element, by 1.5–1.9 eV per electron.

Support for this work was provided by the US-Israel Binational Science Foundation and the Israeli Ministry for Science and Technology. Y.I. was supported by the National Science Foundation through Grant No. PHY-9008627.

References

[1] See, e.g. McWeeny, R., and Sutcliffe, B. T., 1969, *Methods of Molecular Quantum Mechanics* (London: Academic Press), Chap. 8.

[2] See, e.g. Sucher, J., 1989, *Relativistic, Quantum Electrodynamic, and Weak Interaction Effects in Atoms*, edited by W. Johnson, P. Mohr and J. Sucher (New York: American Institute of Physics), p. 28.

[3] Breit, G., 1929, *Phys. Rev.*, **B34**, 553; *ibid.*, 1930, **36**, 383; *ibid.*, 1932, **39**, 616.

[4] Brown, G. E., and Ravenhall, D. G., 1951, *Proc. Roy. Soc.* A, **208**, 552.

[5] Bethe, H. A., and Salpeter, E. E., 1957, *Quantum Mechanics of One- and Two-Electron Atoms* (Berlin: Springer-Verlag).

[6] Sucher, J., 1980, *Phys. Rev.* A, **22**, 348; 1987, *Phys. Scr.*, **36**, 271.

[7] Buchmüller, W., and Dietz, K., 1980, *Z. Phys.* C, **5**, 45.

[8] Lindgren, I., 1989, *Many-Body Methods in Quantum Chemistry*, edited by U. Kaldor, Lecture Notes in Chemistry, Vol. 52 (Heidelberg: Springer-Verlag), p. 293; 1988, *Nucl. Instrum. Methods*, **B31**, 102.

[9] Johnson, W., Mohr, P., and Sucher, J., (eds). 1989, *Relativistic, Quantum Electrodynamic, and Weak Interaction Effects in Atoms* (New York: American Institute of Physics).

[10] Mittleman, M., 1971, *Phys. Rev.* A, **4**, 893; 1972, *ibid.*, **5**, 2395; 1981, *ibid.*, **24**, 1167.

[11] Davydov, A. S., 1966, *Quantum Mechanics* (Peaks Island, Maine: NEO Press), Chap. VIII.

[12] Kim, Y.-K., 1967, *Phys. Rev.*, **154**, 17.

[13] Kagawa, T., 1975, *Phys. Rev.* A, **12**, 2245; 1980, *ibid.*, **22**, 2340.

[14] Johnson, W. R., and Sapirstein, J., 1986, *Phys. Rev. Lett.*, **57**, 1126; Johnson, W. R., Idrees, M., and Sapirstein, J., 1987, *Phys. Rev.* A, **35**, 3218; Blundell, S. A., Johnson, W. R., Liu, Z. W., and Sapirstein, J., 1989, *Phys. Rev.* A, **39**, 3768; Johnson, W. R., Blundell, S. A., and Sapirstein, J. W., 1988, *Phys. Rev.*, A, **37**, 307; 1988, *ibid.*, **37**, 2764; 1990, *ibid.*, **41**, 1689.

[15] Quiney, H. M., Grant, I. P., and Wilson, S., 1987, *J. Phys.* B, **20**, 1413; 1987, *Phys. Scr.*, **36**, 460; 1989, *Many-Body Methods in Quantum Chemistry*, edited by U. Kaldor, Lecture Notes in Chemistry, Vol. 52 (Heidelberg: Springer-Verlag); 1990, *J. Phys.* B, **23**, L271; Grant, I. P., and Quiney, H. M., 1988, *Adv. Atom. Molec. Phys.*, **23**, 37.

[16] Ishikawa, Y., Binning, R. C., and Sekino, H., 1989, *Chem. Phys. Lett.*, **160**, 206; Ishikawa, Y., 1990, *Phys. Rev.* A, **42**, 1142; 1990, *Chem. Phys. Lett.*, **166**, 321; Ishikawa, Y., and Quiney, H. M., 1993, *Phys. Rev.* A, **47**, 1732; Ishikawa, Y., and Koc, K., 1994, *Phys. Rev.* A, **50**, 4733.

[17] Desclaux, J.-P., 1975, *Comput. Phys. Commun.*, **9**, 31.

[18] Grant, I. P., McKenzie, B. J., Norrington, P. H., Mayers, D. F., and Pyper, N. C., 1980, *Comput. Phys. Commun.*, **21**, 207.

[19] For a recent review see Ishikawa, Y., and Kaldor, U., 1996, *Computational Chemistry: Review of Current Trends*, Vol. I, edited by J. Leszczynski (Singapore: World Scientific), p. 1.

[20] Lee, Y.-S., and McLean, A. D., 1982, *J. chem. Phys.*, **76**, 735.

[21] Mark, F., and Schwartz, W. H. E., 1982, *Phys. Rev. Lett.*, **48**, 673; Schwartz, W. H. E., and Wallmeier, H., 1982, *Molec. Phys.*, **46**, 1045.

[22] Wallmeier, H., and Kutzelnigg, W., 1981, *Chem. Phys. Lett.*, **78**, 341; 1983, *Phys. Rev.* A, **28**, 3092.

[23] Ishikawa, Y., Binning, R. C., and Sando, K. M., 1983, *Chem. Phys. Lett.*, **101**, 111; 1984, *ibid.*, **105**, 189; 1985, *ibid.*, **117**, 444; Ishikawa, Y., Baretty, R., and Binning, R. C., 1985, *Chem. Phys. Lett.*, **121**, 130; Ishikawa, Y., and Quiney, H. M., 1987, *Int. J. quant. Chem. Symp.*, **21**, 523.

[24] Stanton, R. E., and Havriliak, S., 1984, *J. chem. Phys.*, **81**, 1910.

[25] Ishikawa, Y., Baretty, R., and Binning, R. C., 1985, *Int. J. quant. Chem. Symp.*, **19**, 285; Ishikawa, Y., and Sekino, H., 1990, *Chem. Phys. Lett.*, **165**, 243.

[26] Dyall, K. G., Grant, I. P., and Wilson, S., 1984, *J. Phys.* B, **17**, 1201.

[27] Aerts, P. J. C., and Nieuwpoort, W. C., 1985, *Chem. Phys. Lett.*, **113**, 165; 986, *ibid.*, **125**, 83.

[28] For a discussion of Fock-space coupled cluster see Kaldor, U., 1991, *Theor. Chim. Acta*, **80**, 427 and reference therein.

[29] Lindgren, I., and Morrison, J., 1986, *Atomic Many-Body Theory*, 2nd Edn (Berlin: Springer Verlag).

[30] Hughes, S. R., and Kaldor, U., 1992, *Chem. Phys. Lett.*, **194**, 99; 1993, *ibid.*, **204**, 339; 1993, *Phys. Rev.* A, **47**, 4705; 1993, *J. chem. Phys.*, **99**, 6773; 1995, *Int. J. quant. Chem.*, **55**, 127.

[31] Salomonson, S., Lindgren, I., and Mårtensson, A.-M., 1980, *Phys. Scripta*, **21**, 351.

[32] Lindroth, E., 1988, *Phys. Rev.* A, **37**, 316.

[33] Blundell, S. A., Johnson, W. R., Liu, Z. W., and Sapirstein, J., 1989, *Phys. Rev.* A, **39**, 3768; 1989, *ibid.*, **40**, 2233; Blundell, S. A., Johnson, W. R., and Sapirstein, J., 1990, *Phys. Rev. Lett.*, **65**, 1411; 1991, *Phys. Rev.* A, **43**, 3407; Liu, Z. W., and Kelly, H. P., 1991, *ibid.*, **43**, 3305.

[34] Salomonson, S., and Öster, P., 1989, *Phys. Rev.* A, **40**, 5548; Lindroth, E., and Salomonson, S., 1990, *ibid.*, **41**, 4659; Hartley, A. C., Lindroth, E., and Mårtensson-Pendrill, A.-M., 1990, *J. Phys.* B, **23**, 1990; Hartley, A. C., and Mårtensson-Pendrill, A.-M., 1990, *Z. Phys.* D, **15**, 309; 1991, *J. Phys.* B, **24**, 1193; Mårtensson-Pendrill, A.-M., Alexander, S. A., Adamowicz, L., Oliphant, N., Olsen, J., Öster, P., Quiney, H. M., Salomonson, S., and Sundholm, D., 1991, *Phys. Rev.* A, **43**, 3355; Lindroth, E., Persson, H., Salomonson, S., and Mårtensson-Pendrill, A.-M., 1992, *Phys. Rev.* A, **45**, 1493; Lindroth, E., and Hvarfner, J., 1992, *ibid.*, **45**, 2771.

[35] Sekino, H., and Bartlett, R. J., 1990, *Int. J. quant. Chem. Symp.*, **24**, 241.

[36] Ilyabaev, E., and Kaldor, U., 1992, *Chem. Phys. Lett.*, **194**, 95.

[37] ILYABAEV, E., and KALDOR, U., 1994, *J. chem. Phys.*, **97,** 8455; 1993, *Phys. Rev.* A, **47,** 137.
[38] ELIAV, E., KALDOR, U., and ISHIKAWA, Y., 1994, *Phys. Rev.* A, **49,** 1724.
[39] ELIAV (ILYABAEV), E., KALDOR, U., and ISHIKAWA, Y., 1994, *Chem. Phys. Lett.*, **222,** 82.
[40] ELIAV, E., KALDOR, U., and ISHIKAWA, Y., 1994, *Phys. Rev.* A, **50,** 1121.
[41] ELIAV, E., KLDOR, U., and ISHIKAWA, Y., 1994, *Int. J. quant. Chem. Symp.*, **28,** 205.
[42] ELIAV, E., KALDOR, U., and ISHIKAWA, Y., 1995, *Phys. Rev.* A, **51,** 225.
[43] ELIAV, E., KALDOR, U., and ISHIKAWA, Y., 1995, *Phys. Rev.* A, **52,** 291.
[44] ELIAV, E., KALDOR, U., and ISHIKAWA, Y., 1995, *Phys. Rev.* A, **52,** 2765.
[45] ELIAV, E., KALDOR, U., and ISHIKAWA, Y., 1995, *Phys. Rev.* A, **53,** 3050.
[46] ELIAV, E., KALDOR, U., ISHIKAWA, Y., SETH, M., and PYYKKÖ, P., 1996, *Phys. Rev.* A, **53,** 3926.
[47] ELIAV, E., KALDOR, U., and ISHIKAWA, Y., 1995, *Phys. Rev. Lett.*, **74,** 1079.
[48] ELIAV, E., KALDOR, U., SCHWERDTFEGER, P., HEß, B. A., and ISHIKAWA, Y., 1994, *Phys. Rev. Lett.*, **73,** 3203.
[49] ELIAV, E., KALDOR, U., ISHIKAWA, Y., and PYYKKÖ, P., 1996, *Phys. Rev. Lett.*, **77,** 5350.
[50] KELLER, O. L., NESTOR, C. W., and FRICKE, B., 1974, *J. phys. Chem.*, **78,** 1945.
[51] ROSE, S. J., GRANT, I. P., and PYPER, N. C., 1978, *J. Phys.* B, **11,** 3499.
[52] DZUBA, V. A., FLAMBAUM, V. V., SILVESTROV, P. G., and SUSHKOV, O. P., 1991, *Phys. Rev.* A, **44,** 2828.
[53] BIEROŃ, J. R., MARCINEK, R., and MIGDAŁEK, J., 1991, *J. Phys.* B, **24,** 31.
[54] MALLI, G. L., DA SILVA, A. B. F., and ISHIKAWA, Y., 1993, *Phys. Rev.* A, **47,** 143.
[55] MOORE, C. E., 1958, *Atomic Energy Levels*, Vol. III, Natl. Bur. Stand. (US) Circ. No. 467 (Washington, DC: US GPO).
[56] HOTOP, H., and LINEBERGER, W. C., 1975, *J. Phys. Chem. Ref. Data*, **4,** 539; 1985, *ibid.*, **14,** 731.

MOLECULAR PHYSICS, 1998, VOL. 94, NO. 1, 189–198

Low-lying singlet and triplet states of all-*trans*(10-s-*cis*)-2,4,6,8,10-undecapentaen-1-al: a theoretical determination

By REMEDIOS GONZÁLEZ-LUQUE and MANUELA MERCHÁN
Departamento de Química Física, Universitat de València, Dr. Moliner 50, Burjassot, E-46100 Valencia, Spain

Ab initio results for the electronic spectra of all-*trans*(10-s-*cis*)-2,4,6,8,10-undecapentaen-1-al are presented. Apart from its intrinsic interest, the system is a reasonable truncated model of all-*trans*-retinal. This paper includes geometry determination of the ground state and the low-lying valence singlet and triplet excited states. Vertical, emission, and non-vertical excitation energies have been computed using multiconfigurational second-order perturbation theory by means of the CASPT2 method. The most intense feature of the computed spectrum is due to the expected strongly dipole-allowed $\pi\pi^*$ transition, placed *in vacuo* at 3.77 eV. The singlet $\pi\pi^*$ state is above the singlet $n\pi^*$ and the A_g-like states by only 0.22 eV. The lowest 0–0 singlet–singlet transition energy corresponds to the A_g-like state, at 2.48 eV. The calculated fluorescence maxima from the $n\pi^*$ and the A_g-like states are found in a similar energy range, at 1.87 eV and 2.06 eV, respectively. The lowest triplet state is of $\pi\pi^*$ character, placed vertically at 1.74 eV, adiabatically at 1.07 eV, with a predicted phosphorescence maximum of 0.75 eV. On the other hand, Rydberg states play a minor role in the description of the low-energy region of the spectra. The results are consistent with available experimental data of the system and related compounds in solution.

1. Introduction

The spectroscopy of retinals is of interest both intrinsically and because of their role in many biological processes of fundamental importance. We have reported an *ab initio* study on the low-lying excited states of retinal, and its truncated model 3-methyl-all-*trans*(10-s-*cis*)-2,4,6,8,10-undecapentaen-1-al, in connection with the 11-*cis*- into all-*trans*-retinal photoisomerization [1]. The theoretical description of the vertical excited states is consistent with experimental evidence, except for the placement of the A_g-like state, which has been vertically computed ~1 eV higher than the maximum observed in the two-photon absorption spectrum. Such deviation could be related to the non-vertical nature of the observed band. On the order hand, the three lowest vertical singlet states are close in energy. The relative ordering in the emission spectra and in the 0–0 transition energies are issues worth addressing from a theoretical point of view. In order to get further insight into the relative energy ordering of the low-lying excited states of long polyenals, results on the vertical, emission, and non-vertical transition energies are examined in the present contribution for all-*trans*(10-s-*cis*)-2,4,6,8,10-undecapentaen-1-al (UND), which contains the same number of double bonds as retinals (figure 1). For this purpose, the study includes geometry determination of the corresponding excited states at the CASSCF level, in addition to the ground-state geometry characterization of the system. The use of flexible basis sets, including diffuse functions for the spectral investigation, also allows determination of the first Rydberg transition.

The excited states of interest are denoted as: $^{1,3}A''(n\pi^*)$, essentially described in a good approximation by a single excitation from a lone-pair orbital of the heteroatom to a π^* orbital; $^{1,3}A'(\pi\pi^*)$, mainly characterized by one-electron promotion from the highest occupied molecular orbital (HOMO) to the lowest unoccupied molecular orbital (LUMO); and $^1A'(\pi - \text{diex})$, with a multiconfigurational character and non-negligible contributions of doubly excited configurations. In terns of the C_{2h} idealized point group of even polyenes, the $^1A'(\pi\pi^*)$ and $^1A'(\pi\text{-diex})$ states can be denoted as B_u- and A_g-like states, respectively.

The absorption maxima of dodecapentaenal have been located at the energy range 3.2–3.3 eV in different solvents [2]. The most intense band in all-*trans*-retinal also has been observed at a similar energy interval [3,4]. On the other hand, the ^1A_g-like state has been placed in all-*trans*-retinal at 2.90 eV in solution (EPA, 77 K) by two-photon spectroscopy [3]. The fluorescence maximum of dodecapentaenal occurs around 2.2 eV. This feature has been assigned by Becker *et al.* [2] to the transition from the $^1A'(\pi\text{-diex})$ to the ground state. The study of the lowest triplet state has been hampered by the absence of phosphorescence for these systems. The lowest triplet state (of $\pi\pi^*$ character) has been located at 1.37 eV above the ground state (assigned to the 0–0 transition) from a singlet–triplet absorption

0026–8976/98 $12·00

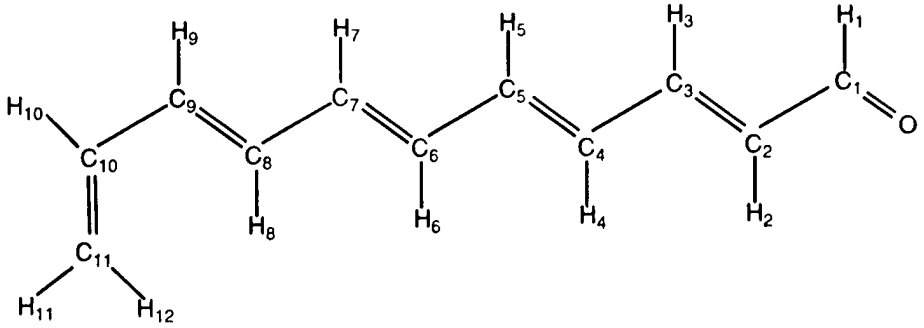

Figure 1. all-*trans*(10-s-*cis*)-2,4,6,8,10-Undecapentaen-1-al atom labelling.

spectrum of dodecapentaenal [5]. The present theoretical findings confirm the overall experimental picture, bringing also results for the singlet and triplet $n\pi^*$ states, where no direct experimental estimate is available.

The spectroscopic study has been performed within the framework of multiconfigurational second-order perturbation CASPT2 theory [6, 7]. The successful performance of the CASPT2 method in computing differential correlation effects for excitation energies has been illustrated in a number of earlier applications (see, e.g. [8, 9]).

2. Methods and computational details

Geometry optimizations have been carried out at the CASSCF level using the generally contracted basis sets of the atomic natural orbital (ANO-S) type obtained from the C,O(10s6p3d)/H(7s) primitive sets [10]. The contraction scheme C,O[3s2p1d]/H[2s] has been used in the present study, which represents a total of 192 basis functions. A full geometry optimization has been performed assuming a planar molecule with C_s symmetry (45 degrees of freedom). In order to include in the spectral study the lowest Rydberg state, the basis set has been supplemented with two s- and p-type diffuse functions (see exponents in [11, 12]), placed at the charge centroid of the ground state, for computation of the vertical transition energies (200 basis functions). When calculating the non-vertical transition energies, the diffuse functions have been located at the corresponding charge centroid of the optimal geometries for the states considered.

The low-lying states have been computed by using multiconfigurational second-order perturbation theory through the CASPT2 method [6, 7]. The complete active space SCF (CASSCF) procedure [13] determines the multiconfigurational single-reference function employed in the perturbational treatment. The molecular orbitals for the excited states have been obtained from state average CASSCF calculations, where the averaging includes all states of interest of a given symmetry. The number of states included in the state average CASSCF calculations, the number of configurations in the CASSCF wavefunction, details on the active spaces used, and the type of state computed are given in table 1.

With the molecule placed in the xy plane, the closed-shell Hartree Fock description of the $C_{11}H_{12}O$ system has (37-6) occupied orbitals of symmetry (a′-a″). The π orbitals belong to the a″ irreducible representation of the point group C_s. For the singlet and triplet states of A′ symmetry the π-valence active space (0-12) has been employed (12π active orbitals with 12π active electrons). An active space comprising all valence π orbitals is the natural choice for a polyene chain. For the $\pi\pi^*$ states the lone pair of the heteroatom behaves as an inactive orbital. The occupation number is close to 2.0 when it is treated as active. The same active space (11 active electrons) has been used to determine the vertical ionization potential to the $1^2A''(\pi$-hole) state. The active space was enlarged to (1-12), with an additional orbital of a′ symmetry, to describe the $^1A''(\pi \rightarrow 3s)$ Rydberg state (12 active electrons). In both cases the remaining orbitals (37-0) were kept inactive. For the $^{1,3}A''(n\pi^*)$ states the active space comprises the lone-pair on the oxygen atom plus the most important π orbitals (1-10) with 14 active electrons, (36-0) inactive orbitals. When exciting away from the lone-pair orbital, the highest unoccupied π^* orbitals for the $n\pi^*$ excited state have a low occupation number and can be moved safely into the virtual space. The same active space (13 active electrons) has been employed to compute the vertical ionization potential to the $1^2A'$(n-hole) state. The energy of each excited state is referred to a ground-state energy computed with the same active space.

For the singlet excited states of A′ symmetry, intruder states weakly interacting with the corresponding π-CASSCF reference function were detected. Level shift corrected perturbation (LS-CASPT2) theory [9, 14, 15] was employed to check their effect on the computed excitation energies. Calibration calculations using level shifts in the range LS = 0.1–0.4 au showed the stability

Table 1. CASSCF wavefunctions with (number of active orbitals[a]) and (number of active electrons) employed to compute the vertical, adiabatic, and emission electronic transtions of all-*trans*(10-s-*cis*)-2,4,6,8,10-undecapentaen-1-al and its vertical ionization potentials.

Wavefunction	States	No. Config.[b]	N_{states}[c]
CASSCF(0-12)(12)	$1^1A'$, $2^1A'$, $3^1A'$, $4^1A'$	226 512	4
CASSCF(0-12)(11)	$1^2A''$(π-hole)	339 768	1
CASSCF(1-10)(14)	$1^1A''$	13 860	1
CASSCF(1-10)(13)	$1^2A'$(n-hole)	34 650	1
CASSCF(1-12)(12)	n^1A''(π3s)	339 768	1
CASSCF(0-12)(12)	$1^3A'$	382 239	1
CASSCF(1-10)(14)	$1^3A''$	23 100	1

[a] Within parentheses the number of active orbitals of symmetry a′–a″ of the point group C_s.
[b] Number of configurations in the CASSCF wavefunction.
[c] States included in the average CASSCF calculation.

of the computed excitation energies for the singlet A′ states with respect to the standard CASPT2 results (LS = 0.0 au). Therefore only the CASPT2 results with no level shift are reported here. In all the cases, CASPT2 calculations have been performed using the full Fock matrix representation of the zero-order Hamiltonian [7]. All electrons except the cores were correlated at the CASPT2 level.

The transition dipole moments have been computed by means of the CASSCF state interaction (CASSI) method [16, 17]. In the formula of the oscillator strength the excitation energy computed at the CASPT2 level was employed [8, 9].

Calculations have been performed using Molcas-3 quantum chemistry software [18].

3. Results and discussion

In this section we shall present and discuss the results obtained for UND. The present findings will be compared with the available experimental data on the UND system and previous theoretical results of related compounds. The study of all-*trans*(10-s-*cis*)-2,4,6,8,10-undecapentaen-1-al is particularly relevant as a truncated model for the all-*trans*-retinal molecule.

Geometry determination of ground-state UND and of its low-lying excited states is considered first and the vertical excitation energies of UND are analysed next. Then the results of the emission and non-vertical transition energies are presented. The computed results are discussed within the framework of the earlier photochemical and photophysical properties of large polyenals.

3.1. *Geometry determinations*

Characterization of the ground-state geometry of UND and the geometries of the low-lying excited states $^1A'(\pi\text{-diex})$, $^1A''(n\pi^*)$, $^3A'(\pi\pi^*)$, and $^3A''(n\pi^*)$ to be employed in the spectral study is considered in this section. All the geometry optimizations have been performed at the CASSCF level, using the active spaces described in the previous section, with the ANO-S type C,O[3s2p1d]/H[2s] basis set. The computed bond distances and bond angles obtained for the corresponding states are collected in table 2.

The most pronounced effect of the non-dynamic π electron correlation on the ground-state geometry of UND occurs for the double bonds. The Hartree–Fock C=O and C=C optimal distances are underestimated by 0.02 Å with respect to the π-CASSCF results. Single C—C bond lengths and bond angles are, however, similar at both levels of theory. Such a situation has been found previously in long polyenes like octatetraene [19]. As discussed in the next section, the computed vertical excitation energies can be expected to be sensitive to the geometry employed for the ground state. It is due to the different topology of the ground-state surface of UND compared with the excited-state surface. The geometry determined at the π-CASSCF level for the ground state of UND has been employed in the calculation of the vertical excitation energies.

The carbonyl bond length increases by 0.13 Å with respect to the ground-state bond distance for the $^{1,3}A''(n\pi^*)$ excited states, in accordance with their electronic nature. In order to better visualize the changes on the carbon–carbon bonds, figure 2 shows the bond distances of the polyene backbone for the $^1A''(n\pi^*)$ and $^3A''(n\pi^*)$ excited states, together with those for the ground state. The polyene chain presents bond alternation of single and double bonds with respect to the ground state mainly for the bonds nearest to the carbonyl group, in both the singlet and the triplet $n\pi^*$ excited states. A similar comparison is performed in figure 3 among the ground state, the $^1A'(\pi\text{-diex})$, and the $^3A'(\pi\pi^*)$ excited states. As expected, the lengths of the double bonds in the excited states $^1A'(\pi\text{-diex})$ and $^3A'(\pi\pi^*)$ increase, while the single

Table 2. Geometrical parameters[a] for the low-lying excited states of the all-*trans*(10-s-*cis*)-2,4,6,8,10-undecapentaen-1-al molecule computed at the CASSCF level (see active space in table 1) using the ANO-S type C,O[3s2p1d]/H[2s] basis set. For comparison, results obtained at the Hartree Fock level for the ground state are included (data within parentheses). Calculations have been performed within the constraints of C_s symmetry.

Parameter	Ground state	$^1A'(\pi$-diex)	$^1A''(n\pi^*)$	$^3A'(\pi\pi^*)$	$^3A''(n\pi^*)$
$r(C_1—O)$	1.205(1.190)	1.216	1.337	1.210	1.336
$r(C_1—C_2)$	1.475(1.474)	1.450	1.327	1.464	1.328
$r(C_2—C_3)$	1.353(1.335)	1.426	1.461	1.388	1.458
$r(C_3—C_4)$	1.458(1.458)	1.383	1.370	1.402	1.373
$r(C_4—C_5)$	1.356(1.336)	1.439	1.426	1.437	1.422
$r(C_5—C_6)$	1.456(1.458)	1.394	1.409	1.367	1.412
$r(C_6—C_7)$	1.357(1.336)	1.423	1.385	1.457	1.383
$r(C_7—C_8)$	1.457(1.458)	1.394	1.447	1.366	1.448
$r(C_8—C_9)$	1.355(1.334)	1.443	1.338	1.440	1.338
$r(C_9—C_{10})$	1.474(1.477)	1.393	1.423	1.415	1.473
$r(C_{10}—C_{11})$	1.350(1.329)	1.416	1.350	1.382	1.350
$\angle(H_1C_1O)$	120.1(120.4)	119.6	111.1	119.8	111.1
$\angle(H_1C_1C_2)$	116.1(115.0)	116.9	123.4	116.5	123.6
$\angle(H_2C_2C_1)$	116.8(116.9)	117.1	119.2	116.9	119.2
$\angle(H_2C_2C_3)$	121.6(122.2)	120.4	118.3	121.0	118.3
$\angle(H_3C_3C_2)$	118.7(118.8)	117.5	117.2	117.8	117.2
$\angle(H_3C_3C_4)$	116.8(116.4)	118.3	119.0	117.7	119.0
$\angle(H_4C_4C_3)$	117.1(117.1)	118.4	118.3	118.4	118.3
$\angle(H_4C_4C_5)$	119.4(119.9)	117.5	117.3	117.9	117.3
$\angle(H_5C_5C_4)$	119.0(119.1)	117.5	118.1	117.2	118.0
$\angle(H_5C_5C_6)$	116.9(116.6)	118.5	118.1	118.7	118.2
$\angle(H_6C_6C_5)$	117.0(116.9)	118.3	117.4	118.8	117.4
$\angle(H_6C_6C_7)$	119.2(119.6)	117.6	118.1	117.1	118.0
$\angle(H_7C_7C_6)$	119.0(119.2)	117.4	118.9	117.1	118.9
$\angle(H_7C_7C_8)$	116.9(116.7)	118.3	117.3	119.0	117.3
$\angle(H_8C_8C_7)$	116.5(116.4)	118.1	116.5	118.1	116.5
$\angle(H_8C_8C_9)$	120.1(120.4)	118.7	119.8	118.2	119.7
$\angle(H_9C_9C_8)$	117.7(117.8)	116.5	117.7	116.7	117.7
$\angle(H_9C_9C_{10})$	115.4(115.1)	117.2	115.3	117.1	115.3
$\angle(H_{10}C_{10}C_9)$	115.0(114.8)	116.4	114.9	115.7	114.9
$\angle(H_{10}C_{10}C_{11})$	117.7(117.8)	116.7	117.6	116.9	117.6
$\angle(H_{11}C_{11}C_{10})$	120.5(120.5)	120.2	120.5	120.4	120.5
$\angle(H_{12}C_{11}C_{10})$	122.5(122.6)	122.3	122.6	122.5	122.6

[a] Bond distances in Å and bond angles in deg: see figure 1 for atom labelling.

bond distances decrease with respect to the ground state. Moreover, the bond alternation decreases in the alternate character of single and double bonds towards the centre of the molecule for the $^1A'(\pi$-diex) state, but increasing for the $^3A'(\pi\pi^*)$ state. No big changes are noted for the bond angles of the excited states, with respect to the ground-state geometry, except for the angles involving the oxygen atom of the $^{1,3}A''(n\pi^*)$ states. The reported geometries optimized at the CASSCF level for the excited states have been used in the computation of the emission and non-vertical transition energies implying the states of interest.

3.2. *Vertical transition energies*

Using the optimized CASSCF geometry for the ground state of the molecule, listed in table 2, and the basis set including diffuse functions, the vertical low-lying singlet–singlet and singlet–triplet transitions from the ground state minimum have been studied. In addition, the first Rydberg state arising from the excitation out of the HOMO to the 3s diffuse orbital has been characterized. The results for the vertical excitation energies computed for UND are collected in table 3, where the first column identifies the different states, the second and third columns give the vertical transition energies obtained by the CASSCF and CASPT2 calculations, respectively, and then come the dipole moment μ, computed at the CASSCF level (in debye), and the oscillator strengths.

The $1^1A''(n\pi^*)$ and $2^1A'(\pi$-diex) states are found to be energetically very close, at the CASPT2 level placed at 3.55 eV and 3.58 eV, respectively. The $3^1A'(\pi\pi^*)$ state is slightly above, at 3.77 eV, with a computed oscillator

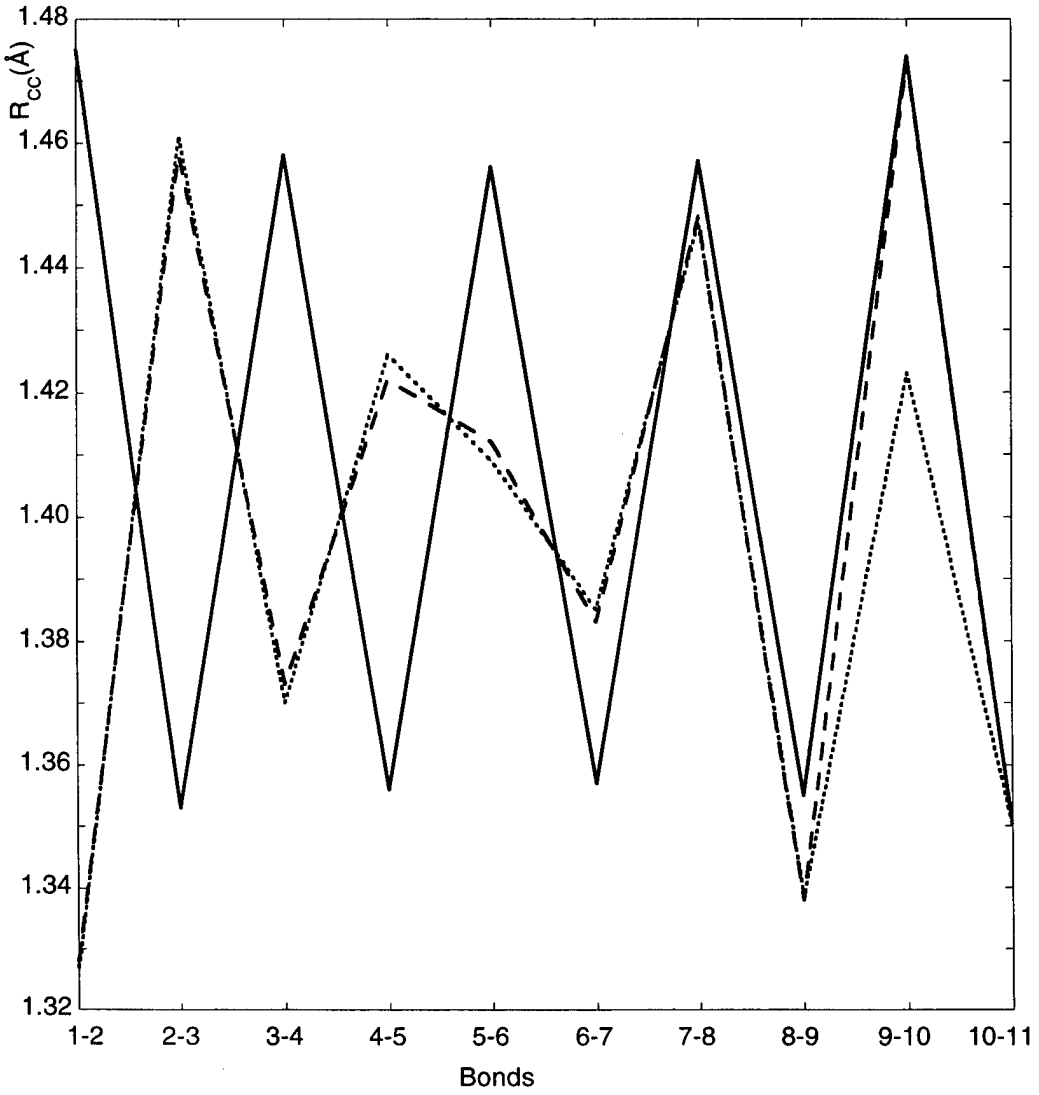

Figure 2. Optimal bond distances of the polyene chain, computed at the CASSCF level, for the ground state (full line), the $^3A''(n\pi^*)$ (dashed line), and the $^1A''(n\pi^*)$ (dotted line) excited states of all-*trans*(10-s-*cis*)-2,4,6,8,10-undecapentaen-1-al.

Table 3. Computed excitation energies (in eV) and other properties of the vertical excited states of all-*trans*(10-s-*cis*)-2,4,6,8,10-undecapentaen-1-al. The optimal ground-state geometry computed at the π-CASSCF level has been employed. The ANO-S type C,O[3s2p1d]/H[2s] enlarged with diffuse functions has been used in the spectral study.

State	CASSCF	CASPT2	μ^a	Osc. str.
Ground state ($1^1A'$)			3.793	
Singlet states				
$1^1A''(n\pi^*)$	3.98	3.55	0.743	0.0000
$2^1A'(\pi\text{-diex})$	4.16	3.58	3.746	0.0003
$3^1A'(\pi\pi^*)$	5.96	3.77	7.115	0.9177
$n^1A''(\pi 3s)$	5.42	5.20	6.068	0.0003
Triplet states				
$1^3A'(\pi\pi^*)$	2.26	1.74	3.882	
$1^3A''(n\pi^*)$	3.76	3.32	0.683	

[a] Dipole moment (CASSCF) in debye.

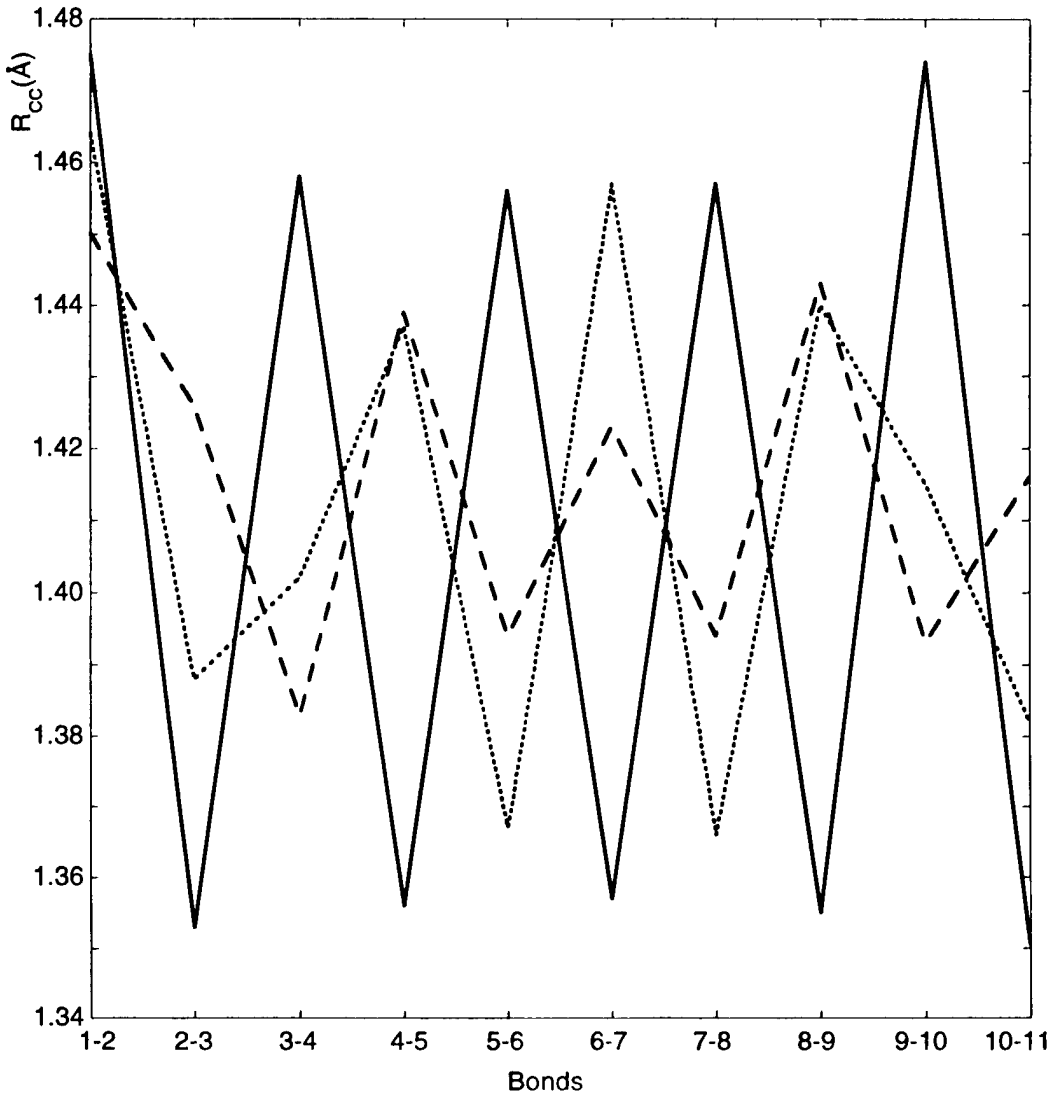

Figure 3. Optimal bond distances of the polyene chain, computed at the CASSCF level, for the ground state (full line), the $^1A'(\pi$-diex) (dashed line), and the $^3A'(\pi\pi^*)$ (dotted line) excited states of all-*trans*(10-s-*cis*)-2,4,6,8,10-undecapentaen-1-al.

strength of 0.9. The $^1A'(\pi\pi^*)$ corresponds to the fourth root of the average CASSCF performed for the singlet states with the same spatial symmetry as the ground state. Indeed, the number of roots in the average CASSCF calculation for the $^1A'$ states was systematically increased to reach the expected intense transition to the $\pi\pi^*$ state. Not until the number of roots was four was the strong optically allowed transition found. Due to the large contribution of the dynamic correlation for this transition, about 2.2 eV, it becomes the third singlet–singlet transition at the CASPT2 level. The extra root computed (not shown in table 3) is placed around 4.5 eV at the CASPT2 level, 0.7 eV lower than at the CASSCF level. It corresponds to a weak transition. On the other hand, the results of the vertical triplet states certainly confirm the $\pi\pi^*$ nature of the lowest triplet state, placed at 1.74 eV. The $1^3A''(n\pi^*)$ state is computed to be 1.58 eV above the $1^3A'(\pi\pi^*)$ state. The singlet–triplet splittings are calculated 0.23 eV ($n\pi^*$) and 2.03 eV ($\pi\pi^*$), in agreement with a larger penetration of the orbitals involved in the latter. It leads to a larger exchange integral between the π and π^*, that is, to a larger predicted stabilization of the $\pi\pi^*$ triplet state within a simple molecular orbital model. As occurs with a number of systems and rationalized elsewhere [1], for the UND system also we note that twice the energy of the $^3A'(\pi\pi^*)$ vertical excitation energy (1.74 eV) gives in a good approximation (within 0.1 eV) of the computed vertical excitation energy of the $^1A'(\pi$-diex) state (3.58 eV).

The lowest vertical ionization potentials with a π-hole and an n-hole are computed to be 7.43(7.54) eV and

8.49(9.17) eV at the CASSCF(CASPT2) levels. Accordingly, the lowest singlet Rydberg state corresponds to the $A''(\pi 3s)$, with a very weak CASPT2 transition energy of 5.20 eV. Dynamic correlation has little influence for this transition, decreasing the CASSCF excitation energy by only 0.22 eV. Therefore Rydberg states play a minor role in the description of the low-energy region of the singlet–singlet spectrum. Transition to the lowest singlet Rydberg state is located more than 1 eV above the most intense feature of the absorption spectrum.

The nature of the valence excited states is similar to the corresponding electronic states studied for 3-methyl-all-*trans*(10-s-*cis*)-2,4,6,8,10-undecapentaen-1-al, discussed elsewhere [1]. On the other hand, as expected, the $A''(\pi 3s)$ state is described mainly by the HOMO $\rightarrow$ 3s singly excited configuration, which has a weight in the CASSCF wavefunction of 77%. To a good approximation, the $1^2A''(\pi\text{-hole})$ and $1^2A'(\text{n-hole})$ states of the cationic UND system also are described well by a single configuration, with weights in the corresponding CASSCF wavefunctions of 78% and 85%, respectively.

The computed vertical excitation energies should be compared with the observed gas-phase data. As far as we know, such experimental data are not available for UND. The absorption spectrum measured in solution has been reported, however [2]. The computed results can be compared with the Franck–Condon maxima of the correspondings bands. Apart from the solvent effects, which can easily affect the band maxima with respect to the theoretical results performed *in vacuo*, one has also to keep in mind that the isomer studied might not have to be the most stable in solution. However, taking into account the dependence of the spectroscopic properties on the all 16 isomers of retinal [20], a minor deviation can be expected between the theoretical and experimental findings for this reason. In the one-photon spectrum of dodecapentaenal the maximum is located in the energy range 3.22–3.31 eV depending on the solvent [2]. Considering the expected bathochromic character for the most intense transition in solution, the CASPT2 result, 3.77 eV, is consistent with the experimental data available.

It is interesting also to compare the present results for UND and those for its 3-methyl homologue reported earlier [1]. Small differences, within 0.02 eV, are found between the vertical transition energies corresponding to the $^1A''(n\pi^*)$, $^3A''(n\pi^*)$, and $^1A'(\pi\pi^*)$ states of the two systems. The transition energies to the $^1A'(\pi\text{-diex})$ and $^3A'(\pi\pi^*)$ states are, however, decreased for the UND system by 0.31 eV and 0.22 eV, respectively. Such a difference could be related to the absence of the methyl group in UND. Nevertheless, it does not seem to be the most likely factor responsible for the additional stabilization of those states, given its small influence on three of the computed transitions. On the other hand, the basis set has been enlarged with diffuse functions in the calculations for UND. However, a minor influence on the computed valence states can be expected from the diffuse functions since the corresponding Rydberg states of the same symmetry lie higher up in energy. Actually, the $^1A'(\pi\pi^*)$ state, where a similar effect due to the diffuse functions could be expected, has a similar placement in both systems. Moreover, the geometry of ground-state UND has been determined at the CASSCF level, whereas an optimized Hartree–Fock structure was employed for its 3-methyl homologue. The relevance of doubly excited configurations in the singlet A_g-like state leads to a higher degree of bond-order reversal, more pronounced than expected for the singlet B_u-like state, as occurs for octatetraene [19]. The computed vertical excitation energy to the $^1A'(\pi\text{-diex})$ state is then more sensitive to the geometry employed for the ground state. Similar arguments can be applied to rationalize the additional stabilization for the $^3A'(\pi\pi^*)$ state of UND with respect to its methyl homologue.

3.3. *Emission and non-vertical transition energies*

Knowledge of the energy hypersurfaces of the ground and low-lying excited states of polyenals is essential for the determination of their static and dynamic properties, which are particularly relevant in an ample group of biologically active chromophores [21–24]. The basic understanding of the spectroscopic behaviour of these compounds requires not only the accurate computation of the vertical states but also the characterization of the emission and non-vertical transition energies.

The basis set (including diffuse functions) and active spaces are the same as those used for the vertical transitions. Then a consistent comparison can be performed between the computed absorption and emission spectra. As described in section 2, the geometries for the ground state and excited state minima have been optimized at the CASSCF level. The computed transitions here involve the energy differences between the minima of the ground state and the excited state (0–0 absorption transition) and the vertical emission, from the excited state minimum vertically to the ground state potential surface (maximum of fluorescence or phosphorescence in the emission band). The study includes determination of the 0–0 transition and emission maxima for the two lowest singlet, $^1A''(n\pi^*)$ and $^1A'(\pi\text{-diex})$, and triplet, $^3A''(n\pi^*)$ and $^3A'(\pi\pi^*)$ states. Attempts to optimize the geometry for $^1A'(\pi\pi^*)$ have failed due to convergence problems. Geometry optimizations are restricted to a given root; no state average is implemented in the

Table 4. Vertical, adiabatic, and emission electronic transitions (in eV) computed for the all-*trans*(10-s-*cis*)-2,4,6,8,10-undecapentaen-1-al molecule. Geometries have been optimized at the CASSCF level (see table 2). The ANO-S type C,O[3s2p1d]/H[2s] enlarged with diffuse functions has been used in the spectral study.

	Vertical absorption		0–0 transition		Emission max.	
State	CASSCF	CASPT2	CASSCF	CASPT2	CASSCF	CASPT2
Singlet–singlet spectra						
$^1A''(n\pi^*)$	3.98	3.55	3.04	2.63	1.58	1.87
$^1A'(\pi$-diex)	4.16	3.58	3.09	2.48	2.30	2.06
Singlet–triplet spectra						
$^3A'(\pi\pi^*)$	2.26	1.74	1.49	1.07	0.75	0.75
$^3A''(n\pi^*)$	3.76	3.32	2.99	2.60	1.58	1.85

available gradient codes of the software employed [18]. Considering that the $^1A'(\pi\pi^*)$ state appears as the fourth root of the valence CASSCF calculation, the convergence problems are easy to understand in such a complex hypersurface. However, based on the octatetraene results [19], the 0–0 transition and emission maximum involving the $^1A'(\pi\pi^*)$ state can safely be predicted to occur at higher energies than those corresponding to the $^1A'(\pi$-diex) state of UND. For octatetraene, owing to symmetry restrictions, the state described mainly by the HOMO → LUMO configuration is the lowest root of B_u symmetry and, therefore, its geometry optimization has been achieved. The 0–0 transition and the emission maximum to/from the 1^1B_u state were found to be about 0.1 eV and 0.3 eV, respectively, below the corresponding vertical transition of the polyene. A much pronounced decrease was, however, obtained for the 2^1A_g state of the same polyene: 0.8 eV (0–0) and 1.4 eV (emission maximum) with respect its vertical excitation energy. As can be deduced from table 4, where the results are collected, the energy differences between the vertical excitation and the 0–0 transition (≈1 eV) and with respect to the emission maximum (≈1.5 eV) for the $^1A'(\pi$-diex) state of UND have a similar order of magnitude as those for the 2^1A_g state of octatetraene.

A weakly allowed state has been observed to be the lowest excited singlet state in the one-photon absorption and excitation spectra of dodecapentaenal. On the basis of the fluorescence quantum yields and intrinsic lifetime data, it has been assigned of A_g-like character by Becker, Das and Kogan [2]. The absorption spectrum of the compound shows, for instance, at 77 K in EPA, a weak but distinctly separated absorption band in the 2.76–2.85 eV region, on the low-energy side of the main absorption band system. This weak absorption band becomes even more clearly visible in the excitation spectrum. The 0–0 transition for the absorption to the $^1A'(\pi$-diex) state has been computed at 2.48 eV, consistent with this energy range. The 0–0 transition involving the $^1A''(n\pi^*)$ state is also close, at 2.63 eV (CASPT2 results). Both states therefore are plausible candidates for the observed weak feature in solution, although *in vacuo* the lowest 0–0 transition implies the A_g-like state. On the other hand, the emission maximum (EPA at 77 K), accordingly assigned to be of A_g-like character, has been observed at 2.19 eV [2]. The present result for the $^1A'(\pi$-diex) state has located the fluorescence maximum at 2.06 eV, in apparent agreement with the experimental result. Note, however, that the emission maximum for the $^1A''(n\pi^*)$ state, at 1.87 eV, is predicted as the lowest *in vacuo*. With such a small energy difference the ordering of the states can be affected readily by the nature of the solvent. The situation is similar for all-*trans*-retinal, where there has been no unequivocal assignment of the lowest excited state (see recent discussion in [25]). Evidence based on fluorescence quantum yields suggests, however, that the S_1 state of all-*trans*-retinal is $n\pi^*$ in aliphatic hydrocarbons and A_g-like in hydrogen-bonding solvents [3,22]. The present results *in vacuo* support that suggestion.

Table 4 lists also the vertical, adiabatic, and phosphorescence maxima for the triplet $n\pi^*$ and $\pi\pi^*$ states. The lowest triplet state clearly corresponds to the $1^3A'(\pi\pi^*)$ state. The lowest 0–0 singlet–triplet transition has been located at 1.07 eV, consistent with the 0–0 assignment in the singlet–triplet absorption bands induced by oxygen at high pressure reported by Evans [5]. The phosphorescence maximum from the $1^3A'(\pi\pi^*)$ state is predicted as about 0.8 eV.

As stated in the introduction, one of the main purposes of this study has been to achieve a better understanding of the behaviour of the A_g-like state, which is vertically located well above its 0–0 transition. With the 0–0 transition and emission maximum energies to hand one is tempted to derive the vertical transition from these data. Let us assume a perfect mirror rule, that is, equal forms for the potential energy surfaces of the ground and the $^1A'(\pi$-diex) states. Using the CASPT2 result for the 0–0 transition, 2.48 eV, and the fluores-

cence maximum, 2.06 eV, one might expect the vertical excitation at 2.90 eV, with perfect mirror rule behaviour. However, it is 0.68 eV below the computed vertical excitation energy, at 3.58 eV. The key point is that the hypersurfaces of the ground and excited states are quite different, and therefore the mirror rule is not fulfilled. The $^1A'(\pi\text{-diex})$ state relaxes by 1.1 eV from the ground-state geometry to the geometry of its minimum, while the ground state relaxes by 0.42 eV from the geometry of the excited state to its optimal one. It leads to a deviation of 0.68 eV from the ideal mirror rule. The topology of the two hypersurfaces is intrinsically different. Small changes in the geometry of the ground state yield significant variations in the computed vertical transition energy.

4. Summary and conclusion

We have presented results for the excitation and emission transitions of the all-*trans*(10-s-*cis*)-2,4,6,8,10-undecapentaen-1-al molecule, by using the CASSCF/CASPT2 method, which is a well established approach for accurate calculations of electronic spectra of organic compounds. The study includes geometry optimization for the ground state and the excited states $^1A'(\pi\text{-diex})$, $^1A''(n\pi^*)$, $^3A''(n\pi^*)$, and $^3A'(\pi\pi^*)$ at the CASSCF level. An ANO-type basis set of split-valence plus polarization quality was employed for the geometry optimizations. It was enlarged with diffuse functions for computation of the spectroscopic properties.

Vertical excitation energies using the optimized ground-state geometry have been computed for the low-lying valence states. The $1^1A''(n\pi^*)$ and $2^1A'(\pi\text{-diex})$ appear nearly degenerate, at 3.55 eV and 3.58 eV, respectively. They are below the $3^1A'(\pi\pi^*)$ state, computed at 3.77 eV, which is related to the most intense feature of the absorption spectrum. The result is consistent with the absorption maximum observed in the absorption spectra in solution. The placement of the lowest Rydberg state at 5.20 eV indicates that Rydberg states have a minor role in the description of the low-energy part of the spectrum *in vacuo*.

The optimized minima for the $^1A'(\pi\text{-diex})$ and $^1A''(n\pi^*)$ excited states have been used to compute the 0–0 absorption and vertical emission transitions. The lowest 0–0 transition corresponds to the $^1A'(\pi\text{-diex})$, at 2.48 eV, and the lowest emission comes from the $^1A''(n\pi^*)$ state, at 1.87 eV. Owing to the small energy difference between the two states in both features, the 0–0 absorption and the fluorescence maximum, the nature of the solvent may easily reverse the predicted state ordering *in vacuo*. Indeed, the computed fluorescence maximum for the $^1A'(\pi\text{-diex})$, 2.06 eV, is in agreement with the observed emission maximum in an alcoholic solvent (EPA at 77 K) at 2.19 eV and, therefore, supports the assignment of the observed feature. The findings also give further support for the $n\pi^*$ state of free all-*trans*-retinal, or in aliphatic hydrocarbons, as the lowest, while the A_g-like state becomes the lowest in hydrogen-bonded solvents. On the other hand, the computed singlet–triplet absorption and emission spectra reveal the lowest triplet state to be of $\pi\pi^*$ character. The $1^3A'(\pi\pi^*)$ state is vertically placed at 1.74 eV, with a singlet–triplet 0–0 transition of 1.07 eV, and a predicted phosphorescence maximum of 0.75 eV.

Similar spectroscopic characteristics can be expected for the corresponding Schiff base of the UND system. Apparently, the lack of $n\pi^*$ states in the low-energy region might simplify the study. A parallel investigation of the simplest protonated Schiff base of UND, together with the corresponding potential energy surfaces along the biologically active twisting coordinates, is currently under way at the same level of theory.

The research reported in this paper has been performed within the framework of the DGICYT Project No. PB94-0986 of Spain and of the European Commission TMR network contract ERB FMRX-CT96-0079 (Quantum Chemistry of the Excited State). Technical assistance by W. Díaz is gratefully acknowledged.

References

[1] Merchán, M., and González-Luque, R., 1997, *J. chem. Phys.*, **106,** 1112.
[2] Becker, R. S., Das, P. K., and Kogan, G., 1979, *Chem. Phys. Lett.*, **67,** 463.
[3] Birge, R. R., Bennett, J. A., Hubbard, L. M., Fang, H., Pierce, B. M., Kliger, D. S., and Leroi, G. E., 1982, *J. Amer. chem. Soc.*, **104,** 2519.
[4] Alex, S., Thanh, H. L., and Vocelle, D., 1992, *Can. J. Chem.*, **70,** 880.
[5] Evans, D. F., 1960, *J. chem. Soc.*, 1735.
[6] Andersson, K., Malmqvist, P.-Å., Roos, B. O., Sadlej, A. J., and Wolinski, K., 1990, *J. phys. Chem.*, **94,** 5483.
[7] Andersson, K., Malmqvist, P.-Å., and Roos, B. O., 1992, *J. chem. Phys.*, **96,** 1218.
[8] Roos, B. O., Fülscher, M. P., Malmqvist,. P.-Å., Merchán, M., and Serrano-Andrés, L., 1995, *Quantum Mechanical Electronic Structure Calculations with Chemical Accuracy*, edited by S. R. Langhoff (Dordrecht: Kluwer) p. 357.
[9] Roos, B. O., Andersson, K., Fülscher, M. P., Malmqvist, P.-Å., Serrano-Andrés, L., Pierloot, K., and Merchán, M., 1996, *Advances in Chemical Physics*, Vol. 93, edited by I. Prigogine and S. A. Rice (New York: Wiley) p. 219.
[10] Pierloot, K., Dumez, B., Widmark, P.-O., and Roos, B. O., 1995, *Theoret. chim. Acta*, **90,** 87.
[11] Rubio, M., Merchán, M., Ortí, E., and Roos, B. O., 1994, *Chem. Phys.*, **179,** 395.
[12] Rubio, M., Merchán, M., Ortí, E., and Roos, B. O., 1995, *Chem. Phys. Lett.*, **234,** 373.

[13] ROOS, B. O., 1987, *Advances in Chemical Physics: Ab Initio Methods in Quantum Chemistry—II*, edited by K. P. Lawley, (Chichester: Wiley), p. 399.
[14] ROOS, B. O., and ANDERSSON, K., 1995, *Chem. Phys. Lett.*, **245**, 215.
[15] ROOS, B. O., ANDERSSON, K., FÜLSCHER, M. P., SERRANO-ANDRÉS, L., PIERLOOT, K., MERCHÁN, M., and MOLINA, V., 1996, *J. molec. Struct. Theochem*, **388**, 257.
[16] MALMQVIST, P.-Å., 1986, *Int. J. Quantum Chem.*, **30**, 479.
[17] MALMQVIST, P.-Å., and ROOS, B. O., 1989, *Chem. Phys. Lett.*, **155**, 189.
[18] ANDERSSON, K., FÜLSCHER, M. P., KARLSTRÖM, G., LINDH, R., MALMQVIST, P.-Å., OLSEN, J., ROOS, B. O., SADLEJ, A. J., BLOMBERG, M. R. A., SIEGBAHN, P. E. M., KELLÖ, V., NOGA, J., URBAN, M., and WIDMARK, P.-O., 1994, MOLCAS Version 3 (Department of Theoretical Chemistry, University of Lund).
[19] SERRANO-ANDRÉS, L., LINDH, R., ROOS, B. O., and MERCHÁN, M., 1993, *J. phys. Chem.*, **97**, 9360.
[20] ZHU, Y., GANAPATHY, S., TREHAN, A., ASATO, A. E., and LIU, R. S. H., 1992, *Tetrahedron*, **48**, 10061.
[21] OTTOLENGHI, M., 1980, *Adv. Photochem.*, **12**, 97.
[22] BECKER, R. S., 1988, *Photochem. Photobiol.*, **48**, 369.
[23] BIRGE, R. R., 1990, *Ann. Rev. phys. Chem.*, **41**, 683.
[24] KOYAMA, Y., and MUKAI, Y., 1993, *Adv. Spectrosc., Biomolec. Spectrosc.*, **21**, 49.
[25] LARSON, E. J., FRIESEN, L. A., and JOHNSON, C. K., 1997, *Chem. Phys. Lett.*, **265**, 161.

MOLECULAR PHYSICS, 1998, VOL. 94, NO. 1, 199–208

Metastability in the sulphur molecule S_2^{2+} and S_2^{3+} cations. A theoretical study

By MIROSLAV URBAN

Department of Physical Chemistry, Faculty of Sciences, Comenius University, Mlynská dolina, SK-842 15 Bratislava, Slovakia

GEERD H. F. DIERCKSEN

Max-Planck-Institute for Astrophysics, Karl-Schwarzschild-Strasse 1, POB 1523, 85740 Garching, Germany

and MICHAEL JUŘEK

J. Heyrovský Institute of Physical Chemistry Academy of Sciences of the Czech Republic, Dolejškova 3, 18223 Prague 8, Czech Republic

Complete active space SCF (CASSCF) calculations followed by second order perturbation calculations (CASPT2) are performed for the ground state and for some low lying excited states of the S_2 molecule di-cation and tri-cation. Spectroscopic values of the S_2 parent molecule and its ions, S_2^+, S_2^{2+}, and S_2^{3+} are calculated from the potential energy curves. The performance of the active space selected for CASPT2 and the ANO (atomic natural orbitals) basis set is verified by coupled cluster CCSD(T) calculations for ionization potential and spectroscopic constants of the S_2 molecule and its S_2^+ cation as well as for ionization potentials of the sulphur atom. Due to a multireference character of the potential energy curve of the doubly and triply charged S_2 cations the performance of CCSD(T) deteriorates at longer distances from the minima and is thus not applicable over the whole surface. The stability of the title ions is discussed in terms of the barrier height and half-widths together with the tunnelling lifetimes for the metastable electronic states. It is shown that the metastable S_2^{2+} and S_2^{3+} cations are the ground states for the respective ions (the closed shell $^1\Sigma_g^+$ state and the $^2\Pi$ state, respectively) and that repulsive curves are far from their low vibrational levels. That means that the depletion mechanism through predissociation is improbable. It is shown that especially the S_2^{3+} ion is able to release a considerable amount of energy, 6.97 eV, after its decay. For the S_2^{2+} ion it is 1.24 eV. The barrier for dissociation is 2.73 eV for S_2^{2+} and 0.66 eV for S_2^{3+}. The lifetimes for both metastable cations are predicted for a few vibrational levels. For both ions, S_2^{2+} and S_2^{3+}, we have also detected additional (excited) metastable states: The $^3\Sigma_u^+$, $^3\Delta_u$ and $^3\Pi_g$ states for S_2^{2+} and the $^2\Sigma_g^+$ state for S_2^{3+}. The stability of the excited metastable states is expected, however, to be lower since they exhibit a lower barrier in comparison to the ground states of both ions. Their eventual experimental detection still appears to be possible.

1. Introduction

This work was primarily inspired by the experimental work of Cornides and co-workers [1] who used spark source mass spectrometry to detect rather unusual S_2^{3+} and other related small molecular ions. At first sight, this triply charged species should readily undergo destruction due to a 'coulomb explosion'. To a lesser extent this also applies to the S_2^{2+} ion to which we also paid attention. This doubly charged species is, however, expected to exist [2] since it is more-or-less valence isoelectronic with the known oxygen di-cation, studied both experimentally and theoretically [3–7]. In analogy to O_2^{2+}, there is also a triple bond in the S_2^{2+} ion since two electrons are removed from the antibonding π_g orbitals of the ground state of the parent S_2 molecule during ionization. This consideration leads to a possibility of the existence of this species. The bond lengths and the energies of the S_2^+ and S_2^{2+} ions relative to the sulphur molecule were calculated at the correlated level by Balaban *et al.* [2]. They did not present any information about the barrier preventing the dissociation of either S_2^{2+} or any other spectroscopic states. The triple charged cation, S_2^{3+}, which is of central interest to this work, seems not to have been investigated by any theoretical method. Yet this is important, since the mass spectrometry experiments only give information about the very

0026–8976/98 $12·00

existence of this species and not about its structure, barrier to dissociation, possible depletion mechanisms, energy obtained after the decay, etc.

All multiply charged ions which we have mentioned so far are *metastable*. The metastabilty in AB^{n+} arises from the existence of a local minimum due to the interaction between an *attractive* channel $A + B^{n+}$ and *repulsive* channels $A^{p+} + B^{q+}$, $p + q = n$, or, in other words, from a competition between an ordinary chemical bond and an essentially electrostatic repulsion. Recent excellent reviews present an overview of both experimental and theoretical developments in this field [8, 9]. The relative *asymptotic* energy (see, for example [10, 11]) is estimated by relative ionization potentials of the fragments A and B. In, for example a specific case of $p, q = 1$, $\Delta E = E[A + B^{2+}] - E[A^+ + B^+] = IP(B^+) - IP(A)$. If such a double charged diatomic cation should have a possibility to show metastability, the second ionization potential of either A or B should be larger than the sum of first IPs of the components, IP(A) + IP(B). In fact, the original idea dates from 1933, when Pauling [12] predicted the existence of the metastable He_2^{2+} ion. Thus, a general chemical and theoretical interest in understanding the unusual chemical phenomenon of metastability is another motivation for this work. In a broader perspective one can mention that metastable molecules are potential candidates as energy storage and energy transfer devices [8, 9, 13]. Understanding of related phenomena at the molecular level with some relation to novel technological applications is in this respect of great potential interest. In general, the metastable species may have energies very much in excess of the global minima corresponding to two separated species (with a lower charge as a metastable molecule). For example, energetical aspects of the He_2^{2+} ion were discussed by Nicolaides [14] who describes its ground state as a 'volcanic' state. He presents a series of possible chemical reactions capable of releasing enormous propulsive energies in the range 230–1000 kcal mol^{-1}. Finally, metastable cations have large oxidation power.

In general, the investigation of metastable multiply charged cations is difficult both experimentally and theoretically. Experimental work encounters difficulties in producing relatively high concentrations of these short living species, and at the same time in detecting them. Due to the experimental difficulties, most of the information about these systems arose from theoretical calculations, even if progress in experimental techniques changes this situation gradually [3, 8, 9]. A theoretical description is difficult as well, and can fail even qualitatively [4, 8–9, 15]. To obtain accurate results the use of multireference techniques is highly desirable in a description of a phenomenon in which a substantial characteristic is a curve crossing. An extended basis set is another requirement. In any reasonable theoretical description one also has to consider that the mechanism of depletion can be based on thermal decomposition, non-radiative transition (i.e. tunnelling through the potential barrier), predissociation resulting from the bound-repulsive crossing, as well as by radiative transitions (for metastable but electronically excited states). These mechanisms were discussed, for example by Bruna and Wright [16] and Lundquist *et al.* [3]. Thus a combination of both theoretical and experimental techniques is very often the most advantageous approach. More general considerations can be found in the literature, see for example [8, 9, 16]. Other related homonuclear diatomics are, for example, B_2^{2+} [10], C_2^{2+} [17], N_2^{2+} [18], F_2^{2+} [19]. Some of the above species are reported as possible ionospheric molecules (e.g. N_2^{2+}). Triply charged homonuclear diatomics are very rare, see e.g. Al_2^{3+} [16]. Even more highly charged diatomics were investigated [20] but usually without any detailed consideration of their potential energy curves, stability, and energetics. Interestingly, relativistic effects are observed in the heteroatomic metastable HBr^{2+} and DBr^{2+} [21].

2. Methods and computational details

All calculations performed within the present study of the S_2 molecule and its ions were carried out with all electrons taken into account. The electronic wave functions are expressed in terms of contracted sets of Gaussian-type orbitals (GTO/CGTO). After some pilot calculations with a series of smaller sets we arrived at the ANO(17s12p5d3f) primitive set contracted to the spherical [7s6p4d3f] set [22], i.e. altogether 132 basis functions. The computational point group was D_{2h}. The computer program MOLCAS-3 [23] was used throughout for all CASPT2 calculations [24].

The CASPT2 calculations rely on the CASSCF wave function which serves as a reference for the second order perturbation theory treatment of the dominant effect from the dynamical correlation whilst the CASSCF wave function itself should be capable of covering all the multireference aspects of the electronic structure, or, in other words, all near-degeneracy effects. These arose in the present case primarily from the effects of the sulphur 3p orbitals. By far the largest CI coefficient in the CAS expansion for both S_2^{2+} and S_2^{3+} is the double excitation from the bonding $2\pi_u$ orbital to the antibonding $2\pi_g$ orbital. Its weight, of course, depends to a large extent on the interatomic distance: near equilibrium it is relatively small, e.g. for S_2^{3+} at $R = 1.95$ A it is 0.044.

The ground electronic state of S_2 is $^3\Sigma_g^-$ with the electron configuration expressed as $1\sigma_g^2 1\sigma_u^2 2\sigma_g^2 2\sigma_u^2$

$3\sigma_g^2 3\sigma_u^2 1\pi_u^4 1\pi_g^4\ 4\sigma_g^2 4\sigma_u^2 5\sigma_g^2\ 2\pi_u^4 2\pi_g^2$. After removing the two antibonding electrons from the $2\pi_g$ orbital we arrive at the formally triple (2.5) bond in the S_2^{2+} (and S_2^{3+}) cation, respectively. In all CASSCF/CASPT2 calculations the electrons in $1\sigma_g^2 1\sigma_u^2 2\sigma_g^2 2\sigma_u^2$ orbitals were frozen. Corresponding electrons were left uncorrelated in all subsequent PT2 calculations as well. The best selection of the active space for the CASSCF calculation would be the (20002000–11101110–42214221) space with ten (nine) active electrons for S_2^{2+} (S_2^{3+}). The notation means (frozen–inactive–active) orbitals with the full CI wave function being created from all possible electron configurations of active electrons distributed in active orbitals which correspond to a desired spectroscopic state. The remaining effects of the dynamical correlation arise from excitations from/to inactive and active orbitals to remaining secondary orbitals and are treated by the second order perturbation theory with the multireference CASSCF zeroth order wave function [24]. The above mentioned active space includes all dominant near-degeneracy effects, and also orbitals dominated by all five sulphur d-orbitals, which appeared in some cases to be relatively important (their occupation numbers approached a value of 0.02). The only inactive ones are the $3\sigma_g 3\sigma_u 1\pi_u 1\pi_g$ which arise from the sulphur 2p orbitals. This active space was, unfortunately, not applicable at the CASPT2 level with the computer resources available to us. It lead to more than a million reference Configuration Space Functions (CFSs). We used it in some comparative calculations for S_2^{3+} at the CASSCF level only. Other active spaces which we have examined were the (20002000–11101110–21102110) space (the smallest possible one), followed by the (20002000–11101110–31103110) active space and the (20002000–21102110–32213221) space. The (31103110) active space has an advantage of considering the $4\sigma_g 4\sigma_u$ orbitals as active but it treats only the two ($3d_0$ and $3d_{2+}$) sulphur correlating d-orbitals, in contrast to the (42214221) active space. Finally, we used the (32213221) active space, applicable in all cases of interest. It exhibits some similar characteristics as the largest (42214221) space but at the price of shifting the $4\sigma_g 4\sigma_u$ orbitals among the inactive and thus reducing the number of active electrons by four. The corresponding excitation coefficients from these $4\sigma_{g,u}$ orbitals appear not to be dangerously large in the PT2 treatment, and the corresponding denominators are in most cases larger than 1.0. The shorthand notation including the active orbitals will only be used in the subsequent text and tables.

The relatively high weight of the dominating reference determinant in the vicinity of the (local) minima of the sulphur molecule and its cations allows the use of the highly sophisticated coupled cluster (CC) calculation in this region. This method in its single reference form is not applicable over the whole potential curves and thus the CC calculations only serve for test purposes of the more generally applicable CASPT2 method. The reason for using CC is that it is supposed to provide a more dynamical correlation and thus more accurate results in cases where the strongly dominating single determinant reference can be defined [25–27]. We used it at a level in which the single and double excitations (CCSD) [28] and perturbative (non-iterative) corrections for triple excitations from the unrestricted SCF HF reference function [29] were included. The particular version of perturbative corrections (T3(CCSD)) to CCSD energies employed in the present study includes an additional fifth order singles–triples term [30] and is referred to by the acronym CCSD(T). All electrons with the exception of the innermost eight $1\sigma_g^2 1\sigma_u^2 2\sigma_g^2 2\sigma_u^2$ electrons were explicitly correlated

The computer program ACES II [31] was used throughout for UHF-CC calculations.

The potential energy curves were used to solve the Schrödinger equation for rotational–vibrational motion of the nuclei by Numerov–Cooley integration [32]. The metastable states arising in the S_2^{2+} and S_2^{3+} ions were treated by using the methodology introduced by LeRoy and co-workers [33]. We used the Airy function criterion for the wave function to find the position of minima and maxima and a semiclassical approach to calculate their widths and lifetimes. The energy levels were fitted to provide standard spectroscopic constants of S_2^{2+} and S_2^{3+}. Rotational and vibrational states 0,0–0,20 were usually used in calculations of B_e and states 0,0–0, v_{max} were used in calculations of ω_e and $\omega_e x_e$. Of course, v_{max} is not the same for different states and changes with the well depth. We have considered all possible vibrational states with the exception of the highest few which would worsen the final fit.

3. Spectroscopic characteristics and ionization potentials of the sulphur atom and the sulphur molecule

3.1. *Spectroscopic characteristics*

It was not the purpose of the present paper to produce as accurate as possible spectroscopic constants of the parent S_2 molecule. Instead we only want to show that the basis set and methods used in this study are capable of providing reliable results at least in cases where experimental values are available. This can partly demonstrate the predictive power of applying the methods to multiply charged ions whose properties are not experimentally known. Still the very good agreement of spectroscopic constants with experiment for S_2 and S_2^+, see table 1, does not guarantee the quality of the active space and the capability of the CASPT2 method to describe correctly the most difficult region around the

Table 1. Energy values and spectroscopic constants for the S_2 molecule in the ground state, ($^3\Sigma_g^-$), and its S_2^+ ion in the $^2\Pi$ state. Interpolated total energies (+195 for S_2 and +194 for S_2^+) in au, dissociation energies in eV, equilibrium distances in 10^{-10} m, other values in cm^{-1}.

	R_e	$-E_{min}$	D_e^a	ω_e	$\omega_e x_e$	B_e	$\Delta G_{1/2}$	$\Delta G_{3/2}$	$\Delta G_{5/2}$
S_2 molecule									
RASSCF-3221	1.890	0.255920	4.173	744	2.51	0.2953	738	733	727
CASPT2-3221	1.892	0.574230	4.575	730	2.60	0.2946	725	720	714
			(4.530)						
CCSD(T)	1.892	0.602465	4.594	735	2.66	0.2945	730	724	719
Selected reference results									
MRCI+Q [34]	1.900	0.45677	4.261	719	2.84	0.292			
CI-SDQ(S) [35]	1.895		3.82				728	724	718
Experimental [36]	1.8892		4.414	726	2.844	0.2955	720	714	709
S_2^+ ion									
RASSCF-3221	1.827	0.930142	5.506	820	2.03	0.3161	817	809	802
CASPT2-3221	1.831	1.231109	5.314	796	2.44	0.3146	791	785	778
			(5.265)						
CASPT2-3110	1.833	1.233051	5.214	793	2.43	0.3139	787	782	775
CCSD(T)	1.827	1.261252	5.468	812	1.62	0.3159	808	803	797
Selected reference results									
CI-SDQ(S) [35]	1.827		4.65				818	812	806
Experimental [36]	1.825		5.42	790					

[a] The ZPE correction is 0.045 ev for the S_2 molecule and 0.049 eV for the S_2^+ ion. Numbers in parentheses include ZPE.

maximum on potential energy curves for the metastable species. Very good agreement of CASPT2(32213221) spectroscopic constants for S_2 and S_2^+ with CCSD(T) results (in this case CCSD(T) is perfectly applicable) also confirms the reliability of our approach. The quality of the basis set can be assessed from the comparison with recent benchmark calculations by Woon and Dunning [34] who used the multiconfiguration CI and the correlated consistent cc-pV5Z basis set of valence quintuple zeta quality. The accuracy of present results, as deduced from the comparison with experiment, is essentially the same as that obtained in Woon and Dunning's study. Good agreement with the experimental values is also found for spectroscopic constants of the S_2^+ ion. The difference of the dissociation energy from experiment is, similarly as with the parent molecule, about 0.1 eV which is considered to be satisfactory for the present purposes. Both the bond distance and, especially, the harmonic vibrational frequency are in excellent agreement with experimental results.

3.2. *Ionization potentials*

The capability of obtaining reasonable ionization potentials is another critical test of the methods used in the investigation of metastable molecules. IPs for the sulphur atom are experimentally known to a high accuracy, while in the S_2 molecule only the first ionization potential is reliably available from experiment. Table 2 shows that again, as with the spectroscopic constants, our methods at the level in which they account for a sufficient fraction of the dynamical correlation (i.e. CCSD(T) and CASPT2) are mutually consistent. The deviation from experiment at the CASPT-32213221 level is largest for the first IP of the sulphur atom, 0.242 eV, i.e. it differs from experiment by about 2.4%. At the CCSD(T) level it is only slightly smaller (0.205 eV). Because ionization potentials with quite different methods are similar, the error must reflect the basis set effect. The second and third atomic IPs are accurate to within 0.07 and 0.10 eV, respectively, which is very satisfactory. The first IP for the sulphur molecule deviates from experiment by only 0.02 eV, which must be considered an excellent but fortuitous agreement. The second IP of the molecule is only estimated [2] and can hardly serve as a test of the method. Where experimental data are available, the agreement of the calculated and experimental values may be considered to be good, at least for the present purposes.

4. The metastability of the S_2^{2+} ion

We have investigated altogether five electronic states of S_2^{2+}. Three of them, the ground state $^1\Sigma_g^+$, $(\ldots 5\sigma_g^2 2\pi_u^4)$ and the two low excited states, the $^3\Sigma_u^+$ $(\ldots 5\sigma_g^2 2\pi_u^3 2\pi_g^1)$ and the $^5\Sigma_g^+$ $(\ldots 5\sigma_g^2 2\pi_u^2 2\pi_g^2)$ dissociate into two sulphur

Table 2. Ionization potentials of the sulphur atom and adiabatic ionization potentials of the sulphur molecule (eV) [a].

Starting/final species	Experiment[b]	CASSCF	CASPT2	CCSD(T)
Sulphur atom (^{3}P)				
$S/S^+(^4S)$	10.360	9.742	10.118	10.159
$S^+/S^{2+}(^3P)$	23.33	23.25	23.40	23.31
$S^{2+}/S^{3+}(^2P)$	34.83	34.40	34.73	34.72
Sulphur molecule ($^3\Sigma g^-$)				
S_2/S_2^+ ($^2\Pi_g$)	9.36	8.865	9.337	9.285
S_2^+/S_2^{2+} ($^1\Sigma_g^+$)	16.6[c]	16.377	16.873	16.845
S_2^{2+}/S_2^{3+} ($^2\Pi_u$)	—	29.171	29.246	29.279

[a] RASSCF and CASPT2 results with the (32213221) active space. UHF-CCSDT(T) with 1s and 2s electrons frozen. Bond lengths as defined in table 2.
[b] Atomic data from [37]; molecular data from [36].
[c] Estimate taken from [2]; vertical ionization potential given in [36] is 15.58 eV.

Table 3. Metastable spectroscopic states of the S_2^{2+} ion and their barrier characteristics: the position of the minima and maxima R_{min}, R_{max} (in 10^{-10} m), the barrier height V_b and the dissociation energy D_e related to the respective fragments (in eV), and spectroscopic constants (in cm^{-1}).

Method/State	R_{min}	R_{max}	V_b^a	$D_e^{a,b}$	ω_e	$\omega_e x_e$	B_e	$\Delta G_{1/2}$	$\Delta G_{3/2}$	$\Delta G_{5/2}^c$
$^1\Sigma_g^+$, the ground state										
CASSCF-31103110	1.809	2.747	2.25	2.05	808	5.45	0.322	796	786	776
CASPT2-31103110	1.793	2.861	2.62	1.36	828	5.18	0.328	816	807	797
CASSCF-32213221	1.781	2.767	2.73	1.59	871	5.14	0.332	859	850	840
CASPT2-32213221	1.789	2.888	2.73	1.24	833	5.19	0.329	822	812	802
$^3\Sigma_u^+$										
CASPT2-32213221	2.037	2.817	0.70	3.37	493	6.44	0.253	481	467	454
CASPT2-31103110			0.63	3.51	494	6.21	0.251	481	470	456
$^3\Delta_u$										
CASPT2-32213221	2.002	3.002	1.33	2.54	559	5.64	0.262	548	535	524
$^3\Pi_g$										
CASPT2-32213221	1.885	2.486	0.85	3.78	641	6.84	0.295	628	612	599

[a] Includes the ZPV correction which is 0.052 eV for the $^1\Sigma_g^+$ ground state; 0.031 eV for the $^3\Sigma_u^+$ state; 0.035 eV for the $^3\Delta_u$ state and 0.040 eV for the $^3\Pi_u$ state with the CASPT2-32213221 method.
[b] Dissociation products are $S^+(^4S) + S^+(^4S)$ for $^1\Sigma_g^+$ and $^3\Sigma_u^+$ states; for the $^3\Delta_u$ and the $^3\Pi_g$ states the products are $S^+(^4S) + S^+(^2D)$.
[c] The potential energy curve supports 37 vibrational levels of the $^1\Sigma_g^+$ state, 14, 25, and 13 vibrational levels of the $^3\Sigma_u^+$, $^3\Delta_u$, and $^3\Pi_u$ states, respectively (CASPT2-32213221 data).

S^+ ions in their ground state, i.e. the ^4S state. The $^1\Sigma_g^+$ and $^3\Sigma_u^+$ states are metastable. Metastability also exhibit the $^3\Delta_u$ state ($\ldots 5\sigma_g^2 2\pi_u^3 2\pi_g^1$) which dissociates into the $S^+(^4S)$ and $S^+(^2D)$ fragments and the $^3\Pi_g$ state ($\ldots 5\sigma_g^1 2\pi_u^4 2\pi_g^1$) with the same dissociation limit. The characteristics of all metastable states are collected in table 3. The potential energy curves are presented in figure 1. Energy characteristics in table 3 show only marginal differences between CASPT2-31103110 and CASPT2-32213221 results. CASSCF results between the two active spaces differ much more, as could be expected. To be more specific, CASSCF-31103110 and CASSCF-32213221 barrier heights and dissociation energies both differ by 0.5 eV between the two active spaces, but the difference at the CASPT2 level is reduced to 0.1 eV. All $\Delta G(n+1/2)$ vibrational levels differ by 63–64 cm^{-1} at the CASSCF level between the two active spaces and are reduced by an order of magnitude to 5–6 cm^{-1} at the CASPT2 level. These differences can be considered as the error bars of our results for a specific quantity.

The ground state of the S_2^{2+} ion with its electronic configuration $\ldots 5\sigma_g^2 2\pi_u^4$ forms a triple bond. It is then not surprising that its bond length is shorter than that of

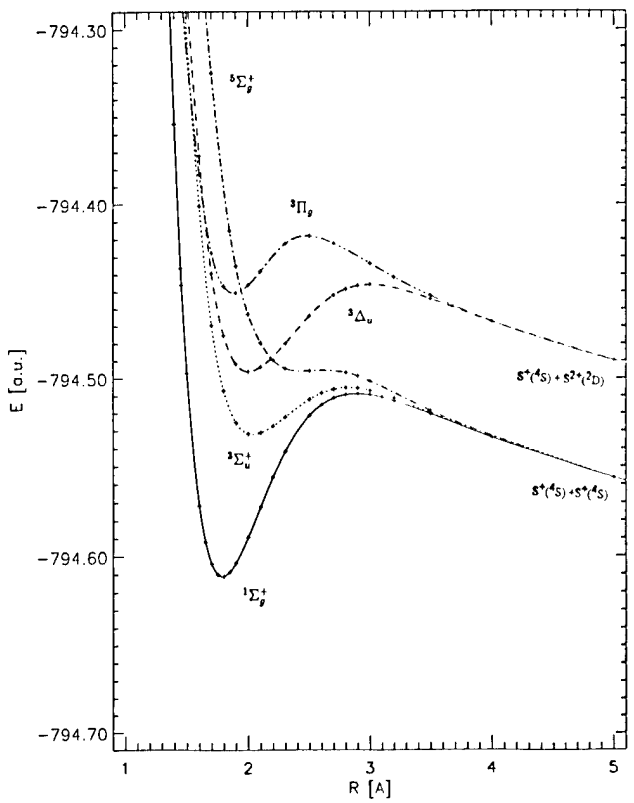

Figure 1. Potential energy curves for the S_2^{2+} cation in its $^1\Sigma_g^+$ ground state and four low lying excited states with the CASPT2-32213221 method.

the parent molecule, S_2 (compare data in tables 1 and 3), by about 0.103 A at the CASPT2 level. The barrier for the ground state is sufficiently high to allow detection since, in adddition to a predicted stability towards the tunnelling (the lifetime in the ground vibrational state is enormously large) it is also not crossed by any other repulsive curve which would lead to decay via predissociation. Similarly as the ground state $^1\Sigma_g^+$, the $^3\Sigma_u^+$ excited state is also not crossed by any repulsive curve. Even if its barrier is much lower than that for the ground state, it still should be sufficiently stable.

A comparison of our calculations with experimental work and theoretical calculations for the valence isoelectronic O_2^{2+} ion is interesting. Lundquist *et al.* (see [3] and references therein) combined an experimental observation of a Doppler free energy release spectrum with sophisticated MR-CI theoretical calculations, but experimentally could describe only the $^3\Delta_u$ excited state and higher states. Also the work by Fournier *et al.* [7] is a combined experimental/theoretical treatment. Let us start with a comparison of states dissociating to $X^+(^4S) + X^+(^4S)$ fragments (X = O or S). For this dissociative channel a comparison of S_2^{2+} and O_2^{2+} ions is more accessible when theoretical results are used for both O_2^{2+} [3–7] and S_2^{2+} ions. The ground state for both molecules is $^1\Sigma_g^+$, and exhibits metastability. The $^5\Sigma_g^+$ is repulsive in both cases (for S_2^{2+} we observe a shoulder, but definitely no local minimum), while the $^3\Sigma_u^+$ state is metastable in S_2^{2+} but repulsive (with a shoulder on the potential energy curve) in the O_2^{2+} ion. This is the most striking difference between the two ions. There was a long lasting discussion about the possibility of the existence of a local minimum for the $^3\Sigma_u^+$ state of O_2^{2+}. Finally this possibility was definitely excluded [5]. It is difficult to speculate about the reason for the existence of the metastable character of the same state in S_2^{2+}. The *non-existence* of the metastability in O_2^{2+} was discussed [7] on the basis of the mixing of the $^3\Sigma_u^+$ state, $\ldots 3\sigma_g^2 1\pi_u^3 1\ \pi_g^1 3\sigma_u^0$ with the much higher state of the same symmetry and multiplicity but with the dominating configuration $\ldots 3\sigma_g^1 1\pi_u^4 1\pi_g^0 3\sigma_u^1$ which is strictly repulsive. The $5\sigma_u$ orbital in S_2^{2+} is analogous to the 'critical' $3\sigma_u$ orbital. We found only small occupation of this orbital (0.05 in the final CASPT2 wave function) in S_2^{2+} at a distance of 2.0 A. To circumvent a possibility of an artefact due to a necessarily limited active space we also present in table 3 calculations with our alternative active space, 31103110, in which $4\sigma_g 4\sigma_u$ orbitals are included in the active space (but not all orbitals to which the sulphur d-orbitals contribute significantly). Energy values obtained with this active space –the barrier height and the dissociation energy –differ from the 32213221 active space by 0.1 eV, but an artefact in our finding of metastability due to the limitation of the active space is definitely excluded. Due to the high quality and the size of the ANO basis set which we used the basis set effect also can be excluded.

Returning to the $^1\Sigma_g^+$ ground state, we can note that the barrier is 2.73 eV for S_2^{2+} compared to a barrier of 3.59 eV for O_2^{2+} and the dissociation energies are 1.24 and 3.92 eV, respectively, for the two ions. The harmonic vibrational frequency for O_2^{2+} is 2147 cm^{-1}, i.e. much higher than is our value from table 3 (we present here values from [5] for O_2^{2+}), but this is a natural consequence of the different atomic masses of the two atoms.

The $^3\Delta_u$ state of S_2^{2+} can be compared with the same state observed in O_2^{2+} experimentally and theoretically [3]. Both are metastable with 25 vibrational levels supported in S_2^{2+} for this state and three levels for O_2^{2+}. The release energy is 2.54 eV in S_2^{2+} and 6.89 eV in O_2^{2+}, the barrier is 1.37 in S_2^{2+} and substantially lower, 0.146 eV in O_2^{2+}. The $^3\Delta_u$ state is crossed by the $^5\Sigma_g^+$ state in both ions (in O_2^{2+} actually at the $v = 0$ level) but no predissociation is observed since the two states do not interact [3].

The $^3\Pi_g$ state is also metastable in both, S_2^{2+} and O_2^{2+} di-cations. Normally they would dissociate to their

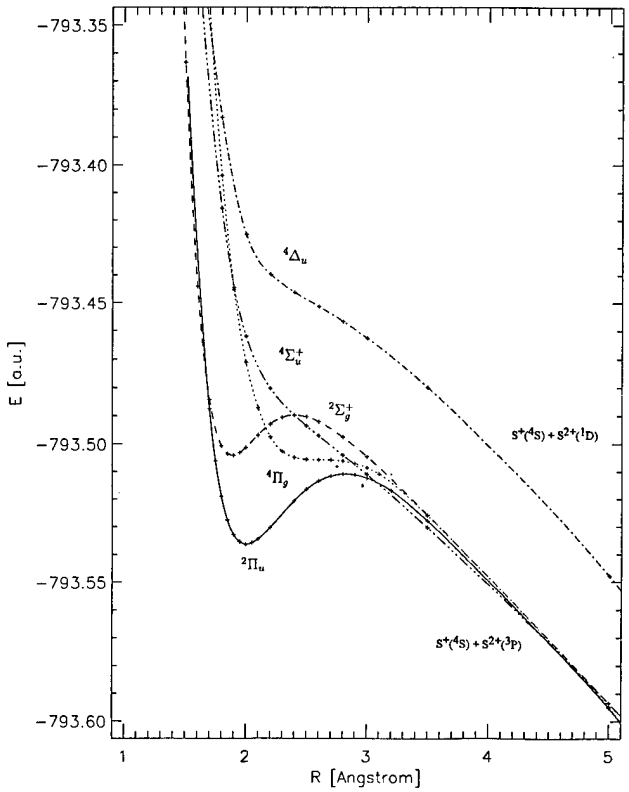

Figure 2. Potential energy curves for the S_2^{3+} cation in its $^2\Pi_u$ ground state and four low lying excited states with the CASPT2-32213221 method.

respective $X^+(^4S)$ and $X^+(^2D)$ fragments, but due to crossing with the $^5\Sigma_g^+$ state predissociation occurs if the spin–orbit coupling is considered. The final products then are the lowest electronic states of the two $X^+(^4S)$ ions. This is experimentally observed [3] in O_2^{2+} and can certainly be expected in S_2^{2+} as well. The $^3\Pi_g$ curve of S_2^{2+} is crossed by the repulsive $^5\Sigma_g^+$ curve very close to its minimum, see figure 1.

5. The metastability of the S_2^{3+} ion

Also for this multiply charged molecular ion we have investigated several electronic states, five altogether. Four of them, the ground state $^2\Pi_u$ $(\ldots 5\sigma_g^2 2\pi_u^3)$ and the three low excited states, the $^2\Sigma_g^+$ $(\ldots 5\sigma_g^1 2\pi_u^4)$, the $^4\Pi_g$ $(\ldots 5\sigma_g^2 2\pi_u^2 2\pi_g^1)$, and the $^4\Sigma_u^+$ $(\ldots 5\sigma_g^1 2\pi_u^3 2\pi_g^1)$ dissociate into the sulphur $S^+(^4S)$ and $S^{2+}(^3P)$ ions, i.e. their ground states. The $^4\Delta_u$ state dissociates into the $S^+(^4S) + S^{2+}(^1D)$ ions.

The ground state $^2\Pi_u$ and the $^2\Sigma_g^+$ states are metastable. The characteristics of both metastable states are collected in table 4. The potential energy curves are presented in figure 2. In figure 3 we present a comparison of CASSCF, CASPT2 curves with three different selections of the active space and the CCSD(T) curve. The CCSD(T) procedure did not converge for distances longer than 2.8 A. For distances a bit shorter there were observed symmetry broken solutions. The fact that single reference MBPT and CC methods, normally very powerful, are not applicable in investigations of the metastable molecules where the truly multireference description is needed, is well known [4, 15]. All three CASPT2 curves show very similar (even if not identical) behaviour and even the CASSCF-32213221 curve is qualitatively correct. The energy characteristics in table 4 demonstrate little sensitivity to the selection of the active space and agree to within 0.02 eV in the barrier height and to within 0.09 eV for the dissociation energy. The vibrational spacing $\Delta G(n+1/2)$ values agree less satisfactorily in the two larger active spaces which, however, does not change the overall picture dramatically. For example, both CASPT2-32213221

Table 4. Metastable spectroscopic states of the S_2^{3+} ion and their barrier characteristics: the position of the minima and maxima R_{min}, R_{max} (in 10^{-10} m), the barrier height V_b and the dissociation energy D_e related to the respective fragments (in eV), and spectroscopic constants (in cm^{-1}).

Method/State	R_{min}	R_{max}	V_b^a	$D_e^{a,b}$	ω_e	$\omega_e x_e$	B_e	$\Delta G_{1/2}$	$\Delta G_{3/2}$	$\Delta G_{5/2}^c$
$^2\Pi_u$, the ground st.										
CASSCF-31103110	2.033	2.780	0.54	7.15	474	7.23	0.254	459	445	431
CASPT2-31103110	2.001	2.782	0.68	7.06	509	6.63	0.262	495	482	470
CASSCF-32213221	1.970	2.773	0.80	7.06	558	7.47	0.270	543	529	514
CASPT2-32213221	2.005	2.818	0.66	6.97	479	6.71	0.261	473	448	436
$^2\Sigma_g^+$										
CASPT2-32213221	1.891	2.402	0.36	7.82	549	14.12	0.293	520	493	463

[a] The difference of energy between products and the respective local minimum. Includes the ZPV correction which is 0.031 eV for the $^2\Pi_u$ ground state and 0.034 eV for the $^2\Sigma_g^+$ state with the CASPT2-32213221 method. In fact with all other methods very similar values are obtained.

[b] Dissociation products are $S^+(^4S) + S^{2+}(^3P)$ for both metastable, $^2\Pi_u$ and $^2\Sigma_g^+$, states.

[c] the potential energy curve supports 14 vibrational levels of the $^2\Pi_u$ state and 6 vibrational levels of the $^2\Sigma_g^+$ state (CASPT2-32213221 data).

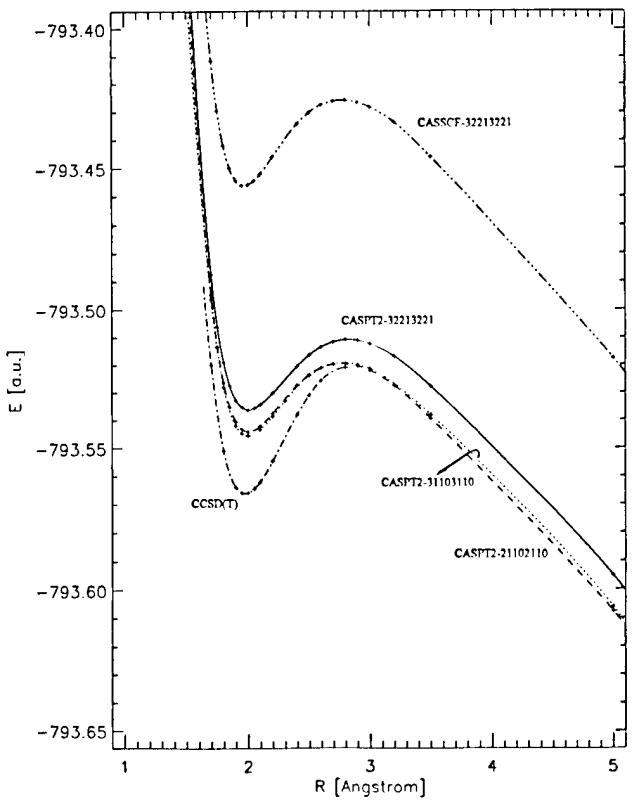

Figure 3. A comparison of the potential energy curves for the $^2\Pi_u$ ground state of the S_2^{3+} cation using the CASSCF and CASPT2 methods with different selections of the active space and with the CCSD(T) curve.

and CASPT2-31103110 curves do support 14 vibrational levels in the $^2\Pi_u$ ground state potential well.

There is no similar triply charged positive homonuclear diatomic molecule known to us with which our results for S_2^{3+} could be compared. Possibly the most closely related ion is Al_2^{3+} [16]. This tri-cation, however, exhibits metastability in highly excited states, which are crossed by dozens of repulsive curves. Its ground state is fully repulsive, in contrast to S_2^{3+}. Also, the ground state of S_2^{3+} is well isolated from any other curve and is not crossed by any repulsive curve considered in the present study. Considering the electronic structure of the $^2\Pi_u$ ground state one can hardly expect any other curve with energies low enough to be able to cross the $^2\Pi_u$ curve at sufficiently low vibrational states. The lifetime (formally more than 10^{60} s for the $v=0$ vibrational level) should be long enough to allow its spectroscopic investigation. The mass spectroscopy detection [1] was succesfully performed long ago, but the experimental investigation of the properties of the metastable states of S_2^{3+} is still missing. Even the low lying metastable $^2\Sigma_g^+$ state may possibly be detected, although its barrier is much lower and correspondingly the lifetime is much shorter than for the ground state.

We present in table 5 lifetimes for selected metastable states as calculated from the halfwidth of the barrier following the standard procedure [33]. We note that the lifetime for, e.g. the $^1\Sigma_g^+$ state of S_2^{2+} is larger than 10^{10} s up to the vibrational quantum number 31, and similarly, for its $^3\Delta_u$ state up to the vibrational quantum number 19. We stress that the lifetimes presented here are lifetimes with respect to a spontaneous non-radiative dissociation. They are often enormously high and have no direct relation to experimentally observed lifetimes. In experimental investigations the stability (and hence the halfwidth) is influenced by phenomena perturbing a metastable state, such as radiative broadening and colli-

Table 5. Lifetimes (in seconds) for selected spectroscopic states[a,b] of metastable S_2^{q+}.

Vibration quantum number	$S_2^{2+}(^3\Sigma_u^+)$	$S_2^{2+}(^3\Pi_g^+)$	$S_2^{3+}(^2\Pi_u)$	$S_2^{3+}(^2\Sigma_g^+)$
0	b	b	b	b
1	b	b	b	b
2	b	b	b	0.99×10^{8}
3	b	b	b	0.32×10^{3}
4	b	b	b	0.40×10^{-2}
5	b	b	b	0.19×10^{-6}
6	b	b	b	
7	b	b	b	
8	b	0.38×10^{7}	b	
9	0.90×10^{9}	0.69×10^{2}	0.10×10^{9}	
10	0.19×10^{5}	0.30×10^{-2}	0.37×10^{4}	
11	0.92×10	0.35×10^{-6}	0.25×10	
12	0.10×10^{-3}	0.13×10^{-9}	0.34×10^{-4}	
13	0.27×10^{-7}		0.11×10^{-7}	

[a] Lifetimes for the S_2^{2+} $^1\Sigma_g^+$ and $^3\Delta_u$ states for lowest 14 vibrational levels are larger than 10^{10} seconds and are not presented.

[b] Only lifetimes smaller than 10^{10} seconds are presented.

sional broadening. Evaluation of these effects goes beyond the scope of the present paper.

6. Conclusion

The electronic ground states of the $S_2^{2+}(^1\Sigma_g^+)$ and $S_2^{3+}(^2\Pi)$ ions are metastable. For S_2^{3+} this confirms the experimental evidence of its very existence, even if properties of this ion remain experimentally unknown. Considering all deficiencies related to approximations involved in our calculations of the lifetimes for these species we believe that they are stable enough to allow a detailed experimental investigation of their properties. This view is supported by a comparison with a similar species, the O_2^{2+} cation, which is experimentally well known. We also conclude that metastable excited states of S_2^{2+}, namely $^3\Sigma_u^+$, $^3\Delta_u$ and $^3\Pi_g$ states, exibit sufficiently high barriers to dissociation. Energy curves support enough vibrational levels (14, 25 and 13, respectively), and estimated lifetimes appear to be sufficiently large to allow experimental detection and investigation of excited metastable states as well. The S_2^{3+} cation also exhibit metastability not only in the ground state but also in its $^2\Sigma_g^+$ state. We believe that for metastable states of S_2^{3+}, similarly and on the basis of the same arguments as with S_2^{2+}, the experimental investigation is possible as well.

The methods used in the present study are considered to be reliable enough to encourage an experimental study of a variety of the electronic states of both S_2^{2+} and S_2^{3+} cations.

Partial support to one of us (M.U.) by the Slovak Grant Agency (Contract No. 1/1455/1994) is gratefully acknowledged. M.U. also thanks G. H. F. Diercksen for his hospitality at the Max-Planck-Institut fur Astrophysik.

References

[1] Morvay, L., and Cornides, I., 1984, *Int. J. Mass Spectrom. Ion Proc.*, **62,** 263; Ujpál, M., Morvay, L., and Cornides, I., 1988, *Rapid. Commun. Mass Spectrom.*, **2,** 162; Morvay, L., and Cornides, I., 1992, *Rapid. Commun. Mass Spectrom.*, **6,** 339.

[2] Balaban, A., DeMaré, G. R., and Poirier, R. A., 1989, *J. molec. Struct.* (THEOCHEM), **183,** 103.

[3] Lundquist, M., Edvardsson, D., Baltzer, P., Larsson, M., and Wannberg, B., 1996, *J. Phys.* B: *At. Molec. Opt. Phys.*, **29,** 499.

[4] Nobes, R. H., Moncrieff, D., Wong, M. W., Gill, P. M. W., and Pople, J. A., 1991, *Chem. Phys. Lett.*, **182,** 216.

[5] Pettersson, L. G. M., and Larsson, M., 1991, *J. chem. Phys.*, **94,** 818.

[6] Yang, H., Hanson, D. M., Trentini, F. V., and Whitten, J. L., 1990, *Chem. Phys.*, **147,** 115.

[7] Fournier, J. Fournier, P. G., Langford, M. L., Mousselmal, Robbe, J. M., and Gandara, G., 1992, *J. chem. Phys.*, **96,** 3594.

[8] Mathur, D., 1993, *Phys. Rep.* **225,** 193.

[9] Larsson, M., 1993, *Comments At. molec. Phys.*, 39.

[10] Bruna, P. B., and Wright, J. S., 1990, *J. chem. Phys.*, **93,** 2617.

[11] Ackermann, J., and Hogreve, H., 1992, *J. Phys.* B: *At. molec. opt. Phys.*, **25,** 4069.

[12] Pauling, L., 1933, *J. chem. Phys.*, **1,** 56.

[13] Boldyrev, A. I., and Simons, J., 1992, *J. chem. Phys.*, **97,** 4272; Gonzales, N., and Simons, J., 1994, *J. chem. Phys.*, **100,** 5778.

[14] Nicolaides, C. A., 1989, *Chem. Phys. Lett.*, **161,** 547.

[15] Nagesha, K., Marathe, V. R., and Mathur, D., 1991, *Chem. Phys.*, **154,** 125.

[16] Bruna, P. B., and Wright, J. S., 1993, *J. Phys.* B: *At. molec. opt. Phys.*, **26,** 1819.

[17] Hogreve, H., 1966, *Chem. Phys.*, **202,** 71.

[18] Taylor, P. R., 1983, *Molec. Phys.*, **49,** 1297; Bennett, F. R., 1995, *Chem. Phys.*, **190,** 53; Lundquist, M., Edvardsson, D., Baltzer, and Wannberg, B., 1996, *J. Phys.* B: *At. molec. opt. Phys.*, **29,** 1489; Senekowitsch, J., O'Neil, S., Knowles, P., and Werner, H.-J., 1991, *J. phys. Chem.*, **95,** 2125.

[19] Senekowitsch, J., and O'Neil, S., 1991, *J. chem. Phys.*, **95,** 1847.

[20] Pyykkö, 1989, *Molec. Phys.*, **67,** 871; Safvan, C. P., and Mathur, D., 1994, *J. Phys.* B: *At. molec. opt. Phys.*, **27,** 4073.

[21] Banichevich, A., Peyerimhoff, S. D., Hess, B. A., and Van Hemert, M. C., 1991, *Chem. Phys.*, **154,** 199.

[22] Widmark, P.-O, Persson, B. J., and Roos, B. O., 1991, *Theor. Chim. Acta*, **79,** 419.

[23] Andersson, K., Blomberg, M. R. A., Fülscher, M., Kellö, V., Lindh, R., Malmqvist, P.-A., Noga, J., Olsen, J., Roos, B. O., Sadlej, A. J., Siegbahn, P. E. M., Urban, M., and Widmark, P.-O., 1994, MOLCAS System of Quantum Chemistry Programs, Release 3. Theoretical Chemistry, University of Lund, Lund Sweden and IBM Sweden.

[24] Andersson, K., Malmqvist, P.-A., Roos, B. O., Sadlej, A. J., and Wolinski, K., 1990, *J. phys. Chem.*, **94,** 5483; Andersson, K., Malmqvist, P.-A., and Roos, B. O., 1992, *J. chem. Phys.*, **96,** 1218.

[25] Urban, M., Černušák, I., Kellö, V., and Noga, J., 1987, *Methods in Computational Chemistry*, Vol. I, edited by S. Wilson (New York: Plenum Press), p. 117.

[26] Bartlett, R. J., 1995, *Advanced Series in Physical Chemistry, Vol. 2, Modern Electronic Structure Theory*, edited by D. R. Yarkony (Singapore: World Scientific), p. 1047.

[27] Lee, T. J., and Scuseria, G. E., 1995, *Quantum Mechanical Electronic Structure Calculations with Chemical Accuracy*, edited by S. R. Langhoff (Dordrecht: Kluwer Academic Publishers), p. 47.

[28] Purvis, G. D., and Bartlett, R. J., 1982, *J. chem. Phys.*, **76,** 1910.

[29] Urban, M., Noga, J., Cole, S. J., and Bartlett, R. J., 1985, *J. chem. Phys.*, **83,** 4041.

[30] Raghavachari, K., Trucks, G. W., Pople, J. A., and Head-Gordon, M., 1989, *Chem. Phys. Lett.*, **157,** 479.

[31] ACES II: STANTON, J. F., GAUSS, J., WATTS, J. D., LAUDERDALE, W. J., and BARTLETT, R. J., 1992, *Int. J. quantum Chem. Symp.*, **26**, 879.
[32] COOLEY, J. W., 1961, *Math. Comput.*, **15**, 363.
[33] LEROY, R. J., and LIU, B., 1978, *J. chem. Phys.*, **69**, 3622; LEROY, R. J., and BERNSTEIN, R. B., *J. phys. Chem.*, **54**, 5114.
[34] WOON, D. E., and DUNNING JR., T. H., 1994, *J. chem. Phys.*, **101**, 8877.
[35] MCLEAN, A. D., LIU, B., and CHANDLER, G. S., 1984, *J. chem. Phys.*, **80**, 5130.
[36] HUBER, K. P., and HERZBERG, G., 1979, *Molecular Spectra and Molecular Structure. IV. Constants of Diatomic Molecules* (New York: Van Nostrand Reinhold).
[37] MOORE, C. E., 1958, *Atomic Energy Levels* (Washington, DC: National Bureau of Standards).

MOLECULAR PHYSICS, 1998, VOL. 94, NO. 1, 209–216

A statistical multireference state-specific dressing of configuration interaction matrices: application to Heisenberg Hamiltonians

By NATHALIE GUIHERY, JEAN-PAUL MALRIEU, DANIEL MAYNAU AND PETER WIND

Laboratoire de Physique Quantique, URA 505, Université Paul Sabatier, 118, route de Narbone, 31062 Toulouse Cedex, France

For an arbitrary (truncated or selected) configuration interaction (CI) space and from a specific eigenvector, one may extract statistical and state specific amplitudes of elementary excitations. These amplitudes are used for the evaluation of the coefficients of the outer-space determinants, leading to a state specific dressing of the CI matrix. The process is repeated to self-consistency. Numerical applications to ground and excited states of a Heisenberg Hamiltonian for conjugated molecules illustrate the efficiency of the method.

1. Introduction

Recently, a simple procedure labelled size-consistent self-consistent $(SC)^2CI$ [1], has been proposed. It consists of the definition of a dressing which makes size-consistent the lowest eigenvalue of any CI matrix. This dressing is of coupled electron pair approximation (CEPA) type [2–4] and exactly treats all exclusion effects. A specific determinant, the Hartree–Fock (HF) ground state one, plays a special role, i.e. the dressing is of single reference nature, even when the CI space is multireference (for instance a MRSDCI or a CASSDCI). A direct transposition of this technique to Heisenberg Hamiltonians has proved to be efficient [5], although the reference determinant ϕ_0, which is a Néel-type determinant (without any spin frustration), has a very small coefficient, while being the largest one. Nevertheless this method can only be applied to alternant (spin non-frustrated) molecules.

The excited roots of the $(SC)^2CI$ matrix have recently been shown to be very accurate for atoms and molecules [6], especially when the CI is a MRSDCI where references are the leading singly (or doubly) excited configurations. This result may be rationalized [7] but it would be convenient to define specific dressing for excited states. The concept of a multireference dressing appears as a desirable task, even for the ground state. For instance, in the case of Heisenberg Hamiltonians, the treatment of spin-frustrated systems requires a multireference dressing since the less frustrated determinants are numerous.

The attemps to define MR-CEPA [8–11], MR-ACPF [12] and MR-AQCC [13] procedures are numerous and follow different strategies. A state-specific $MR(SC)^2CI$ method which appears to be promising from numerical tests [14] has been recently presented [11] by our group, but it remains quite difficult to implement. In the present paper, a very simple procedure to define a state-specific dressing for any CI is proposed. It exploits the eigenvector of interest to define statistical pseudo-amplitudes for the double excitation operations. These pseudo-amplitudes are used to obtain an estimate of the coefficients of the outer-space. The procedure must be iterated to self-consistency. The present paper gives a few exploratory calculations on Heisenberg Hamiltonians, concerning both some non-alternant hydrocarbons, for which the traditional $(SC)^2$ single reference dressing is not conceivable and the excited states of alternant and non-alternant hydrocarbons. Comparison to the full CI results shows the efficiency of the proposed self-consistent statistical state-specific dressing.

2. A statistical state specific dressing

2.1. *The ground state $(SC)^2$ single reference dressing*

We would like to generalize an idea which has been exploited for the ground state when a single determinant ϕ_0 prevails in the wave-function, and which has led to self-consistent size-consistent dressing of CI matrices ($(SC)^2CI$ method [1]), the principle of which will be briefly recalled here.

Consider a CI space S of determinants ϕ_i. This space may be truncated to a certain level of excitations with respect to a single determinantal ground state (closed-shell) reference ϕ_0; it may be a CASSDCI or even a selected CI space. Let P_s be the projector on this space S

$$P_s = \sum_i |\phi_i\rangle\langle\phi_i|. \tag{1}$$

The diagonalization of the corresponding CI matrix gives a zero-order description $\tilde{\Psi}_0$ of the ground state

0026–8976/98 $12·00

eigenvector Ψ_0 and of a zero order estimate $\tilde{E}_0$ of the exact energy E_0

$$P_s H P_s |\tilde{\Psi}_0\rangle = \tilde{E}_0 |\tilde{\Psi}_0\rangle. \quad (2)$$

The method consists of the definition of amplitudes of coefficients of double excitations from the CI wave-function for the ground state.

$$\tilde{\Psi}_0 = C_0^0 \phi_0 + \sum_i C_i^0 \phi_i. \quad (3)$$

ϕ_0 is supposed to satisfy Brillouin's theorem, there is no contribution of the single excitations to the energy and the coefficients of singly excited determinants are weak, and hereafter single excitations will be omitted.

For a double excitation $D_l^+ = a_r^+ a_s^+ a_a a_b$ where the orbitals a and b are occupied and r and s are empty in ϕ_0, one writes

$$f_l^0 = \frac{C^0_{D_l^+ \phi_0}}{C^0_{\phi_0}}, \quad (4)$$

where $C^0_{\phi_0}$ and $C^0_{D_l^+ \phi_0}$ are respectively the coefficients of determinants ϕ_0 and $D_l^+ \phi_0$ in the ground state Ψ_0. This expression may be seen as the amplitude relative to the double excitation D_l^+ in the single reference coupled cluster expansion for the ground state

$$|\Psi_0\rangle = \exp S |\phi_0\rangle \quad (5)$$

since the products of single excitations do not significantly contribute to the coefficient $C_{D_l^+ \phi_0}$. Then one approximates the effect of the outer-space determinants ϕ_α obtained from the determinants ϕ_i by a double excitation D_l^+. The quantity $\sum_{\alpha \notin S} H_{i\alpha} C_\alpha^0$ appearing in the eigenequation relative to ϕ_i

$$\sum_{j \in S} H_{ij} C_j^0 + (H_{ii} - E) C_i^0 + \sum_{\alpha \notin S} H_{i\alpha} C_\alpha^0 = 0 \quad (6)$$

only concerns the determinants ϕ_α obtained from ϕ_i through double excitations

$$\phi_\alpha = D_l^+ \phi_i,$$

$$\sum_{\alpha \notin S} H_{i\alpha} C_\alpha^0 = \sum_{l, \text{ such as } D_l^+ i \neq 0, D_l^+ i \notin S} H_{i, D_l^+ i} C^0_{D_l^+ i}, \quad (7)$$

where $D_l^+ i$ is a compact notation for $D_l^+ \phi_i$, and the crucial approximation consists in writing C_α^0 as

$$C_\alpha^0 = f_l^0 C_i^0. \quad (8)$$

This evaluation of C_α^0 is partial, it includes the part of the complete expansion which is necessary to suppress unliked diagrams. Scheme 1 gives a diagrammatic transposition of this expression where the closed horizontal line represents the multiple excitations leading from $|0\rangle$ to $|i\rangle$.

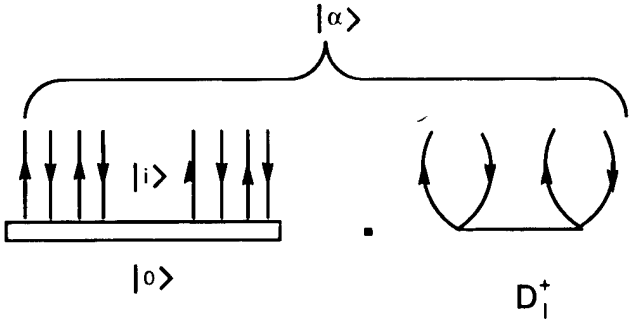

Scheme 1

From these assumptions and noting that for double excitations, $H_{i,D_l^+ i} = H_l = \langle ab|rs\rangle$, i.e. is independent of ϕ_i, one may see that

$$\sum_{\alpha \notin S} H_{i\alpha} C_\alpha^0 = \left(\sum_{l \text{ such as } D_l^+ i \neq 0, D_l^+ i \notin S} f_l^0 H_l \right) C_i^0. \quad (9)$$

This summation may be treated by a proper diagonal energy shift of the CI matrix

$$\tilde{H}_{ii} = H_{ii} + \Delta_{ii}, \quad (10)$$

$$\Delta_{ii} = \sum_{l \text{ such as } D_l^+ i \neq 0, D_l^+ i \notin S} H_l f_l^0. \quad (11)$$

The method presented above is a single reference dressing (with respect to ϕ_0) of a CI matrix which may be a MRCI. The ground state solution is size consistent. Excited roots have shown to be very accurate although they do not strictly satisfy the size extensivity requirements.

2.2. *Multireference generalization*

One may desire to conceive a more consistent procedure, which would be appropriate for the calculation of multireference states, and in particular excited states, i.e.

(i) in which the amplitudes of the double excitations are extracted from the desired excited state wave-function,

(ii) which would accept a multireference zeroth order function (as compulsory for most excited states, but often desirable too for ground state problems).

Such requirements are already fulfilled by a previously proposed $MR(SC)^2$ [11, 14] and some later CC [15, 16] type versions. The method proposed here is a simpler alternative. The variational space is supposed to include all singles and doubles on these references. The interest of the state specificity appears already for an excited state m involving a single determinantal single reference I, such as a $S_z = 1$ triplet singly excited state. The

amplitudes of double excitations on this reference single determinant have no reason to be strictly equal to those appearing in the singlet ground state expansion. It is obvious that the physically meaningful references change from one state to another. Such a state specific extraction of amplitudes is not computationally more demanding than for the ground state. In this case, the amplitude of the double excitation D_l^+ will be calculated as

$$f_{l,I}^{\mathrm{m}} = \frac{C_{D_l^+ I}^{\mathrm{m}}}{C_I^{\mathrm{m}}}. \tag{12}$$

Let us consider now a multiple reference problem, involving several reference determinants I. This reference space might for instance be a complete active space (CAS), involving n electrons in p active orbitals. The information will be extracted from the relevant eigenvector $\tilde{\Psi}_{\mathrm{m}}$ of the MRSDCI matrix. The list of the double excitations D_l^+ is different from one reference to another, although in the case of a CAS, the inactive double excitations are the most numerous and possible on all references. Moreover the values of the ratios $f_{l,I}^{\mathrm{m}}$ have no reason to be identical for the same operation D_l^+ and different references I. It is tempting to consider a reference-independent mean ratio f_l^{m}.

$$f_l^{\mathrm{m}} = \frac{1}{N_l^{\mathrm{m}}} \sum_{I, D_l^+ I \neq 0} f_{l,I}^{\mathrm{m}} (C_I^{\mathrm{m}})^2, \tag{13}$$

where N_l^{m} is a normalization factor

$$N_l^{\mathrm{m}} = \sum_{I, D_l^+ I \neq 0} (C_I^{\mathrm{m}})^2 \tag{14}$$

running on all references I on which the operation D_l^+ is possible, i.e. gives a non-zero result. The averaging takes care of the relative weights of the various references in the wave function. The variance of the distributions of the f_{lI}^{m}'s around their mean value

$$(\Delta f_l^{\mathrm{m}})^2 = \frac{1}{N_l^{\mathrm{m}}} \sum_{I, D_l^+ I \neq 0} (f_{l,I}^{\mathrm{m}} - f_l^{\mathrm{m}})^2 (C_I^{\mathrm{m}})^2 \tag{15}$$

indicates whether the weighted ratios are weakly reference dependent.

The quantities f_l^{m} will replace the ratios f_l^0 used in the single reference $(SC)^2$ dressing. The dressing will concern the MRSDCI matrix where the non-reference determinants will be labelled $|i\rangle$, as before. This new dressing will be obtained by approximating the coefficient of the outer-space determinants $|\alpha\rangle$ interacting with $|i\rangle$ and such that $|\alpha\rangle = D_l^+ |i\rangle$ by

$$C_\alpha^{\mathrm{m}} = f_l^{\mathrm{m}} C_i^{\mathrm{m}}. \tag{16}$$

This result is a state specific diagonal dressing of the CI matrix

$$\Delta_{ii}^{\mathrm{m}} = \sum_{l \text{ such as } D_l^+ i \neq 0, D_l^+ i \notin S} H_l f_l^{\mathrm{m}} \tag{17}$$

which may be seen as a generalization of the ground state $(SC)^2$ dressing (equation (11) using statistical state specific amplitudes.

2.3. *Specification to Heisenberg Hamiltonians*

Let us consider a molecular frame with n centres $(1, \ldots, i, j, \ldots, n)$ and n electrons (half-filled band situation). The Heisenberg Hamiltonian may be written [17] as

$$H = \sum_{i,j} R_{ij} + g_{ij} |i\bar{j} - \bar{i}j\rangle\langle i\bar{j} - \bar{i}j|. \tag{18}$$

The term R_{ij} is a spin-independent scalar function of the distance r_{ij} between i and j and g_{ij} represents the effective exchange between adjacent atoms. It is also a function of r_{ij}. A precise determination of these functions for the treatment of π electrons of conjugated hydrocarbons may be found in [17]. Other parametrization may be found in [18]. The Hamiltonian is an effective Hamiltonian, concerning only neutral valence bond (VB) structures. The dimension of the Full CI space which grows as $C_n^{n/2}$, becomes too large to be handled on a workstation when n reaches 20. A previous work [5] has proposed an energy-based truncation of the CI space, keeping only the spin distributions which present up to a threshold number m of spin frustrations on the bonds. This truncated CI has to be dressed to avoid size-inconsistency, and the $(SC)^2 CI$ procedure has proven to be very efficient, since it divides the error with respect to full CI by a factor about 60 and gives accurate results even when very limited CI spaces are considered [5].

For such a local Hamiltonian, one needs only to determine the amplitudes of the spin exchanges D_l^+ on each bond l which increase the energy (i.e. the number of spin frustrations). This means that the transition energy is positive

$$\Delta E_{l,i} = \langle D_l^+ i | H | D_l^+ i \rangle - \langle i | H | i \rangle > 0.$$

As a refinement, we have taken into account the value of $\Delta E_{l,i}$, since a spin exchange on a given bond l may increase the number of spin frustrations by $1, 2, \ldots, n_l$, where n_l is the number of bonds adjacent to bond l. We have therefore extracted different amplitudes for each bond according to the various energy increase $\Delta E_{l,i}$ characteristic of the various spin environments of the bond l. We therefore must extract from the variational function a few quantities $f_l(\Delta E)$ for each bond. In this precise problem there is no need to identify the minimal number of references I, it is possible to calculate the mean ratio f_l^{m} given by equation (13) where the summa-

tion runs over the whole set of determinants such that $D_I^+ I$ belongs to the model space.

3. Numerical tests

3.1. *Mean amplitudes and variances of the $f_{I,I}^m$ ratios*

On the linear problem $C_{12}H_{14}$ with equal bond lengths the mean values of the $f_{I,I}^m$ ratios and their variances have been calculated for each bond and for the three lowest states. These calculations have been done for three levels of truncations, namely 4, 6 and 10 (full CI) frustrations. Results are reported in table 1, bond numbers are given in scheme 2. For a given state the

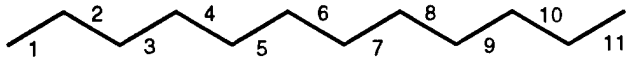

Scheme 2

statistical amplitudes f_I^m vary considerably from one bond to another but are weakly dependent on the level of truncation of the CI. Variances are quite small and they scale on the amplitudes f_I^m. Another very important feature concerns the changes of the f_I^m amplitudes when going from one state to another for the same bond. This result explains the improvment brought by the state specificity of the amplitudes as illustrated below.

3.2. *Multireference ground-state systems*

We have then applied the statistical dressing to the research of the ground state of non-alternant hydrocarbons, for which there is no Néel (spin-non-frustrated) determinant. For instance, in the *para*-di-cyclopentadienyl-benzene (scheme 3) the minimal number of frustrations is two; 26 determinants have the minimal energy and should be considered as references. Some of the determinants obtained by the action of Hamiltonian on these references have up to 6 frustrations, so that it is necessary to start from this minimal number of frustrations to define the smallest reasonable CI space. The bare and dressed CI lowest eigenvalues obtained for the optimized geometry of the ground state appear in table 2 for increasing sizes of the CI space (see also figure 1). The benefit of the dressing is of the same order of magnitude as for the single-reference dressing

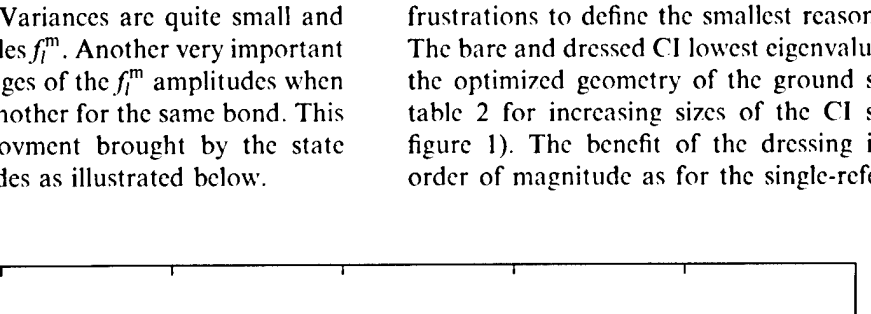

Scheme 3

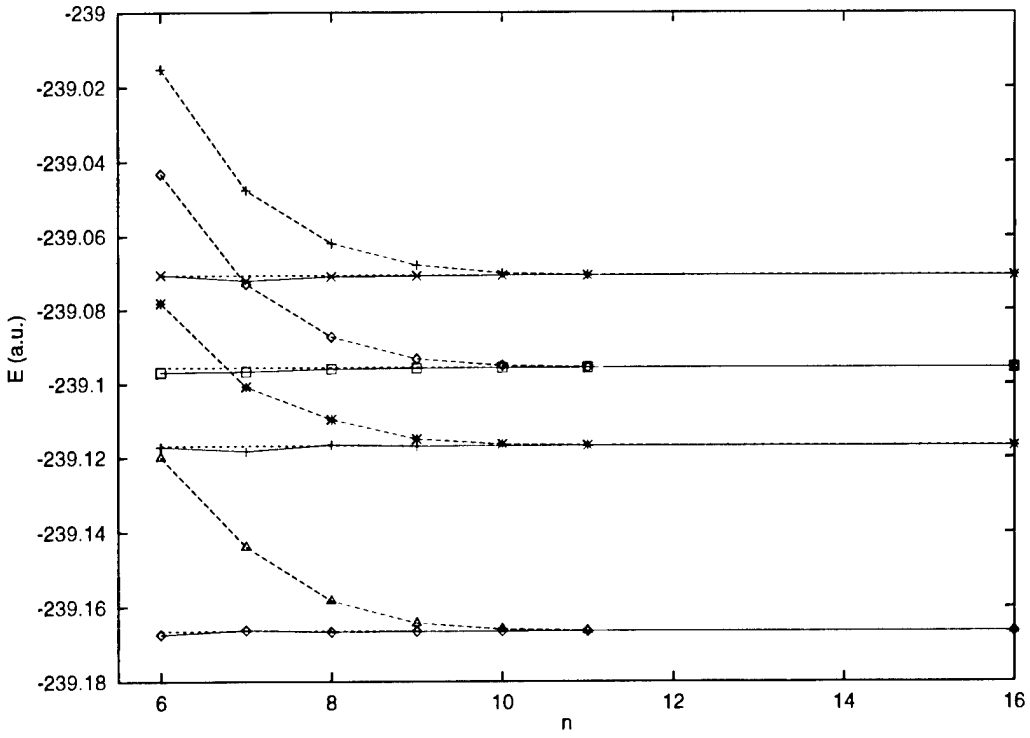

Figure 1. Bare (dashed line) and state specifically dressed (solid line) CI energies obtained for the six lowest eigenvectors of the *para*-di-cyclopentadienyl-benzene as functions of the number of spin frustrations (n) accepted in the CI space.

Table 1. Mean amplitudes of the spin exchange operations and their variances computed for the three lowest states of $C_{12}H_{14}$ polyene. The maximal number of frustrations accepted in the model space is indicated.

Studied state	Model space	Bonds 1 and 11		Bonds 2 and 10		Bonds 3 and 9		Bonds 4 and 8		Bonds 5 and 7		Bond 6	
		f_1	Δf_1	f_1	Δf_1	f_1	Δf_1	f_1	Δf_1	f_1	Δf_1	f_1	Δf_1
State 1	FCI	0.6789	2.31×10^{-2}	0.2970	4.13×10^{-3}	0.4865	5.24×10^{-3}	0.3230	6.96×10^{-3}	0.4665	6.02×10^{-3}	0.3285	4.32×10^{-3}
	6 frust.	0.6787	2.32×10^{-2}	0.2966	4.29×10^{-3}	0.4864	5.56×10^{-3}	0.3229	6.98×10^{-3}	0.4662	6.15×10^{-3}	0.3284	4.36×10^{-3}
	4 frust.	0.6596	2.65×10^{-2}	0.2812	5.21×10^{-3}	0.4684	3.99×10^{-3}	0.3118	4.49×10^{-3}	0.4468	6.27×10^{-3}	0.3174	4.65×10^{-3}
State 1	FCI	0.5336	3.20×10^{-2}	0.3461	2.96×10^{-4}	0.3253	1.09×10^{-2}	0.4025	1.90×10^{-2}	0.2814	8.85×10^{-3}	0.4191	2.50×10^{-2}
	6 frust.	0.5333	3.22×10^{-2}	0.3458	3.65×10^{-4}	0.3253	1.09×10^{-2}	0.4021	1.89×10^{-2}	0.2813	8.98×10^{-3}	0.4189	2.48×10^{-2}
	4 frust.	0.5139	3.60×10^{-2}	0.3316	3.03×10^{-3}	0.3238	1.08×10^{-2}	0.3838	8.09×10^{-3}	0.2803	9.56×10^{-3}	0.3979	1.10×10^{-2}
State 1	FCI	0.4058	1.26×10^{-2}	0.3561	7.32×10^{-3}	0.2907	1.60×10^{-3}	0.3432	8.45×10^{-3}	0.4396	2.85×10^{-2}	0.2776	4.02×10^{-3}
	6 frust.	0.4062	1.28×10^{-2}	0.3544	6.86×10^{-3}	0.2907	1.63×10^{-3}	0.3430	8.27×10^{-3}	0.4384	2.92×10^{-2}	0.2762	3.70×10^{-3}
	4 frust.	0.4170	1.18×10^{-2}	0.3040	6.54×10^{-3}	0.2704	5.25×10^{-4}	0.3137	8.56×10^{-3}	0.4219	2.8×10^{-2}	0.2587	3.52×10^{-3}

Table 2. Errors (in eV) of the lowest eigenvalue of the truncated bare and dressed CI matrices for the *para*-di-cyclopentadienyl-benzene as a function of the number n of spin frustrations accepted in the CI space.

n	Dimension of the CI space	Error of the bare energy	Error of the dressed energy
6	2376	1.26	-0.024
7	4264	0.61	7×10^{-3}
8	6546	0.22	-6×10^{-3}
9	9034	0.056	-1×10^{-3}
10	10870	0.012	-7×10^{-4}
11	11998	1×10^{-3}	-2×10^{-4}
FCI	12870	0	0

for alternant hydrocarbons [5], i.e. a reduction of the error by a factor 60.

3.3. *Quality of excited roots of the ground-state-dressed CI matrix*

We have calculated the ground state and the three lowest excited states of the linear polyene $C_{12}H_{14}$ in its ground state optimized geometry. For further comparison with the method proposed here, the dressing of the CI was first performed according to the $(SC)^2$ method, i.e. considering the Néel determinants as references for the dressing as in [5]. Computations have been performed for several truncations, increasing the number n of spin frustrations accepted in the selected space. Results are given in figure 2. The comparison between eigenenergies of the bare and dressed CI matrices show that, as occurs for *ab initio* calculations [6], the dressing greatly improves the accuracy of the excited roots but is somewhat poorer than that of the ground state, due to the following factors:

the dressing is defined on the ground state vector, if the two fully alternant determinants ϕ_0 and ϕ_0' have the largest coefficients in the ^{1}Ag singlet ground state and the lowest ^{3}Bu triplet state, the two upper triplets cannot be considered as generated from these determinants. Their main components are on determinants having at least two spin frustrations. The CI space including only determinants having up to 4 spin frustrations is therefore minimal.

3.4. *Improved excited roots from state-specific dressings*

The efficiency of the state specific dressing proposed here has been checked on the same $C_{12}H_{14}$ chain. Actually the error to the exact energies is reduced by at least a factor three with respect to the ground state dressing (cf. figure 2).

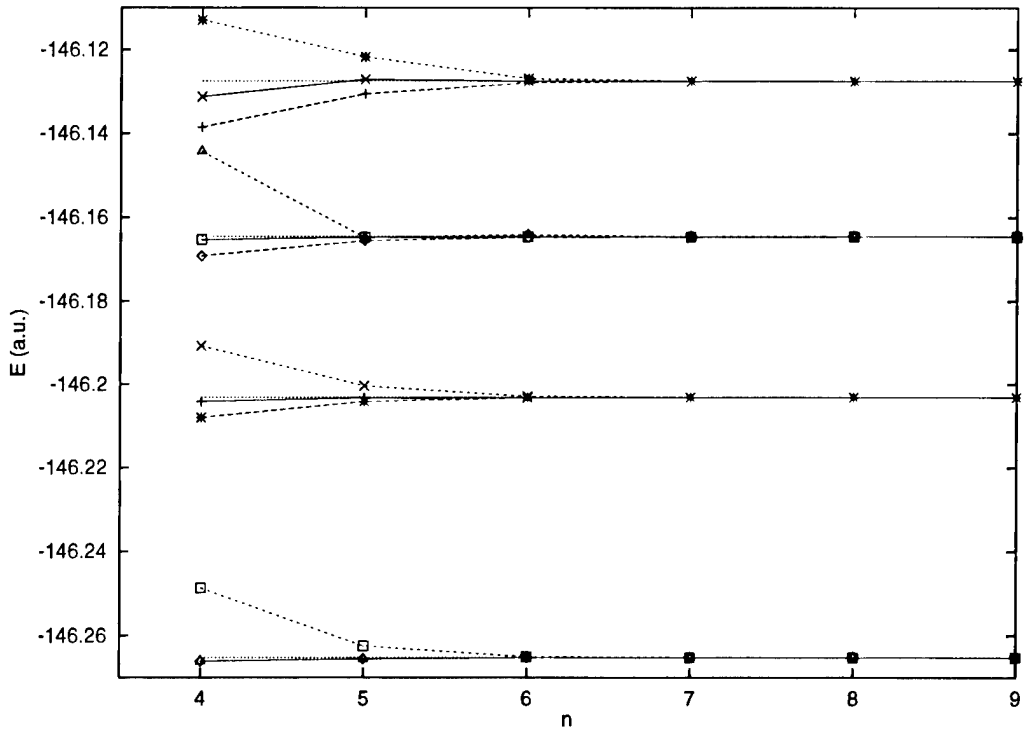

Figure 2. CI energies computed for the ground state and the three lowest excited states of the $C_{12}H_{14}$ linear polyene as functions of the number of spin frustrations (n) accepted in the CI space. The results obtained using the statistical dressing proposed here are represented by the solid line, the bare energies are represented by thin dashed lines and the energies obtained using the $(SC)^2$ ground state dressing are represented by thick dashed lines.

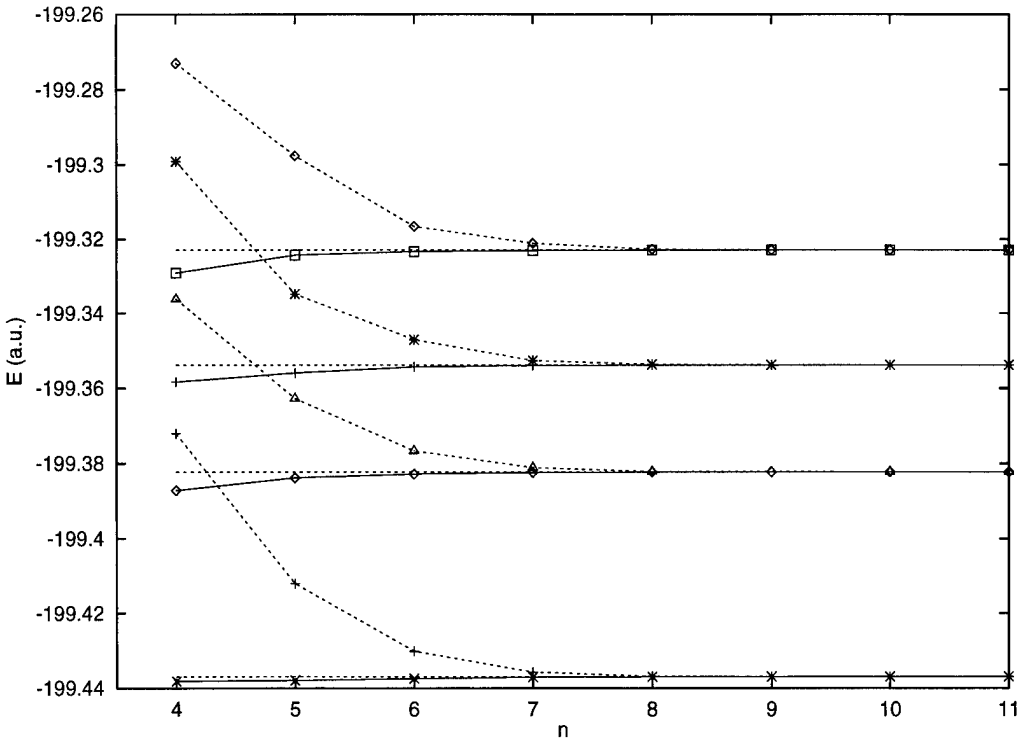

Figure 3. Bare (dashed line) and state specifically dressed (solid line) CI energies obtained for the ground state and the three lowest triplet states of the $C_{16}H_{18}$ linear polyene as functions of the number of spin frustrations (n) accepted in the CI space.

In order to see whether these conclusions were valid for larger systems, the $C_{16}H_{18}$ linear polyene has been studied. The results obtained for this molecule are given in figure 3 for the ground state and the three lowest excited states. The errors for the smallest CI space (4 spin frustrations, 1290 determinants, instead of 12870 in the FCI) is lower than 0.005 au (~0.1 eV) after dressing and for $n=6$ the deviations from the FCI roots are smaller than 0.001 au, i.e. below the accuracy which one may expect from such a semi-empirical Hamiltonian. Actually our statistical dressing insures the same quality for the excited states as the one obtained for the ground state by a single-reference $(SC)^2$ dressing [5].

The triplet states have been approached from the $S_z = 1$ CI space using the same procedure. For the same truncation threshold, the roots for $S_z = 0$ and $S_z = 1$ are significantly different before dressing (notice that such a truncated CI cannot give S^2 eigenfunctions), but the dressing insures the near degeneracy of the two estimates of the triplet state energies. The largest discrepancy (cf. table 3) is lower than 0.004 au for $n=4$ after dressing instead of 0.033 au before dressing for the third triplet state, and for $n=6$ the difference between $S_z = 0$ and $S_z = 1$ is lower than 1.10^{-3} au.

The same type of accuracy is obtained for the excited states of the non-alternant molecule (cf. figure 1). The third and fourth eigenvectors are strictly degenerate, as well as the fifth and sixth ones. The truncation maintains the degeneracy, which is not destroyed by the dressing. The statistical dressing reduces dramatically the error on the excited states energies, and performs as efficiently as it does on the ground state.

The original $(SC)^2$ dressing extracted the amplitudes f_I^m from the coefficients of ϕ_0 and of the D_I^+0 determinants. Our definition of f_I^m uses the full vector given by the truncated CI diagonalization. Between these two extreme procedures, one might extract the quantities f_I^m from a reduced subspace of the CI, which concern only the determinants below another threshold $n' < n$. We have verified that increasing n' from 2 to n improves the dressed energy, and our statistical definition of the amplitudes seems to be optimal. Finally one should recall that when the error on the total energy is lower than 0.001 au, the error on the optimized bond lengths are negligible [5].

4. Conclusion

The so-called $(SC)^2$ dressing of the CI matrices was initially proposed for the calculation of the ground state. The dressing is a single reference one, since one determinant plays a special role, and is ground-state specific. It has been observed that the lowest excited roots are quite

Table 3. Errors (in eV) of the bare and dressed CI eigenvalues computed for $S_z = 0$ and $S_z = 1$, for the three lowest triplet states of the linear polyene $C_{16}H_{18}$; n is the number of spin frustrations accepted in the CI space.

	Bare energy		Dressed energy	
	$S_z = 0$	$S_z = 1$	$S_z = 0$	$S_z = 1$
First triplet state				
$n = 4$	1.25	2.15	−0.13	−0.18
$n = 5$	0.53	0.88	−0.04	−0.08
$n = 6$	0.15	0.28	−0.02	−0.03
$n = 7$	0.03	0.05	-4×10^{-3}	-9×10^{-3}
$n = 8$	3×10^{-3}	6×10^{-3}	-7×10^{-4}	-2×10^{-3}
$n = 9$	1.5×10^{-3}	3×10^{-4}	-8×10^{-5}	-1×10^{-4}
$n = 10$	0	0	0	0
Second triplet state				
$n = 4$	1.49	2.19	−0.12	−0.12
$n = 5$	0.52	0.9	−0.06	−0.04
$n = 6$	0.18	0.29	−0.01	−0.02
$n = 7$	0.03	0.06	-4×10^{-3}	-6×10^{-3}
$n = 8$	4×10^{-3}	7×10^{-3}	-7×10^{-4}	-1×10^{-3}
$n = 9$	2×10^{-3}	4×10^{-4}	-8×10^{-5}	-1×10^{-4}
$n = 10$	0	3×10^{-5}	0	0
Third triplet state				
$n = 4$	1.36	2.24	−0.17	−0.06
$n = 5$	0.69	0.99	−0.04	−0.04
$n = 6$	0.17	0.32	−0.01	−0.01
$n = 7$	0.05	0.08	-4×10^{-3}	-4×10^{-3}
$n = 8$	5×10^{-3}	4×10^{-4}	-6×10^{-4}	-8×10^{-4}
$n = 9$	4×10^{-4}	0	-8×10^{-5}	-8×10^{-5}
$n = 10$	3×10^{-3}	0	0	0

accurate. In this approximation the amplitudes of the double excitations are taken as equal to those of the ground state single reference expansion. A generalization of the $(SC)^2$ type dressing has been proposed here. It is both state-specific and multireference. The method appears to give more accurate results than the ground state dressing technique. It is very simple and the test studies presented here, concerning intrinsically multireference states, show its remarkable efficiency, at least for Heisenberg Hamiltonians. This promising strategy will be applied in the near future to *ab initio* Hamiltonians. It will be shown that the dressing of each determinant may be calculated easily through the storage of partial summations, as already done in the $(SC)^2$ technique [1] preserving the computational simplicity of the procedure. The connection with rigorous $MR(SC)^2$ [11, 14] and MR-CC methods [15, 19 27] will be established later on. A recent paper [16] has shown that one may extract CC amplitudes from the eigenvectors of any CI matrix, and express the MRCC method as a self-consistent dressing of this CI matrix. The present paper has presented a much simpler way of extracting information from a truncated CI vector and to use it in a definition of diagonal self-consistent dressing which approximately restores the size-extensivity.

This work has been supported by the European Commission through the TMR network contract ERBFMRX CT96-0079 (Quantum Chemistry of excited states).

References

[1] Daudey, J. P., Heully, J. L., and Malrieu, J. P., 1993, *J. chem. Phys.*, **89**, 1240.
[2] Kelly, H. P., and Sessler, M. A., 1963, *Phys. Rev.*, **132**, 2091.
[3] Ahlrichs, R., Lischka, H., Staemmler, V., and Kutzelnigg, W., 1975, *J. chem. Phys.*, **62**, 1225.
[4] Meyer, W., 1973, *Int. J. quantum. Chem.*, **58**, 1017.
[5] Guihéry, N., Ben Amor, N., Maynau, D., and Malrieu, J. P., 1996, *J. chem. Phys.*, **104**, 3701.
[6] Heully, J. L., Malrieu, J. P., Nebot Gil, I., and Sanchez Marin, J., 1996, *Chem. Phys. Lett.*, **256**, 589.
[7] Heully, J. L., Malrieu, J. P., Nebot Gil, I., and Sanchez Marin, J., work in progress.
[8] Ruttink, P. J. A., VanLenthe, J. H., Zwaans, R., and Groenenboom, G. C., 1991, *J. chem. Phys.*, **94**, 7212.
[9] Fink, R., and Staemmler, V., 1993, *J. chem. Phys.*, **87**, 129.
[10] Fulde, P., and Stoll, H., 1992, *J. chem. Phys.*, **97**, 4248.
[11] Malrieu, J. P., Daudey, J. P., and Caballol, R., 1994, *J. chem. Phys.*, **101**, 8908.
[12] Gdanitz, R., and Ahlrichs, R., 1988, *Chem. Phys. Lett.*, **143**, 413.
[13] Szalay, P. G., and Bartlett, R. J., 1995, *J. chem. Phys.*, **103**, 3600.
[14] Meller, J., Malrieu, J. P., and Heully, J. L., 1995, *Chem. Phys. Lett.*, **244**, 440.
[15] Meller, J., Malrieu, J. P., and Caballol, R., 1996, *J. chem. Phys.*, **104**, 4068.
[16] Adamowicz, L., Caballol, R., Malrieu, J. P., and Meller, J., 1996, *Chem. Phys. Lett.*, **259**, 619.
[17] Said, M., Maynau, D., Malrieu, J. P., and Garcia Bach, N. A., 1984, *J. Am. chem. Soc.*, **106**, 571.
[18] Bernardi, F., Olivucci, M., and Robb, M., 1992, *J. Am. chem. Soc.*, **114**, 1606.
[19] Mukherjee, D., Matra, R. K., and Mukhopadhyay, A., 1975, *Molec. Phys.*, **30**, 1561.
[20] Mukherjee, D., Matra, R. K., and Mukhopadhyay, A., 1955, *Molec. Phys.*, **33**, 955.
[21] Lindgren, I., 1978, *Int. J. quant. Chem. Symp.*, **12**, 33.
[22] Offermann, R., Ey, W., and Kümmel, H., 1976, *Nucl. Phys.* A, **273**, 349.
[23] Jeziorsky, B., and Monkhorst, H. J., 1981, *Phys. Rev. A*, **24**, 1668.
[24] Mukhopadhyay, A., and Mukherjee, D., 1989 *Chem. Phys. Lett.*, **163**, 171, 1991, *ibid.*, **177**, 544.
[25] Meissner, L., Kucharski, S., and Bartlett, R. J., 1989, *J. chem. Phys.*, **91**, 6187.
[26] Meissner, L., and Bartlett, R. J., 1990, *J. chem. Phys.*, **92**, 561.
[27] Mahapatra, U. S., Datta, B., Bandyopadhyay, B., and Mukherjee, D., *Adv. quant. Chem.* (in the press).

MOLECULAR PHYSICS, 1998, VOL. 94, NO. 1, 217–223

Cumulant approach and coupled-cluster method for many-particle systems

By KLAUS W. BECKER and MATTHIAS VOJTA

Institut für Theoretische Physik, Technische Universität Dresden, D-01062 Dresden, Germany

Cumulants represent a natural language for expressing macroscopic properties of many-body systems. The most important property of cumulants is that of size consistency, i.e. a cumulant expression for an extensive variable scales with the size of the system, independent of possible further approximations used in the evaluation procedure. Cumulants can be considered as a generalization of linked diagrams known from diagrammatic technique of many-body theory. In this paper we outline a recently introduced method based on cumulants in order to derive expressions for zero-temperature properties of many-particle systems, i.e. the ground-state energy, static expectation values and dynamical correlation functions. This cumulant formalism allows one to describe weakly and strongly correlated systems along the same lines. We show that the coupled-cluster method known from quantum chemistry can be derived from our cumulant approach. Finally, we demonstrate the usefulness of the cumulant method by applying it to examples from solid-state physics and quantum chemistry.

1. Introduction

For the investigation of the ground state of many-particle systems the ground-state energy E_0 plays a central role. One basic property of energy is its size consistency, i.e. the energy of two well-separated, but otherwise identical systems equals twice the value of a single system. Each approximation which is used to evaluate E_0 must preserve this property. In diagrammatic approaches size consistency is guaranteed by the fact that in any physical quantity only linked diagrams enter. Usually, a diagram technique is based on Wick's theorem. For time-dependent problems, i.e. the calculation of Green's functions, the use of Wick's theorem is greatly simplified if the unperturbed Hamiltonian is a single-particle Hamiltonian. Therefore, in practice standard diagrammatic approaches are restricted to weakly correlated systems. An alternative approach to evaluate statical and dynamical properties at zero temperature was recently proposed [1–3] and is based on the introduction of cumulants. Cumulants have been known for a long time in mathematical statistics and in probability theory. Kubo has been pivotal in demonstrating and emphasizing their usefulness in diverse branches of physics. Cumulant expressions preserve size consistency, i.e. a cumulant expression for an extensive variable scales with the size of the system (provided that the associated reference function is product-separable) independent of further approximations.

The cumulant method presented here is based on a perturbational approach, i.e. the Hamiltonian is split into H_0 and H_1 with eigenvalues and eigenvectors of H_0 known. One starts from eigenstates of H_0 and includes the effect of H_1 by an exponential ansatz. The unperturbed part H_0 is not restricted to be a single-particle operator. This favours the cumulant method especially for the description of strongly correlated systems though it may be applied as well to weakly correlated systems.

Another approach which avoids the size-consistency problem is the coupled-cluster method [4] which has been used in quantum chemistry and also in solid-state physics. Within the coupled-cluster method the full ground state is written as an exponential operator applied on an reference state which is usually the ground state of an uncorrelated problem (e.g. the Hartree–Fock solution of the Hamiltonian under consideration). However, also correlated reference functions have been used, see e.g. [5].

This paper is organized as follows. In section 2 we summarize the cumulant method for calculating ground-state properties of many-body systems. In section 3 we compare this method with standard variational calculations and with the coupled-cluster method known from quantum chemistry. To demonstrate the applicability of the method we show applications to the the 2D Hubbard model at half-filling and to the method of increments used in quantum chemistry. A discussion and concluding remarks are put in the last section.

0026–8976/98 $12·00

2. Cumulant method for ground-state properties

In this section we shortly present the cumulant method for calculating ground-state properties of many-body systems. For more details see [1–3, 6]. The method starts from the definition of the function

$$f(\lambda) = \ln \langle \phi_0 | \exp[-\lambda(H_0 + H_1)] \exp(\lambda H_0) | \phi_0 \rangle, \quad (1)$$

where H_0 is the unperturbed Hamiltonian H_0 with the ground state $|\phi_0\rangle$ known, i.e. $H_0|\phi_0\rangle = \varepsilon_0|\phi_0\rangle$. In the following we assume that the ground state of H_0 is non-degenerate, for a discussion of the case of degeneracy see Appendix A. The aim is to calculate the ground-state energy E_0 of the full system, $H|\psi_0\rangle = E_0|\psi_0\rangle$. The shift of the ground-state energy $\delta E_0 = E_0 - \varepsilon_0$ due to the perturbation H_1 can be derived in a straightforward way. Introducing the Liouvillian L_0 which is defined by $L_0 A = [H_0, A]$ for any operator A, equation (1) is formally transformed into

$$f(\lambda) = \ln \langle \phi_0 | \exp[-\lambda(H_1 + L_0)] \mathbf{1} | \phi_0 \rangle, \quad (2)$$

where $\mathbf{1}$ is a unity operator in Hilbert space. The exponential is defined as a power series where L_0 acts on the H_1 operators to the right, i.e.

$$\exp[-\lambda(H_1 + L_0)] \mathbf{1} = \mathbf{1} - \lambda H_1 + \frac{\lambda^2}{2}(H_1^2 + L_0 H_1) + \cdots. \quad (3)$$

Note $L_0 \mathbf{1} = 0$. Next, we define the Laplace transform of the function $f(\lambda)$ by:

$$\hat{f}(z) = -\int_0^{+\infty} f(\lambda) \exp(\lambda z)\, \mathrm{d}z, \qquad \Re\{z\} < 0. \quad (4)$$

One can show [1, 6] that the energy shift δE_0 with respect to the unperturbed ground-state energy ε_0 is given by

$$\delta E_0 = \lim_{z \to 0} z^2 \hat{f}(z). \quad (5)$$

On the other side, equation (2) is used to express δE_0 in terms of cumulants

$$\delta E_0 = \lim_{z \to 0} \langle \phi_0 | H_1 \left(1 + \frac{1}{z - H_1 - L_0} H_1 \right) | \phi_0 \rangle^c. \quad (6)$$

Here $\langle \phi_0 | \cdots | \phi_0 \rangle^c$ denotes cumulant expection values with respect to the unperturbed ground state $|\phi_0\rangle$. Cumulant expectation values [7] for a product of arbitrary operators A_i with an arbitrary state $|\phi\rangle$ are defined by:

$$\langle \phi | \prod_i A_i^{n_i} | \phi \rangle^c = \left(\prod_i \left(\frac{\partial}{\partial \lambda_i} \right)^{n_i} \right) \ln \langle \phi | \prod_i \exp(\lambda_i A_i) | \phi \rangle \,|_{\lambda_i = 0 \,\forall\, i}. \quad (7)$$

The quantity inside the bracket of (6) is called wave operator Ω (it has similarity with the Möller operator known from scattering theory),

$$\Omega = 1 + \lim_{z \to 0} \frac{1}{z - H_1 - L_0} H_1. \quad (8)$$

Thus we can rewrite δE_0 as

$$\delta E_0 = \langle \phi_0 | H_1 \Omega | \phi_0 \rangle^c \qquad \text{or} \qquad E_0 = \langle \phi_0 | H \Omega | \phi_0 \rangle^c \quad (9)$$

Treating cumulant expectation values one must distinguish between prime and composite operators. A prime operator is a single entity in the cumulant evaluation procedure. Expanding Ω given in (8) the resulting products of L_0 and H_1 are composite operators in the cumulant ordering. Within cumulants, the operator Ω transforms the ground state $|\phi_0\rangle$ of the unperturbed Hamiltonian H_0 into the full ground state $|\psi_0\rangle$ of H. Expanding (8) into powers of H_1 it can be shown that (9) is equivalent to Rayleigh Schrödinger perturbation theory summed up to infinite order, see e.g. [6].

There is no general rule how to split H into H_0 and H_1 except that the overlap between the unperturbed and the full ground state has to be non-zero, i.e. $\langle \psi_0 | \phi_0 \rangle \neq 0$. The operator Ω describes the influence of H_1 onto $|\phi_0\rangle$. This effect should be a small correction to $|\phi_0\rangle$, i.e. it should be treatable perturbatively in the sense that it can be obtained by summation of a perturbation expansion. This is usually fulfilled if H_0 is the dominant part of the Hamiltonian. Therefore, for strongly correlated systems H_0 should consist of the correlations (or at least part of them) whereas H_1 usually contains the hybridization.

Instead of using the explicit form (8) of the wave operator Ω an exponential ansatz was proposed [8]

$$\Omega = \exp S, \qquad S = \sum_\mu \alpha_\mu S_\mu \quad (10)$$

where $\{S_\mu\}$ is a set of relevant operators. They have to be chosen in such a way that $\exp(\sum_\mu \alpha_\mu S_\mu)|\phi_0\rangle$ (with appropriate parameters α_μ) represents a good approximation of the exact ground state. The yet unknown parameters α_μ are to be determined from the following set of equations

$$\langle \phi_0 | S_\nu^\dagger H \Omega | \phi_0 \rangle^c = 0, \qquad \nu = 1, 2, 3, \ldots. \quad (11)$$

These equations follow from the condition of $\Omega|\phi_0\rangle$ being an eigenstate of H. Note that equations (9), (10) and (11) allow for the computation of the ground-state energy. The result of (9), (10) and (11) is *a priori* size-consistent even if the sum in S is restricted to a finite set of operators S_ν due to the use of cumulants.

The choice of appropriate operators S_ν is most important for actual calculations using the cumulant method. These operators describe fluctuations introduced into

$|\phi_0\rangle$ by successive application of H_1. In principle, they can be derived systematically from the explicit form (8) of the wave operator Ω. For practical applications this might be only of little help especially if the main physical effect comes from higher powers of H_1. In such a case a small set of few relevant operators leads to a far simpler description of the main effect than including a large set of powers H_1^n. The selection of relevant operators for the cumulant method can be seen as similar to the selection of dynamical variables for the Mori–Zwanzig projection technique: Formally, variables can be systematically derived from the Liouvillian, but often choosing variables from physical insight is more useful.

In the past, equations (9), (10) and (11) were used to evaluate ground-state properties of several systems, see for instance [2, 9, 10]. Recently, we have proposed an extension of the formalism which allows one also to evaluate excitation energies [11]. Note that the cumulant formalism can also account for the calculation of dynamical correlation functions [3]. This allows one to treat static and dynamical aspects of the system along the same lines.

3. Comparison with variational calculations and the coupled-cluster method

For practical calculations the cumulant method together with the exponential ansatz for the wave operator Ω consists of selecting an appropriate set of operators S_ν, i.e. writing down an ansatz for the ground-state wavefunction. Then the coefficients α_ν are determined using equations (11). The main advantage of this procedure compared to other methods is that the exponential term occurs only once in all equations.

In a standard variational calculation one uses an ansatz for the wavefunction and minimizes the ground-state energy by variation of the coefficients. In such a calculation the ansatz wavefunction (including the exponential operator) usually occurs four times, $E_0 = \langle\psi_0|H|\psi_0\rangle/\langle\psi_0|\psi_0\rangle$. Furthermore, a wavefunction with an exponential ansatz is usually not normalized to unity. So both numerator and denominator of the energy expression might diverge with an exponential of the system size whereas their ratio should be proportional to the system size. The physical difference between both methods is the following: in a variational calculation the aim is to minimize the total energy of the system whereas in the cumulant method the aim is to find an eigenstate of H. (Note that equation (11) is exactly the condition of $\exp S|\phi_0\rangle$ being an eigenstate of H.)

There is a close relationship of the equations (9), (10) and (11) to the so-called coupled cluster method. This approach which was originally invented for studies in nuclear physics is also size consistent and does not involve Wick's theorem. For a review see [4]. Recently it was shown [8] that the coupled-cluster method can be derived from the cumulant expressions (9) and (11). Comparing practical calculations the cumulant method with an exponential ansatz is again easier to handle than the coupled-cluster scheme because the exponential term occurs only once in the cumulant equations and twice in the coupled-cluster equations.

Usually these different methods lead to different (approximate) results when calculating ground-state quantities. However, if the ansatz for the ground-state wavefunction covers the exact ground state, i.e. if the subspace spanned by the operators S_ν contains the exact ground-state wavefunction, then of course all methods lead to the same exact result. Furthermore, the cumulant and coupled-cluster methods yield the same result provided that they use the same set of operators $\{S_\mu\}$ and that the equations for the coefficients are solved exactly.

In the following we briefly show how to derive coupled-cluster (CC) and variational (V) equations from the cumulant method if one assumes that the exact ground state has the form $|\psi_0\rangle = \exp S|\phi_0\rangle$ with $S = \sum_\nu \alpha_\nu S_\nu$. We note that equation (11) also holds for arbitrary composite operators, e.g., $0 = \langle\phi_0|ABH\Omega|\phi_0\rangle^c$ for arbitrary operators A and B. Inserting (11) into (9) one can transform

$$E_0 = \langle\phi_0|H \exp S|\phi_0\rangle^c \tag{12}$$

into

$$E_0 = \begin{cases} \langle\phi_0| \exp(-S) H \exp S|\phi_0\rangle^c \\ \langle\phi_0| \exp S^\dagger H \exp S|\phi_0\rangle^c. \end{cases} \tag{13}$$

Evaluating the cumulants leads to [11]

$$E_0 = \begin{cases} \langle\phi_0| \exp(-S) H \exp S|\phi_0\rangle & \text{(CC)} \\ \dfrac{\langle\psi_0|H|\psi_0\rangle}{\langle\psi_0|\psi_0\rangle} & \text{(V).} \end{cases} \tag{14}$$

These are the energy expressions for the coupled-cluster and the variational scheme, respectively. The equations for the coefficients are obtained from (11) as follows:

$$0 = \langle\phi_0|S_\nu^\dagger H \exp S|\phi_0\rangle^c = \begin{cases} \langle\phi_0|S_\nu^\dagger \exp(-S) H \exp S|\phi_0\rangle^c \\ \langle\phi_0| \exp S^\dagger S_\nu^\dagger H \exp S|\phi_0\rangle^c. \end{cases} \tag{15}$$

Transforming again the cumulants and using $\langle\phi_0|S_\nu|\phi_0\rangle = 0$ one finds

$$0 = \langle\phi_0|S_\nu^\dagger \exp(-S) H \exp S|\phi_0\rangle \quad \text{(CC)} \tag{16}$$

and

$$0 = \langle\psi_0|S_\nu^\dagger H|\psi_0\rangle^c + \langle\psi_0|HS_\nu|\psi_0\rangle^c = \frac{\partial}{\partial\alpha_\nu} E_0 \quad (\mathrm{V}). \tag{17}$$

These two conditions are the equations for the coefficients α_ν within the coupled-cluster and the variational method. The second step of (17) includes evaluating the new cumulants with $|\psi_0\rangle$ yielding exactly the four terms arising from the differentiation of the energy expression $\langle\psi_0|H|\psi_0\rangle/\langle\psi_0|\psi_0\rangle$ with respect to α_ν [11].

We want to note here that the wave operator (8) of the cumulant approach is not limited to an exponential form (as is the case, for example, in coupled-cluster calculations). So the cumulant method appears to be the more general and powerful scheme for the calculation of ground-state properties. A modified application of the cumulant approach is shown in the next section.

4. Application to the Hubbard model

In this section we demonstrate the application of the cumulant method to the 2D Hubbard model. The following calculation contains two modifications to the scheme presented in the last section, for more details see [9].

The operators $\{S_\nu\}$ may also represent composite operators, i.e. *products* of operators, each of which is an entity in the cumulant ordering.

Noting that the wave-operator Ω, defined in equation (8), obeys the integral equation

$$\Omega = 1 + \lim_{x\to 0} \frac{1}{x - L_0} H_1 \Omega, \tag{18}$$

we may replace equations (9) and (11) by

$$E_0 = \langle\phi_0|H|\phi_0\rangle + \lim_{x\to 0} \left\langle \phi_0|H_1 \frac{1}{x - L_0} H_1 \Omega|\phi_0\right\rangle^c, \tag{19}$$

$$0 = \langle\phi_0|S_\nu^\dagger H_1|\phi_0\rangle^c + \langle\phi_0|S_\nu^\dagger H_0 \Omega|\phi_0\rangle^c + \lim_{x\to 0} \left\langle \phi_0|S_\nu^\dagger H_1 \frac{1}{x - L_0} H_1 \Omega|\phi_0\right\rangle^c. \tag{20}$$

The advantage of recasting (9) and (11) into the new form (19) and (20) is the appearance of the term $H_1\,[1/(x - L_0)]\,H_1$ on the right hand sides. This term may be interpreted as an *effective Hamiltonian* as obtained by second order perturbation theory. As mentioned above, it is understood that the operators S_ν in (19) and (20) may also represent products of operators.

We now turn to the Hubbard model at half-filling on a two-dimensional square lattice. The Hubbard model is given by

$$H = H_0 + H_1 \tag{21}$$

$$H_0 = U \sum_{i=1}^{N} n_{i\uparrow} n_{i\downarrow} \tag{22}$$

$$H_1 = -t \sum_{\langle ij\rangle\sigma} (c_{i\sigma}^\dagger c_{j\sigma} + h.c.)\,. \tag{23}$$

Here, U is the Coulomb repulsion between electrons on the same site. $n_{i\sigma} = c_{i\sigma}^\dagger c_{i\sigma}$ is the occupation-number operator for electrons with spin σ on site i. The symbol $\langle ij\rangle$ denotes pairs of nearest-neighbours. In the case of strong electronic correlations, $U \gg t$, the above Hamiltonian is used as a model system for the electronic degrees of freedom of the CuO_2 planes in high-T_c superconductors. In this limit, double-occupation with two electrons on the same site is strongly suppressed. Then, the Hubbard model can be transformed into the $t - J$ Hamiltonian which acts only in the unitary subspace where double-occupancy is excluded

$$H_{t\text{-}J} = H_J + H_t \tag{24}$$

$$H_J = J \sum_{\langle ij\rangle} \left[\mathbf{S}_i \cdot \mathbf{S}_j - \frac{1}{4}\hat{n}_i\hat{n}_j\right] \tag{25}$$

$$H_t = -t \sum_{\langle ij\rangle\sigma} (\hat{c}_{i\sigma}^\dagger \hat{c}_{j\sigma} + h.c.). \tag{26}$$

The first part of H_J is the antiferromagnetic Heisenberg exchange with $J \equiv 4t^2/U$. H_t is the so-called conditional hopping term since the hopping of electrons is only allowed to a site which was empty before. We have also introduced $\hat{n}_i = \sum_\sigma \hat{c}_{i\sigma}^\dagger \hat{c}_{i\sigma}$ and $\hat{c}_{i\sigma}^\dagger \equiv c_{i\sigma}^\dagger (1 - n_{i\,\sigma})$. For later reference we define $\hat{\hat{c}}_{i\sigma}^\dagger \equiv c_{i\sigma}^\dagger n_{i\,\sigma}$. Note that $\hat{c}_{i\sigma}^\dagger$ describes transitions from empty to singly occupied sites, whereas $\hat{\hat{c}}_{i\sigma}^\dagger$ describes transitions from singly to doubly occupied sites. At half-filling, with one electron at each site, the $t - J$ model reduces to the Heisenberg Hamiltonian since in that case the restricted hopping term H_t cannot act. The ground-state energy of the antiferromagnetic Heisenberg exchange (25) (with $\hat{n}_i = \hat{n}_j = 1$ at half-filling) is not exactly known. From series expansions and numerical methods [12], there is quite general agreement that the correct value of the ground-state energy is close to $-1.17\,NJ$.

We now apply our method to calculate the ground-state energy of the Hubbard model at half-filling. We start from the Néel state as unperturbed ground state $|\phi_0\rangle$. From the above discussion it is evident that in the large U limit only spin-fluctuations reduce the ground-state energy relative to the energy of the Néel state. Charge fluctuations, induced by hopping operators, are important only for decreasing values of U/t. Hence, in the exponent of ansatz (10) for Ω we include

spin-fluctuation operators $S_1, ..., S_4$ and charge fluctuation operators $A_1, ..., A_3$: the resulting ansatz for Ω therefore reads

$$\Omega = \exp\left\{\left[\sum_{\nu=1}^{4} \sigma_\nu S_\nu\right] + \left[\sum_{\nu=1}^{3} \alpha_\nu A_\nu\right]\right\}. \tag{27}$$

Equation (27) is valid for both large and moderate values of U/t.

The spin fluctuation operators S_ν are best found from a perturbative treatment of the Heisenberg model (for instance by use of projection technique) up to fourth order:

$$S_1 = \boxed{\Uparrow_i \quad \Downarrow_j} \tag{28}$$

$$S_2 = (S_1)^2 \tag{29}$$

$$S_3 = \boxed{\begin{matrix} \Uparrow_i & \Downarrow_j \\ \Downarrow_k & \Uparrow_l \end{matrix}} \tag{30}$$

$$S_4 = \boxed{\Uparrow_i \quad \Downarrow_j \quad \Uparrow_k \quad \Downarrow_l} \tag{31}$$

The arrows with double lines $\Uparrow$ or $\Downarrow$ indicate spins which are flipped relative to their original orientation in the Néel state. For instance, the first spin fluctuation operator S_1 is formed by two successive hoppings from site i to a neighbouring site j and back, combined with flipping of the transferred spin. Explicitly, S_1 is written as

$$S_1 = \sum_{\langle ij \rangle} c_{j\downarrow}^\dagger c_{i\downarrow} c_{i\uparrow}^\dagger c_{j\uparrow} = -\sum_{\langle ij \rangle} S_j^- S_i^+; \; j \in \text{sublattice} \uparrow. \tag{32}$$

The sum runs over all pairs of neighbouring sites i, j. In (32) we have again introduced the spin raising and lowering operators $S_i^\sigma = c_{i\sigma}^\dagger c_{i-\sigma}$ ($\sigma = \pm 1$). The remaining operators S_2, S_3 and S_4 are formed by four successive hopping processes. S_2 is the first example for an operator which is *not prime*, but rather a composite operator. It appears here only due to the introduction of cumulants. Applying S_2 is equivalent to applying S_1 twice, and its main contribution comes from two spin-flip processes with overlapping sites. S_3 creates a 2×2 square of flipped spins. Finally, S_4 creates all other 4 site spin-flip configurations connected to each other.

Restricting ourselves first to the case $U \gg t$ we only keep these spin fluctuation operators S_ν in the ansatz for Ω. Inserting the ansatz for Ω into (19) and (20) we obtain a set of equations for the ground-state energy E_0 and the coefficients σ_ν which can be reduced to a quartic equation for σ_1. Details of the calculation are written down in [9]. The values for the coefficients are found to be: $\sigma_1 = 0.1756$, $\sigma_2 = (-)2.32 \times 10^{-3}$, $\sigma_3 = 3.04 \times 10^{-2}$, $\sigma_4 = 8.85 \times 10^{-3}$. The final value for the ground-state energy E_0 for the Hubbard model at half-filling and $U \gg t$ is found to be

$$E_0 = -1.1756 \times N \frac{4t^2}{U}; \qquad U \gg t. \tag{33}$$

It agrees well with that of the Heisenberg model. Note that the coefficients σ_2, σ_3 and σ_4 are smaller by at least one order of magnitude than σ_1. This shows a tendency for rapid convergence when operators for multiple hoppings are added to the ansatz.

For smaller values of U/t we now consider charge fluctuation operators A_ν which will produce states with empty and doubly-occupied sites. The simplest possible operator is

$$A_1 = \sum_{\langle ij \rangle \sigma} \hat{c}_{i\sigma}^\dagger \hat{c}_{j\sigma}; \qquad j \in \text{sublattice } \sigma. \tag{34}$$

The quantity $\hat{c}_{i\sigma}^\dagger$ has been defined already below equation (26). It describes the creation of an electron with spin σ on a site i where an electron with spin $-\sigma$ is already present there. The operator A_1 is written symbolically as

$$A_1 = \boxed{\uparrow\downarrow_i \quad \bigcirc_j} \tag{35}$$

The circle denotes a hole. The opposite-directed arrows indicate two opposite electron spins at the same site. We will also include two operators of second order in the hopping Hamiltonian H_t

$$A_2 = (A_1)^2 \tag{36}$$

$$A_3 = \sum_{\langle ijk \rangle \sigma} \hat{c}_{i-\sigma}^\dagger \hat{c}_{j-\sigma} \hat{c}_{j\sigma}^\dagger \hat{c}_{k\sigma}; \qquad k \in \text{sublattice } \sigma. \tag{37}$$

When evaluated with their respective Hermitian conjugates they are the only second order operators to yield non-zero expectation values. In other words, only those hopping operators of second order are included in the set A_ν which represent *connected diagram* contributions to the energy. In symbols a typical term in A_3 would be

$$A_3 = \boxed{\uparrow\downarrow_i \quad \Uparrow_j \quad \bigcirc_k} \tag{38}$$

where sites i and k ($i \neq k$) are nearest neighbours of site j.

Having defined the operators A_ν we now proceed with the full ansatz (27) for the wave operator Ω. From (20) we obtain again a set of nonlinear equations for the energy and the coefficients σ_ν and α_ν. For brevity we only state here the equation for the energy

$$E_0 = \lim_{x \to 0} \left\langle \phi_0 | H_1 \frac{1}{x - L_0} H_1 [1 + \sigma_1 S_1 + \alpha_2 A_2 + \alpha_3 A_3] | \phi_0 \right\rangle_0^c \tag{39}$$

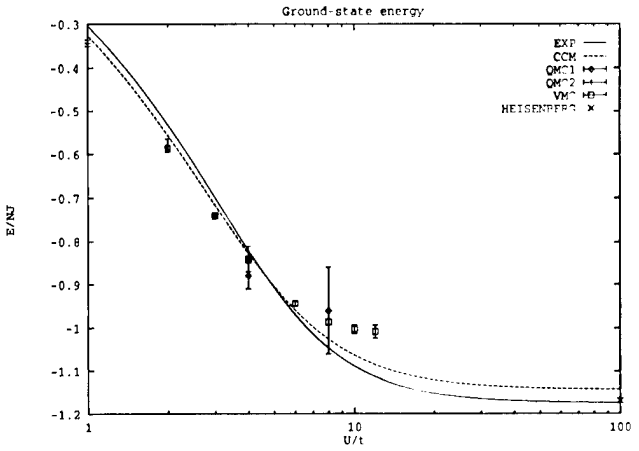

Figure 1. Ground-state energy of the 2D Hubbard model at half-filling. The solid line is the result of the exponential (EXP) ansatz in its new formulation. The dotted line is the result of the coupled-cluster method (CCM). Quantum Monte Carlo (QMC) and variational Monte Carlo (VMC) data are shown as well. The Heisenberg limit is indicated by a cross.

The result for E_0 (in units of $J = 4t^2/U$) is plotted in figure 1 as function of U/t (full line). Quantum Monte Carlo (QMC) results [13] are available only in the weak and intermediate-coupling regime, up to $U/t = 8$. The variational Monte Carlo (VMC) method [14] provided results in the strong-correlation regime too. Both QMC and VMC data points are shown in figure 1. The QMC and VMC results agree well where both are available. However, in the strong-coupling regime the VMC results can only set an upper bound for the ground-state energy. The infinite U value, indicated by a cross on the figure, is the QMC result [12] for the Heisenberg antiferromagnet. For a further discussion of the results see [9].

5. Application to the method of increments

In this section we discuss the method of increments which is useful for high-accuracy correlation calculations of the ground state of periodic systems. We consider a solid with well defined bonds such as diamond or silicon. The result of a SCF calculation is assumed to be done. The resulting SCF ground state $|\phi_{\mathrm{SCF}}\rangle$ of $H_0 = H_{\mathrm{SCF}}$ is expressed in terms of localized molecular orbitals (MO) labelled with index I.

Then we employ the following ansatz for Ω:

$$\Omega = 1 + \sum_I \alpha_I A_I + \sum_{IJ} \alpha_{IJ} A_{IJ}, \tag{40}$$

where the first term with the operators A_I describes one- and two-particle excitations out of bond I, whereas the operators A_{IJ} in the second term create two-particle excitations in bonds I and J.

Note that the applied ansatz (40) for the wave operator Ω does not have an exponential form as suggested in section 2, compare (9). So the wave-function $\Omega|\phi_0\rangle$ obtained with the ansatz (40) looks similar to a configuration-interaction (CI) wavefunction. However, the result for the ground-state energy E_0 obtained using the present approach is size-consistent due to the use of cumulants whereas the results of a CI calculation is not size-consistent.

The method of increments now provides a solution of the cumulant equations for E_0 and the parameters $\{\alpha_I\}$ and $\{\alpha_{IJ}\}$ in terms of successive local approximations. It is based on the following idea. First, all electrons in $|\phi_{\mathrm{SCF}}\rangle$ are kept fixed except the two in one bond I which corresponds to the wave operator

$$\Omega^{(1)} = 1 + \alpha_I^{(1)} A_I. \tag{41}$$

The parameter $\alpha_I^{(1)}$ is obtained from:

$$0 = \langle A_I^\dagger H \Omega^{(1)} \rangle_{\mathrm{SCF}}^c. \tag{42}$$

We can define the correlation energy of bond I:

$$\varepsilon_I^{(1)} = \langle H_{\mathrm{res}} \Omega^{(1)} \rangle_{\mathrm{SCF}}^c \tag{43}$$

$$= \alpha_I^{(1)} \langle H_{\mathrm{res}} A_I \rangle_{\mathrm{SCF}}^c. \tag{44}$$

The total energy of the system including to one-bond correlations is then given by:

$$E_0^{(1)} = \varepsilon_{\mathrm{SCF}} + \sum_I \varepsilon_I^{(1)}. \tag{45}$$

In the second step the electrons in two bonds I, J are released:

$$\Omega^{(2)} = 1 + \alpha_I^{(2)} A_I + \alpha_J^{(2)} A_J + \alpha_{IJ}^{(2)} A_{IJ}. \tag{46}$$

With this wave operator we can define the energy increments from the two bonds as compared with the previous situation as:

$$\varepsilon_{IJ}^{(2)} = \sum_{i=I,J} (\alpha_i^{(2)} - \alpha_i^{(1)}) \langle H_{\mathrm{res}} A_i \rangle_{\mathrm{SCF}}^c + \alpha_{IJ}^{(2)} \langle H_{\mathrm{res}} A_{IJ} \rangle_{\mathrm{SCF}}^c. \tag{47}$$

From this we find the total energy due to one- and two-bond correlations

$$E_0^{(2)} = \varepsilon_{\mathrm{SCF}} + \sum_I \varepsilon_I^{(1)} + \sum_{\langle IJ \rangle} \varepsilon_{IJ}^{(2)}. \tag{48}$$

In the next step one can improve these results by including correlations among electrons on three sites: in most cases this procedure is sufficient to obtain accurate results. By calculating higher and higher increments the exact correlation energy within the common CEPA-0 scheme is obtained. The method of increments is useful if the incremental expansion in terms of local correla-

tions is convergent. It can be applied, for example, to group IV semiconductors, see [15].

6. Conclusion

In this paper we have presented a method for calculating ground-state properties in many-body systems. This method is based on the introduction of cumulants. It can be applied to both weakly and strongly correlated systems. After a brief description of the method we have compared it with variational calculations and with the coupled-cluster method known from quantum chemistry. We have shown that the basic equations for both methods can be derived from our cumulant formalism. Finally, we have presented two applications of the cumulant method: the Hubbard model at half-filling and the method of increments.

It is a pleasure for us to thank B. Paulus, H. Köhler, and G. Polatsek for helpful discussions.

Appendix A: treatment of a degenerate ground state of H_0

If we are faced with a degenerate ground state of H_0 where the degeneracy is lifted by H_1 we have the freedom to choose the initial state $|\phi_0\rangle$ for the cumulant method from the subspace of degenerate states. The operator Ω given by (8) transforms any of these states into the full ground state $|\psi_0\rangle$ provided it has a non-zero overlap with $|\psi_0\rangle$. However, if we use a certain ansatz for the operator Ω then the best choice of $|\phi_0\rangle$ depends on the form of this ansatz. Assume that the states $|\phi_{0_1}\rangle, \ldots, |\phi_{0_m}\rangle$ are the degenerate ground states of H_0 with energy ε_0. The correct state $|\tilde{\phi}_0\rangle$ with $\Omega|\tilde{\phi}_0\rangle$ being the ground state of H (for a certain form of Ω) is a linear combination of the $|\phi_{0_j}\rangle$:

$$|\tilde{\phi}_0\rangle = \sum_{j=1}^{m} \gamma_j |\phi_{0_j}\rangle . \tag{A 1}$$

To find the γ_j one again uses equation (11) provided by the cumulant method. Note that equation (11) also holds for generalized cumulants [16], i.e. defined with a bra vector different from the ket $|\phi_n\rangle$:

$$0 = \langle \Phi | S_\nu^\dagger H \Omega | \phi_0 \rangle^c . \tag{A 2}$$

The arbitrary vector $\langle \Phi|$ should have a non-zero overlap with $|\phi_0\rangle$. Evaluating the cumulants [11] and using the linear combination (A 1) instead of the ket vector $|\phi_0\rangle$ we obtain

$$\sum_j \gamma_j \langle \Phi | S_\nu^\dagger H \Omega | \phi_{0_j} \rangle = E_0 \sum_j \gamma_j \langle \Phi | S_\nu^\dagger \Omega | \phi_{0_j} \rangle . \tag{A 3}$$

For fixed $\Omega = \exp S$ and appropriate operators S_ν, equation (A 3) is a generalized eigenvalue problem for E_0 and $\{\gamma_j\}$ and can be solved by standard methods. The lowest eigenvalue is the ground-state energy, the corresponding eigenvector the desired linear combination of the degenerate ground-state vectors of H_0.

References

[1] Becker, K. W., and Fulde, P., 1988, *Z. Phys.* B, **72,** 423.
[2] Becker, K. W., Won, H., and Fulde, P., 1989, *Z. Phys.* B, **75,** 335.
[3] Becker, K. W., and Brenig, W., 1990, *Z. Phys.* B, **79,** 195.
[4] Bishop, R. F., 1991, *Theor. Chim. Acta*, **80,** 95.
[5] Mukherjee, D., 1996, *Recent Progress in Many-body Theories*, Vol. 10, edited by E. Schachinger, R. Mitter and H. Stormann (Plenum Press); Kutzelnigg, W., and Mukherjee, D., 1997, *J. chem. Phys.*, **107,** 432.
[6] Fulde, P., 1993, *Electron Correlations in Molecules and Solids* (Berlin: Springer).
[7] Kubo, R., 1962, *J. phys. Soc. Jpn*, **17,** 1700.
[8] Schork, T., and Fulde, P., 1992, *J. chem. Phys.*, **97,** 9195.
[9] Polatsek, G., and Becker, K. W., 1996, *Phys. Rev.* B, **54,** 1637.
[10] Vojta, M., and Becker, K. W., 1996, *Phys. Rev.* B, **54,** 15483.
[11] Köhler, H., Vojta, M., and Becker, K. W., 1997, *Phys. Rev.* B, **56,** 6603.
[12] For a recent review on the Heisenberg antiferromagnet, see for instance Manousakis, E., 1991, *Rev. mod. Phys.*, **63,** 1.
[13] Hirsch, J. E., 1983, *Phys. Rev. Lett.*, **51,** 1900; 1985, *Phys. Rev.* B, **31,** 4403; White, S. R., *et al.*, 1989, *Phys. Rev.* B, **40,** 506; Moreo, A., *et al.*, 1990, *Phys. Rev.* B, **41,** 2313.
[14] Yokoyama, H., and Shiba, H., 1987, *J. phys. Soc. Jpn*, **56,** 3582.
[15] Paulus, B., Fulde, P., and Stoll, H., 1995, *Phys. Rev. B*, **51,** 10572.
[16] Kladko, K., and Fulde, P., 1998, *Int. J. quantum. Chem.*, **66,** 377.

MOLECULAR PHYSICS, 1998, VOL. 94, NO. 1, 225–234

The state-selective coupled cluster method for quasi-degenerate electronic states

By LUDWIK ADAMOWICZ
Department of Chemistry, University of Arizona, Tucson, Arizona 85721, USA

PIOTR PIECUCH
Department of Chemistry, University of Toronto, 80 St. George Street, Toronto, Ontario, Canada M5S 3H6

and KEYA B. GHOSE
Lehrstuhl für Theoretische Chemie, Ruhr-Universität, D-44780 Bochum, Germany

This presentation will provide a comprehensive account of the recent developments in the the state-selective coupled cluster method for quasi-degenerate electronic states. We will mention some previous important applications and present new data from our recently finished calculations related to stretching of chemical bonds. We will also discuss some possible future developments.

1. Introduction

Single reference coupled cluster (SRCC) method [1–3] has been largely successful in providing accurate values of energy [4–7] and molecular properties [8–18] for the non-degenerate ground states of closed shell systems as well as of high-spin open-shell systems. In such cases, the zero-order approximation to the exact wave function can be satisfactorily described by a single determinant, which is usually the restricted or unrestricted Hartree–Fock (RHF or UHF) wave function. However, problems that are of chemical interest often correspond to more complicated situations where a few leading configurations of the full configuration interaction (FCI) space contribute almost equally to the wave function of the electronic state of interest (it is important to realize that a configuration composition of a state depends on the particular choice of the molecular orbital basis and a state which is significantly 'multiconfigurational' in one basis may have less of the multi-reference character in the other basis). The proper way to deal with such open-shell/quasi-degenerate situations is to include the dominant configurations in the model/reference space and generate the corresponding exact wave functions by applying a suitable wave operator on this reference space. The genuine multi-reference (MR) CC methods, such as the Fock-space [19–21] and Hilbert-space [22, 23] versions follow such a direction and eventually arrive at an eigenvalue equation involving diagonalization of an effective Hamiltonian defined through the Bloch equation in the model space. Strict application of these approaches leads to simultaneous calculation of several electronic states corresponding to the given reference space.

Another, very diverse class of MRCC methods focuses on a single state at a time. These methods are called the state-selective (SS) or single-state theories [24–31]. Some of these approaches rely on more general multi-reference concepts (e.g. [27]), while aiming at a single electronic state, whereas the others utilize the SRCC concepts (e.g. the SSCC method of [31] or the equation-of-motion (EOM) CC methods [32]). Some SSCC methods combine SRCC ansatz with a CI-like eigenvalue problem, thus allowing evaluation of a number of electronic states in a single calculation (e.g. the EOMCC method [32(a)] and its more recent similarity-transformed modification [32(b)], or the method proposed by Paldus *et al.* [25]).

The state-selective MRCC approach of Oliphant and Adamowicz [33] and Piecuch *et al.* [34] introduces multi-reference character of the wave function through suitable modifications of cluster components defining the SRCC approach. These modifications are introduced in such a way as to provide sufficient flexibility to the wave function in order to handle open-shell and quasi-degenerate situations. We use the term 'multi-reference' in a loose sense, as it is done in the MRCI theory, where the multi-reference description is achieved directly by selecting important configurations and not by employing the Bloch wave operator formalism and the concept of effective Hamiltonians.

In the SSMRCC method of [33–38], the exponential wave operator of SRCC is partitioned into internal and

0026–8976/98 $12·00

external parts such that the former acts on a suitably chosen single-determinantal formal reference to generate a multi-determinantal zero-order wave function. The external part of the exponential SRCC operator acts on this zero-order wave function to generate the exact wave function. Both parts are exponentials of the relevant cluster operators. Another SSMRCC ansatz which we recently proposed [39, 40] to better handle the quasi-degenerate situations arising in excited states, where the cluster structure of the electron correlation effect is expected to be different from the quasi-degeneracy resulting from stretching chemical bonds, has the internal part linearized. Such linearization makes the computation of the internal cluster components simpler.

The advantage of using a partially linearized ansatz in a size-extensive representation of the wave function, rather than a fully exponential one, is to avoid any particular assumption regarding the cluster structure through the exponentiated excitation operator. However, if a linearized ansatz is used, one needs to either consider all the configurations which can be constructed with the use of the active orbitals in the model space (the full CI expansion using core and active orbitals) or use some other means, such as size-extensive corrections to the Hamiltonian matrix, in order to obtain a fully size-extensive theory. In the recently proposed method termed $[(SC)^2 - CI]$ [41, 42], the size-extensivity was achieved through a self-consistent dressing of the diagonal elements of the CI matrix. Such an approach, which proceeds through the construction of an effective Hamiltonian matrix by including contributions from higher excitations in the diagonal elements, offers some potential advantages over the conventional CC approach. One such advantage is reducing the non-linearity of the equations for the configuration amplitudes and solving for the amplitudes using the conventional diagonalization procedure; another being that the method offers a scheme which can be easily implemented within the conventional CI method and can provide size-consistent results not only for the ground state at the equilibrium geometry but also for structures significantly distorted from the equilibrium as well as for excited states. Although for some excited states, which are well described by single excitations from the Hartree–Fock wave function, the EOMCC method based on the single-determinant CC approach provides very good results [32], there are many classes of excited electronic states where a different approach is necessary. Dealing with those states requires that the CC method be extended beyond the single reference case allowing for several determinants to significantly contribute to the reference wave function of the state of interest.

Based on our previous experience, we prefer to consider the state-specific (or state-selective) approach. The state-selective scheme can be applied to determine only one state of the system (this being either the ground or excited state) in a single calculation, while a single multi-state calculation provides results simultaneously on several states. The reason for choosing the state-specific approach is the realization that in most applications one is usually concerned with a single electronic state or a small subset of states. Moreover, if several states are simultaneously considered in a calculation, as it is done in genuine MRCC methods, one either needs to compromise the accuracy of the calculation by having the states share the same active orbitals and the same set of cluster amplitudes (this may be a more reasonable assumption for some states than for the others), or to perform a calculation which, in essence, would be equivalent in complexity and effort to a set of independent calculations, each aiming to determine a different state. On the other hand, if electron excitation spectra are investigated, it certainly is more practical to consider several states in a single calculation, and this mandates a multi-state procedure.

We also find it reasonable to assume that the initial step in our approach will be a complete active space self-consistent field (CASSCF) calculation, which will produce orbitals and the initial reference functions for the state or states under consideration. The CASSCF method [43] is a well established approach, which through implementation of the second-order orbital and configuration optimization procedure has become a popular and effective method to study states with multi-reference character, particularly excited states. At present, however, it seems that a satisfactory method to treat the dynamic electron correlation effects in a size-consistent fashion is still an open problem. In particular, it seems that no satisfactory approach has yet been proposed that equivalently describes the dynamic and non-dynamic electron correlation contributions and allows them to interact in a self-consistent manner. The CASPT2 method, which has been advanced by several groups [43], provides a good account of the dynamic correlation effects for cases where the active orbitals are energetically separated from the virtual orbitals. However, it fails when degeneracies appear in the orbital space. Although 'level shifting' and other types of techniques have been tried to remedy the problem, no 'clean' and general solution has yet been found.

There has been also some development within the MRCI method to correct its lack of size-extensivity. In our recent work [39, 40] we proposed a scheme where the dynamic/non-dynamic electron correlation interaction in a state-specific calculation is introduced by 'dressing' the CI Hamiltonian with the contributions of the

higher excitations. These contributions are determined based on the coupled-cluster representation of the wave function. Another possible approach to determine the size-extensive dressing of the CI Hamiltonian matrix is to develop a procedure for solving the CI problem simultaneously for M states. In this type of approach, which we proposed recently [40], we use a set of M determinants that have the largest contributions to the M states of interest. The CI space then represents the model space and the determinants play the same role as references in the single-state single-reference problem. They form the so-called 'main model space' of the intermediate Hamiltonian theory [44]. The CI eigenstates are expressed in the form which is based on the Jeziorski–Monkhorst (J–M) [22] formulation of the MRCC expansion, with the M determinants being the M references. The coefficients of the outer-space determinant, which contribute to the dressing terms in the Hamiltonian, are calculated from the J–M exponential wave-operator. In the solution of the dressed-CI problem, it is necessary to iterate the CI equation and recalculate the dressing terms in each iteration. The method is particularly applicable to the CAS-SDCI problem (MRCI singles and doubles approach employing CASSCF orbitals). The general concept of the approach is reviewed in greater detail in the following section.

2. State-selective multi-reference CC formalism

In the originally introduced version of the SS MRCC method [33–38], the traditional SRCC exponential wave operator e^T is partitioned into two parts, $\exp T^{(\mathrm{int})}$ and $\exp T^{(\mathrm{ext})}$, such that the former acts on a suitably chosen single-determinantal formal reference function $|0\rangle$ (which is chosen as a Fermi vacuum) to generate the model space reference function $|\Phi^{(\mathrm{int})}\rangle$ being a linear combination of reference determinants and the latter produces excitations outside the model space. The formal reference determinant, $|0\rangle$, can be different for different states. Thus, the exact function is generated as:

$$|\Psi\rangle = \exp T^{(\mathrm{ext})}|\Phi^{(\mathrm{int})}\rangle = \exp T^{(\mathrm{ext})} \exp T^{(\mathrm{int})}|0\rangle. \quad (1)$$

The $T^{(\mathrm{int})}$ and $T^{(\mathrm{ext})}$ operators commute as both of them are expressed in terms of excitation operators relative to $|0\rangle$. In order to specify the orbital indices in these two operators, the spin–orbital space is divided into active and inactive subspaces. The inactive space contains core and virtual orbitals which are always occupied and unoccupied, respectively, in all model space configurations. Active space orbitals are those which have different occupancies for different model space configurations. The formal reference determinant, $|0\rangle$, defines the partitioning of the active space into two subsets, namely, the active hole (occupied in $|0\rangle$) and active particle (not occupied in $|0\rangle$) subspaces. Hole and particle indices in $T^{(\mathrm{int})}$ have fully internal (all active) labelling. Let $N^{(\mathrm{int})}$ denote the highest level of excitation possible in the $T^{(\mathrm{int})}$ operator. For $T^{(\mathrm{ext})}$, the indices are either all external (inactive) or semi-internal (a mixture of internal and external labelling). Let $N^{(\mathrm{ext})}$ denote the highest level of excitation possible in the $T^{(\mathrm{ext})}$ operator, which is equal to the number of all correlated electrons. In this work, we follow the convention of indicating orbitals of different categories: core (inactive holes) **i, j, k, l**; active holes **I, J, K, L**; active particles **A, B, C, D**; and virtual (inactive particles) **a, b, c, d**. If the active or inactive character of a particular spin–orbital is irrelevant, we designate it in italics (holes: ***i, j, k, l***; particles: ***a, b, c, d***). With the use of the above indexing convention, the $T^{(\mathrm{int})}$ and $T^{(\mathrm{ext})}$ operators can be formally written in terms of particle–hole (p–h) excitation operators, $E^{a_1a_2\ldots a_\eta}_{i_1i_2\ldots i_\eta}$ ($|0^{a_1a_2\ldots a_\eta}_{i_1i_2\ldots i_\eta}\rangle = E^{a_1a_2\ldots a_\eta}_{i_1i_2\ldots i_\eta}|0\rangle$), in the following way:

$$T^{(\mathrm{int})} = \sum_{\kappa=1}^{N^{(\mathrm{int})}} T^{(\mathrm{int})}_\kappa, \quad (2)$$

$$T^{(\mathrm{ext})} = \sum_{\eta=1}^{N^{(\mathrm{ext})}} T^{(\mathrm{ext})}_\eta, \quad (3)$$

with

$$T^{(\mathrm{int})}_\kappa = (\kappa!)^{-2} \sum_{\substack{\mathrm{I}_1>\mathrm{I}_2>\cdots>\mathrm{I}_\kappa \\ \mathrm{A}_1>\mathrm{A}_2>\cdots>\mathrm{A}_\kappa}}^{\mathrm{int}} t^{\mathrm{I}_1\mathrm{I}_2\ldots\mathrm{I}_\kappa}_{\mathrm{A}_1\mathrm{A}_2\ldots\mathrm{A}_\kappa} E^{\mathrm{A}_1\mathrm{A}_2\ldots\mathrm{A}_\kappa}_{\mathrm{I}_1\mathrm{I}_2\ldots\mathrm{I}_\kappa}, \quad (4)$$

$$T^{(\mathrm{ext})}_\eta = (\eta!)^{-2} \sum_{\substack{i_1>i_2>\cdots>i_\eta \\ a_1>a_2>\cdots>a_\eta}}^{(\mathrm{ext})} t^{i_1i_2\ldots i_\eta}_{a_1a_2\ldots a_\eta} E^{a_1a_2\ldots a_\eta}_{i_1i_2\ldots i_\eta}, \quad (5)$$

where among the $a_1a_2\ldots a_\eta$ and $i_1i_2\ldots i_\eta$ indices in the above expansion, either at least one label corresponds to an inactive orbital, or all indices are active, but in this case the level of the external excitation is at least one higher than the highest excitation level in $T^{(\mathrm{int})}$. The SS MRCC expressions for determining correlation energy ΔE and amplitudes are obtained with assumption of intermediate normalization $\langle\Psi|0\rangle = \langle 0|0\rangle = 1$ as follows:

$$\langle 0|[H_N \exp T^{(\mathrm{ext})} \exp T^{(\mathrm{int})}]_c|0\rangle = \Delta E, \quad (6)$$

$$\langle \Phi^*|[H_N \exp T^{(\mathrm{ext})} \exp T^{(\mathrm{int})}]_c|0\rangle = 0, \quad (7)$$

where Φ^* are the excited configurations and H_N represents the Hamiltonian in the normal order form ($H_N = H - \langle 0|H|0\rangle$). It is the sum of one- and two-body operators, F_N and V_N, whose matrix elements are the usual one- and two-electron molecular integrals.

For practical use, expansions of $T^{(\mathrm{int})}$ and $T^{(\mathrm{ext})}$ in terms of respective many-body components $T_\kappa^{(\mathrm{int})}$ and $T_\eta^{(\mathrm{ext})}$ have to be truncated. In all the applications performed to date, the internal set was restricted to include only $T_1^{(\mathrm{int})}$ and $T_2^{(\mathrm{int})}$ operators, while the external set contained all possible semi-internal and external, singly and doubly excited amplitudes plus a restricted set of internal and semi-internal three- and four-body amplitudes. The three-body external amplitudes were restricted to carry at least one pair of active hole particle labels and four body amplitudes were restricted to carry at least two active hole–particle pair labels. The approximate version of SS MRCC with all singles and doubles amplitudes and internal and restricted semi-internal types of triple amplitudes is called the SS MRCCSD(T) method. The version which includes internal and restricted semi-internal quadruple amplitudes is termed the SS MRCCSD(TQ) method. These versions have the following ansatz for the wave function:

$$|\Psi^{\mathrm{SSMRCCSD(T)}}\rangle = \exp\left[T_1^{(\mathrm{ext})} + T_2^{(\mathrm{ext})} + T_3\left(\begin{matrix} abC \\ Ijk \end{matrix}\right)\right] \exp\left[T_1^{(\mathrm{int})} + T_2^{(\mathrm{int})}\right]|0\rangle, \quad (8)$$

$$|\Psi^{\mathrm{SSMRCCSD(TQ)}}\rangle = \exp\left[T_1^{(\mathrm{ext})} + T_2^{(\mathrm{ext})} + T_3\left(\begin{matrix} abC \\ Ijk \end{matrix}\right) + T_4\left(\begin{matrix} abCD \\ IJkl \end{matrix}\right)\right] \exp\left[T_1^{(\mathrm{int})} + T_2^{(\mathrm{int})}\right]|0\rangle. \quad (9)$$

It has been shown with a number of examples that the SS MRCCSD method based on the above wave functions handles very well the dissociation process of single- and double-bonds, as well as quasi-degenerate situations in some excited states [45].

In order to more effectively handle the general quasi-degeneracy problem, we recently proposed the use of a linearized form for the internal operator, $\exp T^{(\mathrm{int})}$, while retaining our previous description for the external operator (semi-linear approach) [39]. The resulting ansatz assumes the form:

$$|\Psi\rangle = \exp T^{(\mathrm{ext})}(1 + C^{(\mathrm{int})})|0\rangle. \quad (10)$$

In this case the equations for the amplitudes are linear in terms of $C^{(\mathrm{int})}$. In general, if $T^{(\mathrm{int})}$ includes all possible excitations within the active orbital space, the $\exp T^{(\mathrm{int})}|0\rangle$ and $(1 + C^{(\mathrm{int})})|0\rangle$ wave functions are completely equivalent and only practical reasons may determine which approach will be more effective and convenient in a particular case. However, since in calculations on excited states one usually performs CAS calculations first, it seems more practical to use the linearized form of the wave function, equation (10), rather than convert the CAS wave function to the exponential form, equation (1). Also, the spin adaptation of the wave function of equation (10) (making the function and eigenfunction of the S^2 operator) is more straightforward than for the wave function of equation (1), which makes this ansatz better suited in representing excited states. In order for the ansatz represented by equation (10) to provide a size-extensive wave function, the internal part, $(1 + C^{(\mathrm{int})})|0\rangle$, should include the complete set of the determinants within the manifold of configurations constructed with the use of all active orbitals. Thus, the substitution of $\exp T^{(\mathrm{int})}$ with $(1 + C^{(\mathrm{int})})$ will satisfy the linked cluster theorem and preserve the size-extensivity requirement only if the full CI representation of the internal part of the wave function is assumed and no truncation is made in the $C^{(\mathrm{int})}$ amplitude set. However, because of the exponential nature of the $T^{(\mathrm{ext})}$ operator, the series can be truncated after including any particular level of multi-body operators. For example, including one- and two-body excited operators, $T_1^{(\mathrm{ext})}$ and $T_2^{(\mathrm{ext})}$, is one of the possible choices. In this case the ansatz for the wave function has the following form:

$$|\Psi\rangle = \exp\left[T_1^{(\mathrm{ext})} + T_2^{(\mathrm{ext})} + T_3\left(\begin{matrix} abC \\ Ijk \end{matrix}\right) + T_4\left(\begin{matrix} abCD \\ IJkl \end{matrix}\right) + T_5\left(\begin{matrix} abCDE \\ IJKlm \end{matrix}\right) + \cdots\right](1 + C^{(\mathrm{int})})|0\rangle, \quad (11)$$

where the $C^{(\mathrm{int})}$ operator comprises the following excitations:

$$C_I^A, C_{IJ}^{AB}, C_{IJK}^{ABC}, C_{IJKL}^{ABCD} \ldots \quad (12)$$

and can be defined as:

$$C^{(\mathrm{int})} = \sum_{\kappa=1}^{N^{(\mathrm{int})}} C_\kappa^{(\mathrm{int})}, \quad (13)$$

$$C_\kappa^{(\mathrm{int})} = \sum_{\substack{I_1>I_2>\cdots>I_n \\ A_1>A_2>\cdots>A_n}}^{(\mathrm{int})} c_{A_1A_2\ldots A_n}^{I_1I_2\ldots I_n} E_{I_1I_2\ldots I_n}^{A_1A_2\ldots A_n}. \quad (14)$$

The $T^{(\mathrm{ext})}$ operator comprises the same types of fully external and semi-external amplitudes as in the fully exponential ansatz. The only difference is that, since all fully internal excitations are included in $C^{(\mathrm{int})}$, there is no need to include any higher-level fully internal excitations in $T^{(\mathrm{ext})}$ as was done with the fully exponential ansatz, where the external excitations have to be augmented by internal triple and quadruple excitations, $T_3\left(\begin{matrix} ABC \\ IJK \end{matrix}\right)$ and $T_4\left(\begin{matrix} ABCD \\ IJKL \end{matrix}\right)$, in the SS MRCCSD(T) and SS MRCCSD(TQ) levels of theory to account for connected internal single and double excitations from important singly and doubly excited configurations generated by $T^{(\mathrm{int})}$. If we assume that all the configurations

generated by the action of $(1 + C^{(\mathrm{int})})$ on $|0\rangle$ are equally important then, in principle, one needs to include in $T^{(\mathrm{ext})}$ all fully external and semi-internal excitations which are single and double excitations from all the $(1+C^{(\mathrm{int})})|0\rangle$ configurations. This would necessitate, in the case when $C^{(\mathrm{int})}$ is a κ-body operator, including certain selected $\kappa+1$ and $\kappa+2$ body $T^{(\mathrm{ext})}$ amplitudes. Although there are certainly cases where one cannot avoid high-order connected excitations, one can always make an attempt for the state of interest to reduce the importance of higher excited configurations in the model space manifold. One way of accomplishing this is by transforming the model space CI expansion for the state of interest to an expansion in terms of configurations constructed with the use of natural orbitals determined for this state. With this kind of transformation, it may be possible to reduce the active orbital set (the degree of the reduction can be different for different states) by including only those orbitals which are more significantly occupied. In consequence, one can reduce the level of the $T^{(\mathrm{ext})}$ excitations. There is an additional point which one can make in favour of using the natural orbitals. If they are not used in the calculation, the CAS orbitals are not well defined, which can cause inconsistency in representing different points on the potential energy surface.

The following types of amplitudes are included in the $T^{(\mathrm{ext})}$ operator: three types of single amplitudes:

$$t_{\mathrm{a}}^{\mathrm{I}}, t_{\mathrm{A}}^{\mathrm{i}}, t_{\mathrm{a}}^{\mathrm{i}}, \tag{15}$$

eight types of double-excitation amplitudes:

$$t_{\mathrm{aB}}^{\mathrm{IJ}}, t_{\mathrm{AB}}^{\mathrm{Ij}}, t_{\mathrm{aB}}^{\mathrm{Ij}}, t_{\mathrm{ab}}^{\mathrm{IJ}}, t_{\mathrm{AB}}^{\mathrm{ij}}, t_{\mathrm{ab}}^{\mathrm{Ij}}, t_{\mathrm{aB}}^{\mathrm{ij}}, t_{\mathrm{ab}}^{\mathrm{ij}}, \tag{16}$$

and eight types of triple excitation amplitudes:

$$t_{\mathrm{aBC}}^{\mathrm{IJK}}, t_{\mathrm{ABC}}^{\mathrm{IJk}}, t_{\mathrm{aBC}}^{\mathrm{IJk}}, t_{\mathrm{abC}}^{\mathrm{IJK}}, t_{\mathrm{ABC}}^{\mathrm{Ijk}}, t_{\mathrm{abC}}^{\mathrm{IJk}}, t_{\mathrm{aBC}}^{\mathrm{Ijk}}, t_{\mathrm{abC}}^{\mathrm{ijK}}. \tag{17}$$

From the above it is easy to see how to determine what types of higher order amplitudes should be included if higher order internal excitations become important. Those can be generated by adding one or more active hole–particle label pairs, (L,D), (L,M,D,E), etc., to the above triple amplitudes. The resulting eight classes of the general types of external excitation amplitudes are:

$$t_{\mathrm{aBC...D}}^{\mathrm{IJK...L}}, t_{\mathrm{ABC...D}}^{\mathrm{iJK...L}}, t_{\mathrm{aBC...D}}^{\mathrm{iJK...L}}, t_{\mathrm{abC...D}}^{\mathrm{IJK...L}},$$

$$t_{\mathrm{ABC...D}}^{\mathrm{ijK...L}}, t_{\mathrm{abC...D}}^{\mathrm{iJK...L}}, t_{\mathrm{aBC...D}}^{\mathrm{ijK...L}}, t_{\mathrm{abC...D}}^{\mathrm{ijK...L}}. \tag{18}$$

As one can see, the 'complete' wave function in equation (10) is developed by acting with the excitation operators on a single determinant wave function, $|0\rangle$, which we call the formal reference. As mentioned before this function can be chosen to be different for different states. As a matter of fact, for states which belong to different symmetry representations, the formal references have to be different, since the formal reference is expected to contribute (presumably in a significant way) to the calculated state. The proposal of using different formal references for different states is in line with the role which we consider the coupled cluster method should play in electronic structure calculations, which is to exact the CASSCF results by accounting for the part of the dynamic electron correlation contribution not included at the CASSCF level. In this scheme a separate CC calculation is performed for each state (like in the CASPT2 method).

The approach that we propose is close in spirit to the approach suggested by Paldus and co-workers [25] and, perhaps even closer, to the approach proposed by Nakatsuji and co-workers [26]. In the former approach the authors start form $\exp T|0\rangle$ to describe the ground state, and then generate excited states through the action of a linear CI-like operator W on the ground-state wave function. The internal part of W acting on $|0\rangle$ gives a contribution similar to our $(1+C^{(\mathrm{int})})|0\rangle$. The remaining portion of W includes correlation effects needed to describe the dynamical correlation in the excited state. This effect is described in our approach by $T^{(\mathrm{ext})}$. Nakatsuji and co-workers [26] use an idea which in some respect is similar to our proposal. They start with their symmetry adapted cluster (SAC) expansion theory by defining the ground state wave function in the exponential form: $\Psi_{\mathrm{g}}^{\mathrm{SAC}} = \exp S|0\rangle$, where $S = \sum_I C_I S_I^{\dagger}$ is expressed in terms of symmetry adapted configuration generators, $S_I^{\dagger}$. For the excited, ionized and electron attached states they use the following SAC–CI wavefunction: $\Psi_{\mathrm{ex}}^{\mathrm{SAC-CI}} = \sum_{\mathrm{K}} d_{\mathrm{K}} R_{\mathrm{K}}^{\dagger} \Psi_{\mathrm{g}}^{\mathrm{SAC}}$, where $R_{\mathrm{K}}^{\dagger}$ is a symmetry-adapted excitation, ionization, or electron attachment operator.

For the modified SS MRCC ansatz, the equations for energy and amplitudes may be expressed by projecting the Schrödinger's equation against the vacuum determinant and the configurations $|\Phi_{(\mathrm{int})}^{*}\rangle$ and $|\Phi_{(\mathrm{ext})}^{*}\rangle$, where $|\Phi_{(\mathrm{ext})}^{*}\rangle$ are the configurations corresponding to excitations included in $T^{(\mathrm{ext})}$ and $|\Phi_{(\mathrm{int})}^{*}\rangle$ are all the configurations other than $|0\rangle$ included in the model space formed out of active orbitals. Projecting the Schrödinger's equation to the vacuum, one can write the correlation energy as,

$$\langle 0|H_N \exp T^{(\mathrm{ext})}(1 + C^{(\mathrm{int})})|0\rangle = \Delta E. \tag{19}$$

To obtain the equation for the amplitudes of the $T^{(\mathrm{ext})}$ and $C^{(\mathrm{int})}$ operators, the Schrödinger equation has to be projected onto the set of internally and externally excited states leading to,

$$\langle \Phi_{(\mathrm{int})}^{*}|H_N \exp T^{(\mathrm{ext})}(1 + C^{(\mathrm{int})})|0\rangle = \Delta E c^{(\mathrm{int})},$$

$$c^{(\mathrm{int})} = \langle \Phi_{(\mathrm{int})}^{*}|C^{(\mathrm{int})}|0\rangle, \tag{20}$$

$$\langle \Phi^*_{(\mathrm{ext})} | H_N \exp T^{(\mathrm{ext})} (1 + C^{(\mathrm{int})}) | 0 \rangle = \Delta E c^{(\mathrm{ext})},$$
$$c^{(\mathrm{ext})} = \langle \Phi^*_{(\mathrm{ext})} | C^{(\mathrm{ext})} | 0 \rangle, \quad (21)$$

where $C^{(\mathrm{ext})}$ may be defined as sum of $T^{(\mathrm{ext})}$ of the same rank and all the products of $T^{(\mathrm{ext})}$ and $C^{(\mathrm{int})}$ of the lower ranks that give the same order of excitation as $|\Phi^*_{(\mathrm{ext})}\rangle$.

In general, $(1 + C^{(\mathrm{int})})|0\rangle$ describes a complete set of determinants within the set of active orbitals and thus, as in the full CI case, the disconnected components of the left and right hand side of the equation obtained by the projection to the 'internal' set of configurations, equation (20), cancel among themselves. In such a case, the disconnected components of the left hand side of equation (21) also cancel with the right hand side as in the standard CC method,

$$\langle \Phi^*_{(\mathrm{int})} | [H_N \exp T^{(\mathrm{ext})} (1 + C^{(\mathrm{int})})]_c | 0 \rangle = 0, \quad (22)$$

$$\langle \Phi^*_{(\mathrm{ext})} | [H_N \exp T^{(\mathrm{ext})} (1 + C^{(\mathrm{int})})]_c | 0 \rangle = 0. \quad (23)$$

The above equations have only symbolic meaning. In order to perform cancellation of the disconnected terms on the left and right hand sides of equations (20) and (21) one needs to separate the disconnected terms resulting from the disconnected parts of the $C^{(\mathrm{int})}$ operator. This requires that this operator is expressed in terms of the $T^{(\mathrm{int})}$ operators. However, then the $C^{(\mathrm{int})}$ cannot be directly calculated. Therefore, in the calculations utilizing semi-linear ansatz we will be solving equations (20) and (21) rather than equations (22) and (23).

One may examine the case where $C^{(\mathrm{int})}$ contains an 'incomplete' set of operators in the sense that it is truncated at some lower excitation order, e.g. singles and doubles, so that $(1 + C^{(\mathrm{int})})|0\rangle$ does not represent the full CI expansion within the active space. This modification of the semi-linear ansatz makes it more general and helps include only those configurations in the internal space which are important. This may lead to computational simplicity as well. Unfortunately, truncation of this type would introduce disconnected diagrams to the energy. In each equation of the system of equations (20) and (21) there will be only partial cancellation of the disconnected components. In some special situations one can identify the terms needed to achieve cancellation of disconnected terms. For example, if $C^{(\mathrm{int})}$ and $T^{(\mathrm{ext})}$ operators are truncated at a given order of excitation, say doubles, the disconnected components of the left hand side of equation (20) will consist of disconnected diagrams of the operator $[H_N \exp T^{(\mathrm{ext})}(1 + C^{(\mathrm{int})})]$ with two internal holes and particle lines open. This can only be a product of closed diagrams representing vacuum expectation value of $H_N \exp T^{(\mathrm{ext})}$ and the $c^{(\mathrm{int})}$ coefficient. If we now separate ΔE as,

$$\langle 0 | H_N \exp T^{(\mathrm{ext})} | 0 \rangle + \langle 0 | H_N \exp T^{(\mathrm{ext})} C^{(\mathrm{int})} | 0 \rangle$$
$$= \Delta E^{(\mathrm{ext})} + \Delta E^{(\mathrm{int})} = \Delta E, \quad (24)$$

then one can see that in this special situation, the disconnected components resulting from the left hand side of every equation (20) will cancel with $\Delta E^{(\mathrm{ext})} c^{(\mathrm{int})}$. As for equation (21), the disconnected diagrams with at least one external line are products of the closed diagrams of $[H_N \exp T^{(\mathrm{ext})}(1 + C^{(\mathrm{int})})]$ operator and amplitudes representing $T^{(\mathrm{ext})}$ operator and this cancels with the right hand side fully. However, if one uses different truncation schemes in $C^{(\mathrm{int})}$ and $T^{(\mathrm{ext})}$ operators, as would be done in the semi-linear SSCC ansatz, one must use equations (20) and (21) accepting the fact that certain disconnected terms will not cancel out. Hence for the semi-linear ansatz to formally satisfy the size extensivity, it is necessary that the $C^{(\mathrm{int})}$ operators describe the complete set of excitations within the active orbitals in which case equations (22) and (23) are satisfied.

With many active orbitals, the rank of $C^{(\mathrm{int})}$ operator will be high and in such situations the set of equations to be solved will become very complex. A plausible solution [27] is to keep the $C^{(\mathrm{int})}$ amplitudes (as determined from CASSCF calculation) frozen while solving for the external set of amplitudes, $T^{(\mathrm{ext})}$. This will mean solving for the external amplitudes in the presence of a fixed potential owing to the active orbital set in a decoupled manner. On the other hand, if the number of active orbitals and consequently the number of $C^{(\mathrm{int})}$ amplitudes is small enough to make the corresponding computational exercise feasible, one can solve the coupled set of equations (20) and (21). This line of approach will help relaxing the internal amplitudes in the presence of the external set. Depending on the number of active orbitals needed for a qualitatively correct description of bonding, one needs to choose from above two alternative modes of solving.

Finally, one might consider the complete elimination of the exponential component in the wave function by replacing the external excitation part by the linearized operator:

$$|\Psi\rangle = (1 + C^{(\mathrm{ext})})(1 + C^{(\mathrm{int})})|0\rangle, \quad (25)$$

which, when the $C^{(\mathrm{ext})}$ operator is truncated, leads to a MRCI expansion. In order for the above ansatz to be size-consistent one needs to include the complete set of both internal and external excitations. Obviously, this would lead to the full CI (FCI) wave function.

In the above discussion one point needs to be clarified in order to avoid a contradiction between what is commonly understood as the 'reference function' and the meaning of this term which we use in this work. First, in equation (1) we introduced a single determinantal

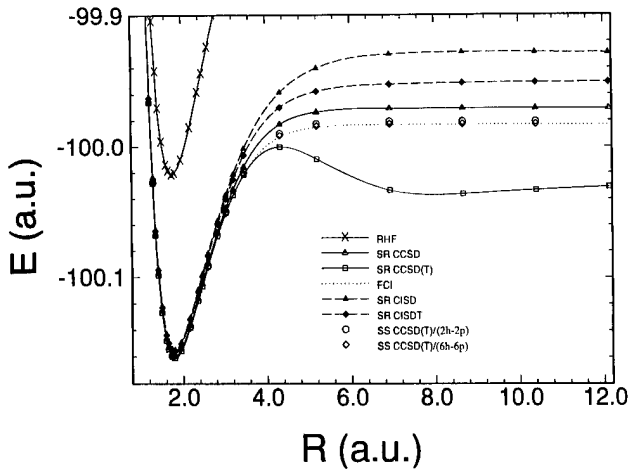

Figure 1. The potential energy curves for the HF molecule calculated at the SRCC and SSCC levels of theory.

wave function $|0\rangle$, which we call the formal reference. Next, we introduced two new functions, $\exp T^{(\mathrm{int})}|0\rangle$ and $(1 + C^{(\mathrm{int})})|0\rangle$, which are defined in the active orbital space and in the commonly used terminology would also be called reference functions (even though they have multi-determinantal character). In the subsequent step we act with $\exp T^{(\mathrm{ext})}$ on those reference functions to introduce the dynamic correlation effects. It is important to distinguish between the formal reference determinant, which is used to establish the partitioning of the orbital space into the active and inactive subspaces and to define the Fermi vacuum, and the reference functions defined in the active configuration manifold with the internal excitation operators. According to the conventional definition, the latter are the 'true' reference functions, which provide the first approximations for the state under consideration. If the CASSCF wave function is used as the 'true' reference, the choice of the formal reference determinant is ambiguous since all active-space configurations are included. Obviously, the formal reference determinant cannot be the one, which does not contribute to the state under consideration. In practical applications one usually chooses one of the leading determinants to be the formal reference.

3. Numerical examples

The results presented in this section have been obtained with the double-exponential SSMRCC wave function of equation (1) at the SSCCSD(T) and SSCCSD(TQ) levels of theory (equations (8) and (9)). First, on figure 1 we present a potential energy curve calculation for the ground state of the HF molecule as a function of the internuclear distance using the double zeta (DZ) basis set. The figure compares the performance of the single reference (SR) CC theory at the CCSD and CCSD(T) [46] levels with the SSCCSD(T) results obtained with two-hole and two-particle active space (σ and σ^* spatial orbitals) and with six-hole and six-particle active space (σ, π_x, π_y, and $\sigma^*, \pi_x^*, \pi_y^*$ spatial orbitals). In describing the active spaces, we use a spin–orbital description, so that two holes correspond to a single spatial orbital, etc. There are a few observations which one can make upon inspection of the results. First, it is clear that the SSCCSD(T) method with both smaller and larger active spaces gives results virtually identical to FCI. Second, the results with the smaller active space are only marginally worse than with the larger space. The SRCCSD method overestimates the dissociation energy and, what is noticeable, the SRCCSD(T) method using RHF orbitals underestimates it and produces a large and unphysical dip in the curve around 5–7 au.

Similar behaviour of the SRCCSD(T) method can be seen for the CO molecule in the results presented in table 1. The differences between the total energies calculated at the particular level of the theory and the FCI results, which are shown at the bottom of the table, indicate that this method performs well near the equilibrium but fails at $2R_e$. The failure of the SRCCSD(T) approach is particularly dramatic when the RHF orbitals are used (SRCCSD(T)/RHF method). Somewhat better results at $R = 2R_e$ are obtained at the SRCCSD(T)/UHF level (i.e. using SRCCSD(T) with

Table 1. A comparison of the SSCCSD(T) energies (in hartree) with FCI, CCSD/RHF, CCSD/UHF, CCSD+T(CCSD)/RHF, CCSD(T)/RHF, and CCSD(T)/UHF results for the CO molecule at the equilibrium ($R = R_e$) and stretched bond lengths R obtained with double zeta (DZ) basis set. In all correlated calculations, the lowest two core orbitals and the highest two virtual orbitals were kept frozen. Δ is the difference with the FCI result.

Method	$R = R_e$[a]	$R = 1.5R_e$	$R = 2.0R_e$
RHF	−112.685 05	−112.439 21	−112.314 40
UHF	−112.685 05	−112.453 83	−112.413 90
SRCCSD/RHF	−112.886 14	−112.715 10	−112.468 51
SRCCSD/UHF	−112.886 14	−112.723 59	−112.609 17
SRCCSD+T(CCSD)	−112.896 10	−112.785 83	−112.480 26
SRCCSD(T)/RHF	−112.893 73	−112.746 15	−112.478 08
SRCCSD(T)/UHF	−112.893 73	−112.745 22	−112.672 25
FCI	−112.895 09	−112.749 93	−112.627 56
SSCCSD(T1)[b]	**−112.892 28**	**−112.744 96**	**−112.635 69**
Δ SRCCSD(T)/RHF	**0.001 4**	**0.003 8**	**0.149 5**
Δ SRCCSD(T)/UHF	**0.001 4**	**0.004 7**	**−0.044 7**
Δ SSCCSD(T)/RHF	**0.002 8**	**0.005 0**	**−0.008 1**

[a] R_e = 2.132 bohr.
[b] SSCCSD(T) calculations with four-hole and four-particle active space consisting of valence π_x, π_y, π_x^* and π_y^* orbitals.

Table 2. A comparison of the FCI, CCSD, SSCCSD(T) and SSCCSD(TQ) energies (au) for C_2 at equilibrium (R_e)[a] and stretched bond length ($1.5R$) obtained with double zeta (DZ) basis set. The lowest two occupied and the highest two virtual orbitals were kept frozen. Δ is the difference with the FCI result.

	$R = R_e$	$R = 1.5R_e$
RHF	−75.356 48	−75.202 68
SRCCSD	−75.621 18	−75.482 24
SSCCSD(T1)[b]	**−75.631 80**	**−75.502 95**
SSCCSD(TQ1)[c]	**−75.633 22**	**−75.506 58**
SSCCSD(T2)[d]	**−75.638 44**	**−75.504 33**
SSCCSD(TQ2)[e]	**−75.639 77**	**−75.508 86**
FCI	−75.641 86	−75.518 41
ΔSRCCSD	0.020 7	0.036 2
ΔSSCCSD(T1)	**0.010 1**	**0.015 5**
ΔSSCCSD(TQ1)	**0.008 6**	**0.011 8**
ΔSSCCSD(T2)	**0.003 4**	**0.014 1**
ΔSSCCSD(TQ2)	**0.002 1**	**0.009 6**

[a] R_e = 2.348 au.
[b] SSCCSD(T) calculations with four-hole four-particle active space (π_{ux}, π_{uy}, π_{gx} and π_{gy}).
[c] SSCCSD(TQ) calculations with four-hole four-particle active space (π_{ux}, π_{uy}, π_{gx} and π_{gy}).
[d] SSCCSD(T) calculations with six-hole six-particle active space (σ_g, π_{ux}, π_{uy}, σ_u, π_{gx} and π_{gy}).
[e] SSCCSD(TQ) calculations with six-hole six-particle active space (σ_g, π_{ux}, π_{uy}, σ_u, π_{gx} and π_{gy}).

the UHF reference), but this is achieved at the expense of not providing a pure spin state. Moreover, the error in the SRCCSD(T)/UHF result (*ca.* 45 millihartree) is still rather large. This is an important observation in view of the popularity of the UHF-based SRCCSD(T) approach.

The SSCCSD(T) method with four-hole and four-particle active space (using only the π and π^* valence orbitals) performs much better and gives only 8.1 millihartree error at $R = 2R_e$ in spite of using the RHF reference. Since three bonds dissociate in CO when the internuclear distance increases, a more accurate description of the process requires larger active space and, probably, the SSCCSD(TQ) level of theory. It is very encouraging to observe that the simplest SSCCSD(T) method using 'minimal' active space performs so well. The resulting wave function is not spin-contaminated as in the SRCCSD(T)/UHF case.

We examine the contribution of the quadruple excitations in calculations for the C_2 molecule in the results presented in table 2. For this system the appropriate active space should contain either four holes and four particles (π_{ux}, π_{uy} and π_{gx}, π_{gy}) or six holes and six particles (σ_g, π_{ux}, π_{uy} and σ_u, π_{gx}, π_{gy}). At the bottom of the table one again can find differences between the total energy provided by the particular SSCC method and the FCI results. These differences systematically decrease when the active space is enlarged and when quadruple excitations are included in the calculations. Also, upon examining the last four rows in the table one sees that including the quadruple excitations makes the energy slope more parallel to the slope obtained with FCI.

4. Conclusions

The SSMRCC method is still in the development stage. Not only the performance of this method in terms of reproducing the FCI results, but also its convergence properties and effectiveness in practical applications will decide about its usefulness in theoretical calculations. At this stage, one can already see that the behaviour of the SSCCSD(T) method is better than in the case of the very popular SRCCSD(T) method even when the latter method uses the UHF reference. We plan to implement the SSMRCC method based on the semi-linear ansatz. We believe that this approach when coupled with the CASSCF method will provide a practical and well converging scheme to generate very accurate results for excited states, as well as for dissociating systems.

This study has been supported by the National Science Foundation under grant No. CHE-9300497. Two of us (L.A. and P.P.) would like to thank Professor Rodney J. Bartlett for inviting them to speak at the 'Coupled Cluster Theory and Electron Correlation' workshop.

References

[1] Coester, F., 1958, *Nucl. Phys.*, **7**, 421; Coester, F., and Kümmel, H., 1960, *ibid.* **17**, 477; Čížek, J., 1966, *J. Chem. Phys.* **45**, 4256; 1969, *Adv. Chem. Phys.* **14**, 35; Čížek, J., and Paldus, J., 1971, *Int. J. Quantum Chem.* **5**, 359; Paldus, J., Čížek, J., and Shavitt, I., 1972, *Phys. Rev.* A **5**, 50.

[2] Bartlett, R. J., 1981, *Ann. Rev. phys. Chem.*, **32**, 359; 1989; *J. phys. Chem.*, **93**, 1697.

[3] Paldus, J., 1981, *Diagrammatic Methods for Many-Fermion Systems* (Holland: University of Nijmegen); Bartlett, R. J., Dykstra, C. E., and Paldus, J., 1984, *Advanced Theories and Computational Approaches to the Electronic Structure of Molecules*, edited by C. E. Dykstra (Dordrecht: Reidel, 1984), pp. 127–159; Paldus, J., 1983, *New Horizons of Quantum Chemistry*, edited by P.-O. Löwdin and B. Pullman (Dordrecht, Reidel), pp. 31–60; Paldus, J., 1992, *Methods in Computational Molecular Physics*, Vol. 293, NATO Advanced Study Institute, Series B: Physics, edited by S. Wilson and G. H. F. Diercksen (New York, Plenum), pp. 99–194.

[4] Purvis III, G. D., and Bartlett, R. J., 1982, *J. chem. Phys.*, **76**, 1910; Trucks, G. W., Noga, J., and

BARTLETT, R. J., 1988, *Chem. Phys. Lett.*, **145,** 548; STANTON, J. F., GAUSS, J., WATTS, J. D., and BARTLETT, R. J., 1991, *J. chem. Phys.*, **94,** 4334; NOGA, J., and BARTLETT, R. J., 1987, *J. chem. Phys.*, **86,** 7041; 1988, *ibid.*, **89,** 3401 (Erratum).

[5] SCUSERIA, G. E., LEE, T. J., and SCHAEFER III, H. F., 1986, *Chem. Phys. Lett.*, **130,** 236; LEE, T. J., and RICE, J. E., 1988, *ibid.*, **150,** 406; SCUSERIA, G. E., JANSSEN, C. L., and SCHAEFER III, H. F., 1988, *J. chem. Phys.*, **89,** 7382; SCUSERIA, G. A., and SCHAEFER III, H. F., 1988, *Chem. Phys. Lett.*, **152,** 382.

[6] CHILES, R. A., and DYKSTRA, C. E., 1981, *J. chem. Phys.*, **74,** 4544; DYKSTRA, C. E., and AUGSPURGER, J. D., 1988, *Chem. Phys. Lett.*, **145,** 545.

[7] NOGA, J., KELLÖ, V., and URBAN, M., 1985, Comenius Technical Report, Comenius University, Bratislava.

[8] MONKHORST, H. J., 1977, *Int. J. quantum Chem. Symp.*, **11,** 421; KONDO, A. E., PIECUCH, P., and PALDUS, J., 1995, *J. chem. Phys.*, **102,** 6511 (1995); 1996, *ibid.*, **104,** 8566; PIECUCH, P., and PALDUS, J., 1997, *J. Math. Chem.*, **21,** 51.

[9] HELGAKER, T., and JØRGENSEN, P., 1992, *Methods in Computational Molecular Physics*, edited by S. Wilson and G. Direcksen (New York: Plenum); JØRGENSSEN, P., and HELGAKER, T., 1988, *J. chem. Phys.*, **89,** 1560; KOCH, H., and JØRGENSEN, P., 1990, *J. chem. Phys.*, **93,** 3333.

[10] JØRGENSEN, P., and SIMONS, J., 1983, *J. chem. Phys.*, **79,** 334; BARTLETT, R. J., 1986, *Geometrical Derivatives of Energy Surfaces and Molecular Properties*, Vol. 166, NATO Advanced Study Institute, Series C: Mathematical and Physical Sciences, edited by P. Jørgensen and J. Simons (Dordrecht: Reidel), pp. 35–61.

[11] ADAMOWICZ, L. A., LAIDIG, W. D., and BARTLETT, R. J., 1984, *Int. J. quantum Chem. Symp.*, **18,** 245.

[12] FITZGERLAD, G., HARRISON, R. J., and BARTLETT, R. J., 1986, *J. chem. Phys.*, **85,** 5143.

[13] SCHEINER, A. C., SCUSERIA, G. E., RICE, J. E., LEE, T. J., and SCHAEFER III, H. F., 1987, *J. chem. Phys.*, **87,** 5361.

[14] HANDY, N. C., and SCHAEFER III, H. F., 1984, *J. chem. Phys.*, **81,** 5031.

[15] NOGA, J., and URBAN, M., 1988, *Theor. Chim. Acta*, **73,** 291; BARTLETT, R. J., and NOGA, J., 1988, *Chem. Phys. Lett.*, **150,** 29; URBAN, M., DIERCKSEN, G. H. F., SADLEJ, A. J., and NOGA, J., 1990, *Theor. Chim. Acta*, **77,** 29; WATTS, J. D., TRUCKS, G. W., and BARTLETT, R. J., 1989, *Chem. Phys. Lett.*, **157,** 359.

[16] SLATER, E. A., TRUCKS, G. W., and BARTLETT, R. J., 1989, *J. chem. Phys.*, **90,** 1752; SALTER, E. A., and BARTLETT, R. J., 1989, *ibid.*, **90,** 1767; SEKINO, H., and BARTLETT, R. J., 1984, *Int. J. quantum Chem. Symp.*, **18,** 255; SEKINO, H., and BARTLETT, R. J., 1986, *J. chem. Phys.*, **84,** 2726; SALTER, E. A., SEKINO, H., and BARTLETT, R. J., 1987, *J. chem. Phys.*, **87,** 502.

[17] PAL, S., 1986, *Phys. Rev.* A, **33,** 2240; GHOSE, K. B., and PAL, S., 1992, *ibid.*, **45,** 1518; PAL, S., 1990, *Phys. Rev.* A, **42,** 4385; GHOSE, K. B., NAIR, P. G., and PAL, S., 1993, *Chem. Phys. Lett.*, **211,** 15; PAL, S., and GHOSE, K. B., 1992, *Current Sci.*, **63,** 667; PAL, S., 1986, *Phys. Rev.* A, **34,** 2682; GHOSE, K. B., and PAL, S., 1987, *ibid.*, **36,** 1539; PAL, S., 1989, *ibid.*, **39,** 2712; VAVAL, N., GHOSE, K. B., and PAL, S., 1994, *J. chem. Phys.*, **101,** 4914; GHOSE, K. B., 1995, *Int. J. quantum Chem.*, **53,** 275.

[18] KOCH, H., JENSEN, H. J. AA., JØRGENSEN, P., HELGAKER, T., SCUSERIA, G. E., and SCHAEFER III, H. F., 1990, *J. chem. Phys.*, **92,** 4924; KOBAYASHI, R., KOCH, H., and JØRGENSEN, P., 1994, *ibid.*, **101,** 4956.

[19] JEZIORSKI, B., and PALDUS, J., 1989, *J. chem. Phys.*, **90,** 2714.

[20] LINDGREN, I., and MUKHERJEE, D., 1987, *Phys. Rep.*, **151,** 93.

[21] MUKHERJEE, D., and PAL, S., 1989, *Adv. quantum Chem.*, **20,** 291.

[22] JEZIORSKI, B., and MONKHORST, H. J., 1981, *Phys. Rev.* A, **24,** 1668.

[23] JEZIORSKI, B., and PALDUS, J., 1988, *J. chem. Phys.*, **88,** 5673; LAIDIG, W. D., SAXE, P., and BARTLETT, R. J., 1987, *J. chem. Phys.*, **86,** 887; MEISSNER, L., JANKOWSKI, K., and WASILEWSKI, J., 1988, *Int. J. quantum Chem.*, **34,** 535; MEISNER, L., KUCHARSKI, S. A., and BARTLETT, R. J., 1987, *J. chem. Phys.*, **91,** 6187; MEISNER, L., and BARTLETT, R. J., 1990, *J. chem. Phys.*, **92,** 561; KUCHARSKI, S. A., and BARTLETT, R. J., 1991, *J. chem. Phys.*, **95,** 8227; PALDUS, J., PYLYPOW, L., and JEZIORSKI, B., 1989, *Many-Body Methods in Quantum Chemistry*, Vol. 52 of Lecture Notes in Chemistry, edited by U. Kaldor (Berlin: Springer), p. 151; PIECUCH, P., and PALDUS, J., 1992, *Theor. Chim. Acta*, **83,** 69; BALKOVÁ, A., KUCHARSKI, S. A., MEISSMER, L., and BARTLETT, R. J., 1991, *Theor. Chim. Acta*, **80,** 335; PALDUS, J., PIECUCH, P., JEZIORSKI, B., and PYLYPOW, L., 1992, *Recent Progress in Many-Body Theories*, Vol. 3, edited by T. L. Ainsworth, C. E. Campbell, B. E. Clements,, and E. Krotschek (New York: Plenum), p. 287; KUCHARSKI, S. A., BALKOVÁ, A., SZALAY, P. G., and BARTLETT, R. J., 1992, *J. chem. Phys.*, **97,** 4289; PALDUS, J., PIECUCH, P., PYLYPOW, L., and JEZIORSKI, B., 1993, *Phys. Rev.* A, **47,** 2738; PIECUCH, P., TOBOŁA, R., and PALDUS, J., 1993, *Chem. Phys. Lett.*, **210,** 243; PIECUCH, P., and PALDUS, J., 1994, *Phys. Rev.* A, **49,** 3479; PIECUCH, P., and PALDUS, J., 1994, *J. chem. Phys.*, **101,** 5875; PIECUCH, P., and PALDUS, J., 1995, *J. phys. Chem.*, **99,** 15354.

[24] HARRIS, F. E., 1977, *Int. J. quantum Chem. Symp.*, **11,** 403.

[25] PALDUS, J., ČÍŽEK, J., SAUTE, M., and LAFORGUE, A., 1978, *Phys. Rev.* A, **17,** 805; SAUTE, M., PALDUS, J., and ČÍŽEK, J., 1979, *Int. J. quantum Chem.*, **15,** 463.

[26] NAKATSUJI, H., 1978, *Chem. Phys. Lett.*, **59,** 362; 1979, *ibid.*, **67,** 329; NAKATSUJI, H., and HIRAO, K., 1978, *J. chem. Phys.*, **68,** 2053, 4279; NAKATSUJI, H., 1983, *Int. J. quantum Chem. Symp.*, **17,** 241; 1985, *J. chem. Phys.*, **83,** 713; 1991, *J. chem. Phys.*, **95,** 4296; 1992, *Acta Chim. Hung.*, **129,** 719.

[27] BANERJEE, A., and SIMONS, J., 1981, *Int. J. quantum Chem.*, **19,** 207; 1982, *J. chem. Phys.*, **76,** 4548.

[28] BAKER, H., and ROBB, M. A., 1983, *Molec. Phys.*, **50,** 20.

[29] TANAKA, R., and TERASHIMA, H., 1984, *Chem. Phys. Lett.*, **106,** 558.

[30] HOFFMAN, M. R., and SIMONS, J., 1988, *J. chem. Phys.*, **88,** 993.

[31] PALDUS, J., and LI, X., 1993, *Symmetries in Science VI*, edited by B. Gruber (New York: Plenum), p. 573; LI, X., and PALDUS, J., 1993, *Int. J. quantum Chem. Symp.*, **27,** 269; 1994, *J. chem. Phys.*, **101,** 8812.

[32] (a) GEERTSEN, J., RITTBY, M., and BARTLETT, R. J., 1989, *Chem. Phys. Lett.*, **164,** 57; STANTON, J. F., and

BARTLETT, R. J., 1993, *J. chem. Phys.*, **98,** 7029; COMEAU, D. C., and BARTLETT, R. J., 1993, *Chem. Phys. Lett.*, **207,** 414; BARTLETT, R. J., and STANTON, J. F., 1994, *Rev. Comp. Chem.*, **5,** 65; NOOIJEN, M., and BARTLETT, R. J., 1995, *J. chem. Phys.*, **102,** 3629; NOOIJEN, M., and BARTLETT, R. J., 1995, *J. chem. Phys.*, **102,** 6735; (b) NOOIJEN, M., and BARTLETT, R. J., 1997, *J. chem. Phys.*, **106,** 6441.

[33] OLIPHANT, N., and ADAMOWICZ, L., 1991, *J. chem. Phys.*, **94,** 1229; OLIPHANT, N., and ADAMOWICZ, L., 1992, *J. chem. Phys.*, **96,** 3739.

[34] PIECUCH, P., OLIPHANT, N., and ADAMOWICZ, L., 1993, *J. chem. Phys.*, **99,** 1875; OLIPHANT, N., and ADAMOWICZ, L., 1993, *Int. Rev. Phys. Chem.*, **12,** 339.

[35] PIECUCH, P., and ADAMOWICZ, L., 1994, *J. chem. Phys.*, **100,** 5792; PIECUCH, P., and ADAMOWICZ, L., 1994, *Chem. Phys. Lett.*, **221,** 121.

[36] OLIPHANT, N., and ADAMOWICZ, L., 1992, *Chem. Phys. Lett.*, **190,** 13; PIECUCH, P., and ADAMOWICZ, L., 1994, *J. chem. Phys.*, **100,** 5857.

[37] GHOSE, K. B., and ADAMOWICZ, L., 1995, *J. chem. Phys.*, **103,** 9324.

[38] GHOSE, K. B., PIECUCH, P., and ADAMOWICZ, L., 1995, *J. chem. Phys.*, **103,** 9331.

[39] ADAMOWICZ, L., and MALRIEU, J.-P, 1996, *J. chem. Phys.*, **105,** 9240.

[40] ADAMOWICZ, L., CABALLOL, R., MALRIEU, J.-P., and MELLER, J., 1996, *Chem. Phys. Lett.*, **259,** 619.

[41] DAUDEY, J.-P., HUELLY, J.-L., and MALRIEU, J.-P., 1990, *J. chem. Phys.*, **99,** 1240.

[42] MALRIEU, J.-P., DAUDEY, J.-P., and CABALLOL, R., 1994, *J. chem. Phys.*, **101,** 8908.

[43] ROOS, B. O., 1992, *Lecture Notes in Quantum Chemistry*, Vol. 58, edited by B. O. Roos (Berlin: Springer), p. 177.

[44] MALRIEU, J.-P., DURAND, PH., and DAUDEY, J.-P., 1985, *J. Phys. A*, **18,** 809.

[45] ALEXANDROV, V., PIECUCH, P., and ADAMOWICZ, L., 1995, *J. chem. Phys.*, **102,** 3301.

[46] RAGHAVACHARI, K., TRUCKS, G. W., POPLE, J. A., and HEAD-GORDON, M., 1989, *Chem. Phys. Lett.*, **157,** 479.

MOLECULAR PHYSICS, 1998, VOL. 94, NO. 1, 235–248

Externally corrected singles and doubles coupled cluster methods for open-shell systems. II. Applications to the low lying doublet states of OH, NH_2, CH_3 and CN radicals

By G. PERIS†, F. RAJADELL†, X. LI‡, J. PLANELLES† and J. PALDUS†‡§

† Departament de Ciències Experimentals, Universitat Jaume I, Apartat 224, E-12080, Castelló, Spain

‡ Department of Applied Mathematics, University of Waterloo, Waterloo, Ontario, Canada N2L 3G1

The externally-corrected singles and doubles coupled cluster (CCSD) method, as implemented for high-spin open shell systems by exploiting the unitary group approach and restricted to the first order interacting space (UGA-CCSD(is)) in Part I (Li, X., *et al.*, 1997, *J. chem. Phys.*, **107**, 90), is applied to several simple radicals in their doublet ground and excited states. The capabilities and limitations of this approach are examined by studying the potential energy surfaces or their suitable cuts involving the dissociation of both single and multiple bonds (OH and CN) or simultaneous dissociation of several single bonds (NH_2 and CH_3). Using low dimensional CAS-FCI and SOCI wave functions for the internal and external active space excitations, it is shown that corrected CCSD energies are superior to the standard ones in all cases, including those obtained with CI spaces of very modest dimension, and are capable of accounting for the presence of higher than pair clusters even in severe cases of quasi-degeneracy.

1. Introduction

In the preceding paper of this series [1] (further referred to as Part I), we have outlined and tested the so-called externally corrected coupled cluster method, restricted to singly and doubly excited cluster amplitudes (CCSD), for open-shell systems, relying on the unitary group approach (UGA-CCSD method) [2–8]. The key idea of any externally corrected CCSD method is based on the fact that the full CC chain of equations can be exactly decoupled at the pair cluster level if we know the 3- and 4-body cluster amplitudes [9–12], assuming that the Hamiltonian involves at most two-body interactions. This idea was first exploited for closed-shell systems in formulating the so-called ACPQ method [9] (approximate coupled pair method with quadruples), which implicitly accounts for connected 4-body clusters T_4 as given by the UHF wave functions of the DODS (different orbitals for different spins) type. An explicit account of these clusters, leading to the so-called CCSDQ' method [13], was achieved only recently. Unfortunately, the UHF wave function of the DODS type for closed-shell systems contains only even-number of times excited clusters. In general, we thus must rely on some easily accessible source of higher than pair clusters when decoupling CCSD equations from the rest of the CC chain, rather than neglecting these clusters altogether as is done when deriving the standard CCSD method. This is particularly important in quasi-degenerate situations that are invariably encountered when we examine systems that are far away from their equilibrium geometry. In such cases we must rely on a suitable, yet computationally easily accessible, wave function that is capable of describing the dissociation or association process under consideration and can provide a reasonable approximation of both T_3 and T_4 cluster components.

In our first attempt exploring the potential of the externally corrected CCSD approach we have used for this purpose a valence bond wave function [10, 11] and the semi-empirical Pariser–Parr–Pople (PPP) π-electron model systems. Later, we employed the complete active space (CAS) SCF wave functions, examining simple *ab initio* models [12]. In Part I of this series we applied this approach to open-shell systems at the *ab initio* level, while exploring CAS-SCF, CAS-FCI, as well as some limited CI wave functions as a source of the 3- and 4-body cluster amplitudes.

§ Also at: Department of Chemistry and $(GWC)^2$—Waterloo Campus, University of Waterloo, Waterloo, Ontario, Canada N2L 3G1.

0026–8976/98 $12·00

In general, the approximate 3- and 4- body clusters $T_3^{(0)}$ and $T_4^{(0)}$, respectively, obtained by the cluster analysis of a suitable wave function, generate corrections to both the absolute and linear terms of the resulting externally corrected CCSD equations, the latter arising from the disconnected $T_1 T_3^{(0)}$ term. As explained in Part I, this term can be treated in either an iterative or a non-iterative way, the latter one representing an additional approximation in which we use the external $T_1^{(0)}$ clusters in the $T_1 T_3^{(0)}$ term, thus replacing it by $T_1^{(0)} T_3^{(0)}$. In this way all corrections simply modify the absolute term of standard CCSD equations, or UGA-CCSD(is) equations in our case. Since the non-iterative treatment of the $T_1 T_3$ term leads, generally, to only a few microhartree error in the energy [1], we use it throughout.

We have also shown in Part I that the type of MOs (ROHF versus CAS-SCF) that are employed is of little importance. Moreover, very similar results are obtained when using the CAS-SCF and CAS-FCI wave functions to generate the external $T_3^{(0)}$ and $T_4^{(0)}$ (and/or $T_1^{(0)}$ for the $T_1 T_3$ term) corrections, although the latter wave function requires less computational effort (roughly one CAS-SCF iteration). All active spaces employed in Part I are rather small. Obviously, the external sources, such as CAS-SCF, CAS-FCI, or limited CIs within the active space, that were used in Part I, can only generate 3- and 4-body connected clusters with all labels restricted to active orbitals, i.e. active space T_3 and T_4. To get more extensive information about the T_3 and T_4 clusters, we would have to employ larger active spaces. For larger systems, however, the use of CAS-SCF or CAS-FCI as an external source for corrections is computationally too demanding and it is worthwhile exploring more affordable schemes relying on other CI-type wave functions. As the first step in this direction, we divide the extended set of active orbitals into the two disjoint subsets of the so-called internal and external active orbitals. We then consider CAS-FCI for internal active orbitals, which will guarantee the correct description of the studied dissociation channel, and account for the effect of the remaining correlating external active orbitals via the second order CI (SOCI). This results in an affordable scheme, requiring CI wave functions of relatively modest dimension, while providing 3- and 4-body corrections of roughly the same quality as the CAS-FCI or CAS-SCF schemes with the extended active space (AS) consisting of both internal and external active orbitals.

In this paper we thus employ as the external source for the $T_3^{(0)}$ and $T_4^{(0)}$ clusters a CI-type wave function obtained by performing FCI within the AS defined by the internal active orbitals (i-CAS-FCI), followed by the second order CI involving single and double excitations into the external active orbital set (e-SOCI). To explore the performance of this scheme in various situations involving stretching or breaking of one or more single bonds, or of a single multiple bond, we examine double zeta (DZ) and DZ plus polarization (DZP) models of the ground and some excited states of the OH, NH_2, CH_3, and CN radicals. After briefly outlining the method employed and computational details in sections 2 and 3, we present and discuss our results in section 4 and draw appropriate conclusions in section 5.

2. Method

We employ the externally corrected UGA-CCSD(is) method, described in Part I and relying on general ideas exposed in [10–12]. However, in contrast to Part I, where we employed as an external source the CAS-FCI or CAS-SCF wave functions, we now exploit the computationally less demanding CI procedure, requiring considerably smaller CI spaces.

The key idea of the externally corrected CCSD methods stems from the fact that our Hamiltonian involves at most two-body potentials, so that CC equations corresponding to projections onto the singly and doubly excited configuration state functions (CSFs) involve at most 3- and 4-body cluster amplitudes. These higher than pair cluster amplitudes are neglected when deriving the standard CCSD equations by decoupling the full CC chain at the double excitation level. However, it is precisely these higher than pair clusters that become important in quasi-degenerate situations. Unfortunately, the reference state of standard CC procedures cannot usually properly describe such situations, particularly the dissociation channels involving open-shell fragments. Such a description can be, however, often achieved with a relatively simple multiconfigurational wave function. It is thus possible to use such a wave function as a source of the required 3- and 4-body clusters, and thus to achieve a more appropriate decoupling of the CC chain at the pair cluster level. Thus, by cluster analysing the chosen external wave function we compute $T_3^{(0)}$ and $T_4^{(0)}$ cluster components and subsequently use them to correct the absolute (and possibly the linear) terms of the standard CCSD approach [10–12].

In Part I, this idea was exploited for open-shell systems by relying on the recently developed UGA-CCSD(is) method and appropriate codes [2–8]. This paper employs the same procedure and software, except that we now rely on a computationally less demanding external source. Instead of using the standard CAS-FCI or CAS-SCF procedure, in which one employs a relatively small set of orbitals as the active ones, we use an extended active orbital set, which is subdivided into the subsets of the so-called internal

and external active orbitals, as already stated above. We then consider CAS-FCI within the internal active space only (i-CAS-FCI), followed by the second order CI involving the external part of the active orbital space (e-SOCI). We shall see that this procedure requires CI of a much smaller dimension than the standard CAS-FCI method, in which all the correlated orbitals are in the active orbital space, while providing the 3- and 4-body cluster amplitudes of approximately the same quality. Thus, when specifying the active orbital space we distinguish between the internal and external active orbitals.

When computing $T_3^{(0)}$ and $T_4^{(0)}$ corrections to CCSD equations, we always get a contribution to the absolute term, except when accounting for the $T_1T_3^{(0)}$ term, which modifies the coefficients at the singly excited cluster amplitudes in the linear terms. It was shown in Part I, however, that a non-iterative treatment of this term, obtained by replacing the CCSD T_1 clusters by the approximate $T_1^{(0)}$ clusters (which are a byproduct of the cluster analysis of the external wave function yielding $T_3^{(0)}$ and $T_4^{(0)}$ clusters), leads to only a very minor change in the resulting energies (usually at a microhartree level). Thus, in all calculations presented here we employ this non-iterative T_1T_3 correction scheme.

Finally, we must mention the procedure that is employed to compute $T_3^{(0)}$ and $T_4^{(0)}$ corrections. The codes that are employed in this paper treat both cluster components in a slightly different manner. For quadruples, we simply compute t_4-amplitudes that are involved in our CI wave function and evaluate their contribution to the absolute term of UGA-CCSD(is) equations. In contrast, for the triply excited cluster components we consider all possible t_3-amplitudes, even when they are not present in the external CI wave function. Assuming, then, that those not present in the CI wave function will have a negligible weight in the external wave function (i.e. $C_3 = 0$ in such cases), we compute corresponding $T_3^{(0)}$ corrections for all triple amplitudes. While this set of codes was used to generate the results presented in this paper, we have now designed a new set of codes that simply assumes that $T_3 = 0$ when the corresponding C_3 is not available. In this way, both T_3 and T_4 amplitudes are treated on the same level. Clearly, this new version is computationally more efficient and will be systematically used in the future. The differences between both versions, at least when used with an active space (AS) of a reasonable size, are less than a millihartree in all cases we examined.

3. Computational details

The ROHF, CAS-SCF, CAS-CI and SOCI calculations providing the external source for the corrections are obtained using the GAMESS system of programs [14]. The UGA-CCSD(is) [2–8], the cluster analysis and computation of corrections to CCSD(is) are carried out using our own codes [1, 11].

Concerning the basis sets, at the double zeta (DZ) level we use the 2s contractions of Huzinaga's 4s primitive set [15] scaled by the factor of 1.2 for the H atom, and Dunning's 4s2p contraction [16] of Huzinaga's 9s5p primitive sets [15] for the C, N and O atoms. For DZ plus polarization (DZP) bases we use the following exponents for the polarization functions: $\alpha_{3d}(C) = 0.51$, $\alpha_{3d}(N) = 0.9$, and $\alpha_{3d}(O) = 0.8$. For hydrogen, we use $\alpha_{2p}(H) = 0.8$ for NH_2 and $\alpha_{2p}(H) = 1.0$ for OH and CH_3. This choice enables us to use some of the existing full CI (FCI) benchmarks [17, 18].

For the $^2\Pi$ state of OH, we use for the equilibrium bond length $R_e = 1.832$ bohr. At the DZP level, we employ Cartesian Gaussians (all six components) and freeze 1s core orbital as well as the corresponding 1s* virtual orbital in all calculations.

For NH_2, both the $^2A_1$ and $^2B_1$ states are considered, using the geometries as well as the benchmark FCI values of [17]. In these calculations, only the nitrogen 1s orbital is frozen, while the corresponding virtual 1s* orbital is correlated.

For CH_3, we examine the $^2A_2''$ ground state, taking for the equilibrium bond length $R_e = 2.06$ bohr as in [18]. Again, all virtual orbitals are correlated, unless a restricted AS is used.

Finally, we chose the $^2\Sigma^+$ and $^2\Pi$ states of CN to examine the stretching of a multiple bond. We employ experimental bond lengths for these states, namely $R_e = 1.1718$ and 1.2333 Å, respectively. In all correlated calculations the 1s orbitals, as well as the corresponding 1s* virtual orbitals of both C and N, are frozen.

Other computational details concerning these systems may be found in [7]. However, in contrast to this paper, we employ all six 3d Cartesian components in all considered cases. For this reason, the CCSD(is) energies for NH_2 and CH_3 at the DZP level given here slightly differ from those of [7].

4. Results and discussion

An accurate description of bond breaking or formation is a challenging problem for any quantum chemical method. This is particularly the case for single reference (SR) CC approaches. It is well known, for example, that the spin–orbital or closed-shell CCSD(T) [19] or CCSD[T] [20] approaches yield excellent results for near equilibrium geometries (as well as for the dissociation energies; cf. e.g. [21]), but invariably fail away from equilibrium in view of their perturbative nature (see, e.g. figure 4 of [22]). In general, breaking of a chemical bond

requires a multi-reference description, and any SR approach will thus involve highly excited cluster components or the corresponding CSFs. However, approximating the higher than pair clusters by extracting them from a suitable external source can substantially extend the excellent performance of CCSD to systems involving highly stretched geometries, as will be illustrated by the following examples.

For all the studied systems, we first present the results obtained with a DZ basis set, where a comparison with the exact or nearly exact FCI results is always possible, followed by realistic DZP results. We will present and discuss the studied systems in order of increasing complexity.

4.1. *Stretching of a single bond*

We employ the $^2\Pi$ state of the OH radical as a model of a single bond stretching. This system was already examined in considerable detail in Part I, where we employed both CAS-SCF and CAS-FCI wave functions as the external source for T_3 and T_4 corrections.

For both DZ and DZP basis sets employed, the ROHF MOs can be labelled as follows†

$$O_{1s}O_{2s}\sigma_{OH}O_{2p_x}O_{2p_y}\sigma^*_{OH}O_{2p'_y}O_{2p'_x}O_{2p'_z}H_{1s^*}O_{2s^*}\mathcal{P}O_{1s^*}, \tag{1}$$

where $\mathcal{P}$ designates the polarization orbitals, so that $\mathcal{P} = \varnothing$ (an empty set) for DZ basis, while

$$\mathcal{P} = H_{2p'_x}H_{2p'_y}H_{2p'_z}O_{3d_1}O_{3d_2}O_{3d_3}O_{3d_4}O_{3d_5}O_{3d_6} \tag{2}$$

for a DZP basis. The orbital ordering given above corresponds to $R = 2R_e$ and may change as the bond is stretched or contracted. The lowest occupied (O_{1s}) and the highest unoccupied (O_{1s^*}) orbitals are kept frozen in all calculations. The corresponding (complete) active space (AS) involving all the (non-frozen) orbitals and yielding the FCI results is designated as the zeroth active space, AS0, while various truncated active subspaces are labelled by ASn, $n = 1, 2, 3, \ldots$. In the present case, (O_{1s}) and (O_{1s^*}) are always frozen, so that we have 7 active electrons (i.e. all the valence electrons) occupying four orbitals O_{2s}, σ_{OH}, O_{2p_x} and O_{2p_y}, which are always included in the (internal) active space and are referred to as occupied MOs. The correlating virtual orbitals that are included in the active space are subdivided into the two subsets of the so-called internal and external active orbitals. In specifying various truncated active spaces ASn, ($n > 0$), we only list the pertinent virtual orbitals, separating the internal and external ones by a double slash. The occupied and internal active virtual orbitals then define the i-CAS-FCI (full configuration interaction involving the complete internal active space orbitals) space, which is then extended by considering the second-order interacting space involving the external active virtual orbitals (e-SOCI). For the OH radical, the following active spaces are considered (in addition to AS0):

$$\begin{aligned}
&\text{AS1}: [\sigma^*_{OH}//O_{2p'_y}O_{2p'_x}O_{2p'_z}H_{1s^*}O_{2s^*}\mathcal{P}],\\
&\text{AS2}: [\sigma^*_{OH}//O_{2p'_y}O_{2p'_x}O_{2p'_z}H_{1s^*}O_{2s^*}],\\
&\text{AS3}: [\sigma^*_{OH}//O_{2p'_y}O_{2p'_x}O_{2p'_z}H_{1s^*}],\\
&\text{AS4}: [\sigma^*_{OH}//O_{2p'_y}O_{2p'_x}O_{2p'_z}].
\end{aligned} \tag{3}$$

For a DZ basis, where $\mathcal{P} = \varnothing$, AS1 ≡ AS2. The dimension of these spaces is always given together with the energetic information (cf. tables 1 and 2). The dimension of the CCSD approach is the same in each case and, at the DZ level equals 113 and at the DZP level to 541.

The resulting total energies as well as the differences relative to the FCI benchmark, representing the exact solution for a given basis set, are listed in tables 1 and 2 for the DZ and DZP basis sets, respectively. The last column in these tables gives the so-called non-parallelism error (NPE), which is defined as the difference between the maximal and minimal positive deviations from the FCI potential energy curve (PEC) (or, should the computed and FCI PECs intersect, as the sum of absolute values of the maximal positive and negative deviations from the FCI PEC). Although we generate only a few points on the PEC (usually $R = R_e$, $R = 1.5R_e$ and $R = 2R_e$), so that the NPE given in our tables is based on this limited information, it nonetheless characterizes the 'parallelism' of the approximate and FCI PECs over the examined interval of internuclear separations, since these curves are smooth and seldom intersect (and if so, then only once). Clearly, if both PECs are 'parallel', i.e. if they differ by a constant energy shift, we have that NPE ≡ 0.

The DZ results given in table 1 clearly indicate that in each case the corrected CCSD method represents an improvement over the standard CCSD(is) one. Already for the smallest AS4 of dimension 268 we find a significant improvement in CCSD energies relative to FCI, particularly for stretched geometries. Correspondingly,

† The molecular orbital labelling employed emphasizes the atomic site on which the atomic orbital having the highest weight is localized by listing first the atomic label. The type of the orbital (1s, 2s, etc.) is then given as a subscript. The unoccupied orbitals in the reference are starred. For the bonding orbitals of the sigma type we either give the atomic labels as subscript or, in the case of orbitals involving more than two centres (as in CH_3), we simply indicate the main component by the single atomic label (e.g. σ_H for the orbital involving hydrogen AOs in CH_3 that is symmetric with respect to the H_3 plane).

Table 1. The total energies E, reported as $-(E+75)$ hartree, and the energy differences ΔE (in millihartree) relative to the exact FCI ≡ CI(AS0) energy, for the $^2\Pi$ state of the OH radical, obtained with a DZ basis set and various externally corrected as well as standard CCSD(is) methods for the three internuclear separations ($R_e = 1.832$ bohr). The dimension of the CI spaces used for the external corrections is given in the second column and the NPE (see the text) in the last column.

		$-(E+75)$ (hartree)			ΔE (mhartree)			
Method	Dim	R_e	$1.5R_e$	$2R_e$	R_e	$1.5R_e$	$2R_e$	NPE
CI(AS0)	3460	0.481 22	0.423 69	0.372 76	0	0	0	0
CCSD-AS2		0.480 51	0.422 61	0.372 62	0.71	1.08	0.14	0.94
CI(AS2)	656	0.478 23	0.420 36	0.369 52	3.00	3.34	3.24	0.34
CCSD-AS3		0.480 46	0.422 09	0.371 26	0.76	1.60	1.50	0.84
CI(AS3)	441	0.457 85	0.398 72	0.346 88	23.38	24.97	25.88	2.51
CCSD-AS4		0.480 47	0.421 79	0.370 44	0.75	1.90	2.32	1.57
CI(AS4)	268	0.439 83	0.391 19	0.339 83	41.40	32.50	32.93	8.90
CCSD(is)	113	0.480 03	0.420 99	0.367 11	1.20	2.71	5.65	4.45

Table 2. Same as table 1 for DZP basis.

		$-(E+75)$ (hartree)			ΔE (mhartree)			
Method	Dim	R_e	$1.5R_e$	$2R_e$	R_e	$1.5R_e$	$2R_e$	NPE
CI(AS0)	441 792	0.568 02	0.492 10	0.432 65	0	0	0	0
CCSD-AS1		0.566 45	0.490 16	0.430 50	1.56	1.95	2.15	0.59
CI(AS1)	3954	0.554 21	0.478 54	0.419 61	13.81	13.56	13.03	0.77
CCSD-AS2		0.566 09	0.488 42	0.424 09	1.92	3.68	8.56	6.63
CI(AS2)	656	0.488 12	0.419 07	0.362 31	79.90	73.03	70.34	9.56
CCSD-AS3		0.566 10	0.488 16	0.423 21	1.91	3.94	9.44	7.53
CI(AS3)	441	0.468 14	0.400 68	0.343 61	99.88	91.42	89.03	10.85
CCSD-AS4		0.566 05	0.487 84	0.422 85	1.97	4.27	9.80	7.83
CI(AS4)	268	0.462 53	0.393 54	0.339 41	105.48	98.56	93.24	12.24
CCSD(is)	541	0.565 58	0.487 05	0.419 95	2.44	5.05	12.70	10.26

the NPE is reduced by a factor of almost three, from 4.5 to 1.6 mhartree. This desired effect of external corrections gets amplified when we increase the size of the AS, as may be seen by comparing the results for AS2 and AS3. Again, this effect is most pronounced for stretched geometries, as could be expected. Thus, at $R = 2R_e$, we find the difference from the FCI energy to gradually decrease from 5.7 mhartree for standard CCSD(is) to 2.3, 1.5 and 0.14 mhartree for AS4, AS3 and AS2, respectively, while this difference at the equilibrium geometry is much smaller and almost constant for all externally corrected CCSD schemes (0.7–0.8 mhartree versus 1.2 mhartree for standard CCSD(is)).

It should also be noted that in all cases the corrected CCSD energies are significantly closer to FCI than the CAS-CI energies corresponding to the wave function that is used as the source of the 3- and 4-body clusters. Of course, this improvement becomes less significant with the increasing dimension of the AS employed since, ideally, the FCI corrections will yield the exact energies (this is always the case for closed-shell systems [11, 12], while for OS cases considered here a small discrepancy arises due to the approximations involved in the UGA-CCSD(is) method, e.g. the consideration of at most quadratic terms in cluster amplitudes, etc. (see Part I for more details)). In this regard, the NPE values may be deceptive, since they only depend on the relative performance of the method at various geometries. Nonetheless, they serve as a useful guide in general.

At the DZP level, we employed all the active spaces, equation (3), with $\mathcal{P}$ given by (2), as well as AS0 corresponding to FCI (with frozen O_{1s} and O_{1s^*} orbitals). The resulting energies as well as the dimensions of the CI spaces corresponding to ASs, equation (3), are given in table 2. We observe the same pattern in performance of the externally corrected CCSD method as for a smaller DZ basis. The improvement in the energy over the standard CCSD(is) value steadily increases and, correspondingly, the NPE decreases, with the size of the AS employed. However, although the use of the low-dimen-

sional ASs improves the CCSD result by several mhartrees once the bond is stretched, a really significant improvement is only found for a rather large AS1, equation (3), that involves polarization functions, as might be expected. In each case, we find again a very significant improvement over the corresponding SOCI result, which is used as the source of 3- and 4-body corrections for our CCSD.

Before proceeding to the next system, let us briefly compare the above presented results with those obtained earlier in Part I. There we have shown that the CAS-FCI or CAS-SCF correction scheme gives very similar results, the former one being significantly less costly. This led us to investigate various limited CI schemes. These preliminary results indicated that it is preferable to employ even severely limited CI based on a large AS, rather than FCI or even CAS-SCF employing a much more modest AS. Indeed, using the CAS-FCI or CAS-SCF schemes used in Part I prevented us from employing ASs involving polarization orbitals. The present paper thus pursues this very idea in various situations, modelling different types of dissociation processes. Let us note that with AS4 (which happens to correspond to AS4 of Part I) and the DZ basis at the three geometries considered (R_e, $1.5R_e$, $2R_e$), the energy differences ΔE relative to FCI of the CCSD-CASFCI, CCSD-CASSCF and the present CCSD-AS4 are, respectively, 0.7, 1.7 and 2.1; 0.7, 1.2 and 1.2; and 0.7, 1.9 and 2.3 mhartree. Similarly, for the DZP basis and AS2 (corresponding to AS6 of Part I), these values are, respectively, 1.9, 3.7 and 8.8; 1.9, 3.6 and 8.7; and 1.9, 3.7 and 8.6 mhartree. Thus, the small i-CAS-CI supplemented by e-SOCI gives practically the same result as the corresponding CAS-FCI or CAS-SCF. Note that in the present case the σ^*_{OH} orbital is always in the internal part (and thus used in CAS-FCI), while all other orbitals are accounted for via SOCI. In contrast, no distinction of internal and external active orbitals was made in Part I, thus leading to larger CI spaces. For example, the AS4, AS3 and AS2 (corresponding to AS1, AS2 and AS3 of Part I) have CI dimensions 268, 441 and 656, while the corresponding CAS-SCF or CAS-FCI of Part I have dimensions 588, 1512 and 3460, respectively.

This reduction in the CI dimension enables us to employ even polarization orbitals in the wave function serving as our external source, while relying on only modest computational requirements. This in turn leads to a very significant improvement for stretched geometries, as we have already seen above. Nonetheless, we must stress that even with the smallest AS4, having roughly half the dimension of CCSD and involving no polarization orbitals, the standard CCSD(is) result is improved by 23% at $2R_e$.

4.2. *Simultaneous stretching of two single bonds*

Here we examine both the $^2B_1$ ground state as well as the lowest $^2A_1$ excited state of the NH_2 radical. The ordering of the ROHF orbitals for the $^2A_1$ state at $2R_e$ is found to be:

$$N_{1s}N_{2s}\sigma_{1NH}N_{2p_x}\sigma_{2NH}\sigma^*_{2NH}\sigma^*_{1NH} N_{2p'_x}N_{2p'_y}N_{2p'_z}N_{2s'}\sigma_H\sigma^*_H\mathcal{P}N_{1s'}, \quad (4)$$

where again $\mathcal{P} = \varnothing$ for a DZ basis, while

$$\mathcal{P} = H_{2p_x}H_{2p_y}H_{2p_z}N_{3d_1}N_{3d_2}N_{3d_3} \times N_{3d_4}N_{3d_5}H_{2p'_x}H_{2p'_y}H_{2p'_z}N_{3d_0} \quad (5)$$

for a DZP basis. We also write $\mathcal{P} = \mathcal{P}'N_{3d_0}$. In this case we freeze only the occupied N_{1s} orbital in all calculations. We thus have 7 active (all valence) electrons and we employ the following ASs for both states, in addition to AS0 corresponding to FCI (with frozen N_{1s} orbital):

$$\begin{aligned}
&\text{AS1}: [\sigma^*_{2NH}\sigma^*_{1NH}//N_{2p'_x}N_{2p'_y}N_{2p'_z}N_{2s'}\sigma_H\sigma^*_H H_{2p_x} \times H_{2p_y}H_{2p_z}N_{3d_1}N_{3d_2}N_{3d_3}N_{3d_4}N_{3d_5}H_{2p'_x}H_{2p'_y}H_{2p'_z}],\\
&\text{AS2}: [\sigma^*_{2NH}\sigma^*_{1NH}//N_{2p'_x}N_{2p'_y}N_{2p'_z}N_{2s'}\sigma_H\sigma^*_H H_{2p_x} \times H_{2p_y}H_{2p_z}N_{3d_1}N_{3d_2}N_{3d_3}N_{3d_4}N_{3d_5}],\\
&\text{AS2}': [\text{AS2} + N_{3d_0}],\\
&\text{AS3}: [\sigma^*_{2NH}\sigma^*_{1NH}//N_{2p'_x}N_{2p'_y}N_{2p'_z}N_{2s'}\sigma_H\sigma^*_H N_{3d_1} \times N_{3d_2}N_{3d_3}N_{3d_4}N_{3d_5}],\\
&\text{AS4}: [\sigma^*_{2NH}\sigma^*_{1NH}//N_{2p'_x}N_{2p'_y}N_{2p'_z}N_{2s'}\sigma_H\sigma^*_H H_{2p_x} \times H_{2p_y}H_{2p_z}],\\
&\text{AS5}: [\sigma^*_{2NH}\sigma^*_{1NH}N_{2p'_x}N_{2p'_y}N_{2p'_z}N_{2s'}],\\
&\text{AS6}: [\sigma^*_{2NH}\sigma^*_{1NH}//N_{2p'_x}N_{2p'_y}N_{2p'_z}N_{2s'}\sigma_H\sigma^*_H],\\
&\text{AS7}: [\sigma^*_{2NH}\sigma^*_{1NH}//N_{2p'_x}N_{2p'_y}N_{2p'_z}N_{2s'}].
\end{aligned} \quad (6)$$

The last three (ASn, $n = 5, 6, 7$) are employed for a DZ basis and those with $n = 1, 2, 2', 3, 4$ and 6 for a DZP basis. We also consider FCI with frozen $N_{1s'}$ orbital, which is referred to as AS0′. Thus, it is really the latter that represents the benchmark for a comparison with the CCSD(is) energies. However, as may be seen from tables 3 and 4, both energies differ by less than 0.2 mhartree for all considered geometries (in spite of the fact that the dimension is almost doubled when correlating the $N_{1s'}$ orbital), so that our conclusions will be the same using either benchmark.

Both the standard and externally corrected CCSD(is) energies, as well as the corresponding SOCI energies and the NPEs obtained with a DZ basis sets are listed in tables 3 and 4 for the $^2A_1$ and $^2B_1$ states, respectively. We find again a systematic improvement in the exter-

Table 3. Same as table 1 for the $^2A_1$ state of the NH_2 radical. The total energies are reported as $-(E+55)$ hartree.

Method	Dim	$-(E+55)$ (hartree)			ΔE (mhartree)			NPE
		R_e	$1.5R_e$	$2R_e$	R_e	$1.5R_e$	$2R_e$	
CCSD-AS0		0.603 35	0.449 78	0.359 77	0.05	0.07	−4.01	4.08
CI(AS0)	27 300	0.603 40	0.449 85	0.355 77	0	0	0	0
CCSD-AS0′		0.603 35	0.449 77	0.359 76	0.06	0.08	−4.00	4.08
CI(AS0′)	14 666	0.603 29	0.449 73	0.355 62	0.11	0.12	0.15	0.04
CCSD-AS5		0.602 82	0.449 21	0.358 57	0.59	0.65	−2.81	3.45
CI(AS5)	3 556	0.565 37	0.439 64	0.346 68	38.04	10.21	9.09	28.95
CCSD-AS6		0.602 78	0.449 13	0.358 22	0.63	0.72	−2.45	3.08
CI(AS6)	2 899	0.600 58	0.447 03	0.353 12	2.83	2.83	2.64	0.18
CCSD-AS7		0.602 66	0.448 73	0.357 35	0.74	1.12	−1.58	2.33
CI(AS7)	1 429	0.564 48	0.437 35	0.344 71	38.93	12.50	11.06	27.87
CCSD(is)	235	0.602 13	0.444 78	0.339 52	1.28	5.07	16.22	14.97

Table 4. Same as table 3 for the $^2B_1$ state of the NH_2 radical.

Method	Dim	$-(E+55)$ (hartree)			ΔE (mhartree)			NPE
		R_e	$1.5R_e$	$1.75R_e$	R_e	$1.5R_e$	$1.75R_e$	
CCSD-AS0		0.645 97	0.534 77	0.480 90	0.06	0.05	−0.25	0.31
CI(AS0)	24 924	0.646 03	0.534 82	0.480 65	0	0	0	0
CCSD-AS0′		0.645 96	0.534 76	0.480 89	0.07	0.06	−0.24	0.30
CI(AS0′)	13 742	0.645 90	0.534 68	0.480 51	0.13	0.14	0.14	0.01
CCSD-AS5		0.645 31	0.533 99	0.480 21	0.72	0.83	0.44	0.40
CI(AS5)	3 430	0.605 63	0.514 39	0.469 29	40.40	20.43	11.36	29.04
CCSD-AS6		0.645 35	0.534 18	0.480 20	0.68	0.64	0.45	0.22
CI(AS6)	2 737	0.643 35	0.532 50	0.478 59	2.68	2.32	2.06	0.62
CCSD-AS7		0.645 18	0.533 73	0.479 72	0.85	1.09	0.93	0.24
CI(AS7)	1 363	0.604 89	0.513 13	0.467 73	41.14	21.69	12.92	28.22
CCSD(is)	219	0.644 69	0.530 37	0.474 62	1.34	4.45	6.03	4.69

nally corrected CCSD(is) energies as the size of the AS employed increases, even though for a highly stretched geometry ($R = 2R_e$) we already find a slight overcorrection. In fact, this overcorrection is largest when using the full AS0 space (about −4 mhartree for the $^2A_1$ state at $2R_e$ and −0.25 mhartree for the $^2B_1$ state at $1.75R_e$), while it is negligible (less than 0.1 mhartree) at less stretched geometries.

Here we must remark again that, in principle, when using the FCI wave function as an external source for high order cluster amplitudes, we should recover the exact energy. This is indeed the case for closed-shell systems where the excitation level is unambiguously defined and we include all the terms (up to and including the quadratic ones) in the CCSD equations [11, 12]. However, CCSD(is) involves several approximations which cause the above mentioned overcorrections. In the first place, at most, quadratic terms are retained and, most importantly, the so-called pseudo-doubles are neglected. Although the latter are approximately taken into account through the external corrections, the decoupling of the full CC chain in the OS case is only approximate when using CCSD(is). Nonetheless, the errors involved are rather small, unless we are far away from the equilibrium geometry, where the external corrections may not be entirely reliable and one may also run into the convergence problems.

For the $^2B_1$ ground state, we face convergence difficulties at the highly stretched geometry ($R = 2R_e$), so that only the results for $R = 1.75R_e$ are reported. In all cases, however, the corrected CCSD energies represent a significant improvement over both the standard CCSD(is) and SOCI ones, the latter being used as a source of higher than pair cluster corrections. Indeed,

Table 5. Same as table 3 for DZP basis.

Method	Dim	$-(E+55)$ (hartree)			ΔE (mhartree)			NPE
		R_e	$1.5R_e$	$2R_e$	R_e	$1.5R_e$	$2R_e$	
CI(AS0)(5d)[a]	3 307 920[b]	0.688 76	0.517 61	0.415 13	0	0	0	0
CCSD-AS1		0.687 84	0.516 90	0.417 53	0.92	0.72	−2.39	3.31
CI(AS1)	19 870	0.681 35	0.510 10	0.408 04	7.41	7.52	7.10	0.42
CCSD-AS2		0.687 56	0.516 33	0.416 37	1.20	1.28	−1.24	2.52
CI(AS2)	13 711	0.663 52	0.500 66	0.401 76	25.24	16.95	13.38	11.87
CCSD-AS2′		0.687 61	0.516 53	0.416 81	1.15	1.08	−1.68	2.83
CI(AS2′)	15 672	0.665 88	0.504 01	0.405 33	22.88	13.61	9.81	13.07
CCSD-AS3		0.687 38	0.515 72	0.415 98	1.38	1.89	−0.85	2.74
CI(AS3)	8 708	0.639 57	0.488 23	0.399 46	49.19	29.39	15.68	33.52
CCSD-AS4		0.687 34	0.514 81	0.409 17	1.42	2.80	5.97	4.55
CI(AS4)	6 008	0.628 48	0.460 83	0.352 14	60.28	56.78	63.00	6.22
CCSD-AS6		0.687 20	0.510 49	0.408 84	1.57	7.13	6.30	5.56
CI(AS6)	2 899	0.609 56	0.451 80	0.350 44	79.20	65.81	64.69	14.51
CCSD(is)	1 013	0.686 59	0.510 59	0.390 64	2.17	7.03	24.49	22.32

[a] Reference [17].
[b] Frozen core, 6 d-orbitals.

Table 6. Same as table 4 for DZP basis.

Method	Dim	$-(E+55)$ (hartree)			ΔE (mhartree)			NPE
		R_e	$1.5R_e$	$2R_e$	R_e	$1.5R_e$	$2R_e$	
CI(AS0)(5d)[a]	3 271 984[b]	0.742 62	0.605 21	0.505 52	0	0	0	0
CCSD-AS1		0.742 27	0.604 67	0.508 60	0.35	0.54	−3.08	3.62
CI(AS1)	19 442	0.734 59	0.598 27	0.499 62	8.03	6.94	5.91	2.12
CCSD-AS2		0.741 92	0.603 74	0.505 38	0.70	1.47	0.15	1.32
CI(AS2)	13 381	0.708 21	0.581 49	0.492 07	34.41	23.72	13.46	20.95
CCSD-AS3		0.741 63	0.602 88	0.504 61	0.99	2.33	0.91	1.41
CI(AS3)	8 464	0.685 91	0.569 48	0.489 95	56.71	35.73	15.57	41.14
CCSD-AS4		0.741 54	0.601 14	0.486 81	1.08	4.07	18.71	17.63
CI(AS4)	5 772	0.682 28	0.548 01	0.446 28	60.34	57.20	59.25	3.13
CCSD-AS6		0.741 33	0.600 53	0.486 24	1.29	4.68	19.28	17.99
CI(AS6)	2 737	0.662 91	0.538 70	0.444 63	79.71	66.51	60.89	18.81
CCSD(is)	990	0.740 76	0.597 36	0.487 00	1.87	7.85	18.52	16.66

[a] Reference [17].
[b] Frozen core, 6 d-orbitals.

even when using the smallest AS7, the NPE of the standard CCSD(is) is reduced by about 85% (while the NPE of the corresponding SOCI is almost twice as large as that of standard CCSD(is)) in the case of the excited state and by 95% for the ground state (again, the SOCI NPE is six times as large as that of CCSD(is)). Thus, the AS7 set, which involves antibonding σ^* orbitals in the internal (active) space and an extra antibonding orbital for each occupied valence orbital in the external space, seems to provide an ideal source for external corrections, since its size is very modest (corresponding CI dimension is less than 1500 in each case) and the computer requirements for CCSD-AS7 exceeds that for standard CCSD(is) by only a couple of iterations.

For a realistic DZP basis set, the results are collected in tables 5 and 6. As benchmark FCI energies we use the results of Bauschlicher *et al.* [17]. We must note, however, that in contrast to [17], we employ Cartesian Gaussians, since we rely on the GAMESS package for the CAS-FCI and SOCI results. Of course, we also employ the same basis set in our CCSD calculations. Thus, in con-

trast to the basis set of [17], our basis set contains an extra s-type d-orbital. Clearly, the inclusion of this orbital produces a lower variational energy, so that the FCI energies of [17] represent only the upper bound to the actual FCI for our basis set. This energy lowering can be estimated not to exceed 2–3 mhartree at $R = 2R_e$ by examining an analogous energy lowering for a smaller basis set that our computing facility can handle. It should also be noted that the nitrogen $3d_s$ orbital is included in all CCSD calculations. For this reason, the CCSD(is) results are slightly different from those of [7] and [23], where this $3d_s$ orbital was eliminated.

Apart from minor differences that we have just outlined, the main conclusions are the same as for a DZ basis set. All correcting schemes, including the very modest AS6, perform well and significantly improve the standard CCSD(is) energies. Comparing, for example, the performance of the largest AS1 and of the smallest AS6 corrected CCSD methods with the standard CCSD(is) one, we find that for the $^2A_1$ state at $R = R_e$, the 2.2 mhartree error is reduced to 0.9 and 1.6 mhartree, respectively, and at $R = 2R_e$, this reduction is from 24.5 mhartree to −2.4 and 6.3 mhartree (see table 5). To achieve a similar reduction for the ground state, we have to employ AS3 or larger active spaces.

In all preceding cases, the size of the corrections increases with the quasi-degeneracy of the state, i.e. with the size of the error of the standard CCSD(is). This feature clearly reduces the NPE and is most desirable. It is worth noting, however, that in spite of the fact that CI energies deviate significantly more from FCI than the corresponding corrected CCSD values (even for the largest AS1), the latter yield a larger NPE in view of the approximations leading to a slight overcorrection at large internuclear separations. Nonetheless, from a practical viewpoint, it is important that already the smallest AS6 gives very desirable results: while the CI(AS6) error for the $^2A_1$ state at $R = R_e$ is 79.2 mhartree, the CCSD-AS6 error is only 1.6 mhartree, and at $R = 2R_e$, these errors are 64.3 and 6.3 mhartree, respectively.

For the $^2B_1$ ground state (table 6) we obtain analogous results as for the $^2A_1$ state, except that the low dimensional AS4 and AS6 schemes give considerably poorer results, as already noted. The reason for this behaviour lies probably in the ROHF optimization scheme that does not work well in this case. Generally, CCSD performs better when using the ROHF rather than CAS-SCF orbitals. However this is not the case at $R = 2R_e$ for the $^2B_1$ state considered here.

4.3. *Simultaneous stretching of three single bonds*

We next consider a symmetric stretching of three single bonds using DZ and DZP models of the $^2A_2''$ state of the CH_3 radical. The ROHF orbitals, ordered by their energies at $R = 2R_e$, form the sequence

$$C_{1s}\sigma_{1CH}\sigma_{2CH}\sigma_{3CH}C_{2p_y}\sigma^*_{1CH}\sigma^*_{2CH}\sigma^*_{3CH} \times C_{2p_y^*}C_{2p_x^*}C_{2p_z^*}C_{2s^*}\sigma^*_{1H}\sigma^*_{2H}\sigma^*_{3H}\mathcal{P}\,C_{1s^*}, \quad (7)$$

where again $\mathcal{P} = \varnothing$ for a DZ basis and

$$\mathcal{P} = C_{3d_1}C_{3d_2}C_{3d_3}C_{3d_4}C_{3d_5}H_{2p_y}H_{2p_x}H_{2p_z}H_{2p'_y} \times H_{2p'_x}H_{2p'_z}H_{2p_y''}H_{2p_x''}H_{2p_z''}C_{3d_s} \quad (8)$$

for a DZP basis. The carbon C_{1s} orbital is kept frozen in all calculations. We thus have 7 active (all valence) electrons distributed over 4 orbitals, $\sigma_{1CH}, \sigma_{2CH}, \sigma_{3CH}$ and C_{2p_y}.

For a DZ basis, we use as a benchmark the FCI energies correlating all orbitals except C_{1s} (AS0) as well as near FCI energies obtained by freezing both the lowest occupied (C_{1s}) and the highest unoccupied (C_{1s^*}) orbitals, designated as CI(AS0′). As may be seen from table 7, the latter CI gives practically the same energies as the former one, while the corresponding dimension is lowered by almost a factor of two. The remaining ASs used with a DZ basis are:

$$\begin{aligned}
&\text{AS4}: [\sigma^*_{1CH}\sigma^*_{2CH}\sigma^*_{3CH}//C_{2p_y^*}C_{2p_z^*}C_{2p_x^*}C_{2s^*}\sigma^*_{1H}\sigma^*_{2H}\sigma^*_{3H}],\\
&\text{AS4}': [\sigma^*_{1CH}\sigma^*_{2CH}\sigma^*_{3CH}C_{2p_y^*}//C_{2p_z^*}C_{2p_x^*}C_{2s^*}\sigma^*_{1H}\sigma^*_{2H}\sigma^*_{3H}],\\
&\text{AS5}: [\sigma^*_{1CH}\sigma^*_{2CH}\sigma^*_{3CH}//C_{2p_y^*}C_{2p_z^*}C_{2p_x^*}C_{2s^*}],\\
&\text{AS5}': [\sigma^*_{1CH}\sigma^*_{2CH}\sigma^*_{3CH}C_{2p_y^*}//C_{2p_z^*}C_{2p_x^*}C_{2s^*}].
\end{aligned} \quad (9)$$

Note that the primed ASs differ from the unprimed ones by the inclusion of the $C_{2p_y^*}$ lone pair orbital amongst the inner active ones, significantly increasing the dimension of the corresponding CI space (see table 7). Note that the y axis is perpendicular to the molecular plane.

For a DZP basis, we use in addition the following ASs involving all or some polarization orbitals:

$$\begin{aligned}
&\text{AS1}: [\sigma^*_{1CH}\sigma^*_{2CH}\sigma^*_{3CH}//C_{2p_y^*}C_{2p_x^*}C_{2p_z^*}C_{2s^*}\sigma^*_{1H}\sigma^*_{2H}\sigma^*_{3H} \times C_{3d_1}C_{3d_2}C_{3d_3}C_{3d_4}C_{3d_5}H_{2p_y}H_{2p_x}H_{2p_z}],\\
&\text{AS2}: [\sigma^*_{1CH}\sigma^*_{2CH}\sigma^*_{3CH}//C_{2p_y^*}C_{2p_x^*}C_{2p_z^*}C_{2s^*}\sigma^*_{1H}\sigma^*_{2H}\sigma^*_{3H} \times C_{3d_1}C_{3d_2}C_{3d_3}C_{3d_4}C_{3d_5}],\\
&\text{AS3}: [\sigma^*_{1CH}\sigma^*_{2CH}\sigma^*_{3CH}//C_{2p_y^*}C_{2p_x^*}C_{2p_z^*} \times C_{2s^*}\sigma^*_{1H}\sigma^*_{2H}\sigma^*_{3H}H_{2p_y}H_{2p_x}H_{2p_z}],
\end{aligned} \quad (10)$$

Table 7. Same as table 1 for the $^2A_2''$ state of the CH_3 radical. The total energies are reported as $-(E+39)$ hartree and $R_e = 2.060$ bohr.

Method	Dimension	$-(E+39)$ (hartree)			ΔE (mhartree)			NPE
		R_e	$1.5R_e$	$2R_e$	R_e	$1.5R_e$	$2R_e$	
CCSD-AS0		0.644 63	0.430 39	0.262 20	0.05	0.27	0.82	0.78
CI(AS0)	70 644	0.644 68	0.430 66	0.263 02	0	0	0	0
CCSD-AS0′		0.644 62	0.430 38	0.262 18	0.05	0.28	0.84	0.79
CI(AS0′)	42 890	0.644 60	0.430 60	0.262 93	0.08	0.07	0.10	0.03
CCSD-AS4		0.644 00	0.430 06	0.261 85	0.67	0.60	1.18	0.58
CI(AS4)	8 796	0.641 86	0.429 16	0.262 05	2.81	1.50	0.97	1.84
CCSD-AS4′		0.644 25	0.430 26	0.262 08	0.43	0.40	0.94	0.54
CI(AS4′)	15 502	0.642 54	0.429 90	0.262 58	2.14	0.76	0.44	1.67
CCSD-AS5		0.643 82	0.429 21	0.259 61	0.86	1.45	3.41	2.55
CI(AS5)	3 478	0.605 48	0.409 29	0.245 75	39.19	21.37	17.28	21.92
CCSD-AS5′		0.643 88	0.429 31	0.259 75	0.80	1.35	3.28	2.48
CI(AS5′)	5 222	0.605 85	0.409 85	0.246 10	38.83	20.82	16.92	21.91
CCSD(is)	322	0.643 42	0.423 89	0.228 73	1.25	6.77	34.29	33.04

as well as ASn', $n = 1, 2, 3$, which again differ by the inclusion of C_{2p_y} amongst the inner active orbitals, i.e.:

$$\begin{aligned}
\mathrm{AS1'}&: [\sigma^*_{1CH}\sigma^*_{2CH}\sigma^*_{3CH}C_{2p'_y}//C_{2p'_x}C_{2p'_z}C_{2s}\cdot\sigma^*_{1H}\sigma^*_{2H}\sigma^*_{3H}\\
&\quad\times C_{3d_1}C_{3d_2}C_{3d_3}C_{3d_4}C_{3d_5}H_{2p_y}H_{2p_x}H_{2p_z}],\\
\mathrm{AS2'}&: [\sigma^*_{1CH}\sigma^*_{2CH}\sigma^*_{3CH}C_{2p'_y}//C_{2p'_x}C_{2p'_z}C_{2s}\cdot\sigma^*_{1H}\sigma^*_{2H}\sigma^*_{3H}\\
&\quad\times C_{3d_1}C_{3d_2}C_{3d_3}C_{3d_4}C_{3d_5}],\\
\mathrm{AS3'}&: [\sigma^*_{1CH}\sigma^*_{2CH}\sigma^*_{3CH}C_{2p'_y}//C_{2p'_x}C_{2p'_z}C_{2s}\cdot\sigma^*_{1H}\\
&\quad\times \sigma^*_{2H}\sigma^*_{3H}H_{2p_y}H_{2p_x}H_{2p_z}].
\end{aligned} \tag{11}$$

The relevant energies, obtained with both the standard and corrected CCSD(is) schemes, as well as the benchmark FCI energies and the NPE values, are given in tables 7 and 8 for DZ and DZP basis sets, respectively. We find again that all the externally corrected CCSD energies represent a significant improvement over the standard ones. Considering, first, the results obtained with a DZ basis, we see that even the AS5 set, having the smallest dimension, gives excellent results: the NPE of the standard CCSD(is) approach is reduced by more than 92%, while the CI(AS5), used as the source of external corrections, reduces this error by less than 34%. We note again that FCI corrected CCSD gives small but non-zero errors, all smaller than 1 mhartree, due to the approximations involved in the CCSD(is) approach.

A completely analogous situation is found for a DZP basis (table 8). We only note that with the smallest AS5 scheme, the NPE of standard CCSD(is) is reduced by more than 75%, while the NPE of CI(AS5) is larger than that of standard CCSD(is).

It is worthwhile to point out that moving the antibonding lone pair ($C_{2p'_y}$) orbital from the external to the internal active space, i.e. by going from ASn to ASn', hardly changes the resulting energies and the NPE, while almost doubling the dimension of the corresponding CI space. This clearly demonstrates that only essential orbitals for the dissociation process need to be included in the internal space, while the remaining correlating orbitals can be moved to the external space, significantly lowering the dimension of CI required for external corrections.

4.4. *Stretching of a triple bond*

We finally consider the most challenging problem of a triple bond stretching, employing DZ and DZP models of the $^2\Sigma^+$ and $^2\Pi$ states of the CN radical. The ROHF orbital sequence for the $^2\Sigma^+$ state is

$$\begin{aligned}
&N_{1s}C_{1s}N_{lp}C_{lp}\pi_1\pi_2\sigma\pi^*_2\pi^*_1\sigma^*C_{2p'_y}C_{2p'_x}C_{2p'_z}N_{2p'_y}\\
&\qquad\times N_{2p'_x}N_{2p'_z}C_{lp}\cdot N_{lp}\cdot\mathcal{P}C_{1s}\cdot N_{1s}\cdot,
\end{aligned} \tag{12}$$

with $\mathcal{P} = \varnothing$ for a DZ basis and

$$\begin{aligned}
\mathcal{P} = {}& C_{3d_1}C_{3d_2}C_{3d_3}C_{3d_4}C_{3d_5}N_{3d_1}N_{3d_2}N_{3d_3}\\
&\times N_{3d_4}N_{3d_5}C_{3d_\cdot}N_{3d_\cdot}
\end{aligned} \tag{13}$$

for a DZP basis. For the $^2\Pi$ state, we find the same ordering of virtual orbital, while the bonding σ orbital now precedes the π orbitals.

The 1s orbitals (N_{1s} and C_{1s}) are frozen in all ASn' schemes, while four additional electrons are kept frozen

Table 8. Same as table 7 for DZP basis.

Method	Dimension	$-(E+39)$ (hartree)			ΔE (mhartree)			NPE
		R_e	$1.5R_e$	$2R_e$	R_e	$1.5R_e$	$2R_e$	
CI(AS0)[a]	~12 230 000	0.721 21	0.482 85	0.303 13	0	0	0	0
CCSD-AS1		0.720 18	0.481 86	0.301 51	1.03	0.99	1.63	0.63
CI(AS1)	37 216	0.700 03	0.470 87	0.296 16	21.18	11.99	6.98	14.20
CCSD-AS2		0.720 08	0.481 73	0.301 54	1.13	1.12	1.60	0.48
CI(AS2)	24 116	0.692 97	0.468 40	0.295 64	28.24	14.46	7.49	20.75
CCSD-AS3		0.719 76	0.479 54	0.295 97	1.45	3.32	7.17	5.71
CI(AS3)	17 348	0.654 01	0.434 82	0.260 10	67.20	48.04	43.03	24.18
CCSD-AS4		0.719 71	0.479 45	0.295 27	1.51	3.40	7.87	6.36
CI(AS4)	8 796	0.649 48	0.433 03	0.261 90	71.73	49.82	41.24	30.50
CCSD-AS5		0.719 53	0.478 43	0.292 68	1.68	4.42	10.46	8.78
CI(AS5)	3 478	0.620 46	0.413 27	0.242 75	100.75	69.59	60.38	40.37
CCSD-AS1′		0.720 48	0.482 15	0.301 83	0.73	0.70	1.30	0.60
CI(AS1′)	70 774	0.700 84	0.471 76	0.296 82	20.37	11.09	6.31	14.06
CCSD-AS2′		0.720 37	0.482 02	0.301 86	0.84	0.84	1.27	0.44
CI(AS2′)	45 310	0.693 76	0.469 27	0.296 30	27.45	13.58	6.83	20.62
CCSD-AS3′		0.719 95	0.479 71	0.296 17	1.26	3.14	6.96	5.70
CI(AS3′)	31 516	0.654 59	0.435 50	0.260 59	66.62	47.35	42.55	24.07
CCSD-AS4′		0.719 89	0.479 63	0.295 51	1.32	3.23	7.62	6.30
CI(AS4′)	15 502	0.650 06	0.433 70	0.262 42	71.16	49.15	40.71	30.45
CCSD-AS5′		0.719 61	0.478 51	0.292 82	1.60	4.34	10.31	8.71
CI(AS5′)	5 222	0.620 82	0.413 75	0.243 11	100.39	69.10	60.02	40.37
CCSD(is)	1 501	0.719 18	0.474 39	0.264 96	2.03	8.47	38.18	36.14

[a] Reference [18].

in the lone pair orbitals N_{lp} and C_{lp} in the ASn schemes. Thus, ASn and ASn' cases involve 5 and 9 active electrons, respectively. Again, we identify these ASs by listing correlating virtual orbitals, subdivided into the internal and external subsets separated by a double slash:

$$\begin{aligned}
\text{AS1}&: [\pi_2^*\pi_1^*\sigma^*//C_{2p_y^*}C_{2p_x^*}C_{2p_z^*}N_{2p_y^*}N_{2p_x^*}N_{2p_z^*}C_{lp^*}N_{lp^*}\\
&\quad\times C_{3d_1}C_{3d_2}C_{3d_3}C_{3d_4}C_{3d_5}N_{3d_1}N_{3d_2}N_{3d_3}N_{3d_4}N_{3d_5}],\\
\text{AS2}&: [\pi_2^*\pi_1^*\sigma^*//C_{2p_y^*}C_{2p_x^*}C_{2p_z^*}N_{2p_y^*}N_{2p_x^*}N_{2p_z^*}C_{3d_1}\\
&\quad\times C_{3d_2}C_{3d_3}C_{3d_4}C_{3d_5}N_{3d_1}N_{3d_2}N_{3d_3}N_{3d_4}N_{3d_5}],\\
\text{AS3}&: [\pi_2^*\pi_1^*\sigma^*//C_{3d_1}C_{3d_2}C_{3d_3}C_{3d_4}C_{3d_5}N_{3d_1}N_{3d_2}\\
&\quad\times N_{3d_3}N_{3d_4}N_{3d_5}],\\
\text{AS4}&: [\pi_2^*\pi_1^*\sigma^*//C_{2p_y^*}C_{2p_x^*}C_{2p_z^*}N_{2p_y^*}N_{2p_x^*}N_{2p_z^*}C_{lp^*}N_{lp^*}],\\
\text{AS5}&: [\pi_2^*\pi_1^*\sigma^*//C_{2p_y^*}C_{2p_x^*}C_{2p_z^*}N_{2p_y^*}N_{2p_x^*}N_{2p_z^*}],\\
\text{AS3}''&: [\pi_2^*\pi_1^*\sigma^*//C_{3d_1}C_{3d_2}C_{3d_3}C_{3d_4}C_{3d_5}N_{3d_1}\\
&\quad\times N_{3d_2}N_{3d_3}N_{3d_4}N_{3d_5}C_{lp^*}N_{lp^*}].
\end{aligned}\tag{14}$$

Only $n = 4$ and 5 ASn schemes are relevant for a DZ basis. We also note that in this case we freeze 1s as well as 1s* orbitals on both C and N in all calculations. As a benchmark, we use a near FCI value [23], obtained by considering all CSFs up to and including sextuples (as well as an unspecified number of higher excited CSFs). In this case, only the $R = R_e$ and $R = 1.5R_e$ are considered.

The standard and corrected CCSD(is) energies, as well as the near FCI values, are given for the $^2\Sigma^+$ and $^2\Pi$ states in tables 9 and 10 for a DZ basis and in tables 11 and 12 for a DZP basis. Although we find again a very significant improvement over the standard CCSD(is) values in all cases, particularly for the stretched geometry, the role of various correlating orbitals seems to be less specific than in other cases. Also, an apparently more efficient reduction of the standard CCSD(is) error for the stretched geometry might be due to a tendency of the externally corrected CCSD(is) to overcorrect in such cases. Inclusion of the virtual lone pair orbitals (AS3 versus AS3′) seems to have little

Table 9. Same as table 1 for the $^2\Sigma^+$ state of the CN radical. The total energies are reported as $-(E+92)$ hartree. Only two internuclear separations ($R_c = 1.1718$ Å and $1.5R_c$) are considered and no NPE values are given.

Method	Dimension	$-(E+92)$ (hartree)		ΔE (mhartree)	
		R_c	$1.5R_c$	R_c	$1.5R_c$
nCI(AS0)[a]	~420 000	0.368 89	0.226 28	0	0
CCSD-AS4		0.362 13	0.212 30	6.77	13.98
CI(AS4)	1 742	0.271 38	0.122 20	97.52	104.08
CCSD-AS5		0.361 90	0.211 98	6.99	14.30
CI(AS5)	1 078	0.266 45	0.119 25	102.44	107.04
CCSD-AS4′		0.363 96	0.224 37	4.93	1.91
CI(AS4′)	56 440	0.363 00	0.222 54	5.89	3.74
CCSD-AS5′		0.361 90	0.222 35	6.99	3.93
CI(AS5′)	33 200	0.311 73	0.192 97	57.17	33.31
CCSD(is)	529	0.358 93	0.190 62	9.96	35.66

[a] Reference [23].

Table 10. Same as table 9 for the $^2\Pi$ state of the CN radical ($R_c = 1.2333$ Å).

Method	Dimension	$-(E+92)$ (hartree)		ΔE (mhartree)	
		R_c	$1.5R_c$	R_c	$1.5R_c$
CI(AS0)[a]	~420 000	0.312 95	0.210 94	0	0
CCSD-AS4		0.308 34	0.209 09	4.61	1.86
CI(AS4)	1 738	0.228 33	0.123 97	84.62	86.97
CCSD-AS5		0.308 15	0.208 75	4.80	2.20
CI(AS5)	1 078	0.221 91	0.120 86	91.05	90.08
CCSD-AS4′		0.311 66	0.215 35	1.29	−4.41
CI(AS4′)	55 860	0.308 06	0.207 82	4.89	3.13
CCSD-AS5′		0.310 99	0.213 16	1.96	−2.22
CI(AS5′)	32 980	0.279 15	0.176 01	33.81	34.93
CCSD(is)	505	0.305 70	0.193 42	7.25	17.52

[a] Reference [23]

effect. On the other hand, freezing the corresponding occupied lone pair orbitals (ASn versus ASn') leads to a significant deterioration of resulting energies, particularly for stretched geometries. Except for these general observations, however, we cannot draw any general conclusion in this case, which must be regarded as a preliminary test of the externally corrected schemes for this difficult problem. In any case, a comparison of the corresponding CI(ASn) and CCSD-ASn energies shows a dramatic improvement in all cases.

Table 11. Same as table 9 for DZP basis.

Method	Dimension	$-(E+92)$ (hartree)		ΔE (mhartree)	
		R_c	$1.5R_c$	R_c	$1.5R_c$
CI(AS0)[a]	~680 000	0.492 43	0.310 05	0	0
CCSD-AS1		0.483 82	0.302 22	8.61	7.83
CI(AS1)	7 450	0.338 60	0.151 40	153.83	158.65
CCSD-AS2		0.483 57	0.302 04	8.87	8.01
CI(AS2)	5 986	0.334 10	0.149 67	158.34	160.38
CCSD-AS3		0.481 38	0.293 57	11.05	16.48
CI(AS3)	2 562	0.286 41	0.095 64	206.02	214.41
CCSD-AS4		0.481 40	0.298 30	11.03	11.75
CI(AS4)	1 742	0.306 93	0.128 81	185.51	181.25
CCSD-AS5		0.481 16	0.298 20	11.27	11.85
CI(AS5)	1 078	0.302 93	0.127 66	189.50	182.39
CCSD-AS3′		0.482 57	0.304 86	9.86	5.19
CI(AS3′)	85 080	0.376 32	0.204 06	116.11	205.99
CCSD-AS3″		0.483 02	0.305 57	9.41	4.48
CI(AS3″)	120 416	0.389 90	0.216 76	102.54	93.29
CCSD-AS4′		0.481 55	0.307 84	10.88	2.21
CI(AS4′)	56 440	0.384 54	0.224 01	107.89	86.04
CSD-AS5′		0.480 78	0.306 58	11.66	3.47
CI(AS5′)	33 200	0.364 02	0.201 27	128.41	108.78
CCSD(is)	1 983	0.479 11	0.279 04	13.32	31.01

[a] Reference [23]

5. Conclusions

In this paper we have studied the performance of the so-called externally corrected UGA based CCSD(is) method in quasi-degenerate situations that arise when exploring various dissociation channels of simple radicals. The method and its implementation was described in Part I of this series. However, instead of using the CAS SCF or CAS FCI wave function as an external source for the 3- and 4-body cluster amplitudes as was done in Part I, we employ here a computationally much less demanding scheme that combines a small internal CAS-FCI with a larger external SOCI, providing a CI-type wave function of modest dimensions, yet properly describing the dissociation channel considered. The handling of 3- and 4-body cluster amplitudes that are obtained by the cluster analysis of the external CI-type wave function, as well as the solution of the resulting externally corrected UGA-CCSD(is) equations, were amply described in Part I. The non-iterative handling of T_1T_3 correction was employed throughout.

This approach was applied to several DZ and DZP models of simple radicals, enabling us to assess its per-

Table 12. Same as table 10 for DZP basis.

Method	Dimension	$-(E+92)$ (hartree)		ΔE (mhartree)	
		R_e	$1.5R_e$	R_e	$1.5R_e$
nCI(AS0)[a]	~680 000	0.454 01	0.308 40	0	0
CCSD-AS1		0.448 03	0.301 48	5.99	6.92
CI(AS1)	7 442	0.306 92	0.157 14	147.09	151.26
CCSD-AS2		0.447 84	0.301 13	6.17	7.27
CI(AS2)	5 982	0.300 78	0.155 03	153.23	153.37
CCSD-AS3		0.446 41	0.294 16	7.60	14.24
CI(AS3)	2 558	0.267 56	0.096 72	186.45	211.68
CCSD-AS4		0.446 70	0.297 90	7.31	10.50
CI(AS4)	1 738	0.276 80	0.134 03	177.21	174.37
CCSD-AS5		0.446 56	0.297 67	7.45	10.73
CI(AS5)	1 078	0.271 63	0.132 64	182.38	175.76
CCSD-AS3′		0.449 04	0.301 19	4.97	7.21
CI(AS3′)	84 788	0.351 07	0.183 10	102.95	125.30
CCSD-AS3″		0.449 34	0.301 83	4.67	6.57
CI(AS3″)	119 764	0.366 06	0.195 68	87.96	112.71
CCSD-AS4′		0.449 19	0.303 03	4.83	5.37
CI(AS4′)	55 860	0.343 68	0.211 15	110.33	97.24
CCSD-AS5′		0.448 65	0.301 50	5.36	6.90
CI(AS5′)	32 980	0.321 44	0.187 64	132.57	120.76
CCSD(is)	1 939	0.444 78	0.284 63	9.23	23.77

[a] Reference [23]

formance when stretching or breaking one single (OH) or one multiple (CN) bond, or when simultaneously stretching two (NH_2) or three (CH_3) single bonds. For the OH and CN radicals, both the ground as well as the lowest excited state of another symmetry species were considered. In all cases, the externally corrected CCSD(is) energies not only represent a significant improvement over the standard CCSD(is) values, but also significantly improve the shape of the computed potential energy surface as measured by the so-called NPE, since the magnitude of these corrections increases with the increasing quasi-degeneracy. The corrected CCSD(is) energies are also much closer to the corresponding FCI values than the CI energies corresponding to the wave function serving as a source of 3- and 4-body corrections. The corrected CCSD(is) NPEs are also generally smaller than those corresponding to the limited CI energies. Most importantly, the former ones behave in a much more systematic way than the latter, which are sometimes poorer than those associated with the standard CCSD(is) energies.

In this regard we must also mention our recent work [23] that accounts for the effect of 3-body connected clusters (both pseudo-doubles and genuine triples) perturbatively, along similar lines as is done in, nowadays, standard CCSD(T) [19] or CCSD + T(CCSD) ≡ CCSD[T] [20] approaches within the closed-shell or spin–orbital formalisms. Although these corrections provide very good results in the neighbourhood of the equilibrium geometry (cf. e.g. [21]), they generally fail once the quasi-degeneracy effects become significant, just as in the closed-shell case (see e.g. figure 4 of [22]). Thus, the externally corrected CCSD approaches, that also account for connected quadruples, represent a much more reliable and effective method having a considerably larger range of applicability.

Although the above presented results are most encouraging, the search for computationally inexpensive, yet efficient and reliable, sources of external corrections should be continued. We are currently examining [24] a similar scheme for the low spin systems that is based on multireference CI wave functions of modest dimensions.

J. Paldus wishes to acknowledge the Generalitat Valenciana 7I028.02 grant. G. Peris thanks to the Generalitat Valenciana for granting him a fellowship. Continued support from the Generalitat Valenciana project GV-2230/94, Universitat Jaume I - Fundació Caixa de Castelló, project P1B 96-11 (J. Planelles) and the National Science and Engineering Research Council of Canada (J. Paldus) are gratefully acknowledged.

References

[1] Li, X., Peris, G., Planelles, J., Rajadell, F., and Paldus, J., 1997, *J. chem. Phys.*, **107,** 90.
[2] Paldus, J., and Li., X., 1993, *Symmetries in Science VI*, edited by B. Gruber (New York: Plenum), pp. 573–591.
[3] Li, X., and Paldus, J., 1993, *Int. J. quantum chem. Symp.*, **27,** 269.
[4] Li, X., and Paldus, J., 1994, *J. chem. Phys.*, **101,** 8812.
[5] Jeziorski, B., Paldus, J., and Jankowski, P., 1995, *Int. J. quantum Chem.*, **56,** 129.
[6] Li, X., Piecuch, P., and Paldus, J., 1994, *Chem. Phys. Lett.*, **224,** 267; Piecuch, P., Li, X., and Paldus, J., 1994, *Chem. Phys. Lett.*, **230,** 377; Li, X., and Paldus, J., 1994, *Chem. Phys. Lett.*, **231,** 1; Li, X., and Paldus, J., 1995, *J. chem. Phys.*, **102,** 2013; Li, X., and Paldus, J., 1995, *J. chem. Phys.*, **102,** 8059; Li, X., and Paldus, J., 1995, *J. chem. Phys.*, **103,** 1024; Li, X., and Paldus, J., 1995, *J. chem. Phys.*, **103,** 6536; Paldus, J., and Li, X., 1996, *Can. J. Chem.*, **74,** 918.
[7] Li, X., and Paldus, J., 1995, *J. chem. Phys.*, **102,** 8897.
[8] Li, X., and Paldus, J., 1996, *J. chem. Phys.*, **104,** 9555.
[9] Paldus, J., Čížek, J., and Takahashi, M., 1984, *Phys. Rev.* A, **30,** 2193.
[10] Paldus, J., and Planelles, J., 1994, *Theor. Chim. Acta*, **89,** 13.
[11] Planelles, J., Paldus, J., and Li, X., 1994, *Theor. Chim. Acta*, **89,** 33, 59.

[12] PERIS, G., PLANELLES, J., and PALDUS, J., 1997, *Int. J. quantum Chem.*, **62,** 137.
[13] PIECUCH, P., TOBOŁA, R., and PALDUS, J., 1996, *Phys. Rev.* A, **54,** 1210.
[14] GAMESS, SCHMIDT, M. W., BALDRIDGE, K. K., BOATZ, J. A., ELBERT, S. T., GORDON, M. S., JENSEN, J. H., KOSEKI, S., MATSUNAGA, N., NGUYEN, K. A., SU, S. J., WINDUS, T. L., together with DUPUIS, M., and MONTGOMERY, J. A., 1993, *J. comput. Chem.*, **14,** 1347.
[15] HUZINAGA, S., 1965, *J. chem. Phys.*, **42,** 1293.
[16] DUNNING, T. H., 1970, *J. chem. Phys.*, **53,** 2823.
[17] BAUSCHLICHER, C. W., LANGHOFF, S. R., TAYLOR, P. R., HANDY, N. C., and KNOWLES, P. J., 1986, *J. chem. Phys.*, **85,** 1469.
[18] BAUSCHLICHER, C. W., and TAYLOR, P. R., 1987, *J. chem. Phys.*, **86,** 5600.
[19] RAGHAVACHARI, K., TRUCKS, G. W., POPLE, J. A., and HEAD-GORDON, M., 1989, *Chem. Phys. Lett.*, **157,** 479.
[20] URBAN, M., NOGA, J., COLE, S. J., and BARTLETT, R. J., 1985, *Chem. Phys. Lett.*, **83,** 4041.
[21] WOON, D. E., and DUNNING, JR, T. H., 1994, *J. chem. Phys.*, **101,** 8877.
[22] PIECUCH, P., KONDO, A. E., ŠPIRKO, V., and PALDUS, J., 1996, *J. chem. Phys.*, **104,** 4699.
[23] LI, X., and PALDUS, J., 1998, *Molec. Phys.* **94,** 41.
[24] LI, X., and PALDUS, J., 1997, *J. chem. Phys.*, **107,** 6257; 1998, *ibid.* **108,** 637; 1998, *Chem. Phys. Lett.* (in the press).

MOLECULAR PHYSICS

An international journal in the field of chemical physics

*Submitting a paper to **Molecular Physics***

Molecular Physics publishes full-length papers describing original work of an experimental and theoretical nature on the structure and properties of atomic and molecular physics. The breadth of the editors' experience encourages papers in all branches of chemical physics.

Before preparing your submission, please contact Taylor & Francis for a complete style guide, or visit our web page; contact details are given below.

Papers for consideration (three copies) should be sent to any of the Editors, at the particular editorial office, addresses given below.

Papers are accepted for consideration on condition that:

- the work is original;
- you own the copyright;
- you have secured the permission of all named co-authors, and have agreed the order of names for publication;
- you have secured all permissions for the reproduction of original or derived material from a copyright source;
- the paper has not been previously published;
- the paper is not under consideration elsewhere;
- you will transfer copyright to Taylor & Francis Ltd if the paper is accepted for publication.

There are no page charges in ***Molecular Physics***.

Fifty complimentary offprints of your article will be sent to the principal or sole author. Larger quantities may be ordered at a special discount price. The order form that accompanies the proof must be completed and returned, irrespective of whether you require additional copies.

Contact addresses:

Style guides
Lora Sharples, Editorial Assistant Journals, Taylor & Francis Ltd, One Gunpowder Square, London EC4A 3DE, UK

`http://www.tandf.co.uk`

Editorial offices
Professor H. F. Schaefer III, Center for Computational Quantum Chemistry, University of Georgia, Athens, Georgia 30602, USA; fax (1) 706 542 0406; email, "hfsiii@uga.cc.uga.edu".

Professor A. Bauder, Laboratorium für Physikalische Chemie, Eidgenössische Technische Hochschule Zürich, Universitätstrasse 22, ETH Zentrum, CH-8092 Zürich, Switzerland; fax (41) 632 1021; email, "bauder@mw.phys.chem.ethz.ch".

Professor N. C. Handy, Department of Chemistry, University of Cambridge, Lensfield Road, Cambridge CB2 1EW; fax (44) (0)1223 336362; email, "nch1@cus.cam.ac.uk".

Professor R. M. Lynden-Bell, Atomistic Simulation Group, School of Maths and Physics, The Queen's University, Belfast BT7 1NN; fax (44) (0)1232 241958; email, "molphys@qub.ac.uk".

Professor I. M. Mills, Department of Chemistry, University of Reading, Whiteknights, Reading RG6 2AD; fax (44) (0)118 9316331; email, "i.m.mills@rdg.ac.uk".

British Library Supplementary Publications Scheme
now renamed British Library Document Supply Centre (BLDSC)

Several years ago the British Library Lending Division, in consultation with journal editors, developed a scheme for the storage and distribution of material which supplements articles in scientific journals. The depositing of the details of investigations, both experimental and theoretical, means that the average length of papers is reduced and as a consequence that the number of papers published is increased. It also makes the details of the investigation available to the expert. This reduction in length is not intended to detract from the paper's general methods and conclusions which may be of interest to a large audience. However, it does enable those readers who are concerned with the details to obtain them.

Under the scheme authors submit articles and their supplementary material to the journal editor simultaneously and both are refereed. On acceptance of the paper the supplementary material is sent by the editor to the British Library Document Supply Centre. The paper should describe the material contained in the Supplementary Publication.

Supplementary material is stored in the form in which it is deposited. Inclusion of some introductory text is recommended. Pages should be numbered. The first page of a table should carry a self-explanatory heading and column headings should be repeated on continuation pages. The optimum page size is 29·7 cm × 21 cm (A4 size): the maximum is 33 cm × 24 cm for typescript and 39 cm × 28·5 cm for diagrams and graphs. Clear computer print-out is acceptable.

Copies of supplementary publications may be obtained from

The British Library, Document Supply Centre,
Boston Spa, Wetherby, Yorkshire LS23 7BQ,
England.

Registered users of the BLDSC, both in the UK and overseas, should submit the appropriate number of request forms and coupons. Other organizations and individuals in the UK and overseas can obtain copies directly from Boston Spa; they should apply to the User Services Section for a quotation.

Continued from outside back cover

MOLECULAR PHYSICS

Volume 94 Number 1 MAY 1998 ISSN 0026-8976

Continued on inside back cover

0026-8976(1998)94:1;1-P